



Provided by the author(s) and University of Galway in accordance with publisher policies. Please cite the published version when available.

Title	Fibrin-in-fibrin intervention for enhanced dopaminergic graft survival in Parkinson's disease: Special focus on brain N-glycans
Author(s)	Samal, Juhi
Publication Date	2019-11-07
Publisher	NUI Galway
Item record	http://hdl.handle.net/10379/15552

Downloaded 2024-05-14T22:10:03Z

Some rights reserved. For more information, please see the item record link above.





**Fibrin-in-Fibrin Intervention for Enhanced
Dopaminergic Graft Survival in Parkinson's disease:
Special Focus on Brain *N*-Glycans**

A thesis submitted to the National University of Ireland for the degree of Doctor of
Philosophy

Juhi Samal

October 2019

Centre for Research in Medical Devices, National University of Ireland, Galway

Research Supervisors: Prof. Abhay Pandit and Dr Eilis Dowd

Table of Contents

Table of Contents	I
List of Figures	IX
List of Tables	XIII
Acknowledgements	XVI
List of Abbreviations	XIX
Abstract	XXI

Chapter 1: Introduction

1.1 Brain as a delivery target.....	1
1.2 Design of the biomaterial intervention for therapeutic delivery in the brain.....	5
a. Cell-substrate interactions.....	6
b. Mechanical cues.....	7
c. Chemical cues.....	7
d. Topographical cues.....	8
1.3 Parkinson's Disease : Introduction.....	9
1.4 Neurotrophic factor therapy (NFT) for PD.....	13
a. GDNF in prevention of neurodegeneration.....	16
b. Biomaterial augmentation of the GDNF therapy.....	18
1.5 Cellular therapies for PD.....	28
a. Cell sources for transplantation.....	28
b. Limitations of ventral mesencephalic cells.....	30
c. Biomaterial augmentation of the cell therapy.....	31
d. Injectable hydrogels as a biomaterial scaffold.....	32
e. Injectable fibrin gel.....	33
1.6 Glycomics in neurodegeneration.....	41
a. Glycans in brain.....	42
b. Glycans in neurodegeneration.....	44
1.7 Objectives and hypothesis.....	46
a. Phase I.....	46
b. Phase II.....	47
c. Phase III.....	47
d. Phase IV.....	49
e. Phase V.....	49
1.8 References.....	50

Chapter 2: Hollow Fibrin Microsphere Reservoirs for Neurotrophic Factors

2.1 Introduction.....	94
2.2 Materials and methods.....	95
2.2.1 Fabrication of hollow fibrin microspheres.....	95
2.2.2 Morphological characterization of fibrin hollow spheres.....	96
2.2.3 Analysis of template removal.....	96
2.2.4 Size and zeta potential analysis of fibrin microspheres.....	96
2.2.5 Fluorescent labelling of NGF and fibrin.....	96
2.2.6 Loading of hollow fibrin microspheres with NGF.....	97
2.2.7 Release profile of NGF from hollow fibrin spheres.....	97
2.2.8 Internalization study of fibrin spheres using rMSCs.....	97
2.2.9 Cytotoxicity of hollow fibrin spheres.....	98
2.2.10 Bioactivity of released NGF.....	98
2.2.11 Immunostaining for neurites.....	98
2.2.12 Analysis of neurite lengths.....	99
2.2.13 In vivo analysis.....	99
2.2.14 Surgery and perfusion.....	99
2.2.15 Peroxidase-based immunohistochemistry.....	99
2.2.16 Statistical Analysis.....	101
2.3 Results.....	101
2.3.1 Fabrication and morphological characterization of hollow fibrin spheres.....	101
2.3.2 Stability of hollow fibrin microspheres.....	103
2.3.3 Loading and release profile from hollow fibrin spheres.....	103
2.3.4 Internalization of hollow fibrin spheres.....	106
2.3.5 Impact of fibrin spheres on cellular viability.....	106
2.3.6 Assessment of bioactivity of released NGF.....	107
2.3.7 <i>In vivo</i> assessment of hollow fibrin spheres.....	111
2.4 Discussion.....	115
2.5 Conclusions.....	117
2.6 References.....	118
Chapter 3: Fibrin-in-Fibrin Intervention for Enhanced Dopaminergic Graft Survival	
3.1 Introduction.....	123

3.2 Materials and methods.....	125
3.2.1 Fabrication of fibrin hollow microspheres.....	125
3.2.2 Morphological characterisation of fibrin hollow microspheres.....	125
3.2.3 Size and zeta potential analysis of fibrin microspheres.....	126
3.2.4 Loading of hollow fibrin microspheres with GDNF.....	126
3.2.5 Fabrication of the fibrin-in-fibrin intervention.....	126
3.2.6 Release profile of GDNF from hollow fibrin spheres and fibrin-in-fibrin platform	127
3.2.7 Rheological characterisation of the fibrin-in-fibrin system and rat brains.....	127
3.2.8 Cell viability and apoptosis analysis.....	127
3.2.9 Immunohistochemistry.....	128
3.2.10 Gene expression analysis.....	128
3.2.11 Quantification of the paracrine response.....	129
3.2.12 Statistical analysis.....	129
3.3 Results.....	129
3.3.1 Fabrication and physiochemical characterisation of the fibrin hollow microspheres using LbL assembly.....	129
3.3.2 Stability of hollow fibrin microspheres.....	131
3.3.3 Loading and release profile from hollow fibrin spheres.....	131
3.3.4 Impact of fibrin spheres on cellular viability.....	133
3.3.5 Optimisation of fibrin-in-fibrin platform for maximal graft survival.....	133
3.3.6 Rheological compatibility of the optimised fibrin-in-fibrin platform with the rodent brain.....	137
3.3.7 Immunohistochemical analysis for neuronal and inflammatory markers.....	137
3.3.8 Gene expression analysis for neuronal and inflammatory markers.....	138
3.3.9 Modulation of VM secretome with platform parameters.....	138
3.4 Discussion.....	140
3.5 Conclusion.....	146
3.6 References.....	146
Chapter 4: Complete Spatial Characterisation of Rat Brain N-Glycans and Modulation of Tissue Glycosignature with 6-OHDA Induced Parkinsonism	
4.1 Introduction.....	133
4.2 Materials and methods.....	135
4.2.1 Chemicals and reagents.....	135

4.2.2 Animals.....	136
4.2.3 Extraction of striatal and nigral tissues from rat brain.....	136
4.2.4 Perfusion.....	136
4.2.5 Tissue homogenization.....	136
4.2.6 Release of <i>N</i> -glycans from striatal and nigral tissue homogenates.....	137
4.2.7 2-AB labeling of <i>N</i> -glycans.....	137
4.2.8 Ultra-Performance Liquid Chromatography (UPLC).....	137
4.2.9 Weak Anion Exchange (WAX)-(UPLC).....	138
4.2.10 Glycan nomenclature.....	138
4.2.11 Exoglycosidase digestions.....	138
4.2.12 Liquid Chromatography Mass Spectrometry.....	139
4.2.13 Lectin histochemistry.....	139
4.3 Results and Discussion.....	140
4.3.1 Development of a robust glycol-analytical platform.....	140
4.3.2 Protocol verification and reproducibility.....	140
4.3.3 Glycosylation features.....	142
4.3.4 Fucosylation.....	142
4.3.5 Sialylation.....	142
4.3.6 Galactosylation.....	144
4.3.7 Mannosylation.....	144
4.3.8 Spatial regulation of <i>N</i> -glycosylation.....	144
4.3.9 Lectin histochemistry.....	147
4.4 Discussion.....	147
4.5 Conclusion.....	161
4.6 References.....	161
Chapter 5: Modulation of Brain Molecular Signature with the 6-OHDA Induction of Parkinsonism	
5.1 Introduction.....	171
5.2 Materials and methods.....	174
5.2.1 Chemicals and reagents.....	174
5.2.2 Animals.....	174
5.2.3 6-OHDA lesions, transplantation and rotational behaviour.....	175
5.2.4 Extraction of striatal and nigral tissues from rat brain for HILIC-UPLC.....	175

5.2.5 Perfusion.....	175
5.2.6 Tissue homogenization	176
5.2.7 Release of N-glycans from striatal and nigral tissue homogenates.....	176
5.2.8 2-AB labelling of N-glycans	176
5.2.9 Ultra-Performance Liquid Chromatography (UPLC).....	176
5.2.10 Tissue processing for MALDI-MSI	177
5.2.11 Deparaffinization and rehydration	177
5.2.12 N-glycan MALDI-MSI.....	178
5.2.13 Glycan nomenclature.....	178
5.2.14 Lectin histochemistry.....	182
5.2.15 Statistical analysis.....	204
5.3 Results.....	204
5.3.1 Glycosylation trends in healthy vs diseased rodent brains.....	204
5.3.2 Temporal modulation of glycosylation traits.....	204
5.3.3 Mannosylation.....	207
5.3.4 Fucosylation.....	210
5.3.5 Sialylation.....	210
5.3.6 Lectin histochemical characterisation of the disease glyco-phenotype.....	210
5.3.7 MALDI-MSI analysis of the disease glyco-phenotype.....	214
5.4 Discussion.....	218
5.5 Conclusions.....	222
5.6 References.....	222
Chapter 6: Fibrin-in-Fibrin Intervention for Enhanced Graft Survival and Glyco-modulation in 6-OHDA Parkinson’s Model	
6.1 Introduction.....	229
6.2 Materials and methods.....	231
6.2.1 Fabrication of fibrin hollow microspheres.....	231
6.2.2 Loading of hollow fibrin microspheres with NGF.....	232
6.2.3 Fabrication of the fibrin-in fibrin intervention.....	232
6.2.4 Isolation of VM cells.....	232
6.2.5 <i>In vivo</i> study.....	233
6.2.6 6-OHDA lesion and transplant surgery.....	233
6.2.7 Behavioural analysis.....	233

6.2.8 Peroxidase-based immunohistochemistry.....	234
6.2.9 Tissue processing for MALDI imaging.....	235
6.2.10 Deparaffinization and rehydration.....	235
6.2.11 <i>In vitro</i> glycan MALDI-MSI.....	235
6.2.12 Glycan nomenclature.....	236
6.2.13 Statistical analysis.....	238
6.3 Results.....	238
6.3.1 <i>In vivo</i> experimental design.....	238
6.3.2 Impact of the fibrin-in-fibrin intervention on the motor function recovery.....	238
6.3.3 Impact of the fibrin-in-fibrin intervention on striatal microgliosis.....	240
6.3.4 Impact of the fibrin-in-fibrin intervention on striatal astrocytosis.....	240
6.3.5 Biodegradability of the fibrin-in-fibrin intervention.....	245
6.3.6 GDNF release from the fibrin-in-fibrin intervention <i>in vivo</i>	245
6.3.7 Improvement in striatal re-innervation using fibrin-in-fibrin intervention.....	245
6.3.8 Improvement in dopaminergic cell survival using fibrin-in-fibrin intervention...	250
6.3.9 Impact of the fibrin-in-fibrin intervention on the modulation of host brain glyco-phenotype.....	250
6.4 Discussion.....	255
6.5 Conclusions.....	259
6.6 References.....	260
Chapter 7: Summary	
7.1 Introduction.....	267
7.2 Summary.....	268
7.2.1 Phase I –Fibrin-based hollow reservoirs for neurotrophic factor delivery.....	268
7.2.2 Phase II – Fibrin-in-fibrin intervention for enhanced VM graft survival.....	270
7.2.3 Phase III – Complete spatial resolution of rodent brain N-glycans.....	271
7.2.4 Phase IV - Modulation of brain glycol-signature with the 6-OHDA induced Parkinsonism.....	272
7.2.5 Phase V – Fibrin-in-fibrin intervention for enhanced functional recovery in 6-OHDA Parkinson’s model.....	272
7.3 Limitations.....	273
7.3.1 Phase I – Fibrin-based hollow reservoirs for neurotrophic factor delivery.....	273
7.3.2 Phase II –Fibrin-in-fibrin intervention for enhanced VM graft survival.....	274

7.3.3 Phase III& IV – Complete spatial resolution of rodent brain N-glycans and Modulation of brain glyco- signature with the 6-OHDA induced Parkinsonism.....	274
7.3.4 Phase V – Fibrin-in-fibrin intervention for enhanced graft survival and glyco-modulation in 6-OHDA Parkinson’s model.....	275
7.4 Future Rirections.....	276
7.4.1 Delivery of mesenchymal stem cell (MSCs) and dendritic cell (DC)-derived exosomes	276
7.4.2 Directed differentiation of human-induced pluripotent stem cells to dopaminergic cells on microgels.....	277
7.4.3 Glyco-engineered hydrogel system	281
7.4.4 Spatio-temporal proteomic analysis for PD progression.....	283
7.5 References	283

Appendices

A. List of reagents.....	288
B. Fibrin hydrogel fabrication.....	289
C. Isolation of Ventral Mesencephalic cells.....	289
a. Preparation of complete media.....	289
b. Plating media for E14 rat VM cultures.....	289
c. Poly-d-lysine coating.....	290
d. Ventral mesencephalon dissection.....	290
e. E14 rat VM cultures.....	290
D. Immunocytochemistry.....	291
E. RNA extraction.....	291
a. Cell lysis.....	291
b. RNA isolation.....	292
c. RNA quantification.....	292
F. Synthesis of cDNA by Reverse Transcription.....	292
G. RT-qPCR Analysis.....	293
H. 6-OHDA Parkinsonian rat model induced by stereotactic injection.....	295
I. Injection of fibrin hydrogel in 6-OHDA Parkinsonian rat model.....	295
J. Behavioural analysis – drug induced rotations.....	296
K. Tissue processing.....	297
a. Preparation of 4% paraformaldehyde solution.....	297
b. Tissue processing for cryopreservation.....	297
c. Tissue processing for embedding in paraffin.....	298
d. Tissue sectioning using the cryostat.....	298

e. Tissue sectioning using the microtome.....	299
L. Tissue histochemistry.....	299
a. Periodate treatment of bovine serum albumin for lectin histochemistry...	299
b. Lectin histochemistry on cryosections.....	300
c. Immunohistochemistry on paraffin-embedded sections.....	301
M. Lectin microarray on brain samples.....	302
N. Glycoprotein extraction.....	303
O. <i>N</i> -glycans isolation and detection.....	303
P. Exoglycosidase digestion of <i>N</i> -glycans.....	305
Q. MALDI imaging.....	307
R. Supplementary data.....	311
S. Journal publications, conference proceedings and awards.....	344

List of figures

Chapter 1

Figure 1.1	Schematic representation of the brain's protective shield.....	3
Figure 1.2	Schematic representation of the disease pathophysiology in PD.....	11
Figure 1.3	Biomaterials in neurotrophic factor delivery.....	14
Figure 1.4	Study outline.....	48

Chapter 2

Figure 2.1	A schematic outline of the modified template charge manipulation method used for the fabrication of hollow fibrin spheres	100
Figure 2.2	Fabrication of the fibrin hollow microspheres	102
Figure 2.3	Physical characterization and stability of the fibrin hollow microspheres.....	104
Figure 2.4	Characterization of the loading and release profile.....	105
Figure 2.5	Interaction of fibrin hollow spheres with cells.....	108
Figure 2.6	Impact of fibrin hollow spheres on cellular viability.....	109
Figure 2.7	Assessment of bioactivity of NGF released from hollow fibrin spheres using PC-12 cells.....	110
Figure 2.8	Sustained release of NGF and degradability of fibrin spheres <i>in vivo</i>	111, 112
Figure 2.9	Host responses to hollow fibrin microspheres.....	114

Chapter 3

Figure 3.1	Schematic outline of the experimental design.....	130
Figure 3.2	Fibrin microsphere characterization.....	132
Figure 3.3	Stability of fibrin microspheres and impact on cellular metabolic activity..	134
Figure 3.4	Loading and release kinetics of fibrin-in-fibrin intervention.....	135
Figure 3.5	Rheological assessment of the fibrin-in-fibrin intervention.....	137
Figure 3.6	Viability analysis for fibrin-in-fibrin platform.....	139
Figure 3.7	Better neuronal survival in optimised fibrin-in-fibrin intervention	141

Figure 3.8	Modulation of the paracrine and gene expression profiles.....	143
Chapter 4		
Figure 4.1	A schematic outline of the developed multi-faceted glyco-analytical platform for the qualitative and quantitative spatial analysis of rodent brain <i>N</i> -glycans.....	161
Figure 4.2	Reproducibility of the glyco-analytical platform.....	163
Figure 4.3	HILIC-UPLC and LC-MS analysis <i>N</i> - glycan compositions.....	166
Figure 4.4	Relative abundances represented as percentages of total <i>N</i> -glycans belonging to each of the three biosynthetic classes.....	168
Figure 4.5	Percentage fractions of fucosylated <i>N</i> -glycans in striatum and SN.....	169
Figure 4.6	Percentage fractions of sialylated <i>N</i> -glycans in striatum and SN.....	170
Figure 4.7	Lectin histochemical analysis for <i>N</i> -glycosylation modulation.....	173
Figure 4.8	Schematic representation of spatial resolution of <i>N</i> -glycans in striatum and SN in the rodent brain.....	179
Chapter 5		
Figure 5.1	Schematic outline of the study to elucidate the spatio-temporal modulation of <i>N</i> -glycosylation in the 6-OHDA PD model.....	201
Figure 5.2	Overall modulation of major <i>N</i> -glycans classes in the rodent brain.....	203
Figure 5.3	<i>N</i> -glycosylation modulation at Day 21.....	205
Figure 5.4	<i>N</i> -glycosylation modulation at Day 7.....	206
Figure 5.5	Temporal <i>N</i> -glycosylation modulation in SN.....	208
Figure 5.6	Temporal <i>N</i> -glycosylation modulation in striatum.....	209
Figure 5.7	Modulation of fucosylation and sialylation in striatum and SN.....	211
Figure 5.8	Lectin histochemical analyses for <i>N</i> -glycosylation modulation in PD....	212,213
Figure 5.9	MALDI-MSI resolution of <i>N</i> -glycan modulation in SN in the healthy vs diseased brains.....	216
Figure 5.10	MALDI-MSI resolution of <i>N</i> -glycan modulation in striatum in the healthy vs diseased brains	217

Chapter 6

Figure 6.1	<i>In vivo</i> assessment of the impact of a GDNF-loaded fibrin-in-fibrin platform on the survival and efficacy of primary dopaminergic neurons.....	237
Figure 6.2	Impact of the GDNF-loaded collagen hydrogel on graft functionality.....	239
Figure 6.3	Microglial response to the biomaterial intervention.....	241
Figure 6.4	Astrocytic response to the biomaterial intervention.....	243
Figure 6.5	Biodegradability of the fibrin-in-fibrin intervention.....	246
Figure 6.6	GDNF release <i>in vivo</i> from the fibrin-in-fibrin intervention.....	247
Figure 6.7	Enhanced striatal re-innervation by fibrin-in-fibrin intervention.....	248
Figure 6.8	Enhanced dopaminergic cell survival by fibrin-in-fibrin intervention.....	249
Figure 6.9	Modulation of SN glyco-phenotype by fibrin-in-fibrin intervention.....	252
Figure 6.10	Modulation of striatal glyco-phenotype by fibrin-in-fibrin intervention...	253
Figure 6.11	Modulation of major N-glycan classes in response to the biomaterial intervention.....	254

Chapter 7

Figure 7.1	Schematic representation of the milestones achieved during the study. Each phase of study is correlated towards the development of a biomaterial intervention to promote graft survival in a PD model.....	269
Figure 7.2	Schematic representing the combinatorial biomaterial therapy for augmenting the VM cell survival and promoting functional repair by minimising the neuro-inflammation by modulating the cellular paracrine response.....	278
Figure 7.3	Schematic representing the directed differentiation of human iPSCs on a 3D fibrin gel platform to VM cells to form a cellular ‘micro-graft’ for testing the potency of cellular therapies in a PD model.....	280
Figure 7.4	Schematic representation of the glycosylation approaches targeted by the biomaterial therapies to ‘tune’ the paracrine profile of the target cells to promote tissue repair.....	282

Appendices

Figure A1	Photo of rat undergoing stereotaxic surgeries.....	295
Figure A2	Parkinsonian rat exhibiting turning behaviour.....	296
Figure A3	Cylinder test for Parkinsonian rats.....	297
Figure S 5.1	Segmentation analysis in SN for comparison between healthy and diseased brains.....	334
Figure S 5.2	MALDI-MSI analysis of SN glyco-phenotype between healthy and diseased brains.....	335
Figure S 5.3	MALDI-MSI analysis of striatal glyco-phenotype between healthy and diseased brains.....	336
Figure S 5.4	Lectin microarray analysis of glyco-phenotype between healthy and diseased rodent brains.....	337
Figure S 6.1	Motor function analysis for the pilot study.....	340
Figure S 6.2	Lectin histochemical analysis for N-glycosylation modulation by the biomaterial intervention.....	341
Figure S6.3	MALDI-MSI analysis for N-glycosylation modulation in striatum by the biomaterial intervention.....	342
Figure S6.4	MALDI-MSI analysis for N-glycosylation modulation in striatum by the biomaterial intervention.....	343

List of Tables

Table 1.1	Summary of the biomaterial-augmented neurotrophic factor delivery in the pre-clinical models with the therapeutic outcomes.....	19
Table 1.2	Summary of biomaterial-augmented cellular therapies in the brain with the therapeutic outcomes.....	35
Table 2.1	Targets and antibodies used for immunohistochemistry of rat brain sections.....	100
Table 4.1	A) N-glycome of SN separated into 26 chromatographic peaks by HILIC chromatography. Structures of major glycans in each chromatographic peak and the average percentage of individual peak areas (%) as determined by HILIC-UPLC and validated by LC-MS have been represented.....	175
	B) N-glycome of striatum separated into 26 chromatographic peaks by HILIC chromatography. Structures of major glycans in each chromatographic peak and the average percentage of individual peak areas (%) as determined by HILIC-UPLC and validated by LC-MS have been represented.....	177
Table 4.2	Summary of quantifiable differences in <i>N</i> -glycosylation patterns of striatum and SN detected using the elaborate glycoanalytical platform.....	180
Table 5.1	Summary of the lectins used for tissue histochemistry with their binding specificity, assay concentration and inhibitory carbohydrate (150 mM)....	202
Table 6.1	MALDI-MSI detection of N-glycan modulation.....	251
<i>Appendices</i>		
Table A1	Summary of the phenotypic markers and antibodies used for detection....	291
Table A2	Master mix composition of reverse transcription.....	293
Table A3	Reverse transcription program in DNA engine.....	293
Table A4	PCR master mix for SYBR [®] Green.....	294
Table A5	qPCR program for TH, B-tubulin, GFAP and 18s primers.....	294
Table A6	qPCR primers for TH, B-tubulin, GFAP.....	294
Table A7	Routine program overnight for tissue processor.....	299
Table A8	Binding specificity and haptenic sugars of lectins for profiling of tissue glycosylation.....	301

Table A9	List of enzymes used for exoglycosidase digestions.....	306
Table A10	Digestion volumes used per tube for exoglycosidase digestions.....	307
Table S4.1	Calculation of derived traits.....	311
Table S4.2	Mass spectrometry tables for glycan peak identification.....	319
Table S4.3	Summary of the techniques used in the glyco-analytical platform.....	334

I certify that the thesis is all my own work and have not obtained a degree in this
University, or elsewhere, on the basis of this work

Acknowledgements

गुरु ब्रम्हा गुरु विष्णू, गुरुः देवो महेश्वरा

गुरु शाक्षात परब्रम्हा, तस्मै श्री गुरुवे नमः

I would like to dedicate the above verse as an acknowledgement to my supervisor, Professor Abhay Pandit for his valued mentorship and excellent opportunities offered throughout my PhD. I would like to express my tremendous gratitude towards Prof. Pandit who fostered my scientific aptitude by prompting me to ponder about the unanswered research questions and the constructive scientific evaluation as a peer reviewer. The constant drive to seek out more than I deemed possible and to aim high would be the ‘take-home’ from your training for me. I would like to extend a heartfelt gratitude to Dr Eilis Dowd, the ‘Parkinsonian expert’ for this study for my training in the neurobiology part of the investigation. My special thanks also to the members of the Graduate Research Committee, Dr Una Fitzgerald, Dr Dimitrios Zeugolis and Dr Manus Biggs for their valuable support during these years. A special thanks to Dr. Sunny Abbah-Akogwu for his tremendous help with the daunting *in vivo* studies performed at CÚRAM. I would like to thank Science Foundation Ireland (SFI) and the European Regional Development Fund (Grant Number 13/RC/2073) and Hardiman Fellowship for providing funding for this project.

A huge vote of thanks for Dr Oliver Carroll for being forever patient with all of us and going out of his way to help the students and researchers in the lab. I would like to reserve a special mention to our graphic designer Maciek Doczyk for contributing a lot to the figures in the thesis. Many thanks to Anthony Sloan for his timely help with the editing of this thesis and my manuscripts. I cannot express enough gratitude for his timely comments on all the documents that were sent to him and of course, the lovely morning coffee chats. I would like to thank Vidoja Kovačević for his help with the ordering and delivery as well as for the warm banter through these years. A special mention to Keith Feerick, who was one of the most hard-working professionals here at CÚRAM. He had helped each one of us tremendously and we will never forget all that he had done for us. You were always a very special part of us and you will be always be missed. May your soul rest in peace. A special vote of thanks to all the administrative professionals in CÚRAM I had the pleasure to work with: Tara Cosgrave, Mairéad Uí

Fhátharta, Dr Stefania Spada, Carmel McGroarty-Mitchell and Dr Iain Shaw. It was a pleasure as well to be involved in education and public engagement activities by Claire Riordan and Andrea Fitzpatrick. Tara, you are the ROCK solid support for all of us here at CÚRAM and we all owe you a big time for managing everything in such a nice way.

‘There are friends, there is family; and then there are friends that become family’. Such has been the experience of this PhD in CÚRAM. It’s been one hell of a journey and along the way I was blessed to have crossed path with some of the nicest people that are now a part of my ‘Galway Family’. A heartfelt thanks to all these people who were there to pick me up every step of the way and helped me grow, both professionally and personally. Shout out to Ana Lucia Rebelo (aka banana) and Dr Merari Chevalier (aka my crazy Argentinian) for their unparalleled help, love and inspiration that literally drove me to finish the thesis. I will forever cherish the memories we have made, the stories we have shared and the many moments of hysterical laughter on the inside jokes. You have to know that you are the ‘FAMILY’ that I chose and glad that you guys chose me back and tolerated me all this time. I would also like to thank Shubhasmin Rana for feeding my way out of the not-so-great days and being a true friend in need for all the bleak moments. There are no words enough to express my gratitude towards you girls! I would like to reserve a special mention to Dr Paolo Contessotto, an exceptional researcher and a friend for a lifetime, to have constantly supported me with his sarcasm, coffees and great food. A warm thanks to Alessia Di Nubila, Dr Sergio Martin Saldana, Dr Mihai Lomora and Gillian Murphy for completing my lab crew and family! A sincere thanks to Dr Shane Browne and Dr Isma Liza Mohd Isa for guiding my way through this journey. Shane, thanks for being my most ‘unexpected’ but one of the most valued people. Both of you have been really good friends and mentors, not to forget the no-sugar coating rule! A beautiful journey, that this PhD turned out to be, would not have been as exciting without some people that moved on to do better things in their life from here. A huge thanks to Dr Diana Gaspar, Dr Aitor Larranaga, Dr Christos Tapeinos and Dr Akshay Srivastava for sharing laughs with me and lab banter. Last but not the least, a special mention to Adrian Stefan Ungureanu for being such a support system for me in the last months and supporting me in every way. Words were never my forte but know that I really appreciate what you are to me! It only feels right to say ‘how lucky am I to have something that makes saying goodbye so hard’. You all are my ‘something’!

My final acknowledgements go to my family, for their unwavering support and inspiration. This, like everything else in my life would never have been possible without you; people who

have cherished with me every great moment and provided unconditional support and love all these years. I would like to thank my brother Gaur Samal, my sister-in-law, Preeti Roy Samal and our little bundle of joy, Gappi (Samaanvi) for their love and support. All gratitude is incommensurate when it comes to the love, faith and fearlessness that my dad, Mr. Ganeswar Samal and mom, Mrs. Jayanti Samal have instilled in me. Papa, you are and will always be the BEST MAN of my life and my pillar of strength. Thank you for raising me the way you did and making me the person I am today. I owe all of it to you! Also, I love you, a LOT! Maa, you're the strongest person that I know in this world and I would consider it a huge success if I live to be half as dignified and caring as you are to all of us. Past few years have been rough, but you're still the glue that holds us together. I will forever be indebted to both of you for giving me life, unconditional love and nurture. I dedicate this thesis to my parents, especially to you MAA! I hope I've made you proud.

List of commonly used abbreviations

DAPI	4',6-Diamidine-2'-phenylindole dihydrochloride.
6-OHDA	6-Hydroxydopamine
AAA	Anguilla Anguilla Lectin
ANOVA	Analysis Of Variance
AP	Anterio-Posterior
ATP	Adenosine Triphosphate
BBB	Blood-Brain-Barrier
BTDS	Brain-targeting delivery systems
BDNF	Brain-Derived Neurotropic Factor
CD11b	Integrin Alpha M/ CR3
CNS	Central Nervous System
Con A	Concavalin A
DAB	Diaminobenzidine Tetra Hydrochloride
°C	Degrees Celsius
DV	Dorso-Ventral
E	Embryonic Day
ECM	Extracellular Membrane
ESC	Embryonic Stem Cell
FCS	Fetal Calf Serum
GDNF	Glial-Derived Neurotrophic Factor
GFAP	Glial Fibrillary Acidic Protein
GFR	GDNF Family Receptor
GS-β14	Griffonia Simplicifolia Lectin
HA	Hyaluronic Acid
HBSS	Hank' s Balanced Salt Solution
H ₂ O ₂	Hydrogen Peroxide
ICC	Immunocytochemistry
i.p	Intraperitoneal
iPSC	Induced Pluripotent Stem Cell
IHC	Immunohistochemistry
IF	Immunofluorescence

LC-MS/MS	Liquid Chromatography- Mass Spectrometry
MALDI-MSI	Matrix-Assisted Laser Desorption/Ionization-Mass Spectrometric Imaging
MCT-1	Monocarboxylate Transporter 1
MFB	Medial Forebrain Bundle
ML	Medial-Lateral
MSC	Mesenchymal Stem Cell
µg	Microgram
µl	Microliter
mg	Milligram
MPTP	1-Methyl-4-Phenyl-1,2,3,6-Tetrahydropyridine
ng	Nanogram
NGF	Nerve Growth Factor
nm	Nanometre
6-OHDA	6-Hydroxydopamine
OX42	Integrin Alpha M
PBS	Phosphate Buffer Saline
PD	Parkinson's Disease
PEG	Polyethylene glycol
PFA	Paraformaldehyde
rMSCs	Rat Mesenchymal Stem Cells
ROS	Reactive Oxygen Species
SEM	Standard Error ± Mean
SN	Substantia Nigra
TBS	Tris-Buffered Saline
TH	Tyrosine Hydroxylase
TNF	Tumour Necrosis Factor
UPDRS	Unified Parkinsons Disease Rating Scale
UPLC	Ultra-Performance Liquid Chromatography
VM	Ventral Mesencephalon
WGA	Wheat Germ Agglutinin

Most abbreviations, other than commonly used expressions, are also defined at the first point of occurrence in the text.

Abstract

Parkinson's disease (PD) is a chronic, progressive neurodegenerative disorder caused due to the selective loss of dopaminergic neurons in substantia nigra pars compacta (SN) translating into the classical motor symptoms of tremors, rigidity, akinesia and postural instability. The worldwide burden of PD has more than doubled over the last 26 years, from 2.6 million to 6.1 million. This is chiefly attributed to the increased ageing of the population stemming from the increase in life expectancy, and the possible changes in the environmental and social risk factors. Most of the available therapeutic strategies in PD focus on the management of the motor and non-motor symptoms and primarily rely on dopamine replacement strategies. However, there is a major unmet clinical need to address the underlying cause of PD. i.e. the loss of dopaminergic neurons.

Comprehensive pre-clinical and clinical assessment have proven the potential of primary dopaminergic neurons to survive, integrate with the host system, re-equilibrate the striatal dopamine content and promote functional recovery. However, their routine use as a clinical therapy is hindered by the poor graft survival after transplantation and the subsequent ethical concerns with the use of multiple fetal donors for each patient. An injectable biomaterial intervention has the potential to provide a solution to this problem in a multi-faceted way by improving the engraftment of encapsulated cells through the provision of a supportive and growth factor-rich environment which effectively shields the cells from the host immune-response. To this end, the overall aim of this project was to assess the effect of a multimodal, glial-derived neurotrophic factor (GDNF)-loaded fibrin-in fibrin intervention on the survival dopaminergic neurons and the functional recovery after transplantation into the Parkinsonian brain.

The first step in the project was to fabricate and characterise *in vivo* the fibrin-based hollow microspheric reservoirs for the controlled release of neurotrophic factors. Following this, the fibrin-in-fibrin platform was optimised for the intra-cranial delivery of primary dopaminergic neurons through an exhaustive *in vitro* analysis. *In vitro* studies showed that altering the macromolecular, cell and microspheric concentration can tune the paracrine responses of the encapsulated cells. The success of biomaterial therapy is usually governed by the careful investigation and manipulation of inter-cellular and cell-matrix signalling, wherein the cell surface *N*-glycans play a consequential role. To this end, investigation of the variations in the glycosylation patterns of proteins at cellular and matrix level in brain could lead to the

identification of molecular targets for devising efficient therapeutic targets and their modulation with biomaterial therapies. This led to the next stage of the project which dealt with the complete spatial resolution of *N*-glycans in striatum and SN of the healthy and diseased brains. To the best of our knowledge, this was the first study elucidating the spatio-temporal patterns of *N*-glycosylation modulation in PD brains. This study holds tremendous potential in deciphering the glycan cues implicated in PD pathophysiology and to develop viable biomaterial therapies harnessing the ‘glyco-code’ elucidated in this study.

Further, to test for therapeutic potential of the fibrin-in-fibrin intervention, 6-hydroxydopamine (6-OHDA) rodent model was used as a relevant pre-clinical animal model as it is the most suited model to validate the experimental therapies. In summary, it was demonstrated that the optimised fibrin-in-fibrin intervention is well tolerated in the brain and successfully augmented the engrafted cell survival along with the neurite outgrowth. The intervention acted as an effective shield to attenuate the host response against the implanted cells. Building on this, a pilot analysis showed that the encapsulation of embryonic day (E) 14 VM cells in a GDNF-loaded fibrin-in-fibrin platform mediates a dramatic five-fold increase in the survival, which translated into a significant improvement in the functional recovery in the rotational behaviour and limb placement asymmetry. Additionally, this study represented the dynamic re-modelling of the brain glyco-environment using the fibrin-in-fibrin intervention away from the diseased phenotype and towards the healthy brain glyco-phenotype using matrix-assisted laser desorption/ionization mass spectrometric imaging (MALDI-MSI). To summarise, this thesis attempts to address some major biological and clinical lacunae in the field by the application of a multidimensional approach through the investigation of the implication of glycosylation in a relevant model of PD, the application of an ECM-inspired fibrin-based, brain-targeted intervention and elucidating the mechanistic story.

Chapter 1

Biomaterial intervention of therapeutic and cellular delivery to the brain in PD

Sections of this chapter are published as:

Samal J*, Rebelo AL*, Pandit A.P. (2019). "A window into the brain: Tools to assess pre-clinical efficacy of biomaterials-based therapies on central nervous system disorders." *Advanced Drug Delivery Reviews* (in press).

1.1 Brain as a delivery target

The brain is befittingly protected by layers of fluidic and solid processes along with the cerebrospinal fluid (CSF) that function together to buffer and protect it from challenges in the external environment that might result in brain injuries [1,2]. About 11% of the world population is currently suffering from disorders of the central nervous system which is anticipated to increase to 14% by 2020 [3]. A major proportion of this is the elderly population over 70 years of age, where the incidence of central nervous system (CNS) disorders is 50% or more [4]. Two major causes of the CNS disorders are neurodegeneration and neuroinflammation. Neurodegenerative disorders like Alzheimer's disease (AD), Parkinson's disease (PD), Huntington's disease (HD), and Amyotrophic Lateral Sclerosis (ALS) are a substantial proportion of CNS disorders that are characterized by age-related progressive loss of neuronal function followed by cell death [5]. There are many causes and mechanism of neurodegeneration involving a cascade of molecular changes that makes devising an efficient treatment very complicated [6].

Maintenance of brain homeostasis and the exchange of molecules between peripheral circulation and brain is stringently regulated by three interfaces or barriers: the blood-brain barrier (BBB), the choroid plexus epithelium and the arachnoid epithelium. The BBB is a sieving layer composed of cerebrovascular endothelial cells, astrocytes end-feet, pericytes and basal lamina characterised by the presence of tight junctions between the endothelial cells, transmembrane protein-complexes and minimal fenestra [7]. Molecules in circulation have access through the BBB subject to following criteria (i) low molecular weight lipid-soluble molecules (MW <400 Da) or (ii) endogenous BBB transporter mediated transport. The role of these barriers and various strategies to circumvent them have been represented in **Figure 1.1**.

Efficient drug delivery to the brain remains a challenging domain because of the various physical and biological aspects involved in delivery. The majority of the large-molecule drug candidates for various brain disorders have restricted clinical translation because of their inability to reach the site of interest in the brain at therapeutically relevant concentrations. The impact that any nanoparticle (NP) or therapeutic molecule can have depends on their interaction with target cells. This has given way to extensive research on the metabolic fate of therapeutics after administration, their distribution and targeting capacities. Major limitations to targeted brain delivery can be broadly categorized into (I) physical factors like blood flow, particle size, CSF turnover and the ratio of diseased to healthy cells in the brain and (II) biological factors including the absence of tissue-specific transporters, biomarkers or the presence of specific

exclusions including perineuronal nets or pH differences around certain neurons. The invasive nature of direct delivery to the diseased site makes the drug administration in blood a safer option which means its dilution in 4.7-5l of blood in the human body. This is followed by their distribution over 100,000 km of blood vessels [8] during which in every blood cycle they extravasate and accumulate in the tissues. This process of extravasation takes place for hydrophilic molecules in the size range of 5-12 nm for most tissues such as the liver. Free extravasation in the brain, however, is allowed for molecules or particles of 1 nm or less in diameter and the others are under stringent regulation of transcellular pathways [9]. Further dilution of drugs/delivery systems occurs in 150 ml of CSF [10] after crossing the blood brain barrier (BBB) followed by distribution over 1.5 litres of brain volume for an average adult [11], where the regular turnover of CSF plays a crucial role in their clearance from the brain. All these factors make it very difficult to arrive at a specific dosage of drugs/ delivery vehicles to successfully achieve a therapeutic effect or prevent the nanoparticle- associated toxicity and this gives rise to a major concern in designing the drug-delivery vehicles.

To address this, there is mounting research interest in developing biomaterial-based strategies to overcome these physical and biological barriers to therapeutic transport for CNS disorders. These biomaterial therapies provide a solution more suited to the invasive neural surgeries to deliver therapeutics to a target site in the brain and can be fabricated using natural or synthetic polymers. The biomaterial-based delivery systems show inherent diversification in their architecture dictated by the fabrication protocols, drug-loading properties, mechanism of brain-targeting, target specificity and stability of the system. Biomaterial-based platforms offer an advantage over other delivery systems in terms of the magnitude of therapeutic loading [12]. Encapsulated therapeutics are sheltered against chemical or enzymatic action when these systems are delivered into the body and are in contact with the circulation, thereby increasing the odds of their delivery at a pharmacologically relevant concentration. Multiple surface modifications could be used to tailor the therapeutic platform for target specificity [13,14]. An effective biomaterial platform for brain delivery would be a meticulously tailored balance of parameters including stability, immunogenicity and degradation profile. These would enable the transport of a high payload in a spatiotemporally regulated manner. **Figure 1.1** represents the physical and biological barriers for therapeutic delivery into the brain and elucidation of different brain-targeting delivery systems (BTDS) with their mechanism of evading the BBB.

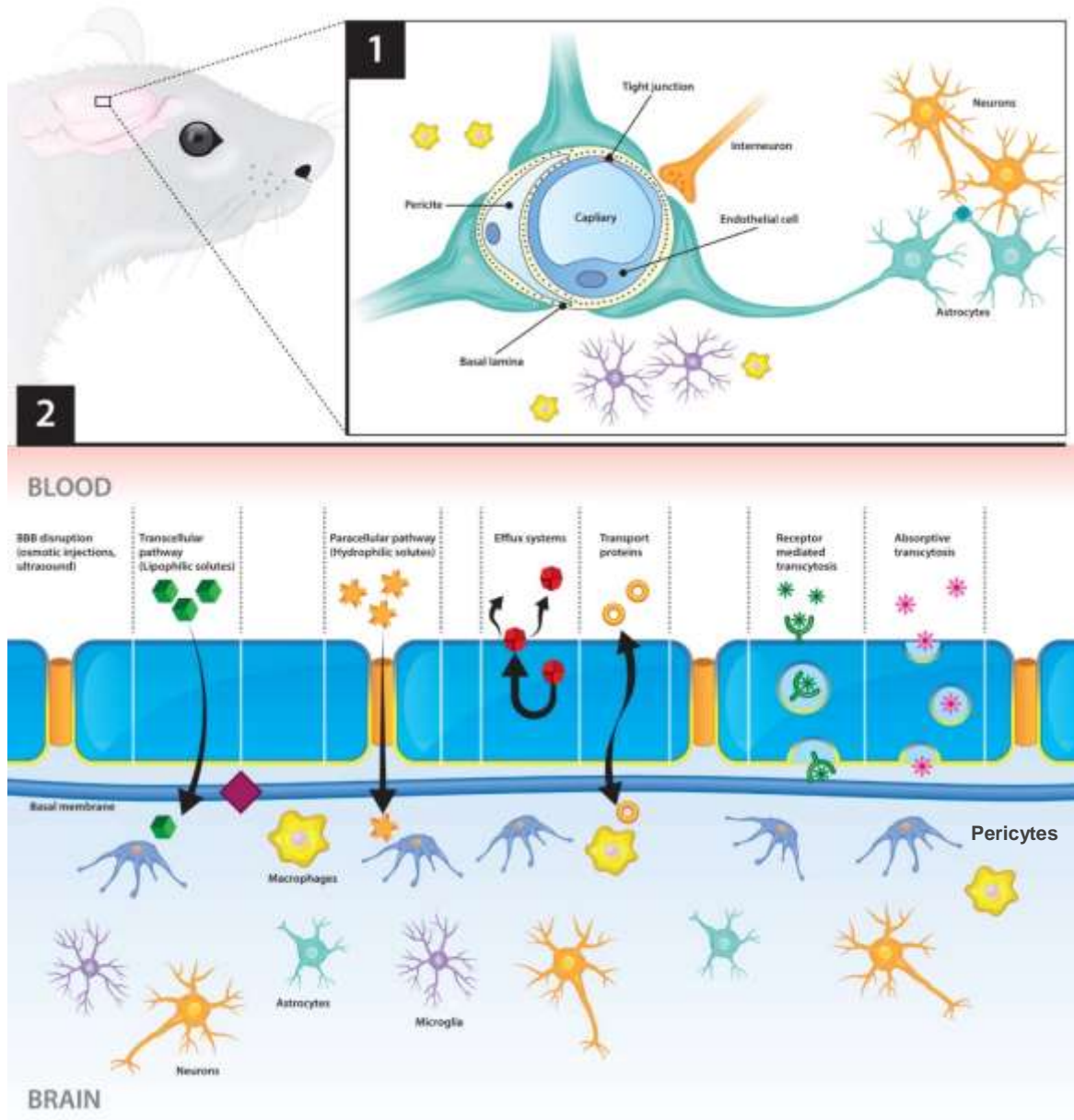


Figure 1.1: Schematic representation of the brain's protective shield: (1) Representation of blood-brain barrier (BBB) that effectively masks the brain from free access to the molecules in circulation and (2) Mechanisms of evasion of the BBB used by various delivery systems to facilitate the molecules in circulation to gain access to the brain.

Any nanoparticle or therapeutic targeted to the brain in a systemic injection are faced with the BBB. It acts like a filter with a certain cutoff, thereby limiting the entrance of certain molecules into the brain. It is composed of cerebrovascular endothelial cells, astrocytes end-feet, pericytes and basal lamina providing the mechanical support and segregation from neighboring tissues. The junctions between the endothelial cells act as a selective passage for the molecules carried by the blood [15]. Brain interstitial fluid is accessed by molecules in the circulation only if they meet any one of these conditions (i) either they are lipid-soluble molecules with a molecular weight <400 Da, or (ii) they are transported across the endothelium via an endogenous BBB transporter. Smaller molecules like nutrients, vitamins etc. are carried across the BBB via endogenous carrier-mediated transport (CMT) [16] whereas larger molecules like neurotrophins and cytokines are carried across the BBB via saturable receptor-mediated transport (RMT) and absorptive endocytosis [17]. The saturable transport can be unidirectional (brain to blood or blood to brain) or bidirectional. The process can be either an active transport or facilitated diffusion depending on the energy used in the course of transport. Absorptive endocytosis chiefly involves electrostatic interactions between the positively charged moieties of peptides or glycoproteins with the negatively charged plasma membrane. Absorptive endocytosis has been demonstrated to be involved in the transport of various therapeutic peptides such as the adrenocorticotrophic hormone (ACTH) analogue, ebitatide as a therapeutic option for Alzheimer's [18] and E-2078, dynorphin- like analgesic peptide [19]. This mode of transport across the BBB is favorable only for those peptides which are amenable to chemical modifications to make them cationic and show stability against enzymatic degradation. Besides, it is not a very target-specific mode of delivery because of lower affinity and non-specific binding in other tissues.

Further, larger proteins and peptides are transported across the BBB by using the receptor-mediated saturable systems. This is most evidently demonstrated by the transport of enzyme GUS which, despite of its huge size (300 KDa), is transported by a saturable mannose-6-phosphate receptor (M6PR) across the neonatal BBB into the brain [20]. Besides the physical barriers, the impact of filtration is further boosted by the enzymatic and transporter functions such as P-glycoproteins which eliminate small molecules before reaching the basal side [21]. This restricts the accumulation of cytotoxic molecules in the brain. Several other efflux systems have been also characterized like monocarboxylate transporter 1 (MCT1), related receptors for probenecid homeostasis [22] and organic anion transporting polypeptide (oatp2) for digoxin detoxification from the brain [23].

1.2 Design of the biomaterial intervention for therapeutic delivery in the brain

Recent advances in molecular and pathway analyses are constantly improving the current understanding of neurodegenerative diseases, yet an effective repair of the damaged brain still remains a daunting task. A better understanding of the underlying disease pathology taken together with cell-based therapeutics and tissue engineering approaches aim at effectively replacing the damaged neurons or prompting the neuronal circuits to regenerate. The blueprint to achieve an effective brain protection, repair and recovery includes the therapeutic delivery of neuroprotective compounds, remodelling the tissue- microenvironment using tissue engineering, cellular therapies to replace lost cells and directed efforts at enhancing neuronal plasticity to promote the ability of the brain to regenerate and reorganize. Each of these strategies is faced with considerable challenges to overcome for clinical translation. About 90% of the neuroprotective drugs are inactive following systemic administration because they are sieved out by the blood–brain barrier or they have very short half-lives [24,25]. Cell-based therapies have poor cell survival and integration in the host circuitry post-implantation and fall short of recapitulating the explicit architecture and functional wiring present host brain [26]. Poor regulation of cellular growth processes, differentiation and migration to the appropriate location limits the success of the strategies aimed at modulating the brain's inherent plasticity.

Tissue-engineered scaffolds offer some lucrative solutions for the treatment of neurodegenerative disorders. However, currently the design and fabrication of these scaffolds are still in its initial stages and must comply with several preconditions before their standardised employment in treatment regimen. Towards their use in the neurodegenerative disorders, scaffolds should be able to support neural cells (either transplanted or endogenous) through optimization of surface functionality, mechanical properties, and biological activity. In other words, the successful fabrication of a tissue engineered scaffold to mimic the cellular microenvironment is one of the prime challenges. Fabricating a scaffold to overcome the morphological (porosity, stiffness etc.) and biological (toxicity, biocompatibility etc.) limitations is a daunting task. More importantly, the biological function of the scaffold should be customised to address the necessities of individual disease processes due to the varied pathophysiology. It is, therefore, imperative to optimise the physical attributes like porosity

and functionalisation with neurotrophic cues with appropriate mechanical compatibility to make it well suited for *in vivo* applications.

a. Cell-substrate interactions

The CNS ECM is particularly enriched in proteoglycans such as chondroitin sulfate proteoglycans (CSPGs), glycosaminoglycans such as hyaluronic acid (HA), and proteins such as laminin and collagen [27]. The survival of the engrafted cells can be maximised by carefully tailoring the biomaterial substrates to closely mimic the ECM. A biomaterial substrate usually acts as a blank palette which can be decorated with the biological cues to promote specific cell–substrate interactions. ECM proteins are recognized by cell surface receptors and are involved in dictating the cellular fate such as proliferation, differentiation, and migration. Fibronectin is one such component of the CNS ECM that interacts with integrins to promote cell adhesion and viability [28]. Despite its presence in a limited amount in the healthy CNS matrix, it plays a pivotal role in promoting axonal regeneration of adult neurons [29]. This paved the way to the development of several ECM-derived synthetic, integrin interacting peptides that boosted cell adhesion and viability [30,31]. Similarly, there have been previous reports about synthetic laminin-derived peptides and their ability to promote neural cell adhesion and neurite outgrowth: tyrosine–isoleucine–glycine–serine–arginine (YIGSR) [32] and isoleucine–lysine–valine–alanine–valine (IKVAV) [33], respectively. Another instance representing the role of ECM peptide mimetics is the neural cell adhesion molecule (NCAM)-derived amino-acid sequence, EVYVVAENQQGKSKA, which actuates neurite outgrowth and increases neuronal survival[34].

To promote the cell–substrate interactions, these cell-adhesive peptides have been unified with biomaterial strategies. The conformation of the peptide and the presentation of the immobilized peptide is critical to its binding with the corresponding integrin receptor. Peptide adsorption and/or non-specific conjugation disrupts peptide conformation, resulting in poor receptor binding and irreproducible results. Regulated bio-orthogonal, water-based reactions act as a superb immobilization strategy, as it relies on specific coupling chemistry yielding controlled biomolecule orientation [35]. These peptide mimetic-based hydrogels functionalized with RGD have been shown to enhance the dorsal root ganglia neurite outgrowth [36]. Similar results were observed with the acrylate-modified dextran hydrogels functionalized with thiolated YIGSR and IKVAV peptides [37].

b. Mechanical cues

To enhance the engrafted cell survival, a matrix support mimicking the physical properties similar to the native environment (i.e. the brain) must be offered to cells and axons. This presents a major design obstacle given the native brain tissue has an elastic modulus of 0.5–1 kPa.[38,39]. Previous proof-of-concept studies have demonstrated that the neural cells respond to the mechanical properties through migration, biased differentiation and varied neurite trajectory and development [40–42].

An ideal tissue-engineered scaffold for brain tissue engineering will also emulate the physical and mechanical properties of the tissue. In this regard, a seminal study by Leipzig et al. (2009) showed that gel stiffness affected the differentiation profile of rat neural stem cells where softer (<1 kPa) methacrylamide chitosan hydrogels promoted the differentiation into astrocytes and neurons, whereas stiffer gels (>7 kPa) differentiated them into oligodendrocytes [43]. Gel stiffness also impacted the proliferation with an intermediate stiffness (3.5 kPa) exhibiting the greatest amount of proliferation. Another study by Sur et al (2013) reported that the gel stiffness could tune the differentiation of the embryonic dissociated hippocampal cells to neuronal phenotypes [44]. This study showed that the cells cultured on softer peptide amphiphilic hydrogels (~7 kPa) showed significantly higher neuronal differentiation, maturation, and synapse density compared with cells cultured on stiffer hydrogels (~25 kPa). An intriguing observation was the phenotype shift that the modulation of the scaffold could affect in the MSCs. On soft substrates, with moduli comparable to that of the brain (0.1–1 kPa), MSCs showed a preferential differentiation to neuronal phenotype[45]. Moreover, the stiffness of substrates also effects cell viability which was found to be higher on softer hydrogels [46]. The response of different cell types to their physical environment is highly cell-specific, thereby informing effective bioengineering strategies to customise the materials for tissue repair. To conclude, a subtle modulation of the mechanical properties can significantly transform the cell fate, making it consequential in therapeutic scaffold design.

c. Chemical cues

Better intercellular signalling and bioactivity is observed as a consequence of the synergy between immobilized growth factors and cell adhesion molecules leading to the cell receptor activation [47]. A synergistic effect of multiple growth factors on fibrin backbone (ie, platelet-derived growth factor (PDGF), vascular endothelial growth factor (VEGF), and bone morphogenetic protein-2 (BMP-2) resulted in greater bioactivity when compared with binding them on separate polymer backbones [48]. A similar effect was observed by Tam et al (2012)

in the domain of differentiation of NSPCs into oligodendrocytes where the combined therapeutic effect of PDGF-A and RGD peptide resulted in better differentiation compared with controls of each bioactive molecule alone or even both on separate polymeric backbones [49]. Together, the studies demonstrate that cell–substrate interactions are influenced not only by the presence of specific ligands but also by their spatial orientation relative to each other. The requirement of specific ligands for promoting specific cellular responses such as adhesion and/or differentiation as well as their orientation in the substrates are important considerations when designing biomaterials to promote repair *in vivo*.

Complimentary to the bio-affinity of ECM components, microarchitecture also plays a pivotal role in directly modulating the immobilised growth factor activity and cell fate during tissue repair. Inert biocompatible RADA₁₆-functionalised peptide hydrogel (G' 300 Pa) was reported for recovery of cerebral neocortex injury in a rat brain surgery model where it filled up the cavity and promoted reduced astrogliosis [50]. Similar peptide-functionalised hydrogel was shown to promote the cellular viability and outgrowth of spiral ganglion neurites compared to the unmodified hydrogel [51]. IKVAV peptide hydrogel containing peptide-amphiphile nanofibers exhibiting a multimodal architectural support when tested in *in vivo* mouse spinal cord injury model enhanced cell viability (~two fold) at the site of injury and promoted development of motor neurons [52,53]. Methacrylamide chitosan (MAC) scaffold functionalized with interferon- γ (IFN- γ) for neurons, platelet derived growth factor-AA (PDGF-AA) for oligodendrocytes, or Bone morphogenetic protein-2 (BMP-2) for astrocytes modulated the differentiation of subcutaneously implanted NPCs into different lineages. One of the chief observations of this study was the enhanced differentiation potential observed as a function of tethering the ligands to the scaffolds rather than providing them in solution [54]. 3D microtopographic scaffolds incorporating tunable electrospun microfibers that promote *in situ* stem cell neuronal showed a ~38-fold improvement *in vivo* cell viability and 3.5-fold improvement in neurite outgrowth [55]. Alginate-based capillary hydrogels seeded with brain-derived neurotrophic factor (BDNF) expressing bone marrow stromal cells (BMSCs) were found to guide the axon extension and affected a 3–4 fold increase in the axon length at the lesion site [56]. All these studies are well representative of the combinatorial impact of the substrate architecture with functionalisation in promoting the neural regeneration.

d. Topographical cues

The microarchitecture of the native ECM emanates from the dynamic remodelling achieved as a consequence of the cells secreting and degrading structural molecules to construct the 3D

niche imperative for cellular functions [57]. These ECM structures manifested as fibers, pores, and ridges, provide the essential structural support for cellular alignment and physical cues for cellular interactions [58]. These topographical cues have been shown to direct stem cell fate, but their impact on the lineage commitment and subsequent maturation stages of dopaminergic (DA) cells have been less investigated. A recent study by Tan et al (2018) applied topographical patterns sequentially to human induced pluripotent stem cells (iPSCs) during differentiation stages to test their ability to influence the yield and functionality of subtype-specific DA neurons [59]. Gratings showed higher yield of DA neurons and pillars yielded better network formation and functionality. Earlier studies have shown that relatively larger clustered ECM molecules promote proliferation while small clusters induce apoptosis, thus demonstrating the paramount importance of the size and shape of the ECM molecules in influencing cellular fate and function [60]. Alignment is another topographical aspect of particular interest in the development of scaffolds intended highly organized tissue repair like the CNS where it exerts substantial effects on the guidance and orientation of neural cells and their processes [61,62]. Moreover, the fiber diameter also has a significant impact on the orientation of process outgrowth, where small-diameter, high surface curvature fibers prompted an increasing tendency for neurite outgrowth [63].

Cell–substrate interactions could be manipulated up to a sub-micron level with the recent advances in nanotechnology and electrospinning [63]. A study by Tsai et al (2004) demonstrated that PMMA hydrogel channels were used to promote tissue regeneration of transected rat spinal cords [64]. The authors showed an enhanced axonal regeneration by contact guidance cues provided by the cord stumps in the hydrogel channels while limiting the growth of scar tissue. A seminal analysis was performed by Moore et al (2006) where they synthesized multi-channelled scaffolds with tunable properties to support the growth and guidance of multiple cell types within a single scaffold in a spatio-specific manner [65]. All these studies taken together highlight the importance of understanding of cell–substrate interactions, as well as cell–cell interactions for the optimal design of biomaterial- and cell-based treatment strategies intended to promote functional repair

1.3 Parkinson’s Disease: Introduction

Parkinson’s disease (PD) is the second most common neurodegenerative disease after Alzheimer disease. First described by Dr. James Parkinson in 1817 as a “shaking palsy”, PD is

characterized by a progressive loss of dopaminergic neurons in the SN pars compacta which translates to both motor and non-motor symptoms. In PD, there is a long latency between the first damage to cells in at-risk nuclei of the nervous system, and the onset of clinical symptoms. Although the incidence of PD is more common in the elderly, there have been cases of individuals reported with PD at 30 or 40 years of age [66]. Very interestingly, the gender differences in the incidence of PD are reflected in the delayed onset in the females attributed chiefly to the neuroprotective effects of estrogen which translates to a 3:2 ratio of males to females diagnosed with PD [67]. The manifestation of the motor symptoms of the disease only occurs after the loss of about 70–80% of dopaminergic neurons [68]. This accentuates the need of identifying patients in the period amid the onset of dopaminergic cell loss and the appearance of clinical manifestations for the development of effective neuroprotective treatment strategies [69]. PD is hypothesized to be the result of an interaction between several genetic and environmental factors. The interplay of genetic predisposition and environmental factors induces the mitochondrial failure and oxidative stress within SN neurons [70]. The hypothesis of exogenous toxins as causative factors in PD gained recognition from the induction of Parkinsonian syndrome by 1-methyl-4-phenyl-1,2,3,6-tetrahydropyridine (MPTP) [71] and pesticides related in structure to MPTP [72]. Accumulation of 1-methyl-4-phenylpyridine (MPP⁺) in dopaminergic neurons mediates the toxicity of MPTP by inhibiting complex 1 of the mitochondrial respiratory chain. This depletes the neurons of energy, ultimately causing cell death. Earlier studies showed that there is an impairment of enzymes that form complex 1 in PD [73]. Another cardinal reason for the development of PD is a deficient antioxidant system. Glutathione mediates the clearance of the peroxide ions generated by the oxidative metabolism of dopamine by monoamine-oxidase (MAO). Reduced glutathione levels in PD leads to the accumulation of more toxic free oxygen radicals, which damage the dopaminergic neurons [74,75].

Another factor implicated in neurodegeneration in PD is the decreased activity of the proteasome resulting in reduced ability to clear proteins to clear excess or misfolded

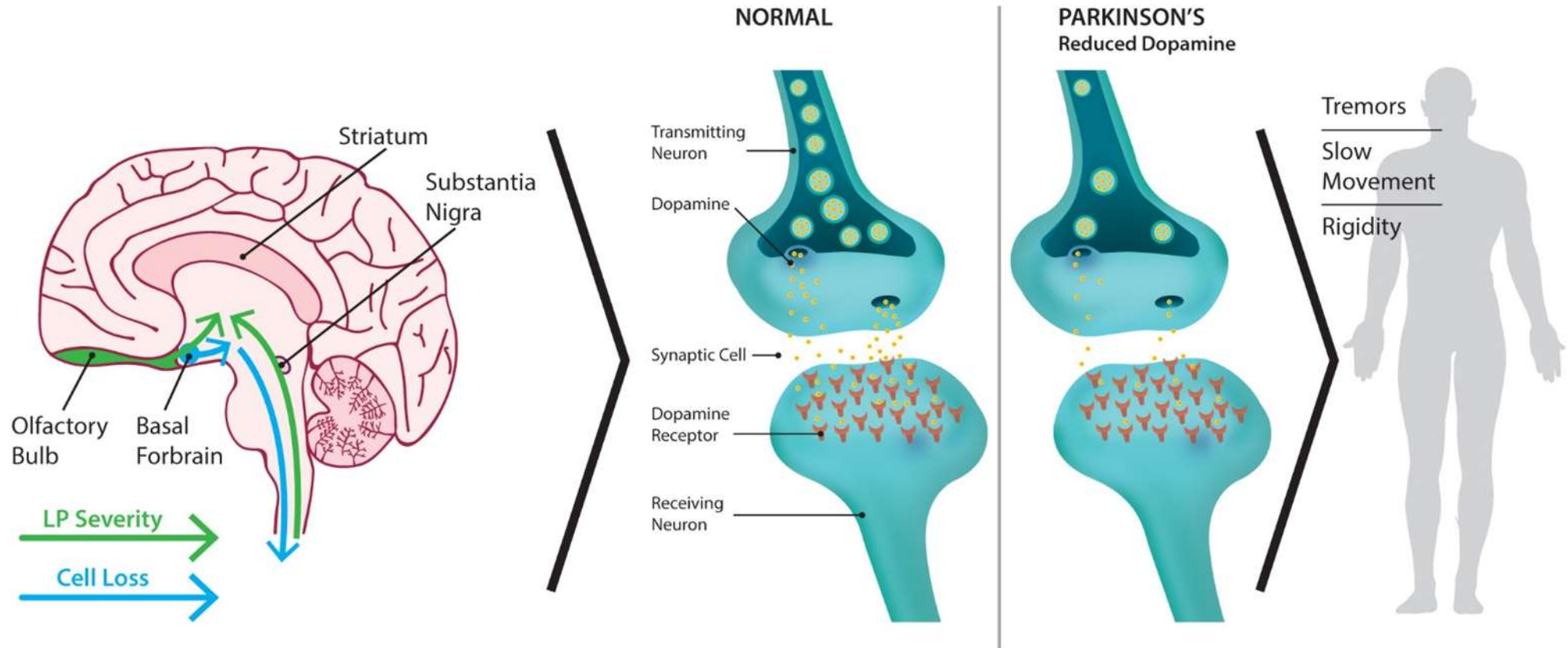


Figure 1.2: Schematic representation of the disease pathophysiology in PD: Schematic representation of the regions in the brain affected by the induction of Parkinson's disease with the green arrow indicative of progression in lewy pathology (LP) and the blue arrow indicative of the subsequent loss of dopaminergic neurons. This translates to an aberrant dopamine signalling manifesting in the brain translating into the motor manifestations of tremors, rigidity, akinesia and postural instability.

proteins from the brain [76]. Several genetic mutations have been demonstrated to cause parkinsonian syndromes that closely resemble idiopathic PD. The characterisation of single-gene mutations in some cases of familial PD has highlighted the three main disease mechanisms caused by these gene mutations implicated in PD as dysfunction of the UPS, abnormalities of the oxidative stress response and mitochondrial defects [77]. Activated host glial cells (astrocytes and microglia) are known to intervene in the neurodegeneration by amplifying the primary neuronal stress and mediating neuronal degeneration [78].

A major histopathological hallmark of chronic neurodegenerative diseases including PD is the presences of lewy bodies (LBs) (**Figure 1.2**), described as intracellular cytoplasmic inclusions composed of proteins, lipids, and other materials. Six neuropathological stages of this disease based on the localization of the affected neurons and the involved brain regions revealed six pathological stages of this disease [79]. The pathology initiates in the lower medulla oblongata, specifically the dorsal motor nucleus of the vagal nerve, and the anterior olfactory structures and is characterised as stage 1. Stage 2 is often characterized by the lesions in the dorsal motor nucleus worsening, inclusions developing in the lower raphe nuclei, and Lewy neurites in the locus ceruleus. Stage 3 affects the SN followed by stage 4 where lesions appear in the cortex. Stage 5 is characterized by the propagation of the pathology in the adjoining temporal neocortical fields, while in stage 6 cortical involvement is evident. These pathological stages are well correlated with the cognitive decline.

There is an urgent need to find reliable molecular biomarkers to distinguish PD from other neurodegenerative/ psychotic conditions, monitor its progression, or monitor its response to therapeutic intervention [80]. α -Synuclein (α -Syn) aggregates are toxic to the dopaminergic neurons in the SN, and can readily facilitate the transmission of toxic α -syn from affected cells to adjacent healthy cells, thereby promoting progressive neuronal death [81,82]. The propagation of α -syn between cells is usually a commonplace phenomenon. However, in the presence of a stress cue, pre-aggregated α -syn acts as a 'seed' to induce the aggregation of soluble α -syn within the receiver cells in a 'prion-like' fashion [70]. Furthermore, any malfunction in lysosomal-clearance mechanisms could cause the spread of PD pathology through exosomes and other inter-cellular communication pathways because α -syn aggregates are normally cleared by the proteasome system or by the lysosomes. Exosomes facilitate the clearance of unwanted proteins from the healthy neurons which explains the release of α -syn from neurons in normal conditions. Any cellular or environmental trigger that leads to higher α -syn secretion could be transmitted to other adjacent cells and promote neuronal degeneration.

This necessitates the identification of more reliable molecular markers that are closely related to the neuropathology and can be used to diagnose the disease with precision as well as monitor the efficacy of therapeutic interventions.

1.4 Neurotrophic factor therapy (NTF) for PD

NTFs are small secreted proteins that regulate the induction, survival and maturation of developing neurons and play a crucial part in regulating neurite branching, synaptic plasticity, and neuronal phenotype through the binding and activation of their receptors. NTFs are also involved in supporting and protecting the mature neuronal populations in an adult brain and providing a conducive environment to survive. Additionally, as NTF deficiency has been associated with progressive loss of dopaminergic neurons in PD, several factors have been investigated for their neurotrophic and protective impact on dopaminergic neurons. This is demonstrated by several studies investigating the replacement or enhancement of NTF signalling mediating the neuronal protection in both cellular and preclinical PD models [83]. Currently available NTF-based therapeutic approaches aim at the attenuation of the severity of symptoms in the PD, rather than addressing the cause of the disease. However, ongoing research has been focusing on disease-modifying biomaterial-based strategies using the NTFs to alter the natural course of the disease by modulating the cellular phenotypes (**Figure 1.3**). The aim of this therapeutic approach would be to apply the NTFs which can effectively halt or reverse the progressive degeneration of nigrostriatal dopaminergic neurons, thus addressing the underlying cause of PD. Another important aspect of the NTF delivery in the clinical scenario is to deliver the NTFs to the patients in a prolonged, safe and targeted manner. The NTF superfamily is subdivided into four major groups: (1) the neurotrophin family; (2) the glial cell line-derived neurotrophic factor (GDNF) family of ligands (GFLs); (3) neurotrophic cytokines (neurokinines); and (4) the family of cerebral dopamine neurotrophic factor (CDNF) and mesencephalic astrocyte-derived neurotrophic factor (MANF) [83]. The neurotrophin family in the mammals comprises of nerve growth factor (NGF), brain-derived neurotrophic factor (BDNF), neurotrophin-3 (NT-3), and neurotrophin4/5 (NT-4). The activation of the cognate tropomyosin-related kinase receptor (TrkA, TrkB or TrkC), or the p75 neurotrophin receptor (p75^{NTR}) mediates the biological activity of the neurotrophins, by modulating the Trk activation and downstream signalling [84,85]. Reduced levels of NGF were detected in the SN, cerebrospinal fluid and serum of PD patients [86]. NGF was also shown to augment the survival of the adrenal medullary cells engrafted in the basal ganglia of PD patients [87].

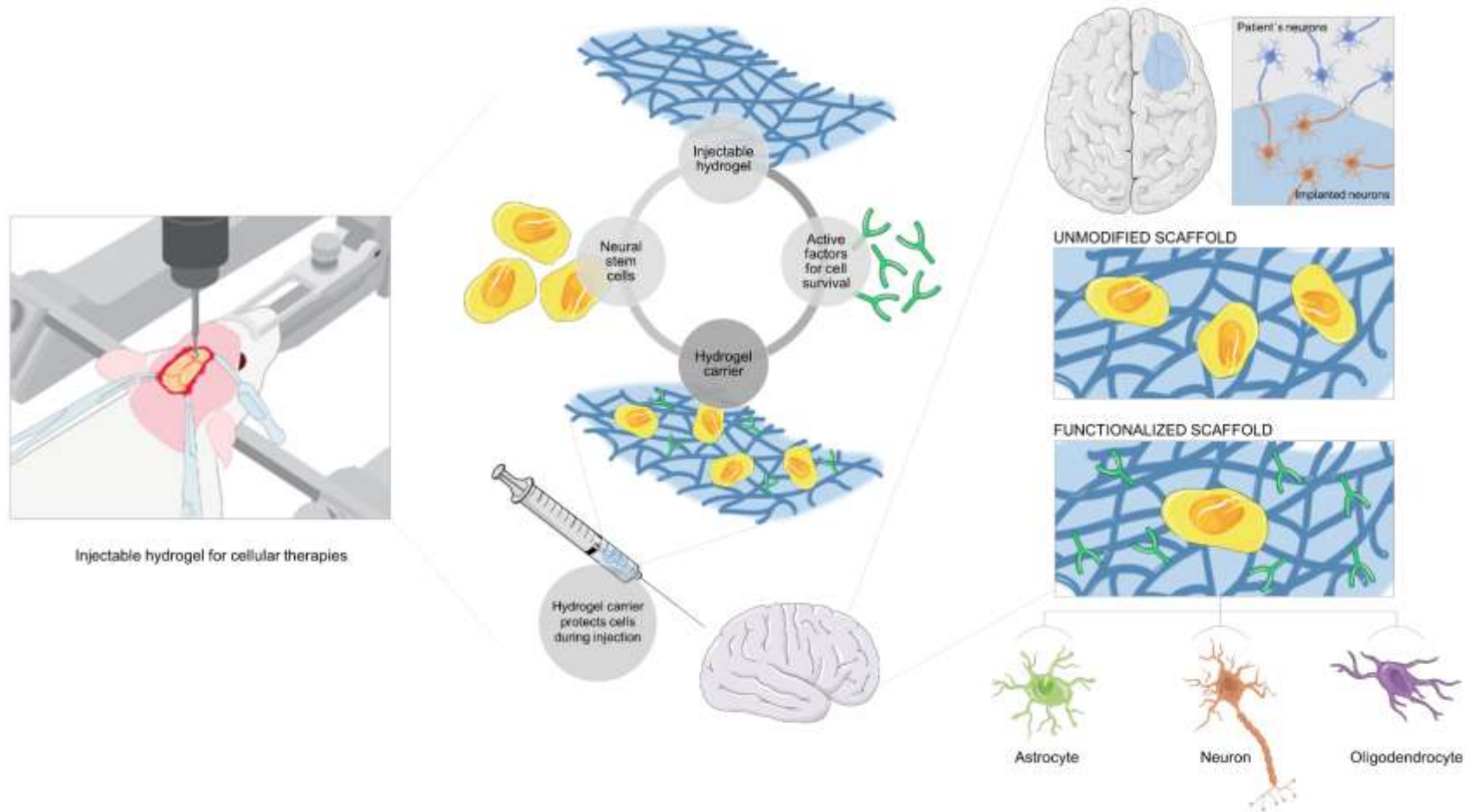


Figure 1.3: Biomaterials in neurotrophic factor delivery: Neurotrophic factor therapy augmented using the biomaterial platforms in combination with cellular therapies to promote selective differentiation into specific phenotypes.

A recent study by Rahmani et al. (2017) showed that the PD patients had reduced serum BDNF levels compared to those of the healthy individuals. The study also revealed a proportional correlation between motor progression and serum BDNF downregulation in PD, thus emphasizing its implication in the disease pathophysiology [88]. Besides, the therapeutic application of BDNF [89,90] and NT-3 [91,92] have shown significant trophic effects, attenuation of progressive neurodegeneration, reversal of the behavioural deficits and protection of the engrafted neurons in several disease models for PD.

Amongst the lesser investigated NTFs are CDNF, together with its closest relative MANF, which are localized mainly to the lumen of endoplasmic reticulum (ER) [93,94], comprise of a novel family of structurally and mechanistically distinct NTFs. The chief mode of action for CDNF and MANF is the modulation of the unfolded protein response (UPR) pathway [95,96]. The presence of a prolonged and aggravated ER stress activates cellular signals leading to cell death and this has been suggested to be involved in neurodegenerative diseases, such as Parkinson's disease, Alzheimer's disease, and is an important target for therapeutic modulation [97,98]. Intraputamenally administered recombinant human CDNF has shown robust neurorestorative effects in a number of small and large animal models of PD, and had a good safety profile in preclinical toxicology studies [99]. Injection of CDNF in the rat [95,100,101] and non-human primate [99] 6-OHDA and MPTP model of PD, resulted in robust recovery of motor functions, and showed specific neuro-protective and regenerative effects towards tyrosine hydroxylase (TH)-positive dopamine neurons. Currently, intraputamenal infusions of CDNF using a neurosurgically implanted drug delivery system similar to the one used in the Bristol GDNF phase II study [102,103], are being tested in a randomized placebo-controlled phase I-II clinical study in moderately advanced PD patients [104]. Similarly, MANF has been tested in both 6-OHDA and MPTP rodent models of PD and shown significant neuroprotection of the dopaminergic neurons and functional recovery through the inhibition of the oxidative stress [105,106]. Interestingly, GDNF and neuritin failed to show a functional impact and neuroprotection in the α -synuclein model, which can better mimic the progression of human PD. A recent study by Zhang et al. (2018) overexpressed MANF specifically in DA neurons by using an α -synuclein *Caenorhabditis elegans* (*C. elegans*) model and showed MANF successfully alleviated progressive neuronal degeneration and motor function deficits [107].

A very limited number of studies cater to the investigation of neurokinines like ciliary neurotrophic factor (CNTF), leukemia inhibiting factor (LIF) etc. as a potential therapeutic in PD. Nam et al. (2015) investigated the role of astrocyte-produced CNTF on the active

minimization of the loss of the dopaminergic neurons and facilitates behavioural recovery through CNTF receptor alpha (CNTFR α) in both the MPTP and adeno-associated virus α -synuclein rat models of PD [107]. However, the role of CNTF in attenuating neurodegeneration has been better explored in Huntington's disease [108,109]. Considering that these NTFs have selective effects on dopaminergic neurones including GDNF, neurturin, growth/differentiation factor (GDF) 5, MANF and (CDNF) represent the ideal candidates for this therapy.

a. GDNF in prevention of neurodegeneration

GDNF belongs to a family of related proteins, called GDNF family of ligands (GFL) which comprises of four proteins: GDNF, neurturin, persephin and artemin. The members of GFL family bind to the glycosylphosphatidylinositol (GPI)-linked receptors (GFR α) receptors, thereby activating a transmembrane tyrosine kinase, c-Ret, and downstream signalling via the MAP kinase pathway and phospholipase C γ pathway [110]. GDNF is known to induce downstream responses through c-Ret-independent mechanisms such as the activation of Src family tyrosine kinases and receptor interaction with neural cell adhesion molecule (NCAM) [110].

The prototypical member of this family, GDNF, was isolated from a rat glial cell line B49 and was shown to exert neurotrophic effects on cultured dopaminergic neurones [111]. Besides dopaminergic neurons, GDNF is also involved in the maintenance of other neuronal subtypes like motor, sympathetic, parasympathetic, sensory and enteric neurons as well as the regulation of the kidney development and spermatogenesis outside the nervous system [112,113]. Several studies have investigated the application of GDNF to promote the survival and differentiation of dopaminergic neurones *in vitro* [114–116] and in the pre-clinical models to protect the neurons from dopaminergic toxins, MPP⁺ and 6-OHDA [117–119]. An attenuation in apoptosis in dopaminergic neurons cultured from embryonic rat [114,120] and human [121] midbrain following GDNF treatment was observed indicating the therapeutic potential of GDNF application in the *in vivo* models. GDNF has also been shown to confer neuroprotection to the dopaminergic neurones in a neuroinflammation model of LPS neurotoxicity [122,123]. It has been shown that the embryonic dopaminergic neurons deprived of GDNF undergo cell death via a death receptor- and caspase-dependent, but mitochondria-independent, pathway [124] indicating that GDNF promotes neuronal survival by inhibiting the death receptor pathway. Regarding the *in vivo* impact of GDNF treatment, a single injection of GDNF into either the SN or striatum significantly boosted the levels of dopamine and its metabolites [121]. Since then several studies have reported neuroprotective and reversal of

functional deficits in adult animal models of PD through the application of GDNF therapy [125].

Due to the high potency of GDNF in the pre-clinical models, GDNF has been investigated in several clinical trials. The first clinical study as reported by Nutt et al (2003) was a multicenter, randomized, double-blind, placebo-controlled trial (RDBCT) that compared the effects of monthly intracerebroventricular administration of placebo and increasing doses of GDNF in 50 subjects with PD for 8 months [126]. There was no improvement in the 'on' and 'off' total and motor Unified Parkinson's Disease Rating Scale (UPDRS) scores. However, the treated patients showed common adverse symptoms like nausea, vomiting and paresthesias. Sixteen of these patients underwent an extended open-label study for up to 20 months, without any significant motor improvement. The lack of any detectable therapeutic ability of GDNF was chiefly attributed to the poor diffusion into the parenchyma from the ventricular source of injection. The side effects were postulated to be a result of the wide non-specific dispersal throughout CSF triggering the non-motor pathway receptors [127]. A subsequent open-label study that enrolled 5 PD patients investigated the effects of intraputamen delivery of GDNF via implanted catheters connected to an extracranial pump system [128]. There was a significant reduction in the clinical side effects, a 39% improvement in the off-medication UPDRS motor scores and a 61% improvement in the activities of daily living subscore. A significant reduction by over 60% in dyskinetic movement was detected while on medication and no dyskinetic movements off medication was observed. Besides, positron emission tomography (PET) scans of [¹⁸F]dopa uptake showed a significant increase in DA storage 18 month post-treatment. A follow up study by Patel et al (2013) investigated the motor function recovery in one of the patients with bilateral GDNF infusions for 39 months with functional analysis up to 36 months post-treatment cessation. Based on UPDRS ratings, a general preservation in the clinical effects of GDNF were preserved for 36 months post-GDNF cessation with a 74% and 76% improvement in the UPDRS-III and UPDRS-II scores "off" medication [129]. Slevin et al (2005) reported another open-label clinical trial with a 6-month unilateral intraputaminal GDNF 'dose-escalated' infusion in ten patients with advanced PD [130]. A significant improvement by 34 and 33%, respectively, was observed for UPDRS total scores in the on and off states at 24 weeks and this correlated well with the improvement in the UPDRS motor scores at the same time points. However, these benefits dissolved with cessation of the GDNF treatment. In order to confirm the results from the smaller pilot analysis reported by Gill et al (2003) [128], a placebo-controlled randomized trial with 34 PD patients was

performed with bilateral intraputamenal GDNF infusion or placebo via continuous infusion. Six months post-treatment a significant 32.5% increase in putamenal [¹⁸F]dopa uptake was observed in the GDNF-treatment with no significant improvement in the UPDRS scores [131]. Real-time convection-enhanced delivery of adeno-associated virus serotype 2 (AAV2)- GDNF was modelled in non-human primates by Richardson et al. (2011) [132] which formed the basis for the development of an ongoing phase 1 clinical trial with 24 patients for advanced PD (NIH trial No. [NCT01621581](#)).

b. ***Biomaterial augmentation of the GDNF therapy***

Clinical trials of GDNF have employed catheter-pump systems that can achieve a prolonged and regulated release of GDNF. The use of the catheter-pumps, however, generated considerable device-related complications in participants of the study, including a need for catheter repositioning, infections, discomfort or pain due to the pump being implanted in abdominal area [128] [131]. Besides, other studies failed due to poor GDNF targeting to the brain and side-effects of non-specific diffusion to other regions of the brain [133][131]. GDNF is a protein with a short *in vivo* half-life of approximately 34 h in the cerebrospinal fluid and 3–4 days into the brain [134]. Furthermore, it has an impaired ability to cross the blood brain barrier, thus, requiring an effective drug delivery strategy to reach the brain. Therefore, in order to use GDNF effectively as a therapeutic agent for PD, it is mandatory to develop a safe and effective brain delivery system. To address the problem of delivery, several biomaterial formulations like hydrogels and microspheres have been investigated till date (**Table 1.1**).

The biomaterial systems for controlled delivery of neurotrophic factors have been classified into affinity-based and reservoir-based systems. Affinity-based systems harness the interactions between the biomaterial system and the therapeutic factors to tune the loading and release properties [135][136,137]. Reservoir-based delivery systems, on the other hand, employ a polymer structure surrounding the drug with its release being modulated by the material properties [138–141]. In these systems, drugs are non-covalently embedded into the porous polymer structure of the biomaterial and released with the progressive loss of polymeric structure post-implantation. Table 1.1 presents a summary of the biomaterial-based delivery systems for neurotrophic factors for therapeutic delivery to the brain in different disease targets. With GDNF, several studies involving microspheres and hydrogels have shown improved functional recovery in the animals treated with the biomaterial-based delivery systems as compared to the bolus treatment of the neurotrophic factors [135,140–143].

Table 1.1: Summary of the biomaterial-augmented neurotrophic factor delivery in the pre-clinical models with the therapeutic outcomes delivery in the pre-clinical models with the therapeutic outcomes.

Neurotrophic factor	<i>In vitro</i>	<i>In vivo</i>	Biomaterial intervention	Mode of delivery	Outcomes	Reference
GDNF	PC-12	6-OHDA SD model	PLGA microspheres	Intrastriatal injection	<ul style="list-style-type: none"> Decrease on the number of net amphetamine induced turns 4 weeks post-treatment. Increase in TH immunostaining showing striatal innervation 	[138]
	C17.2 neural progenitor cells	LFP SD brain injury model	-	Peri-lesion injection	<ul style="list-style-type: none"> GDNF-expressing NPCs promotes graft survival, migration, neuronal differentiation Improved cognitive outcome in composite neuroscore, beam balance and rotating pole tests 	[144]
	-	SD	PLGA microparticles in PEG hydrogel	SN injection	<ul style="list-style-type: none"> Controlled spatio-temporal release Inhibition of microglial and astrocytic recruitment 	[139]
	PC-12	<i>Macaca fascicularis</i> MPTP PD model	PLGA microspheres	Stereotactic brain injection	<ul style="list-style-type: none"> CRS score decrease observed after GDNF administration Fine motor hand improvement in GDNF-microspheres treatment Increase in TH immunostaining showing striatal innervation 	[141]
	-	TBI Wistar rat model	Gelatin-hydroxyphenylpropionic acid (Gtn-HPA) hydrogel	SVZ injection	<ul style="list-style-type: none"> Higher attenuation of gliosis in the presence of Gtn-HPA hydrogel and GDNF Higher migration of Dcx+ neuroblasts to the GDNF loaded hydrogel 	[142]
	VM cells	6-OHDA SD model	PLGA microspheres	Intrastriatal injection	<ul style="list-style-type: none"> GDNF-loaded MS treated group showed a decrease of ipsiversive turns per minute in amphetamine-induced rotations Significant reduction in the delay in reaction in sensorimotor orientation test in GDNF-loaded MS treatment More TH+ fibres directed towards MS found in GDNF-loaded MS treatment 	[140]

Table 1.1: Summary of the biomaterial-augmented neurotrophic factor delivery in the pre-clinical models with the therapeutic outcomes delivery in the pre-clinical models with the therapeutic outcomes.

Neurotrophic factor	<i>In vitro</i>	<i>In vivo</i>	Biomaterial intervention	Mode of delivery	Outcomes	Reference
GDNF	-	SD	Fibrin hydrogel	Intrastriatal injection	<ul style="list-style-type: none"> Fibrin scaffold allowed for GDNF diffusion from the cells No significant microgliosis and impact on MSC morphology observed 	[143]
	-	MPTP- C57BL/6J mice	TAT-CS-NLC	Intranasal	<ul style="list-style-type: none"> CS-NLC-TAT-GDNF led to a significant improvement of the locomotor activity in rotarod test Highest regeneration of dopaminergic neurons in CS-NLC-GDNF and CS-NLC-TAT-GDNF treatments. Decreased microgliosis observed in CS-NLC-TAT-GDNF treatment 	[135]
	VM cells	6-OHDA SD model	Collagen hydrogel	Intrastriatal	<ul style="list-style-type: none"> Enhanced survival, re-innervation and functional recovery in collagen gel encapsulated VM cells Decreased astrocytosis and microgliosis in collagen hydrogel treatment 	[145]
	GDNF-transfected MSCs	MCAO SD model	-	Intravenous	<ul style="list-style-type: none"> Reduced lesion and infarct volumes in both MSC and MSC-GDNF treatment Increased treadmill velocity after 7 days post treatment with MSC-GDNF Increased GDNF release in vivo in MSC-GDNF treatment compared to other controls 	[146]
	NSPCs	MCAO Wistar rat model	-	Intracerebral	<ul style="list-style-type: none"> GDNF transfected NSPCs migrate more towards the ischemic core Better survival of transfected cells and enhanced in vivo secretion of GDNF NSPC-GDNF group showed suppressed microglial activation Significant improvement in LPT and cylinder test performance in NSPC-GDNF group 	[147]

Table 1.1: Summary of the biomaterial-augmented neurotrophic factor delivery in the pre-clinical models with the therapeutic outcomes delivery in the pre-clinical models with the therapeutic outcomes.

Neurotrophic factor	<i>In vitro</i>	<i>In vivo</i>	Biomaterial intervention	Mode of delivery	Outcomes	Reference
	PC-12	6-OHDA SD model	PLGA microspheres	Intrastriatal	<ul style="list-style-type: none"> GDNF-MS- and VEGF + GDNF-MS-treated groups showed best functional recovery in rotational tests. Improved recovery of the lesion (TH+ neurons) in the group receiving the combined therapy (VEGF + GDNF-MS) compared to the control groups 	[148]
Table 1.1 contd.						
GDNF						
	Mice primary cortical cells	Wistar rats	Electrospun PCL scaffolds	Intrastriatal	<ul style="list-style-type: none"> GDNF immobilized scaffolds promoted GFP+ neuronal survival and the migration of host neurons towards the scaffold GDNF tethering enhanced the graft innervation and integration in the host circuitry while minimising microgliosis 	[149]
	-	Rotenone SD model	Lactoferrin (Lf) modified PAMAM dendrimers	Intravenous	<ul style="list-style-type: none"> Multiple injections of Lf-modified NPs showed higher GDNF expression than that of a single injection over 10 days. Multiple dose regimen improved locomotor activity compared to rotenone controls in open field test Significant neurorestoration observed only with multiple dose regime of Lf-NPs with <i>h</i>GDNF 	[136]
GDNF	Brain capillary endothelial cells and SH-SY5Y	Rotenone SD model	DGL-PEG-angiopoep (DPA)vectors	Intravenous	<ul style="list-style-type: none"> DPA/<i>h</i>GDNF NPs achieved best locomotor activity improvement of rats in open field test where no differences were detected in rearing, head dipping and defecating between different groups. TH recovery was observed with DPA/<i>h</i>GDNF NPs treatment and comparable to oil-treated controls. 	[137]

Table 1.1: Summary of the biomaterial-augmented neurotrophic factor delivery in the pre-clinical models with the therapeutic outcomes delivery in the pre-clinical models with the therapeutic outcomes.

Neurotrophic factor	<i>In vitro</i>	<i>In vivo</i>	Biomaterial intervention	Mode of delivery	Outcomes	Reference
GDNF	Rat primary astrocytes and MSCs	SD model	Collagen hydrogel	Intrastriatal	<ul style="list-style-type: none"> No loss of striatal tissue by collagen hydrogel No impact on the loss of MSCs after implantation or adverse impact of graft survival with no impedance to the release of GDNF in the striatum 	[150]
	VM cells	6-OHDA Swiss mice model	Electrospun PLLA/xyloglucan scaffolds	Intrastriatal	<ul style="list-style-type: none"> No impedance in cell migration to the scaffold and increased dopaminergic cell density in the implanted grafts Better implanted cell survival and integration in GDNF functionalized scaffold treatment group 	[151]
	E12 VM cells	6-OHDA SD model	Collagen hydrogel	Intrastriatal	<ul style="list-style-type: none"> Improvement in TH+ cell survival in GDNF-collagen treatment compared to GDNF or collagen only treatments Improved rotational behaviour in GDNF-collagen treatment compared to other groups 	[152]
	-	Wistar brain injury model	PCL scaffolds with BDNF mimetics	Medio-lateral craniotomy	<ul style="list-style-type: none"> PCL scaffolds with BDNF mimetic significantly reduced the microglial cells within 100 µm of injury site No glial scar was found at the implant boundary Increased migration and survival of the neuroblasts on the BDNF-PCL scaffolds if the scaffolds directly impinged on the SVZ Neurite sprouting observed at the tissue-implant interface of PCL-BDNF implants at both 8 and 21 dpi 	[153]
	-	SD	PLGA microparticles in PEG hydrogel	SN injection	<ul style="list-style-type: none"> Enhanced BDNF immunoreactivity till 56 days post implantation upto 250 µm from the site of injection 	[139]

Table 1.1: Summary of the biomaterial-augmented neurotrophic factor delivery in the pre-clinical models with the therapeutic outcomes delivery in the pre-clinical models with the therapeutic outcomes.

Neurotrophic factor	<i>In vitro</i>	<i>In vivo</i>	Biomaterial intervention	Mode of delivery	Outcomes	Reference
BDNF					<ul style="list-style-type: none"> Higher GFAP + cells at both rostral and caudal ends of the BDNF-microparticle-gel implanted Reduction in CD68+ cells at both rostral and caudal ends of the BDNF-microparticle-gel implanted 	
	✓hUC- MSCs ^{CXCR4/GFP}	SD TBI model	Chitosan scaffolds	Cortical implantation	<ul style="list-style-type: none"> Higher migration of MSCs towards the lesion in scaffolds with MSCs^{CXCR4/GFP} compared to that of MSCs^{GFP} Scaffold filled the tissue cavity preventing the tissue loss observed in saline treatment group Number of GFP and MAP-2 + cells was higher in the hUCMSC^{CXCR4/GFP}/scaffold as compared to the hUC-MSC^{GFP}/scaffold group in lesion boundary showing higher migration and neuronal differentiation at lesion boundary 	[154]
	PC12-TrkB	SD	Alginate microspheres PVA matrices	Hippocampal injection	<ul style="list-style-type: none"> Reduced immobility and increased swimming behaviour observed in BDNF infusion and BDNF-microsphere treatment but not for BDNF-matrix treatment in FST Increasing dose and duration of BDNF exposure increased total TrkB, ERK and CREB, phosphorylated ERK and phosphorylated CREB was decreased 	[155]
	-	SD	Liposomes	Intravenous	<ul style="list-style-type: none"> Dose dependant expression of BDNF and BDNF mRNA in both hemispheres with enhanced expression in cortex observed for Tf-pGFAP-BDNF-PEG and Tf-pCMV-BDNF-PEG groups 	[156]

Table 1.1: Summary of the biomaterial-augmented neurotrophic factor delivery in the pre-clinical models with the therapeutic outcomes delivery in the pre-clinical models with the therapeutic outcomes.

Neurotrophic factor	<i>In vitro</i>	<i>In vivo</i>	Biomaterial intervention	Mode of delivery	Outcomes	Reference
BDNF		<i>Macaca fascicularis</i> MCAO model, C57BL6 focal or photothrombotic stroke model	Hyaluronan (HA) hydrogel	Stroke cavity injection	<ul style="list-style-type: none"> Sustained BDNF release from HA gels over 3 weeks in striatal and cortical stroke compared to bolus BDNF injections Improved performance of HA-BDNF treatment in impaired forelimb use in rearing (Cylinder task) and in gait (grid walking task) compared to controls Significant axonal sprouting from peri-infarct motor cortex to contralateral striatum and promotion of neurogenesis in HA-BDNF treatment BDNF levels are elevated after hydrogel-BDNF in peri-infarct tissue in frontal, parietal, and temporal cortex in the non-human primate model 	[157]
BDNF	-	Fischer 344 rats	Lipid (Glyceryl tripalmitate) matrices	Intrastriatal	<ul style="list-style-type: none"> No overt behavioral changes, obvious neurological deficits or weight loss observed due to matrix implantation Very few $\alpha\beta$ T-cell receptor and Natural killer cells observed around the implants 	[158]
	-	SD MCAO model	Collagen binding domain conjugation	Intra-ventricular	<ul style="list-style-type: none"> Significantly retention of CBD-BDNF in the infarcted hemisphere compared to NAT-BDNF Significant improvement in mNSS score two and four weeks post MCAO in CBD-BDNF compared to other controls CBD-BDNF group showed the smallest metabolic asymmetry in PET scans 	[159]
	hCMEC/D3	CD mice and LPS-induced encephalitis mice model	Macrophage exosomes	Carotid artery injection	<ul style="list-style-type: none"> Increased influx of exosomes in the inflamed brains due to increased ICAM-1 expression Accumulation of exosome-formulated BDNF (ExoBDNF) in the brain-inflamed mice was significantly 	[160]

Table 1.1: Summary of the biomaterial-augmented neurotrophic factor delivery in the pre-clinical models with the therapeutic outcomes delivery in the pre-clinical models with the therapeutic outcomes.

Neurotrophic factor	<i>In vitro</i>	<i>In vivo</i>	Biomaterial intervention	Mode of delivery	Outcomes	Reference
					increased compared to the same formulation in the healthy animals	
	-	C57BL6 mice	Diblock copolypeptide hydrogels (DCH)	Caudate putamen injection	<ul style="list-style-type: none"> • NGF dissolved in either K180L20 or E180L20 provided significantly longer delivery of NGF bioactivity, maintaining hypertrophy of local forebrain cholinergic neurons for 4 weeks and inducing hypertrophy up to 5 mm from injection sites • Tunable platform to match the rheological properties to that of the brain 	[161]
NGF	PC-12, MSCs	SD rats	Fibrin microspheres	Intrastratial	<ul style="list-style-type: none"> • No exaggerated host response to fibrin spheres in vivo • Sustained release of NGF over 14 days through fibrin microspheres 	[162]
	-	SD rats	PLGA microparticles	Intraseptal	<ul style="list-style-type: none"> • Significant protection of AChE neurons by PLGA-NGF microparticle treatment at two and six week post implantation 	[163]
	NT2N neurons	C57BL/6 CCI injury model	-	Intraseptal	<ul style="list-style-type: none"> • No apparent impact on motor function recovery in NGF transduced NT2N treatment group • Mice engrafted with NGF-expressing NT2N neurons showed significantly shorter mean learning latencies than non-transduced NT2N treatment 	[164]
	PC-12	Quinolinic acid treated SD	PLGA microspheres	Intrastratial	<ul style="list-style-type: none"> • Lesion size in NGF-releasing microspheres treatment was reduced by 40% • Increased survival of ChAT – immunoreactive neurons in NGF-PLGA microsphere treatment compared to that of the controls 	[165]

Table 1.1: Summary of the biomaterial-augmented neurotrophic factor delivery in the pre-clinical models with the therapeutic outcomes delivery in the pre-clinical models with the therapeutic outcomes.

Neurotrophic factor	<i>In vitro</i>	<i>In vivo</i>	Biomaterial intervention	Mode of delivery	Outcomes	Reference
NGF	NGC0211	Göttingen minipigs	PET scaffold	MRI guided neurosurgery	<ul style="list-style-type: none"> • Specific diffusive NGF-immunoreactive signal was detected around NsG0202.1 devices to cover the clinically relevant area • Marked increase in NGF release compared to previous generation device • Host response reactivity was limited close to the site of implantation and not expresses at sites remote from the implantation site 	[166]
	-	CA1 removed Wistar rat model	Chitosan particles	Intra-hippocampal	<ul style="list-style-type: none"> • Significant reduction in glial scar formation in NT-3-chitosan treatment compared to that of the controls • NT-3-chitosan carriers group had a significantly larger amount of NF-positive axons and cells and BDA-positive fibers than the blank chitosan carriers group showing the re-establishment of neural circuitry • The latency of the NT-3-chitosan carriers group and the blank chitosan carriers group in MWM test was significantly different from that of the lesion control group 	[167]
	RBMECs and iPSCs	ICH	PBCA NPs	Intravenous	<ul style="list-style-type: none"> • FITC-PBCA NP/cmvNT-3-HRE complexes appeared in mouse brain cells near the blood vessels • Up-regulation of NT-3 protein expression FITC-PBCA NP/cmvNT-3-HRE treatment • AIF and cleaved caspase-3 expression in the order ICH > cmvNT-3-HRE > PBCA NP/cmvNT-3-HRE complexes = sham group 	[168]

Table 1.1: Summary of the biomaterial-augmented neurotrophic factor delivery in the pre-clinical models with the therapeutic outcomes delivery in the pre-clinical models with the therapeutic outcomes.

Neurotrophic factor	<i>In vitro</i>	<i>In vivo</i>	Biomaterial intervention	Mode of delivery	Outcomes	Reference
NT-3						

Abbreviations:

6-OHDA: 6-Hydroxydopamine, AchE: Acetylcholinesterase , BDA: Biotinylated dextran amine, BDNF: Brain derived neurotrophic factor, CCI: Chronic constriction injury , ChAT: Choline Acetyl transferase, Dcx: Doublecortin, DCH: Diblock copolypeptide hydrogels , FST: Forced swim test, GDNF: Glial cell derived neurotrophic factor, hUC-MSCs^{CXCR4/GFP}: Human MSCs expressing chemokine (C-X-C motif) receptor , hCMEC/D3 :Brain microvascular endothelial cell line , ICH: Intracerebral haemorrhage , iPSCs: Induced pluripotent stem cells, MCAO: Middle cerebral artery occlusion, mNSS: Modified neurological severity score, MSC: Mesenchymal stem cells, MWM: Morris water maze, NF: Neurofilament, NGF: Nerve growth factor, NPC: Neural progenitor cells,NPs: Nanoparticles, NPSC: Neural stem and progenitor cells ,NT-3:Neurotrophin-3, LFP: lateral fluid percussion, LPS: Lipopolysaccharide , LPT: Limb placement test, PAMAM: Polyamidoamine , PC-12: Pheochromocytoma cell line, PCL: Poly ε-caprolactone, PD: Parkinson’s disease, PEG: Polyethylene glycol, PET: Polyethylene terephthalate, PLGA: poly (lactic-co-glycolic) acid, PLLA: Poly(l-lactic acid), PVA: Polyvinyl acetate , RBMECs:Rat brain-microvascular endothelial cells, SD: Sprague Dawley, SN: Substantia nigra, SVZ: Subventricular zone, TAT-CS-NLC: Transactivator of transcription-chitosan-nanolipid carriers, TBI: Traumatic brain injury, TH: Tyrosine hydroxylase, VM: Ventral mesencephalon

1.5 Cellular therapies for PD

a. Cell sources for transplantation

The origin of cell therapy for PD began with the transplantation of fetal rat DA-containing neurons which improved the functional abnormalities in the rat PD model and showed good survival of grafts and axonal outgrowth in 1979. It has been almost three decades since the VM cells were first tested clinically in the PD patients in 1988. Fetal nigral cell transplantation were partly successful in achieving synapse formation between transplanted donor cells and host neurons as well as to compensate for the DA loss. However, there were significant immunological problems and ethical issues involved centred around the use of aborted fetuses. The positive outcomes of fetal nigral cell transplantation using a cell suspension were reported compared to the solid tissue transplantation used in the previous randomized, double-blind studies [169]. Two patients showed improvement in motor function, reduction in levodopa (L-DOPA)-induced dyskinesia, and no dyskinesia in the off state. A long term postmortem analysis after four years showed that many transplanted cells had survived with subtle immune reactions. A follow up analysis over an extended time period (ten years) demonstrated that some PD patients receiving fetal nigral cell transplantation showed a continuous improvement of motor symptoms [170]. All the aforementioned studies show that subject to appropriate patient selection, transplantation protocol, and optimal trial design, VM transplantation might exert strong therapeutic effects over an extended period.

Different types of stem cells have been explored for their *in vivo* therapeutic efficacy in PD. They offer the edge in cellular therapies as they are easily harvested and amplified via differentiation capacity. Dezawa et al. (2004) reported a protocol for highly specific induction of cells with neuronal characteristics, alleviating any glial differentiation from both rat and human MSCs using gene transfection with Notch intracellular domain (NICD) followed by the treatment with a cocktail of bFGF, forskolin, and ciliary neurotrophic factor [171]. This supplemented with GDNF treatment increased the fraction of DA neurons. Furthermore, multilineage-differentiating stress-enduring (Muse) cells with stage-specific embryonic antigen-3 (SSEA-3) have been identified and show tremendous potential to be harnessed in the PD cell therapy as their isolation and culture is less time and labor-consuming [172]. To date, there have been no successful clinical trials involving MSCs for PD patients. However, several *in vivo* transplantation studies show their potential in promoting functional repair in PD [173,174]

Towards the application for PD, embryonic stem cells (ESCs) have also been studied tremendously. There are two different neuronal differentiation protocols from ESCs that were reported. Kawasaki et al (2000) found that the co-culture of ESCs and stromal cells (stromal cell-derived inducing activity [SDIA] method) promotes the development of a neuronal phenotype with a higher inclination towards DA neuron-like cells [175]. This method was subjected to pre-clinical trials in a non-human primate model [176,177]. The second protocol was described by Lee et al (2000) which was a method that involves going through the embryoid body where the CNS progenitors were expanded and differentiated into dopaminergic and serotonergic neurons by mitogens and specific signalling molecules [178]. Samata et al (2016) reported a double selection strategy for cells expressing both CORIN and LMX1A::GFP, and reported a cell surface marker to enrich mDA progenitors, leucine-rich repeat and transmembrane domains 1 (LRTM1) to enrich the differentiated cell population in DA neurons and minimise the tumorigenic cells [179]. The ethical issues and tumor formation are the chief hurdles in the clinical translation of the ESCs. However, several studies are underway to minimise their tumorigenicity. Neural stem cells (NSCs) are another well investigated cell source for functional recovery in PD models [180,181]. NSCs exert the neuro-reparative effect by the secretion of trophic factors as well as neuronal differentiation. NSCs have been implemented in a phase I study of transplantation of NSCs for PD patients from Turkey [182]. Twenty-one PD patients were bilaterally transplanted with NSCs at specific intervals, and the motor function of the patients improved significantly (UPDRS scores: 72.76 ± 13.81 from 80.71 ± 15.48) with no tumor formation.

iPSC technology has flourished rapidly after the first establishment of mouse- and human-derived iPSCs were established [183,184]. Tumorigenesis is a major concern in terms of the clinical application of iPSCs, and various modifications have been developed to reduce the risk of tumor formation. The first approved clinical trial harnessing iPSCs for the treatment of PD started in Melbourne, Australia, by the International Stem Cell Corporation in 2016 [185]. The other aim of the use of iPSC technology is also expected to reveal the disease pathophysiology using patient-derived iPSCs. Using PD patient-derived iPSCs and differentiated DAergic neurons, an *ex vivo* disease model could be set up to investigate the genetic alteration, reaction to therapies, and fate of the cells to elucidate critical mechanistic aspects for PD pathogenesis [186,187]. Drug discoveries from iPSC technology are highly anticipated. Very recently, Kikuchi et al. demonstrated the successful application of dopaminergic neurons derived from human iPSCs as midbrain dopaminergic neurons for an extended period of time (two years) in

an MPTP primate model of Parkinson's disease where they showed enhanced survival and motor function recovery [188]. All these studies taken together show the potential of stem cell therapies in PD. However, multiple optimisations to minimise the tumor formations and the genetic manipulations are required before using the stem cells as a therapy in the clinic.

b. Limitations of Ventral mesencephalic cells

A major hurdle in the use of VM tissue for cell transplantation studies is its fetal origin which raises ethical concerns about collecting tissues from elective abortion and the complication of obtaining multiple donors for a single transplant. Hagell et al (2001) showed that to achieve clinical efficacy at least 3 to 5 VMs need to be transplanted per hemisphere [189]. Several studies have shown that the level of striatal re-innervation required for the amelioration of motor symptoms is positively correlated to number of dopaminergic neurons in the VM transplant. VM grafts, however, are a heterogeneous population of cells of which only 30-40% are dopaminergic neurons. Amongst this, only about 1-20% of the transplanted cells survival the procedure and this can partly explain the extremely poor survival of dopaminergic neurons after transplantation [190].

Poor survival of engrafted VM cells is caused by an interplay of a multitude of factors. Contrary to the previous assumption of necrosis during tissue dissection and transplantation process as being key player in the cell death in VM grafts, the large extent of cell death in VM grafts occurs post-transplantation through apoptosis. Apoptotic cell death is provoked at various points of the grafting process by factors including but not limited to I) cell detachment from the ECM, also referred to as anoikis [191] growth factor deprivation in the adult host brain [192] and III) the recruitment of host neuro-immune cells. This apoptotic loss of engrafted cells is primarily a function of external factors in the cellular microenvironment rather than a physiological insult [193,194]. VM cell therapy involves the removal of fetal dopaminergic neurons from the trophic factor-rich VM of the developing embryo and subsequent transplantation into the trophic factor-depleted adult striatum. The trophic activity of the brain and in particular, the striatum, is known to decrease with age [195]. Numerous studies suggest that it could take up to four days post-transplantation to form a stabilised network and about 80-90% of dopaminergic neurons die within that time period [196,197]. This is augmented by the fact that the transplanted cells undergo trophic deprivation of the factors normally present throughout target innervation and development. Identification of a foreign object results in the activation of host immune cells and the subsequent release of a myriad of pro-inflammatory

molecules and cytokines, including TNF- α , IL-1 β and INF- γ , causing cell death as a result of this cascade activation. Immune activation following the cell engraftment was detected in the post-mortem analysis from the double-blind, placebocontrolled clinical trials, where a prominent activated microglial staining around the graft site was detected [198,199]. This is one of the major causes of the implanted cell death and consequently had an effect on the clinical efficacy. The specific impact was highlighted in the Olanow et al. (2003) trial where a sharp decline in the clinical benefit began after the withdrawal of immunosuppression [199]. The outcomes of this trial were reinforced by a recent study where that long-term immunosuppression (up to 2 years) corresponded to the long term relief of motor symptoms [200]. However, randomized, double-blind studies revealed the insufficient functional recovery of older patients and delayed graft-induced dyskinesia in some patients [199]. These represent the major challenges that need to be circumvented to ensure the successful clinical translation of VM cells.

c. Biomaterial augmentation of the cell therapy

Biomaterial therapy augments the targeted delivery of therapeutic proteins and cells to the brain, while promoting regeneration and repairing damaged neuronal pathways, to direct motor function recovery. However, the brain as a therapeutic target is very sensitive and any material used for intracranial delivery should fulfil certain criteria including but not limited to (a) being minimally invasive; (b) not eliciting an exaggerated host response or promoting neuroinflammation; (c) being very close to the natural ECM to support the cell survival and integration; (d) being structurally stable for the therapeutic interval but capable of degrading without any toxic remnants; (e) being tunable in terms of physical and topographical properties; and (f) being capable of a sustained therapeutic delivery [201,202]. All these criteria for an ideal biomaterial intervention for therapeutic delivery are fulfilled to a greater extent by the injectable hydrogels. A summary of different biomaterial platforms used for promoting the brain repair in conjugation with cellular therapy is presented in **Table 1.2**. Several different biomaterial platforms like scaffolds [152,203–205], microspheres [206–208], liposomes [209] and exosomes [210] have been investigated in both rodent and non-human primate PD models to augment the cell survival post-implantation. These platforms were either tested on their own [203,211–215] or facilitated the delivery of a therapeutic agent [206,208,216–218] towards the enhancement of cellular survival. Most of these studies highlight the impact of biomaterial therapies on enhancing the graft survival and promoting functional recovery as demonstrated by the motor analyses. Huang et al (2013) designed an angiopep-conjugated dendrigraft poly-

L-lysine (DGL)-based gene delivery system for hGDNF delivery in a chronic rotenone PD model where five injections of DPA/hGDNF NPs showed best functional recovery and enhanced survival of dopaminergic neurons. Biomaterials in the format of hydrogel [217,219–221] and fibers [198][222] were also investigated in several studies for their impact on the motor function recovery in the rodent models of PD. Table 1.2 summarises the outcomes of all the studies investigating biomaterials in different formats and their impact on the transplanted dopaminergic neurons survival as well as functional recovery.

d. Injectable hydrogels as a biomaterial scaffold

Injectable hydrogels are three-dimensional networks of hydrophilic polymers which can be chemically cross-linked and can be formed *in situ* in response to temperature and pH changes that makes them injectable and facilitating their noninvasive intracranial delivery [223]. Furthermore, the physical properties of the hydrogels are tunable by modulating their cross-linking. Hydrogels provide an edge as therapeutic intervention for clinical applications in neuroregeneration as they can circumvent the problems associated with both cell- and growth factor-therapies. Hydrogels can serve as reservoirs for several therapeutic and signaling molecules directly to the injury site, and act as scaffolds providing suitable physical support, adhesion substrate, optimal nutrient and oxygen exchange, and immune-protection to the implanted cells [224,225]. The focus of the use of the hydrogels in neuroregeneration is to carefully regulate the host neural tissue and transplanted cells by supporting their attachment, survival and subsequent integration with host neural circuitry [226].

These hydrogels for CNS applications can be derived from either natural materials or synthetic materials. Natural materials originate from biological sources including, chitosan, hyaluronan, fibrin and collagen. The leverage of the natural biomaterials stems from their natural origin and involvement in the biological system. They contain endogenous ligands to promote cellular adhesion and their origin usually minimises the activation of the host immune response [211]. However, the synthetic materials are chemically fabricated and offer a better control over standardisation [227]. Interestingly, another class of bio-hybrid hydrogels are available nowadays where natural materials, such as alginate, fibrin or collagen, are cross-linked with synthetic polymers, such as polymer polyethylene glycol (PEG), offering a combination of the biological properties of the protein and the mechanical stability [228].

Injectable hydrogels have been most widely investigated and are promising candidates for the delivery of therapeutic agents and/or cells to the brain [212]. The alteration of a hydrogel's porous structure allows for the modulated control on the nutrient and oxygen infusion to encapsulated cells and therapeutic factor release to surrounding tissues, while effectively shielding the encapsulated cells from the host immune response [229]. These scaffolds can also be functionalised by the growth factors/ therapeutic cues to support cell adhesion, migration or differentiation [230]. Additionally, the degradation and persistence of these scaffolds *in vivo* could be manipulated by modulating the degree of crosslinking. An intriguing observation was that the growth factors can be added to further support cell survival and function after transplantation *in vivo* with a temporal control over their release [231], thereby facilitating the *in vivo* regenerative processes.

e. Injectable fibrin gel

Fibrin is a natural biodegradable protein involved in the blood clotting cascade following injury, which is produced by enzymatic lysis of fibrinogen by thrombin [226,232]. When derived from an autologous donor, it represents a highly compatible biomaterial for cell/therapeutic delivery [226,233]. Fibrin glue has several features, which make it a very viable option towards the application of controlled release of therapeutic molecules. Firstly, it is relatively easy to tune several of the parameters of the components to change the gel's structure and mechanical properties. Most formulations of fibrin glue include antifibrinolytic agents like epsilon-aminocaproic acid, C1-esterase inhibitor, tranexamic acid and aprotinin, of which aprotinin is most commonly used to attune gel degradation [234]. Together with the tunability of fibrin as a delivery platform, it is an attractive drug delivery system owing to the interactions it can have with endogenous growth factors, thereby modulating their release from the gel. Fibrin serves as a docking agent for several growth factors like vascular endothelial growth factor (VEGF) [235], transforming growth factor-B1 (TGF- β 1) [236], basic fibroblastic growth factor (bFGF) [237], and growth factor-binding agents like insulin-like growth factor-binding protein-3 for insulin-like growth factor (IGF) [238]]. There have been several studies *in vitro* and *in vivo* showing the suitability of fibrin for therapeutic application in the PNS and spinal cord injury models. In an SCI investigation by Willerth et al. (2007), ES-NPCs cultured in the fibrin gel with a cocktail of different growth factors showed an effective differentiation towards the neuronal phenotype. [239]. Man et al. (2011) studied the impact of the biophysical properties of the fibrin gel on the mouse neonatal DRG behavior where the increase in NaCl

and/or fibrinogen concentrations made the matrix stiffer and inhibited neurite outgrowth [240]. Several studies have used the fibrin-based therapeutic reservoirs for drug or growth factor delivery to the brain and have shown no exaggerated host response to these systems [241,242] while obtaining a sustained release of the cargo *in vivo* [243].

Table 1.2: Summary of biomaterial-augmented cellular therapies in the brain with the therapeutic outcomes.

Animal model	Cell source	Site of transplantation	Biomaterial	Growth factor (gene/proteins) +/-	Outcomes	Reference
6-OHDA rat model (SD)	Human MSCs	Intrastriatal	PLGA microspheres	NT3	<ul style="list-style-type: none"> Improved rotational behaviour for the animals treated with PAM-NT3-MSCs complex compared to control groups Significantly higher density of TH+ fibres in the lesioned striatum with with PAM-NT3-MSCs No strong inflammatory response and phagocytosis was observed to PAM-NT3-MSCs 	[206]
6-OHDA rat model (SD)	Human retinal pigment epithelial (RPE) cells	Intrastriatal	Dextran microcarriers coated with gelatin	-	<ul style="list-style-type: none"> Microcarriers-RPE grafted animals displayed a significant reduction in AIR GDNF and BDNF levels are found significantly higher (41.2% and 68.1%) in the RPE cell-grafted tissues compared to that of controls 	[207]
Rotenone rat model (SD)	-	Intravenous	DGL-PEG-angiopep (DPA) nanocarriers	hGDNF gene	<ul style="list-style-type: none"> Five injections of DPA/hGDNF NPs showed best locomotor activity improvement of rats in open field tests Five injections of DPA/hGDNF NPs showed no apparent difference with the oil-treated group in TH+ immunostaining 	[208]
6-OHDA mice model (C57BL/6)	-	Intravenous/ intranasal	Raw 264.7 macrophages derived exosomes	Catalase	<ul style="list-style-type: none"> Significant reduction in apomorphine induced rotational behaviour in exo-CAT treated group when compared to the saline treatment Exosomes delivered upon the i.n. administration was greater than i.v. injection I.n. administration of exoCAT caused 3-fold increase in survived DA neurons 	[216]
6-OHDA rat model (SD)	GDNF secreting 3T3 fibroblasts	Intrastriatal	Alginate-poly-L-lysine-alginate (APA) microcapsules	-	<ul style="list-style-type: none"> Microcapsules containing GDNF secreting cells significantly reduced the number of apomorphine- induced rotations. No significant differences in amphetamine induced rotations between treatment and controls. 	[210]

Table 1.2: Summary of biomaterial-augmented cellular therapies in the brain with the therapeutic outcomes.

Animal model	Cell source	Site of transplantation	Biomaterial	Growth factor (gene/proteins) +/-	Outcomes	Reference
					<ul style="list-style-type: none"> GDNF immunoreactivity in the striatal tissue surrounding the capsules detected upto 6 months No significant changes in the levels of dopamine (DA), DOPAC or HVA 	
6-OHDA mice model (Swiss mice)	VM cells	Intrastriatal	Xyloglucan and poly-l-lactide acid (PLLA) scaffolds	GDNF	<ul style="list-style-type: none"> Xyloglucan, but not PLLA short fibers, significantly increased graft volume Dual presentation of GDNF enhanced graft-induced striatal reinnervation and the volume of innervation/GFP+ cells 	[217]
6-OHDA rat model (SD)	-	Intravenous	TfR targeting liposomes (THLs)	GDNF plasmid DNA	<ul style="list-style-type: none"> Dose-dependent decrease in apomorphine-induced rotations with THL treatment 19-fold increase in striatal TH enzyme activity in dose-responsive and time-responsive way was observed. 	[218]
xia6-OHDA rat model (SD)	VM cells	Intrastriatal	PLGA microcarriers	GDNF	<ul style="list-style-type: none"> Early and sustained amelioration of rotational deficits by the VM adhered to GDNF loaded PLGA microcarriers GDNF-loaded microspheres release GDNF 6 weeks after grafting and TH+ cells were comparable in unloaded and GDNF loaded microspheres Reinnervation intense near the graft and sparse at a distance from the graft 	[209]
SD rats	GDNF overexpressing BM-MSCs	Intracerebral	Type I collagen hydrogel	-	<ul style="list-style-type: none"> Microgliosis and astrocytosis were comparable in collagen treatment and control animals No impact of collagen gel on GDNF-MSC graft survival in the rat brain No impact of collagen on striatal penetrability of GDNF Collagen gel was biodegradable 	[215]

Table 1.2: Summary of biomaterial-augmented cellular therapies in the brain with the therapeutic outcomes.

Animal model	Cell source	Site of transplantation	Biomaterial	Growth factor (gene/proteins) +/-	Outcomes	Reference
6-OHDA rat model (SD)	PC-12 cells	Intrastriatal	PAN-PVC capsules	-	<ul style="list-style-type: none"> • Significant reduction in the apomorphine-induced rotational response observed with cell-containing capsules which was sustained for 24 weeks. No significant reduction observed for empty polymer capsules • Encapsulated PC-12s were not tumorigenic and TH+ • Extracellular DA near implants was comparable to the control unlesioned brains 	[214]
MPTP primate (cynomologous monkey) model	PC-12 cells	Caudate nucleus and putamen	Poly-l-lysine adsorbed alginate capsules	-	<ul style="list-style-type: none"> • Significant behavioural improvement was detected in Sinemet challenge only for the group treated with PC-12 loaded capsules • Minimal host response to the capsules and the cells were well-preserved and strongly immunopositive for TH 	[244]
6-OHDA rat model (SD)	BHK cells	Intrastriatal	Polymeric polysulfone capsules	hNGF	<ul style="list-style-type: none"> • No obvious change in the spontaneous behaviour. • Significant reduction of rotational behaviour for up to 6 months in BHK-GDNF group compared to other groups 	[213]
MPTP primate (<i>Papio anubis</i> baboons) model	C2C12 cells	Lateral ventricle	PVA matrices in polyethersulfone capsules	hGDNF	<ul style="list-style-type: none"> • Total distance moved (TDM) improved for GDNF-releasing capsules compared to other controls over week 30 and 45. • No differences in other parkinsonian symptoms observed between the groups. • When assessing TH+ cell volumes, a significant increase was observed in GDNF-treated animals compared to both control and MPTP-only animals 	[245]
Fischer rats	hESC-derived midbrain	Intrastriatal	HA hydrogel	-	<ul style="list-style-type: none"> • 5 fold increase in hydrogel-encapsulated mDA neuronal survival after transplantation 	[203]

Table 1.2: Summary of biomaterial-augmented cellular therapies in the brain with the therapeutic outcomes.

Animal model	Cell source	Site of transplantation	Biomaterial	Growth factor (gene/proteins) +/-	Outcomes	Reference
	dopaminergic neurons				<ul style="list-style-type: none"> Negligible serotonergic neurons, GABAergic neurons, and glial cells within the graft 	
6-OHDA rat model (SD)	VM cells	Intrastriatal	PLGA MS	GDNF	<ul style="list-style-type: none"> Improvement in the rotational behaviour by GDNF-MS treatment both implanted at a distance from or mixed with VM cells 3-fold increase in survival of TH+ cells in GDNF-MS treatment at a distance from VM cell implantation compared to other treatment groups 	[246]
Fischer rats	hPSC derived DA cells	Intrastriatal	PNIPAAm-PEG gels	-	<ul style="list-style-type: none"> 40-fold increase in the total number of cells surviving and a 30-fold increase in the number of TH+ neurons surviving from the 3D platform seeded mDA cell implantation Enhanced integration into host neuronal circuit detected by the expression of synaptophysin throughout the graft and between graft and host cells 	[221]
6-OHDA rat model (SD)	VM cells	Intrastriatal	Collagen hydrogel	GDNF	<ul style="list-style-type: none"> Enhanced survival, re-innervation and functional recovery in collagen gel encapsulated VM cells Decreased astrogliosis and microgliosis in collagen hydrogel treatment VM cells in a GDNF-loaded collagen hydrogel showed functional recovery in rotational analysis at 9 and 12 weeks post-transplantation compared to other treatments 	[220]
6-OHDA rat model (SD)	E12 VM cells	Intrastriatal	Collagen hydrogel	GDNF	<ul style="list-style-type: none"> Improvement in TH+ cell survival in GDNF-collagen treatment compared to GDNF or collagen only treatments Improved rotational behaviour in GDNF-collagen treatment compared to other groups 	[219]
Wistar rats	NSC	Intrastriatal	Star-PEG-heparin hydrogel	FGF-2	<ul style="list-style-type: none"> RGD and FGF-2 promoted the NSC differentiation to neuronal subtypes 	[205]

Table 1.2: Summary of biomaterial-augmented cellular therapies in the brain with the therapeutic outcomes.

Animal model	Cell source	Site of transplantation	Biomaterial	Growth factor (gene/proteins) +/-	Outcomes	Reference
					<ul style="list-style-type: none"> injected gel retained its shape after 3 weeks in the rat brain with no chronic host versus graft rejection 	
SD rats	PC-12s	Intrastriatal	PVC macro and alginate microcapsules	Dopamine	<ul style="list-style-type: none"> Significant improvement in apomorphine-induced rotational behaviour in macro- and micro-encapsulated cell treatment groups over control with no significant differences between the techniques of encapsulation Modest host response to micro- and no adverse response to macro-capsules was observed Cells didn't form tumor indicating effective sequestration and were found to be TH+ 	[222]
MPTP cynomolgus monkey model	PC-12s	Caudate nucleus and putamen injection	PVC fibres	-	<ul style="list-style-type: none"> PC12 cell grafted monkeys recovered performance on the hand reach task to near normal levels No host-derived sprouting response of catecholaminergic or indolaminergic fibers in the grafted striatum High levels of levodopa and dopamine secretion <i>in vivo</i> by the encapsulated cells 	[198]
6-OHDA rat model (SD)	Chromaffin cells	Intrastriatal	Alginate microcapsules	-	<ul style="list-style-type: none"> 60% reduction in apomorphine-induced rotation in cell laden microcapsule treatment Host reaction to the implanted microcapsules was minimal encapsulated chromaffin cells were strongly immunopositive for TH and were over 90% viable 	[247]
Hartley guinea pig model	PC-12s	Intrastriatal	PAN-PVC hollow fibres	-	<ul style="list-style-type: none"> Intact PC12 cell-loaded polymer capsules showed no lymphocytic infiltration and a mild astrocytic reaction Encapsulated cells were immunopositive for TH 	[248]

Table 1.2: Summary of biomaterial-augmented cellular therapies in the brain with the therapeutic outcomes.

Animal model	Cell source	Site of transplantation	Biomaterial	Growth factor (gene/proteins) +/-	Outcomes	Reference
					<ul style="list-style-type: none"> Unencapsulated PC12 cells did not survive transplantation 	
Hartley guinea pig model, 6-OHDA rat model (SD)	PC-12s	Intrastriatal	Alginate microcapsules	-	<ul style="list-style-type: none"> Post-implantation turning rate in apomorphine induced rotations was significantly different in treatment groups with capsules containing PC12 cells and the empty capsules No tumor formation in implanted animals Encapsulated cells stained TH+ with mild astrocytic reaction to the capsules 	[249]
SD rats	PC-12s	Forebrain	PVA fibres	-	<ul style="list-style-type: none"> Encapsulated cells show high immunoreactivity for TH and AcHE and higher survival than unencapsulated cells 	[250]

Abbreviations

AIR: Apomorphine induced rotations, mDA: Midbrain dopaminergic cells, DA: Dopamine, DGL: dendrigraft poly-L-lysine, DOPAC: 3,4-dihydroxyphenylacetic acid, FGF-2: Fibroblast growth factor-2, HA: Hyaluronic acid, hGDNF: human glial cell line-derived neurotrophic factor, hPSC: Human pluripotent stem cells, HVA: Homovanillic acid, MS: Microspheres, NSC: Neural stem cells, PAN-PVC: Poly acrylonitrile vinyl chloride copolymer, PNIPAm: Poly(N-isopropylacrylamide), PEG: polyethylene glycol, PVC: Poly(acrylonitrile vinyl chloride), SD: Sprague Dawley rats, PLLA: poly-L-lactide acid, VM: ventral mesencephalon, TfR: Transferrin receptor, TH: Tyrosine hydroxylase, PAN-PVC fibre: polyacrylonitrile-polyvinylchloride

1.6 Glycomics in neurodegeneration

Glycosylation represents the most common and complicated form of post-translational modifications (PTMs) that play a crucial role in modulating the activities and functions of most proteins in biological systems [251]. The importance of glycosylation as a PTM is reflected in the fact that 50–60% of proteins in the human body are modified by glycosylation [252]. Glycoproteins manifest multiple glycosylation sites on them, each of which can be modified with multiple oligosaccharide moieties with varying structures that are usually developmentally and metabolically regulated. These glycoproteins are synthesized mainly in the endoplasmic reticulum and Golgi *via* cascade of reactions that involve sugar nucleotide synthases, transporters, glycosyltransferases and glycosidases. These structures are usually very dynamic and can be altered by modulation of the cell physiology [253,254]. The amino acids that tether the glycan moieties to proteins are asparagine, arginine, serine, threonine, proline, hydroxyproline, tryptophan, and tyrosine [255]. The amino acid of attachment of the glycans categorises the glycoproteins into *N*- and *O*- linked glycoproteins. The most frequent type of glycosylation, *N*-linked glycosylation, is characterized by the attachment of the glycan to an asparagine side chain of the protein. In *O*-linked glycosylation, the glycan is attached to the serine/threonine side chain of the proteins.

N-linked glycans play a significant role in the secretory pathway by influencing protein folding, quality control and trafficking [256]. The roles played by *N*-linked glycosylation extracellularly are significantly less understood, given their pleiotropic and complex nature and non-amenability to *ex vivo* analyses. Most of the extracellular effects of the *N*-glycans are mediated by the interactions with lectins that show specific binding to different glycan structures [257]. Lectins carry the code necessary for cell-cell recognition and can interact with sugars on apposing cells. This results in cellular adhesion via glycans and specific cell-surface receptors. This carbohydrate-directed cell adhesion is crucial in many intercellular activities. *N*-glycosylation also stabilizes functional protein conformations and masks the proteins from active proteolysis [258].

There are three major structural types of *N*-glycans depending on the branching in glycan chains: oligomannose, complex-type (*N*-acetylglucosamine) and hybrid type (mannose and *N*-acetylglucosamine). Cell surface *N*-glycans are involved in several essential cellular functions including cellular and cell–matrix interactions. They also play crucial roles in cell adhesion, differentiation, synaptogenesis and myelinogenesis during the development of central nervous system (CNS) [259].

a. Glycans in the brain

Human congenital disorders of glycosylation (CDGs) highlight the critical involvement of N-glycosylation in the development of the nervous system. These studies highlighted the close correlation between the mutations in the N-glycosylation pathway and severe neurological abnormalities [260]. Genes involved in the glycan production and processing form an estimated 1% of genes in the mammalian genome, most of which code for glycosyltransferases and glycosidases that construct the cellular glycan repertoire.

Although a massive proportion of mammalian N-glycans are complex type, some cells show higher expression of the hybrid and high-mannose forms. Mice and humans inheriting defective *Mgat1* or *Mgat2* alleles have an essential requirement for hybrid and complex N-glycan branching for embryonic development and postnatal function. Defective *Mgat1* or *Mgat2* alleles results in defects in formation of N-glycan branching patterns causing neurologic defects. Ye et al. (2004) performed a detailed *in vivo* analysis by blocking the hybrid and complex N-glycan branching specifically among neuronal cells using Cre-loxP conditional mutagenesis to identify the functional impact of glycan branching [261]. This translated to a specific pattern of neuronal glycoprotein deficiency concurrent with caspase 3 activation and apoptosis. There were also severe locomotor deficits and early postnatal death observed as a result of the aberration in *Mgat1*. Interestingly, no such changes were observed for the *Mgat 2* mutagenesis in terms of phenotypic neuronal markers or locomotor dysfunction.

There is a broad spectrum of cell surface and extracellular matrix (ECM) glycoproteins participating in cell adhesion and signalling in the nervous system [262,263]. Rodent brains were found to be particularly enriched in oligomannosidic N-glycans with 50% of the neutral N-glycans being oligomannosides. There was an interesting concentration of oligomannosides in the synapses of the adult brain [264]. Mannose-binding lectins were found to be concentrated in glutamatergic synapses and oligomannosides are present on both the NMDA (N-methyl-D-aspartate) and AMPA subtypes of glutamate receptors [265]. Another significant and functionally relevant molecule at synapses is the ion pump Na⁺/K⁺-ATPase, which is sorted subcellularly to the dendritic compartment. AMOG is the regulatory subunit of this enzyme which requires glycosylation for the transport of the catalytically active α -subunit to the cell surface as an $\alpha 2\beta 2$ heterodimer [266]. A striking 80% of the glycans of AMOG are

oligomannosides, which are postulated to have a significant functional role in the interplay between this molecule and glycan-binding partners.

Laminins, integrins and receptor protein tyrosine phosphatases, which are glycosylated outside the nervous system, have significant consequences in neuronal migration, axonal growth, myelination, synaptogenesis, neuromuscular junction development and neuronal survival [267,268]. A potent example of the significance of the modulation of N-glycosylation in regulation of cell mobility and adhesion was the impact of β 1,6-branching GlcNAc modifications on the functions of laminin 332 and α 3 β 1 integrins [269,270]. In the cancerous cells, an increase of beta1,6-GlcNAc in laminin 332 catalyzed by N-acetylglucosaminyltransferase V (GnT-V) is related to the promotion of cancer cell motility. Contrarily, bisecting GlcNAc catalyzed by N-acetylglucosaminyltransferase III (GnT-III) suppresses the further branching, and the elongation of N-glycans which decreases cellular migration, an effect which is mediated by impaired alpha3beta1 integrin clustering and resultant focal adhesion formation.

The N-glycans in the brain are predominantly decorated with α 2,3-linked sialic acid, with little or no α 2,6-linked sialic acid [271]. The first molecule in the nervous system that was shown to bind α 2,3-linked sialic acid was myelin-associated glycoprotein (MAG), which is involved in myelin formation and maintenance [272,273]. MAG is known to enhance *in vitro* neurite outgrowth at early developmental stages [274], but inhibits neurite outgrowth in the adult, thereby facilitating a non-conductive environment for neuronal regeneration [275]. α 2, 6-sialylation, on the other hand, plays a significant role in modulating the molecular interactions. It impacts the functions of α 4 β 1 integrins and receptor protein tyrosine phosphatase CD45 by modifying their conformation or manipulating their interactions with functionally important receptors in immune cells [276,277]. Interestingly, a binding domain for α 2,3-linked sialic acid was identified in the first fibronectin type III-homologous domain of L1, where it functions as a glycan acceptor to interact with CD24. This cross-talk between L1 and CD24 has been suggested to be implicated in neurite outgrowth and signal transduction. The CD24-induced promotion or inhibition of neurite outgrowth is mediated by L1 and depends on α 2,3-linked sialic acids mediated interactions with CD24 [278]. The abnormalities in this lectin domain have been associated with abnormalities of brain function in their mutated forms. For instance, the mutations in the putative sialic acid binding motif in L1 results in a severe case of mental retardation and spastic paraplegia [279,280]. On the other hand, α 2,6-linked sialic acids play a crucial role as negative regulators of galectin binding, impacting several cellular and molecular

functions influenced by galectin signalling [281]. The homopolymers of α 2,8-linked sialic acid (PSA) have only been demonstrated to be present on the NCAM specifically in developing tissues such as brain [282], heart [283] and kidney [284] where they exhibit a highly regulated expression pattern. In the brain, PSA expression is correlated to the regions that exhibit physiological plasticity suggesting that these might be related to developmental processes [285]. The aforementioned studies and several others provide cumulative evidence of the glycan-dependent regulatory mechanisms operative in the nervous system.

b. Glycans in neurodegeneration

The structural elucidation of the glycoproteins implicated as a function of glycosylation in human neurodegenerative diseases remains a challenge because of their inherent complexity and heterogeneity in biological systems. Despite several studies have highlighted the importance of glycosylation in the disease processes of AD and PD, there has not been a detailed investigation of the implications of N-glycans in the disease pathophysiology. Sihlbom et al. (2004) performed a 2d gel electrophoretic analysis and FT-ICR MS to characterize different glycosylated isomers of α -1-antitrypsin, β -trace and apolipoprotein J [286]. A more recent study by Gizaw et al. (2016) performed a glycoblot analysis for human Alzheimer's disease brain, serum and cerebrospinal fluid to identify potential glycan-based markers of disease progression [287]. They reported no detectable differences in the total expression levels of the glycans between the brain tissues of the AD patients and healthy controls. However, N-glycans such as bisect-type and multiply branched glycoforms were increased significantly in AD patient group in the serum compared to that of healthy controls. Interestingly, the levels of some gangliosides appeared to be differentially regulated in AD patient brain and serum samples when compared with the healthy controls. The same group previously investigated a detailed glycomic profile of Huntington's disease transgenic mice [288]. They reported 87 and 58 N-glycans in HD transgenic mice and healthy controls respectively and a differential modulation in the O-glycans in the HD transgenic mice in a gender-dependant manner. They also reported GD1a in brain and GM2-NeuGc serum levels as new biomarkers of HD.

Specific protein glycosylation is of significant consequence and has been relatively well elucidated for certain molecular targets like acetylcholinesterase (AChE). It is one of the critical enzyme targets in AD, which is widely distributed in the brain and hydrolyzes the neurotransmitter acetylcholine at cholinergic synapses. Previous studies have reported the modulation of glycosylation of AChE in the *post-mortem* brain and CSF of AD patients

[289,290]. This modulation of AChE glycosylation appears to be a hallmark for AD as it is not seen in other neurological diseases. Similar modulation of a related enzyme, butyrylcholinesterase (BuChE) was observed in the CSF of the AD patients. However, the sensitivity of diagnosing AD with AChE and BuChE in the CSF fails to meet the desired standards to qualify as a disease biomarker [291,292]. Another essential protein involved in AD pathogenesis is microtubule-associated protein (MAP) which undergoes several PTMs, and aggregates into paired helical filaments. Hyperphosphorylation of tau is a pathological hallmark of AD and it was shown that N-linked glycosylation facilitates the process [293].

To date, there is limited information on the role of glycosylated proteins in PD. Some preliminary studies by Farrer and colleagues established a connection between parkin dysfunction, an E3 ubiquitin ligase involved in targeting the proteins for degradation by the proteasomal complex, and the formation of α -synuclein inclusions [294]. It has been hypothesized that parkin-mediated ubiquitination of an O-linked glycosylated form of α -synuclein underlies this process [295]. A seminal study by Varadi et al. (2019) reported reduced sialylation and increased fucosylation in Parkinson's disease patients on tri-antennary glycans with 2 and 3 terminal sialic acids [296]. Another important study by Russell et al (2017) investigated the overall N-glycosylation of IgG as a potential biomarker for PD and its role in mediating the antibody-dependent cell cytotoxicity and a possible state of low-grade inflammation in individuals with Parkinson's disease [297]. A crucial therapeutic intervention for PD would aim at prevention of aggregation of α -synuclein which is modified by O-GlcNAc at at least nine different positions *in vivo*, with currently unknown biological significance. A detailed analysis by Levine et al (2019) used the synthesis of site-specific O-GlcNAcylated forms of α -synuclein to inhibit the aggregation of an aggressive mutant of α -synuclein, suggesting that therapies that increase this modification might be applied *in vivo* for the α -synuclein model [298].

All these studies are suggestive of glycosylation and glycoproteins as crucial players in both physiological conditions as well as in neurodegenerative disorders like in AD and PD. There is a big gap in the field in terms of the absence of any systematic analysis of glycosylation in relevant disease models or a detailed analysis of brain N-glycans in PD patients. Thus, in this study, a detailed spatio-temporal analysis of the rodent brain N-glycans as well as in 6-OHDA PD model is reported using an elaborate glycoanalytical platform.

1.7 Objectives and hypothesis

The aim of this study was to develop a therapeutic fibrin-in-fibrin intervention as a combination cellular and neurotrophic factor therapy and to investigate its efficacy in enhancing the VM graft survival and functional recovery via glycome modulation in a 6-OHDA Parkinson model.

This thesis consists of five research phases (**Figure 1.4**):

- I) Development of fibrin-based reservoir system for neurotrophic factor delivery to the brain (Chapter 2),
- II) Establishment and characterization of fibrin-in-fibrin intervention (Chapter 3)
- III) Complete spatial characterization of rodent brain N-glycome (Chapter 4).
- IV) Spatio-temporal modulation of N-glycosylation in Parkinson's Disease in rodent model of PD (Chapter 5)
- V) Fibrin-in-fibrin intervention for functional recovery in 6-OHDA PD model (Chapter 6)

a. Phase I

Overall aim

To develop a fibrin-based hollow microspheric reservoir for the controlled delivery of neurotrophic factors *in vivo*.

Hypothesis

Fibrin based ECM- mimicking reservoir platform can be fabricated by the manipulation of template charge to obtain a controlled delivery of neurotrophic factors in the brain.

Objectives

- I. Fabricate and characterize the fibrin-based reservoir system
- II. Evaluate the loading and release profiles and investigate interaction with cells
- III. Assess the impact of neurotrophin encapsulation on bioactivity and release *in vitro*
- IV. Perform a preliminary *in vivo* assessment of the host compatibility and release properties of the system in the rodent brains

b. Phase II

Overall aim

To develop and validate a fibrin-in-fibrin intervention for VM cell transplantation to enhance the survival of the engrafted cells by modulating their paracrine secretion profile while conferring them the required immune-protection.

Hypothesis

Manipulation of the biophysical microenvironment can enhance the dopaminergic precursor ventral mesencephalic (VM) graft survival by promoting cell-cell and cell-matrix interactions and minimising the inflammatory response.

Objectives

- I. Fabricate and characterise the fibrin-in-fibrin intervention
- II. Investigate the loading and release of GDNF from the fibrin-in-fibrin platform using ELISA
- III. Investigate the cellular behaviour on tuneable parameters such as hydrogel concentration, cell density and microsphere concentration.
- IV. Investigate the modulation of paracrine response and gene expression of the encapsulated grafts to optimise the conditions of treatment to be tested *in vivo*

c. Phase III

Overall aim

To develop a standardised and reproducible glyco-analytical platform for the complete characterisation of N- glycans from striatum and substantia nigra (SN) in the rodent brains.

Hypothesis

The spatial resolution of *N*-glycans isolated from striatum and SN could give us an insight into their involvement in regulation of striatal and nigral cues for establishment and pathophysiological degeneration of neural circuitry in Parkinson's disease.

Objectives

- I. Optimisation of the of *N*- glycans isolation protocol from rat striatum and SN

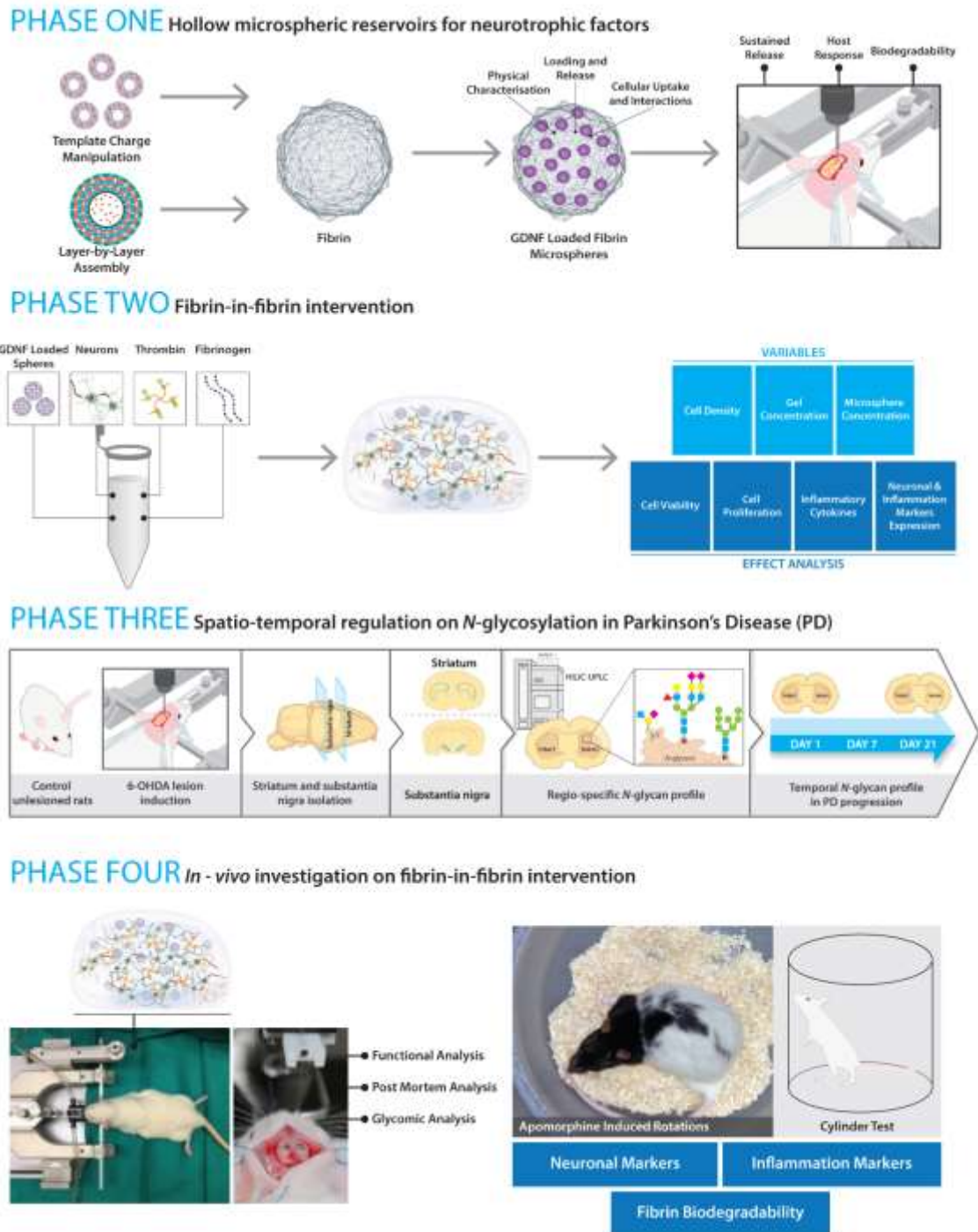


Figure 1.4: Study outline: Schematic representation of the major phases of the study aimed towards the investigation of an optimized fibrin-in-fibrin therapeutic intervention in 6-OHDA model of Parkinson's disease.

- II. Resolution and relative quantitation of *N*- glycome using ultra performance liquid chromatography (UPLC), weak anion exchange UPLC (WAX-UPLC) and liquid chromatographic mass spectrometry
- III. Lectin histochemical analyses visual and semi-quantitative representation of N-glycan modulation

d. Phase IV

Overall aim

To investigate the modulation of *N*-glycosylation of rodent brain with the progression of PD using the spatio-specific glycoanalytical technology.

Hypothesis

Spatiotemporal resolution of *N*-glycans isolated from striatum and SN over the time course of the disease progression in a Parkinson's model could give us an insight into the structures and implications of the glycan cues involved in the pathophysiological degeneration and therapeutic restoration of the neural circuitry.

Objectives

- I. *In vivo* analysis for 6-OHDA PD induction over a period of 21 days
- II. Detailed comparative spatio-temporal analysis of relative abundances of *N*-type glycans in the SN and striatum of 6-OHDA treated rat brains using the previously developed glyco-analytical platform
- III. Lectin histochemical analyses for visual and semi-quantitative representation of N-glycan modulation in PD.

e. Phase V

Overall aim

To assess the fibrin-in-fibrin intervention for the controlled delivery of glial cell derived neurotrophic factor (GDNF) in fibrin hollow microspheres towards the transplantation of primary dopaminergic neurons to the Parkinsonian brain using a fibrin hydrogel.

Hypothesis

A tuneable fibrin-in-fibrin intervention would act as a temporally-controlled local GDNF reservoir and immunoprotect the transplanted cells, thereby improving the overall survival and re-innervation of primary dopaminergic neurons after intra-striatal transplantation and lead to motor function recovery in a 6-OHDA PD model.

Objectives

- I. Fabricate and test the fibrin-in-fibrin system in a 6-OHDA rat model for the survival of dopaminergic cells
- II. Investigate functional recovery using cylinder test and apomorphine-induced rotations
- III. Investigate the impact of the fibrin-in-fibrin intervention on the molecular signature and *N*-glycosignature of the rodent brains through MALDI-MSI and lectin histochemistry (Ongoing)

1.8 References

- [1] L. Sakka, G. Coll, J. Chazal, Anatomy and physiology of cerebrospinal fluid, *Eur. Ann. Otorhinolaryngol. Head Neck Dis.* 128 (2011) 309–316. doi:10.1016/j.anorl.2011.03.002.
- [2] R. Weller, M. Christodoulides, *Meningitis: cellular and molecular basis*, 2013. <https://www.cabi.org/bookshop/book/9781780641621> (accessed January 15, 2018).
- [3] J. Ghersi-Egea, Y. Sugiyama, Drug transfer in the choroid plexus. Multiplicity and substrate specificities of transporters, *Adv. Drug Deliv. Rev.* 56 (2004) 1693–1890. doi:10.1016/j.addr.2004.07.004.
- [4] K.-T. Callixte, T.B. Clet, D. Jacques, Y. Faustin, D.J. François, T.-T. Maturin, The pattern of neurological diseases in elderly people in outpatient consultations in Sub-Saharan Africa., *BMC Res. Notes.* 8 (2015) 159. doi:10.1186/s13104-015-1116-x.
- [5] C. Glorioso, S. Oh, G.G. Douillard, E. Sibille, Brain molecular aging, promotion of neurological disease and modulation by Sirtuin5 longevity gene polymorphism, *Neurobiol. Dis.* 41 (2011) 279–290. doi:10.1016/j.nbd.2010.09.016.
- [6] T.M. Barchet, M.M. Amiji, Challenges and opportunities in CNS delivery of therapeutics for neurodegenerative diseases, *Expert Opin. Drug Deliv.* 6 (2009) 211–225. doi:10.1517/17425240902758188.
- [7] P. Ballabh, A. Braun, M. Nedergaard, The blood–brain barrier: an overview, *Neurobiol. Dis.* 16 (2004) 1–13. doi:10.1016/j.nbd.2003.12.016.
- [8] S. Vogel, *Vital circuits : on pumps, pipes, and the workings of circulatory systems*, Oxford University Press, 1992. https://books.google.ie/books?id=oIFeDvRwh2gC&printsec=copyright&redir_esc=y#v=onepage&q&f=false (accessed March 5, 2017).
- [9] H. Sarin, Physiologic upper limits of pore size of different blood capillary types and another perspective on the dual pore theory of microvascular permeability, *J.*

- Angiogenes. Res. 2 (2010) 14. doi:10.1186/2040-2384-2-14.
- [10] E.R. Kandel, Principles of neural science, n.d. <https://www.mhprofessional.com/9780071390118-usa-principles-of-neural-science-fifth-edition-group> (accessed March 5, 2017).
- [11] D.A. Drachman, Do we have brain to spare?, *Neurology*. 64 (2005) 2004–2005. doi:10.1212/01.WNL.0000166914.38327.BB.
- [12] J. Kreuter, Nanoparticles—a historical perspective, *Int. J. Pharm.* 331 (2007) 1–10. doi:10.1016/J.IJPHARM.2006.10.021.
- [13] H.B. Newton, Advances in strategies to improve drug delivery to brain tumors, *Expert Rev. Neurother.* 6 (2006) 1495–1509. doi:10.1586/14737175.6.10.1495.
- [14] S.P. Vyas, A. Singh, V. Sihorkar, Ligand-receptor-mediated drug delivery: an emerging paradigm in cellular drug targeting., *Crit. Rev. Ther. Drug Carrier Syst.* 18 (2001) 1–76.
- [15] P. Ballabh, A. Braun, M. Nedergaard, The blood-brain barrier: An overview: Structure, regulation, and clinical implications, *Neurobiol. Dis.* 16 (2004) 1–13. doi:10.1016/j.nbd.2003.12.016.
- [16] W.M. Pardridge, Transport of small molecules through the blood-brain barrier: biology and methodology, *Adv. Drug Deliv. Rev.* 15 (1995) 5–36. doi:10.1016/0169-409X(95)00003-P.
- [17] W.A. Banks, Delivery of peptides to the brain: Emphasis on therapeutic development, *Biopolymers.* 90 (2008) 589–594. doi:10.1002/bip.20980.
- [18] T. Terasaki, S. Takakuwa, A. Saheki, S. Moritani, T. Shimura, S. Tabata, A. Tsuji, Absorptive-mediated endocytosis of an adrenocorticotrophic hormone (ACTH) analogue, ebratide, into the blood-brain barrier: studies with monolayers of primary cultured bovine brain capillary endothelial cells., *Pharm. Res.* 9 (1992) 529–34. <http://www.ncbi.nlm.nih.gov/pubmed/1323100> (accessed March 6, 2017).
- [19] T. Terasaki, K. Hirai, H. Sato, Y.S. Kang, A. Tsuji, Absorptive-mediated endocytosis of a dynorphin-like analgesic peptide, E-2078 into the blood-brain barrier., *J. Pharmacol. Exp. Ther.* 251 (1989) 351–7. <http://www.ncbi.nlm.nih.gov/pubmed/2571724> (accessed March 6, 2017).
- [20] A. Urayama, J.H. Grubb, W.S. Sly, W.A. Banks, Developmentally regulated mannose 6-phosphate receptor-mediated transport of a lysosomal enzyme across the blood-brain barrier., *Proc. Natl. Acad. Sci. U. S. A.* 101 (2004) 12658–63. doi:10.1073/pnas.0405042101.
- [21] D.J. Begley, Delivery of therapeutic agents to the central nervous system: the problems and the possibilities., *Pharmacol. Ther.* 104 (2004) 29–45. doi:10.1016/j.pharmthera.2004.08.001.
- [22] Y. Deguchi, K. Nozawa, S. Yamada, Y. Yokoyama, R. Kimura, Quantitative evaluation of brain distribution and blood-brain barrier efflux transport of probenecid in rats by microdialysis: possible involvement of the monocarboxylic acid transport system., *J. Pharmacol. Exp. Ther.* 280 (1997) 551–60. <http://www.ncbi.nlm.nih.gov/pubmed/9023263> (accessed March 6, 2017).

- [23] B. Noé, B. Hagenbuch, B. Stieger, P.J. Meier, Isolation of a multispecific organic anion and cardiac glycoside transporter from rat brain., *Proc. Natl. Acad. Sci. U. S. A.* 94 (1997) 10346–50. <http://www.ncbi.nlm.nih.gov/pubmed/9294213> (accessed March 6, 2017).
- [24] W.M. Pardridge, Drug targeting to the brain, *Pharm. Res.* 24 (2007) 1733–1744. doi:10.1007/s11095-007-9324-2.
- [25] W.M. Pardridge, Molecular biology of the blood–brain barrier, *Mol. Biotechnol.* 30 (2005) 057–070. doi:10.1385/MB:30:1:057.
- [26] O. Lindvall, A. Björklund, Cell therapy in Parkinson’s disease., *NeuroRx.* 1 (2004) 382–393. doi:10.1602/neurorx.1.4.382.
- [27] D.R. Zimmermann, M.T. Dours-Zimmermann, Extracellular matrix of the central nervous system: from neglect to challenge, *Histochem. Cell Biol.* 130 (2008) 635–653. doi:10.1007/s00418-008-0485-9.
- [28] A.B.J. Prowse, F. Chong, P.P. Gray, T.P. Munro, Stem cell integrins: Implications for ex-vivo culture and cellular therapies, *Stem Cell Res.* 6 (2011) 1–12. doi:10.1016/j.scr.2010.09.005.
- [29] D.A. Tonge, H.T. de Burgh, R. Docherty, M.J. Humphries, S.E. Craig, J. Pizzey, Fibronectin supports neurite outgrowth and axonal regeneration of adult brain neurons in vitro, *Brain Res.* 1453 (2012) 8–16. doi:10.1016/J.BRAINRES.2012.03.024.
- [30] U. Hersel, C. Dahmen, H. Kessler, RGD modified polymers: biomaterials for stimulated cell adhesion and beyond., *Biomaterials.* 24 (2003) 4385–415. doi:10.1016/s0142-9612(03)00343-0.
- [31] M.D. Pierschbacher, E. Ruoslahti, Cell attachment activity of fibronectin can be duplicated by small synthetic fragments of the molecule, *Nature.* 309 (1984) 30–33. doi:10.1038/309030a0.
- [32] J. Graf, R.C. Ogle, F.A. Robey, M. Sasaki, G.R. Martin, Y. Yamada, H.K. Kleinman, A pentapeptide from the laminin B1 chain mediates cell adhesion and binds to 67000 laminin receptor, *Biochemistry.* 26 (1987) 6896–6900. doi:10.1021/bi00396a004.
- [33] K. Tashiro, G.C. Sephel, B. Weeks, M. Sasaki, G.R. Martin, H.K. Kleinman, Y. Yamada, A synthetic peptide containing the IKVAV sequence from the A chain of laminin mediates cell attachment, migration, and neurite outgrowth., *J. Biol. Chem.* 264 (1989) 16174–82. <http://www.ncbi.nlm.nih.gov/pubmed/2777785> (accessed August 18, 2019).
- [34] J.L. Neiiendam, L.B. Kohler, C. Christensen, S. Li, M.V. Pedersen, D.K. Ditlevsen, M.K. Kornum, V. V. Kiselyov, V. Berezin, E. Bock, An NCAM-derived FGF-receptor agonist, the FGL-peptide, induces neurite outgrowth and neuronal survival in primary rat neurons, *J. Neurochem.* 91 (2004) 920–935. doi:10.1111/j.1471-4159.2004.02779.x.
- [35] M.A. Azagarsamy, K.S. Anseth, Bioorthogonal click chemistry: An indispensable tool to create multifaceted cell culture scaffolds, *ACS Macro Lett.* 2 (2013) 5–9. doi:10.1021/mz300585q.
- [36] K.J. Lampe, A.L. Antaris, S.C. Heilshorn, Design of three-dimensional engineered protein hydrogels for tailored control of neurite growth, *Acta Biomater.* 9 (2013)

- 5590–5599. doi:10.1016/J.ACTBIO.2012.10.033.
- [37] S.G. Lévesque, M.S. Shoichet, Synthesis of cell-adhesive dextran hydrogels and macroporous scaffolds, *Biomaterials*. 27 (2006) 5277–5285. doi:10.1016/J.BIOMATERIALS.2006.06.004.
- [38] A. Gefen, S.S. Margulies, Are in vivo and in situ brain tissues mechanically similar?, *J. Biomech*. 37 (2004) 1339–52. doi:10.1016/j.jbiomech.2003.12.032.
- [39] I. Levental, P.C. Georges, P.A. Janmey, Soft biological materials and their impact on cell function, *Soft Matter*. 3 (2007) 299–306. doi:10.1039/B610522J.
- [40] A.P. Balgude, X. Yu, A. Szymanski, R. V Bellamkonda, Agarose gel stiffness determines rate of DRG neurite extension in 3D cultures., *Biomaterials*. 22 (2001) 1077–84. doi:10.1016/s0142-9612(00)00350-1.
- [41] F.X. Jiang, B. Yurke, B.L. Firestein, N.A. Langrana, Neurite outgrowth on a DNA crosslinked hydrogel with tunable stiffnesses, *Ann. Biomed. Eng*. 36 (2008) 1565–1579. doi:10.1007/s10439-008-9530-z.
- [42] K. Saha, A.J. Keung, E.F. Irwin, Y. Li, L. Little, D. V. Schaffer, K.E. Healy, Substrate modulus directs neural stem cell behavior, *Biophys. J*. 95 (2008) 4426–4438. doi:10.1529/biophysj.108.132217.
- [43] N.D. Leipzig, M.S. Shoichet, The effect of substrate stiffness on adult neural stem cell behavior, *Biomaterials*. 30 (2009) 6867–6878. doi:10.1016/j.biomaterials.2009.09.002.
- [44] S. Sur, C.J. Newcomb, M.J. Webber, S.I. Stupp, Tuning supramolecular mechanics to guide neuron development, *Biomaterials*. 34 (2013) 4749–4757. doi:10.1016/j.biomaterials.2013.03.025.
- [45] A.J. Engler, S. Sen, H.L. Sweeney, D.E. Discher, Matrix elasticity directs stem cell lineage specification, *Cell*. 126 (2006) 677–689. doi:10.1016/j.cell.2006.06.044.
- [46] S.Q. Liu, Q. Tian, J.L. Hedrick, J.H. Po Hui, P.L. Rachel Ee, Y.Y. Yang, Biomimetic hydrogels for chondrogenic differentiation of human mesenchymal stem cells to neocartilage, *Biomaterials*. 31 (2010) 7298–7307. doi:10.1016/J.BIOMATERIALS.2010.06.001.
- [47] P.M. Comoglio, C. Boccaccio, L. Trusolino, Interactions between growth factor receptors and adhesion molecules: breaking the rules, *Curr. Opin. Cell Biol*. 15 (2003) 565–571. doi:10.1016/S0955-0674(03)00096-6.
- [48] M.M. Martino, F. Tortelli, M. Mochizuki, S. Traub, D. Ben-David, G.A. Kuhn, R. Müller, E. Livne, S.A. Eming, J.A. Hubbell, Engineering the growth factor microenvironment with fibronectin domains to promote wound and bone tissue healing., *Sci. Transl. Med*. 3 (2011) 100ra89. doi:10.1126/scitranslmed.3002614.
- [49] R.Y. Tam, M.J. Cooke, M.S. Shoichet, A covalently modified hydrogel blend of hyaluronan–methyl cellulose with peptides and growth factors influences neural stem/progenitor cell fate, *J. Mater. Chem*. 22 (2012) 19402–19411. doi:10.1039/c2jm33680d.
- [50] T.-Y. Cheng, M.-H. Chen, W.-H. Chang, M.-Y. Huang, T.-W. Wang, Neural stem cells encapsulated in a functionalized self-assembling peptide hydrogel for brain tissue engineering, *Biomaterials*. 34 (2013) 2005–2016.

- doi:10.1016/J.BIOMATERIALS.2012.11.043.
- [51] C. Frick, M. Müller, U. Wank, A. Tropitzsch, B. Kramer, P. Senn, H. Rask-Andersen, K.-H. Wiesmüller, H. Löwenheim, Biofunctionalized peptide-based hydrogels provide permissive scaffolds to attract neurite outgrowth from spiral ganglion neurons, *Colloids Surfaces B Biointerfaces*. 149 (2017) 105–114. doi:10.1016/J.COLSURFB.2016.10.003.
- [52] W. Sun, T. Incitti, C. Migliaresi, A. Quattrone, S. Casarosa, A. Motta, Viability and neuronal differentiation of neural stem cells encapsulated in silk fibroin hydrogel functionalized with an IKVAV peptide, *J. Tissue Eng. Regen. Med.* 11 (2017) 1532–1541. doi:10.1002/term.2053.
- [53] H. Cui, M.J. Webber, S.I. Stupp, Self-assembly of peptide amphiphiles: From molecules to nanostructures to biomaterials, *Biopolymers*. 94 (2010) 1–18. doi:10.1002/bip.21328.
- [54] H. Li, A.M. Koenig, P. Sloan, N.D. Leipzig, In vivo assessment of guided neural stem cell differentiation in growth factor immobilized chitosan-based hydrogel scaffolds, *Biomaterials*. 35 (2014) 9049–9057. doi:10.1016/J.BIOMATERIALS.2014.07.038.
- [55] A.L. Carlson, N.K. Bennett, N.L. Francis, A. Halikere, S. Clarke, J.C. Moore, R.P. Hart, K. Paradiso, M. Wernig, J. Kohn, Z.P. Pang, P. V. Moghe, Generation and transplantation of reprogrammed human neurons in the brain using 3D microtopographic scaffolds, *Nat. Commun.* 7 (2016) 10862. doi:10.1038/ncomms10862.
- [56] M.I. Günther, N. Weidner, R. Müller, A. Blesch, Cell-seeded alginate hydrogel scaffolds promote directed linear axonal regeneration in the injured rat spinal cord, *Acta Biomater.* 27 (2015) 140–150. doi:10.1016/J.ACTBIO.2015.09.001.
- [57] S.-H. Kim, J. Turnbull, S. Guimond, Extracellular matrix and cell signalling: the dynamic cooperation of integrin, proteoglycan and growth factor receptor, *J. Endocrinol.* 209 (2011) 139–151. doi:10.1530/JOE-10-0377.
- [58] D. Hoffman-Kim, J.A. Mitchel, R. V. Bellamkonda, Topography, cell response, and nerve regeneration, *Annu. Rev. Biomed. Eng.* 12 (2010) 203–231. doi:10.1146/annurev-bioeng-070909-105351.
- [59] K.K.B. Tan, W.W.M. Lim, C. Chai, M. Kukumberg, K.L. Lim, E.L.K. Goh, E.K.F. Yim, Sequential application of discrete topographical patterns enhances derivation of functional mesencephalic dopaminergic neurons from human induced pluripotent stem cells, *Sci. Rep.* 8 (2018) 9567. doi:10.1038/s41598-018-27653-1.
- [60] R. Singhvi, A. Kumar, G. Lopez, G. Stephanopoulos, D. Wang, G. Whitesides, D. Ingber, Engineering cell shape and function, *Science* (80-.). 252 (1994) 1164–1167. doi:10.1126/science.252.5009.1164.
- [61] M. Lietz, L. Dreesmann, M. Hoss, S. Oberhoffner, B. Schlosshauer, Neuro tissue engineering of glial nerve guides and the impact of different cell types, *Biomaterials*. 27 (2006) 1425–1436. doi:10.1016/J.BIOMATERIALS.2005.08.007.
- [62] E. Schnell, K. Klinkhammer, S. Balzer, G. Brook, D. Klee, P. Dalton, J. Mey, Guidance of glial cell migration and axonal growth on electrospun nanofibers of poly- ϵ -caprolactone and a collagen/poly- ϵ -caprolactone blend, *Biomaterials*. 28 (2007)

- 3012–3025. doi:10.1016/J.BIOMATERIALS.2007.03.009.
- [63] R.M. Smeal, P.A. Tresco, The influence of substrate curvature on neurite outgrowth is cell type dependent, *Exp. Neurol.* 213 (2008) 281–292. doi:10.1016/J.EXPNEUROL.2008.05.026.
- [64] E.C. Tsai, P.D. Dalton, M.S. Shoichet, C.H. Tator, Synthetic Hydrogel Guidance Channels Facilitate Regeneration of Adult Rat Brainstem Motor Axons after Complete Spinal Cord Transection, *J. Neurotrauma.* 21 (2004) 789–804. doi:10.1089/0897715041269687.
- [65] M.J. Moore, J.A. Friedman, E.B. Lewellyn, S.M. Mantila, A.J. Krych, S. Ameenuddin, A.M. Knight, L. Lu, B.L. Currier, R.J. Spinner, R.W. Marsh, A.J. Windebank, M.J. Yaszemski, Multiple-channel scaffolds to promote spinal cord axon regeneration, *Biomaterials.* 27 (2006) 419–429. doi:10.1016/J.BIOMATERIALS.2005.07.045.
- [66] L.M. de Lau, M.M. Breteler, Epidemiology of Parkinson's disease, *Lancet Neurol.* 5 (2006) 525–535. doi:10.1016/S1474-4422(06)70471-9.
- [67] I.N. Miller, A. Cronin-Golomb, Gender differences in Parkinson's disease: Clinical characteristics and cognition, *Mov. Disord.* 25 (2010) 2695–2703. doi:10.1002/mds.23388.
- [68] O.M.A. El-Agnaf, S.A. Salem, K.E. Paleologou, M.D. Curran, M.J. Gibson, J.A. Court, M.G. Schlossmacher, D. Allsop, Detection of oligomeric forms of α -synuclein protein in human plasma as a potential biomarker for Parkinson's disease, *FASEB J.* 20 (2006) 419–425. doi:10.1096/fj.03-1449com.
- [69] H.W. Berendse, J. Booij, C.M. Francot, P.L. Bergmans, R. Hijman, J.C. Stoof, E.C. Wolters, Subclinical dopaminergic dysfunction in asymptomatic Parkinson's disease patients' relatives with a decreased sense of smell., *Ann. Neurol.* 50 (2001) 34–41. <http://www.ncbi.nlm.nih.gov/pubmed/11456307> (accessed August 13, 2019).
- [70] M.E. Bernis, J.T. Babila, S. Breid, K.A. Wüsten, U. Wüllner, G. Tamgüney, Prion-like propagation of human brain-derived alpha-synuclein in transgenic mice expressing human wild-type alpha-synuclein, *Acta Neuropathol. Commun.* 3 (2015) 75. doi:10.1186/s40478-015-0254-7.
- [71] J.W. Langston, L.S. Forno, J. Tetrad, A.G. Reeves, J.A. Kaplan, D. Karluk, Evidence of active nerve cell degeneration in the substantia nigra of humans years after 1-methyl-4-phenyl-1,2,3,6-tetrahydropyridine exposure, *Ann. Neurol.* 46 (1999) 598–605. doi:10.1002/1531-8249(199910)46:4<598::AID-ANA7>3.0.CO;2-F.
- [72] J.A. Firestone, T. Smith-Weller, G. Franklin, P. Swanson, W.T. Longstreth, H. Checkoway, Pesticides and risk of Parkinson Disease, *Arch. Neurol.* 62 (2005) 91–95. doi:10.1001/archneur.62.1.91.
- [73] A.H. V. Schapira, J.M. Cooper, D. Dexter, J.B. Clark, P. Jenner, C.D. Marsden, Mitochondrial complex I deficiency in Parkinson's Disease, *J. Neurochem.* 54 (1990) 823–827. doi:10.1111/j.1471-4159.1990.tb02325.x.
- [74] P. Jenner, C.W. Olanow, Oxidative stress and the pathogenesis of Parkinson's disease, *Neurology.* 47 (1996) 161S–170S. doi:10.1212/WNL.47.6_Suppl_3.161S.
- [75] J. Sian, D.T. Dexter, A.J. Lees, S. Daniel, Y. Agid, F. Javoy-Agid, P. Jenner, C.D. Marsden, Alterations in glutathione levels in Parkinson's disease and other

- neurodegenerative disorders affecting basal ganglia, *Ann. Neurol.* 36 (1994) 348–355. doi:10.1002/ana.410360305.
- [76] K.P. St McNaught, R. Belizaire, O. Isacson, P. Jenner, C. Warren Olanow, Altered proteasomal function in sporadic Parkinson’s Disease, *179 (2002) 38–46*. doi:10.1006/exnr.2002.8050.
- [77] E.-K. Tan, L.M. Skipper, Pathogenic mutations in Parkinson disease, *Hum. Mutat.* 28 (2007) 641–653. doi:10.1002/humu.20507.
- [78] A.L. Bartels, K.L. Leenders, Neuroinflammation in the pathophysiology of Parkinson’s disease: Evidence from animal models to human *in vivo* studies with [¹¹C]-PK11195 PET, *Mov. Disord.* 22 (2007) 1852–1856. doi:10.1002/mds.21552.
- [79] H. Braak, K. Del Tredici, U. Rüb, R.A.I. de Vos, E.N.H. Jansen Steur, E. Braak, Staging of brain pathology related to sporadic Parkinson’s disease., *Neurobiol. Aging.* 24 (n.d.) 197–211. <http://www.ncbi.nlm.nih.gov/pubmed/12498954> (accessed August 13, 2019).
- [80] A. Siderowf, D. Aarsland, B. Mollenhauer, J.G. Goldman, B. Ravina, Biomarkers for cognitive impairment in Lewy body disorders: Status and relevance for clinical trials, *Mov. Disord.* 33 (2018) 528–536. doi:10.1002/mds.27355.
- [81] K.C. Luk, V. Kehm, J. Carroll, B. Zhang, P. O’Brien, J.Q. Trojanowski, V.M.-Y. Lee, Pathological α -synuclein transmission initiates Parkinson-like neurodegeneration in nontransgenic mice, *Science* (80-.). 338 (2012) 949–953. doi:10.1126/science.1227157.
- [82] J.A. Steiner, E. Quansah, P. Brundin, The concept of alpha-synuclein as a prion-like protein: ten years after, *Cell Tissue Res.* 373 (2018) 161–173. doi:10.1007/s00441-018-2814-1.
- [83] T.M. Rodrigues, A. Jerónimo-Santos, T.F. Outeiro, A.M. Sebastião, M.J. Diógenes, Challenges and promises in the development of neurotrophic factor-based therapies for parkinson’s disease, *Drugs and Aging.* 31 (2014) 239–261. doi:10.1007/s40266-014-0160-x.
- [84] K.K. Teng, S. Felice, T. Kim, B.L. Hempstead, Understanding proneurotrophin actions: Recent advances and challenges, *Dev. Neurobiol.* 70 (2010) NA-NA. doi:10.1002/dneu.20768.
- [85] D.R. Kaplan, D. Martin-Zanca, L.F. Parada, Tyrosine phosphorylation and tyrosine kinase activity of the trk proto-oncogene product induced by NGF, *Nature.* 350 (1991) 158–160. doi:10.1038/350158a0.
- [86] M. Mogi, A. Togari, T. Kondo, Y. Mizuno, O. Komure, S. Kuno, H. Ichinose, T. Nagatsu, Brain-derived growth factor and nerve growth factor concentrations are decreased in the substantia nigra in Parkinson’s disease., *Neurosci. Lett.* 270 (1999) 45–48. doi:10.1016/s0304-3940(99)00463-2.
- [87] I. Date, T. Ohmoto, Neural transplantation and trophic factors in Parkinson’s Disease: special reference to chromaffin cell grafting, NGF support from pretransected peripheral nerve, and encapsulated dopamine-secreting cell grafting, *Exp. Neurol.* 137 (1996) 333–344. doi:10.1006/exnr.1996.0034.
- [88] F. Rahmani, A. Saghazadeh, M. Rahmani, A.L. Teixeira, N. Rezaei, V. Aghamollaii,

- H.E. Ardebili, Plasma levels of brain-derived neurotrophic factor in patients with Parkinson disease: A systematic review and meta-analysis, *Brain Res.* 1704 (2019) 127–136. doi:10.1016/j.brainres.2018.10.006.
- [89] T. Tsukahara, M. Takeda, S. Shimohama, O. Ohara, N. Hashimoto, Effects of brain-derived neurotrophic factor on 1-Methyl-4-phenyl-1,2,3,6-tetrahydropyridine-induced parkinsonism in monkeys, *Neurosurgery.* 37 (1995) 733–741. doi:10.1227/00006123-199510000-00018.
- [90] M. Levivier, S. Przedborski, C. Bencsics, U.J. Kang, Intrastratial implantation of fibroblasts genetically engineered to produce brain-derived neurotrophic factor prevents degeneration of dopaminergic neurons in a rat model of Parkinson's disease., *J. Neurosci.* 15 (1995) 7810–7820. <http://www.ncbi.nlm.nih.gov/pubmed/8613721> (accessed August 11, 2019).
- [91] C.A. Altar, C.B. Boylan, M. Fritsche, B.E. Jones, C. Jackson, S.J. Wiegand, R.M. Lindsay, C. Hyman, Efficacy of brain-derived neurotrophic factor and neurotrophin-3 on neurochemical and behavioral deficits associated with partial nigrostriatal dopamine lesions, *J. Neurochem.* 63 (2002) 1021–1032. doi:10.1046/j.1471-4159.1994.63031021.x.
- [92] S. Gu, H. Huang, J. Bi, Y. Yao, T. Wen, Combined treatment of neurotrophin-3 gene and neural stem cells is ameliorative to behavior recovery of Parkinson's disease rat model, *Brain Res.* 1257 (2009) 1–9. doi:10.1016/j.brainres.2008.12.016.
- [93] M. Lindahl, P. Lindholm, Unconventional neurotrophic factors CDNF and MANF: Structure, physiological functions and therapeutic potential, *Neurobiol. Dis.* 97 (2017) 90–102. doi:10.1016/J.NBD.2016.07.009.
- [94] C.C. Glembotski, D.J. Thuerauf, C. Huang, J.A. Vekich, R.A. Gottlieb, S. Doroudgar, Mesencephalic astrocyte-derived neurotrophic factor protects the heart from ischemic damage and is selectively secreted upon sarco/endoplasmic reticulum calcium depletion., *J. Biol. Chem.* 287 (2012) 25893–25904. doi:10.1074/jbc.M112.356345.
- [95] P. Lindholm, M.H. Voutilainen, J. Laurén, J. Peränen, V.-M. Leppänen, J.-O. Andressoo, M. Lindahl, S. Janhunen, N. Kalkkinen, T. Timmusk, R.K. Tuominen, M. Saarma, Novel neurotrophic factor CDNF protects and rescues midbrain dopamine neurons in vivo, *Nature.* 448 (2007) 73–77. doi:10.1038/nature05957.
- [96] P.S. Petrova, A. Raibekas, J. Pevsner, N. Vigo, M. Anafi, M.K. Moore, A.E. Peaire, V. Shridhar, D.I. Smith, J. Kelly, Y. Durocher, J.W. Commissiong, MANF: A new mesencephalic, astrocyte-derived neurotrophic factor with selectivity for dopaminergic neurons, *J. Mol. Neurosci.* 20 (2003) 173–188. doi:10.1385/JMN:20:2:173.
- [97] D. Lindholm, H. Wootz, L. Korhonen, ER stress and neurodegenerative diseases, *Cell Death Differ.* 13 (2006) 385–392. doi:10.1038/sj.cdd.4401778.
- [98] H.L. Smith, G.R. Mallucci, The unfolded protein response: mechanisms and therapy of neurodegeneration, *Brain.* 139 (2016) 2113–2121. doi:10.1093/brain/aww101.
- [99] H.J. Huttunen, M. Saarma, CDNF protein therapy in Parkinson's Disease, *Cell Transplant.* 28 (2019) 349–366. doi:10.1177/0963689719840290.
- [100] M.H. Voutilainen, S. Bäck, J. Peränen, P. Lindholm, A. Raasmaja, P.T. Männistö, M. Saarma, R.K. Tuominen, Chronic infusion of CDNF prevents 6-OHDA-induced

- deficits in a rat model of Parkinson's disease, *Exp. Neurol.* 228 (2011) 99–108. doi:10.1016/J.EXPNEUROL.2010.12.013.
- [101] M. Airavaara, B.K. Harvey, M.H. Voutilainen, H. Shen, J. Chou, P. Lindholm, M. Lindahl, R.K. Tuominen, M. Saarma, B. Hoffer, Y. Wang, CDNF protects the nigrostriatal dopamine system and promotes recovery after MPTP treatment in mice, *Cell Transplant.* 21 (2012) 1213–1223. doi:10.3727/096368911X600948.
- [102] O. Lewis, M. Woolley, D. Johnson, A. Rosser, N.U. Barua, A.S. Bienemann, S.S. Gill, S. Evans, Chronic, intermittent convection-enhanced delivery devices, *J. Neurosci. Methods.* 259 (2016) 47–56. doi:10.1016/J.JNEUMETH.2015.11.008.
- [103] N.U. Barua, M. Woolley, A.S. Bienemann, D.E. Johnson, O. Lewis, M.J. Wyatt, C. Irving, S. O'Sullivan, G. Murray, C. Fennelly, P. Skinner, S.S. Gill, Intermittent convection-enhanced delivery to the brain through a novel transcutaneous bone-anchored port, *J. Neurosci. Methods.* 214 (2013) 223–232. doi:10.1016/J.JNEUMETH.2013.02.007.
- [104] H.J. Huttunen, A first-in-human clinical study to test the safety and preliminary efficacy of CDNF in Parkinson's disease, (2018). <https://researchportal.helsinki.fi/en/publications/a-first-in-human-clinical-study-to-test-the-safety-and-preliminar> (accessed August 12, 2019).
- [105] Y. Liu, J. Zhang, M. Jiang, Q. Cai, J. Fang, L. Jin, MANF improves the MPP+/MPTP-induced Parkinson's disease via improvement of mitochondrial function and inhibition of oxidative stress., *Am. J. Transl. Res.* 10 (2018) 1284–1294. <http://www.ncbi.nlm.nih.gov/pubmed/29887945> (accessed August 12, 2019).
- [106] M.H. Voutilainen, S. Bäck, E. Pörsti, L. Toppinen, L. Lindgren, P. Lindholm, J. Peränen, M. Saarma, R.K. Tuominen, Mesencephalic astrocyte-derived neurotrophic factor is neurorestorative in rat model of Parkinson's disease., *J. Neurosci.* 29 (2009) 9651–9. doi:10.1523/JNEUROSCI.0833-09.2009.
- [107] Z. Zhang, Y. Shen, H. Luo, F. Zhang, D. Peng, L. Jing, Y. Wu, X. Xia, Y. Song, W. Li, L. Jin, MANF protects dopamine neurons and locomotion defects from a human α -synuclein induced Parkinson's disease model in *C. elegans* by regulating ER stress and autophagy pathways, *Exp. Neurol.* 308 (2018) 59–71. doi:10.1016/j.expneurol.2018.06.016.
- [108] A.-C. Bachoud-Lévi, N. Déglon, J.-P. Nguyen, J. Bloch, C. Bourdet, L. Winkel, P. Rémy, M. Goddard, J.-P. Lefaucheur, P. Brugières, S. Baudic, P. Cesaro, M. Peschanski, P. Aebischer, Neuroprotective gene therapy for Huntington's disease using a polymer encapsulated BHK cell line engineered to secrete human CNTF, *Hum. Gene Ther.* 11 (2000) 1723–1729. doi:10.1089/10430340050111377.
- [109] D.F. Emerich, S.R. Winn, P.M. Hantraye, M. Peschanski, E.-Y. Chen, Y. Chu, P. McDermott, E.E. Baetge, J.H. Kordower, Protective effect of encapsulated cells producing neurotrophic factor CNTF in a monkey model of Huntington's disease, *Nature.* 386 (1997) 395–399. doi:10.1038/386395a0.
- [110] H. Sariola, Novel functions and signalling pathways for GDNF, *J. Cell Sci.* 116 (2003) 3855–3862. doi:10.1242/jcs.00786.
- [111] L.F. Lin, D.H. Doherty, J.D. Lile, S. Bektesh, F. Collins, GDNF: a glial cell line-derived neurotrophic factor for midbrain dopaminergic neurons., *Science.* 260 (1993)

- 1130–1132. doi:10.1126/science.8493557.
- [112] M.S. Airaksinen, M. Saarma, The GDNF family: Signalling, biological functions and therapeutic value, *Nat. Rev. Neurosci.* 3 (2002) 383–394. doi:10.1038/nrn812.
- [113] G. Paratcha, F. Ledda, GDNF and GFR α : a versatile molecular complex for developing neurons, *Trends Neurosci.* 31 (2008) 384–391. doi:10.1016/j.tins.2008.05.003.
- [114] E.D. Clarkson, W.M. Zawada, C.R. Freed, GDNF reduces apoptosis in dopaminergic neurons in vitro., *Neuroreport.* 7 (1995) 145–149. <http://www.ncbi.nlm.nih.gov/pubmed/8742438> (accessed August 12, 2019).
- [115] D.L. Choi-Lundberg, Q. Lin, Y.N. Chang, Y.L. Chiang, C.M. Hay, H. Mohajeri, B.L. Davidson, M.C. Bohn, Dopaminergic neurons protected from degeneration by GDNF gene therapy., *Science.* 275 (1997) 838–841. doi:10.1126/science.275.5301.838.
- [116] K.D. Beck, J. Valverde, T. Alexi, K. Poulsen, B. Moffat, R.A. Vandlen, A. Rosenthal, F. Hefti, Mesencephalic dopaminergic neurons protected by GDNF from axotomy-induced degeneration in the adult brain, *Nature.* 373 (1995) 339–341. doi:10.1038/373339a0.
- [117] C. Winkler, H. Sauer, C.S. Lee, A. Björklund, Short-term GDNF treatment provides long-term rescue of lesioned nigral dopaminergic neurons in a rat model of Parkinson's disease., *J. Neurosci.* 16 (1996) 7206–7215. doi:10.1523/JNEUROSCI.16-22-07206.1996.
- [118] C. Rosenblad, D. Kirik, B. Devaux, B. Moffat, H.S. Phillips, A. Björklund, Protection and regeneration of nigral dopaminergic neurons by neurturin or GDNF in a partial lesion model of Parkinson's disease after administration into the striatum or the lateral ventricle, *Eur. J. Neurosci.* 11 (1999) 1554–1566. doi:10.1046/j.1460-9568.1999.00566.x.
- [119] B.J. Hoffer, A. Hoffman, K. Bowenkamp, P. Huettl, J. Hudson, D. Martin, L.-F.H. Lin, G.A. Gerhardt, Glial cell line-derived neurotrophic factor reverses toxin-induced injury to midbrain dopaminergic neurons in vivo, *Neurosci. Lett.* 182 (1994) 107–111. doi:10.1016/0304-3940(94)90218-6.
- [120] H. Sawada, M. Ibi, T. Kihara, M. Urushitani, M. Nakanishi, A. Akaike, S. Shimohama, Neuroprotective mechanism of glial cell line-derived neurotrophic factor in mesencephalic neurons, *J. Neurochem.* 74 (2000) 1175–1184. doi:10.1046/j.1471-4159.2000.741175.x.
- [121] E.D. Clarkson, W.M. Zawada, C.R. Freed, GDNF improves survival and reduces apoptosis in human embryonic dopaminergic neurons in vitro, *Cell Tissue Res.* 289 (1997) 207–210. doi:10.1007/s004410050867.
- [122] B. Xing, T. Xin, L. Zhao, R.L. Hunter, Y. Chen, G. Bing, Glial cell line-derived neurotrophic factor protects midbrain dopaminergic neurons against lipopolysaccharide neurotoxicity, *J. Neuroimmunol.* 225 (2010) 43–51. doi:10.1016/J.JNEUROIM.2010.04.010.
- [123] D.B. Hoban, L. Howard, E. Dowd, GDNF-secreting mesenchymal stem cells provide localized neuroprotection in an inflammation-driven rat model of Parkinson's disease, *Neuroscience.* 303 (2015) 402–411. doi:10.1016/J.NEUROSCIENCE.2015.07.014.

- [124] L. -y. Yu, M. Saarma, U. Arumae, Death receptors and caspases but not mitochondria are activated in the GDNF- or BDNF-deprived dopaminergic neurons, *J. Neurosci.* 28 (2008) 7467–7475. doi:10.1523/JNEUROSCI.1877-08.2008.
- [125] J.H.K. S. Ramaswamy, K.E. Soderstrom, Neurotrophic factors for the treatment of Parkinson's disease, *Cytokine Growth Factor Rev.* 22 (2011) 157–165. doi:10.1016/J.CYTOGFR.2011.05.001.
- [126] J.G. Nutt, K.J. Burchiel, C.L. Comella, J. Jankovic, A.E. Lang, E.R. Laws, A.M. Lozano, R.D. Penn, R.K. Simpson, M. Stacy, G.F. Wooten, the I.G.S. ICV GDNF Study Group. Implanted intracerebroventricular. Glial cell line-derived neurotrophic factor, Randomized, double-blind trial of glial cell line-derived neurotrophic factor (GDNF) in PD., *Neurology.* 60 (2003) 69–73. doi:10.1212/wnl.60.1.69.
- [127] J.P. Golden, R.H. Baloh, P.T. Kotzbauer, P.A. Lampe, P.A. Osborne, J. Milbrandt, E.M. Johnson, Expression of neurturin, GDNF, and their receptors in the adult mouse CNS, *J. Comp. Neurol.* 398 (1998) 139–150. doi:10.1002/(SICI)1096-9861(19980817)398:1<139::AID-CNE9>3.0.CO;2-2.
- [128] S.S. Gill, N.K. Patel, G.R. Hotton, K. O'Sullivan, R. McCarter, M. Bunnage, D.J. Brooks, C.N. Svendsen, P. Heywood, Direct brain infusion of glial cell line-derived neurotrophic factor in Parkinson disease, *Nat. Med.* 9 (2003) 589–595. doi:10.1038/nm850.
- [129] N.K. Patel, N. Pavese, S. Javed, G.R. Hotton, D.J. Brooks, S.S. Gill, Benefits of putaminal GDNF infusion in Parkinson disease are maintained after GDNF cessation, *Neurology.* 81 (2013) 1176–1178. doi:10.1212/WNL.0b013e3182a55ea5.
- [130] J.T. Slevin, G.A. Gerhardt, C.D. Smith, D.M. Gash, R. Kryscio, B. Young, Improvement of bilateral motor functions in patients with Parkinson disease through the unilateral intraputamenal infusion of glial cell line—derived neurotrophic factor, *J. Neurosurg.* 102 (2005) 216–222. doi:10.3171/jns.2005.102.2.0216.
- [131] A.E. Lang, S. Gill, N.K. Patel, A. Lozano, J.G. Nutt, R. Penn, D.J. Brooks, G. Hotton, E. Moro, P. Heywood, M.A. Brodsky, K. Burchiel, P. Kelly, A. Dalvi, B. Scott, M. Stacy, D. Turner, V.G.F. Wooten, W.J. Elias, E.R. Laws, V. Dhawan, A.J. Stoessl, J. Matcham, R.J. Coffey, M. Traub, Randomized controlled trial of intraputamenal glial cell line-derived neurotrophic factor infusion in Parkinson disease, *Ann. Neurol.* 59 (2006) 459–466. doi:10.1002/ana.20737.
- [132] R.M. Richardson, A.P. Kells, K.H. Rosenbluth, E.A. Salegio, M.S. Fiandaca, P.S. Larson, P.A. Starr, A.J. Martin, R.R. Lonser, H.J. Federoff, J.R. Forsayeth, K.S. Bankiewicz, Interventional MRI-guided putaminal delivery of AAV2-GDNF for a planned clinical trial in Parkinson's disease., *Mol. Ther.* 19 (2011) 1048–1057. doi:10.1038/mt.2011.11.
- [133] J.G. Nutt, K.J. Burchiel, C.L. Comella, J. Jankovic, A.E. Lang, E.R. Laws, A.M. Lozano, R.D. Penn, R.K. Simpson, M. Stacy, G.F. Wooten, Randomized, double-blind trial of glial cell line-derived neurotrophic factor (GDNF) in PD, *Neurology.* 60 (2003) 69–73. doi:10.1212/WNL.60.1.69.
- [134] M. Luz, E. Mohr, H.C. Fibiger, GDNF-induced cerebellar toxicity: A brief review, *Neurotoxicology.* 52 (2016) 46–56. doi:10.1016/J.NEURO.2015.10.011.
- [135] S. Hernando, E. Herran, J. Figueiro-Silva, J.L. Pedraz, M. Igartua, E. Carro, R.M.

- Hernandez, Intranasal administration of TAT-conjugated lipid nanocarriers loading GDNF for Parkinson's Disease, *Mol. Neurobiol.* 55 (2018) 145–155. doi:10.1007/s12035-017-0728-7.
- [136] R. Huang, W. Ke, Y. Liu, D. Wu, L. Feng, C. Jiang, Y. Pei, Gene therapy using lactoferrin-modified nanoparticles in a rotenone-induced chronic Parkinson model, *J. Neurol. Sci.* 290 (2010) 123–130. doi:10.1016/J.JNS.2009.09.032.
- [137] R. Huang, H. Ma, Y. Guo, S. Liu, Y. Kuang, K. Shao, J. Li, Y. Liu, L. Han, S. Huang, S. An, L. Ye, J. Lou, C. Jiang, Angiopep-conjugated nanoparticles for targeted long-term gene therapy of Parkinson's Disease, *Pharm. Res.* 30 (2013) 2549–2559. doi:10.1007/s11095-013-1005-8.
- [138] E. Garbayo, C.N. Montero-Menei, E. Ansorena, J.L. Lanciego, M.S. Aymerich, M.J. Blanco-Prieto, Effective GDNF brain delivery using microspheres—A promising strategy for Parkinson's disease, *J. Control. Release.* 135 (2009) 119–126. doi:10.1016/J.JCONREL.2008.12.010.
- [139] K.J. Lampe, D.S. Kern, M.J. Mahoney, K.B. Bjugstad, The administration of BDNF and GDNF to the brain via PLGA microparticles patterned within a degradable PEG-based hydrogel: Protein distribution and the glial response, *J. Biomed. Mater. Res. Part A.* 96A (2011) 595–607. doi:10.1002/jbm.a.33011.
- [140] C. Jollivet, A. Aubert-Pouessel, A. Clavreul, M.-C. Venier-Julienne, S. Remy, C.N. Montero-Menei, J.-P. Benoit, P. Menei, Striatal implantation of GDNF releasing biodegradable microspheres promotes recovery of motor function in a partial model of Parkinson's disease, *Biomaterials.* 25 (2004) 933–942. doi:10.1016/S0142-9612(03)00601-X.
- [141] E. Garbayo, E. Ansorena, H. Lana, M. del M. Carmona-Abellan, I. Marcilla, J.L. Lanciego, M.R. Luquin, M.J. Blanco-Prieto, Brain delivery of microencapsulated GDNF induces functional and structural recovery in parkinsonian monkeys, *Biomaterials.* 110 (2016) 11–23. doi:10.1016/J.BIOMATERIALS.2016.09.015.
- [142] D. Fon, A. Al-Aboodi, P.P.Y. Chan, K. Zhou, P. Crack, D.I. Finkelstein, J.S. Forsythe, Effects of GDNF-loaded injectable gelatin-based hydrogels on endogenous neural progenitor cell migration, *Adv. Healthc. Mater.* 3 (2014) 761–774. doi:10.1002/adhm.201300287.
- [143] T.C. Moloney, M. Ní Fhlathartaigh, M. Kulkarni, A. Pandit, E. Dowd, Fibrin as a scaffold for delivery of GDNF overexpressing stem cells to the adult rat brain, *ACS Biomater. Sci. Eng.* 1 (2015) 559–566. doi:10.1021/acsbiomaterials.5b00049.
- [144] M. Aalberts, F.M.. van Dissel-Emiliani, N.P.. van Adrichem, M. van Wijnen, M.H.. Wauben, T.A.. Stout, W. Stoorvogel, Identification of Distinct Populations of Prostatomes That Differentially Express Prostate Stem Cell Antigen, Annexin A1, and GLIPR2 in Humans1, *Biol. Reprod.* 86 (2012) 82. doi:10.1095/biolreprod.111.095760.
- [145] N. Moriarty, A. Pandit, E. Dowd, Encapsulation of primary dopaminergic neurons in a GDNF-loaded collagen hydrogel increases their survival, re-innervation and function after intra-striatal transplantation, *Sci. Rep.* 7 (2017) 16033. doi:10.1038/s41598-017-15970-w.
- [146] Y. Horita, O. Honmou, K. Harada, K. Houkin, H. Hamada, J.D. Kocsis, Intravenous administration of glial cell line-derived neurotrophic factor gene-modified human

- mesenchymal stem cells protects against injury in a cerebral ischemia model in the adult rat, *J. Neurosci. Res.* 84 (2006) 1495–1504. doi:10.1002/jnr.21056.
- [147] M. Kameda, T. Shingo, K. Takahashi, K. Muraoka, K. Kurozumi, T. Yasuhara, T. Maruo, T. Tsuboi, T. Uozumi, T. Matsui, Y. Miyoshi, H. Hamada, I. Date, Adult neural stem and progenitor cells modified to secrete GDNF can protect, migrate and integrate after intracerebral transplantation in rats with transient forebrain ischemia, *Eur. J. Neurosci.* 26 (2007) 1462–1478. doi:10.1111/j.1460-9568.2007.05776.x.
- [148] E. Herrán, J.Á. Ruiz-Ortega, A. Aristieta, M. Igartua, C. Requejo, J.V. Lafuente, L. Ugedo, J.L. Pedraz, R.M. Hernández, In vivo administration of VEGF- and GDNF-releasing biodegradable polymeric microspheres in a severe lesion model of Parkinson's disease, *Eur. J. Pharm. Biopharm.* 85 (2013) 1183–1190. doi:10.1016/J.EJPB.2013.03.034.
- [149] T.-Y. Wang, J.S. Forsythe, D.R. Nisbet, C.L. Parish, Promoting engraftment of transplanted neural stem cells/progenitors using biofunctionalised electrospun scaffolds, *Biomaterials.* 33 (2012) 9188–9197. doi:10.1016/J.BIOMATERIALS.2012.09.013.
- [150] D.B. Hoban, B. Newland, T.C. Moloney, L. Howard, A. Pandit, E. Dowd, The reduction in immunogenicity of neurotrophin overexpressing stem cells after intrastriatal transplantation by encapsulation in an in situ gelling collagen hydrogel, *Biomaterials.* 34 (2013) 9420–9429. doi:10.1016/J.BIOMATERIALS.2013.08.073.
- [151] T.-Y. Wang, K.F. Bruggeman, J.A. Kauhausen, A.L. Rodriguez, D.R. Nisbet, C.L. Parish, Functionalized composite scaffolds improve the engraftment of transplanted dopaminergic progenitors in a mouse model of Parkinson's disease, *Biomaterials.* 74 (2016) 89–98. doi:10.1016/J.BIOMATERIALS.2015.09.039.
- [152] N. Moriarty, S. Cabré, V. Alamilla, A. Pandit, E. Dowd, Encapsulation of young donor age dopaminergic grafts in a GDNF-loaded collagen hydrogel further increases their survival, reinnervation, and functional efficacy after intrastriatal transplantation in hemi-Parkinsonian rats, *Eur. J. Neurosci.* 49 (2019) 487–496. doi:10.1111/ejn.14090.
- [153] D. Fon, K. Zhou, F. Ercole, F. Fehr, S. Marchesan, M.R. Minter, P.J. Crack, D.I. Finkelstein, J.S. Forsythe, Nanofibrous scaffolds releasing a small molecule BDNF-mimetic for the re-direction of endogenous neuroblast migration in the brain, *Biomaterials.* 35 (2014) 2692–2712. doi:10.1016/j.biomaterials.2013.12.016.
- [154] C. Huang, L. Zhao, J. Gu, D. Nie, Y. Chen, H. Zuo, W. Huan, J. Shi, J. Chen, W. Shi, The migration and differentiation of hUC-MSCs (CXCR4/GFP) encapsulated in BDNF/chitosan scaffolds for brain tissue engineering, *Biomed. Mater.* 11 (2016) 035004. doi:10.1088/1748-6041/11/3/035004.
- [155] R.W. Sirianni, P. Olausson, A.S. Chiu, J.R. Taylor, W.M. Saltzman, The behavioral and biochemical effects of BDNF containing polymers implanted in the hippocampus of rats, *Brain Res.* 1321 (2010) 40–50. doi:10.1016/J.BRAINRES.2010.01.041.
- [156] Y. Xing, C.-Y. Wen, S.-T. Li, Z.-X. Xia, Non-viral liposome-mediated transfer of brain-derived neurotrophic factor across the blood-brain barrier., *Neural Regen. Res.* 11 (2016) 617–22. doi:10.4103/1673-5374.180747.
- [157] D.J. Cook, C. Nguyen, H.N. Chun, I. L Llorente, A.S. Chiu, M. Machnicki, T.I. Zarebinski, S.T. Carmichael, Hydrogel-delivered brain-derived neurotrophic factor

- promotes tissue repair and recovery after stroke, *J. Cereb. Blood Flow Metab.* 37 (2017) 1030–1045. doi:10.1177/0271678X16649964.
- [158] S. Koennings, A. Sapin, T. Blunk, P. Menei, A. Goepferich, Towards controlled release of BDNF — Manufacturing strategies for protein-loaded lipid implants and biocompatibility evaluation in the brain, *J. Control. Release.* 119 (2007) 163–172. doi:10.1016/J.JCONREL.2007.02.005.
- [159] J. Guan, W. Tong, W. Ding, S. Du, Z. Xiao, Q. Han, Z. Zhu, X. Bao, X. Shi, C. Wu, J. Cao, Y. Yang, W. Ma, G. Li, Y. Yao, J. Gao, J. Wei, J. Dai, R. Wang, Neuronal regeneration and protection by collagen-binding BDNF in the rat middle cerebral artery occlusion model, *Biomaterials.* 33 (2012) 1386–1395. doi:10.1016/J.BIOMATERIALS.2011.10.073.
- [160] D. Yuan, Y. Zhao, W.A. Banks, K.M. Bullock, M. Haney, E. Batrakova, A. V. Kabanov, Macrophage exosomes as natural nanocarriers for protein delivery to inflamed brain, *Biomaterials.* 142 (2017) 1–12. doi:10.1016/J.BIOMATERIALS.2017.07.011.
- [161] B. Song, J. Song, S. Zhang, M.A. Anderson, Y. Ao, C.-Y. Yang, T.J. Deming, M. V. Sofroniew, Sustained local delivery of bioactive nerve growth factor in the central nervous system via tunable diblock copolypeptide hydrogel depots, *Biomaterials.* 33 (2012) 9105–9116. doi:10.1016/J.BIOMATERIALS.2012.08.060.
- [162] J. Samal, D.B. Hoban, C. Naughton, R. Concannon, E. Dowd, A. Pandit, Fibrin-based microsphere reservoirs for delivery of neurotrophic factors to the brain, *Nanomedicine.* 10 (2015) 765–783. doi:10.2217/nmm.14.221.
- [163] J.-M. Péan, P. Menei, O. Morel, C.N. Montero-Menei, J.-P. Benoit, Intraseptal implantation of NGF-releasing microspheres promote the survival of axotomized cholinergic neurons, *Biomaterials.* 21 (2000) 2097–2101. doi:10.1016/S0142-9612(00)00141-1.
- [164] L. Longhi, D.J. Watson, K.E. Saatman, H.J. Thompson, C. Zhang, S. Fujimoto, N. Royo, D. Castelbuono, R. Raghupathi, J.Q. Trojanowski, V.M.-Y. Lee, J.H. Wolfe, N. Stocchetti, T.K. McIntosh, *Ex Vivo* Gene Therapy Using Targeted Engraftment of NGF-Expressing Human NT2N Neurons Attenuates Cognitive Deficits Following Traumatic Brain Injury in Mice, *J. Neurotrauma.* 21 (2004) 1723–1736. doi:10.1089/neu.2004.21.1723.
- [165] P. Menei, J.M. Pean, V. Nerrière-Daguin, C. Jollivet, P. Brachet, J.P. Benoit, Intracerebral implantation of NGF-releasing biodegradable microspheres protects striatum against excitotoxic damage, *Exp. Neurol.* 161 (2000) 259–272. doi:10.1006/exnr.1999.7253.
- [166] L. Fjord-Larsen, P. Kusk, M. Torp, J. Christian, H. Sørensen, K. Etrup, C.R. Bjarkam, J. Törnøe, B. Juliusson, L.U. Wahlberg, Encapsulated cell biodelivery of transposon-mediated high-dose NGF to the göttingen mini pig basal forebrain, *Open Tissue Eng. Regen. Med. J.* 5 (2012) 35–42. doi:10.2174/1875043501205010035.
- [167] L. Mo, Z. Yang, A. Zhang, X. Li, The repair of the injured adult rat hippocampus with NT-3-chitosan carriers, *Biomaterials.* 31 (2010) 2184–2192. doi:10.1016/J.BIOMATERIALS.2009.11.078.
- [168] C.-Y. Chung, J.-T. Yang, Y.-C. Kuo, Polybutylcyanoacrylate nanoparticles for

- delivering hormone response element-conjugated neurotrophin-3 to the brain of intracerebral hemorrhagic rats, *Biomaterials*. 34 (2013) 9717–9727. doi:10.1016/J.BIOMATERIALS.2013.08.083.
- [169] I. Mendez, R. Sanchez-Pernaute, O. Cooper, A. Viñuela, D. Ferrari, L. Björklund, A. Dagher, O. Isacson, Cell type analysis of functional fetal dopamine cell suspension transplants in the striatum and substantia nigra of patients with Parkinson's disease, *Brain*. 128 (2005) 1498–1510. doi:10.1093/brain/awh510.
- [170] Y. Ma, S. Peng, V. Dhawan, D. Eidelberg, Dopamine cell transplantation in Parkinson's disease: challenge and perspective, *Br. Med. Bull.* 100 (2011) 173–189. doi:10.1093/bmb/ldr040.
- [171] M. Dezawa, H. Kanno, M. Hoshino, H. Cho, N. Matsumoto, Y. Itokazu, N. Tajima, H. Yamada, H. Sawada, H. Ishikawa, T. Mimura, M. Kitada, Y. Suzuki, C. Ide, Specific induction of neuronal cells from bone marrow stromal cells and application for autologous transplantation, *J. Clin. Invest.* 113 (2004) 1701–1710. doi:10.1172/JCI20935.
- [172] Y. Kuroda, S. Wakao, M. Kitada, T. Murakami, M. Nojima, M. Dezawa, Isolation, culture and evaluation of multilineage-differentiating stress-enduring (Muse) cells, *Nat. Protoc.* 8 (2013) 1391–1415. doi:10.1038/nprot.2013.076.
- [173] L. Danielyan, S. Beer-Hammer, A. Stolzing, R. Schäfer, G. Siegel, C. Fabian, P. Kahle, T. Biedermann, A. Lourhmati, M. Buadze, A. Novakovic, B. Proksch, C.H. Gleiter, W.H. Frey, M. Schwab, Intranasal delivery of bone marrow-derived mesenchymal stem cells, macrophages, and microglia to the brain in mouse models of Alzheimer's and Parkinson's disease, *Cell Transplant.* 23 (2014) 123–139. doi:10.3727/096368914X684970.
- [174] M. Salama, M. Sobh, M. Emam, A. Abdalla, D. Sabry, M. El-Gamal, A. Lotfy, M. El-Husseiny, M. Sobh, A. Shalash, W.M. Mohamed, Effect of intranasal stem cell administration on the nigrostriatal system in a mouse model of Parkinson's disease, *Exp. Ther. Med.* 13 (2017) 976–982. doi:10.3892/etm.2017.4073.
- [175] H. Kawasaki, K. Mizuseki, S. Nishikawa, S. Kaneko, Y. Kuwana, S. Nakanishi, S.I. Nishikawa, Y. Sasai, Induction of midbrain dopaminergic neurons from ES cells by stromal cell-derived inducing activity., *Neuron*. 28 (2000) 31–40. <http://www.ncbi.nlm.nih.gov/pubmed/11086981> (accessed August 20, 2019).
- [176] Y. Takagi, J. Takahashi, H. Saiki, A. Morizane, T. Hayashi, Y. Kishi, H. Fukuda, Y. Okamoto, M. Koyanagi, M. Ideguchi, H. Hayashi, T. Imazato, H. Kawasaki, H. Suemori, S. Omachi, H. Iida, N. Itoh, N. Nakatsuji, Y. Sasai, N. Hashimoto, Dopaminergic neurons generated from monkey embryonic stem cells function in a Parkinson primate model, *J. Clin. Invest.* 115 (2005) 102–109. doi:10.1172/JCI21137.
- [177] D. Doi, A. Morizane, T. Kikuchi, H. Onoe, T. Hayashi, T. Kawasaki, M. Moton, Y. Sasai, H. Saiki, M. Gomi, T. Yoshikawa, H. Hayashi, M. Shinoyama, M.M. Refaat, H. Suemori, S. Miyamoto, J. Takahashi, Prolonged Maturation Culture Favors a Reduction in the Tumorigenicity and the Dopaminergic Function of Human ESC-Derived Neural Cells in a Primate Model of Parkinson's Disease, *Stem Cells*. 30 (2012) 935–945. doi:10.1002/stem.1060.
- [178] S.-H. Lee, N. Lumelsky, L. Studer, J.M. Auerbach, R.D. McKay, Efficient generation

- of midbrain and hindbrain neurons from mouse embryonic stem cells, *Nat. Biotechnol.* 18 (2000) 675–679. doi:10.1038/76536.
- [179] B. Samata, D. Doi, K. Nishimura, T. Kikuchi, A. Watanabe, Y. Sakamoto, J. Kakuta, Y. Ono, J. Takahashi, Purification of functional human ES and iPSC-derived midbrain dopaminergic progenitors using LRTM1, *Nat. Commun.* 7 (2016) 13097. doi:10.1038/ncomms13097.
- [180] F. Zuo, F. Xiong, X. Wang, X. Li, R. Wang, W. Ge, X. Bao, Intraatrial Transplantation of Human Neural Stem Cells Restores the Impaired Subventricular Zone in Parkinsonian Mice, *Stem Cells.* 35 (2017) 1519–1531. doi:10.1002/stem.2616.
- [181] Y. Yao, C. Huang, P. Gu, T. Wen, Combined MSC-Secreted Factors and Neural Stem Cell Transplantation Promote Functional Recovery of PD Rats, *Cell Transplant.* 25 (2016) 1101–1113. doi:10.3727/096368915X689938.
- [182] L. Lige, T. Zengmin, Transplantation of neural precursor cells in the treatment for parkinson disease: an efficacy and safety analysis, *Turk. Neurosurg.* 26 (2015) 378–83. doi:10.5137/1019-5149.JTN.10747-14.4.
- [183] K. Takahashi, S. Yamanaka, Induction of Pluripotent Stem Cells from Mouse Embryonic and Adult Fibroblast Cultures by Defined Factors, *Cell.* 126 (2006) 663–676. doi:10.1016/j.cell.2006.07.024.
- [184] K. Takahashi, K. Tanabe, M. Ohnuki, M. Narita, T. Ichisaka, K. Tomoda, S. Yamanaka, Induction of Pluripotent Stem Cells from Adult Human Fibroblasts by Defined Factors, *Cell.* 131 (2007) 861–872. doi:10.1016/j.cell.2007.11.019.
- [185] R.A. Barker, M. Parmar, A. Kirkeby, A. Björklund, L. Thompson, P. Brundin, Are stem cell-based therapies for Parkinson’s Disease ready for the clinic in 2016?, *J. Parkinsons. Dis.* 6 (2016) 57–63. doi:10.3233/JPD-160798.
- [186] M.J. Devine, M. Ryten, P. Vodicka, A.J. Thomson, T. Burdon, H. Houlden, F. Cavaleri, M. Nagano, N.J. Drummond, J.-W. Taanman, A.H. Schapira, K. Gwinn, J. Hardy, P.A. Lewis, T. Kunath, Parkinson’s disease induced pluripotent stem cells with triplication of the α -synuclein locus, *Nat. Commun.* 2 (2011) 440. doi:10.1038/ncomms1453.
- [187] N. Xia, P. Zhang, F. Fang, Z. Wang, M. Rothstein, B. Angulo, R. Chiang, J. Taylor, R.A. Reijo Pera, Transcriptional comparison of human induced and primary midbrain dopaminergic neurons, *Sci. Rep.* 6 (2016) 20270. doi:10.1038/srep20270.
- [188] T. Kikuchi, A. Morizane, D. Doi, H. Magotani, H. Onoe, T. Hayashi, H. Mizuma, S. Takara, R. Takahashi, H. Inoue, S. Morita, M. Yamamoto, K. Okita, M. Nakagawa, M. Parmar, J. Takahashi, Human iPSC cell-derived dopaminergic neurons function in a primate Parkinson’s disease model, *Nature.* 548 (2017) 592–596. doi:10.1038/nature23664.
- [189] P. Hagell, P. Brundin, Cell survival and clinical outcome following intraatrial transplantation in Parkinson Disease, *J. Neuropathol. Exp. Neurol.* 60 (2001) 741–752. doi:10.1093/jnen/60.8.741.
- [190] P. Brundin, J. Karlsson, M. Emgård, G.S.K. Schierle, O. Hansson, Å. Petersén, R.F. Castilho, Improving the survival of grafted dopaminergic neurons: a review over current approaches, *Cell Transplant.* 9 (2000) 179–195.

- doi:10.1177/096368970000900205.
- [191] P.J. Reddig, R.L. Juliano, Clinging to life: cell to matrix adhesion and cell survival, *Cancer Metastasis Rev.* 24 (2005) 425–439. doi:10.1007/s10555-005-5134-3.
- [192] T.J. Collier, C.E. Sortwell, Therapeutic potential of nerve growth factors in Parkinson's Disease, *Drugs Aging.* 14 (1999) 261–287. doi:10.2165/00002512-199914040-00003.
- [193] C.E. Sortwell, B.F. Daley, M.R. Pitzer, S.O. McGuire, J.R. Sladek Jr., T.J. Collier, Oligodendrocyte-type 2 astrocyte-derived trophic factors increase survival of developing dopamine neurons through the inhibition of apoptotic cell death, *J. Comp. Neurol.* 426 (2000) 143–153. doi:10.1002/1096-9861(20001009)426:1<143::AID-CNE10>3.0.CO;2-8.
- [194] W.M. Zawada, M.K. Meintzer, P. Rao, J. Marotti, X. Wang, J.E. Esplen, E.D. Clarkson, C.R. Freed, K.A. Heidenreich, Inhibitors of p38 MAP kinase increase the survival of transplanted dopamine neurons., *Brain Res.* 891 (2001) 185–96. doi:10.1016/s0006-8993(00)02965-6.
- [195] T.J. Collier, Z. Dung Ling, P.M. Carvey, A. Fletcher-Turner, D.M. Yurek, J.R. Sladek, J.H. Kordower, Striatal trophic factor activity in aging monkeys with unilateral MPTP-induced parkinsonism, *Exp. Neurol.* 191 (2005) S60–S67. doi:10.1016/J.EXPNEUROL.2004.08.018.
- [196] S.O. McGuire, Z.D. Ling, J.W. Lipton, C.E. Sortwell, T.J. Collier, P.M. Carvey, Tumor Necrosis Factor α is toxic to embryonic mesencephalic dopamine neurons, *Exp. Neurol.* 169 (2001) 219–230. doi:10.1006/exnr.2001.7688.
- [197] M. Emgård, J. Karlsson, O. Hansson, P. Brundin, Patterns of cell death and dopaminergic neuron survival in intrastriatal nigral grafts, *Exp. Neurol.* 160 (1999) 279–288. doi:10.1006/exnr.1999.7198.
- [198] J.H. Kordower, Y.-T. Liu, S. Winn, D.F. Emerich, Encapsulated PC12 cell transplants into hemiparkinsonian monkeys: A behavioral, neuroanatomical, and neurochemical analysis, *Cell Transplant.* 4 (1995) 155–171. doi:10.1016/0963-6897(95)90031-4.
- [199] C.W. Olanow, C.G. Goetz, J.H. Kordower, A.J. Stoessl, V. Sossi, M.F. Brin, K.M. Shannon, G.M. Nauert, D.P. Perl, J. Godbold, T.B. Freeman, A double-blind controlled trial of bilateral fetal nigral transplantation in Parkinson's disease, *Ann. Neurol.* 54 (2003) 403–414. doi:10.1002/ana.10720.
- [200] Z. Kefalopoulou, M. Politis, P. Piccini, N. Mencacci, K. Bhatia, M. Jahanshahi, H. Widner, S. Rehncrona, P. Brundin, A. Björklund, O. Lindvall, P. Limousin, N. Quinn, T. Foltynie, Long-term clinical outcome of fetal cell transplantation for Parkinson disease: two case reports., *JAMA Neurol.* 71 (2014) 83–87. doi:10.1001/jamaneurol.2013.4749.
- [201] G. Orive, E. Anitua, J.L. Pedraz, D.F. Emerich, Biomaterials for promoting brain protection, repair and regeneration, *Nat. Rev. Neurosci.* 10 (2009) 682–692. doi:10.1038/nrn2685.
- [202] T. Wang, J. Forsythe, C. Parish, D. Nisbet, Biofunctionalisation of polymeric scaffolds for neural tissue engineering, *J. Biomater. Appl.* 27 (2012) 369–390. doi:10.1177/0885328212443297.

- [203] M.M. Adil, T. Vazin, B. Ananthanarayanan, G.M.C. Rodrigues, A.T. Rao, R.U. Kulkarni, E.W. Miller, S. Kumar, D. V. Schaffer, Engineered hydrogels increase the post-transplantation survival of encapsulated hESC-derived midbrain dopaminergic neurons, *Biomaterials*. 136 (2017) 1–11. doi:10.1016/J.BIOMATERIALS.2017.05.008.
- [204] N. Moriarty, A. Pandit, E. Dowd, Encapsulation of primary dopaminergic neurons in a GDNF-loaded collagen hydrogel increases their survival, re-innervation and function after intra-striatal transplantation, *Sci. Rep.* 7 (2017) 16033. doi:10.1038/s41598-017-15970-w.
- [205] U. Freudenberg, A. Hermann, P.B. Welzel, K. Stirl, S.C. Schwarz, M. Grimmer, A. Zieris, W. Panyanuwat, S. Zschoche, D. Meinhold, A. Storch, C. Werner, A star-PEG–heparin hydrogel platform to aid cell replacement therapies for neurodegenerative diseases, *Biomaterials*. 30 (2009) 5049–5060. doi:10.1016/J.BIOMATERIALS.2009.06.002.
- [206] G.J.-R. Delcroix, E. Garbayo, L. Sindji, O. Thomas, C. Vanpouille-Box, P.C. Schiller, C.N. Montero-Menei, The therapeutic potential of human multipotent mesenchymal stromal cells combined with pharmacologically active microcarriers transplanted in hemi-parkinsonian rats, *Biomaterials*. 32 (2011) 1560–1573. doi:10.1016/J.BIOMATERIALS.2010.10.041.
- [207] M. Ming, X. Li, X. Fan, D. Yang, L. Li, S. Chen, Q. Gu, W. Le, Retinal pigment epithelial cells secrete neurotrophic factors and synthesize dopamine: possible contribution to therapeutic effects of RPE cell transplantation in Parkinson’s disease, *J. Transl. Med.* 7 (2009) 53. doi:10.1186/1479-5876-7-53.
- [208] R. Huang, H. Ma, Y. Guo, S. Liu, Y. Kuang, K. Shao, J. Li, Y. Liu, L. Han, S. Huang, S. An, L. Ye, J. Lou, C. Jiang, Angiopep-Conjugated Nanoparticles for Targeted Long-Term Gene Therapy of Parkinson’s Disease, *Pharm. Res.* 30 (2013) 2549–2559. doi:10.1007/s11095-013-1005-8.
- [209] V.M. Tatard, L. Sindji, J. (Godbee) Branton, A. Aubert-Pouëssel, J. Colleau, J.-P. Benoit, C.N. Montero-Menei, Pharmacologically active microcarriers releasing glial cell line – derived neurotrophic factor: Survival and differentiation of embryonic dopaminergic neurons after grafting in hemiparkinsonian rats, *Biomaterials*. 28 (2007) 1978–1988. doi:10.1016/J.BIOMATERIALS.2006.12.021.
- [210] L. Grandoso, S. Ponce, I. Manuel, A. Arrúe, J.A. Ruiz-Ortega, I. Ulibarri, G. Orive, R.M. Hernández, A. Rodríguez, R. Rodríguez-Puertas, M. Zumárraga, G. Linazasoro, J.L. Pedraz, L. Ugedo, Long-term survival of encapsulated GDNF secreting cells implanted within the striatum of parkinsonized rats, *Int. J. Pharm.* 343 (2007) 69–78. doi:10.1016/J.IJPHARM.2007.05.027.
- [211] V.A. Kornev, E.A. Grebenik, A.B. Solovieva, R.I. Dmitriev, P.S. Timashev, Hydrogel-assisted neuroregeneration approaches towards brain injury therapy: A state-of-the-art review., *Comput. Struct. Biotechnol. J.* 16 (2018) 488–502. doi:10.1016/j.csbj.2018.10.011.
- [212] J.A. Burdick, R.L. Mauck, S. Gerecht, To serve and protect: hydrogels to improve stem cell-based therapies, *Cell Stem Cell*. 18 (2016) 13–15. doi:10.1016/j.stem.2015.12.004.

- [213] T. Shingo, I. Date, H. Yoshida, T. Ohmoto, Neuroprotective and restorative effects of intrastriatal grafting of encapsulated GDNF-producing cells in a rat model of Parkinson's disease, *J. Neurosci. Res.* 69 (2002) 946–954. doi:10.1002/jnr.10375.
- [214] P.A. Tresco, S.R. Winn, S. Tan, C.B. Jaeger, L.A. Greene, P. Aebischer, Polymer-Encapsulated PC12 Cells: Long-Term Survival and Associated Reduction in Lesion-Induced Rotational Behavior, *Cell Transplant.* 1 (1992) 255–264. doi:10.1177/0963689792001002-307.
- [215] D.B. Hoban, B. Newland, T.C. Moloney, L. Howard, A. Pandit, E. Dowd, The reduction in immunogenicity of neurotrophin overexpressing stem cells after intrastriatal transplantation by encapsulation in an in situ gelling collagen hydrogel, *Biomaterials.* 34 (2013) 9420–9429. doi:10.1016/J.BIOMATERIALS.2013.08.073.
- [216] M.J. Haney, N.L. Klyachko, Y. Zhao, R. Gupta, E.G. Plotnikova, Z. He, T. Patel, A. Piroyan, M. Sokolsky, A. V. Kabanov, E. V. Batrakova, Exosomes as drug delivery vehicles for Parkinson's disease therapy, *J. Control. Release.* 207 (2015) 18–30. doi:10.1016/j.jconrel.2015.03.033.
- [217] T.-Y. Wang, K.F. Bruggeman, J.A. Kauhausen, A.L. Rodriguez, D.R. Nisbet, C.L. Parish, Functionalized composite scaffolds improve the engraftment of transplanted dopaminergic progenitors in a mouse model of Parkinson's disease, *Biomaterials.* 74 (2016) 89–98. doi:10.1016/J.BIOMATERIALS.2015.09.039.
- [218] C.-F. Xia, R.J. Boado, Y. Zhang, C. Chu, W.M. Pardridge, Intravenous glial-derived neurotrophic factor gene therapy of experimental Parkinson's disease with Trojan horse liposomes and a tyrosine hydroxylase promoter, *J. Gene Med.* 10 (2008) 306–315. doi:10.1002/jgm.1152.
- [219] N. Moriarty, S. Cabré, V. Alamilla, A. Pandit, E. Dowd, Encapsulation of young donor age dopaminergic grafts in a GDNF-loaded collagen hydrogel further increases their survival, reinnervation, and functional efficacy after intrastriatal transplantation in hemi-Parkinsonian rats, *Eur. J. Neurosci.* 49 (2019) 487–496. doi:10.1111/ejn.14090.
- [220] N. Moriarty, A. Pandit, E. Dowd, Encapsulation of primary dopaminergic neurons in a GDNF-loaded collagen hydrogel increases their survival, re-innervation and function after intra-striatal transplantation, *Sci. Rep.* 7 (2017) 16033. doi:10.1038/s41598-017-15970-w.
- [221] M.M. Adil, G.M.C. Rodrigues, R.U. Kulkarni, A.T. Rao, N.E. Chernavsky, E.W. Miller, D. V. Schaffer, Efficient generation of hPSC-derived midbrain dopaminergic neurons in a fully defined, scalable, 3D biomaterial platform, *Sci. Rep.* 7 (2017) 40573. doi:10.1038/srep40573.
- [222] P. Aebischer, S.R. Winn, P.A. Tresco, C.B. Jaeger, L.A. Greene, Transplantation of polymer encapsulated neurotransmitter secreting cells: effect of the encapsulation technique, *J. Biomech. Eng.* 113 (1991) 178–183. doi:10.1115/1.2891231.
- [223] M.M. Pakulska, B.G. Ballios, M.S. Shoichet, Injectable hydrogels for central nervous system therapy, *Biomed. Mater.* 7 (2012) 024101. doi:10.1088/1748-6041/7/2/024101.
- [224] P. Zhuang, A.X. Sun, J. An, C.K. Chua, S.Y. Chew, 3D neural tissue models: From spheroids to bioprinting, *Biomaterials.* 154 (2018) 113–133. doi:10.1016/j.biomaterials.2017.10.002.

- [225] O.A. Carballo-Molina, I. Velasco, Hydrogels as scaffolds and delivery systems to enhance axonal regeneration after injuries., *Front. Cell. Neurosci.* 9 (2015) 13. doi:10.3389/fncel.2015.00013.
- [226] X. Li, E. Katsanevakis, X. Liu, N. Zhang, X. Wen, Engineering neural stem cell fates with hydrogel design for central nervous system regeneration, *Prog. Polym. Sci.* 37 (2012) 1105–1129. doi:10.1016/J.PROGPOLYMSCI.2012.02.004.
- [227] M.P. Lutolf, J.A. Hubbell, Synthetic biomaterials as instructive extracellular microenvironments for morphogenesis in tissue engineering, *Nat. Biotechnol.* 23 (2005) 47–55. doi:10.1038/nbt1055.
- [228] L.M. Delgado, Y. Bayon, A. Pandit, D.I. Zeugolis, To cross-link or not to cross-link? Cross-linking associated foreign body response of collagen-based devices., *Tissue Eng. Part B. Rev.* 21 (2015) 298–313. doi:10.1089/ten.TEB.2014.0290.
- [229] S. Lee, X. Tong, F. Yang, The effects of varying poly(ethylene glycol) hydrogel crosslinking density and the crosslinking mechanism on protein accumulation in three-dimensional hydrogels, *Acta Biomater.* 10 (2014) 4167–4174. doi:10.1016/j.actbio.2014.05.023.
- [230] U. Hersel, C. Dahmen, H. Kessler, RGD modified polymers: biomaterials for stimulated cell adhesion and beyond., *Biomaterials.* 24 (2003) 4385–4415. doi:10.1016/s0142-9612(03)00343-0.
- [231] K.F. Bruggeman, A.L. Rodriguez, C.L. Parish, R.J. Williams, D.R. Nisbet, Temporally controlled release of multiple growth factors from a self-assembling peptide hydrogel, *Nanotechnology.* 27 (2016) 385102. doi:10.1088/0957-4484/27/38/385102.
- [232] Z.Z. Khaing, C.E. Schmidt, Advances in natural biomaterials for nerve tissue repair, *Neurosci. Lett.* 519 (2012) 103–114. doi:10.1016/J.NEULET.2012.02.027.
- [233] H. Itosaka, S. Kuroda, H. Shichinohe, H. Yasuda, S. Yano, S. Kamei, R. Kawamura, K. Hida, Y. Iwasaki, Fibrin matrix provides a suitable scaffold for bone marrow stromal cells transplanted into injured spinal cord: A novel material for CNS tissue engineering, *Neuropathology.* 29 (2009) 248–257. doi:10.1111/j.1440-1789.2008.00971.x.
- [234] E. Cholewinski, M. Dietrich, T.C. Flanagan, T. Schmitz-Rode, S. Jockenhoevel, Tranexamic acid—An alternative to aprotinin in fibrin-based cardiovascular tissue engineering, *Tissue Eng. Part A.* 15 (2009) 3645–3653. doi:10.1089/ten.tea.2009.0235.
- [235] A. Sahni, C.W. Francis, Vascular endothelial growth factor binds to fibrinogen and fibrin and stimulates endothelial cell proliferation., *Blood.* 96 (2000) 3772–8. <http://www.ncbi.nlm.nih.gov/pubmed/11090059> (accessed August 20, 2019).
- [236] I. Catelas, J.F. Dwyer, S. Helgersson, Controlled release of bioactive transforming growth factor Beta-1 from fibrin gels in vitro, *Tissue Eng. Part C Methods.* 14 (2008) 119–128. doi:10.1089/ten.tec.2007.0262.
- [237] A. Sahni, T. Odriljin, C.W. Francis, Binding of basic fibroblast growth factor to fibrinogen and fibrin, *J. Biol. Chem.* 273 (1998) 7554–7559. doi:10.1074/jbc.273.13.7554.
- [238] P.G. Campbell, S.K. Durham, J.D. Hayes, A. Suwanichkul, D.R. Powell, Insulin-like growth factor-binding protein-3 binds fibrinogen and fibrin, *J. Biol. Chem.* 274 (1999)

- 30215–30221. doi:10.1074/jbc.274.42.30215.
- [239] S.M. Willerth, T.E. Fixel, D.I. Gottlieb, S.E. Sakiyama-Elbert, The effects of soluble growth factors on embryonic stem cell differentiation inside of fibrin scaffolds., *Stem Cells*. 25 (2007) 2235–2244. doi:10.1634/stemcells.2007-0111.
- [240] A.J. Man, H.E. Davis, A. Itoh, J.K. Leach, P. Bannerman, Neurite outgrowth in fibrin gels is regulated by substrate stiffness, *Tissue Eng. Part A*. 17 (2011) 2931–2942. doi:10.1089/ten.tea.2011.0030.
- [241] S. Anai, T. Hide, T. Takezaki, J. Kuroda, N. Shinojima, K. Makino, H. Nakamura, S. Yano, J. Kuratsu, Antitumor effect of fibrin glue containing temozolomide against malignant glioma, *Cancer Sci*. 105 (2014) 583–591. doi:10.1111/cas.12397.
- [242] X. Wang, Q. Zhang, L. Lv, J. Fu, Y. Jiang, H. Xin, Q. Yao, Glioma and microenvironment dual targeted nanocarrier for improved antiglioblastoma efficacy, *Drug Deliv*. 24 (2017) 1401–1409. doi:10.1080/10717544.2017.1378940.
- [243] J. Samal, D.B. Hoban, C. Naughton, R. Concannon, E. Dowd, A. Pandit, Fibrin-based microsphere reservoirs for delivery of neurotrophic factors to the brain, *Nanomedicine*. 10 (2015) 765–783. doi:10.2217/nmm.14.221.
- [244] P. Aebischer, M. Goddard, A.P. Signore, R.L. Timpson, Functional Recovery in Hemiparkinsonian Primates Transplanted with Polymer-Encapsulated PC12 Cells, *Exp. Neurol*. 126 (1994) 151–158. doi:10.1006/exnr.1994.1053.
- [245] H. Kishima, T. Poyot, J. Bloch, J. Dauguet, F. Condé, F. Dollé, F. Hinnen, W. Pralong, S. Palfi, N. Déglon, P. Aebischer, P. Hantraye, Encapsulated GDNF-producing C2C12 cells for Parkinson’s disease: a pre-clinical study in chronic MPTP-treated baboons, *Neurobiol. Dis*. 16 (2004) 428–439. doi:10.1016/J.NBD.2004.03.012.
- [246] A. Clavreul, L. Sindji, A. Aubert-Pouëssel, J.-P. Benoît, P. Menei, C.N. Montero-Menei, Effect of GDNF-releasing biodegradable microspheres on the function and the survival of intrastriatal fetal ventral mesencephalic cell grafts, *Eur. J. Pharm. Biopharm*. 63 (2006) 221–228. doi:10.1016/J.EJPB.2005.11.006.
- [247] P. Aebischer, P.A. Tresco, J. Sagen, S.R. Winn, Transplantation of microencapsulated bovine chromaffin cells reduces lesion-induced rotational asymmetry in rats, *Brain Res*. 560 (1991) 43–49. doi:10.1016/0006-8993(91)91212-J.
- [248] P. Aebischer, P.A. Tresco, S.R. Winn, L.A. Greene, C.B. Jaeger, Long-term cross-species brain transplantation of a polymer-encapsulated dopamine-secreting cell line., *Exp. Neurol*. 111 (1991) 269–75. doi:10.1016/0014-4886(91)90093-r.
- [249] S.R. Winn, P.A. Tresco, B. Zielinski, L.A. Greene, C.B. Jaeger, P. Aebischer, Behavioral recovery following intrastriatal implantation of microencapsulated PC12 cells, *Exp. Neurol*. 113 (1991) 322–329. doi:10.1016/0014-4886(91)90022-5.
- [250] C.B. Jaeger, L.A. Greene, P.A. Tresco, S.R. Winn, P. Aebischer, Polymer encapsulated dopaminergic cell lines as “alternative neural grafts”., *Prog. Brain Res*. 82 (1990) 41–46. <http://www.ncbi.nlm.nih.gov/pubmed/2290954> (accessed August 9, 2019).
- [251] D. Aarsland, J.P. Larsen, K. Karlsen, N.G. Lim, E. Tandberg, Mental symptoms in Parkinson’s disease are important contributors to caregiver distress., *Int. J. Geriatr. Psychiatry*. 14 (1999) 866–874. <http://www.ncbi.nlm.nih.gov/pubmed/10521886>

- (accessed August 14, 2019).
- [252] R. Apweiler, H. Hermjakob, N. Sharon, On the frequency of protein glycosylation, as deduced from analysis of the SWISS-PROT database, *Biochim. Biophys. Acta - Gen. Subj.* 1473 (1999) 4–8. doi:10.1016/S0304-4165(99)00165-8.
- [253] R.S. Haltiwanger, J.B. Lowe, Role of glycosylation in development, *Annu. Rev. Biochem.* 73 (2004) 491–537. doi:10.1146/annurev.biochem.73.011303.074043.
- [254] J.B. Lowe, J.D. Marth, A genetic approach to mammalian glycan function, *Annu. Rev. Biochem.* 72 (2003) 643–691. doi:10.1146/annurev.biochem.72.121801.161809.
- [255] R.G. Spiro, Protein glycosylation: nature, distribution, enzymatic formation, and disease implications of glycopeptide bonds, *Glycobiology.* 12 (2002) 43R–56R. doi:10.1093/glycob/12.4.43R.
- [256] A. Helenius, and M. Aebi, Intracellular functions of N-linked glycans, *Science (80-.).* 291 (2001) 2364–2369. doi:10.1126/SCIENCE.291.5512.2364.
- [257] A. Varki, M.E. Etzler, R.D. Cummings, J.D. Esko, *Discovery and classification of glycan-binding proteins*, Cold Spring Harbor Laboratory Press, 2009. <http://www.ncbi.nlm.nih.gov/pubmed/20301249> (accessed August 14, 2019).
- [258] A.J. Wittwer, S.C. Howard, Glycosylation at Asn-184 inhibits the conversion of single-chain to two-chain tissue-type plasminogen activator by plasmin, *Biochemistry.* 29 (1990) 4175–4180. doi:10.1021/bi00469a021.
- [259] T.R. Henion, A.A. Faden, T.K. Knott, G.A. Schwarting, 3GnT2 maintains adenylyl cyclase-3 signaling and axon guidance molecule expression in the olfactory epithelium, *J. Neurosci.* 31 (2011) 6576–6586. doi:10.1523/JNEUROSCI.0224-11.2011.
- [260] H.H. Freeze, E.A. Eklund, B.G. Ng, M.C. Patterson, Neurology of inherited glycosylation disorders., *Lancet. Neurol.* 11 (2012) 453–66. doi:10.1016/S1474-4422(12)70040-6.
- [261] Z. Ye, J.D. Marth, N-glycan branching requirement in neuronal and postnatal viability, *Glycobiology.* 14 (2004) 547–558. doi:10.1093/glycob/cwh069.
- [262] R. Kleene, M. Schachner, Glycans and neural cell interactions, *Nat. Rev. Neurosci.* 5 (2004) 195–208. doi:10.1038/nrn1349.
- [263] A. Dityatev, M. Schachner, P. Sonderegger, The dual role of the extracellular matrix in synaptic plasticity and homeostasis, *Nat. Rev. Neurosci.* 11 (2010) 735–746. doi:10.1038/nrn2898.
- [264] A. MATUS, S. DE PETRIS, M.C. RAFF, Mobility of Concanavalin A receptors in myelin and synaptic membranes, *Nat. New Biol.* 244 (1973) 278–280. doi:10.1038/newbio244278a0.
- [265] R.A.C. Clark, J.W. Gurd, N. Bissoon, N. Tricaud, E. Molnar, S.E. Zamze, R.A. Dwek, R.A.J. McIlhinney, D.R. Wing, Identification of lectin-purified neural glycoproteins, GPs 180, 116, and 110, with NMDA and AMPA receptor subunits: conservation of glycosylation at the synapse, *J. Neurochem.* 70 (2002) 2594–2605. doi:10.1046/j.1471-4159.1998.70062594.x.

- [266] S. Gloor, H. Antonicek, K.J. Sweadner, S. Pagliusi, R. Frank, M. Moos, M. Schachner, The adhesion molecule on glia (AMOG) is a homologue of the beta subunit of the Na,K-ATPase, *J. Cell Biol.* 110 (1990) 165–174. doi:10.1083/jcb.110.1.165.
- [267] C.S. Barros, S.J. Franco, U. Muller, Extracellular matrix: functions in the nervous system, *Cold Spring Harb. Perspect. Biol.* 3 (2011) a005108–a005108. doi:10.1101/cshperspect.a005108.
- [268] C.L. Tan, J.C.F. Kwok, R. Patani, C. Ffrench-Constant, S. Chandran, J.W. Fawcett, Integrin activation promotes axon growth on inhibitory chondroitin sulfate proteoglycans by enhancing integrin signaling, *J. Neurosci.* 31 (2011) 6289–6295. doi:10.1523/JNEUROSCI.0008-11.2011.
- [269] Y. Kariya, R. Kato, S. Itoh, T. Fukuda, Y. Shibukawa, N. Sanzen, K. Sekiguchi, Y. Wada, N. Kawasaki, J. Gu, N-glycosylation of laminin-332 regulates its biological functions, *J. Biol. Chem.* 283 (2008) 33036–33045. doi:10.1074/jbc.M804526200.
- [270] Y. Zhao, T. Nakagawa, S. Itoh, K. Inamori, T. Isaji, Y. Kariya, A. Kondo, E. Miyoshi, K. Miyazaki, N. Kawasaki, N. Taniguchi, J. Gu, N-Acetylglucosaminyltransferase III antagonizes the effect of N-Acetylglucosaminyltransferase V on $\alpha\beta 1$ integrin-mediated cell migration, *J. Biol. Chem.* 281 (2006) 32122–32130. doi:10.1074/jbc.M607274200.
- [271] I.J. Ji, S. Hua, D.H. Shin, N. Seo, J.Y. Hwang, I.-S. Jang, M.-G. Kang, J.-S. Choi, H.J. An, Spatially-resolved exploration of the mouse brain glycome by tissue glyco-capture (TGC) and nano-LC/MS, *Anal. Chem.* 87 (2015) 2869–2877. doi:10.1021/ac504339t.
- [272] M. Schachner, U. Bartsch, Multiple functions of the myelin-associated glycoprotein MAG (siglec-4a) in formation and maintenance of myelin., *Glia.* 29 (2000) 154–165. <http://www.ncbi.nlm.nih.gov/pubmed/10625334> (accessed August 15, 2019).
- [273] S. Tang, Y.J. Shen, M.E. DeBellard, G. Mukhopadhyay, J.L. Salzer, P.R. Crocker, M.T. Filbin, Myelin-associated glycoprotein interacts with neurons via a sialic acid binding site at ARG118 and a distinct neurite inhibition site, *J. Cell Biol.* 138 (1997) 1355–1366. doi:10.1083/jcb.138.6.1355.
- [274] M.T. Filbin, Myelin-associated glycoprotein: a role in myelination and in the inhibition of axonal regeneration?, *Curr. Opin. Neurobiol.* 5 (1995) 588–595. <http://www.ncbi.nlm.nih.gov/pubmed/8580710> (accessed August 15, 2019).
- [275] U. Bartsch, C.E. Bandtlow, L. Schnell, S. Bartsch, A.A. Spillmann, B.P. Rubin, R. Hillenbrand, D. Montag, M.E. Schwab, M. Schachner, Lack of evidence that myelin-associated glycoprotein is a major inhibitor of axonal regeneration in the CNS., *Neuron.* 15 (1995) 1375–1381. <http://www.ncbi.nlm.nih.gov/pubmed/8845160> (accessed August 15, 2019).
- [276] A. V. Woodard-Grice, A.C. McBrayer, J.K. Wakefield, Y. Zhuo, S.L. Bellis, Proteolytic shedding of ST6Gal-I by BACE1 regulates the glycosylation and function of $\alpha 4\beta 1$ integrins, *J. Biol. Chem.* 283 (2008) 26364–26373. doi:10.1074/jbc.M800836200.
- [277] M. Amano, M. Galvan, J. He, L.G. Baum, The ST6Gal I sialyltransferase selectively modifies N-glycans on CD45 to negatively regulate galectin-1-induced CD45 clustering, phosphatase modulation, and T cell death, *J. Biol. Chem.* 278 (2003) 7469–7475. doi:10.1074/jbc.M209595200.

- [278] R. Kleene, H. Yang, M. Kutsche, M. Schachner, The neural recognition molecule L1 is a sialic acid-binding lectin for CD24, which induces promotion and inhibition of neurite outgrowth., *J. Biol. Chem.* 276 (2001) 21656–21663. doi:10.1074/jbc.M101790200.
- [279] U. Finckh, J. Schröder, B. Ressler, A. Veske, A. Gal, Spectrum and detection rate of L1CAM mutations in isolated and familial cases with clinically suspected L1-disease., *Am. J. Med. Genet.* 92 (2000) 40–46. <http://www.ncbi.nlm.nih.gov/pubmed/10797421> (accessed August 15, 2019).
- [280] Y.-Z. Du, A.K. Srivastava, C.E. Schwartz, Multiple exon screening using restriction endonuclease fingerprinting (REF): Detection of six novel mutations in the L1 cell adhesion molecule (L1CAM) gene, *Hum. Mutat.* 11 (1998) 222–230. doi:10.1002/(SICI)1098-1004(1998)11:3<222::AID-HUMU7>3.0.CO;2-J.
- [281] Y. Zhuo, S.L. Bellis, Emerging role of α 2,6-sialic acid as a negative regulator of galectin binding and function, *J. Biol. Chem.* 286 (2011) 5935–5941. doi:10.1074/jbc.R110.191429.
- [282] J. Finne, Occurrence of unique polysialosyl carbohydrate units in glycoproteins of developing brain., *J. Biol. Chem.* 257 (1982) 11966–11970. <http://www.ncbi.nlm.nih.gov/pubmed/7118922> (accessed January 24, 2019).
- [283] P.M. Lackie, C. Zuber, J. Roth, Expression of polysialylated N-CAM during rat heart development, *Differentiation.* 47 (1991) 85–98. doi:10.1111/J.1432-0436.1991.TB00226.X.
- [284] J. Roth, D.J. Taatjes, D. Bitter-Suermann, J. Finne, Polysialic acid units are spatially and temporally expressed in developing postnatal rat kidney., *Proc. Natl. Acad. Sci. U. S. A.* 84 (1987) 1969–73. <http://www.ncbi.nlm.nih.gov/pubmed/3470771> (accessed January 24, 2019).
- [285] T. Seki, Y. Arai, Distribution and possible roles of the highly polysialylated neural cell adhesion molecule (NCAM-H) in the developing and adult central nervous system, *Neurosci. Res.* 17 (1993) 265–290. doi:10.1016/0168-0102(93)90111-3.
- [286] C. Sihlbom, P. Davidsson, M.R. Emmett, A.G. Marshall, C.L. Nilsson, Glycoproteomics of cerebrospinal fluid in neurodegenerative disease, *Int. J. Mass Spectrom.* 234 (2004) 145–152. doi:10.1016/J.IJMS.2004.02.016.
- [287] S.T. Gizaw, T. Ohashi, M. Tanaka, H. Hinou, S.-I. Nishimura, Glycoblotting method allows for rapid and efficient glycome profiling of human Alzheimer’s disease brain, serum and cerebrospinal fluid towards potential biomarker discovery, *Biochim. Biophys. Acta - Gen. Subj.* 1860 (2016) 1716–1727. doi:10.1016/J.BBAGEN.2016.03.009.
- [288] S.T. Gizaw, T. Koda, M. Amano, K. Kamimura, T. Ohashi, H. Hinou, S.-I. Nishimura, A comprehensive glycome profiling of Huntington’s disease transgenic mice, *Biochim. Biophys. Acta - Gen. Subj.* 1850 (2015) 1704–1718. doi:10.1016/J.BBAGEN.2015.04.006.
- [289] J. Sáez-Valero, G. Sberna, C.A. McLean, D.H. Small, Molecular isoform distribution and glycosylation of Acetylcholinesterase are altered in brain and cerebrospinal fluid of patients with Alzheimer’s Disease, *J. Neurochem.* 72 (2001) 1600–1608. doi:10.1046/j.1471-4159.1999.721600.x.

- [290] J. Saez-Valero, M.S. Barquero, A. Marcos, C.A. McLean, D.H. Small, Altered glycosylation of acetylcholinesterase in lumbar cerebrospinal fluid of patients with Alzheimer's disease, *J. Neurol. Neurosurg. Psychiatry*. 69 (2000) 664–667. doi:10.1136/jnnp.69.5.664.
- [291] J. Sáez-Valero, D.H. Small, Acetylcholinesterase and butyrylcholinesterase glycoforms are biomarkers of Alzheimer's disease., *J. Alzheimers. Dis.* 3 (2001) 323–328. <http://www.ncbi.nlm.nih.gov/pubmed/12214053> (accessed August 15, 2019).
- [292] J. Sáez-Valero, L.R. Fodero, M. Sjögren, N. Andreasen, S. Amici, V. Gallai, H. Vanderstichele, E. Vanmechelen, L. Parnetti, K. Blennow, D.H. Small, Glycosylation of acetylcholinesterase and butyrylcholinesterase changes as a function of the duration of Alzheimer's disease, *J. Neurosci. Res.* 72 (2003) 520–526. doi:10.1002/jnr.10599.
- [293] F. Liu, T. Zaidi, K. Iqbal, I. Grundke-Iqbal, R.K. Merkle, C.X. Gong, Role of glycosylation in hyperphosphorylation of tau in Alzheimer's disease., *FEBS Lett.* 512 (2002) 101–106. doi:10.1016/s0014-5793(02)02228-7.
- [294] M. Farrer, P. Chan, R. Chen, L. Tan, S. Lincoln, D. Hernandez, L. Forno, K. Gwinn-Hardy, L. Petrucelli, J. Hussey, A. Singleton, C. Tanner, J. Hardy, J.W. Langston, Lewy bodies and parkinsonism in families with parkin mutations., *Ann. Neurol.* 50 (2001) 293–300. <http://www.ncbi.nlm.nih.gov/pubmed/11558785> (accessed August 15, 2019).
- [295] H. Shimura, M.G. Schlossmacher, N. Hattori, M.P. Frosch, A. Trockenbacher, R. Schneider, Y. Mizuno, K.S. Kosik, D.J. Selkoe, Ubiquitination of a new form of alpha-synuclein by parkin from human brain: implications for Parkinson's Disease, *Science* (80-.). 293 (2001) 263–269. doi:10.1126/science.1060627.
- [296] C. Váradi, K. Nehéz, O. Hornyák, B. Viskolcz, J. Bones, Serum N-glycosylation in Parkinson's Disease: A novel approach for potential alterations, *Molecules*. 24 (2019) 2220. doi:10.3390/molecules24122220.
- [297] A.C. Russell, M. Šimurina, M.T. Garcia, M. Novokmet, Y. Wang, I. Rudan, H. Campbell, G. Lauc, M.G. Thomas, W. Wang, The N-glycosylation of immunoglobulin G as a novel biomarker of Parkinson's disease, *Glycobiology*. 27 (2017) 501–510. doi:10.1093/glycob/cwx022.
- [298] P.M. Levine, A. Galesic, A.T. Balana, A.-L. Mahul-Mellier, M.X. Navarro, C.A. De Leon, H.A. Lashuel, M.R. Pratt, α -Synuclein O-GlcNAcylation alters aggregation and toxicity, revealing certain residues as potential inhibitors of Parkinson's disease, *Proc. Natl. Acad. Sci.* 116 (2019) 1511–1519. doi:10.1073/PNAS.1808845116.
- [299] A.H. Schapira, P. Jenner, Etiology and pathogenesis of Parkinson's Disease, *Mov. Disord.* 26 (2011) 1049–1055. doi:10.1002/mds.23732.
- [300] O. Lindvall, A. Björklund, Cell therapy in Parkinson's Disease., *NeuroRx*. 1 (2004) 382–393. doi:10.1602/neurorx.1.4.382.
- [301] M. Emgård, L. Holmberg, E.-B. Samuelsson, B.A. Bahr, S. Falci, Å. Seiger, E. Sundström, Human neural precursor cells continue to proliferate and exhibit low cell death after transplantation to the injured rat spinal cord, *Brain Res.* 1278 (2009) 15–26. doi:10.1016/j.brainres.2009.04.012.
- [302] L.F. Lin, D.H. Doherty, J.D. Lile, S. Bektesh, F. Collins, GDNF: a glial cell line-

- derived neurotrophic factor for midbrain dopaminergic neurons., *Science*. 260 (1993) 1130–2. doi:10.1126/SCIENCE.8493557.
- [303] J.G. Hou, L.F. Lin, C. Mytilineou, Glial cell line-derived neurotrophic factor exerts neurotrophic effects on dopaminergic neurons in vitro and promotes their survival and regrowth after damage by 1-methyl-4-phenylpyridinium., *J. Neurochem*. 66 (1996) 74–82. doi:10.1046/j.1471-4159.1996.66010074.x.
- [304] A. Tomac, E. Lindqvist, L.-F.H. Lin, S.O. Ögren, D. Young, B.J. Hoffer, L. Olson, Protection and repair of the nigrostriatal dopaminergic system by GDNF in vivo, *Nature*. 373 (1995) 335–339. doi:10.1038/373335a0.
- [305] R. Grondin, Z. Zhang, A. Yi, W.A. Cass, N. Maswood, A.H. Andersen, D.D. Elsberry, M.C. Klein, G.A. Gerhardt, D.M. Gash, Chronic, controlled GDNF infusion promotes structural and functional recovery in advanced parkinsonian monkeys, *Brain*. 125 (2002) 2191–2201. doi:10.1093/brain/awf234.
- [306] D.M. Gash, Z. Zhang, Y. Ai, R. Grondin, R. Coffey, G.A. Gerhardt, Trophic factor distribution predicts functional recovery in parkinsonian monkeys, *Ann. Neurol*. 58 (2005) 224–233. doi:10.1002/ana.20549.
- [307] R. Grondin, O.M. Littrell, Z. Zhang, Y. Ai, P. Huettl, F. Pomerleau, J.E. Quintero, A.H. Andersen, M.J. Stenslik, L.H. Bradley, J. Lemmon, M.J. O’Neill, D.M. Gash, G.A. Gerhardt, GDNF revisited: A novel mammalian cell-derived variant form of GDNF increases dopamine turnover and improves brain biodistribution, *Neuropharmacology*. 147 (2019) 28–36. doi:10.1016/J.NEUROPHARM.2018.05.014.
- [308] S.J. Allen, J.J. Watson, D.K. Shoemark, N.U. Barua, N.K. Patel, GDNF, NGF and BDNF as therapeutic options for neurodegeneration, *Pharmacol. Ther.* 138 (2013) 155–175. doi:10.1016/j.pharmthera.2013.01.004.
- [309] D. V. Volodkin, N.I. Larionova, G.B. Sukhorukov, Protein encapsulation via porous CaCO₃ microparticles templating, *Biomacromolecules*. 5 (2004) 1962–1972. doi:10.1021/bm049669e.
- [310] J. Grossmann, Molecular mechanisms of “detachment-induced apoptosis—Anoikis,” *Apoptosis*. 7 (2002) 247–260. doi:10.1023/A:1015312119693.
- [311] P.C. Georges, W.J. Miller, D.F. Meaney, E.S. Sawyer, P.A. Janmey, Matrices with compliance comparable to that of brain tissue select neuronal over glial growth in mixed cortical cultures, *Biophys. J.* 90 (2006) 3012–3018. doi:10.1529/BIOPHYSJ.105.073114.
- [312] A. Gefen, N. Gefen, Q. Zhu, R. Raghupathi, S.S. Margulies, Age-dependent changes in material properties of the brain and braincase of the rat, *J. Neurotrauma*. 20 (2003) 1163–1177. doi:10.1089/089771503770802853.
- [313] K. Miller, K. Chinzei, G. Orsengo, P. Bednarz, Mechanical properties of brain tissue in-vivo: experiment and computer simulation, *J. Biomech.* 33 (2000) 1369–1376. doi:10.1016/S0021-9290(00)00120-2.
- [314] K. Hirakawa, K. Hashizume, T. Hayashi, Viscoelastic property of human brain -for the analysis of impact injury (author’s transl)., *Brain and Nerve*. 33 (1981) 1057–65.
- [315] R.W.P. Rodrigues, V.C. Gomide, G. Chadi, Astroglial and microglial reaction after a partial nigrostriatal degeneration induced by the striatal injection of different doses of

- 6-Hydroxydopamine, *Int. J. Neurosci.* 109 (2009) 91–126.
doi:10.3109/00207450108986528.
- [316] R.A. Hauser, T.B. Freeman, B.J. Snow, M. Nauert, L. Gauger, J.H. Kordower, C.W. Olanow, Long-term evaluation of bilateral fetal nigral transplantation in Parkinson Disease., *Arch. Neurol.* 56 (1999) 179–187. doi:10.1001/archneur.56.2.179.
- [317] P. Brundin, O. Pogarell, P. Hagell, P. Piccini, H. Widner, A. Schrag, A. Kupsch, L. Crabb, P. Odin, B. Gustavii, A. Björklund, D.J. Brooks, C.D. Marsden, W.H. Oertel, N.P. Quinn, S. Rehncrona, O. Lindvall, Bilateral caudate and putamen grafts of embryonic mesencephalic tissue treated with lazarooids in Parkinson's disease, *Brain*. 123 (2000) 1380–1390. doi:10.1093/brain/123.7.1380.
- [318] P. Hagell, A. Schrag, P. Piccini, M. Jahanshahi, R. Brown, S. Rehncrona, H. Widner, P. Brundin, J.C. Rothwell, P. Odin, G.K. Wenning, P. Morrish, B. Gustavii, A. Björklund, D.J. Brooks, C.D. Marsden, N.P. Quinn, O. Lindvall, Sequential bilateral transplantation in Parkinson's disease. Effects of the second graft, *Brain*. 122 (1999) 1121–1132. doi:10.1093/brain/122.6.1121.
- [319] R.A. Barker, H. Widner, Immune problems in central nervous system cell therapy, *NeuroRX*. 1 (2004) 472–481. doi:10.1602/neurorx.1.4.472.
- [320] C.E. Sortwell, M.R. Pitzer, T.J. Collier, Time course of apoptotic cell death within mesencephalic cell suspension grafts: implications for improving grafted dopamine neuron survival, *Exp. Neurol.* 165 (2000) 268–277. doi:10.1006/EXNR.2000.7476.
- [321] X. Liu, W. Peng, Y. Wang, M. Zhu, T. Sun, Q. Peng, Y. Zeng, B. Feng, X. Lu, J. Weng, J. Wang, Synthesis of an RGD-grafted oxidized sodium alginate–N-succinyl chitosan hydrogel and an in vitro study of endothelial and osteogenic differentiation, *J. Mater. Chem. B*. 1 (2013) 4484. doi:10.1039/c3tb20552e.
- [322] A.S. Wolberg, Thrombin generation and fibrin clot structure, *Blood Rev.* 21 (2007) 131–142. doi:10.1016/j.blre.2006.11.001.
- [323] M. Ehrbar, A. Metters, P. Zammaretti, J.A. Hubbell, A.H. Zisch, Endothelial cell proliferation and progenitor maturation by fibrin-bound VEGF variants with differential susceptibilities to local cellular activity, *J. Control. Release*. 101 (2005) 93–109. doi:10.1016/j.jconrel.2004.07.018.
- [324] H. Yasuda, S. Kuroda, H. Shichinohe, S. Kamei, R. Kawamura, Y. Iwasaki, Effect of biodegradable fibrin scaffold on survival, migration, and differentiation of transplanted bone marrow stromal cells after cortical injury in rats, *J. Neurosurg.* 112 (2010) 336–344. doi:10.3171/2009.2.JNS08495.
- [325] L.A. Flanagan, Y.-E. Ju, B. Marg, M. Osterfield, P.A. Janmey, Neurite branching on deformable substrates., *Neuroreport*. 13 (2002) 2411–2415.
doi:10.1097/01.wnr.0000048003.96487.97.
- [326] P.C. Georges, W.J. Miller, D.F. Meaney, E.S. Sawyer, P.A. Janmey, Matrices with compliance comparable to that of brain tissue select neuronal over glial growth in mixed cortical cultures, *Biophys. J.* 90 (2006) 3012–3018.
doi:10.1529/biophysj.105.073114.
- [327] S.E. Sakiyama, J.C. Schense, J.A. Hubbell, Incorporation of heparin-binding peptides into fibrin gels enhances neurite extension: an example of designer matrices in tissue

- engineering, *FASEB J.* 13 (1999) 2214–2224. doi:10.1096/fasebj.13.15.2214.
- [328] Alexei A. Antipov, Gleb B. Sukhorukov, A. Edwin Donath, H. Möhwald, Sustained release properties of polyelectrolyte multilayer capsules, *Adv Colloid Interface Sci.* 111 (2001) 49–61. doi:10.1021/JP002184+.
- [329] H. Ai, S.A. Jones, M.M. de Villiers, Y.M. Lvov, Nano-encapsulation of furosemide microcrystals for controlled drug release, *J. Control. Release.* 86 (2003) 59–68. doi:10.1016/S0168-3659(02)00322-X.
- [330] A. Larrañaga, I.L.M. Isa, V. Patil, S. Thamboo, M. Lomora, M.A. Fernández-Yague, J.-R. Sarasua, C.G. Palivan, A. Pandit, Antioxidant functionalized polymer capsules to prevent oxidative stress, *Acta Biomater.* 67 (2018) 21–31. doi:10.1016/J.ACTBIO.2017.12.014.
- [331] D. V. Volodkin, A.I. Petrov, A. Michelle Prevot, G.B. Sukhorukov, Matrix polyelectrolyte microcapsules: new system for macromolecule encapsulation, *Langmuir.* 20 (2004) 3398–3406. doi:10.1021/LA036177Z.
- [332] H. Kraskiewicz, B. Breen, T. Sargeant, S. McMahon, A. Pandit, Assembly of protein-based hollow spheres encapsulating a therapeutic factor, *ACS Chem. Neurosci.* 4 (2013) 1297–1304. doi:10.1021/cn400080h.
- [333] T.M. Odrljic, C.W. Francis, L.A. Sporn, L.A. Bunce, V.J. Marder, P.J. Simpson-Haidaris, Heparin-binding domain of fibrin mediates its binding to endothelial cells, *Arterioscler. Thromb. Vasc. Biol.* 16 (1996) 1544–1551. doi:10.1161/01.ATV.16.12.1544.
- [334] N. Nevalainen, M. Chermenina, A. Rehnmark, E. Berglöf, F. Marschinke, I. Strömberg, Glial cell line-derived neurotrophic factor is crucial for long-term maintenance of the nigrostriatal system, *Neuroscience.* 171 (2010) 1357–1366. doi:10.1016/j.neuroscience.2010.10.010.
- [335] S.K. Seidlits, Z.Z. Khaing, R.R. Petersen, J.D. Nickels, J.E. Vanscoy, J.B. Shear, C.E. Schmidt, The effects of hyaluronic acid hydrogels with tunable mechanical properties on neural progenitor cell differentiation, *Biomaterials.* 31 (2010) 3930–3940. doi:10.1016/j.biomaterials.2010.01.125.
- [336] Y.-B. Lu, K. Franze, G. Seifert, C. Steinhauser, F. Kirchhoff, H. Wolburg, J. Guck, P. Janmey, E.-Q. Wei, J. Kas, A. Reichenbach, Viscoelastic properties of individual glial cells and neurons in the CNS, *Proc. Natl. Acad. Sci.* 103 (2006) 17759–17764. doi:10.1073/pnas.0606150103.
- [337] J. Zhong, A. Chan, L. Morad, H.I. Kornblum, G. Guoping Fan, S.T. Carmichael, Hydrogel matrix to support stem cell survival after brain transplantation in stroke, *Neurorehabil. Neural Repair.* 24 (2010) 636–644. doi:10.1177/1545968310361958.
- [338] P. Lu, Y. Wang, L. Graham, K. McHale, M. Gao, D. Wu, J. Brock, A. Blesch, E.S. Rosenzweig, L.A. Havton, B. Zheng, J.M. Conner, M. Marsala, M.H. Tuszynski, Long-Distance growth and connectivity of neural stem cells after severe spinal cord injury, *Cell.* 150 (2012) 1264–1273. doi:10.1016/j.cell.2012.08.020.
- [339] D. Thomas, G. Fontana, X. Chen, C. Sanz-Nogués, D.I. Zeugolis, P. Dockery, T. O’Brien, A. Pandit, A shape-controlled tuneable microgel platform to modulate angiogenic paracrine responses in stem cells, *Biomaterials.* 35 (2014) 8757–8766.

- doi:10.1016/j.biomaterials.2014.06.053.
- [340] K.W. Moremen, M. Tiemeyer, A. V. Nairn, Vertebrate protein glycosylation: diversity, synthesis and function, *Nat. Rev. Mol. Cell Biol.* 13 (2012) 448–462. doi:10.1038/nrm3383.
- [341] Y. Zhang, H. Yin, H. Lu, Recent progress in quantitative glycoproteomics, *Glycoconj. J.* 29 (2012) 249–258. doi:10.1007/s10719-012-9398-x.
- [342] B.D. Shur, S. Roth, Cell surface glycosyltransferases, *BBA - Rev. Biomembr.* 415 (1975) 473–512. doi:10.1016/0304-4157(75)90007-6.
- [343] S. Roseman, The synthesis of complex carbohydrates by multiglycosyltransferase systems and their potential function in intercellular adhesion, *Chem. Phys. Lipids.* 5 (1970) 270–297. doi:10.1016/0009-3084(70)90024-1.
- [344] E.C. Collin, M. Kilcoyne, S.J. White, S. Grad, M. Alini, L. Joshi, A.S. Pandit, Unique glycosignature for intervertebral disc and articular cartilage cells and tissues in immaturity and maturity, *Sci. Rep.* 6 (2016) 23062. doi:10.1038/srep23062.
- [345] R.S. Haltiwanger, J.B. Lowe, Role of glycosylation in development, *Annu. Rev. Biochem.* 73 (2004) 491–537. doi:10.1146/annurev.biochem.73.011303.074043.
- [346] S.D. Szajda, A. Jankowska, K. Zwierz, Carbohydrate markers in colon carcinoma., *Dis. Markers.* 25 (2008) 233–242. doi:10.1155/2008/206510.
- [347] S. Liedtke, H. Geyer, M. Wuhrer, R. Geyer, G. Frank, R. Gerardy-Schahn, U. Zahringer, M. Schachner, Characterization of N-glycans from mouse brain neural cell adhesion molecule, *Glycobiology.* 11 (2001) 373–384. doi:10.1093/glycob/11.5.373.
- [348] M. Natalia Lobanovskaya, Tamara Zharkovsky, Külli Jaako, A.Z. Jürgenson, Anu Aonurm-Helm, PSA modification of NCAM supports the survival of injured retinal ganglion cells in adulthood, *Brain Res.* 1625 (2015) 9–17. doi:10.1016/J.BRAINRES.2015.08.008.
- [349] P.T. Kelly, C.W. Cotman, Identification of glycoproteins and proteins at synapses in the central nervous system., *J. Biol. Chem.* 252 (1977) 786–793. <http://www.ncbi.nlm.nih.gov/pubmed/833152> (accessed October 5, 2017).
- [350] J.W. Gurd, S.C. Fu, Concanavalin A receptors associated with rat brain synaptic junctions are high mannose-type oligosaccharides, *J. Neurochem.* 39 (1982) 719–725. doi:10.1111/j.1471-4159.1982.tb07951.x.
- [351] Y. Takeuchi, J. Morise, I. Morita, H. Takematsu, S. Oka, Role of site-specific N-glycans expressed on GluA2 in the regulation of cell surface expression of AMPA-type glutamate receptors, *PLoS One.* 10 (2015) e0135644. doi:10.1371/journal.pone.0135644.
- [352] J. Hu, W. Reutter, H. Fan, Significance of N-glycosylation and sialylation of GABA Transporter 1, *J. Carbohydr. Chem.* 30 (2011) 206–217. doi:10.1080/07328303.2011.604455.
- [353] A.S. Kristensen, J. Andersen, T.N. Jorgensen, L. Sorensen, J. Eriksen, C.J. Loland, K. Stromgaard, U. Gether, SLC6 neurotransmitter transporters: structure, function, and regulation, *Pharmacol. Rev.* 63 (2011) 585–640. doi:10.1124/pr.108.000869.

- [354] M. Pučić, S. Pinto, M. Novokmet, A. Knežević, O. Gornik, O. Polašek, K. Vlahoviček, W. Wang, P.M. Rudd, A.F. Wright, H. Campbell, I. Rudan, G. Lauc, Common aberrations from the normal human plasma N-glycan profile, *Glycobiology*. 20 (2010) 970–975. doi:10.1093/glycob/cwq052.
- [355] S. Grünewald, The clinical spectrum of phosphomannomutase 2 deficiency (CDG-Ia), *Biochim. Biophys. Acta - Mol. Basis Dis.* 1792 (2009) 827–834. doi:10.1016/j.bbadis.2009.01.003.
- [356] M.A. Haeuptle, T. Hennet, Congenital disorders of glycosylation: an update on defects affecting the biosynthesis of dolichol-linked oligosaccharides, *Hum. Mutat.* 30 (2009) 1628–1641. doi:10.1002/humu.21126.
- [357] R. Kleene, M. Schachner, Glycans and neural cell interactions, *Nat. Rev. Neurosci.* 5 (2004) 195–208. doi:10.1038/nrn1349.
- [358] S. Zamze, D.J. Harvey, Y.J. Chen, G.R. Guile, R.A. Dwek, D.R. Wing, Sialylated N-glycans in adult rat brain tissue--a widespread distribution of disialylated antennae in complex and hybrid structures., *Eur. J. Biochem.* 258 (1998) 243–70. doi:10.1046/j.1432-1327.1998.2580243.x.
- [359] Y.J. Chen, D.R. Wing, G.R. Guile, R.A. Dwek, D.J. Harvey, S. Zamze, Neutral N-glycans in adult rat brain tissue--complete characterisation reveals fucosylated hybrid and complex structures., *Eur. J. Biochem.* 251 (1998) 691–703. doi:10.1046/j.1432-1327.1998.2510691.x.
- [360] D.R. Wing, T.W. Rademacher, M.C. Field, R.A. Dwek, B. Schmitz, G. Thor, M. Schachner, Use of large-scale hydrazinolysis in the preparation of N-linked oligosaccharide libraries: application to brain tissue, *Glycoconj. J.* 9 (1992) 293–301. doi:10.1007/BF00731089.
- [361] S.T. Eshghi, S. Yang, X. Wang, P. Shah, X. Li, H. Zhang, Imaging of N-Linked glycans from formalin-fixed paraffin-embedded tissue sections using MALDI mass spectrometry, *ACS Chem. Biol.* 9 (2014) 2149–2156. doi:10.1021/cb500405h.
- [362] R. Raghunathan, N.K. Polinski, J.A. Klein, J.D. Hogan, C. Shao, K. Khatri, D. Leon, M.E. McComb, F.P. Manfredsson, C.E. Sortwell, J. Zaia, Glycomic and proteomic changes in aging brain nigrostriatal pathway, *Mol. Cell. Proteomics.* 17 (2018) 1778–1787. doi:10.1074/mcp.RA118.000680.
- [363] H. Stöckmann, R. O'flaherty, B. Adamczyk, R. Saldova, P.M. Rudd, Automated, high-throughput serum glycoprofiling platform, *Integ.Biol.* 7 (2015) 1026–1032. doi:10.1039/x0xx00000x.
- [364] L. Royle, C.M. Radcliffe, R.A. Dwek, P.M. Rudd, Detailed Structural Analysis of N-Glycans Released From Glycoproteins in SDS-PAGE Gel Bands Using HPLC Combined With Exoglycosidase Array Digestions, in: *Glycobiol. Protoc.*, Humana Press, New Jersey, 2006: pp. 125–144. doi:10.1385/1-59745-167-3:125.
- [365] L. Royle, M.P. Campbell, C.M. Radcliffe, D.M. White, D.J. Harvey, J.L. Abrahams, Y.-G. Kim, G.W. Henry, N.A. Shadick, M.E. Weinblatt, D.M. Lee, P.M. Rudd, R.A. Dwek, HPLC-based analysis of serum N-glycans on a 96-well plate platform with dedicated database software, *Anal. Biochem.* 376 (2008) 1–12. doi:10.1016/j.ab.2007.12.012.

- [366] B. Küster, S.F. Wheeler, A.P. Hunter, R.A. Dwek, D.J. Harvey, Sequencing of N-linked oligosaccharides directly from protein gels: in-gel deglycosylation followed by Matrix-Assisted Laser Desorption/Ionization Mass Spectrometry and normal-phase High-Performance Liquid Chromatography, *Anal. Biochem.* 250 (1997) 82–101. doi:10.1006/abio.1997.2199.
- [367] J.C. Bigge, T.P. Patel, J.A. Bruce, P.N. Goulding, S.M. Charles, R.B. Parekh, Nonselective and efficient fluorescent labeling of glycans using 2-amino benzamide and anthranilic acid, *Anal. Biochem.* 230 (1995) 229–238. doi:10.1006/abio.1995.1468.
- [368] L. Royle, C.M. Radcliffe, R.A. Dwek, P.M. Rudd, Detailed structural analysis of N-glycans released from glycoproteins in SDS-PAGE gel bands using HPLC combined with exoglycosidase array digestions, in: *Glycobiol. Protoc.*, Humana Press, New Jersey, 2006: pp. 125–144. doi:10.1385/1-59745-167-3:125.
- [369] T. Krusius, J. Finne, Structural features of tissue glycoproteins. Fractionation and methylation analysis of glycopeptides derived from rat brain, kidney and liver., *Eur. J. Biochem.* 78 (1977) 369–379. doi:10.1111/j.1432-1033.1977.tb11749.x.
- [370] L.J. Lawson, V.H. Perry, P. Dri, S. Gordon, Heterogeneity in the distribution and morphology of microglia in the normal adult mouse brain., *Neuroscience.* 39 (1990) 151–170. doi:10.1016/0306-4522(90)90229-w.
- [371] R.L. Schnaar, A. Suzuki, P. Stanley, *Glycosphingolipids*, 2009. doi:doi:10.1101/glycobiology.3e.011.
- [372] I.J. Ji, S. Hua, D.H. Shin, N. Seo, J.Y. Hwang, I.-S. Jang, M.-G. Kang, J.-S. Choi, H.J. An, Spatially-resolved exploration of the mouse brain glycome by tissue glyco-capture (TGC) and Nano-LC/MS, *Anal. Chem.* 87 (2015) 2869–2877. doi:10.1021/ac504339t.
- [373] H. Shimizu, K. Ochiai, K. Ikenaka, K. Mikoshiba, S. Hase, Structures of N-Linked sugar chains expressed mainly in mouse brain, 1993. doi:10.1093/oxfordjournals.jbchem.a124177.
- [374] S. -i. Nakakita, S. Natsuka, J. Okamoto, K. Ikenaka, S. Hase, Alteration of brain type N-glycans in neurological mutant mouse brain, *J. Biochem.* 138 (2005) 277–283. doi:10.1093/jb/mvi125.
- [375] L. Royle, M.P. Campbell, C.M. Radcliffe, D.M. White, D.J. Harvey, J.L. Abrahams, Y.-G. Kim, G.W. Henry, N.A. Shadick, M.E. Weinblatt, D.M. Lee, P.M. Rudd, R.A. Dwek, HPLC-based analysis of serum N-glycans on a 96-well plate platform with dedicated database software, *Anal. Biochem.* 376 (2008) 1–12. doi:10.1016/j.ab.2007.12.012.
- [376] S. Takasaki, T. Mizuochi, A. Kobata, [17] Hydrazinolysis of asparagine-linked sugar chains to produce free oligosaccharides, *Methods Enzymol.* 83 (1982) 263–268. doi:10.1016/0076-6879(82)83019-X.
- [377] T. Merry, S. Astrautsova, Chemical and enzymatic release of glycans from glycoproteins, in: *Capill. Electrophor. Carbohydrates*, Humana Press, New Jersey, 2003: pp. 27–40. doi:10.1385/1-59259-294-5:27.
- [378] S.R. Kronewitter, M.L.A. de Leoz, K.S. Peacock, K.R. McBride, H.J. An, S. Miyamoto, G.S. Leiserowitz, C.B. Lebrilla, Human serum processing and analysis

- methods for rapid and reproducible N-glycan mass profiling., *J. Proteome Res.* 9 (2010) 4952–4959. doi:10.1021/pr100202a.
- [379] Y. Kita, Y. Miura, J. Furukawa, M. Nakano, Y. Shinohara, M. Ohno, A. Takimoto, S.-I. Nishimura, Quantitative glycomics of human whole serum glycoproteins based on the standardized protocol for liberating N-glycans, *Mol. Cell. Proteomics.* 6 (2007) 1437–1445. doi:10.1074/mcp.T600063-MCP200.
- [380] D.H. Dube, C.R. Bertozzi, Glycans in cancer and inflammation — potential for therapeutics and diagnostics, *Nat. Rev. Drug Discov.* 4 (2005) 477–488. doi:10.1038/nrd1751.
- [381] A. V Everest-Dass, M.T. Briggs, G. Kaur, M.K. Oehler, P. Hoffmann, N.H. Packer, N-glycan MALDI imaging mass spectrometry on formalin-fixed paraffin-embedded tissue enables the delineation of ovarian cancer tissues., *Mol. Cell. Proteomics.* 15 (2016) 3003–3016. doi:10.1074/mcp.M116.059816.
- [382] A. Varki, Sialic acids in human health and disease, *Trends Mol. Med.* 14 (2008) 351–360. doi:10.1016/J.MOLMED.2008.06.002.
- [383] Q. Chai, J.W. Arndt, M. Dong, W.H. Tepp, E.A. Johnson, E.R. Chapman, R.C. Stevens, Structural basis of cell surface receptor recognition by botulinum neurotoxin B, *Nature.* 444 (2006) 1096–1100. doi:10.1038/nature05411.
- [384] U. Rutishauser, A. Acheson, A. Hall, D. Mann, J. Sunshine, The neural cell adhesion molecule (NCAM) as a regulator of cell-cell interactions, *Science* (80-.). 240 (1988) 53–57. doi:10.1126/science.3281256.
- [385] T. Quirico-Santos, C.O. Fonseca, J. Lagrota-Candido, Brain sweet brain: importance of sugars for the cerebral microenvironment and tumor development., *Arq. Neuropsiquiatr.* 68 (2010) 799–803. doi:10.1590/S0004-282X2010000500024.
- [386] M. Kontou, W. Weidemann, K. Bork, R. Horstkorte, Beyond glycosylation: sialic acid precursors act as signaling molecules and are involved in cellular control of differentiation of PC12 cells., *Biol. Chem.* 390 (2009) 575–579. doi:10.1515/BC.2009.058.
- [387] B. Wang, Sialic acid is an essential nutrient for brain development and cognition, *Annu. Rev. Nutr.* 29 (2009) 177–222. doi:10.1146/annurev.nutr.28.061807.155515.
- [388] J.A. Rodriguez, E. Piddini, T. Hasegawa, T. Miyagi, C.G. Dotti, Plasma membrane ganglioside sialidase regulates axonal growth and regeneration in hippocampal neurons in culture., *J. Neurosci.* 21 (2001) 8387–8395. doi:10.1523/JNEUROSCI.21-21-08387.2001.
- [389] T. Kawano, S. Koyama, H. Takematsu, Y. Kozutsumi, H. Kawasaki, S. Kawashima, T. Kawasaki, A. Suzuki, Molecular cloning of cytidine monophospho-N-acetylneuraminic acid hydroxylase. Regulation of species- and tissue-specific expression of N-glycolylneuraminic acid., *J. Biol. Chem.* 270 (1995) 16458–63. doi:10.1074/jbc.270.27.16458.
- [390] L.R.L. Davies, O.M.T. Pearce, M.B. Tessier, S. Assar, V. Smutova, M. Pajunen, M. Sumida, C. Sato, K. Kitajima, J. Finne, P. Gagneux, A. Pshezhetsky, R. Woods, A. Varki, Metabolism of vertebrate amino sugars with N-glycolyl groups, *J. Biol. Chem.* 287 (2012) 28917–28931. doi:10.1074/jbc.M112.365056.

- [391] L.R.L. Davies, A. Varki, Why is N-Glycolylneuraminic acid rare in the vertebrate brain?, in: *Top Curr Chem*, Springer, Berlin, Heidelberg, 2013: pp. 31–54. doi:10.1007/128_2013_419.
- [392] H. Geyer, U. Bahr, S. Liedtke, M. Schachner, R. Geyer, Core structures of polysialylated glycans present in neural cell adhesion molecule from newborn mouse brain, 2001. doi:10.1046/j.0014-2956.2001.02613.x.
- [393] T. Nomura, T. Yabe, E.S. Rosenthal, M. Krzan, J.P. Schwartz, PSA-NCAM distinguishes reactive astrocytes in 6-OHDA-lesioned substantia nigra from those in the striatal terminal fields, *J. Neurosci. Res.* 61 (2000) 588–596. doi:10.1002/1097-4547(20000915)61:6<588::AID-JNR2>3.0.CO;2-M.
- [394] J.Z. Kiss, C. Wang, G. Rougon, Nerve-dependent expression of high polysialic acid neural cell adhesion molecule in neurohypophysial astrocytes of adult rats, *Neuroscience.* 53 (1993) 213–221. doi:10.1016/0306-4522(93)90299-U.
- [395] H. Shimizu, K. Ochiai, K. Ikenaka, K. Mikoshiba, S. Hase, Structures of N-linked sugar chains expressed mainly in mouse brain., *J. Biochem.* 114 (1993) 334–8. <http://www.ncbi.nlm.nih.gov/pubmed/8282722> (accessed February 26, 2019).
- [396] S. Hua, H.N. Jeong, L.M. Dimapasoc, I. Kang, C. Han, J.-S. Choi, C.B. Lebrilla, H.J. An, Isomer-specific LC/MS and LC/MS/MS profiling of the mouse serum N-glycome revealing a number of novel sialylated N-glycans., *Anal. Chem.* 85 (2013) 4636–43. doi:10.1021/ac400195h.
- [397] S.-Y. Lin, Y.-Y. Chen, Y.-Y. Fan, C.-W. Lin, S.-T. Chen, A.H.-J. Wang, K.-H. Khoo, Precise mapping of increased sialylation pattern and the expression of acute phase proteins accompanying murine tumor progression in BALB/c mouse by integrated sera proteomics and glycomics., *J. Proteome Res.* 7 (2008) 3293–303. doi:10.1021/pr800093b.
- [398] R.K. Margolis, R.U. Margolis, DISPOSITION OF FUCOSE IN BRAIN, *J. Neurochem.* 19 (1972) 1023–1030. doi:10.1111/j.1471-4159.1972.tb01422.x.
- [399] S. Toghi Eshghi, W. Yang, Y. Hu, P. Shah, S. Sun, X. Li, H. Zhang, Classification of Tandem Mass Spectra for Identification of N- and O-linked Glycopeptides, *Sci. Rep.* 6 (2016) 37189. doi:10.1038/srep37189.
- [400] F. Angenstein, H. Matthies, S. Staeck, K.G. Reymann, S. Staak, The maintenance of hippocampal long-term potentiation is paralleled by a dopamine-dependent increase in glycoprotein fucosylation., *Neurochem. Int.* 21 (1992) 403–8. <http://www.ncbi.nlm.nih.gov/pubmed/1338901> (accessed January 22, 2018).
- [401] W. Wetzel, N. Popov, B. Lössner, S. Schulzeck, R. Honza, H. Matthies, Effect of L-fucose on brain protein metabolism and retention of a learned behavior in rats, *Pharmacol. Biochem. Behav.* 13 (1980) 765–771. doi:10.1016/0091-3057(80)90204-X.
- [402] T. Fukuda, H. Hashimoto, N. Okayasu, A. Kameyama, H. Onogi, O. Nakagawasai, T. Nakazawa, T. Kurosawa, Y. Hao, T. Isaji, T. Tadano, H. Narimatsu, N. Taniguchi, J. Gu, α 1,6-Fucosyltransferase-deficient Mice Exhibit Multiple Behavioral Abnormalities Associated with a Schizophrenia-like Phenotype, *J. Biol. Chem.* 286 (2011) 18434–18443. doi:10.1074/jbc.M110.172536.

- [403] R. Horstkorte, M. Schachner, J.P. Magyar, T. Vorherr, B. Schmitz, The fourth immunoglobulin-like domain of NCAM contains a carbohydrate recognition domain for oligomannosidic glycans implicated in association with L1 and neurite outgrowth., *J. Cell Biol.* 121 (1993) 1409–21. doi:10.1083/JCB.121.6.1409.
- [404] M. Jadot, L. Lin, D.E. Sleat, I. Sohar, M.S. Hsu, J. Pintar, F. Dubois, S. Wattiaux-De Coninck, R. Wattiaux, P. Lobel, Subcellular localization of mannose 6-phosphate glycoproteins in rat brain., *J. Biol. Chem.* 274 (1999) 21104–13. <http://www.ncbi.nlm.nih.gov/pubmed/10409663> (accessed March 5, 2019).
- [405] D.E. Sleat, H. Lackland, Y. Wang, I. Sohar, G. Xiao, H. Li, P. Lobel, The human brain mannose 6-phosphate glycoproteome: A complex mixture composed of multiple isoforms of many soluble lysosomal proteins, *Proteomics.* 5 (2005) 1520–1532. doi:10.1002/pmic.200401054.
- [406] D. Chiasserini, S. Paciotti, P. Eusebi, E. Persichetti, A. Tasegian, M. Kurzawa-Akanbi, P.F. Chinnery, C.M. Morris, P. Calabresi, L. Parnetti, T. Beccari, Selective loss of glucocerebrosidase activity in sporadic Parkinson's disease and dementia with Lewy bodies, *Mol. Neurodegener.* 10 (2015) 15. doi:10.1186/s13024-015-0010-2.
- [407] E.C. Collin, M. Kilcoyne, S.J. White, S. Grad, M. Alini, L. Joshi, A.S. Pandit, Unique glycosignature for intervertebral disc and articular cartilage cells and tissues in immaturity and maturity., *Sci. Rep.* 6 (2016) 23062. doi:10.1038/srep23062.
- [408] J.Q. Gerlach, M. Kilcoyne, S. Eaton, V. Bhavanandan, L. Joshi, Non-carbohydrate-Mediated Interaction of Lectins with Plant Proteins, in: *Adv. Exp. Med. Biol.*, 2011: pp. 257–269. doi:10.1007/978-1-4419-7877-6_12.
- [409] G. Szumanska, A.W. Vorbrodt, T.I. Mandybur, H.M. Wisniewski, Leetin histochemistry of plaques and tangles in Alzheimer's disease, 1987. <https://link.springer.com/content/pdf/10.1007%2FBF00695495.pdf> (accessed May 14, 2019).
- [410] R.K.T. Kam, T.C.W. Poon, The potentials of glycomics in biomarker discovery, *Clin. Proteomics.* 4 (2008) 67–79. doi:10.1007/s12014-008-9017-9.
- [411] S. BarbariĆ, V. Mrsa, B. Ries, P. Mildner, Role of the carbohydrate part of yeast acid phosphatase., *Arch. Biochem. Biophys.* 234 (1984) 567–75. doi:10.1016/0003-9861(84)90305-9.
- [412] Y. Tsuji, K. Yamamoto, T. Tochikura, Formation of deglycosylated alpha-L-fucosidase by endo-beta-N-acetylglucosaminidase in *Fusarium oxysporum*., *Appl. Environ. Microbiol.* 56 (1990) 928–33. doi:10.1074/jbc.M114.583286.
- [413] V. Belalcazar, R. Gutiérrez Gallego, E. Llop, J. Segura, J.A. Pascual, Assessing the instability of the isoelectric focusing patterns of erythropoietin in urine, *Electrophoresis.* 27 (2006) 4387–4395. doi:10.1002/elps.200500891.
- [414] F.K. Chu, F. Maley, Stabilization of the structure and activity of yeast carboxypeptidase Y by its high-mannose oligosaccharide chains., *Arch. Biochem. Biophys.* 214 (1982) 134–9. doi:10.1016/0003-9861(82)90015-7.
- [415] K. Sarter, C. Mierke, A. Beer, B. Frey, B.G. Führnrohr, C. Schulze, S. Franz, Sweet clearance: Involvement of cell surface glycans in the recognition of apoptotic cells, *Autoimmunity.* 40 (2007) 345–348. doi:10.1080/08916930701356804.

- [416] J. Gu, T. Isaji, Q. Xu, Y. Kariya, W. Gu, T. Fukuda, Y. Du, Potential roles of N-glycosylation in cell adhesion, *Glycoconj. J.* 29 (2012) 599–607. doi:10.1007/s10719-012-9386-1.
- [417] D. Shental-Bechor, Y. Levy, Folding of glycoproteins: toward understanding the biophysics of the glycosylation code, *Curr. Opin. Struct. Biol.* 19 (2009) 524–533. doi:10.1016/j.sbi.2009.07.002.
- [418] M.N. Fukuda, H. Sasaki, L. Lopez, M. Fukuda, Survival of recombinant erythropoietin in the circulation: the role of carbohydrates., *Blood.* 73 (1989) 84–9. <http://www.ncbi.nlm.nih.gov/pubmed/2910371> (accessed June 12, 2019).
- [419] J. Jaeken, H. Carchon, Congenital disorders of glycosylation: a booming chapter of pediatrics., *Curr. Opin. Pediatr.* 16 (2004) 434–9. doi:10.1097/01.mop.0000133636.56790.4a.
- [420] M.M. Fuster, J.D. Esko, The sweet and sour of cancer: glycans as novel therapeutic targets, *Nat. Rev. Cancer.* 5 (2005) 526–542. doi:10.1038/nrc1649.
- [421] B. Thomas, M.F. Beal, Parkinson’s disease, *Hum. Mol. Genet.* 16 (2007) R183–R194. doi:10.1093/hmg/ddm159.
- [422] M.R. Cookson, THE biochemistry of Parkinson’s Disease, *Annu. Rev. Biochem.* 74 (2005) 29–52. doi:10.1146/annurev.biochem.74.082803.133400.
- [423] P. Davidsson, A. Westman-Brinkmalm, C.L. Nilsson, M. Lindbjer, L. Paulson, N. Andreasen, M. Sjögren, K. Blennow, Proteome analysis of cerebrospinal fluid proteins in Alzheimer patients., *Neuroreport.* 13 (2002) 611–615. <http://www.ncbi.nlm.nih.gov/pubmed/11973456> (accessed June 13, 2019).
- [424] Z. Zhang, Y. Takeda-Uchimura, T. Foyez, S. Ohtake-Niimi, H. Akatsu, K. Nishitsuji, M. Michikawa, T. Wyss-Coray, K. Kadomatsu, K. Uchimura, Deficiency of a sulfotransferase for sialic acid-modified glycans mitigates Alzheimer’s pathology, *Proc Natl Acad Sci U S A.* 114 (2017) E2947–E2954. doi:10.1073/pnas.1615036114.
- [425] J.M. Hatcher, K.D. Pennell, G.W. Miller, Parkinson’s disease and pesticides: a toxicological perspective, *Trends Pharmacol. Sci.* 29 (2008) 322–329. doi:10.1016/J.TIPS.2008.03.007.
- [426] H. Hwang, J. Zhang, K.A. Chung, J.B. Leverenz, C.P. Zabetian, E.R. Peskind, J. Jankovic, Z. Su, A.M. Hancock, C. Pan, T.J. Montine, S. Pan, J. Nutt, R. Albin, M. Gearing, R.P. Beyer, M. Shi, J. Zhang, Glycoproteomics in neurodegenerative diseases, 29 (2010) 79–125. doi:10.1002/mas.20221.
- [427] L.B. Moran, L. Hickey, G.J. Michael, M. Derkacs, L.M. Christian, M.E. Kalaitzakis, R.K.B. Pearce, M.B. Graeber, Neuronal pentraxin II is highly upregulated in Parkinson’s disease and a novel component of Lewy bodies, *Acta Neuropathol.* 115 (2008) 471–478. doi:10.1007/s00401-007-0309-3.
- [428] W.J. Brackenbury, T.H. Davis, C. Chen, E.A. Slat, M.J. Detrow, T.L. Dickendesher, B. Ranscht, L.L. Isom, Voltage-gated Na⁺ channel 1 subunit-mediated neurite outgrowth requires Fyn Kinase and contributes to postnatal CNS development in vivo, *J. Neurosci.* 28 (2008) 3246–3256. doi:10.1523/JNEUROSCI.5446-07.2008.
- [429] H. Miyazaki, F. Oyama, H.-K. Wong, K. Kaneko, T. Sakurai, A. Tamaoka, N. Nukina, BACE1 modulates filopodia-like protrusions induced by sodium channel β 4 subunit,

- Biochem. Biophys. Res. Commun. 361 (2007) 43–48. doi:10.1016/j.bbrc.2007.06.170.
- [430] T. Zhou, Z. Zhang, J. Liu, J. Zhang, B. Jiao, Glycosylation of the sodium channel $\beta 4$ subunit is developmentally regulated and involves in neuritic degeneration, *Int. J. Biol. Sci.* 8 (2012) 630–639. doi:10.7150/ijbs.3684.
- [431] A. Russell, A. Drozdova, W. Wang, M. Thomas, The impact of dementia development concurrent with Parkinson's disease: a new perspective., *CNS Neurol. Disord. Drug Targets.* 13 (2014) 1160–1168. doi:10.2174/1871527313666140917122739.
- [432] A.C. Russell, M. Šimurina, M.T. Garcia, M. Novokmet, Y. Wang, I. Rudan, H. Campbell, G. Lauc, M.G. Thomas, W. Wang, The N-glycosylation of immunoglobulin G as a novel biomarker of Parkinson's disease, *Glycobiology.* 27 (2017) 501–510. doi:10.1093/glycob/cwx022.
- [433] T.W. Powers, B.A. Neely, Y. Shao, H. Tang, D.A. Troyer, A.S. Mehta, B.B. Haab, R.R. Drake, MALDI imaging mass spectrometry profiling of N-glycans in formalin-fixed paraffin embedded clinical tissue blocks and tissue microarrays, *PLoS One.* 9 (2014) e106255. doi:10.1371/journal.pone.0106255.
- [434] T.W. Powers, E.E. Jones, L.R. Betesh, P.R. Romano, P. Gao, J.A. Copland, A.S. Mehta, R.R. Drake, Matrix assisted laser desorption ionization imaging mass spectrometry workflow for spatial profiling analysis of N-linked glycan expression in tissues, *Anal. Chem.* 85 (2013) 9799–9806. doi:10.1021/ac402108x.
- [435] D.S. Cornett, M.L. Reyzer, P. Chaurand, R.M. Caprioli, MALDI imaging mass spectrometry: molecular snapshots of biochemical systems, *Nat. Methods.* 4 (2007) 828–833. doi:10.1038/nmeth1094.
- [436] O.J.R. Gustafsson, M.T. Briggs, M.R. Condina, L.J. Winderbaum, M. Pelzing, S.R. McColl, A. V. Everest-Dass, N.H. Packer, P. Hoffmann, MALDI imaging mass spectrometry of N-linked glycans on formalin-fixed paraffin-embedded murine kidney, *Anal. Bioanal. Chem.* 407 (2015) 2127–2139. doi:10.1007/s00216-014-8293-7.
- [437] U. Ungerstedt, G.W. Arbuthnott, Quantitative recording of rotational behavior in rats after 6-hydroxy-dopamine lesions of the nigrostriatal dopamine system., *Brain Res.* 24 (1970) 485–493. doi:10.1016/0006-8993(70)90187-3.
- [438] C. Váradi, K. Nehéz, O. Hornyák, B. Viskolcz, J. Bones, C. Váradi, K. Nehéz, O. Hornyák, B. Viskolcz, J. Bones, Serum N-glycosylation in Parkinson's Disease: A novel approach for potential alterations, *Molecules.* 24 (2019) 2220. doi:10.3390/molecules24122220.
- [439] T. Fukuda, H. Hashimoto, N. Okayasu, A. Kameyama, H. Onogi, O. Nakagawasai, T. Nakazawa, T. Kurosawa, Y. Hao, T. Isaji, T. Tadano, H. Narimatsu, N. Taniguchi, J. Gu, $\alpha 1,6$ -Fucosyltransferase-deficient mice exhibit multiple behavioral abnormalities associated with a schizophrenia-like phenotype, *J. Biol. Chem.* 286 (2011) 18434–18443. doi:10.1074/jbc.M110.172536.
- [440] K. Kollmann, M. Damme, S. Markmann, W. Morelle, M. Schweizer, I. Hermans-Borgmeyer, A.K. Röchert, S. Pohl, T. Lübke, J.-C. Michalski, R. Käkälä, S.U. Walkley, T. Bräulke, Lysosomal dysfunction causes neurodegeneration in mucopolipidosis II 'knock-in' mice, *Brain.* 135 (2012) 2661–2675. doi:10.1093/brain/aws209.

- [441] A. Członkowska, M. Kohutnicka, I. Kurkowska-Jastrzebska, A. Członkowski, Microglial reaction in MPTP (1-methyl-4-phenyl-1,2,3,6-tetrahydropyridine) induced Parkinson's disease mice model., *Neurodegeneration*. 5 (1996) 137–143. doi:10.1006/neur.1996.0020.
- [442] S.F. Wheeler, P. Domann, D.J. Harvey, Derivatization of sialic acids for stabilization in matrix-assisted laser desorption/ionization mass spectrometry and concomitant differentiation of α (2 \rightarrow 3)- and α (2 \rightarrow 6)-isomers, *Rapid Commun. Mass Spectrom.* 23 (2009) 303–312. doi:10.1002/rcm.3867.
- [443] B. Linnartz, L.-G. Bodea, H. Neumann, Microglial carbohydrate-binding receptors for neural repair, *Cell Tissue Res.* 349 (2012) 215–227. doi:10.1007/s00441-012-1342-7.
- [444] H.J. Crespo, J.T.Y. Lau, P.A. Videira, Dendritic cells: a spot on sialic acid, *Front. Immunol.* 4 (2013). doi:10.3389/fimmu.2013.00491.
- [445] D. Johnson, M.L. Montpetit, P.J. Stocker, E.S. Bennett, The sialic acid component of the beta1 subunit modulates voltage-gated sodium channel function., *J. Biol. Chem.* 279 (2004) 44303–10. doi:10.1074/jbc.M408900200.
- [446] T.H. Davis, C. Chen, L.L. Isom, Sodium channel β 1 subunits promote neurite outgrowth in cerebellar granule neurons, *J. Biol. Chem.* 279 (2004) 51424–51432. doi:10.1074/jbc.M410830200.
- [447] X.-J. Wang, Z.-Q. Yan, G.-Q. Lu, S. Stuart, S.-D. Chen, Parkinson disease IgG and C5a-induced synergistic dopaminergic neurotoxicity: Role of microglia, *Neurochem. Int.* 50 (2007) 39–50. doi:10.1016/J.NEUINT.2006.07.014.
- [448] S.H. Appel, W.-D. Le, J. Tajti, L.J. Haverkamp, J.I. Engelhardt, Nigral damage and dopaminergic hypofunction in mesencephalon-immunized guinea pigs, *Ann. Neurol.* 32 (1992) 494–501. doi:10.1002/ana.410320403.
- [449] Y. He, W.-D. Le, S.H. Appel, Role of Fc γ receptors in nigral cell injury induced by Parkinson Disease immunoglobulin injection into mouse substantia nigra, *Exp. Neurol.* 176 (2002) 322–327. doi:10.1006/EXNR.2002.7946.
- [450] N. Uozumi, S. Yanagidani, E. Miyoshi, Y. Ihara, T. Sakuma, C.-X. Gao, T. Teshima, S. Fujii, T. Shiba, N. Taniguchi, Purification and cDNA cloning of porcine brain GDP-L-Fuc: N -Acetyl- β -D-Glucosaminide α 1 \rightarrow 6Fucosyltransferase, *J. Biol. Chem.* 271 (1996) 27810–27817. doi:10.1074/jbc.271.44.27810.
- [451] S. i. Nakakita, S. Natsuka, K. Ikenaka, S. Hase, Development-dependent expression of complex-type sugar chains specific to mouse brain, *J. Biochem.* 123 (1998) 1164–1168. doi:10.1093/oxfordjournals.jbchem.a022056.
- [452] D.J. Becker, J.B. Lowe, Fucose: biosynthesis and biological function in mammals, *Glycobiology*. 13 (2003) 41R–53R. doi:10.1093/glycob/cwg054.
- [453] T. Okajima, A. Xu, L. Lei, K.D. Irvine, Chaperone activity of protein O-fucosyltransferase 1 promotes notch receptor folding., *Science*. 307 (2005) 1599–603. doi:10.1126/science.1108995.
- [454] S. Nishihara, H. Iwasaki, K. Nakajima, A. Togayachi, Y. Ikehara, T. Kudo, Y. Kushi, A. Furuya, K. Shitara, H. Narimatsu, alpha1,3-Fucosyltransferase IX (Fut9) determines Lewis X expression in brain, *Glycobiology*. 13 (2003) 445–455. doi:10.1093/glycob/cwg048.

- [455] J. Pruszek, W. Ludwig, A. Blak, K. Alavian, O. Isacson, CD15, CD24 and CD29 define a surface biomarker code for neural lineage differentiation of stem cells, *Stem Cells*. 27 (2009) 2928–2940. doi:10.1002/stem.211.
- [456] T. Kudo, T. Fujii, S. Ikegami, K. Inokuchi, Y. Takayama, Y. Ikehara, S. Nishihara, A. Togayachi, S. Takahashi, K. Tachibana, S. Yuasa, H. Narimatsu, Mice lacking α 1,3-fucosyltransferase IX demonstrate disappearance of Lewis x structure in brain and increased anxiety-like behaviors, *Glycobiology*. 17 (2007) 1–9. doi:10.1093/glycob/cwl047.
- [457] E.M. Sajdel-Sulkowska, Immunofluorescent detection of CD15-fucosylated glycoconjugates in primary cerebellar cultures and their function in glial-neuronal adhesion in the central nervous system., *Acta Biochim. Pol.* 45 (1998) 781–790. <http://www.ncbi.nlm.nih.gov/pubmed/9918505> (accessed July 29, 2019).
- [458] P. Contessotto, B.W. Ellis, C. Jin, N.G. Karlsson, P. Zorlutuna, M. Kilcoyne, A. Pandit, Distinct glycosylation in membrane proteins within neonatal versus adult myocardial tissue, *Matrix Biol.* (2019). doi:10.1016/J.MATBIO.2019.05.001.
- [459] N. Sharon, H. Lis, History of lectins: from hemagglutinins to biological recognition molecules, *Glycobiology*. 14 (2004) 53R–62R. doi:10.1093/glycob/cwh122.
- [460] J. Dorszewska, M. Predecki, M. Lianeri, W. Kozubski, Molecular effects of L-dopa therapy in Parkinson’s Disease., *Curr. Genomics*. 15 (2014) 11–7. doi:10.2174/1389202914666131210213042.
- [461] O. Lindvall, A. Björklund, Cell therapy in Parkinson’s disease., *NeuroRx*. 1 (2004) 382–93. doi:10.1602/neurorx.1.4.382.
- [462] J.L. Eriksen, Z. Wszolek, L. Petrucelli, Molecular pathogenesis of Parkinson Disease, *Arch. Neurol.* 62 (2005) 353. doi:10.1001/archneur.62.3.353.
- [463] S. Tabbal, S. Fahn, S. Frucht, Fetal tissue transplantation in Parkinson’s disease, *Curr. Opin. Neurol.* 11 (1998) 341–349. doi:10.1097/00019052-199808000-00010.
- [464] S.R. Sinclair, J.W. Fawcett, S.B. Dunnett, Delayed implantation of nigral grafts improves survival of dopamine neurones and rate of functional recovery, *Neuroreport*. 10 (1999) 1263–1267. doi:10.1097/00001756-199904260-00020.
- [465] S.R. Sinclair, C.N. Svendsen, E.M. Torres, D. Martin, J.W. Fawcett, S.B. Dunnett, GDNF enhances dopaminergic cell survival and fibre outgrowth in embryonic nigral grafts, *Neuroreport*. 7 (1996) 2547–2552. doi:10.1097/00001756-199611040-00029.
- [466] A.M. Sullivan, J. Pohl, S.B. Blunt, Growth/differentiation factor 5 and glial cell line-derived neurotrophic factor enhance survival and function of dopaminergic grafts in a rat model of Parkinson’s disease., *Eur. J. Neurosci.* 10 (1998) 3681–3688. doi:10.1046/j.1460-9568.1998.00378.x.
- [467] P. Brundin, A. Björklund, Survival, growth and function of dopaminergic neurons grafted to the brain., *Prog. Brain Res.* 71 (1987) 293–308. doi:10.1016/S0079-6123(08)61832-4.
- [468] S. Glozman, E. Yavin, Lipid peroxides are generated by the fetal rat brain after episodes of global ischemia in utero, *Neurochem. Res.* 22 (1997) 201–208. doi:10.1023/A:1027371725159.

- [469] R.A. Barker, H. Widner, Immune problems in central nervous system cell therapy, *NeuroRX*. 1 (2004) 472–481. doi:10.1602/neurorx.1.4.472.
- [470] D.R. Lynch, T.M. Dawson, Secondary mechanisms in neuronal trauma, *Curr. Opin. Neurol.* 7 (1994) 510–516. doi:10.1097/00019052-199412000-00007.
- [471] R.S. Ghirnikar, Y.L. Lee, L.F. Eng, Inflammation in traumatic brain injury:role of cytokines and chemokines, *Neurochem. Res.* 23 (1998) 329–340. doi:10.1023/A:1022453332560.
- [472] R.D. Azbill, X. Mu, A.J. Bruce-Keller, M.P. Mattson, J.E. Springer, Impaired mitochondrial function, oxidative stress and altered antioxidant enzyme activities following traumatic spinal cord injury., *Brain Res.* 765 (1997) 283–90. doi:10.1016/s0006-8993(97)00573-8.
- [473] T.J. Collier, C.E. Sortwell, Therapeutic Potential of Nerve Growth Factors in Parkinson's Disease, *Drugs Aging.* 14 (1999) 261–287. doi:10.2165/00002512-199914040-00003.
- [474] C. Mouritzen, M. Drömer, H.O. Keinecke, The effect of fibrin glueing to seal bronchial and alveolar leakages after pulmonary resections and decortications., *Eur. J. Cardiothorac. Surg.* 7 (1993) 75–80. doi:10.1016/1010-7940(93)90184-d.
- [475] G. Zhang, C.T. Drinnan, L.R. Geuss, L.J. Suggs, Vascular differentiation of bone marrow stem cells is directed by a tunable three-dimensional matrix, *Acta Biomater.* 6 (2010) 3395–3403. doi:10.1016/j.actbio.2010.03.019.
- [476] L. Andereggen, M. Meyer, R. Guzman, A.D. Ducray, H.R. Widmer, Effects of GDNF pretreatment on function and survival of transplanted fetal ventral mesencephalic cells in the 6-OHDA rat model of Parkinson's disease, *Brain Res.* 1276 (2009) 39–49. doi:10.1016/j.brainres.2009.04.021.
- [477] M. Espejo, B. Cutillas, E. Arenas, S. Ambrosio, Increased survival of dopaminergic neurons in striatal grafts of fetal ventral mesencephalic cells exposed to Neurotrophin-3 or Glial Cell Line-Derived Neurotrophic Factor, *Cell Transplant.* 9 (2000) 45–53. doi:10.1177/096368970000900107.
- [478] S.B. Dunnett, A. Björklund, Basic neural transplantation techniques. I. Dissociated cell suspension grafts of embryonic ventral mesencephalon in the adult rat brain, *Brain Res. Protoc.* 1 (1997) 91–99. doi:10.1016/S1385-299X(96)00015-3.
- [479] T. Schallert, S.M. Fleming, J.L. Leasure, J.L. Tillerson, S.T. Bland, CNS plasticity and assessment of forelimb sensorimotor outcome in unilateral rat models of stroke, cortical ablation, parkinsonism and spinal cord injury, *Neuropharmacology.* 39 (2000) 777–787. doi:10.1016/S0028-3908(00)00005-8.
- [480] R.-J. Su, J.-L. Zhen, W. Wang, J.-L. Zhang, Y. Zheng, X.-M. Wang, Time-course behavioral features are correlated with Parkinson's disease-associated pathology in a 6-hydroxydopamine hemiparkinsonian rat model., *Mol. Med. Rep.* 17 (2018) 3356–3363. doi:10.3892/mmr.2017.8277.
- [481] P. Brundin, O.G. Nilsson, R.E. Strecker, O. Lindvall, B. Astedt, A. Björklund, Behavioural effects of human fetal dopamine neurons grafted in a rat model of Parkinson's disease., *Exp. Brain Res.* 65 (1986) 235–40. doi:10.1007/bf00243848.

- [482] A. Björklund, S.B. Dunnett, U. Stenevi, M.E. Lewis, S.D. Iversen, Reinnervation of the denervated striatum by substantia nigra transplants: Functional consequences as revealed by pharmacological and sensorimotor testing, *Brain Res.* 199 (1980) 307–333. doi:10.1016/0006-8993(80)90692-7.
- [483] E. Dowd, S.B. Dunnett, Deficits in a lateralized associative learning task in dopamine-depleted rats with functional recovery by dopamine-rich transplants, *Eur. J. Neurosci.* 20 (2004) 1953–1959. doi:10.1111/j.1460-9568.2004.03637.x.
- [484] O. Lindvall, S. Rehnström, P. Brundin, B. Gustavii, B. Astedt, H. Widner, T. Lindholm, A. Björklund, K.L. Leenders, J.C. Rothwell, R. Frackowiak, D. Marsden, B. Johnels, G. Steg, R. Freedman, B.J. Hoffer, A. Seiger, M. Bygdeman, I. Strömberg, L. Olson, Human fetal dopamine neurons grafted into the striatum in two patients with severe Parkinson's Disease, *Arch. Neurol.* 46 (1989) 615. doi:10.1001/archneur.1989.00520420033021.
- [485] T.J. Mahalik, W.E. Hahn, G.H. Clayton, G.P. Owens, Programmed cell death in developing grafts of fetal substantia nigra, *Exp. Neurol.* 129 (1994) 27–36. doi:10.1006/EXNR.1994.1144.
- [486] T.A.E. Ahmed, R. Ringuette, V.A. Wallace, M. Griffith, Autologous fibrin glue as an encapsulating scaffold for delivery of retinal progenitor cells, *Front. Bioeng. Biotechnol.* 2 (2015) 85. doi:10.3389/fbioe.2014.00085.
- [487] M.A. Chernousov, D.J. Carey, α V β 8 integrin is a Schwann cell receptor for fibrin, *Exp. Cell Res.* 291 (2003) 514–524. doi:10.1016/S0014-4827(03)00409-9.
- [488] A. Salsmann, E. Schaffner-Reckinger, F. Kabile, S. Plançon, N. Kieffer, A new functional role of the fibrinogen RGD motif as the molecular switch that selectively triggers integrin α IIb β 3-dependent RhoA activation during cell spreading., *J. Biol. Chem.* 280 (2005) 33610–9. doi:10.1074/jbc.M500146200.
- [489] U. Ungerstedt, Postsynaptic supersensitivity after 6-Hydroxy-dopamine induced degeneration of the nigro-striatal dopamine system, *Acta Physiol. Scand.* 82 (1971) 69–93. doi:10.1111/j.1365-201X.1971.tb11000.x.
- [490] Z. Wen, Z. Yan, K. Hu, Z. Pang, X. Cheng, L. Guo, Q. Zhang, X. Jiang, L. Fang, R. Lai, Odorranalectin-conjugated nanoparticles: Preparation, brain delivery and pharmacodynamic study on Parkinson's disease following intranasal administration, *J. Control. Release.* 151 (2011) 131–138. doi:10.1016/J.JCONREL.2011.02.022.
- [491] U. Ungerstedt, G.W. Arbuthnott, Quantitative recording of rotational behavior in rats after 6-hydroxy-dopamine lesions of the nigrostriatal dopamine system, *Brain Res.* 24 (1970) 485–493. doi:10.1016/0006-8993(70)90187-3.
- [492] R. Iancu, P. Mohapel, P. Brundin, G. Paul, Behavioral characterization of a unilateral 6-OHDA-lesion model of Parkinson's disease in mice, *Behav. Brain Res.* 162 (2005) 1–10. doi:10.1016/J.BBR.2005.02.023.
- [493] K. Hu, Y. Shi, W. Jiang, J. Han, S. Huang, X. Jiang, Lactoferrin conjugated PEG-PLGA nanoparticles for brain delivery: Preparation, characterization and efficacy in Parkinson's disease, *Int. J. Pharm.* 415 (2011) 273–283. doi:10.1016/J.IJPHARM.2011.05.062.
- [494] C. Saraiva, J. Paiva, T. Santos, L. Ferreira, L. Bernardino, MicroRNA-124 loaded

- nanoparticles enhance brain repair in Parkinson's disease, *J. Control. Release.* 235 (2016) 291–305. doi:10.1016/J.JCONREL.2016.06.005.
- [495] Y.-Z. Zhao, R.-R. Jin, W. Yang, Q. Xiang, W.-Z. Yu, Q. Lin, F.-R. Tian, K.-L. Mao, C.-Z. Lv, Y.-X.J. Wang, C.-T. Lu, Using gelatin nanoparticle mediated intranasal delivery of neuropeptide Substance P to enhance neuro-recovery in hemiparkinsonian rats, *PLoS One.* 11 (2016) e0148848. doi:10.1371/journal.pone.0148848.
- [496] S.B. Dunnett, I.Q. Whishaw, D.C. Rogers, G.H. Jones, Dopamine-rich grafts ameliorate whole body motor asymmetry and sensory neglect but not independent limb use in rats with 6-hydroxydopamine lesions., *Brain Res.* 415 (1987) 63–78.
- [497] J.M. Klug, A.B. Norman, Long-term sensitization of apomorphine-induced rotation behavior in rats with dopamine deafferentation or excitotoxin lesions of the striatum., *Pharmacol. Biochem. Behav.* 46 (1993) 397–403.
- [498] A. Abuirmeileh, R. Lever, A.E. Kingsbury, A.J. Lees, I.C. Locke, R.A. Knight, H.S. Chowdrey, C.S. Biggs, P.S. Whitton, The corticotrophin-releasing factor-like peptide urocortin reverses key deficits in two rodent models of Parkinson's disease, *Eur. J. Neurosci.* 26 (2007) 417–423. doi:10.1111/j.1460-9568.2007.05653.x.
- [499] E.B. Torres, K.M. Heilman, H. Poizner, Impaired endogenously evoked automated reaching in Parkinson's disease., *J. Neurosci.* 31 (2011) 17848–17863. doi:10.1523/JNEUROSCI.1150-11.2011.
- [500] K.E. Glajch, S.M. Fleming, D.J. Surmeier, P. Osten, Sensorimotor assessment of the unilateral 6-hydroxydopamine mouse model of Parkinson's disease., *Behav. Brain Res.* 230 (2012) 309–316. doi:10.1016/j.bbr.2011.12.007.
- [501] O.-B. Tysnes, A. Storstein, Epidemiology of Parkinson's disease, *J. Neural Transm.* 124 (2017) 901–905. doi:10.1007/s00702-017-1686-y.
- [502] P.A. LeWitt, Levodopa therapy for Parkinson's disease: pharmacokinetics and pharmacodynamics, *Mov. Disord.* 30 (2015) 64–72. doi:10.1002/mds.26082.
- [503] M.A. Hely, J.G.L. Morris, W.G.J. Reid, R. Trafficante, Sydney multicenter study of Parkinson's disease: Non-L-dopa-responsive problems dominate at 15 years, *Mov. Disord.* 20 (2005) 190–199. doi:10.1002/mds.20324.
- [504] P. Brundin, R.E. Strecker, O. Lindvall, O. Isacson, O.G. Nilsson, G. Barbin, A. Prochiantz, C. Forni, A. Nieoull, H. Widner, F.H. Gage, A. Bjorklund, Intracerebral grafting of dopamine neurons., *Ann. N. Y. Acad. Sci.* 495 (1987) 473–495. doi:10.1111/j.1749-6632.1987.tb23695.x.
- [505] R.A. Barker, J. Barrett, S.L. Mason, A. Björklund, Fetal dopaminergic transplantation trials and the future of neural grafting in Parkinson's disease, *Lancet Neurol.* 12 (2013) 84–91. doi:10.1016/S1474-4422(12)70295-8.
- [506] S. Browne, G. Fontana, B.J. Rodriguez, A. Pandit, A protective extracellular matrix-based gene delivery reservoir fabricated by electrostatic charge manipulation, *Mol. Pharm.* 9 (2012) 3099–3106. doi:10.1021/mp300231d.
- [507] A.F. Williams, R.B. Parekh, D.R. Wing, A.C. Willis, A.N. Barclay, R. Dalchau, J.W. Fabre, R.A. Dwek, T.W. Rademacher, Comparative analysis of the *N*-glycans of rat, mouse and human Thy-1. Site-specific oligosaccharide patterns of neural Thy-1, a member of the immunoglobulin superfamily, *Glycobiology.* 3 (1993) 339–348.

- doi:10.1093/glycob/3.4.339.
- [508] Y. Mechref, M. V. Novotny, C. Krishnan, Structural characterization of oligosaccharides using Maldi-TOF/TOF tandem mass spectrometry, *Anal. Chem.* 75 (2003) 4895–4903. doi:10.1021/ac0341968.
- [509] P.B. O'Connor, E. Mirgorodskaya, C.E. Costello, High pressure matrix-assisted laser desorption/ionization Fourier transform mass spectrometry for minimization of ganglioside fragmentation, *J. Am. Soc. Mass Spectrom.* 13 (2002) 402–407. doi:10.1016/S1044-0305(02)00351-3.
- [510] P.B. O'Connor, C.E. Costello, A high pressure matrix-assisted laser desorption/ionization Fourier transform mass spectrometry ion source for thermal stabilization of labile biomolecules, *Rapid Commun. Mass Spectrom.* 15 (2001) 1862–1868. doi:10.1002/rcm.447.
- [511] A. Schober, Classic toxin-induced animal models of Parkinson's disease: 6-OHDA and MPTP, *Cell Tissue Res.* 318 (2004) 215–224. doi:10.1007/s00441-004-0938-y.
- [512] R. Betarbet, T.B. Sherer, J.T. Greenamyre, Animal models of Parkinson's disease, *BioEssays.* 24 (2002) 308–318. doi:10.1002/bies.10067.
- [513] M.A. Cenci, I.Q. Whishaw, T. Schallert, Animal models of neurological deficits: how relevant is the rat?, *Nat. Rev. Neurosci.* 3 (2002) 574–579. doi:10.1038/nrn877.
- [514] W.M. Pardridge, Drug transport across the blood-brain barrier., *J. Cereb. Blood Flow Metab.* 32 (2012) 1959–1972. doi:10.1038/jcbfm.2012.126.
- [515] G.A. Silva, Nanotechnology applications and approaches for neuroregeneration and drug delivery to the central nervous system., *Ann. N. Y. Acad. Sci.* 1199 (2010) 221–230. doi:10.1111/j.1749-6632.2009.05361.x.
- [516] Q. Peng, S. Zhang, Q. Yang, T. Zhang, X.-Q. Wei, L. Jiang, C.-L. Zhang, Q.-M. Chen, Z.-R. Zhang, Y.-F. Lin, Preformed albumin corona, a protective coating for nanoparticles based drug delivery system., *Biomaterials.* 34 (2013) 8521–8530. doi:10.1016/j.biomaterials.2013.07.102.
- [517] R.C. Lai, R.W.Y. Yeo, K.H. Tan, S.K. Lim, Exosomes for drug delivery - a novel application for the mesenchymal stem cell., *Biotechnol. Adv.* 31 (2013) 543–51. doi:10.1016/j.biotechadv.2012.08.008.
- [518] Y. Tian, S. Li, J. Song, T. Ji, M. Zhu, G. Anderson, J. Wei, G. Nie, A doxorubicin delivery platform using engineered natural membrane vesicle exosomes for targeted tumor therapy., *Biomaterials.* 35 (2014) 2383–2390. doi:10.1016/J.BIOMATERIALS.2013.11.083.
- [519] L. Alvarez-Erviti, Y. Seow, H. Yin, C. Betts, S. Lakhali, M.J.A. Wood, Delivery of siRNA to the mouse brain by systemic injection of targeted exosomes., *Nat. Biotechnol.* 29 (2011) 341–5. doi:10.1038/nbt.1807.
- [520] T.L. Lentz, Rabies virus binding to an acetylcholine receptor alpha-subunit peptide., *J. Mol. Recognit.* 3 (1990) 82–88. doi:10.1002/jmr.300030205.
- [521] K. Hira, Y. Ueno, R. Tanaka, N. Miyamoto, K. Yamashiro, T. Inaba, T. Urabe, H. Okano, N. Hattori, Astrocyte-derived exosomes treated with a Semaphorin 3A inhibitor enhance stroke recovery via Prostaglandin D2 synthase., *Stroke.* 49 (2018)

- 2483–2494. doi:10.1161/STROKEAHA.118.021272.
- [522] M.A. Lopez-Verrilli, A. Caviedes, A. Cabrera, S. Sandoval, U. Wyneken, M. Khoury, Mesenchymal stem cell-derived exosomes from different sources selectively promote neuritic outgrowth, *Neuroscience*. 320 (2016) 129–139. doi:10.1016/J.NEUROSCIENCE.2016.01.061.
- [523] J. Wei, Y. Chen, C. Xue, B. Ma, Y. Shen, J. Guan, X. Bao, H. Wu, Q. Han, R. Wang, C. Zhao, Protection of nerve injury with exosome extracted from mesenchymal stem cell., *Zhongguo Yi Xue Ke Xue Yuan Xue Bao*. 38 (2016) 33–36. doi:10.3881/j.issn.1000-503X.2016.01.006.
- [524] J.P. de Rivero Vaccari, F. Brand, S. Adamczak, S.W. Lee, J. Perez-Barcena, M.Y. Wang, M.R. Bullock, W.D. Dietrich, R.W. Keane, Exosome-mediated inflammasome signaling after central nervous system injury, *J. Neurochem*. 136 (2016) 39–48. doi:10.1111/jnc.13036.
- [525] K. Takahashi, S. Yamanaka, Induction of pluripotent stem cells from mouse embryonic and adult fibroblast cultures by defined factors, *Cell*. 126 (2006) 663–676. doi:10.1016/j.cell.2006.07.024.
- [526] K. Landsteiner, C.P. Miller, Serological studies on the blood of the primates : II. The blood groups in anthropoid apes., *J. Exp. Med*. 42 (1925) 853–862. doi:10.1084/jem.42.6.853.
- [527] X. Yang, J. Tang, C.E. Rogler, P. Stanley, C. Rogler, P. Stanley, Reduced hepatocyte proliferation is the basis of retarded liver tumor progression and liver regeneration in mice lacking N-acetylglucosaminyltransferase III., *Cancer Res*. 63 (2003) 7753–7759. doi:10.1158/0008-5472.can-09-2719.
- [528] L. Russo, A. Sgambato, M. Lecchi, V. Pastori, M. Raspanti, A. Natalello, S.M. Doglia, F. Nicotra, L. Cipolla, Neoglycosylated collagen matrices drive neuronal cells to differentiate, *ACS Chem. Neurosci*. 5 (2014) 261–265. doi:10.1021/cn400222s.
- [529] A. Didonna, F. Benetti, Post-translational modifications in neurodegeneration, *AIMS Biophys*. 3 (2015) 27–49. doi:10.3934/biophys.2016.1.27.
- [530] Y. Li, G. Wu, G.S. Dawe, L. Zeng, S. Cui, G. Loers, T. Tilling, L. Sun, M. Schachner, Z.-C. Xiao, Cell surface sialylation and fucosylation are regulated by L1 via phospholipase C γ and cooperate to modulate neurite outgrowth, cell Survival and migration, *PLoS One*. 3 (2008) e3841. doi:10.1371/journal.pone.0003841.
- [531] I.L. Mohd Isa, S.A. Abbah, M. Kilcoyne, D. Sakai, P. Dockery, D.P. Finn, A. Pandit, Implantation of hyaluronic acid hydrogel prevents the pain phenotype in a rat model of intervertebral disc injury, *Sci. Adv*. 4 (2018) eaaq0597. doi:10.1126/sciadv.aaq0597.

Chapter 2

Fibrin-based microsphere reservoirs for delivery of neurotrophic factors to the brain

Sections of this chapter have been published:

Samal J., Hoban D.B., Naughton M., Concannon R., Dowd E., Pandit A.P. (2015). "Fibrin-based microsphere reservoirs for delivery of neurotrophic factors to the brain." *Nanomedicine* 10(5): 765-783.

2.1 Introduction

Neurotrophic factors promote the differentiation, growth and phenotypic maintenance of neurons. These factors are required both for an initial phase of development of the neuronal circuitry and in the later phase for the maintenance and modulation of neurons essential to proper functioning of the brain [1]. Several studies have shown that neurotrophic factors can modulate neuronal dysfunction. Neurotrophic factors also confer protection to specific neuronal populations by suppression of apoptotic gene expression [2, 3]. Nerve growth factor (NGF), targets the basal forebrain cholinergic and sympathetic neurons [4]. Several studies in rodents [5, 6, 7] and primates [8] have shown the efficacy of NGF in preventing the degenerative changes to cholinergic neurons. Clinically the administration of NGF has resulted in reduction of neuronal death in the basal forebrain of AD patients [9]. There are studies which have shown that NGF plays a role in generation of pain and hyperalgesia by sensitizing the nociceptors and NGF-Trk A signalling interaction which enhances acute and chronic pain by regulating several receptors and signalling molecules [10, 11]. However, in several clinical assays the elevated levels of NGF have been correlated to chronic pain syndromes [12, 13]. However, there is still a potential deficit in designing a suitable delivery vehicle for neurotrophic factors that sustain their therapeutic effects *in vivo*. A significant hurdle in neurotrophic factor delivery is their inability to cross the blood- brain- barrier (BBB) due their size and polarity. In clinical settings, neurotrophic factors must be delivered in significant doses and targeted to the site of interest to avoid any adverse response. Besides, neurotrophic factors have a short half-life, which renders them unsuitable for any clinical applications [14].

In order to increase the efficacy of neurotrophic factors, it is required to devise a delivery platform to ensure the constant delivery of therapeutically relevant doses at the target site. Cellular therapies have been investigated in this context [15, 16]. These strategies either aim at the replacement of lost neuronal subtypes or provide suitable environmental cues for supporting host neurons. Stem cells have been engineered to achieve the production of several neurotrophic factors (e.g. BDNF, GDNF) which have been shown to achieve functional recovery in pre-clinical models of several neurodegenerative disorders such as Parkinson's disease, Alzheimer disease [17, 18]. However, stem cells show limited differentiation potential and show poor graft survival [19]. To circumvent these issues associated with the traditional cell-based therapies, a biomaterials-based approach has significant merit.

Several biomaterials-based delivery systems have been reported for the delivery of neurotrophic factors. These systems can be broadly classified into affinity-based systems and reservoir-based systems [20]. Both synthetic [21, 22] and natural polymers [23] have been used for the fabrication of such systems. There is a growing interest in the development of extracellular matrix (ECM)-mimicking delivery systems which have an impact on cellular signalling while delivering therapeutic molecules [24].

Fibrin has been used as a surgical sealant [25] for over two decades and more recently as an encapsulation platform for cells, owing to its ability to support cell growth and direct their differentiation to different phenotypes [26]. The physiological process of polymerization of fibrin involves cross-linking fibrinogen using thrombin and factor XIII. The use of these *in-situ* polymers and enzymes allows the formation of an autologous delivery system that obviates any concerns relating to immune response. It was therefore considered as the biomaterial of choice in this study for developing a reservoir-based delivery platform for NGF. In this study, it was hypothesized that a modification of the template charge manipulation method [27, 28, 29] can be used to fabricate a fibrin based ECM-mimicking reservoir platform to obtain a controlled delivery of neurotrophic factors. The specific objectives were to fabricate and characterize the fibrin-based reservoir system, evaluate the loading and release profiles, investigate its interaction with cells, assess the impact of neurotrophin encapsulation on its bioactivity and perform a preliminary *in vivo* assessment of the system at the targeted site.

2.2 Materials & Methods

2.2.1 Fabrication of hollow fibrin microspheres

Hollow fibrin microspheres were fabricated using a modified template charge manipulation method as represented in **Figure 2.1** [27]. Briefly, polystyrene beads (Gentaur, Chicago, Illinois) of defined sizes (0.5 μm , 0.8 μm , 1.24 μm and 4 μm) (5% w/v) were spun down at 4500 rpm. This was followed by the resuspension of the beads in poly-L-lysine (PLL) solution (1 mg/ml) for three h to impart a strong positive charge. The beads were then washed with deionised water followed by resuspension in fibrinogen solution (10 mg/ml in 130 KIU/ml solution of aprotinin) (Sealer protein concentrate, TISSEEL^R kit, Baxter Healthcare) for four h with stirring at room temperature followed by three washes with deionised water. Cross-linking of the fibrinogen coating was performed using an equal volume of thrombin solution (4IU, TISSEEL^R kit, Baxter Healthcare). The mixture was agitated for one h at room temperature. To produce the hollow spheres, the polystyrene core was dissolved by washing the coated beads

with tetrahydrofuran (THF). THF was added to the solution of fibrin coated polystyrene templates in 1:1 ratio and agitated for 30 minutes. This step was repeated twice to ensure complete removal of polystyrene. Hollow spheres were washed twice with deionised water and twice with 70% ethanol to ensure removal of any traces of THF.

2.2.2 Morphological characterization of fibrin hollow spheres

The morphology of the polystyrene template, fibrinogen coated polystyrene templates and hollow microspheres were evaluated using scanning electron microscopy (SEM) (Hitachi S-4700 field emission microscope operating with a beam voltage of 15 kV). The samples were placed on carbon tabs mounted on the SEM specimen stubs and then dried. This was followed by gold-coating using an Emitech K550 coating system (Derby, England, U.K.). Transmission electron microscopy was done for morphological characterization of hollow fibrin microspheres using Hitachi H7500 Transmission Electron Microscope.

2.2.3 Analysis of template removal

Removal of the polystyrene template following THF treatment was confirmed using infrared spectrum analysis of the spheres. The characteristic peaks of polystyrene and their absence in the fibrin microspheres was noted. Samples were vacuum dried and subsequently analysed using a Fourier transform infrared spectrometer (Varian 660-IR).

2.2.4 Size and zeta potential analysis of fibrin microspheres

The size of the microspheres was monitored during the process of fabrication using dynamic light scattering (DLS) (Zeta sizer (Malvern, Nano-ZS90). Also, zeta potential measurements were performed to analyze the charge on microspheres as well as the charge on the template during the process of fabrication. The stability of the hollow fibrin spheres was studied over a period of seven days in phosphate buffered saline (PBS) and Dulbecco's Minimal Essential Medium (DMEM) by measuring size and zeta potential over this time period. Similar measurements were performed for assessing the stability of the spheres over a range of pH and ionic strengths.

2.2.5 Fluorescent labelling of NGF and fibrin

Human β NGF (Alomone Laboratories, Jerusalem, Israel) was chosen as a model protein to demonstrate loading and release rates from the hollow fibrin spheres. Fluorescent labelling of NGF and fibrin hollow microspheres was used to facilitate detection of the loading process. Rhodamine B isothiocyanate (Sigma-aldrich) was used to fluorescently tag NGF. Fluorescent

labelling of fibrin microspheres was done by incubating one milligram of hollow fibrin spheres with 1 mg/mL fluorescein isothiocyanate (Invitrogen, Dublin, Ireland) for four h on a shaker RT and followed by washing with ethanol and deionised water.

2.2.6 Loading of hollow fibrin microspheres with NGF

Microspheres were loaded with NGF by re-suspending 1 mg of hollow fibrin spheres in 300 μ l of PBS–0.05% Tween solution (loading buffer) containing different amounts of NGF (2, 4, 6, 8 and 10 μ g). The hollow fibrin spheres were then incubated on a shaker at room temperature for 24 h to allow the growth factor to diffuse into the hollow spheres. Spheres of different sizes (0.5 μ m, 0.8 μ m, 1.24 μ m and 4 μ m) were tested for their loading efficiency using the same procedure. Samples were then spun down for 20 minutes at 14000 rpm to collect the loaded hollow spheres and supernatant was analysed using NGF-ELISA (R&D Systems, Abingdon, U.K.). Calculation of loading efficiency of different sizes of hollow fibrin spheres and doses of NGF was done on the basis of NGF detected in supernatant. Visual detection of growth factor loading onto the hollow spheres was done by fluorescent labelling of the spheres and growth factor and observing the loaded hollow spheres under an inverted fluorescence microscope (Olympus IX81, Mason Technologies, Dublin, Ireland).

2.2.7 Release profile of NGF from hollow fibrin spheres

Characterization of release profile from fibrin spheres was done in release buffer (PBS–0.05% Tween 20) at 37 °C as an acellular release system. Growth factor-loaded microspheres (1 mg) were incubated with 300 μ l of the release buffer, and at different time points microspheres were spun down and supernatant was collected. The collected supernatant was frozen at –20 °C until ELISA was conducted.

2.2.8 Internalization study of fibrin spheres using rMSCs

FITC-labelled fibrin hollow spheres were incubated with rMSCs on a four well chamber slide for 24 h. The medium was then removed and the wells were washed with hanks balanced salt solution (HBSS) to remove any non- internalized spheres. Cells were then fixed with 4% paraformaldehyde, permeablized with 1% Triton-X, and stained with rhodamine-phalloidin and DAPI before being mounted. Cells were then examined under an inverted fluorescence microscope.

2.2.9 Cytotoxicity of hollow fibrin spheres

The toxicity of different doses of fibrin spheres (10 µg, 50 µg, 100 µg, 200 µg, 500 µg/ well) was evaluated using PC-12 cells cultured in DMEM, 10% horse serum and 5% fetal bovine serum, 0.7% L glutamine, 1% pen/strep as well as rMSCs cultured in 1:1 DMEM: alpha MEM, 10% FBS, 1% pen/strep. Cells were seeded in 24-well plates for live/dead assay (Molecular Probes) and alamarBlue™ assay (Invitrogen, Dublin, Ireland). Cells were exposed to the specified doses of fibrin microspheres in culture and imaged using inverted fluorescence microscope after 48 hours. Live cells were stained green with calcein and ethidium homodimer stained the dead cells red. Impact on the metabolic activity of the cells was measured using alamarBlue™ assay at 24 and 48 h post treatment with microspheres. Non- treated cells and 10% DMSO-treated cells were used as controls.

2.2.10 Bioactivity of released NGF

The impact of growth factor loading on the bioactivity of NGF released from hollow fibrin spheres was evaluated using a neurite outgrowth assay using PC-12 cells. NGF-loaded fibrin spheres were added to PC-12 cells seeded on coverslips in 24-well plate and cells were incubated at 37 °C. The change in morphology of PC-12 cells in response to NGF treatment and released NGF from fibrin spheres was observed by examining cells under an inverted light microscope every second day. Supernatants were collected for ELISA analysis to determine the release of NGF from fibrin spheres in the cellular-release system. At the final time point, after collection of supernatant, cells were fixed with ice-cold methanol and stored at -20 °C before immunostaining them for neurites.

2.2.11 Immunostaining of neurites

Cells fixed on coverslips were washed twice in PBS for five minutes at RT. The samples were then incubated in blocking buffer (2% BSA in PBS) for one hour. The cells were then incubated with a neuron-specific βIII tubulin monoclonal antibody (Millipore, Cat. MAB1637) at a 1:200 dilution in blocking buffer. Following overnight incubation with primary antibody at 4 °C, coverslips were washed and secondary fluorescent antibody Alexa FluorR 488 donkey anti-mouse (Invitrogen) was used for one h at room temperature. Coverslips were washed twice in PBS and incubated with DAPI–PBS solution (1 µg/mL) for five min. After washing in PBS, coverslips were mounted on slides with Vectashield™ (Labkem, Ireland) and stored at 4 °C before image analysis. Imaging was done using an inverted fluorescent microscope (Olympus IX81, Mason Technologies, Dublin, Ireland).

2.2.12 Analysis of neurite length

Neurite outgrowth from differentiated PC12 cells was determined from images stained with β III tubulin using ImageJ software (MosaicJ, Philippe Thevenaz). The length of neurites was measured manually for the test and control groups. Thirty neurites were measured per group.

2.2.13 In vivo study

All procedures were carried out in accordance with the Cruelty to Animals Act 1876 under an animal licence (B100/3827) issued by the Irish Department of Health and Children. Procedures were carried out in accordance with European Union Directive 2010/63/EU and S.I. No. 543 of 2012, and were approved by the Animal Ethics Committee of the National University of Ireland, Galway. Thirty six male Sprague Dawley rats were divided into three groups for each of the four time points (day 1, 4, 7, 14) for intrastriatal injections with NGF, fibrin spheres and NGF-loaded fibrin spheres (n=3 per group per time-point). The animals were then sacrificed at the respective time points and the brains were collected for the subsequent analysis of NGF release and host response.

2.2.14 Surgery and perfusion

NGF, hollow fibrin spheres and NGF-loaded fibrin spheres were injected into the striatum bilaterally under isoflurane anaesthesia (5% in oxygen for induction and 2% in oxygen for maintenance) at stereotaxic coordinates AP = 0.0, ML \pm 3.7 and DV -5.0 mm from bregma with the nose bar set to -2.3 mm. Fibrin spheres were resuspended in 5 μ l of phosphate buffered saline (PBS) for injection. Pentobarbital injection (100 mg/kg i.p.) was given to rats for terminal anaesthesia. This was followed by transcardial perfusion with 100 ml of heparinised saline (5000 units/litre) and 150 ml of ice cold 4% paraformaldehyde in phosphate buffer. Brains were dissected out and post-fixation was done for four h at room temperature. The brains were then transferred to 25% sucrose in phosphate buffer. Serial brain sections (30 μ m) were obtained using a freezing stage sledge microtome (Bright, Cambridgeshire, UK). Sections were stored at 4°C in tris-azide buffer until used for immunohistochemistry.

2.2.15 Peroxidase-based immunohistochemistry

Immunohistochemical staining for NGF, fibrin, GFAP and OX-42 was completed on a 1:12 series of sections using a peroxidase-based method. Briefly, quenching of endogenous

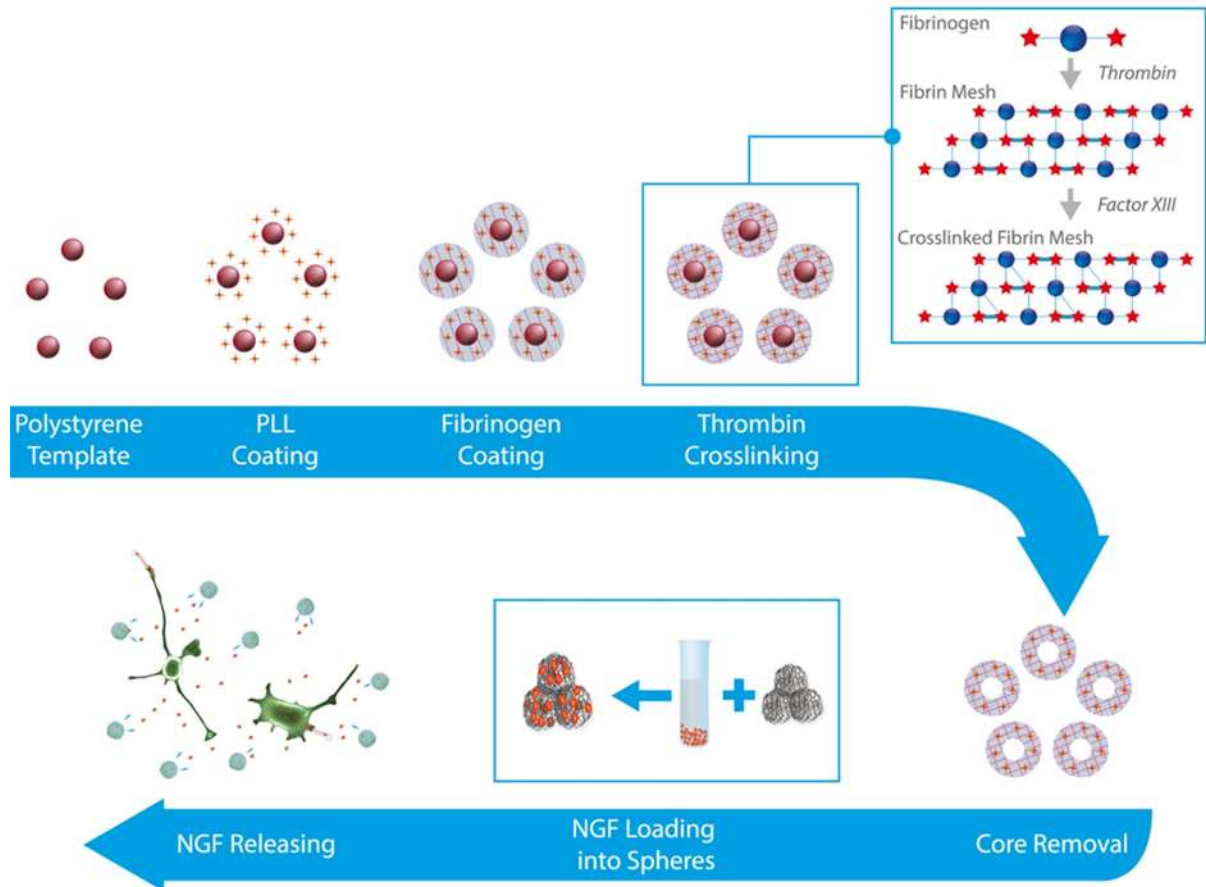


Figure 2.1: A schematic outline of the modified template charge manipulation method used for the fabrication of hollow fibrin spheres which were used as a controlled delivery platform for NGF.

Table 2.1: Targets and antibodies used for immunohistochemistry of rat brain sections.

Target	Primary Antibody	Secondary Antibody
Fibrin	Mouse anti-fibrin (Merck, MABS2155),(1:1000)	Horse anti-mouse (1:200)
NGF	Rabbit anti-NGF (Abcam, ab6199),(1:1000)	Goat anti-rabbit (1:200)
Rat Microglia	Mouse anti-OX-42 (Chemicon, CBL1512) (1:2000)	Horse anti-mouse (1:200)
Rat Astrocytes	Rabbit anit-GFAP (DAKO, N1506), (1:200)	Goat anti-rabbit (1:200)

peroxidase activity was done with a solution of 3% hydrogen peroxide and 10% methanol in distilled water. The sections were incubated in a 3% solution of the appropriate normal serum to avoid the nonspecific binding of the antibody. Overnight incubation of the sections was performed in the relevant primary antibodies at room temperature (**Table 2.1**). The incubation was followed by incubation in biotinylated secondary antibody for three h as represented in **Table 2.1**. The sections were then incubated with streptavidin-biotin-peroxidase complex for two h and developed with 3, 3'-diaminobenzidine (DAB). Developed sections were mounted on gelatin-coated slides and were dehydrated through a series of alcohol concentrations and cleared using xylene before being coverslipped using DPX mountant.

2.2.16 Statistical analysis

All data is presented as mean \pm SD. Single factor paired one tailed students t-test was used for the analysis of the significance of the variations. The groups with $p \leq 0.05$ were considered significantly different.

2.3 Results

2.3.1 Fabrication and morphological characterization of hollow fibrin spheres

Hollow fibrin spheres were fabricated using the template method developed in our laboratory. A modification of this method was used in this study for the fabrication of fibrin spheres as represented by **Figure 2.1**. **Figure 2.2A** shows the SEM images of different stages of fabrication process. The spheres so formed showed a smooth, round morphology in SEM images and fairly uniform size distribution. **Figure 2.2B** represents the magnified SEM image of fibrin spheres showing the hollow cavity of the spheres. The TEM image shows overlaps between the spheres indicating a hollow core (**Figure 2.2C**). Any traces of polystyrene remaining in the core will result in an unfavourable host response. The complete polystyrene core removal was confirmed using ATR-FTIR. The samples after the THF dissolution step did not show the characteristic polystyrene peaks as highlighted in **Figure 2.3A** which indicated the absence of a polystyrene core whereas amide I, amide II and amide III peaks characteristic of proteins were seen in the samples. This augmented the results from SEM and TEM, thereby confirming the lack of polystyrene core which is potentially toxic *in vivo*.

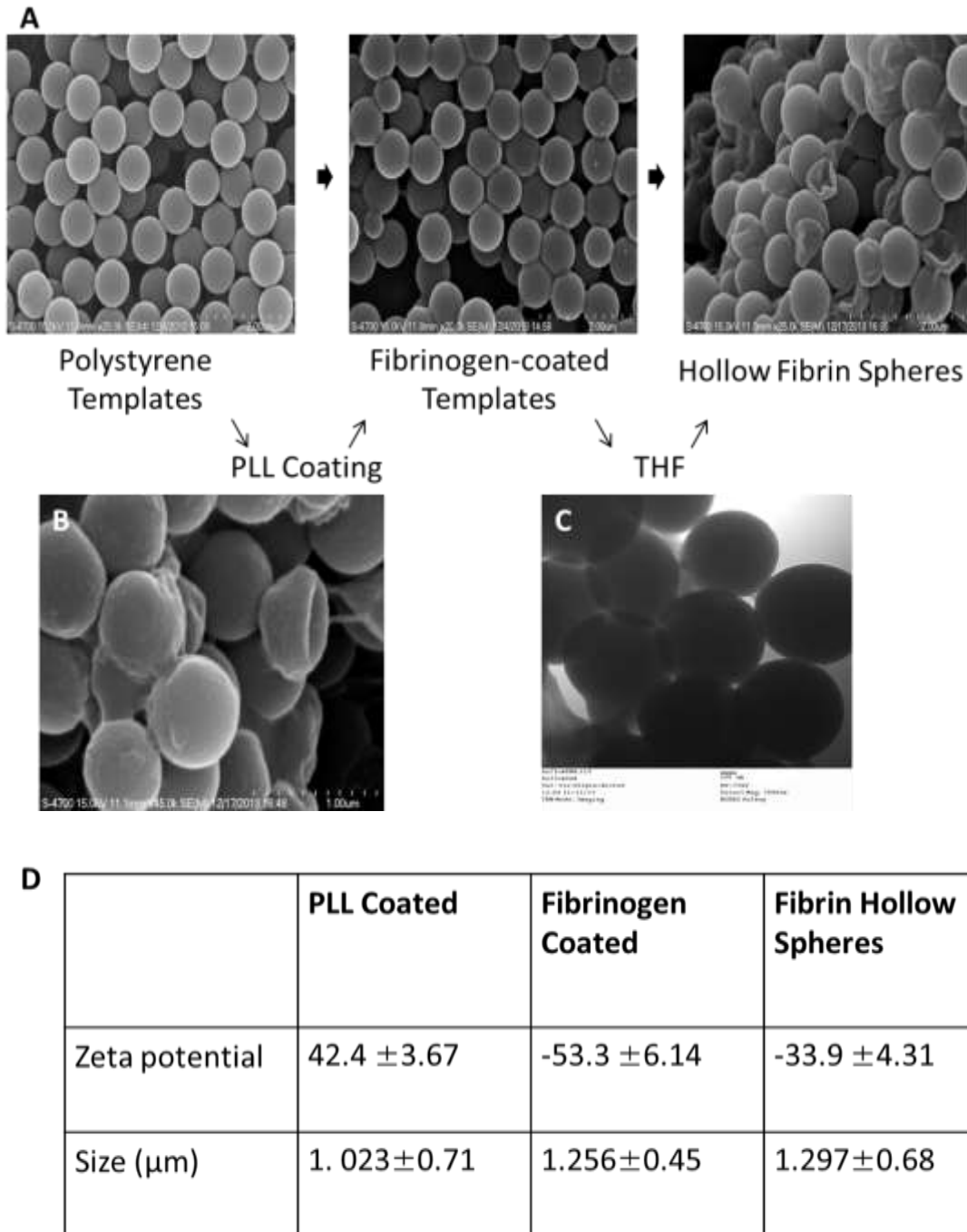


Figure 2.2: Fabrication of the fibrin hollow microspheres. A) Different stages of microspheres fabrication represented by SEM images of polystyrene template, fibrinogen-coated templates and hollow fibrin spheres obtained after cross-linking fibrinogen coating with thrombin and core dissolution using THF, B) Magnified SEM image representing hollow cavity of fibrin spheres C) TEM image showing overlap between the spheres indicative of the absence of solid core. D) Changes in size and zeta potential obtained during different stages of hollow sphere fabrication using a 1.08 μm polystyrene template. PLL coating imparts a positive charge to the template which changes to negative charge after fibrinogen coating (n=8).

2.3.2 Stability of hollow fibrin microspheres

There were detectable changes in the size and zeta potential of polystyrene templates through the process of fabrication as represented in **Figure 2.2D** which were indicative of the formation of hollow spheres. The zeta potential on the spheres was found to be around -33.9 mV under physiological conditions. The stability of the hollow fibrin spheres was tested under a wide range of conditions to assess its suitability as a delivery platform for a wide range of therapeutic applications. There was an increase in the zeta potential when the spheres were tested against 100 mM-1000 mM NaCl (**Figure 2.3B**) which was due to the presence and adsorption of high concentration of ions in the solution which alters the surface charge on the spheres. Zeta potential varied from -16.51 mV to -12.39 mV. However, the spheres retained sufficient negative potential to form a stable suspension. Since the isoelectric point of fibrinogen is around 5.4, the spheres were found to have positive zeta potential below this pH and strong negative zeta above pH 5.4 (**Figure 2.3C**). The values varied from 30.47 mV to -31.35 mV. However, the spheres were found to be stable over a period of seven days in both PBS as well as cell culture media showing a sufficiently negative zeta potential (**Figure 2.3D, E**). The zeta potential was less negative in cell culture media due to the masking impact of proteins present in culture media [33]. The spheres were, therefore, found to be stable over a wide range of physiological conditions.

2.3.3 Loading and release profile from hollow fibrin spheres

Human β -NGF was taken as a model neurotrophic factor to demonstrate the loading efficiency and release profile from the fibrin spheres. To illustrate the protein loading onto the fibrin spheres, NGF and fibrin spheres were fluorescently labelled. **Figure 2.4A** shows the co-localisation of fluorescent signals from NGF and fibrin which is indicative of protein loading. Also, ELISA was performed to determine the amount of NGF loaded as a function of size of the spheres, keeping the concentration of protein constant and dose of NGF using 4 μ m templated fibrin spheres. Highest loading efficiency (~90%) was observed for 4 μ m-templated fibrin spheres and this was found to remain more or less constant for all doses of NGF $\geq 6\mu$ g (Figure 3B,C, * $p \leq 0.05$).

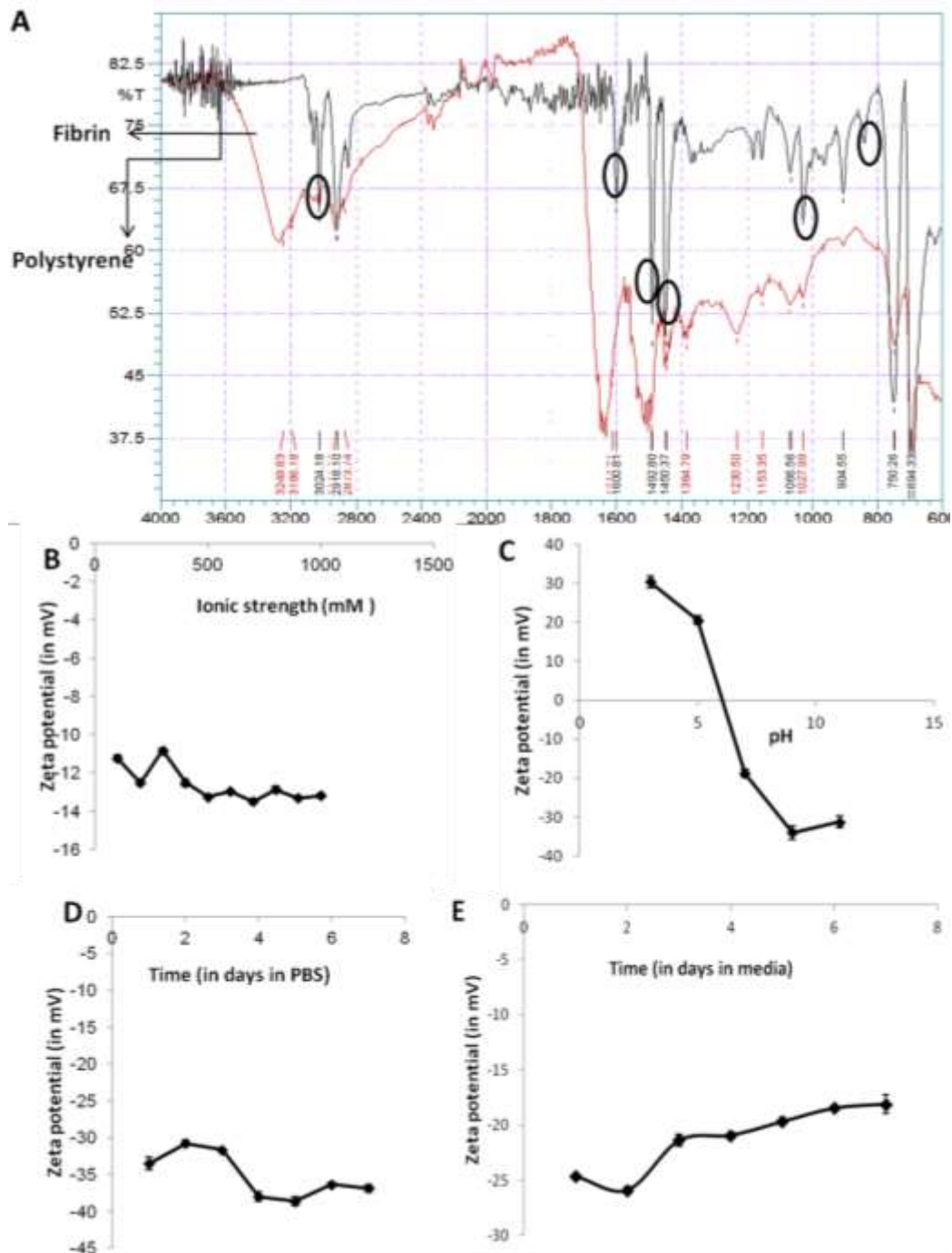


Figure 2.3: Physical characterization and stability of the fibrin hollow microspheres. A) ATR-FTIR spectral analysis (black: polystyrene shells, red: fibrin spheres) representing the absence of characteristic polystyrene peaks in hollow fibrin spheres indicative of complete core removal. Stability analysis of the hollow fibrin spheres performed for over a range of **B)** ionic strengths (100- 1000 mM NaCl), **C)** pH (3.0-11.0) and over a period of seven days in **D)** PBS and **E)** DMEM culture medium. A strong negative charge despite the presence of high concentration of salts and proteins shows the stability of microsphere system (n=8).

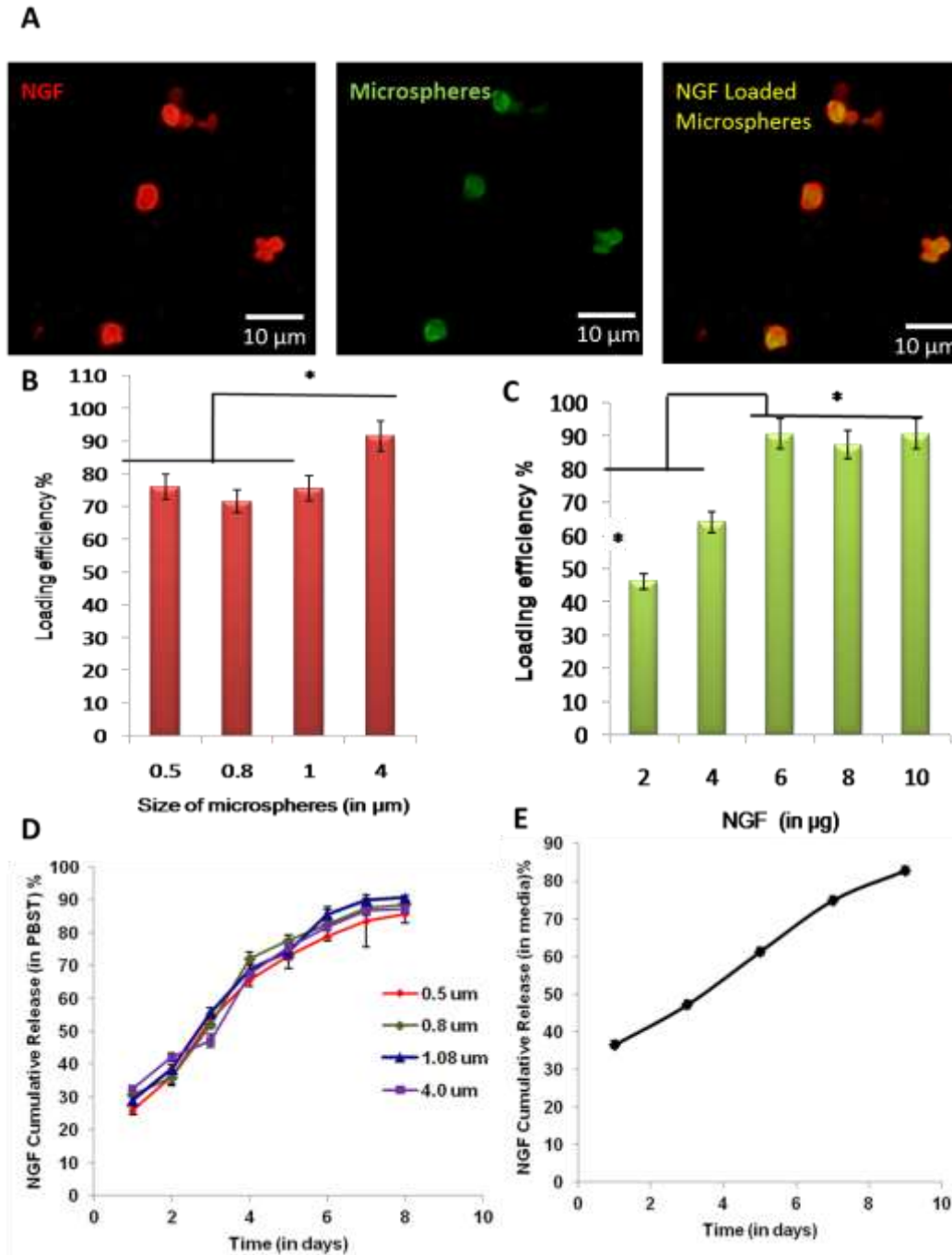


Figure 2.4: Characterization of the loading and release profiles. A) Process of loading of NGF onto hollow fibrin spheres as depicted by fluorescent microscopic images. Co-localization (yellow) in merged image represents that TRITC-labeled NGF (red) was loaded into the FITC-labeled spheres (green). Loading efficiency of hollow spheres after overnight incubation with NGF represented as a function of **B**) size of spheres and **C**) doses of NGF using $4\ \mu\text{m}$ hollow fibrin spheres. ($n=3$, $*p<0.05$), Release profiles of NGF observed from hollow fibrin spheres observed in **D**) PBS for different sizes of spheres and **E**) presence of PC-12 cells using $4\ \mu\text{m}$ hollow fibrin spheres representing initial burst release and release of therapeutic doses of NGF thereafter in both systems ($n=6$).

Release kinetics of NGF from the hollow fibrin spheres was also studied in cellular system using PC-12 cells and acellular PBST system. In the acellular system, hollow fibrin spheres of different sizes were evaluated for NGF release over a period of eight days. There was no significant difference observed in release profiles of spheres of different sizes and there was an initial burst release observed in first six days followed by a stable release of NGF (**Figure 2.4D**). Four micron size of the spheres was tested for release in cellular system because of their high loading efficiency. An initial burst release was observed in cellular system for 24 h which was followed by a linear release profile up to nine days (**Figure 2.4E**).

2.3.4 Internalization of hollow fibrin spheres

Since the fibrin spheres serve as a delivery platform for neurotrophic factors to target cells, it is required that they are not taken up by cells and persist at the target site to achieve the controlled release over a desired time period. In terms of loading capacity, 4 μm - templated spheres had the highest loading capacity. Therefore, 4 and 1.08 μm -templated spheres were tested for the cellular uptake by using FITC-labelled spheres and incubating them with rMSCs. Fluorescent microscopy images (**Figure 2.5 B, C**) show that there was no apparent internalization of 4 μm spheres but the immediate lower size of 1.08 μm was taken up by cells.

Also, the spheres did not have any adverse impact after 48 h of incubation with the cells as there was no change in the morphology of cells observed when compared to a PBS-control (**Figure 2.5A**). Based on the high loading efficiency and non-internalization of the 4 μm -templated spheres, these were used for subsequent experiments.

2.3.5 Impact of fibrin spheres on cellular viability

Six different doses (10, 50, 100, 200 and 500 μg / well) of hollow fibrin spheres were tested for their impact on the metabolic activity of both primary cells (rMSCs) and cell line (PC-12 cells). It was found that at high concentration; the spheres did not have an adverse impact on the metabolic activity of both cell types as demonstrated by alamar BlueTM assay (Fig 4D, E). There was no significant difference in metabolic activity when compared to PBS controls (* $p \leq 0.01$). It was essential to test the different doses of microspheres for their impact on the viability, hence a live/dead assay was performed. **Figure 2.6A, B** show that at high doses, there was no toxicity observed for either rMSCs or PC-12s compared to control.

2.3.6 Assessment of bioactivity of released NGF

Impact of the process of NGF loading and retention into hollow fibrin spheres on its bioactivity was shown using the neurite outgrowth assay. It was shown that the released NGF can promote neuronal cell differentiation. For this study, PC-12 cells were used which undergo differentiation into neurons in the presence of NGF. Fibrin spheres loaded with NGF were incubated with PC-12 cells for a period of six days. Light microscopic images show that there was a significant neurite outgrowth indicative of PC-12 differentiation observed after six days in the cells treated with NGF- loaded spheres when compared to untreated PC-12 cells which retain their round morphology and show no neurite formation (Figure 6A). Neurite formation was found to be comparable in the group treated with the loaded spheres as well as regular NGF treatment group. This showed that a sustained release of NGF was obtained over this period of time from the loaded spheres as opposed to single NGF treatment group. Single NGF treatment group showed initial neurite formation which did not extend or branch further. There was no neurite outgrowth observed for the group where the cells were treated with unloaded fibrin spheres. To quantify these observations, β III tubulin immunostaining was performed for all the test groups after a period of six days (Figure 6B). Significant ($*p \leq 0.05$) and comparable neurite outgrowth was observed in regular NGF treatment and NGF loaded fibrin spheres when compared to untreated and fibrin spheres-treated groups where no neurite formation was observed (**Figure 2.7C**).

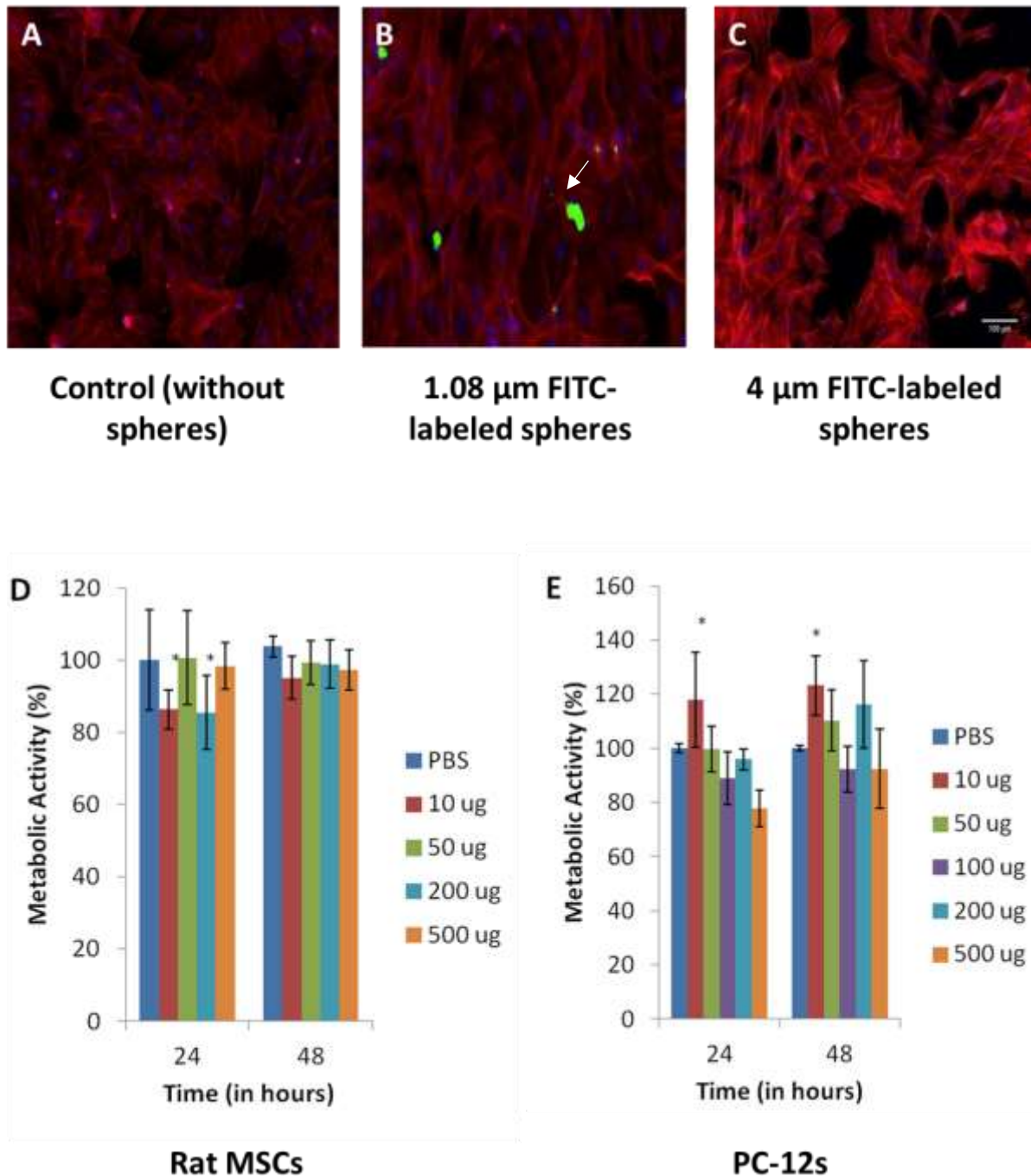


Figure 2.5: Interaction of fibrin hollow spheres with cells. Particle internalization study performed using FITC- labeled spheres incubated with rMSCs for 72 hours. Cells were stained with Rhodamine- phalloidin after washing to show **B**) 1.08 μm spheres were being internalized and **C**) no internalization was observed for 4 μm spheres. Fibrin spheres did not have any adverse impact on cell morphology when compared to **A**) PBS- treated control. alamarBlueTM assay performed for assessment of metabolic activity of **D**) rMSCs and **E**) PC-12s shows that there is no adverse impact of hollow fibrin microspheres even at very high concentrations (500 μg) (n=3, *p<0.05)

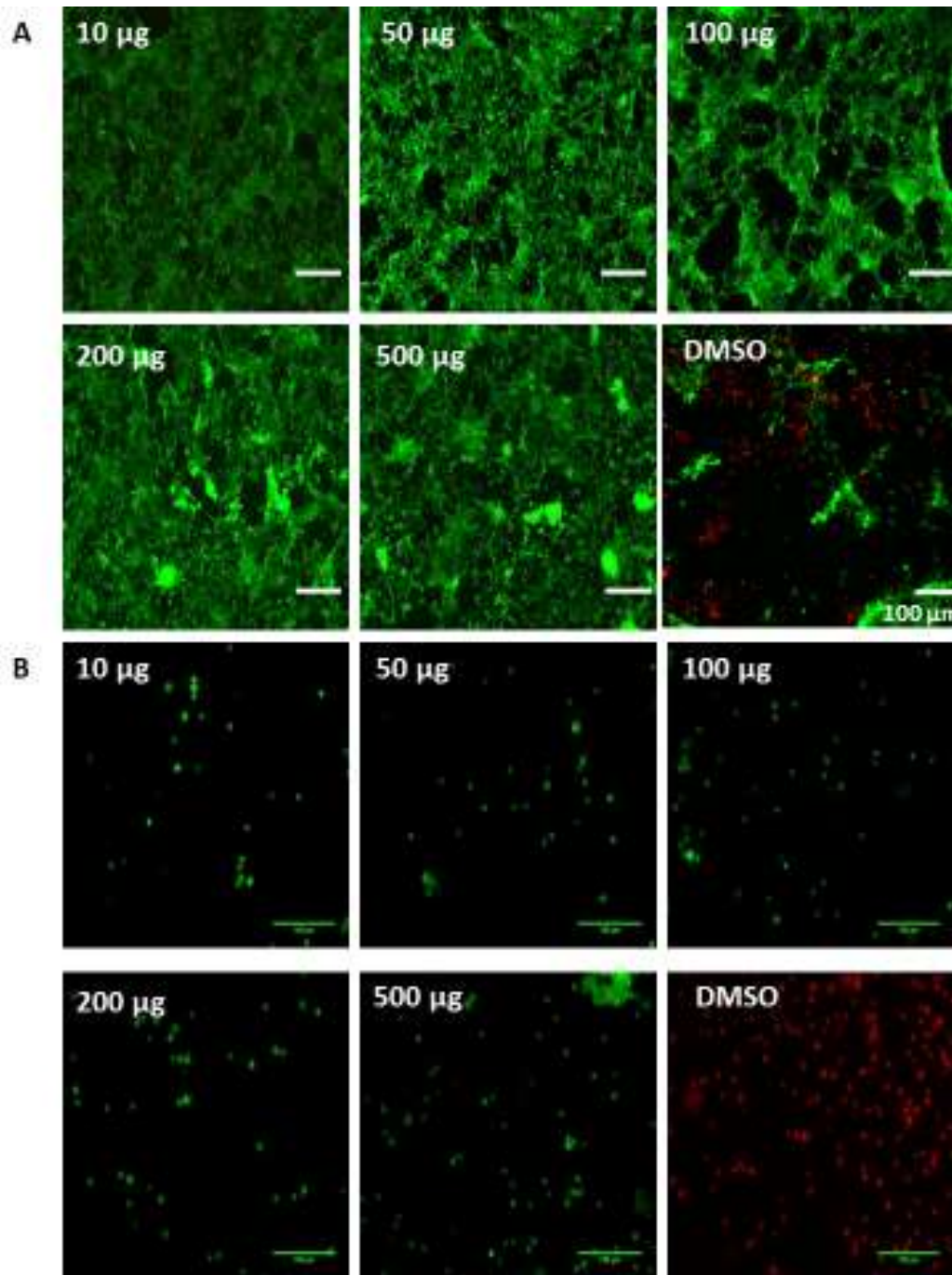


Figure 2.6: Impact of fibrin hollow spheres on cellular viability. Fluorescent microscopic images representing the impact of different doses of hollow fibrin spheres (10, 50, 100, 200, 500 µg/ well) on the viability of **A)** rMSCs and **B)** PC-12 cells compared against DMSO treated controls 48 h post- treatment and tested using Live/Dead assay (Calcein (green): live cells/ EtBr (red): dead cells)

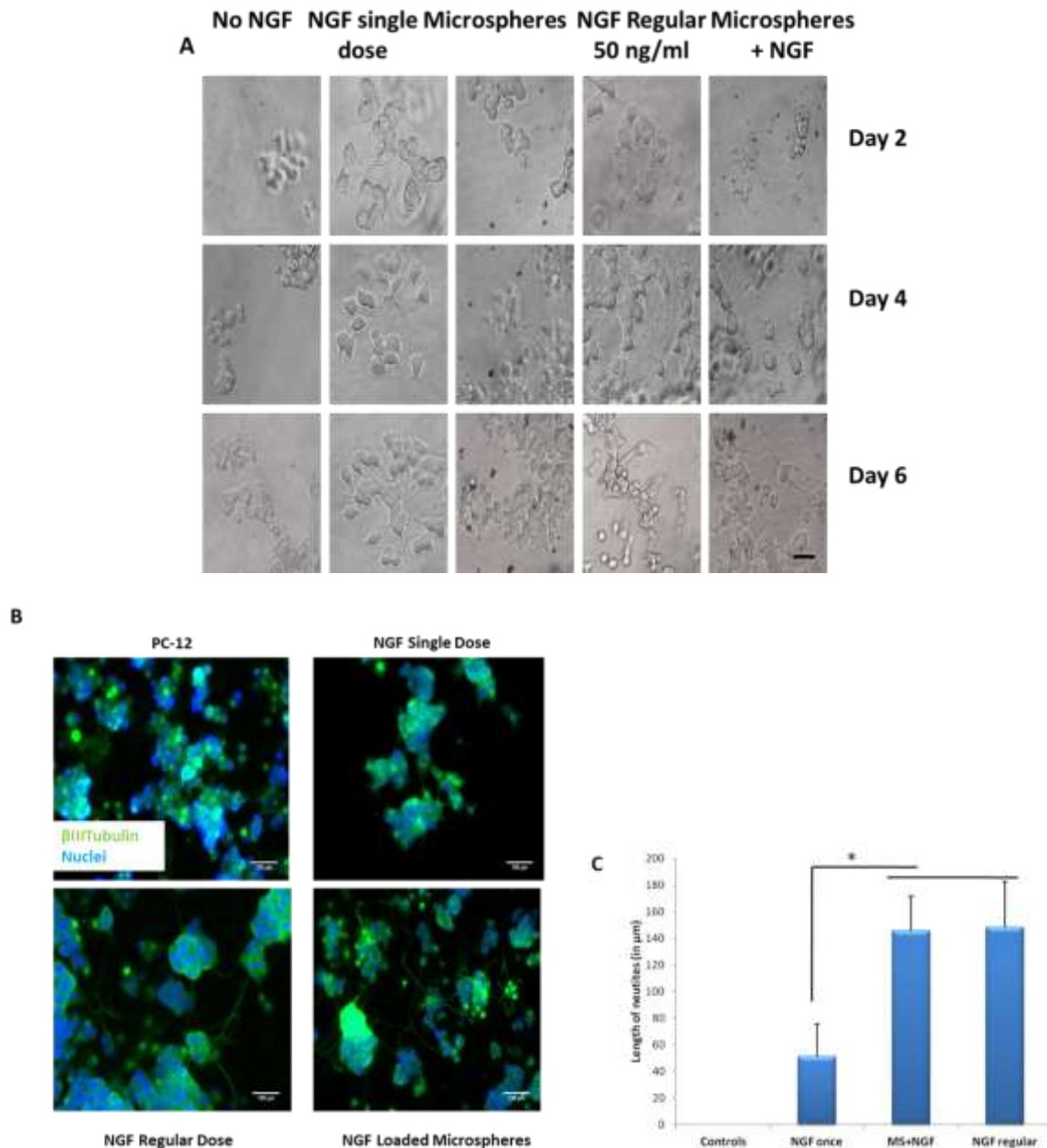


Figure 2.7: Assessment of bioactivity of NGF released from hollow fibrin spheres using PC-12 cells. **A)** Light microscopic images of PC-12s cultured over a period of 6 days and treated with PBS, 50 ng/ml of NGF once and regularly, unloaded spheres and spheres loaded with 275 ng of NGF. Significant and comparable neurite outgrowth was seen in groups with regular NGF treatment and NGF released from fibrin spheres when compared to controls. Neuronal outgrowth in PC12 cells following culture with NGF-loaded spheres (β -III tub staining (green) of differentiated cells). **B)** Representative image of non-treated cells, single treatment with 50 ng/mL NGF, constant treatment with 50 ng/mL NGF, hollow fibrin spheres treatment loaded with 275 ng of NGF. **C)** Significant ($*p < 0.05$) neuronal outgrowth was observed in constant NGF treatment and in all groups treated with NGF-loaded spheres measured in terms of length of neurites using Image J software. Data represents mean \pm SD, $n = 30$ (neurites per group).

2.3.7 *In vivo* assessment of hollow fibrin spheres

In vivo analysis of the fibrin spheres as a delivery system for neurotrophic factors was performed to show the release profile of NGF and host response. Quantitative analysis of NGF release over a period of 14 days showed that a sustained release of NGF was detected in the striatum of the rats injected with NGF-loaded hollow fibrin spheres. Immunohistochemical analysis showed that NGF bolus injected into the striatum was lost after four days post-injection whereas in the group with NGF- loaded fibrin spheres. NGF can be detected after 14 days post-injection (**Figure 2.8A**). Quantification of NGF-positive immunostaining using Image J showed that there was a significant reduction in the immunostained area at Day 4 which reduced to almost no detectable NGF immunostaining at Day 7 in the group injected with NGF. Contrary to this, the immunostained area increased significantly at day 4 when compared to day 1 in the group injected with NGF-loaded fibrin spheres. Positive immunostaining was detected at 14 days post-surgery which indicates the sustained release of NGF from fibrin spheres over this period (**Figure 2.8B**) whereas there is no positive immunostaining is detected in the group injected with fibrin hollow spheres. This was well correlated with the degradation of fibrin spheres as represented in **Figure 2.8C**. The immunohistochemical analysis for fibrin in the brain sections revealed the presence of trace amounts of fibrin around day 14 which supports the controlled release of NGF over a prolonged period of time. The quantifications did not show much differences in the degradation pattern for NGF- loaded and empty fibrin microspheres upon injection in the rat brain (**Figure 2.8D**).

Another important prerequisite for using any growth factor delivery system is that it should not elicit an unfavourable host response. The host response was evaluated qualitatively over a period of 14 days in terms of the microglial and astrocyte migration. The microglial or astrocyte infiltration observed in the striatum after the injection of fibrin spheres was found to be comparable in all three test groups as shown in **Figure 2.9A, B**. This shows that fibrin spheres do not elicit any significant immunogenicity when compared to response caused by injection of NGF. It can thus be concluded that the fibrin hollow spheres are not significantly immunogenic.

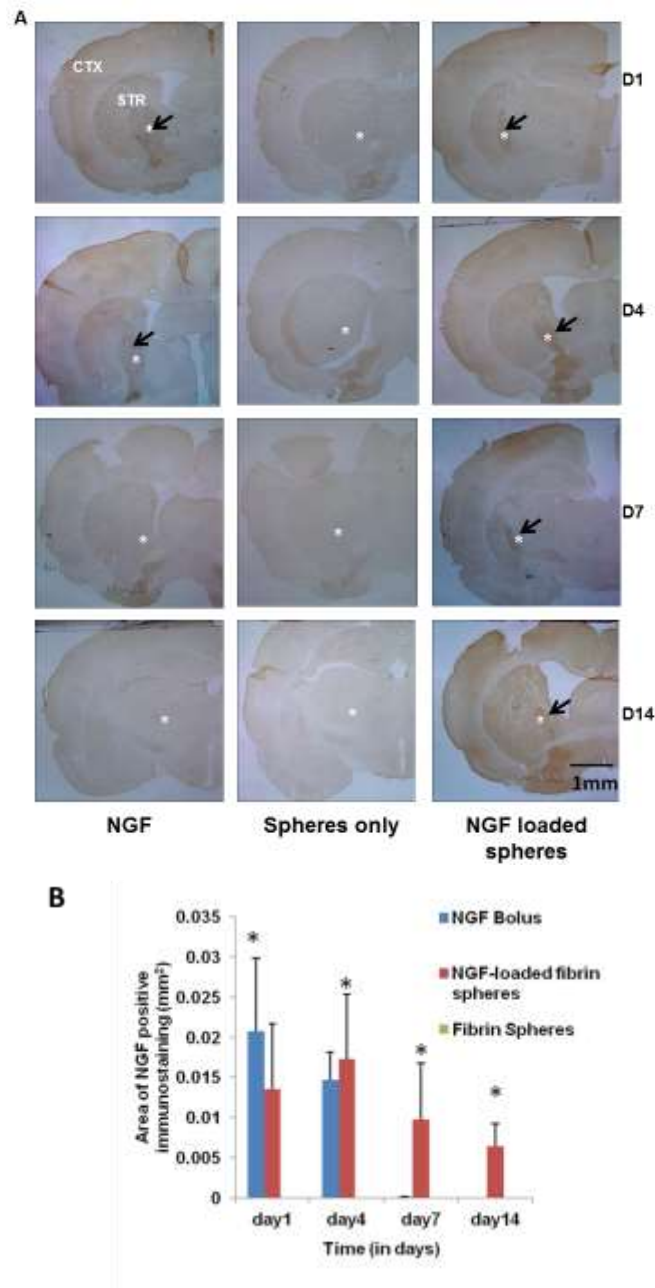


Figure 2.8: Sustained release of NGF *in vivo*. A) Immunohistochemical analyses showing that the experimental group treated with NGF-treated hollow fibrin spheres had a sustained NGF release over a period of 14 days in comparison to NGF bolus which was lost after 4 days of injection. The arrows indicate positive immunostaining for NGF. * indicates the region of implant in striatum where NGF, fibrin spheres and NGF- loaded fibrin spheres were injected (CTX: Cortex, STR: Striatum; Stereotaxic coordinates: AP = 0.0, ML \pm 3.7 and DV -5.0 mm from bregma with the nose bar set to -2.3 mm). Scale bar= 1mm B) Quantification of NGF-positive immunostaining area using Image J software reveals that NGF is detectable after 14 days showing a sustained release of NGF from fibrin spheres. (n=6, *p \leq 0.05).

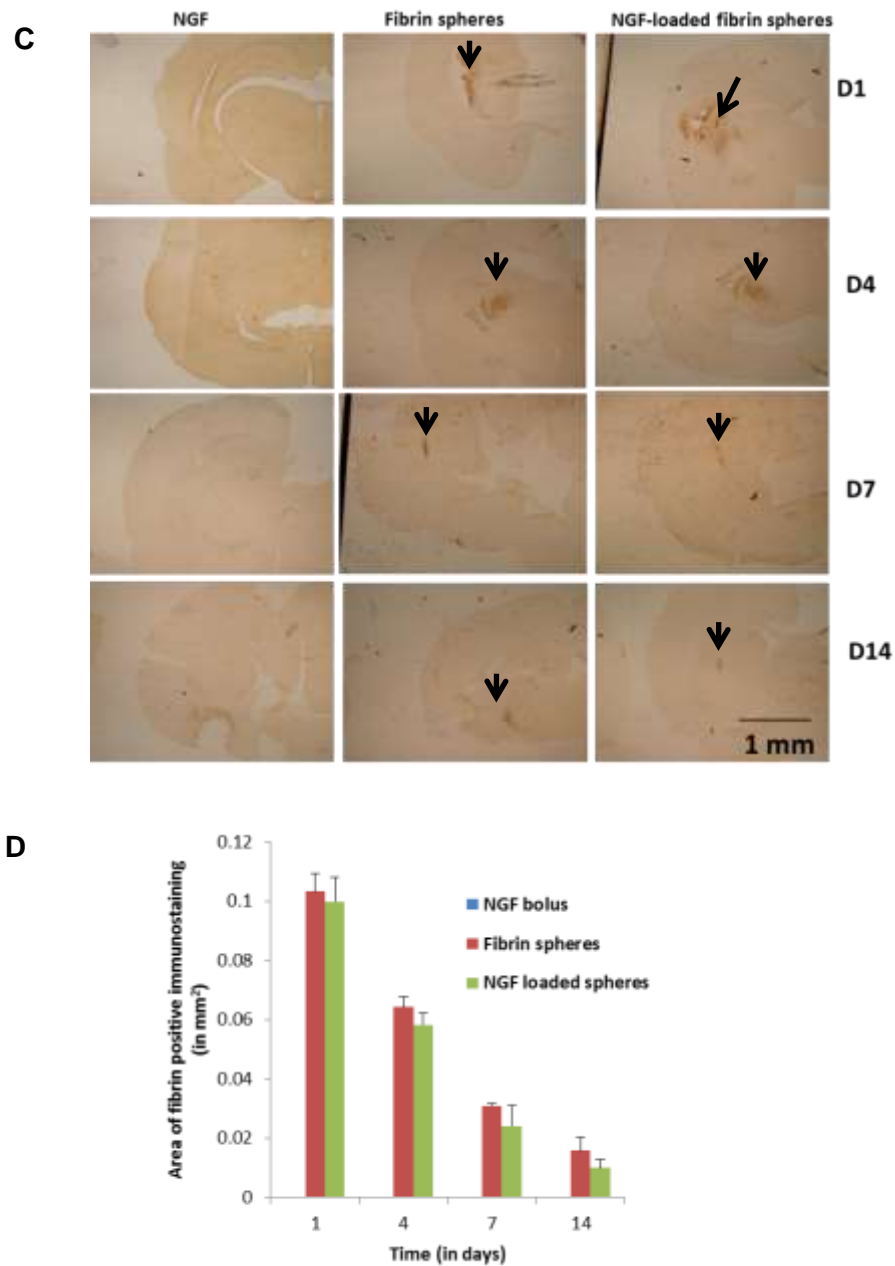


Figure 2.8: *In vivo* degradation of fibrin spheres C) Immunohistochemical analyses showing that the experimental group treated with NGF-treated hollow fibrin spheres showed the traces of fibrin over a period of 14 days in comparison to NGF bolus. The arrows indicate positive immunostaining for fibrin. The region of implant was striatum where NGF, fibrin spheres and NGF- loaded fibrin spheres were injected (CTX: Cortex, STR: Striatum; Stereotaxic coordinates: AP = 0.0, ML \pm 3.7 and DV -5.0 mm from bregma with the nose bar set to -2.3 mm). Scale bar= 1mm D) Quantification of fibrin- positive immunostaining area using Image J software reveals that fibrin- spheres were traceable up to 14 days post-implantation. (n=6, *p \leq 0.05).

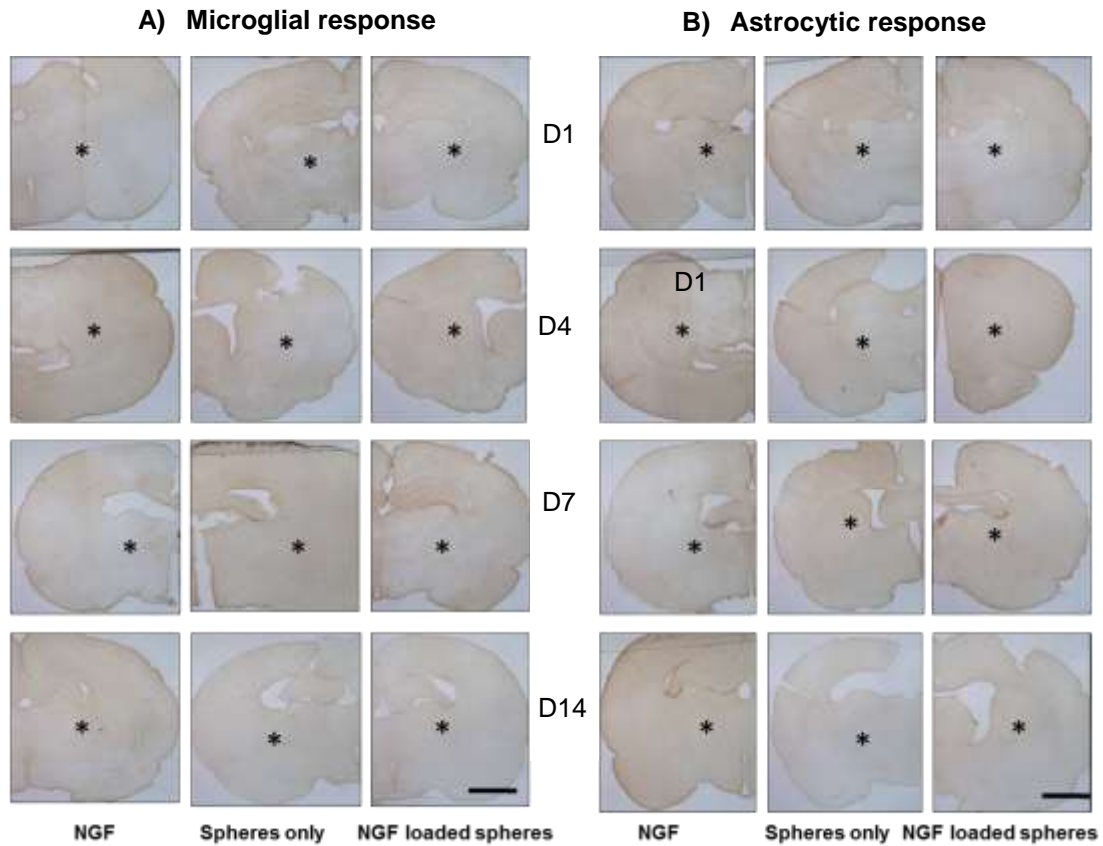


Figure 2.9: Host responses to hollow fibrin microspheres. **A)** microglial (Iba-1) and **B)** astrocytic (GFAP) response in the striatum over a period of 14 days. Qualitative analysis reveals that there was no adverse immune response specific to the hollow fibrin spheres injection over the different time points. * indicates the region of implant in striatum where NGF, fibrin spheres and NGF- loaded fibrin spheres were injected (Stereotaxic coordinates: AP = 0.0, ML \pm 3.7 and DV -5.0 mm from bregma with the nose bar set to -2.3 mm). Scale bar= 1mm.

2.4 Discussion

Neurotrophic factors are a family of growth factors involved in the regulation of the growth and differentiation of the vertebrate nervous system. Their overall levels and the presence of receptors that are expressed plays a key role in determining the spatio-temporal balance between neuronal survival and death [30]. However, their use as a potent therapy to restore neuronal function in central nervous system (CNS) disorders is severely hindered by the presence of the blood brain barrier (BBB) that makes it almost impossible for large proteins and complex compounds to cross from the blood into the brain. This study addresses the issues of delivery and dose from a different perspective. The aim is to modulate their delivery in terms of rate and retention within the microenvironment by using biomaterial-based hollow reservoir system.

The sacrificial template method has been previously used for the fabrication of microsphere reservoirs from extracellular matrix based proteins such as collagen [27, 31] and elastin [29]. The templates were imparted an overall positive charge by PLL coating to allow for fibrinogen binding. Since fibrinogen has an overall negative charge at physiological pH [32], the template charge was manipulated to allow it to interact favourably with polystyrene template. A layer of fibrin was formed around these templates by harnessing the mechanism of clot formation whereby thrombin acts on fibrinogen to form fibrin monomers which are acted upon by factor XIII a to form a cross-linked fibrin mesh. This layer was then cross-linked using thrombin and THF was used to dissolve the polystyrene core. Low concentration of THF and optimized dissolution time prevented the aggregation of fibrin to form larger clumps. Different sizes of polystyrene templates (0.5, 0.8, 1.08 and 4 μm) were used for this purpose.

The SEM and TEM images post-fabrication of the microspheres showed that hollow fibrin spheres can be obtained successfully by manipulating the electrostatic interactions between template and coated macromolecule. The rate of formation and degradation of these fibrin spheres can be regulated as well as their porosity altered in order to control the rates of growth factor loading thus altering the release kinetics [33]. The hollow fibrin spheres developed using this method form an ECM-mimicking system which can be used for controlled delivery purposes and lacks the use of any chemical cross-linkers which have been used for the preparation of microsphere reservoirs. The rationale for the development of a hollow fibrin-based reservoir system was based on the fact that hollow spheres show greater loading capacity compared to solid spheres of the same dimensions [29]. The stability of fibrin hollow spheres

is characterized by their size and zeta potential. An increase in the size and drop in zeta potential is indicative of particle aggregation. The fibrin hollow spheres were tested for stability over a wide range of physio-chemical conditions and time and were found to be stable over varied range of conditions.

Moreover, the hollow structure of these spheres allowed ease of diffusion of NGF into the spheres. The earlier studies have showed comparable loading efficiency can be obtained using the collagen hollow spheres [31]. This system showed a better and sustained release profile compared to collagen hollow spheres in the presence of PC-12 cells where almost 60% of the loaded growth factor was lost in two days [31]. Interestingly, a comparative analysis between the cellular and acellular release showed that the NGF release at subsequent time points was less in cellular system due to NGF uptake by the cells. The uptake was functionally demonstrated by the bioactivity assay in this study. Based on the loading and release kinetics, it was found that 4 μm - templated hollow fibrin spheres showed the best loading capacity and a suitable release profile over the other sizes of spheres.

Furthermore, the impact of these microspheres on the viability and metabolic activity of rat MSCs and PC-12s was also investigated. It was found that even at high doses, there was no significant adverse impact of the microspheres on the viability or metabolic activity of the cells. A potential use of the fibrin hollow spheres in neurodegenerative disorders can be as an adjunct to the existing cell therapy to enhance the survival of engrafted cells by controlled release of neurotrophic factors. It has been shown that NGF treated- MSCs show better engraftment and functional recovery in rodent model of traumatic brain injury [35]. rMSCs were used in this study because transplantation of MSCs in animal models of neurodegenerative diseases resulted in significant behavioural recovery [36, 37] which can be attributed to either neuronal cell replacement or neurotrophic effect of MSCs [38]. Also, MSCs are easily expanded *in vitro* and are capable of trans- differentiating into neuronal cells [39]. This result is in agreement with the previous studies where fibrin was reported to support the viability and growth of mesenchymal stem cells while maintaining their ability to differentiate [40]. It has been shown that by regulating the concentration of fibrinogen and thrombin, fibrin promotes neuronal cell growth [41], neurite extension and branching [42]. Mooney *et al* (2010) showed the specific impact of tailored fibrin gels in selectively promoting the neuronal growth over glial populations [41] which is suggestive of the potential of these microspheres to be used as a therapeutic intervention for neurotrophic factor delivery in various CNS disorders. In order to investigate any potential adverse impact of the loading and release process on the

bioactivity of the released growth factor, an *in vitro* neurite outgrowth assay was performed using PC-12 cells. The results suggested that there was no negative impact of growth factor loading and retention in the fibrin spheres on its bioactivity as a sustained formation and elongation of neurites was observed by the treatment of microsphere-loaded NGF when compared to the bolus NGF.

Previous studies using natural polymers for the fabrication of similar delivery systems for growth factor delivery were never tested for their *in vivo* efficacy [27-29]. To the best of our knowledge, this is the first study evaluating the therapeutic efficacy of a natural-polymer based reservoirs for brain delivery of growth factors *in vivo*. NGF release in the brain was obtained due to diffusion through and degradation of fibrin hollow spheres. The *in vitro* degradation of fibrin hollow spheres is mediated chiefly by matrix metalloproteinases. *In vivo* degradation of fibrin spheres is mediated by the activation of plasminogen by binding to specific sites on fibrin surface that exposes the peptide bond of plasminogen [43]. This is inhibited by aprotinin, a serine protease inhibitor, which is incorporated into fibrin hollow spheres. It forms a reversible complex with active serine residue of plasmin [44], thus providing a controlled release of NGF by controlling the degradation of fibrin hollow spheres. The release of neurotrophic factors can be modulated by tuning the concentrations of fibrinogen and thrombin which makes the system well-adaptable to different release profiles that might be needed for varied therapeutic ends. The immunohistochemical analysis revealed that hollow fibrin microspheres can act as a suitable delivery platform showing no adverse host response while obtaining a sustained growth factor release. This data provides a proof-of-concept study for fibrin hollow spheres platform that can be used for controlled delivery for therapeutic purposes.

2.5 Conclusions

Fibrin hollow microspheres act as a delivery platform for neurotrophic factors showing high loading efficiency for neurotrophic factors and sustained release for a period of 14 days. Also, these microspheres did not show any adverse interactions with both primary cells and neuronal cell line. The bioactivity of neurotrophic factors was not compromised by their loading or release from the fibrin microspheres. When tested qualitatively *in vivo*, fibrin spheres did not elicit any adverse immune response in the host and a sustained release of NGF was observed. Besides, the absence of any chemical cross-linkers in this system offers an advantage over other biomaterial systems used in similar applications. The use of harsh chemicals like THF for the template dissolution and the discontinuation of the polystyrene templates used in the current

by the supplier motivated the investigation of layer-by-layer (LbL) assembly method for the fabrication of hollow fibrin microspheres in the next chapters.

2.7 References

- [1] Weismiller AM, Wu C. Current advances in using neurotrophic factors to treat neurodegenerative disorders. *Transl Neurodegener.*, 1(14), (2012).
- [2] Johnson EM, Chang JY, Koike T, Martin DP. Why do neurons die when deprived of trophic factors? *Neurobiol Aging.*, 10(5), 549-552 (1989).
- [3] Kristiansen M, Ham J. Programmed cell death during neuronal development: the sympathetic neuron model. *Cell Death and Differentiation*, 21(7), 1025-1035 (2014).
- [4] Levi-Montalcini, R. The nerve growth factor 35 years later. *Science*, 237 (4819), 1154–1162 (1987).
- [5] Hefti F. Nerve growth factor (NGF) promotes survival of septal cholinergic neurons after fimbrial transection. *J Neurosci.*, 6(8), 2155- 2162 (1986).
- [6] Kromer LF. Nerve growth factor treatment after brain injury prevents neuronal death. *Science*, 235(4785), 214-216(1987).
- [7] Williams LR, Varon S, Peterson GM, Wictorin K, Fisher W, Bjorklund A, Gage FH. Continuous infusion of nerve growth factor prevents basal forebrain neuronal death. *Proc Natl Acad Sci U S A.*, 83(23), 9231-9235, (1986).
- [8] Tuszynski MH, U HS, Amaral DG, Gage FH. Nerve Growth Factor Infusion in the Primate Brain Reduces Lesion-Induced Cholinergic Neuronal Degeneration. *J Neurosci.*, 10(11), 3604-3614 (1990).
- [9] Saffran BN. Should intracerebroventricular nerve growth factor be used to treat Alzheimer's disease? *Perspect. Biol. Med.*, 35 (4), 471–486 (1992).
- [10] Mantyh PW, Koltzenburg M, Mendell LM, Tive L, Shelton DL. Antagonism of Nerve Growth Factor-trkA Signaling and the Relief of Pain. *Anesthesiology*, 115(1), 189-204 (2011).
- [11] McKelvey L, Shorten GD, O'Keeffe GW. Nerve growth factor-mediated regulation of pain signalling and proposed new intervention strategies in clinical pain management. *J Neurochem.*, 124(3), 276-289 (2013).
- [12] Liu HT, Tyagi P, Chancellor MB, Kuo HC. Urinary nerve growth factor level is increased in patients with interstitial cystitis/bladder pain syndrome and decreased in responders to treatment. *BJU Int.*, 104(10), 1476–1481 (2009).

- [13] Indo Y, Tsuruta M, Hayashida Y, Karim MA, Ohta K, Kawano T, Mitsubuchi H, Tonoki H, Awaya Y, Matsuda I. Mutations in the TRKA/NGF receptor gene in patients with congenital insensitivity to pain with anhidrosis. *Nat Genet.*, 13(4), 485–488 (1996).
- [14] McCall J, Weidner N, Blesch A. Neurotrophic factors in combinatorial approaches for spinal cord regeneration. *Cell Tissue Res.* 349(1), 27–37 (2012).
- [15] Lo B, Parham L. Resolving ethical issues in stem cell clinical trials: the example of Parkinson disease. *J Law Med Ethics.* 38(2), 257–266 (2010).
- [16] Moloney TC, Rooney GE, Barry FP, Howard L, Dowd E. Potential of rat bone marrow-derived mesenchymal stem cells as vehicles for delivery of neurotrophic factors to the Parkinsonian rat brain. *Brain Res.*, 1359, 33–43 (2010).
- [17] Xiong N, Zhang Z, Huang J, Chen C, Zhang Z, Jia M, Xiong J, Liu X, Wang F, Cao X, Liang Z, Sun S, Lin Z, Wang T. VEGF-expressing human umbilical cord mesenchymal stem cells, an improved therapy strategy for Parkinson's disease. *Gene Ther.*, 18(4), 394–402 (2012).
- [18] Lee HJ, Lim IJ, Park SW, Kim YB, Ko Y, Kim SU. Human neural stem cells genetically modified to express human nerve growth factor (NGF) gene restore cognition in the mouse with ibotenic acid-induced cognitive dysfunction. *Cell Transplant.*, 21(11), 2487–2496 (2012).
- [19] Iso Y, Rao KS, Poole CN. Priming with ligands secreted by human stromal progenitor cells promotes grafts of cardiac stem/progenitor cells after myocardial infarction. *Stem Cells.*, 32(3), 674–683(2014).
- [20] Mohtaram NK, Montgomery A, Willerth SM. Biomaterial-based drug delivery systems for the controlled release of neurotrophic factors. *Biomed Mater.*, 8(2), 022001 (2013).
- [21] Sinha V R, Bansal K, Kaushik R, Kumria R, Trehan A. Poly-epsilon-caprolactone microspheres and nanospheres: an overview. *Int. J. Pharm.*, 278(1), 1–23(2004).
- [22] Andrieu-Soler C, Aubert-Pouëssel A, Doat M, Picaud S, Halhal M, Simonutti M, Venier-Julienne MC, Benoit JP, Behar-Cohen F. Intravitreal injection of PLGA microspheres encapsulating GDNF promotes the survival of photoreceptors in the rd1/rd1 mouse. *Mol. Vis.*, 11(120), 118–120 (2005).
- [23] Madduri S, Feldman K, Tervoort T, Papaloizos M, Gander B. Collagen nerve conduits releasing the neurotrophic factors GDNF and NGF. *J. Control. Release*, 143(2), 168–174 (2010).
- [24] Cross M, Dexter TM. Growth factors in development, transformation, and tumorigenesis. *Cell*, 64(2), 271–280 (1991).

- [25] Mouritzen C, Dromer M, Keinecke HO. The effect of fibrin gluing to seal bronchial and alveolar leakages after pulmonary resections and decortications. *Eur J Cardiothorac Surg.*, 7(2), 75–80 (1993).
- [26] Zhang G, Drinnan CT, Geuss LR, Suggs LJ. Vascular differentiation of bone marrow stem cells is directed by a tunable three-dimensional matrix. *Acta Biomater.*, 6(9),3395-3403 (2010).
- [27] Browne S, Fontana G, Rodriguez BJ, Pandit A. A protective extracellular matrix-based gene delivery reservoir fabricated by electrostatic charge manipulation. *Mol. Pharmaceutics.*, 9(11), 3099–2106 (2012).
- [28] Rethore G, Mathew A, Naik H, Pandit A. Preparation of chitosan/polyglutamic acid spheres based on the use of polystyrene template as a nonviral gene carrier. *Tissue Eng., Part C*, 15(4), 605–613 (2009).
- [29] Dash BC, Mahor S, Carroll O, Mathew A, Wang W, Woodhouse KA, Pandit A. Tunable elastin-like polypeptide hollow sphere as a high payload and controlled delivery gene depot. *J. Controlled Release*, 152(3), 382–392(2011).
- [30] Weissmiller AM, We C. Current advances in using neurotrophic factors to treat neurodegenerative disorders. *Transl Neurodegener*, 1(1), 1-14(2012).
- [31] Kraskiewicz H, Breen B, Sargeant T, McMahon S, Pandit A. Assembly of protein-based hollow spheres encapsulating a therapeutic factor. *ACS Chem Neurosci.*, 4(9), 1297-1304 (2013).
- [32] Salim M, O'Sullivan B, McArthur SL, Wright PC. Characterization of fibrinogen adsorption onto glass microcapillary surfaces by ELISA. *Lab Chip.*, 7(1), 64-70 (2007).
- [33] Spicer PP, Mikos AG. Fibrin glue as a drug delivery system. *J Control Release.*, 148(1), 49–55 (2010).
- [34] Leclerc L, Rima W, Boudard D, Pourchez J, Forest V, Bin V, Mowat P, Perriat P, Tillement O, Grosseau P, Bernache-Assollant D, Cottier M. Size of submicrometric and nanometric particles affect cellular uptake and biological activity of macrophages *in vitro*. *Inhal Toxicol.*, 24(9), 580-588 (2012).
- [35] Mahmood A, Lu D, Wang L, Chopp M. Intracerebral transplantation of marrow stromal cells cultured with neurotrophic factors promotes functional recovery in adult rats subjected to traumatic brain injury. *J Neurotrauma.*, 19(12), 1609-1617 (2002).
- [36] Bae JS, Han HS, Youn DH, Carter JE, Mudo M, Schuchman EH, Jin HK. Bone marrow-derived mesenchymal stem cells promote neuronal networks with functional

- synaptic transmission after transplantation into mice with neurodegeneration. *Stem Cells.*, 25(5), 1307-1316 (2007).
- [37] Bouchez G, Sensebe L, Vourc'h P, Garreau L, Bodard S, Rico A, Guilloteau D, Charbord P, Besnard JC, Chalon S. Partial recovery of dopaminergic pathway after graft of adult mesenchymal stem cells in a rat model of Parkinson's disease. *Neurochem Int.*, 52(7), 1332-1342 (2008).
- [38] Chen Q, Long Y, Yuan X, Zou L, Sun J, Chen S, Perez-Polo JR, Yang K. Protective effects of bone marrow stromal cell transplantation in injured rodent brain: synthesis of neurotrophic factors. *J Neurosci Res.*, 80(5), 611-619 (2005).
- [39] Moloney TC, Dockery P, Windebank AJ, Barry FP, Howard L, Dowd E. Survival and immunogenicity of mesenchymal stem cells from the green fluorescent protein transgenic rat in the adult rat brain. *Neurorehabil Neural Repair.*, 24(7), 645-656 (2010).
- [40] Proulx MK, Carey SP, Ditroia LM et al. Fibrin microthreads support mesenchymal stem cell growth while maintaining differentiation potential. *J Biomed Mater Res A.*, 96(2), 301-312 (2011).
- [41] Mooney R, Tawil B, Mahoney M. Specific fibrinogen and thrombin concentrations promote neuronal rather than glial growth when primary neural cells are seeded within plasma-derived fibrin gels. *Tissue Eng Part A.*, 16(5), 1607-1619 (2010).
- [42] Ju YE, Janmey PA, McCormick ME, Sawyer ES, Flanagan LA. Enhanced neurite growth from mammalian neurons in three-dimensional salmon fibrin gels. *Biomaterial.*, 28(12), 2097-2108 (2007).
- [43] Anglés-Cano E. Overview on fibrinolysis: plasminogen activation pathways on fibrin and cell surfaces. *Chem Phys Lipids.*, 67 (68), 353-362 (1994).
- [44] Kang HM1, Kalnoski MH, Frederick M, Chandler WL. The kinetics of plasmin inhibition by aprotinin in vivo. *Thromb Res.*, 115(4), 327-340 (2005).

Chapter 3

Fibrin-in-fibrin intervention for enhanced dopaminergic graft survival

Sections of this chapter are in preparation for publication:

Samal J., Abbah S.A., Lucia A.R., Black A., Drake R., Pandit A. “Fibrin-in-fibrin intervention for enhanced graft survival in Parkinson’s disease: special focus on brain *N*-glycans.”

3.1 Introduction

Parkinson's disease (PD) results primarily from the loss of the dopaminergic (DA) neurons of the substantia nigra (SN) and is associated with cytoplasmic "Lewy body" inclusions in some of the surviving neurons. Selective loss of dopaminergic neurons in a defined region of the brain (SN) makes PD an ideal candidate for cell therapy [1]. It aims at the replacement of what is lost by transplanting dopamine-producing cells into the patients, and thereby reversing the loss of function and initiating regeneration of function. Fetal ventral mesencephalon (VM) is the most commonly used donor source for clinical cell therapy in PD. The donor cells are usually grafted into the striatum as it is the physiological target of the dopamine release. The release is dependent on the graft-derived dopamine neurons making local synaptic connections with the host neurons.

Several studies in the past have shown that embryonic VM grafts can survive, re-innervate the host brain and provide functional compensation in both rodent and primate models of the disease as well as in the human subjects. One of the main problems associated with these grafts is that only 5—10% of implanted dopamine cells survive transplantation [2]. The present requirement for large numbers of human embryonic donors to provide tissue for each host patient and the reliability of dopamine (DA) neuron content of this tissue, are major factors limiting the use of these grafts as a clinical therapy [3]. Previous studies suggest that most of the dopaminergic neurons die within the first week of transplantation. It has been reported that in grafts of ventral mesencephalic tissue the surviving dopaminergic neurons are localized at the periphery of the transplants. This cell death following transplantation can be chiefly attributed to the unavailability of required trophic support and vascularization. In a detailed study performed by Emgard et al. [4], they showed that death of most of grafted neurons occurs within the first 2 weeks after grafting, with a maximum at the shortest time point six days after surgery, and decreases thereafter. The total number of surviving TH-positive neurons or the volume of the transplants at the four time points studied: 6, 10, 14, and 42-days after graft implantation remains more or less unaltered.

One major research strategy to promote dopamine cell survival in grafts has been the application of trophic factors. Glial cell-line derived trophic factor (GDNF) has been found to be particularly effective in promoting dopamine neuron survival *in vitro*. Studies in animals showed that the recombinant protein enhanced survival of midbrain dopamine (DA) neurons and caused sprouting of dopaminergic fibers, increasing neurite outgrowth and cell body size of tyrosine hydroxylase (TH)-positive neurons. It also protected against DA cell neurotoxicity

from 6-hydroxydopamine. Wildtype GDNF of bacterial origin has been shown to have both neurorestorative and neuroprotective properties [5,6] *in vitro* as well as *in vitro* in the rodent [7] and in non-human primate models [8,9], strongly backing up the use of GDNF as potential therapy for PD. GDNF exerts strong therapeutic actions in the animal models of PD by enhancing the phosphorylation of tyrosine hydroxylase which is the rate-limiting enzyme in dopamine synthesis, and mediates an increase in dopamine neuron perikaryal size and the number of neurites [10]. However, GDNF does not cross the blood-brain barrier and the best form of delivery is the direct intra-parenchymal administration into the brain, thereby achieving targeted delivery and minimising the risks of unwanted side-effects caused by the systemic exposure. The major limitation in the translation of GDNF as a clinical therapy stems from its rapid rate of degradation, size and molecular weight that hinder its ability to cross the blood-brain barrier (BBB), thus necessitating the search for alternative routes to bypass the BBB [11].

To this end, the modification of the cellular milieu and modulation of the host environment in terms of biophysical properties and/or biochemical cues like neurotrophins could enhance the survival of transplanted cells in the host. We aim to develop an injectable biomaterial-based intervention which will improve the survival of engrafted dopaminergic progenitor cells by providing adequate physical and trophic support through controlled spatio-temporal release of glial-cell derived neurotrophic factor (GDNF). The fibrin-in-fibrin system comprises of GDNF-loaded fibrin microspheres allowing a controlled release of the growth factor that promotes the survival of the hydrogel- encapsulated VM cells. The fibrin microspheres used for controlled spatio-temporal release of GDNF are fabricated using the layer-by-layer (LbL) assembly by deposition of multiple polyelectrolyte layers to form the template for deposition of fibrin [12]. This was another method of fabrication that was investigated in this project in addition to the template charge manipulation for the fabrication of fibrin hollow microspheres. These degradation and diffusion-based delivery systems can provide sustained release for tunable times.

The natural polymers like collagen, fibrin and silk allow the development of delivery systems that act at the molecular level and minimize inflammation. The encapsulation of cells in tunable fibrin gels could modulate the paracrine secretion profile while providing them with the required immunoprotection to help them survive the initial transplantation phase. We hypothesize that manipulation of the biophysical microenvironment can enhance the dopaminergic precursor ventral mesencephalic (VM) graft survival by promoting cell-cell and cell-matrix interactions and minimising the inflammatory response. Specific objectives of the

study were the fabrication and characterisation of a fibrin-based reservoir system *in vivo*, investigating the loading and release of GDNF using ELISA and to investigate the cellular behaviour on tuneable parameters such as hydrogel concentration, cell densities and microsphere concentrations. A schematic outline of the study design is represented in **Figure 3.1**.

3.2 Materials & Methods

3.2.1 Fabrication of fibrin hollow microspheres

Fibrin hollow microspheres were fabricated via the LbL approach using CaCO₃ microbeads as a sacrificial template and polyarginine (PAR) (Sigma-Aldrich, Dublin) and dextran sulfate (DS) (Sigma-Aldrich, Dublin) as polyelectrolytes. For the fabrication of the sacrificial microbead templates, 0.66 mL of a 1 M Na₂CO₃ solution was mixed with an equal volume of 1 M CaCl₂ solution. After vigorous stirring of these solutions together for 30 s, the obtained dispersion was centrifuged to collect the microbeads followed by washing them three times with a 0.005 M NaCl (wash buffer). This was followed by coating the particles with a 2 mg/mL PA solution of pH 6.5 while stirring. After 15 minutes of incubation, the particles were centrifuged and washed three times with the wash buffer. Then, particles were stirred in a 2 mg/mL DS solution at pH 6.5 for 15 minutes. This process was repeated until two layers of DS and two layers of PA were alternately deposited rendering PA as the pre-final layer to electrostatically support the final layer of fibrinogen. Finally, the particles were suspended in a 3 mg/mL fibrinogen solution at pH 6.5 and incubated for 30 minutes. This was followed by three washes and suspension of the coated particles in 0.1 M EDTA solution for template dissolution. The particles were collected by centrifugation after incubation with EDTA solution for five minutes. This was repeated three times to ensure complete template removal. This was followed by cross-linking the fibrinogen layer on the hollow microspheres with thrombin by incubating them in the cross-linking solution (40 U/ml in TBS and 50 mM CaCl₂) for 10 minutes at 37°C. The resulting fibrin hollow microspheres were washed three times with PBS before the morphological and physiochemical characterization.

3.2.2 Morphological characterisation of fibrin hollow microspheres

For the morphometric analysis, hollow fibrin microspheres were evaluated using scanning electron microscopy (SEM) (Hitachi S-4700 field emission microscope operating with a beam voltage of 15 kV). The samples were placed on carbon tabs mounted on the SEM specimen stubs and then dried. This was followed by gold-coating using an Emitech K550 coating system

(Derby, England, U.K.). Transmission electron microscopy was done for morphological characterization of hollow fibrin microspheres using Hitachi H7500 Transmission Electron Microscope.

3.2.3 Size and zeta potential analysis of fibrin microspheres

The size of the hollow fibrin microspheres was monitored during the process of fabrication using dynamic light scattering (DLS) (Zeta sizer (Malvern, Nano-ZS90). Charge on the templates and template coated with different layers of polyelectrolytes was analysed by the zeta potential measurements during the process of fabrication. Zeta potential measurements were also performed to investigate the stability of the hollow fibrin spheres in phosphate buffered saline (PBS) and Dulbecco's Minimal Essential Medium (DMEM) over a period of seven days. Similar measurements were performed for assessing the stability of the spheres over a range of pH and ionic strengths to evaluate the overall stability of the hollow fibrin microspheres over a broad range of physiological conditions [13].

3.2.4 Loading of hollow fibrin microspheres with GDNF

Fibrin hollow microspheres were loaded with GDNF by re-suspending 1 mg of hollow fibrin spheres in 300 μ l of PBS–0.05% Tween solutions (loading buffer) containing different amounts of GDNF (1, 2, 5 and 10 μ g). The hollow fibrin spheres were then incubated on a shaker at room temperature for 24 h to allow the growth factor to diffuse into the hollow spheres. Samples were then spun down for 20 minutes at 14000 rpm to collect the loaded hollow spheres and supernatant was analysed using GDNF E_{max} ImmunoAssay System (Promega). The loading efficiency of spheres for different doses of GDNF was calculated by detecting the amount of GDNF left in the supernatant.

3.2.5 Fabrication of the fibrin-in fibrin intervention

The fibrin-in-fibrin (FNF) platform was designed by reconstituting human fibrinogen (20 mg/ml) in TBS (1X) with a defined concentration of GDNF-loaded microspheres and VM cells. The FNF gels were then fabricated by cross-linking the fibrinogen component by an equal volume of thrombin crosslinking solution (40 U/ml of human thrombin in TBS with 50 mM $CaCl_2$). The gels were then allowed to incubate at 37°C for ten minutes to stabilize the cross-linking. The volume of the gels (6 μ l) designed were kept consistent with that used in the preclinical model of PD to improve the *in vitro* translation of the *in vitro* optimized parameters. To fabricate and collect the gels efficiently, they were micro-dispensed on a hydrophobic

(commercial Teflon[®] tape) and incubated there for stable cross-linking. The gels were then collected by scraping off the hydrophobic surface using a sterile spatula. The microgels were then resuspended in the cell culture media to incubate them with the VM cells for further experiments.

3.2.6 Release profile of GDNF from hollow fibrin spheres and fibrin-in-fibrin platform

Characterization of the release profile from fibrin spheres and fibrin-in-fibrin platform was done in release buffer (PBS–0.05%Tween 20) at 37 °C as an acellular release system. Growth factor-loaded microspheres (1 mg) were incubated with 300 µl of the release buffer, and at different time points microspheres were spun down and supernatant was collected. For the characterization in a cellular system, the fibrin microspheres and the FNF gels were incubated with VM cells plated on the 48-well tissue culture dish for seven days. The media was collected from each well and spun down to collect the supernatant for analysis using EISA. The collected supernatants from both cellular and acellular systems were frozen at –20 °C until ELISA was conducted.

3.2.7 Rheological characterization of the FNF system and rat brains

The flow properties of hollow microsphere dispersions in silk hydrogels were characterized using an AR2000 rheometer (TA Instruments). The measurements were performed using flat plate geometry (steel) (8 mm diameter) at 37 °C with 100 µm of gap distance. Firstly, oscillatory stress and strain sweep analysis were performed to establish the linear viscoelastic region for every sample. Subsequently, the storage modulus (G'), loss modulus (G'') and $\tan(\delta)$ were determined by doing an oscillatory time sweep test for 10 minutes at a constant frequency of 1 Hz and constant strain of 2%. All the tests were performed in triplicates ($n = 3$).

3.2.8 Cell viability and apoptosis analysis

Embryonic ventral mesencephalic (VM) cells seeded in the gels were extracted by treating the gels with collagenaseP for 30 minutes. The protocol for VM cell extraction and maintenance is described in **Appendices, Section C**. Briefly, 10^5 cells were washed twice with phosphate-buffered saline (PBS), and stained with 2 ml of Annexin V FITC and 10 ml of PI in binding buffer (10 mM HEPES, 150 mM NaCl, 5mM KCl, 1mM MgCl₂, and 1.8mM CaCl₂, pH 7.4) for 15 minutes on the ice in the dark. The apoptotic cells were determined using a Becton Dickinson FACS Canto Flow Cytometer (Mansfield, MA, USA). Live cells (annexin V-negative, PI-negative), early apoptotic cells (annexin V-positive, PI-negative) and dead cells

(annexin V-negative and PI-positive) cells were included for analysis using FlowJo software 8.5.2 (Tree Star, Ashland, OR).

DNA quantification was carried out using Quant-iT™ PicoGreen® dSDNA assay kit (Invitrogen, Ireland) according to the manufacturer's protocol. Briefly, DNA was extracted using three freeze-thaw cycles after adding 200 µl of nucleic acid free water per well (24 well plate). The cell suspension was subsequently transferred to cold Eppendorf tubes and was centrifuged for five minutes at 12,000 rpm. 25 µl was then transferred into a 96-well plate containing 75 µl of 1 × TE buffer. A standard curve was generated using 0, 7.8, 15.6, 31.2, 62.5, 125, 250 and 500 µg/mL DNA concentrations. 100 µl of a 1:200 dilution of Quant-iT™ PicoGreen® reagent was added to each sample and the plate was read using a micro-plate reader (Varioskan Flash, Thermo Scientific, Ireland) with an excitation wavelength of 480 nm and an emission wavelength of 525 nm.

3.2.9 Immunohistochemistry

Following fixation of gels for 10 minutes using 100% ice-cold methanol, cells were washed 3 x 5 minutes using 10 mM phosphate-buffered saline (PBS) containing 0.02% Triton X (PBS-Tx), followed by blocking of non-specific secondary antibody binding for 1 h (using 5% bovine serum albumin in 10 mM PBS) at RT. Gels were then incubated overnight at 4°C in primary antibodies against tyrosine hydroxylase (mouse anti-TH, 1:1000), β tubulin (1:200) and GFAP(1:200) in antibody diluent (1% bovine serum albumin in 10 mM PBS). The gels were washed 3 x 5 minutes using PBS and then incubated for 3 h at room temperature in rabbit anti-mouse Alexa fluor 488 in antibody diluent (1% bovine serum albumin in 10 mM PBS). The cells were then washed 3 x 5 minutes using PBS, counterstained for five minutes using DAPI in 10 mM PBS, and finally washed 3 x 5 minutes using PBS. Imaging was done using a confocal microscope.

3.2.10 Gene expression analysis

VM cells were cultured in the fibrin gels under different test conditions. After a seven-day treatment, total RNA was extracted from cells in culture using TRIzol reagent (Invitrogen) and miRNeasy mini kit following the manufacturer's protocol. Total RNA was reverse-transcribed with random primer (Promega) and subsequently with reverse transcriptase (Promega) in a 20 µL reaction mixture using PTC DNA Engine System (PTC-200, Peltier Thermal Cycler, MJ Research Inc., U.S.A.). A summary of the primers used in this experiment is provided in the **Appendices, Table A6**. The cDNA products were amplified using SYBR green PCR Master

Mix (Promega) and following specific primers. Reactions were conducted in triplicate using StepOnePlus Real-Time PCR System (Applied Biosystems). The results were analyzed using the $2^{-\Delta\Delta C_t}$ method and presented as fold change (relative gene expression) normalized to GAPDH and basal control.

3.2.11 Quantitation of the paracrine response

The paracrine response modulation by manipulating the cellular microenvironments was investigated by using the Quantibody[®] Rat Inflammation Array 1 (RayBiotech, GA, USA). The levels of cytokines present in the supernatants or whole cell extracts were taken from cell embedded microgels or cells alone and estimated using the kit. The assay was performed according to the manufacturer's protocol. Briefly, 100 μ l of the samples or cytokine standards was added to assay diluent in a 96-well assay plate. Following the incubation for two hours, the plate was then washed and incubated with a biotinylated antibody cocktail as per the manufacturer's instructions. This was followed by incubation with Cy3-labelled streptavidin and an incubation at room temperature for an hour. After this, the slide was scanned using the fluorescence detector for Cy3 (Agilent). Cytokines, including interleukin-1 β (IL-1 β), IL-1 α , IL-4, IL-10 and IL-13 were analysed. The data were quantified using a standard curve generated from the kit calibrators for each of the cytokines.

3.2.12 Statistical analysis

Statistical analyses were performed using GraphPad Prism[®] Version 5 (USA) and IBM SPSS[®] Version 21. Data were compared using one-way or two-way analysis of variance (ANOVA) based on the number of factors analysed, followed by a BonFerroni post-hoc comparison test. Statistical significance was set at $p < 0.05$ (*).

3.3 Results

3.3.1 Fabrication and physiochemical characterisation of the fibrin hollow microspheres using LbL assembly

Hollow fibrin spheres were fabricated using the LbL assembly. CaCO₃ microbeads were used as a sacrificial template and dextran sulfate (DS) and polyarginine (PAR) were used as polyelectrolyte layers for the fabrication of the hollow fibrin microspheres. **Figure 2A** shows the SEM images of the fabricated hollow spheres. A smooth, round morphology was observed for the microspheres in SEM images with a uniform size distribution. **Figure 2B** shows a magnified SEM image of fibrin spheres representing the hollow cavity of the spheres.

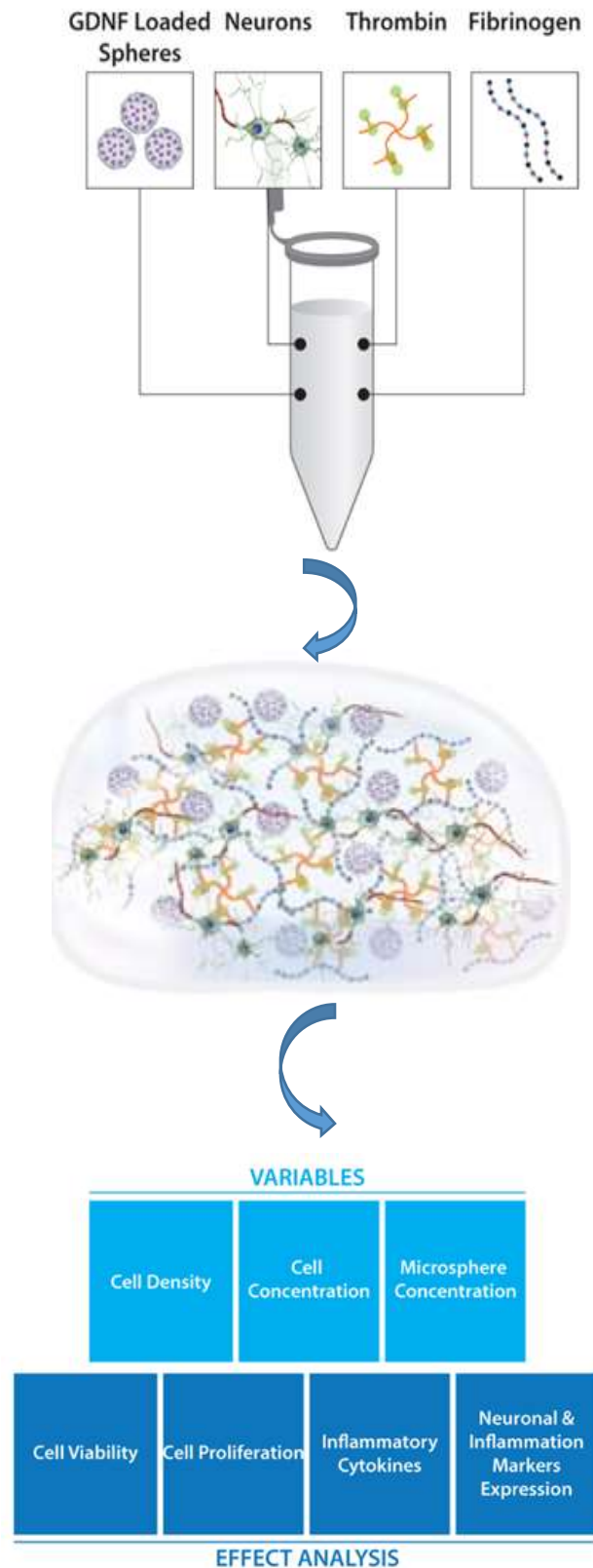


Figure 3.1: Schematic outline of the experimental design. Schematic representation of the experimental design for the optimisation of the fibrin-in-fibrin platform for the therapeutic delivery of dopaminergic progenitors in the PD model.

The template initially showed a positive surface charge at pH 6.5. Accordingly, for the LbL approach, the template was first incubated with DS and the surface charge shifted from the initial value of 10.2 ± 1.8 mV to -20.02 ± 1.4 mV (**Figure 2C**). Thereafter, the particles were alternately incubated in PAR and DS solutions and the surface charge changed from negative to positive as expected. After the deposition of five layers (PAR-DS-PAR-DS-PAR), particles were coated with fibrinogen which formed an electrostatic interaction with PAR as it's negatively charged at pH 6.5. This was followed by the template dissolution using EDTA. As observed by SEM images, there was no evidence of the CaCO₃ core. The particles fabricated using this protocol were around 4 μm in size.

3.3.2 Stability of hollow fibrin microspheres

There were detectable changes in the zeta potential of calcium carbonate templates through the process of fabrication and the deposition of polyelectrolyte layers as represented in **Figure 3.2C** which were indicative of the formation of hollow spheres. The zeta potential on the spheres was found to be around -18.80 mV under physiological conditions. To assess the suitability of the fibrin spheres for a wide range of therapeutic applications, the stability of the hollow fibrin spheres was tested under a wide range of physiological conditions. Zeta potential varied from -16.79 mV to -14.90 mV over a period of seven days in PBS. However, the spheres retained sufficient negative potential to form a stable suspension. The stability of the spheres was investigated over a period of seven days in both PBS as well as in cell culture media and the spheres showed a sufficiently negative zeta potential (**Figure 3.3A, B**). The masking impact of proteins in the cell culture media resulted in less negative zeta potential in the cell culture media [33]. Since the isoelectric point of fibrinogen is around 5.4, the spheres were found to have positive zeta potential below and strong negative zeta above pH 5.4 (**Figure 3.3C**). The values varied from 11.89 mV to -14.26 mV. In all these conditions, the fibrin hollow spheres were found to be stable and therefore, adaptable to various therapeutic applications in varying physiological conditions.

3.3.3 Loading and release profile from hollow fibrin spheres

The loading efficiency and release kinetics of GDNF were investigated from the hollow fibrin microspheres and the fibrin-in-fibrin intervention. The amount of GDNF loaded in the microspheres was determined using GDNF- ELISA. The microspheres showed a high loading efficiency of $\approx 88\%$ and this remained constant for all doses of GDNF > 2 μg (**Figure 3.4A**)

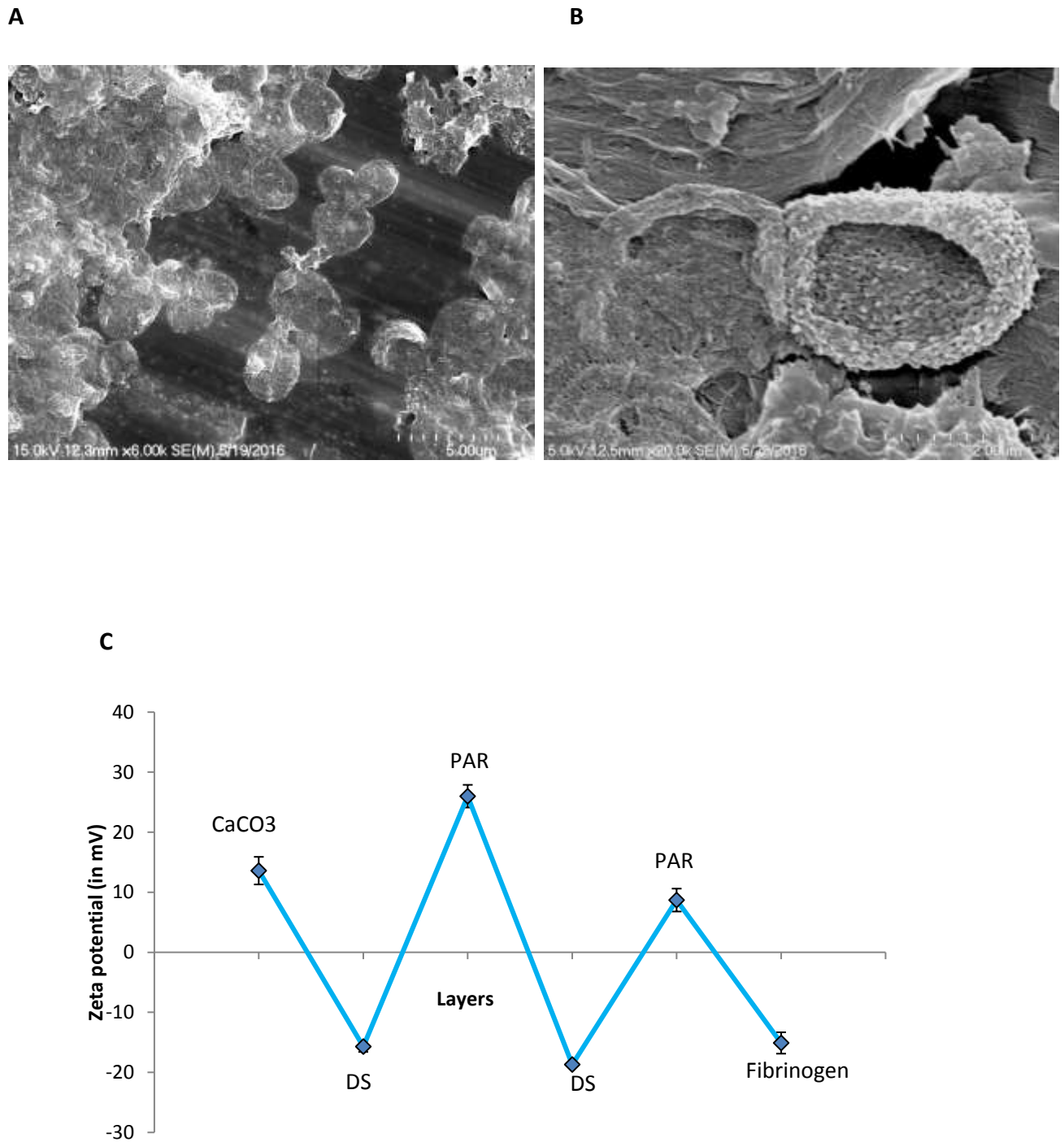


Figure 3.2: Fibrin microsphere characterization. (A) Scanning electron micrographs representing the fibrin microspheres fabricated using layer-by-layer assembly followed by template dissolution, (B) High magnification scanning electron micrographs representing the lack of solid core in the microspheres (C) Layer-by-layer deposition of polyelectrolytes to form the fibrin microspheres represented by the modulation of zeta potential (n=6).

Release kinetics of GDNF from the hollow fibrin spheres was also studied in a cellular system using ventral mesencephalic cells and the acellular PBST system. In the acellular system, the release of GDNF from the microspheres was studied for over a period of two weeks. An initial burst release was observed in the first five days followed by a stable release of GDNF (**Figure 3.4B**). Interestingly, the encapsulation of the fibrin microspheres in the hydrogel system reduced the release of GDNF at the corresponding time points. An initial burst release was still observed for seven days followed by a more sustained release. Similar release kinetics were observed in the cell culture media in the presence of cells. An initial burst release was observed in the cellular system for a week which was followed by a sustained release for 14 days (**Figure 3.4C**).

3.3.4 Impact of fibrin spheres on cellular viability

Four different doses (0.5, 0.1, 1, 10 μ g/ well) of hollow fibrin spheres were tested for their impact on the metabolic activity of both primary neuronal cells (VM cells) and neuronal cell line (PC-12 cells). It was found that even at high concentrations, the spheres did not have an adverse impact on the metabolic activity of either cell type as demonstrated by alamarBlueTM assay (**Figure 3.3D**). There was no significant difference in metabolic activity when compared to PBS controls (* $p \leq 0.05$) except at the highest concentration for VM cells.

3.3.5 Optimisation of fibrin-in-fibrin platform for maximal graft survival

Different concentrations of fibrin microspheres were re-suspended in the fibrinogen solution in tris buffered saline (TBS) along with different cellular concentrations. The graft survival was investigated as a function of fibrinogen concentration, cell concentration and microsphere density. The gels were formed and investigated in 6 μ l microgel (relevant for *in vitro* analysis) and 50 μ l hydrogel formats. The gels were crosslinked using 40 U/ml of thrombin solution in TBS-CaCl₂ buffer. These gels were then subjected to viability and proliferation analyses to optimise the conditions for graft survival *in vitro*.

To investigate cell survival on the microgels, different cell densities such as 0.01, 0.1, 0.5 and 1.0 million cells/ ml were tested with varying fibrinogen and microsphere concentrations. To examine cell survival, cells embedded in microgels were extracted by mild collagenase digestion and were stained with Annexin V-FITC and PI. This was followed by the flow cytometric analysis of viability, early apoptosis and cell death. The cells showed about 70% viability over two weeks, across all fibrinogen concentrations and cell densities except at 60

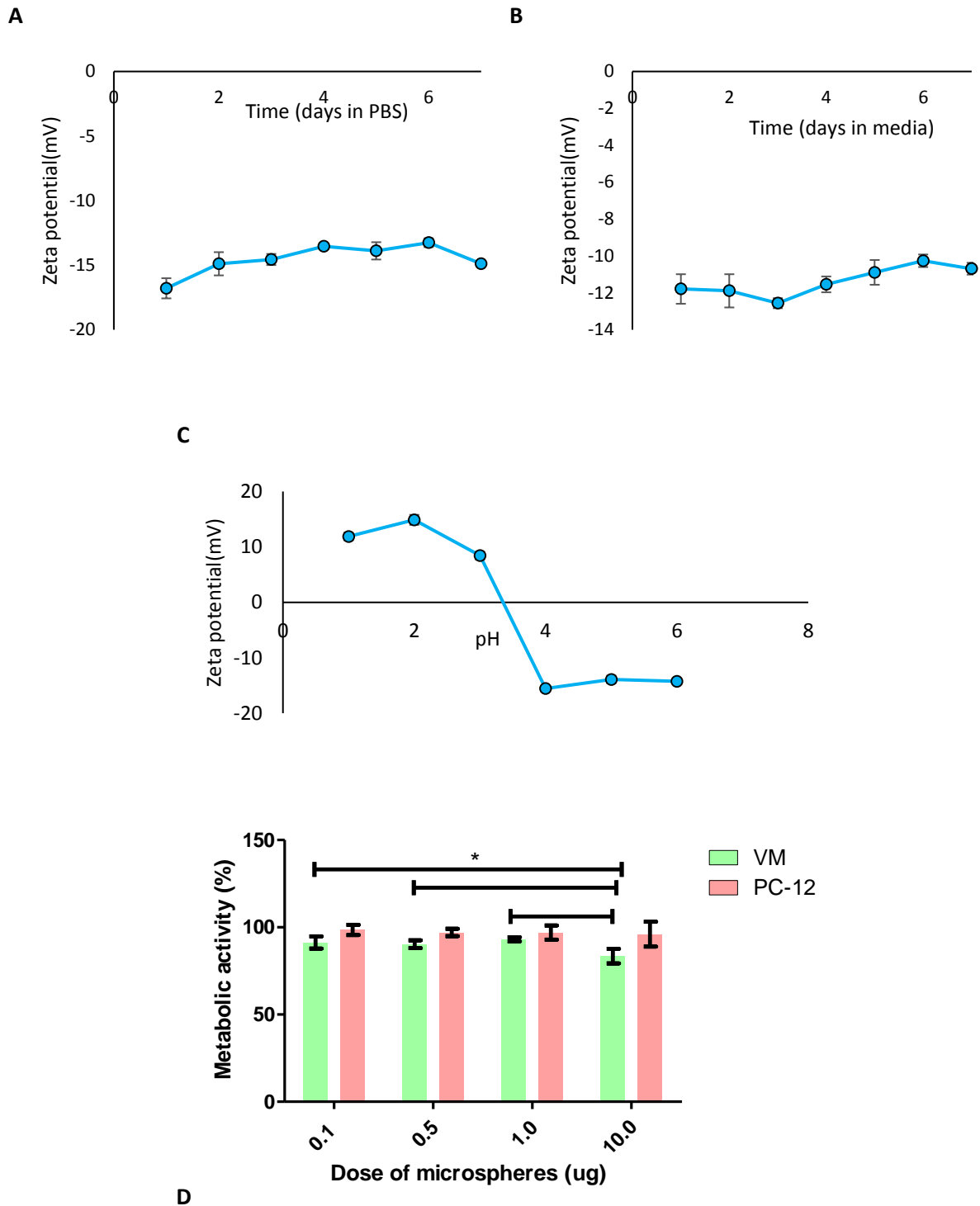
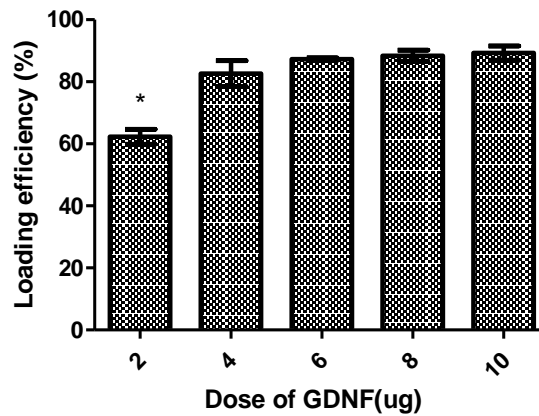


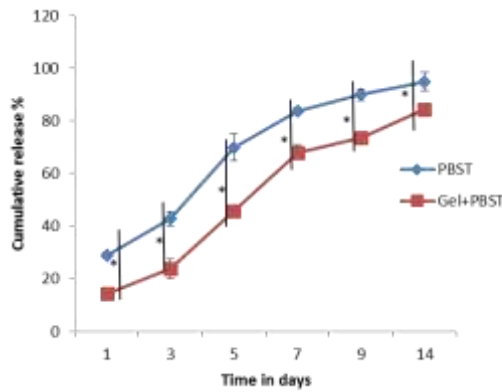
Figure 3.3: Stability of fibrin microspheres and impact on cellular metabolic activity.

Fibrin microspheres investigated using the zeta potential measurements as a function of (A) time in PBS, (B) in media and (C) pH. A strong negative charge despite the presence of a high concentration of salts and proteins is indicative of the stability of microsphere system. (D) No adverse impact on metabolic activity of primary neurons and neuronal cell lines was found.

A



B



C

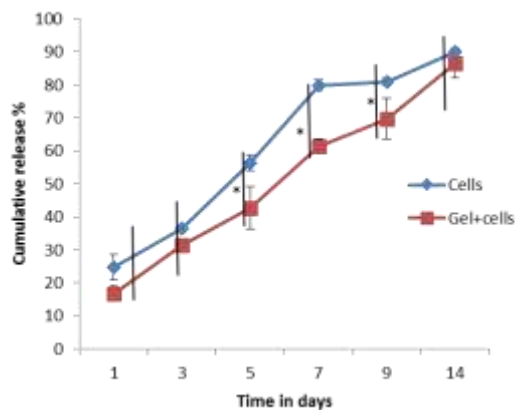


Figure 3.4: Loading and release kinetics of fibrin-in-fibrin intervention. (A) Loading capacity of the microspheres investigated as a function of the dose of GDNF. Time course analysis of GDNF release from the fibrin-in-fibrin system in (B) acellular buffer system and (C) cellular system representing a sustained temporal release over a period 14 days (n=8, *p<0.05)

mg/ml and 10^6 cells/ml (**Figure 3.6A, B, C**). These results were supported by Quant-iT™ PicoGreen™ dsDNA Assay (Thermo-Fischer, UK). The cells were homogeneously dispersed in the microgels with neurites forming an interconnected mesh. These results were supported by PicoGreen® assay. The cells were homogeneously dispersed in the microgels with neurites forming an interconnected mesh. The focus of this analyses was to probe the impact of fibrin microgel on the cellular microenvironment and mediation of processes like apoptosis [14]. Annexin V was used as a marker for early cell apoptosis. The data suggests that across all the fibrinogen, cellular and microsphere concentrations, only 15% of cells underwent apoptosis over two weeks except at the highest concentrations for fibrinogen and cells. Higher apoptosis and cell death was observed at 10 μ g of microspheres on VM cells as detected by alamarBlue™ reduction (n=6, *p<0.05) death was observed at high fibrinogen concentrations which can be attributed to the poor diffusion of nutrients and oxygen in a tight mesh network for the hydrogel. However, the percentage of apoptotic cells in 20 mg/ml of fibrin gel, 5×10^5 cells/ml and 1 μ g of microspheres was found to be minimal amongst the other combination of parameters.

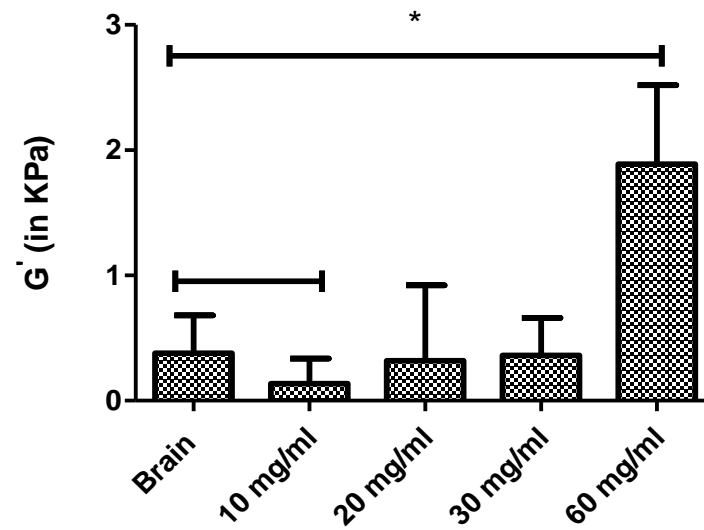
3.3.6 Rheological compatibility of the optimised fibrin-in-fibrin platform with the rodent brain

Previous studies have indicated that brain tissue is extremely soft, with moduli ranging from around 0.2-0.5 kPa [15–18]. In the current study, a strain controlled rheometer was used for the viscoelastic measurements and the results verified that shear moduli (G') of fibrin gels varied as a function of the protein concentration. Whole rat brains were also investigated to determine their shear moduli within two h of their isolation from adult rats. The storage moduli of the brain averaged to 400 Pa which was closer to the moduli for 20 and 30 mg/ml of the fibrin gels with microspheres (**Figure 3.5A, B**). The stiffest gel (60 mg/ml) with the microspheres had a much higher storage modulus. The results from the viscoelastic measurements show that the optimised fibrin-in-fibrin intervention should be compatible to be used as an *in vivo* cellular delivery platform in the rat Parkinsonian model. The easy tuneability of these properties also offer an advantage to the use of fibrin scaffolds for augmenting cell therapies in PD.

3.3.7 Immunohistochemical analysis for neuronal and inflammatory markers

Different microgel variants were subjected to immunohistochemical analyses for investigating the neuronal survival and the survival of dopaminergic progenitors. Also, the survival and proliferation of the astrocytic cells as a function of varied parameters was investigated. The

A



B

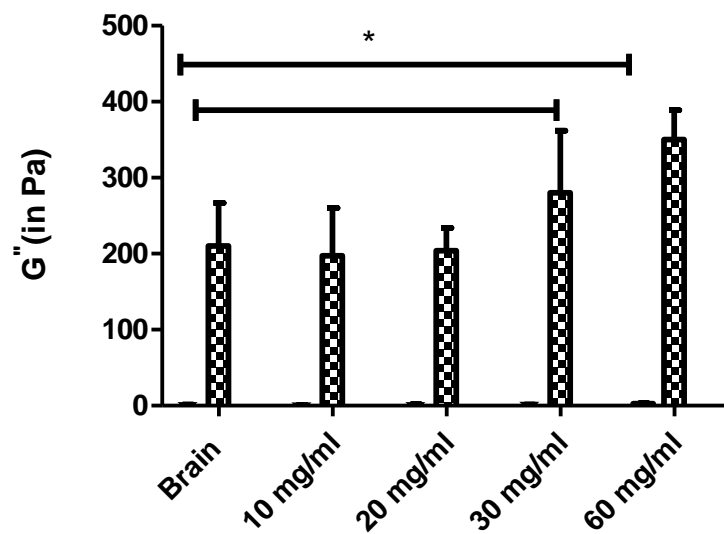


Figure 3.5: Rheological assessment of the fibrin-in-fibrin intervention. Comparative analysis between the (A) storage and (B) loss modulus of the different hydrogel concentrations with 5 μg microspheres revealed that the properties of 20 mg/ml of the fibrin gel with microspheres are closest to those of the rat brain (n=3, *p<0.05).

optimised fibrinogen, cell and microsphere concentration were found to be 20 mg/ml, 5×10^5 cells/ gel and 5 μg of the microspheres. These conditions maximised the neuronal survival, specifically the survival of dopaminergic progenitors and minimised the proliferation of inflammatory cells as indicated by GFAP immunostaining (**Figure 3.7A**). Quantifications of the immunohistochemical analyses for dopaminergic progenitors, neurons and GFAP taken together lead to the determination of the optimised parameters for a fibrin-in-fibrin platform to be tested *in vitro* (**Figure 3.7B, C, D**). Lower hydrogel concentration and higher cell density were used in case there were no significant differences in the neuronal survival and astrocytic proliferation to minimise the polymer content and maximise the cellular delivery using the fibrin-in-fibrin platform.

3.3.8 Gene expression analysis for neuronal and inflammatory markers

To analyse the impact of the fibrin-in-fibrin platform on the expression of neuronal and inflammatory markers as a function of the platform parameters, RT-PCR analyses was performed. Trizol extraction was performed to isolate the RNA from a different combination of hydrogel parameters, and the extracted RNA was subjected to cDNA synthesis. This was followed by RT-PCR analyses for neuronal marker (β III tubulin), dopaminergic cell marker (TH) and astrocytic marker (GFAP). Increased expression of the inflammatory marker (GFAP) was observed at 60 mg/ml of fibrinogen concentration and with 10^6 cells/ml (**Figure 3.8D**). Enhanced proliferation of the astrocytes drives the paracrine phenotype to be more pro-inflammatory as was detected by the investigation of the modulation of the secretome of the engrafted cells. Interestingly, there was no impact on the GFAP expression observed in response to the different concentrations (0.1, 0.5, 1 and 5 μg) of the fibrin microspheres (**Figure 3.8F**) which further supports the hypothesis that these microspheres can be used as a delivery platform in the brain.

3.3.9 Modulation of VM secretome with platform parameters

Previous studies have shown that the activation of glial cells following the striatal lesioning regulates the paracrine trophic responses to dopaminergic neurons [19]. The central question in this paradigm of investigation was whether the interplay of pro- and anti-inflammatory cytokines could be triggered in the favour of enhancing the survival of dopaminergic neurons and minimising the inflammatory cues. Therefore, we hypothesized that paracrine responses of the engrafted cells can be modulated in a tuneable microgel environment by varying polymer concentration, cell density and microsphere concentration. . Interestingly, there was a distinct

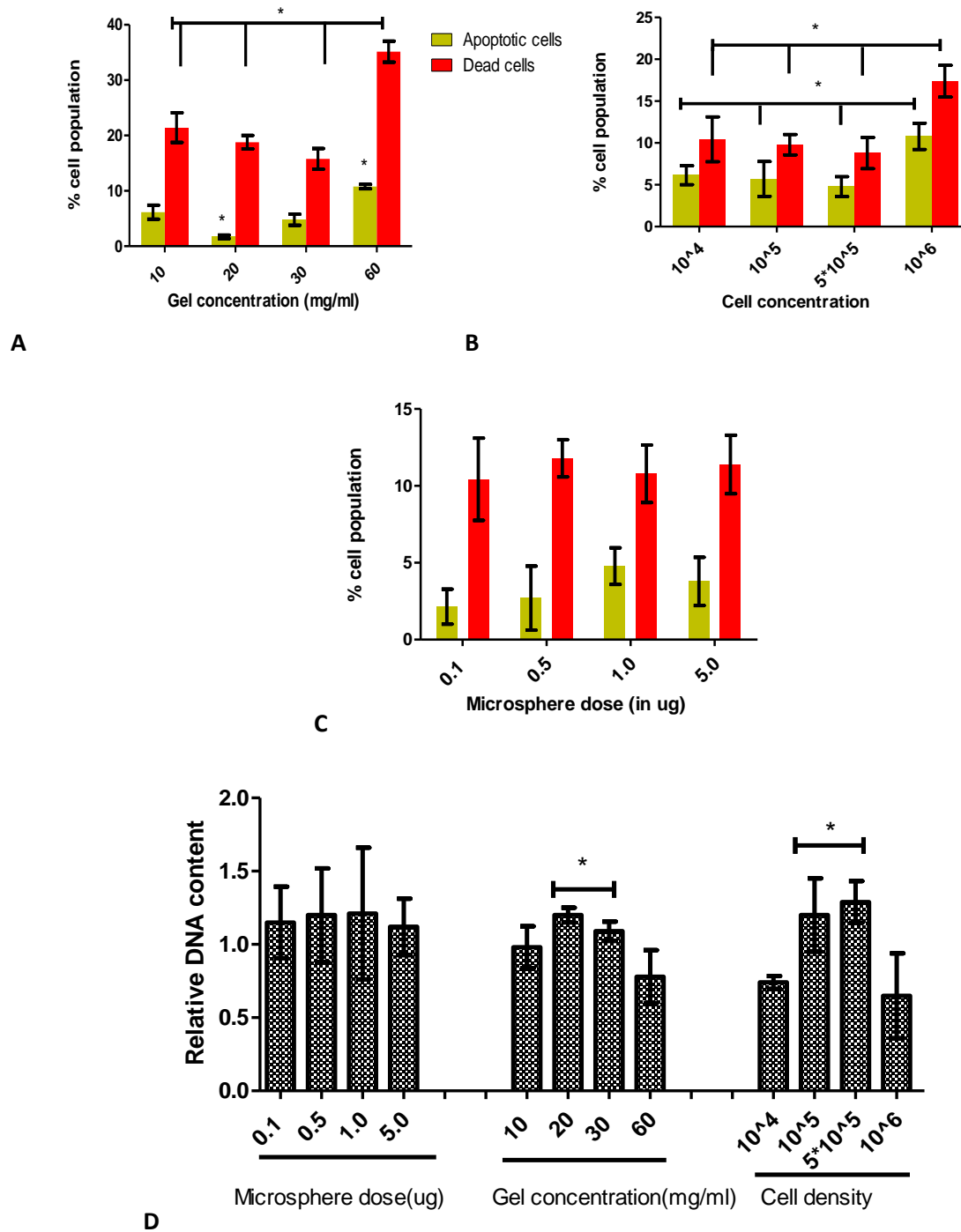


Figure 3.6: Viability analysis for fibrin-in-fibrin platform. Analysis of cellular viability as a function of (A) fibrinogen concentration, (B) cell density and (C) microsphere dose using FITC-AnnexinV-PI staining followed by flow cytometric analysis reveals <30% dead and apoptotic cells for all the combinatorial platform parameters except highest fibrinogen concentration at day 7 post encapsulation. (D) PicoGreen[®] assay represents no adverse impact which included both pro and anti-inflammatory cytokines measured over a range of conditions.

modulation of the paracrine phenotype of the engrafted cells with the modulation of the different platform parameters. VM-embedded microgels of varying fibrinogen, cell and microsphere concentrations (**Figure 3.8 A, B, C**) were screened using rat inflammation array, which included both pro and anti-inflammatory cytokines measured over a range of conditions. Strikingly, at seven days post-encapsulation, we could observe significant differences in the levels of pro- and anti-inflammatory cytokine production between the different fibrinogen, cell and microsphere concentrations, with significant differences in the cytokine levels of IL-1 β , IFN- γ , IL-4, IL-10 and IL-13. The effect of the paracrine output became increasingly clear with the highest cell and polymer densities that were tested. There was a clear shift towards a more pro-inflammatory phenotype that was observed in these conditions. A perfect balance cellular survival and modulation of the paracrine response of the encapsulated cells was observed with 20 mg/ml fibrinogen, 5×10^5 cells and 5 μ g microspheres, which minimised the pro-inflammatory cues while promoting the anti-inflammatory phenotype.

3.4 Discussion

Parkinson's disease (PD) is the second most prevalent chronic neurodegenerative disorder characterized by the physical manifestations of tremor, rigidity, akinesia and postural instability. The underlying pathology involves a selective loss of dopaminergic neurons translating to an aberrant dopamine signalling in the striatum. The paradigm of cell therapy as a long-lasting treatment in PD patients is based on the hypothesis that restoration of striatal DA transmission by engrafting dopaminergic neurons would induce clinical improvement in the PD patients by re-innervating the denervated striatum and forming functional synaptic contacts[20].

The first studies with the use of VM tissues in the PD patients started in 1987 and since then, over the past three decades several clinical trials have provided evidence that dopaminergic neurons isolated from the foetal ventral mesencephalon can survive, integrate with the host circuitry and lead to functional recovery after transplantation into Parkinsonian brains [21–23]. However, the chief hurdle in the clinical translation of VM cell therapy is the poor availability and survival of the engrafted cells in the host brain which calls for an unethically high number of embryos for transplantation. Major reasons underlying the

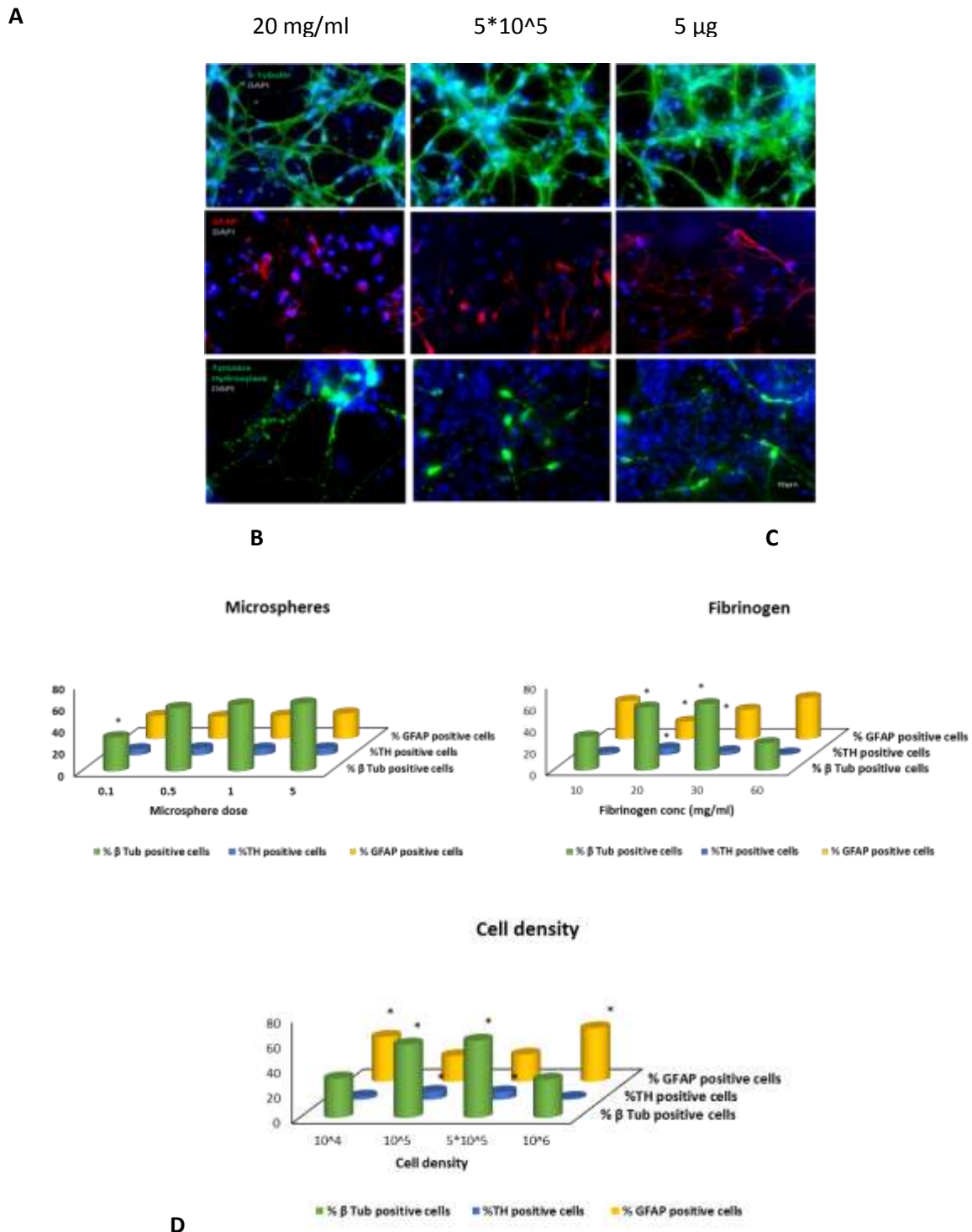


Figure 3.7: Neuronal survival in optimised fibrin-in-fibrin intervention. (A) Representative fluorescent micrographs for immunohistochemical analyses of neuronal and astrocytic growth in the optimised fibrin-in-fibrin intervention (neurons: β -tubulin, dopaminergic neurons: TH, astrocytes: GFAP). Quantification of the positively immunostained cells for a range of (B) microsphere doses, (C) fibrinogen concentrations and (D) cell density to evaluate the optimal set of parameters. 20 mg/ml of fibrin gel with 5 μ g microspheres and a cell density of 5×10^5 best supports the neuronal survival and minimises the inflammatory response ($n=6$, $*p<0.05$, student t-test).

poor graft survival is the loss of cell-cell and cell-matrix interactions caused by the matrix detachment, exposure to a growth factor deprived niche, host immune response to the graft and induction of apoptosis and cell death during the process of transplantation [24–27]. Interestingly, these issues can be well circumvented by the use of biomaterial intervention for the delivery of the cells into the brain. Amongst the natural biopolymer-based scaffolds, protein-based scaffolds such as fibrin, collagen etc. present endogenous binding sites for cell adhesion unlike other scaffolds like chitosan, agarose etc. that usually require modification with specific cell-attachment moieties to promote cell adhesion and proliferation [28].

Fibrin is a degradable natural biopolymer formed by mimicking the last step of the blood coagulation cascade and crosslinking the fibrinogen by thrombin. This is followed by thrombin mediated removal of fibrinopeptides [29]. Plasmin-mediated fibrinolysis results in the eventual degradation of the fibrin clots *in vitro*. This clot has been shown to provide several sites for cell attachment, migration, and proliferation to promote tissue regeneration [30]. Moreover, it presents several advantages for tissue engineering applications in terms of enhanced tissue binding potential, biocompatibility and biodegradability. A distinct advantage in using the autologous fibrin scaffolds is the minimal foreign body reaction. Furthermore, easy tuneability of fibrin scaffolds and their physiological flexibility makes them well suited to a wide range of therapeutic application including the neural tissue engineering [31]. In the context of neural tissue engineering, several studies have shown that varying concentrations of fibrinogen can be used to form fibrin gels that can promote neurite extension and branching [32,33]. The ability to be modified by the exogenous ligands such as growth factors and cytokines makes fibrin an ideal candidate for the brain tissue engineering [34].

In this study, we fabricated hollow fibrin microspheres by using the layer by layer assembly of polyelectrolytes on the sacrificial calcium carbonate templates. Layer-by-layer assembly has been used in several studies to fabricate core-shell particles used for the delivery of several biomolecules and drugs [35–37]. The cores in this case are used as decomposable supports that can be eliminated by physicochemical means such as solvents, pH change, thermal dissolution or decomposition. The porous nature of the CaCO₃ microparticles offers the possibility to obtain a matrix with chemistry similar to that of shell within the core. Volodkin et al. showed that the the extraction of CaCO₃ core with a chelating agent post formation of a polyelectrolyte multilayer shell by the LbL assembly resulted in the fabrication of a capsule with a defined matrix-type interior [38]. With the pI of 8.5 [12], CaCO₃ particles had an overall positive charge at pH=6.0. This was followed by the deposition of different layers of DS and PAR through

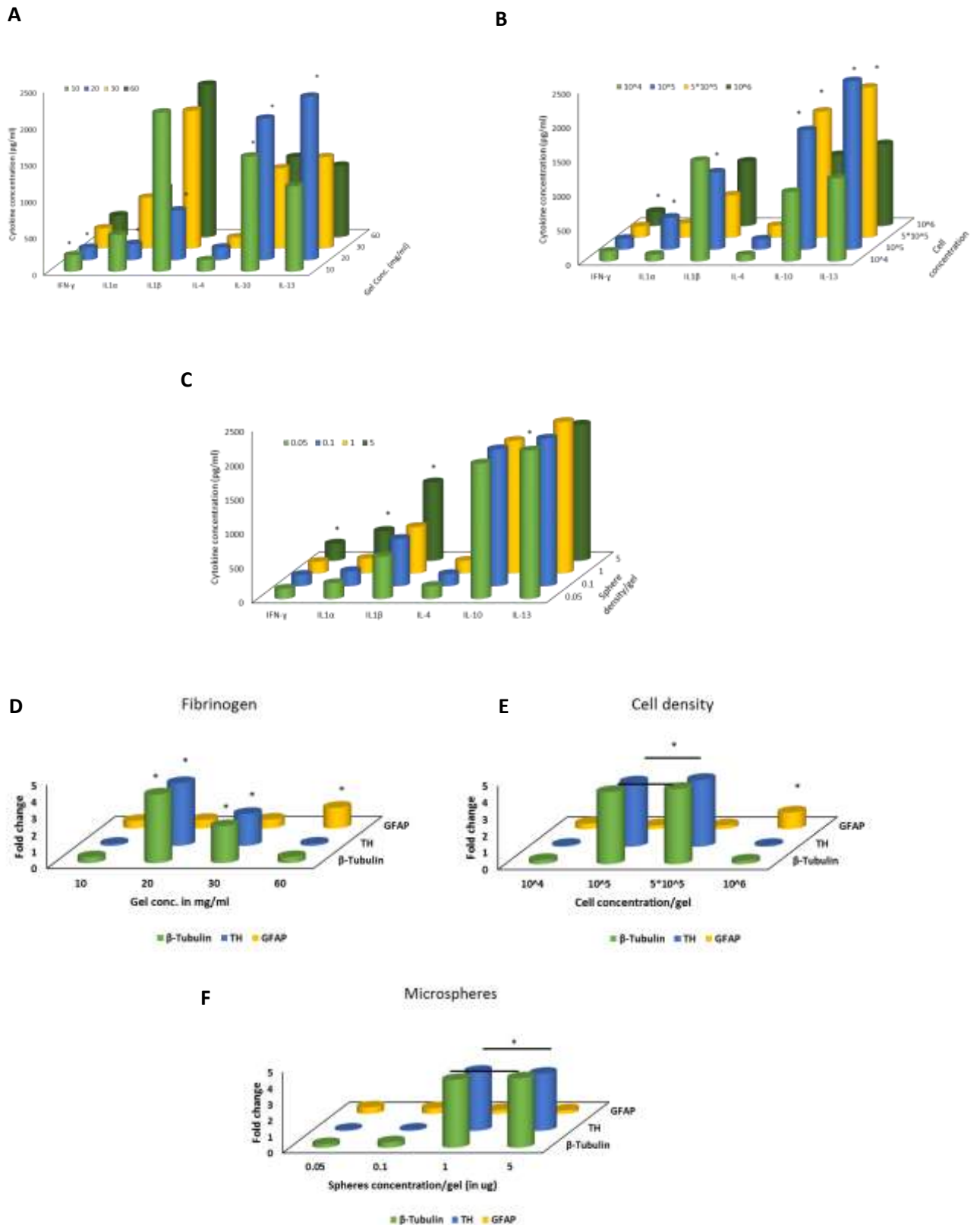


Figure 3.8: Modulation of the paracrine and gene expression profiles. Impact of the (A) fibrinogen concentration, (B) cell density and (C) microsphere dose on the paracrine profile and on the expression of neuronal and inflammatory markers (D, E, F) of the encapsulated cells. There was a shift towards an anti-inflammatory phenotype observed with 20 mg/ml of fibrin gel with 5 ug microspheres and a cell density of 5×10^5 ($n=6$, $*p<0.05$)

electrostatic interactions. The overall negative charge of fibrinogen at pH=6.0 facilitates its deposition as the final layer on the PAR by facilitating it to interact favourably with PAR layer. This was followed by core dissolution using EDTA. A layer of fibrin was formed around the polyelectrolyte shell by harnessing the mechanism of clot formation whereby thrombin acts on fibrinogen to form fibrin monomers which are acted upon by factor XIII a to form a cross-linked fibrin mesh. These fibrin spheres were then tested for their stability over a wide range of physiological conditions and were found to be stable over a broad spectrum of the conditions that were being tested. These microspheres were also tested for their loading efficiency and release properties in both cellular and acellular systems. The microspheres showed comparable loading efficiency to the fibrin and collagen spheres fabricated using the template charge manipulation method in the previous studies [13,39]. Interestingly, sustained release profile was observed in both cellular and acellular systems where the GDNF availability at subsequent time points was less in the cellular system due to its uptake by the cells.

The current study reports on the fabrication of a fibrin-in-fibrin platform for controlled temporal release of neurotrophic factors to promote the survival of the engrafted dopaminergic progenitors. An injectable, biopolymer-based hydrogel can offer multi-faceted support for the enhanced delivery of primary dopaminergic neurons. Several studies have suggested that most of the implanted dopaminergic neurons (80-90%) die within the first four days of implantation into the host. This initial cell death and apoptosis has been found to be mediated by a range of factors including the loss of cell-matrix interactions during cell preparation and transplantation and host immune response [24,27]. While synthetic scaffolds require chemical modifications to enhance cell binding, fibrin as a scaffold offers an advantage of being intrinsically modified with heparin-binding domains that promote cell adhesion and migration [40], thereby facilitating an efficient cell delivery. The host response to the engrafted cells is one of the most important triggers for apoptosis post implantation [24], fibrin gel as a delivery platform offers the advantage of being autologous and does not evoke a strong host response. Moreover, the fibrin gel forms a physical immune-barrier between the ventral mesencephalic graft and the host immune cells, thereby, minimising the cell loss due to immune rejection. Another significant factor that can trigger apoptotic cell death in the established graft is the trophic factor deprivation in the adult Parkinsonian striatum [41]. The controlled delivery of GDNF through the fibrin microspheres supplements the trophic support in a regulated manner to assist the stabilisation of the implanted neurons.

However, the survival and integration of the engrafted cells depend on a multitude of factors including the polymer, microsphere and cell concentration. This study investigates the optimised parameters for the fibrin-in-fibrin intervention that maximises the survival of the implanted neurons while minimising the inflammatory cues by modifying the paracrine responses of the engrafted cells towards an anti-inflammatory phenotype. Viability testing showed that the engrafted cells exhibited high viability and low apoptosis even two weeks post encapsulation (<30%).

Previous studies have highlighted the significance of hydrogels as the scaffolding materials of choice for drug and growth factor delivery as well as for cell transplantation applications for CNS repair. This can be largely attributed to their ability to be adaptable and conform to the mechanical properties of the brain or other CNS tissues [42,43]. Several studies have provided the proof-of-concept that the delivery of cells with a hydrogel carrier maximises their survival *in vivo* when compared to the cells that are transplanted without any matrix support [44,45]. Seidlits et al. (2010) demonstrated the modulation of differentiation of ventral midbrain NPCs into neuronal cells and astrocytes by modulating the stiffness of hyaluronic acid based hydrogels [42]. In this study, we also found a correlation between the gel stiffness and modulation of the neuronal and astrocytic phenotype of the engrafted VM cells both at the gene expression level and in the modulation of paracrine response of the cells. It was found that there was a shift towards the pro-inflammatory phenotype with the highest fibrinogen concentration (60mg/ml) and cell density (10^6 cells) investigated in the current study. However, there was no adverse impact of the highest sphere density tested on the graft survival or the modulation of paracrine phenotype of the cells. In this study, a balance between graft survival and paracrine profile modulation was used to optimise the fibrin-in-fibrin platform parameters.

We also studied the influence on the engrafted cell secretome within the fibrin-in-fibrin construct by varying the fibrinogen, microsphere and cell concentration. Significant differences were observed between the levels of pro-and anti-inflammatory factors secreted by the cells embedded in different conditions. There was a notable spike of pro-inflammatory cytokines with higher fibrinogen concentrations and cell density suggestive of the enhanced proliferation of the inflammatory cells and a drift towards the pro-inflammatory phenotype in those conditions. With low levels of the pro-inflammatory cytokines and higher skewing of the engrafted cell secretome towards the anti-inflammatory phenotype with a higher secretion of IL-4, IL-10 and IL-13, specifically for 20 mg/ml of fibrinogen with 1 ug microspheres and 0.5

million cell density were found to be optimal to enhance the neuronal survival. In line with other studies that have been conducted earlier [46], this study further provides the proof-of-concept that it is possible to modulate cell behaviour by altering the cellular microenvironment in terms of the macromolecular modulation on a tuneable fibrin-in-fibrin platform.

3.5 Conclusion

In this study, a tuneable fibrin-in-fibrin platform for enhanced graft survival was fabricated and characterised. It was shown that there is an evident modulation of the paracrine response of the encapsulated VM grafts by the manipulation of the fabrication parameters influencing the cellular microenvironment. This study highlights the development of a brain –targeted cell delivery platform using the natural biopolymers by modulating the cell-cell and cell-matrix interactions.

3.6 References

- [1] A.H. Schapira, P. Jenner, Etiology and pathogenesis of Parkinson’s Disease, *Mov. Disord.* 26 (2011) 1049–1055. doi:10.1002/mds.23732.
- [2] P. Brundin, J. Karlsson, M. Emgård, G.S.K. Schierle, O. Hansson, Å. Petersén, R.F. Castilho, Improving the survival of grafted dopaminergic neurons: a review over current approaches, *Cell Transplant.* 9 (2000) 179–195. doi:10.1177/096368970000900205.
- [3] N. Moriarty, A. Pandit, E. Dowd, Encapsulation of primary dopaminergic neurons in a GDNF-loaded collagen hydrogel increases their survival, re-innervation and function after intra-striatal transplantation, *Sci. Rep.* 7 (2017) 16033. doi:10.1038/s41598-017-15970-w.
- [4] M. Emgård, L. Holmberg, E.-B. Samuelsson, B.A. Bahr, S. Falci, Å. Seiger, E. Sundström, Human neural precursor cells continue to proliferate and exhibit low cell death after transplantation to the injured rat spinal cord, *Brain Res.* 1278 (2009) 15–26. doi:10.1016/j.brainres.2009.04.012.
- [5] L.F. Lin, D.H. Doherty, J.D. Lile, S. Bektesh, F. Collins, GDNF: a glial cell line-derived neurotrophic factor for midbrain dopaminergic neurons., *Science.* 260 (1993) 1130–2. doi:10.1126/SCIENCE.8493557.
- [6] J.G. Hou, L.F. Lin, C. Mytilineou, Glial cell line-derived neurotrophic factor exerts

- neurotrophic effects on dopaminergic neurons in vitro and promotes their survival and regrowth after damage by 1-methyl-4-phenylpyridinium., *J. Neurochem.* 66 (1996) 74–82. doi:10.1046/j.1471-4159.1996.66010074.x.
- [7] A. Tomac, E. Lindqvist, L.-F.H. Lin, S.O. Ögren, D. Young, B.J. Hoffer, L. Olson, Protection and repair of the nigrostriatal dopaminergic system by GDNF in vivo, *Nature.* 373 (1995) 335–339. doi:10.1038/373335a0.
- [8] R. Grondin, Z. Zhang, A. Yi, W.A. Cass, N. Maswood, A.H. Andersen, D.D. Elsberry, M.C. Klein, G.A. Gerhardt, D.M. Gash, Chronic, controlled GDNF infusion promotes structural and functional recovery in advanced parkinsonian monkeys, *Brain.* 125 (2002) 2191–2201. doi:10.1093/brain/awf234.
- [9] D.M. Gash, Z. Zhang, Y. Ai, R. Grondin, R. Coffey, G.A. Gerhardt, Trophic factor distribution predicts functional recovery in parkinsonian monkeys, *Ann. Neurol.* 58 (2005) 224–233. doi:10.1002/ana.20549.
- [10] R. Grondin, O.M. Littrell, Z. Zhang, Y. Ai, P. Huettl, F. Pomerleau, J.E. Quintero, A.H. Andersen, M.J. Stenslik, L.H. Bradley, J. Lemmon, M.J. O’Neill, D.M. Gash, G.A. Gerhardt, GDNF revisited: A novel mammalian cell-derived variant form of GDNF increases dopamine turnover and improves brain biodistribution, *Neuropharmacology.* 147 (2019) 28–36. doi:10.1016/J.NEUROPHARM.2018.05.014.
- [11] S.J. Allen, J.J. Watson, D.K. Shoemark, N.U. Barua, N.K. Patel, GDNF, NGF and BDNF as therapeutic options for neurodegeneration, *Pharmacol. Ther.* 138 (2013) 155–175. doi:10.1016/j.pharmthera.2013.01.004.
- [12] D. V. Volodkin, N.I. Larionova, G.B. Sukhorukov, Protein encapsulation via porous CaCO₃ microparticles templating, *Biomacromolecules.* 5 (2004) 1962–1972. doi:10.1021/bm049669e.
- [13] J. Samal, D.B. Hoban, C. Naughton, R. Concannon, E. Dowd, A. Pandit, Fibrin-based microsphere reservoirs for delivery of neurotrophic factors to the brain, *Nanomedicine.* 10 (2015) 765–783. doi:10.2217/nmm.14.221.
- [14] J. Grossmann, Molecular mechanisms of “detachment-induced apoptosis—Anoikis,” *Apoptosis.* 7 (2002) 247–260. doi:10.1023/A:1015312119693.
- [15] P.C. Georges, W.J. Miller, D.F. Meaney, E.S. Sawyer, P.A. Janmey, Matrices with

- compliance comparable to that of brain tissue select neuronal over glial growth in mixed cortical cultures, *Biophys. J.* 90 (2006) 3012–3018. doi:10.1529/BIOPHYSJ.105.073114.
- [16] A. Gefen, N. Gefen, Q. Zhu, R. Raghupathi, S.S. Margulies, Age-dependent changes in material properties of the brain and braincase of the rat, *J. Neurotrauma.* 20 (2003) 1163–1177. doi:10.1089/089771503770802853.
- [17] K. Miller, K. Chinzei, G. Orssengo, P. Bednarz, Mechanical properties of brain tissue in-vivo: experiment and computer simulation, *J. Biomech.* 33 (2000) 1369–1376. doi:10.1016/S0021-9290(00)00120-2.
- [18] K. Hirakawa, K. Hashizume, T. Hayashi, Viscoelastic property of human brain -for the analysis of impact injury (author's transl)., *Brain and Nerve.* 33 (1981) 1057–65.
- [19] R.W.P. Rodrigues, V.C. Gomide, G. Chadi, Astroglial and microglial reaction after a partial nigrostriatal degeneration induced by the striatal injection of different doses of 6-Hydroxydopamine, *Int. J. Neurosci.* 109 (2009) 91–126. doi:10.3109/00207450108986528.
- [20] O. Lindvall, A. Björklund, Cell therapy in Parkinson's Disease., *NeuroRx.* 1 (2004) 382–393. doi:10.1602/neurorx.1.4.382.
- [21] R.A. Hauser, T.B. Freeman, B.J. Snow, M. Nauert, L. Gauger, J.H. Kordower, C.W. Olanow, Long-term evaluation of bilateral fetal nigral transplantation in Parkinson Disease., *Arch. Neurol.* 56 (1999) 179–187. doi:10.1001/archneur.56.2.179.
- [22] P. Brundin, O. Pogarell, P. Hagell, P. Piccini, H. Widner, A. Schrag, A. Kupsch, L. Crabb, P. Odin, B. Gustavii, A. Björklund, D.J. Brooks, C.D. Marsden, W.H. Oertel, N.P. Quinn, S. Rehncrona, O. Lindvall, Bilateral caudate and putamen grafts of embryonic mesencephalic tissue treated with lazarooids in Parkinson's disease, *Brain.* 123 (2000) 1380–1390. doi:10.1093/brain/123.7.1380.
- [23] P. Hagell, A. Schrag, P. Piccini, M. Jahanshahi, R. Brown, S. Rehncrona, H. Widner, P. Brundin, J.C. Rothwell, P. Odin, G.K. Wenning, P. Morrish, B. Gustavii, A. Björklund, D.J. Brooks, C.D. Marsden, N.P. Quinn, O. Lindvall, Sequential bilateral transplantation in Parkinson's disease. Effects of the second graft, *Brain.* 122 (1999) 1121–1132. doi:10.1093/brain/122.6.1121.

- [24] R.A. Barker, H. Widner, Immune problems in central nervous system cell therapy, *NeuroRX*. 1 (2004) 472–481. doi:10.1602/neurorx.1.4.472.
- [25] T.J. Collier, C.E. Sortwell, Therapeutic potential of nerve growth factors in Parkinson's Disease, *Drugs Aging*. 14 (1999) 261–287. doi:10.2165/00002512-199914040-00003.
- [26] C.E. Sortwell, M.R. Pitzer, T.J. Collier, Time course of apoptotic cell death within mesencephalic cell suspension grafts: implications for improving grafted dopamine neuron survival, *Exp. Neurol*. 165 (2000) 268–277. doi:10.1006/EXNR.2000.7476.
- [27] P.J. Reddig, R.L. Juliano, Clinging to life: cell to matrix adhesion and cell survival, *Cancer Metastasis Rev*. 24 (2005) 425–439. doi:10.1007/s10555-005-5134-3.
- [28] X. Liu, W. Peng, Y. Wang, M. Zhu, T. Sun, Q. Peng, Y. Zeng, B. Feng, X. Lu, J. Weng, J. Wang, Synthesis of an RGD-grafted oxidized sodium alginate–N-succinyl chitosan hydrogel and an in vitro study of endothelial and osteogenic differentiation, *J. Mater. Chem. B*. 1 (2013) 4484. doi:10.1039/c3tb20552e.
- [29] A.S. Wolberg, Thrombin generation and fibrin clot structure, *Blood Rev*. 21 (2007) 131–142. doi:10.1016/j.blre.2006.11.001.
- [30] M. Ehrbar, A. Metters, P. Zammaretti, J.A. Hubbell, A.H. Zisch, Endothelial cell proliferation and progenitor maturation by fibrin-bound VEGF variants with differential susceptibilities to local cellular activity, *J. Control. Release*. 101 (2005) 93–109. doi:10.1016/j.jconrel.2004.07.018.
- [31] H. Yasuda, S. Kuroda, H. Shichinohe, S. Kamei, R. Kawamura, Y. Iwasaki, Effect of biodegradable fibrin scaffold on survival, migration, and differentiation of transplanted bone marrow stromal cells after cortical injury in rats, *J. Neurosurg*. 112 (2010) 336–344. doi:10.3171/2009.2.JNS08495.
- [32] L.A. Flanagan, Y.-E. Ju, B. Marg, M. Osterfield, P.A. Janmey, Neurite branching on deformable substrates., *Neuroreport*. 13 (2002) 2411–2415. doi:10.1097/01.wnr.0000048003.96487.97.
- [33] P.C. Georges, W.J. Miller, D.F. Meaney, E.S. Sawyer, P.A. Janmey, Matrices with compliance comparable to that of brain tissue select neuronal over glial growth in mixed cortical cultures, *Biophys. J*. 90 (2006) 3012–3018. doi:10.1529/biophysj.105.073114.
- [34] S.E. Sakiyama, J.C. Schense, J.A. Hubbell, Incorporation of heparin-binding peptides

- into fibrin gels enhances neurite extension: an example of designer matrices in tissue engineering, *FASEB J.* 13 (1999) 2214–2224. doi:10.1096/fasebj.13.15.2214.
- [35] Alexei A. Antipov, Gleb B. Sukhorukov, A. Edwin Donath, H. Möhwald, Sustained release properties of polyelectrolyte multilayer capsules, *Adv Colloid Interface Sci.* 111 (2001) 49–61. doi:10.1021/JP002184+.
- [36] H. Ai, S.A. Jones, M.M. de Villiers, Y.M. Lvov, Nano-encapsulation of furosemide microcrystals for controlled drug release, *J. Control. Release.* 86 (2003) 59–68. doi:10.1016/S0168-3659(02)00322-X.
- [37] A. Larrañaga, I.L.M. Isa, V. Patil, S. Thamboo, M. Lomora, M.A. Fernández-Yague, J.-R. Sarasua, C.G. Palivan, A. Pandit, Antioxidant functionalized polymer capsules to prevent oxidative stress, *Acta Biomater.* 67 (2018) 21–31. doi:10.1016/J.ACTBIO.2017.12.014.
- [38] D. V. Volodkin, A.I. Petrov, A. Michelle Prevot, G.B. Sukhorukov, Matrix polyelectrolyte microcapsules: new system for macromolecule encapsulation, *Langmuir.* 20 (2004) 3398–3406. doi:10.1021/LA036177Z.
- [39] H. Kraskiewicz, B. Breen, T. Sargeant, S. McMahon, A. Pandit, Assembly of protein-based hollow spheres encapsulating a therapeutic factor, *ACS Chem. Neurosci.* 4 (2013) 1297–1304. doi:10.1021/cn400080h.
- [40] T.M. Odrljín, C.W. Francis, L.A. Sporn, L.A. Bunce, V.J. Marder, P.J. Simpson-Haidaris, Heparin-binding domain of fibrin mediates its binding to endothelial cells, *Arterioscler. Thromb. Vasc. Biol.* 16 (1996) 1544–1551. doi:10.1161/01.ATV.16.12.1544.
- [41] N. Nevalainen, M. Chermenina, A. Rehnmark, E. Berglöf, F. Marschinke, I. Strömberg, Glial cell line-derived neurotrophic factor is crucial for long-term maintenance of the nigrostriatal system, *Neuroscience.* 171 (2010) 1357–1366. doi:10.1016/j.neuroscience.2010.10.010.
- [42] S.K. Seidlits, Z.Z. Khaing, R.R. Petersen, J.D. Nickels, J.E. Vanscoy, J.B. Shear, C.E. Schmidt, The effects of hyaluronic acid hydrogels with tunable mechanical properties on neural progenitor cell differentiation, *Biomaterials.* 31 (2010) 3930–3940. doi:10.1016/j.biomaterials.2010.01.125.

- [43] Y.-B. Lu, K. Franze, G. Seifert, C. Steinhauser, F. Kirchhoff, H. Wolburg, J. Guck, P. Janmey, E.-Q. Wei, J. Kas, A. Reichenbach, Viscoelastic properties of individual glial cells and neurons in the CNS, *Proc. Natl. Acad. Sci.* 103 (2006) 17759–17764. doi:10.1073/pnas.0606150103.
- [44] J. Zhong, A. Chan, L. Morad, H.I. Kornblum, G. Guoping Fan, S.T. Carmichael, Hydrogel matrix to support stem cell survival after brain transplantation in stroke, *Neurorehabil. Neural Repair.* 24 (2010) 636–644. doi:10.1177/1545968310361958.
- [45] P. Lu, Y. Wang, L. Graham, K. McHale, M. Gao, D. Wu, J. Brock, A. Blesch, E.S. Rosenzweig, L.A. Havton, B. Zheng, J.M. Conner, M. Marsala, M.H. Tuszynski, Long-Distance growth and connectivity of neural stem cells after severe spinal cord injury, *Cell.* 150 (2012) 1264–1273. doi:10.1016/j.cell.2012.08.020.
- [46] D. Thomas, G. Fontana, X. Chen, C. Sanz-Nogués, D.I. Zeugolis, P. Dockery, T. O'Brien, A. Pandit, A shape-controlled tuneable microgel platform to modulate angiogenic paracrine responses in stem cells, *Biomaterials.* 35 (2014) 8757–8766. doi:10.1016/j.biomaterials.2014.06.053.

Chapter 4

Complete spatial resolution of neutral and charged *N*-glycans in rodent brain

Sections of this chapter are under submission:

Samal J., Saldova R., Rudd P.M., Pandit A.P., O'Flaherty R. (2019). "Complete spatial resolution of neutral and charged *N*-glycans in rodent brain."

4.1 Introduction

The biological roles of glycans cover a broad spectrum of protective, organizational and barrier functions making them crucial for the growth and survival of the host organism. *N*-glycosylation represents the most frequent type of post-translational modification in eukaryotic cells [340,341], which involves the attachment of oligosaccharide chains to asparagine residues on proteins. There are three major structural types of *N*-glycans depending on the branching in glycan chains: oligomannose, complex-type (*N*-acetylglucosamine) and hybrid type (mannose and *N*-acetylglucosamine). Cell surface *N*-glycans are involved in several essential cellular functions including cellular and cell–matrix interactions. They also play crucial roles in cell adhesion, differentiation, synaptogenesis and myelinogenesis during the development of central nervous system (CNS) [3].

Early predictions for glycans mediating neural cell interactions in the developing and adult nervous system were based on the cell-specific complex gangliosides and cell- surface glycosyltransferases expressed by neural cells [4,5]. The ubiquitous distribution of glycosylation in the CNS and its facilitation of functional processes that depend on cell recognition, such as migration, neurite outgrowth, synapse formation and stabilization has drawn significant investigation of the biological implications in developmental processes [6,7] and disease pathophysiology [8]. One of the well-studied examples of *N*-glycan involvement in CNS developmental processes is polysialic acid (PSA) and its complexation with the *N*-glycans of neural cell adhesion molecule (NCAM) or CD 56. PSA is a homopolymer of α -2,8-linked sialic acid associated with a *N*-glycan core that is linked with NCAM at 5 and 6 glycosylation sites in the fifth immunoglobulin-like domain of the protein [9]. PSA-NCAM was also shown to promote retinal ganglion cell (RGC) survival in transgenic mice deficient in sialyltransferases or NCAM or post endoneuraminidase (Endo-*N*) administration [10]. Similarly, poly-*N*-acetylglucosamine oligosaccharides (PLN) represent another example of *N*-glycosylation that plays a crucial role in neural development. Targeted genetic inactivation of the β 3GnT2 glycosyltransferase responsible for elongation of PLN results in numerous abnormalities in axonal guidance and glomeruli formation in the olfactory system of mice [3].

Investigations of the role of glycosylation in regulating the communication between neurons in CNS involved sequential extraction and analysis of synaptosomes from brain which revealed the presence of oligomannose *N*-glycan structures [11,12]. Neurotransmitter receptors play a key role in synaptic transmission by acting as ligand-gated channel proteins and facilitating neuronal communication within the nervous system. These receptors generally bear several *N*-

glycans attached to their extracellular domains. The surface expression and intracellular trafficking of AMPA-type glutamate receptor (AMPA) which mediates the majority of rapid excitatory synaptic transmissions in the nervous system and modulates synaptic plasticity has shown to be regulated by site-specific *N*-glycosylation [13]. *N*-glycosylation has been shown to play an important role in the regulation of the function of neurotransmitter transporters, which determines the concentration of neurotransmitters in the synaptic cleft. GABA transporter 1 (GAT1) is a chief GABA transporter in the brain which regulates the reuptake of GABA from the synaptic cleft. It is an *N*-glycosylated protein where the *N*-glycans are involved in regulation of stability, trafficking and GABA-uptake activity of the transporter[14]. Alterations in *N*-glycosylation of a subfamily of transporters from SLC6 (solute carrier) family of membrane proteins reduces the number of transporters expressed at cell surface. This was correlated to the decreased stability of these transporters and impaired transport of non-glycosylated transporters to the cell surface [15].

Alteration in *N*-glycosylation can essentially alter the structure and function of the glycoprotein. The cardinal role of *N*-glycans for the nervous system is brought forth by congenital glycosylation diseases [16], resulting in different neuropathological symptoms like mental retardation, seizures and epilepsy. Examples of such congenital *N*-glycosylation disorders targeting the central nervous system include PMM2-CDG (CDG-Ia) [17,18] and ALG6-CDG (CDG-Ic) [18]. Thorough understanding of the identity and functional roles of glycans in the nervous system will endow us with better perspective on nervous system function[19]. Investigation on the variations in the glycosylation patterns of proteins at cellular and matrix level in brain can lead to the identification of molecular targets for devising efficient therapeutic targets.

Previous studies have reported the conservation of *N*-glycan processing in rodents [20–22]. Different studies have highlighted the spatially specific regulation of *N*-glycans in different regions of the brain of healthy and glioblastoma mouse models using matrix-assisted laser desorption/ionization (MALDI)-MSI [23]. These studies emphasize further the need of a detailed *in vivo* analysis for specific regions in the brain to elucidate further the correlation of glycosylation with the regulation of biological functions. A preliminary analysis of the differential regulation of *N*-glycosylation in the nigrostriatal pathway with age of the animals has been reported [24]. These studies provide ample ground to support the working hypothesis of this study and for further detailed investigation into the structure-specific glycan compositions in these regions of the brain. Most of the brain glycan investigations were

conducted more than twenty years ago and include outdated *N*-glycan methodologies such as hydrazinolysis for *N*-glycan release, separate studies for charged/neutral *N*-glycans (which limits the comparability of these glycans to each other) and/or the use of normal phase HPLC for separation of *N*-glycans. In addition, there is a lack of spatial resolution of these glycan profiles as the tissue samples were homogenized intact for these studies. Since the biosynthesis of *N*-glycans undergoes a stringent spatio-temporal regulation within the tissue, it is hypothesized that the spatial resolution of *N*-glycans isolated from striatum and substantia nigra (SN) could give an insight into their involvement in regulation of striatal and nigral cues for establishment and pathophysiological degeneration of neural circuitry in Parkinson's disease. In this study, the first spatio-specific glycoanalytical technology to analyse the overall *N*-glycosylation of rodent brain is presented. Using a combination of hydrophilic interaction chromatography (HILIC) ultra-performance liquid chromatography (UPLC), electrospray ionization-mass spectrometry (ESI-MS), exoglycosidase sequencing and lectin histochemistry, we present a detailed comparative spatial analysis of relative abundances of *N*-type glycans in SN and striatum of adult rat brains. Analysis using this robust platform revealed regio-specific modulation of *N*-glycosylation in the rodent brains as alterations of features like sialylation and fucosylation and this was well correlated to the regional cellular composition and their projected biological significance. To date, this is the first study and most comprehensive platform for spatial resolution of *N*-glycans in the rodent brains to extensively characterise and compare the *N*-glycome of striatum and SN. This is of great relevance in postulating the possible correlation of *N*-glycosylation and its modulation in the neurodegenerative disorders like Parkinson's disease involving these regions of brain.

4.2 Materials & Methods

The *in vivo* analysis and brain tissue collection and processing for protein extraction was performed at Centre for Research in Medical Devices (CÚRAM), National University of Ireland, Galway. The glyco-analytical platform was developed and used for the investigation of the *N*-glycans in the striatum and substantia nigra of the rodent brains at The National Institute for Bioprocessing Research and Training (NIBRT), University College Dublin. This platform included multiple analytical techniques including HILIC-UPLC, WAX-UPLC, LC-MS/MS and exoglycosidase sequencing performed at NIBRT under the supervision of Dr. Roisin O'Flaherty and Dr. Radka Saldova Fahey. Lectin histochemical analysis was performed at CÚRAM, NUIG.

4.2.1 Chemicals and Reagents

Formic acid (FA) and Tris were obtained from AnalaR, VWR (Dublin, Ireland). Sodium bicarbonate (NaHCO₃) and ammonium bicarbonate (NH₄HCO₃) were obtained from HiPerSolv, BDH (Dublin, Ireland). Protogel was purchased from National Diagnostics, Hessele, Hull, UK. Ammonium persulfate (APS) was purchased from AnalaR; BDH and *N,N,N',N'*-tetramethylethane-1,2-diamine (TEMED) from Sigma-Aldrich. Iodoacetamide (IAA) and dithiothreitol (DTT) were obtained from Sigma-Aldrich. Sodium dodecyl sulfate (SDS), acetonitrile and sucrose were obtained from Sigma Aldrich. Ultrapure water was obtained from Arium[®] ProUV (Sartorius stedum). 2-aminobenzamide (2-AB) labeling of *N*-glycans was performed using fluorescent labeling mix (50 µL, 350 mM 2-AB (Sigma), 1 M sodium cyanoborohydride (Sigma) in acetic acid (Sigma)/dimethyl sulfoxide (Sigma) (30:70) [25].

4.2.2 Animals

Female Sprague–Dawley rats (Charles River, UK) were used in this study (n=35), weighing 225–250 gm at the start of the experiment. Animals were housed in groups of four per cage, on a 12:12-h light:dark cycle, at 19–23 °C, with the humidity level of the room maintained between 40% and 70%, and food and water available *ad libitum* throughout the course of the experiment. All procedures were carried out in accordance with the European Union Directive 2010/73/EU and S.I. No. 543 of 2012, were completed under CAA license (B100/3827) issued to Dr. Eilís Dowd by the Irish Department of Health and Children, and were reviewed and approved by The Animal Care and Research Ethics Committee of the National University of Ireland, Galway.

4.2.3 Extraction of striatal and nigral tissues from rat brain

Intact brains from adult rats were snap frozen and lyophilized. Lyophilized brains were then sectioned into 300 µm slices using the Microm HM 505 E cryostat (GMI) after being mounted on the cryostat chuck using OCT. The sections were collected on SuperFrost[™] Plus Adhesion slides (ThermoFischer Scientific). Relevant sections for striatum and nigra were identified using a brain atlas. Micron biopsy punch of 2 mm and 0.5 mm (Harvard apparatus) were used to punch out striatum and nigra respectively from brain sections. The tissue punches were collected in microcentrifuge tubes and stored at -80 °C until processed further.

4.2.4 Perfusion

Rats were anaesthetised with pentobarbital (1 ml/kg) and transcardially perfused with 100 ml of ice-cold heparinised saline (5000 U/L) followed by 150 ml of 4% paraformaldehyde (pH 7.4). Their brains were removed and placed into 4% paraformaldehyde overnight for post-fixation prior to transfer to 30% sucrose. After 48 h equilibration in sucrose solution, 30 µm serial sections of the fixed brains were cut using a freezing sledge microtome and lectin staining was performed.

4.2.5 Tissue homogenization

Tissue homogenates for *N*-glycan isolation and profiling were obtained by using Tris-SDS lysis buffer [364]. Briefly, collected tissue samples were re-suspended in Tris-SDS lysis buffer (62.5 mM TRIS pH 6.6, 2% SDS) for 20 minutes on ice followed by aspiration thrice and a further 20 minutes incubation. This was followed by homogenization using automated bead homogenizer (Qiagen TissueLyser LT) for complete lysis (40 Hz, six min). Supernatant was collected after centrifugation at 16,860 G for 20 minutes at 4 °C and dried overnight under vacuum centrifugation. Protein concentration in the samples were estimated using bicinchoninic acid (BCA) protein assay (PierceTM BCA Protein Assay Kit, ThermoFischer Scientific).

4.2.6 Release of *N*-glycans from striatal and nigral tissue homogenates

N-glycans were released from dried tissue samples using the high-throughput method described by Royle *et al* [27] with a slight modification. Briefly, samples were immobilized in SDS-gel blocks to minimise the sample loss during transfer, reduced and alkylated in 96-well plates and then washed. The *N*-linked glycans were released using peptide *N*-glycanase F (500,000 U/ mL, NEB) as previously described [28].

4.2.7 2-AB labeling of *N*-glycans

N-glycans were fluorescently labeled with 2-AB by reductive amination [29]. Briefly, 2-AB labeling mixture was added to the released glycans, followed by agitation for five min to ensure proper mixing. This was followed by an incubation at 65°C for 30 min and five min agitation. The samples were then incubated at 65°C for 1.5 hours. Excess

2-AB reagent was removed on Whatman 3MM paper (Clifton, NJ) with acetonitrile and final elution of glycans was performed in water [30].

4.2.8 Ultra-Performance Liquid Chromatography (UPLC)






UPLC was performed using a BEH Glycan 1.7 μm particles in 2.1×150 mm column (Waters, Milford, MA) on an Acquity UPLC (Waters) equipped with a Waters temperature control module and a Waters Aquity fluorescence detector. Solvent A was 50 mM formic acid adjusted to pH 4.4 with ammonia solution. Solvent B was acetonitrile. The column temperature was set to 40 °C. A 30minutesmethod was used with a linear gradient of 30–47% with buffer A at 0.56 mL/min flow rate for 23minutesfollowed by 47–70% A and then to 30% A. Samples were injected in 70% acetonitrile. Fluorescence detection was performed using $\lambda_{\text{excitation}}$: 320 nm and $\lambda_{\text{emission}}$: 420 nm. The system was calibrated using an external standard of hydrolyzed and 2 AB-labeled glucose oligomers to create a dextran ladder, as described previously [26].

4.2.9 Weak anion exchange (WAX)-(UPLC)

Weak anion exchange (WAX)-HPLC was performed using a 10 μm Biosuite DEAE (7.5 mm x 75 mm) column (Waters) on a 2795 Alliance separations module with a Waters 2475 fluorescence detector ($\lambda_{\text{excitation}}$: 330 nm, $\lambda_{\text{emission}}$: 420 nm). Solvent A was 20% MeCN, and solvent B was 25 mM Ammonium Acetate buffer adjusted to pH 7.0. Gradient conditions were as follows: a linear gradient of 100% A to 100% B over 50minutesat a flow rate of 0.75 mL/min. Samples were injected in water. α -fetuin N-glycan standard was used for calibration.

4.2.10 Glycan nomenclature

All N-glycans have two core GlcNAcs attached to trimannosyl; F at the start of the abbreviation indicates a core $\alpha(1,6)$ -fucose linked to the inner GlcNAc; otherwise F indicates an outer arm $\alpha(1,3)$ or $\alpha(1,4)$ -fucose linked to antenna or galactose; Mx, number (x) of mannose on core GlcNAcs; Ax, number of antenna (GlcNAc) on trimannosyl core; A2, biantennary with both GlcNAcs as $\beta(1,2)$ -linked; A3, triantennary with a GlcNAc linked $\beta(1,2)$ - to both mannose and a third GlcNAc linked $\beta(1,4)$ - to the $\alpha(1,3)$ -linked mannose; A4, GlcNAcs linked as A3 with additional GlcNAc- $\beta(1,6)$ -linked to $\alpha(1,6)$ -mannose; Gx, number (x) of $\beta(1,4)$ -linked galactose on the antenna; Galx, number (x) of $\alpha(1,3/4/6)$ -linked galactose on $\beta(1,4)$ -linked galactose; Sx, number (x) of sialic acids linked to galactose; the number 3 or 6 in parentheses after S indicates whether the sialic acid is in an $\alpha(2,3)$ - or $\alpha(2,6)$ -linkage; Sx, number (x) of neuraminic acids

linked to galactose; the number 3, 6 or 8 in parentheses after S indicates whether the sialic acid is in an $\alpha(2,3)$ -, $\alpha(2,6)$ - or $\alpha(2,8)$ - linkage; Gcx, number (x) of glycolylneuraminic acids linked to galactose; the number 3, 6 or 8 in parentheses after S indicates whether the sialic acid is in an $\alpha(2,3)$ -, $\alpha(2,6)$ - or $\alpha(2,8)$ - linkage; Acx, number (x) of acetyl groups; Lacx, the number (x) of repeating poly-*N*-acetylglucosamine repeats containing GlcNAc linked $\beta(1,4)$ - to Gal; Px, the number (x) of phosphorous groups. Symbols representative of different glycan moieties in the structures are represented as follows:  , N-acetylglucosamine;  , Mannose;  , Fucose;  , Galactose;  , N-acetylneuraminic acid (sialic acid).

4.2.11 Exoglycosidase digestions

All enzymes were purchased from Prozyme (San Leandro, CA, USA) or New England Biolabs (Ipswich, MA, USA). The 2AB-labeled glycans were digested in a volume of 10 μ L for 18 h at 37 °C in 50 mM sodium acetate buffer, pH 5.5 using arrays of the following enzymes: *Arthrobacter ureafaciens* sialidase (ABS, Prozyme, 0.5 U/mL); bovine testes β -galactosidase (BTG, Prozyme, 1 U/mL); N-acetylneuraminic acid glycohydrolase (NAN1, NEB, 800 U/mL); bovine kidney α -fucosidase (BKF, Prozyme, 1 U/mL); β -N-acetylglucosaminidase cloned from *S. pneumonia*, expressed in *Escherichia coli* (GUH, NEB, 800 U/ml and Prozyme, 8 U/ml); coffee bean α -galactosidase (CBG, NEB, 800 U/ml); almond meal α -fucosidase (AMF, Prozyme, 0.4 mU/ml). After incubation, enzymes were removed by filtration through 10 kDa protein-binding EZ filters (Pall NANOSEP 10K OMEGA). *N*-glycans were then analyzed by UPLC.

4.2.12 Liquid chromatography mass spectrometry

Online coupled fluorescence (FLR)-mass spectrometry detection was performed using a Waters Xevo G2 QTof with Acquity® UPLC (Waters Corporation, Milford, MA, USA) and BEH Glycan column (1.0 x 150mm, 1.7 μ m particle size). For MS acquisition data the instrument was operated in negative-sensitivity mode with a capillary voltage of 1.8kV. The ion source block and nitrogen desolvation gas temperatures were set at 120 °C and 400 °C, respectively. The desolvation gas was set to a flow rate of 600 L/h. The cone voltage was maintained at 50 V. Full-scan data for glycans were acquired over m/z range of 450 to 2500. Data collection and processing were controlled by MassLynx 4.1 software (Waters Corporation, Milford, MA, USA). The fluorescence detector settings were as follows: λ excitation: 320 nm, λ emission: 420 nm; data rate was 1pts/second and a PMT gain = 10. Sample injection volume was 10 μ L (75% MeCN). The flow rate was 0.150 mL/min and column temperature was maintained at 60°C; solvent A was 50 mM ammonium formate (pH

4.4) and solvent B was MeCN. A 40minuteslinear gradient was used and was as follows: 28% A for one min, 28-43% A for 30 min, 43-70% A for one min, 70 % A for three min, 70-28% solvent A for oneminutesand 28% A for four min. To avoid contamination of system, flow was sent to waste for the first 1.2minutesand after 32 min.

4.2.13 Lectin histochemistry

Brains were dissected out and post-fixation was performed for four h at room temperature. They were then transferred to 25% sucrose in phosphate buffer. For lectin histochemistry, slides were washed with Tris-buffered saline supplemented with Ca^{2+} and Mg^{2+} (TBS; 20 mM Tris-HCl, 100 mM NaCl, 1 mM CaCl_2 , 1 mM MgCl_2 , pH 7.2) with 0.05% Triton X-100 (TBS-T) and then blocked with 2% periodate-treated BSA (Sigma-Aldrich[®]) in TBS for one hour. All washes were three times for five minutes each, all steps performed at room temperature in a humidity chamber unless otherwise stated. Sections were washed then incubated with four different fluorescein isothiocyanate (FITC)- conjugated lectins (EY Labs Inc., UK) in TBS for one h (**Appendices, Table A7**). Inhibitory controls were carried out in parallel to verify lectin binding specificity by pre- (for one hour) and co-incubating lectins in 100 mM of the appropriate haptenic sugar in TBS (**Appendices, Table A7**). Sections were washed five times with TBS-T and counterstained with 4' 6-diamidino-2-phenylindole dihydrochloride (DAPI) for 20 minutes. The slides were washed in TBS-T before mounting the coverslip with ProLong[®] Gold antifade (Life Technologies).

4.2.14 Statistical analysis

Statistical analyses were performed using GraphPad Prism[®] Version 5 (USA) and IBM SPSS[®] Version 21. Data were compared using one-way or two-way analysis of variance (ANOVA) based on the number of factors analysed, followed by a BonFerroni post-hoc comparison test. Statistical significance was set as * $p < 0.05$, ** $p < 0.01$, *** $p < 0.001$.

4.3 Results

4.3.1 Development of a robust glyco-analytical platform

This study represents the first initiative to develop an extensive glycoanalytical platform for the assessment of the spatial regulation of *N*-glycosylation occurring in the striatum and SN. Here, the total *N*-glycome including all of the major neutral and charged *N*-linked glycans expressed in the striatum and SN of adult rat was characterised using a combination of HILIC-UPLC, exoglycosidase sequencing and LC-MS as represented in **Figure 4.1**.

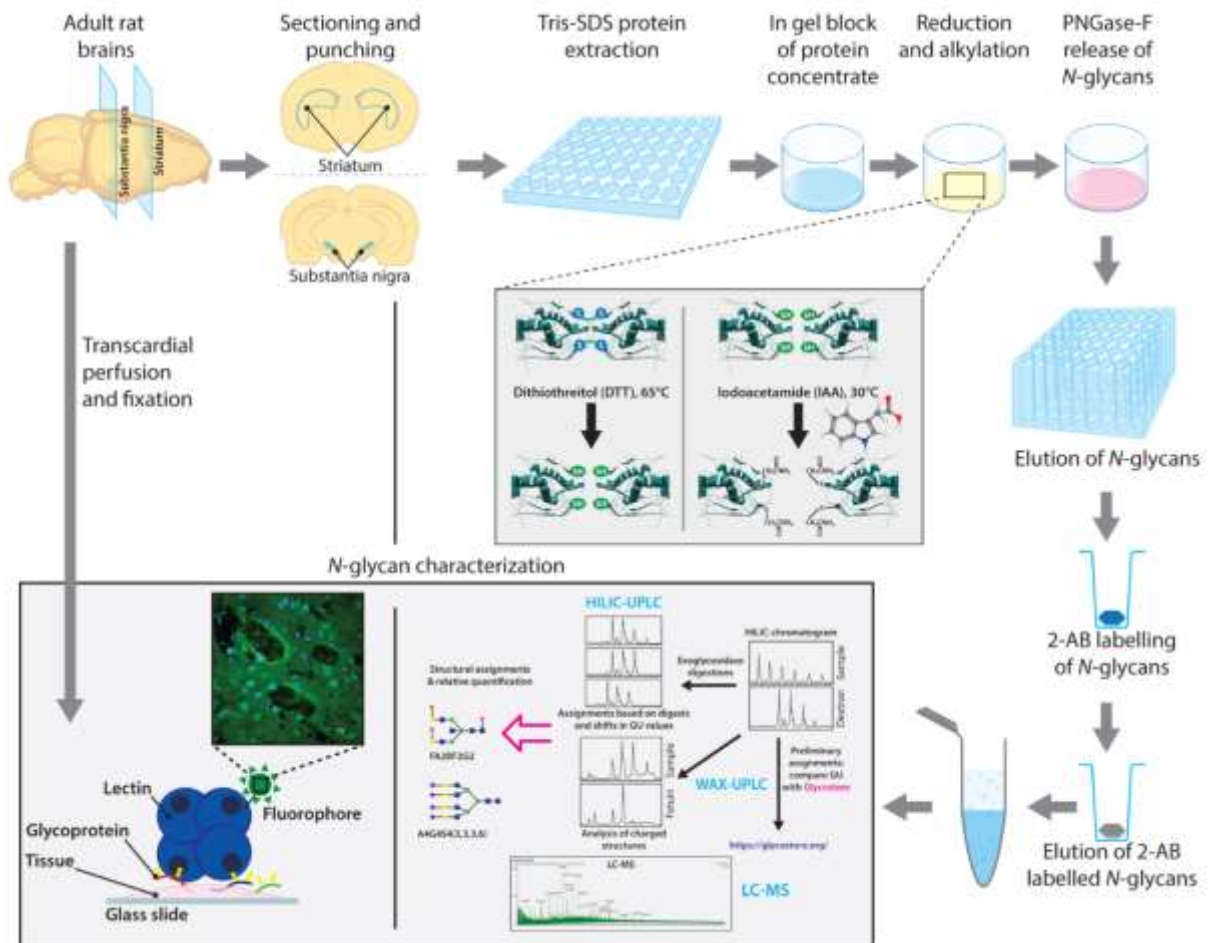


Figure 4.1: Schematic outline of the developed multi-faceted glyco-analytical platform for the qualitative and quantitative spatial analysis of rodent brain *N*-glycans. The schematic outlines different stages of protein isolation and *N*-glycan isolation followed by different analytical techniques used to establish the platform including HILIC-UPLC, WAX-UPLC, exoglycosidase digestions and LC-MS. Lectin histochemical analyses were performed to semi-quantitatively represent the changes in *N*-glycosylation over the two regions of the brain.

4.3.2 Protocol verification and reproducibility

For protocol verification, seven samples from pooled striatal and nigral *N*-glycans were prepared respectively using the newly developed in-gel-block (IGB) glycoanalytical approach [27]. *N*-glycans from both tissue types were then analyzed on a UPLC system equipped with BEH HILIC glycan column and fluorescent detection. Complete overlay of the glycoprofiles is shown in **Figure 4.2A** and is indicative of reproducibility of the protocol optimised for *N*-glycan isolation from brain tissues. Seven biological replicates for each tissue type were ran using the developed technology and visualized on HILIC-UPLC. The coefficients of variation (C_v) between the samples for both tissue types were below 10% for all major peaks, i.e. those peaks with a relative percentage area above 5% (**Figure 4.2B, C**). Only one peak was above 20% of variance in striatum and two peaks showed values of variance above 20% in SN. Higher coefficients of variance ($C_v > 20\%$) were biased towards the small peaks at the beginning and end of the profile of very low intensity.

4.3.3 Glycosylation Features

Representative chromatograms from striatum and SN along with the corresponding major peak assignments are shown in **Figure 4.3A, B**. For feature analysis, major glycan constituents of each peak were considered the representative feature for that peak. The glycosylation traits were calculated from the sum of glycan peaks (GP1-GP26) each of which combined the glycans with the same structural features. The chief glycosylation features like sialylation, galactosylation, fucosylation, oligomannose and branched *N*-glycans were investigated for both striatum and SN. The trends were calculated by summation of the relevant dominant species in each peak for a glycan trait and these are presented in detail in **Supplementary file S1**. All the major glycan species for both striatum and SN in the 26 glycan peaks are represented in **Table 4.1 A, B**. The overall distribution of detected *N*-glycans according to the major structural classes in striatum and SN are represented in **Figure 4.4A, B**. Spatial regulation of *N*-glycosylation can be observed in the distribution of these major structural classes of *N*-glycans in both tissue types. As a general trend, the first glycan species to be eluted as represented in the chromatograms are smaller neutral glycans, followed by larger sialylated and highly fucosylated charged glycans.

4.3.4 Fucosylation

Fucosylated *N*-glycans from both tissue types were classified on the basis of the degree of fucosylation and a difference in spatial distribution of differentially fucosylated species was

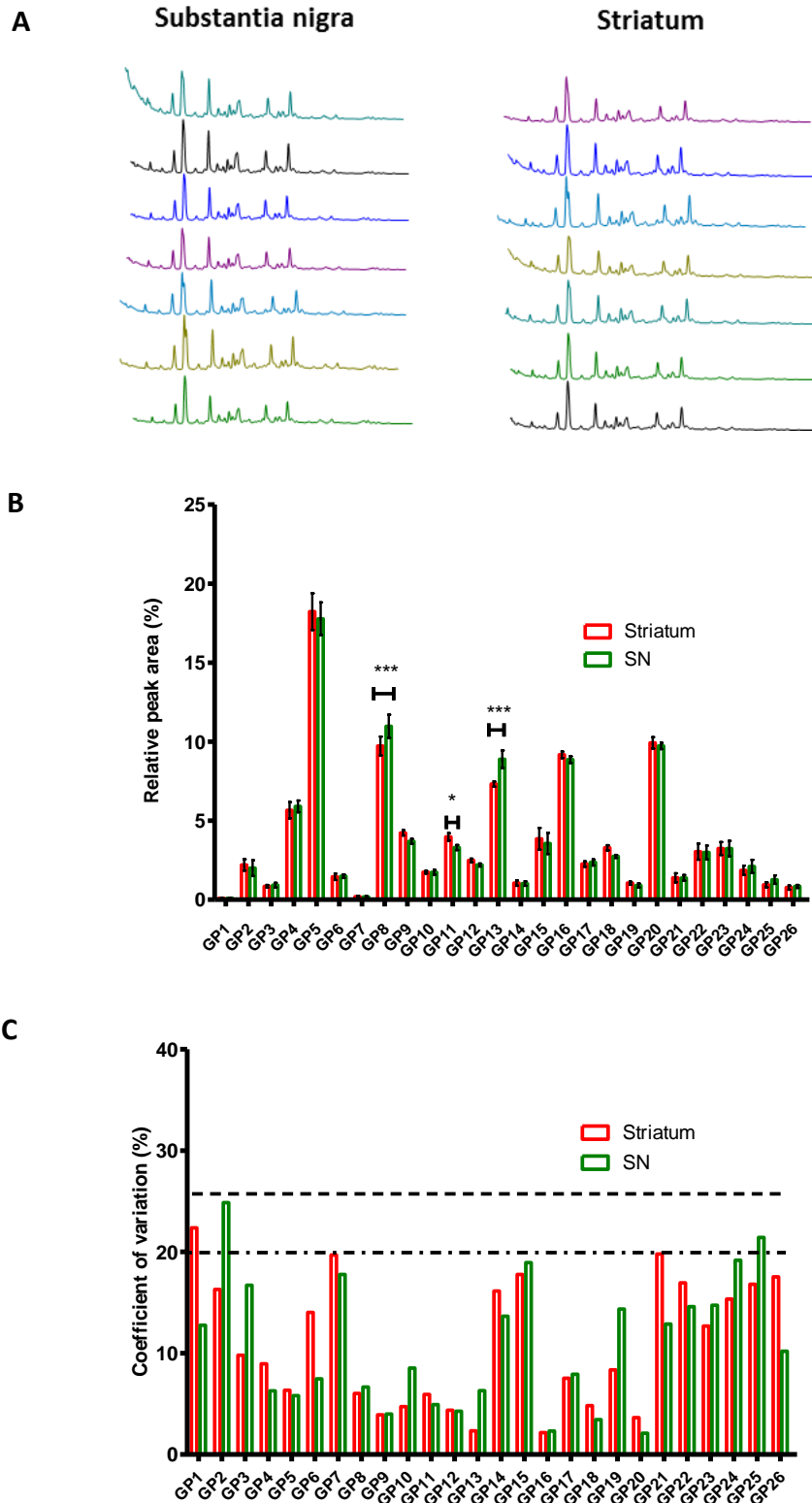


Figure 4.2 Reproducibility of the glycol-analytical platform A) Reproducibility of the platform represented by the overlay of seven biological replicates (biological replicates have been assigned different colours), B) Comparison of the glycan peak areas from striatum and SN of seven samples, C) Comparison of the glycan area coefficients of variation for seven samples for striatum and SN using the in-gel-block (IGB) method followed by HILIC-UPLC. GP: glycan peak number.

identified (**Figure 4.5C**). As represented in **Figure 4.5C**, relatively high abundances of multiple-fucose (up to four fucose residues) substituted *N*-glycans were detected in striatum (31%) and SN (25%). Also, varied proportions of core fucosylated and outer arm fucosylated species were detected in both striatum and SN as represented in **Figure 4.5A, B**.

4.3.5 Sialylation

WAX-UPLC analysis of the *N*-glycans extracted from striatum and SN revealed that major proportion of isolated glycans were neutral (81% for striatum and 83% for SN) as represented in **Figure 4.6A, B**. This distribution of neutral and sialylated species in both tissue types aligned closely with the results from exoglycosidase digestions. From this analysis, it was observed that the *N*-glycans isolated from SN show a lower overall sialylation when compared to the striatum. These differences are more pronounced in the mono-sialylated and tri-sialylated *N*-glycans as opposed to the di- and tetra- sialylated glycans as represented in **Figure 4.6A, B**. A major proportion of sialylated *N*-glycans in both tissue types was, however, constituted by mono- to tri- sialylated species. Higher sialylated *N*-glycans with four Neu5Ac substitutions were also detected in SN which weren't very significant in striatal *N*-glycans. In terms of the Neu5Ac linkage to galactose, this study was in agreement with previous studies investigating the charged *N*-glycans in rodent brains[20,31] which showed that Neu5Ac in $\alpha(2-3)$ -linkage to galactose was much more abundant than in $\alpha(2-6)$ -linkage (**Figure 4.6C**).

4.3.6 Galactosylation

Another extensively investigated glycosylation feature of the glycoproteins is galactosylation. In the current study, there was significant differences detected in the galactosylation patterns of striatum and SN. Major proportion of *N*-glycans in both striatum (65%) and SN (59%) were without galactoses (G0). This comprised of both the neutral and charged *N*-glycans. Four other classes of galactosylated *N*-glycans with one (G1), two (G2), three (G3) and four (G4) terminal galactose residues were also differentially regulated across the two regions of the brain as represented in supplementary information (**Appendices, Section R, Table S4.1: Derived traits**). In terms of antennary distribution, there was an overall abundance of bi- and tri-antennary structures when compared to mono- and tetra- antennary *N*-glycans. As represented in **Figure 4.4B**, there is distinctive spatial regulation of tri-antennary/ bi-antennary glycans with bisect between striatum and SN which includes both the neutral and charged species.

4.3.7 Mannosylation

A distinctive spatial regulation of oligomannose glycans was observed in the current study where a higher proportion of SN *N*-glycans (41%) were observed to be mannosylated as compared to striatum (36%). Another significant feature detected in our study that has not been reported in any broad-spectrum analysis of brain *N*-glycans till date is the presence of mannose-6-phosphorylation (Man 6-P) of the oligomannose *N*-glycans. Interestingly, this feature was only detected in the SN glycans and was not confirmed as a major glycosylation feature in the striatum.

4.3.8 Spatial regulation of *N*-glycosylation

This study outlined the major differences in major *N*-glycosylation traits in the aforementioned sections. Specific differences detected in the *N*-glycan species between striatum and SN were localized in glycan peaks GP14, 18, 22, 24 and 26 in the HILIC-UPLC chromatogram. The typical features of glycosylation being regionally altered in these peaks include fucosylation, sialylation and mannosylation. These differentially regulated glycan species are highlighted in **Table 4.2** and the LC-MS spectra in **Figure 4.3C, D**. The major glycan species detected in each of these peaks were significantly different for striatum and SN. Another observation made by comparing the peak areas for these tissue types was that there was a significant difference in GP8, 11 and 13 (**Figure 4.2B**) between striatum and SN which is a reflective of the fact that the major glycan species in these peaks might be differentially regulated in their expression in these regions of the brain.

4.3.9 Lectin histochemistry

For fucosylation, striatum and SN showed differential binding profile with *Anguilla anguilla* lectin (AAA) (**Figure 4.7A**). This lectin binds to Fuc- α -(1-6) and Fuc- α -(1-3) glycan moieties. The lectin binding profile further supports our observation of the distinct spatial distribution of fucosylated *N*-glycans with striatum showing a more diffused, higher binding intensity than SN. In agreement with analysis, a higher binding intensity was observed for Con A in the SN as compared to striatum indicative of a higher expression of oligomannosidic *N*-glycans. WGA strongly binds to the microglial population and SN is densely populated by it as compared to striatum[32]. The quantified lectin histochemistry analysis is presented in **Figure 4.7B** which is in line with the previous analysis in this study. This presents a very strong evidence on the hypothesized correlation of the *N*-glycosylation patterns in different regions of the brain with their sub-cellular composition and biological functions.

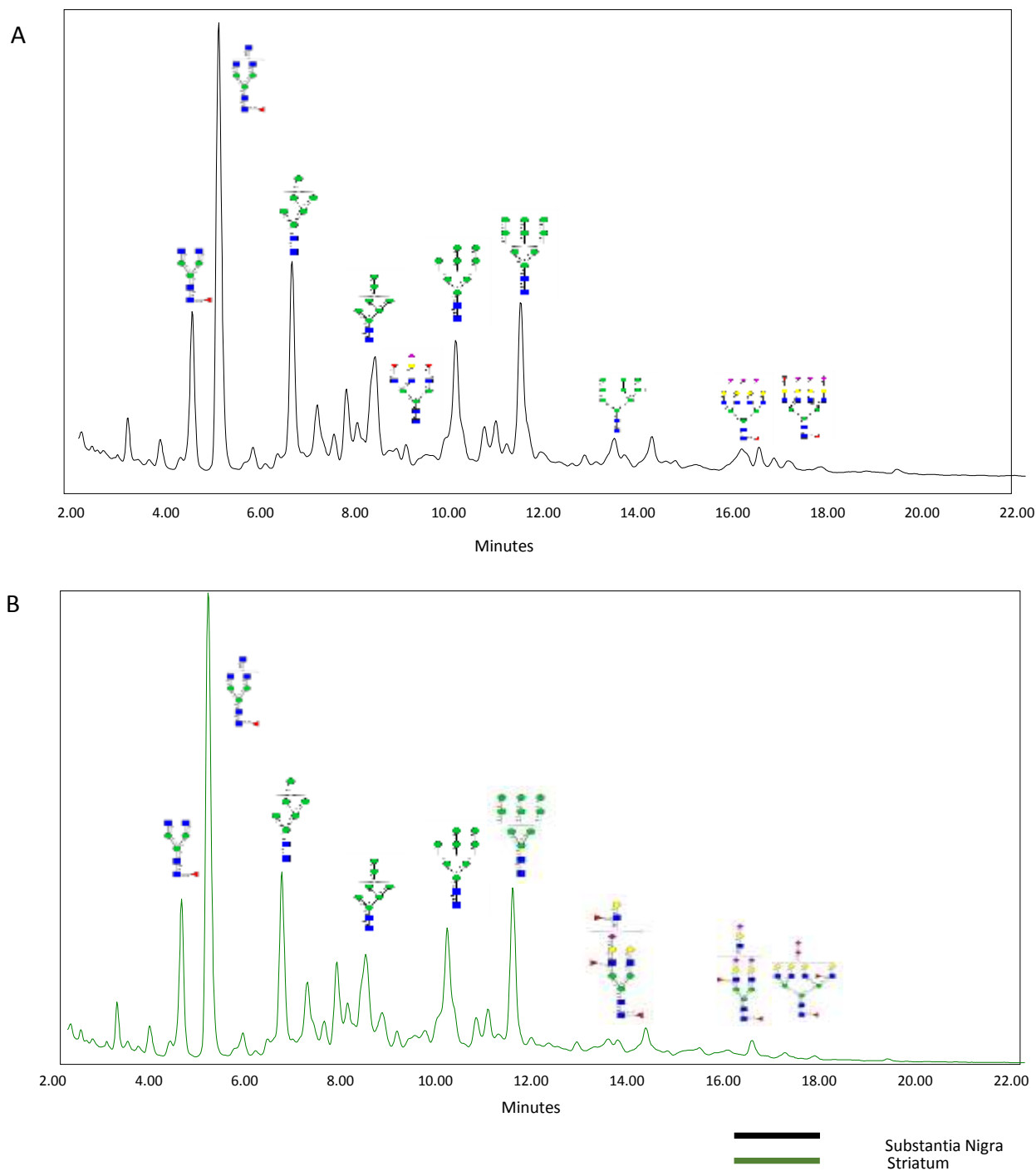


Figure 4.3 HILIC-UPLC analysis N- glycan compositions. N-glycan analysis of **A)** SN and **B)** striatum from rodent brains representing the major glycan peaks for both regions of the brain. The N-glycome for both these regions was separated into 26 chromatographic peaks. Detailed composition analysis for each of these peaks has been summarized in Table 4.1 A,B for SN and striatum.

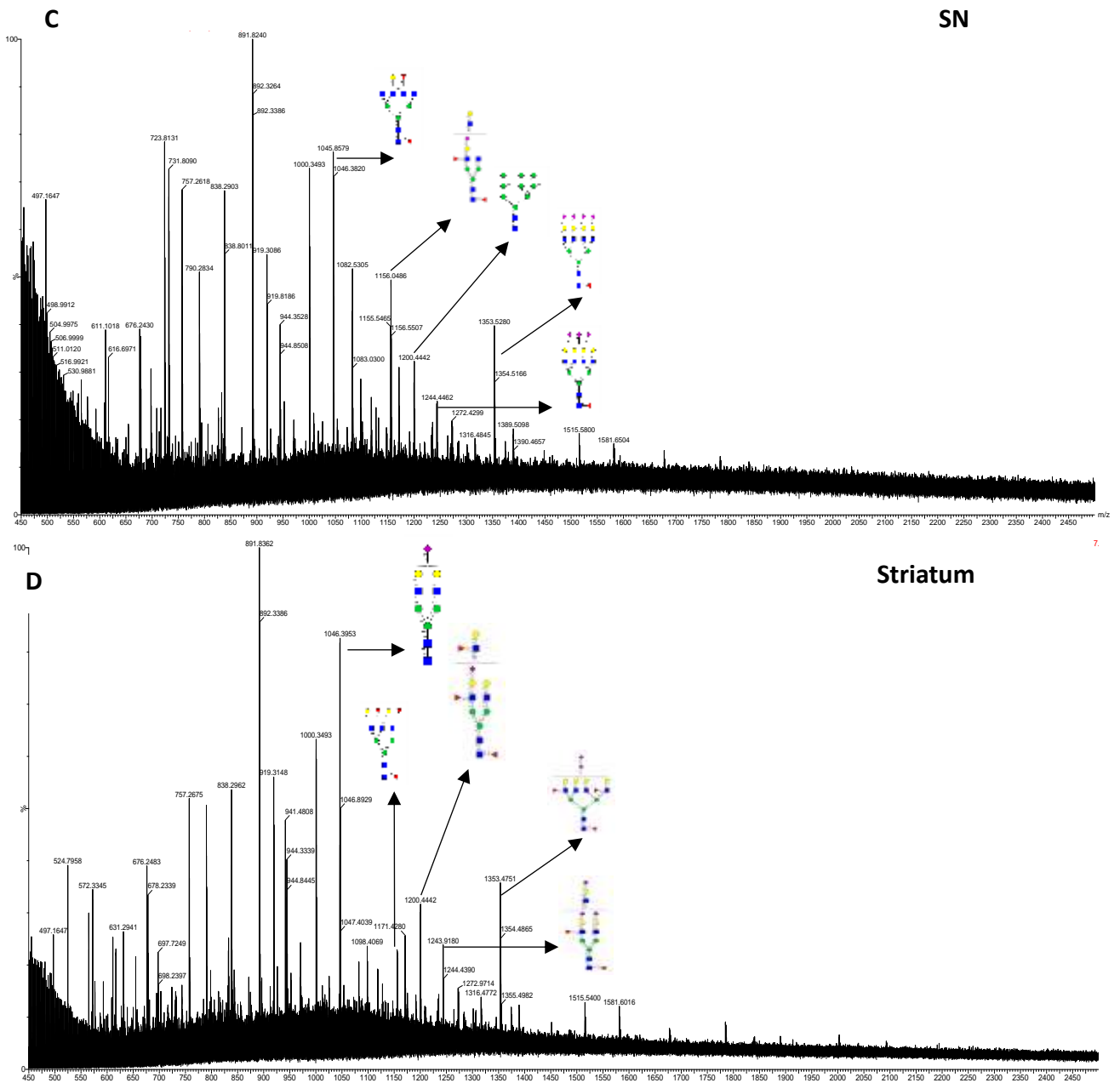


Figure 4.3: Negative mode CID of the *N*-linked glycans released from **C)** SN and **D)** striatum from the rodent brains representing the differentially expressed glycans for both regions of the brain.

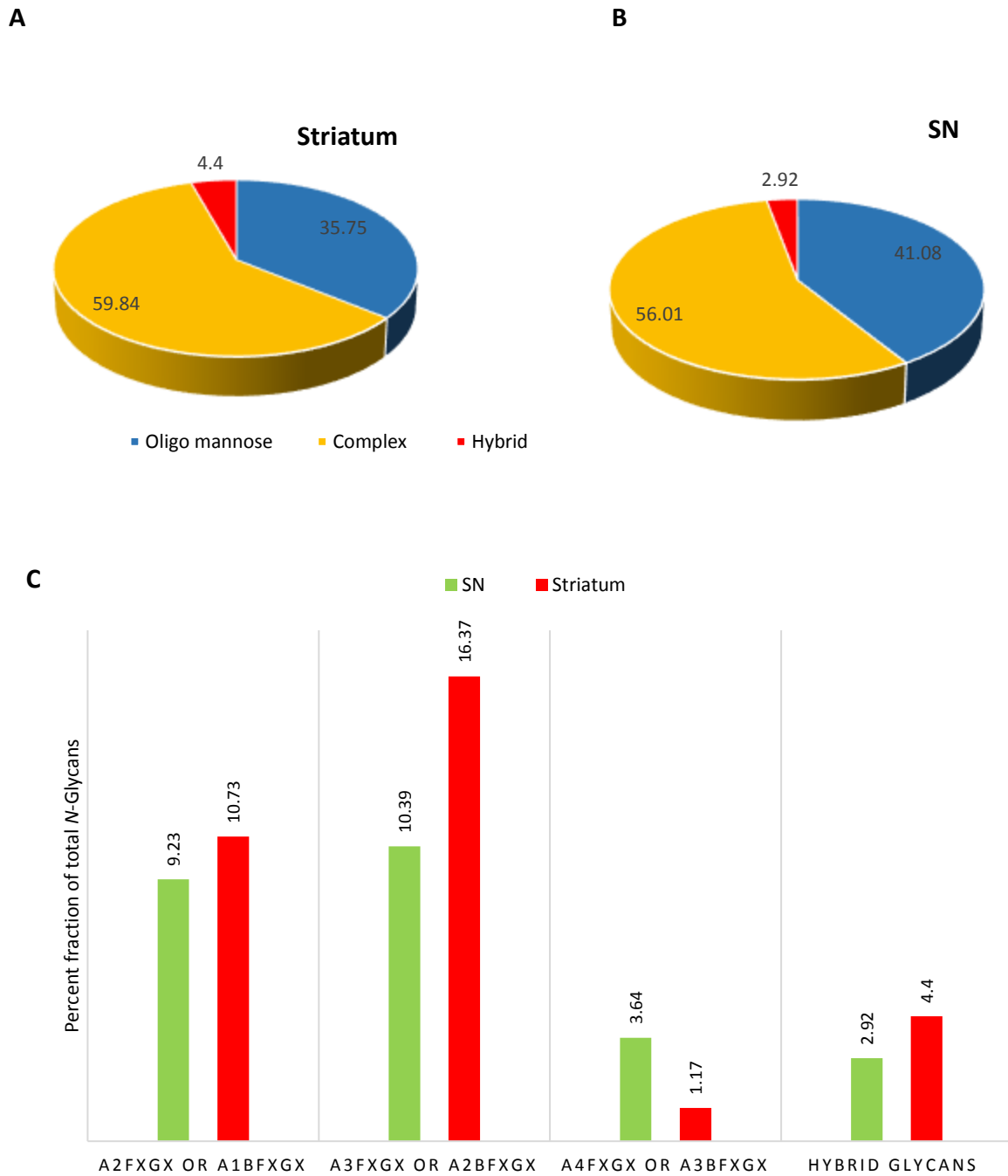


Figure 4.4 Relative abundances represented as percentages of total *N*-glycans belonging to each of the three biosynthetic classes: oligomannose, complex and hybrid in **A)** striatum and **B)** SN of the rat brain indicating a clear spatial distribution of *N*-glycosylation. **C)** Classification of total *N*-glycans based on their antennary distribution (including bisects) in striatum and SN in rat brains. The classifications were derived from the exoglycosidase digestions and detailed assignments all the chromatographic peaks from HILIC-UPLC where the major species in each peak was used for all subsequent trait calculations.

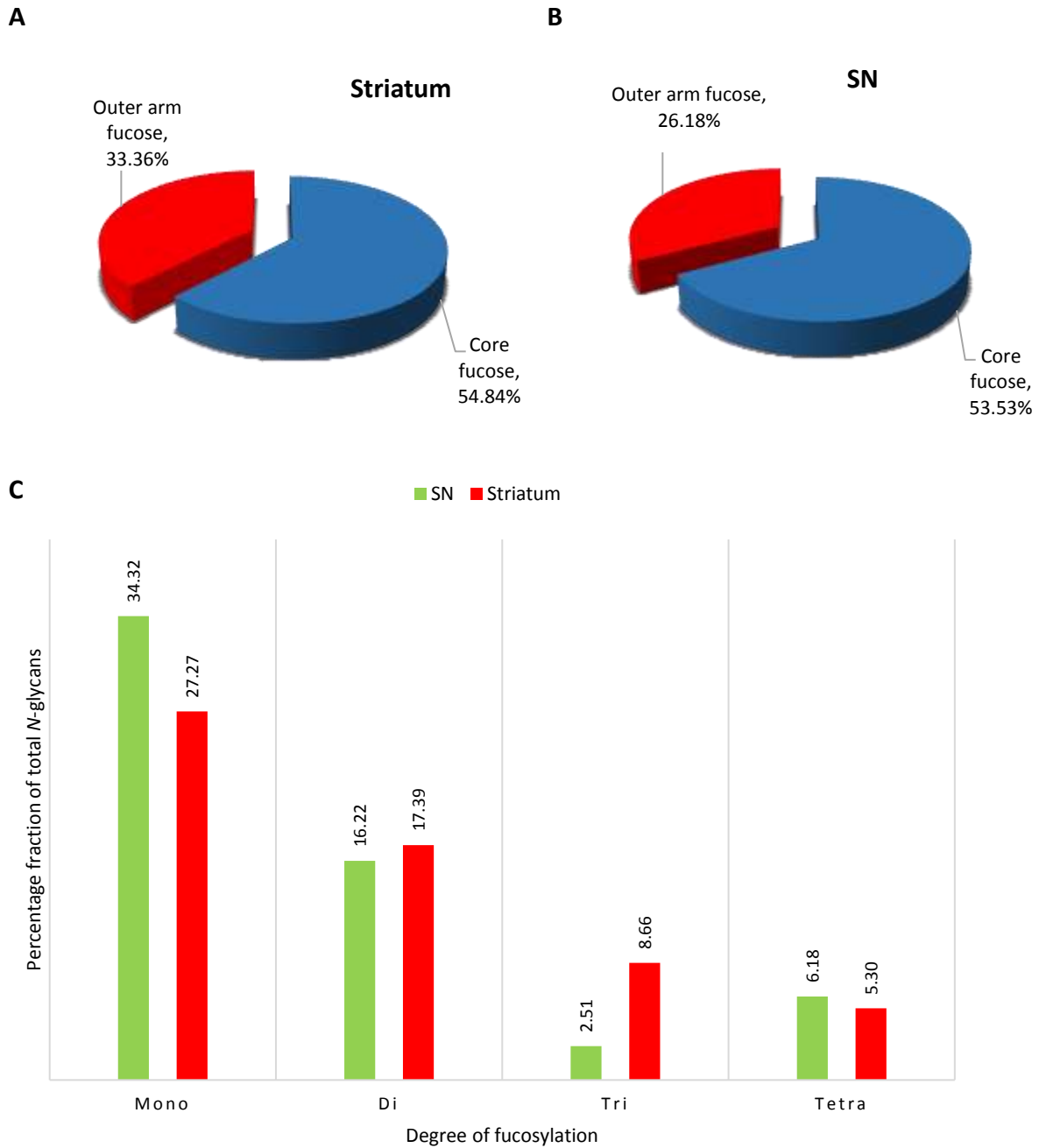


Figure 4.5 Percentage fractions of fucosylated N-glycans. Fucosylated N-glycans in **A)** striatum and **B)** SN of the rat brain differentiated by core and outer arm fucosylation indicating a clear spatial distribution between the two regions. **C)** Classification of fucosylated N-glycans represented as percentages, according to degree of fucosylation (n = 1, 2, 3, 4) which includes both sialylated and unsialylated fucosylated glycans.

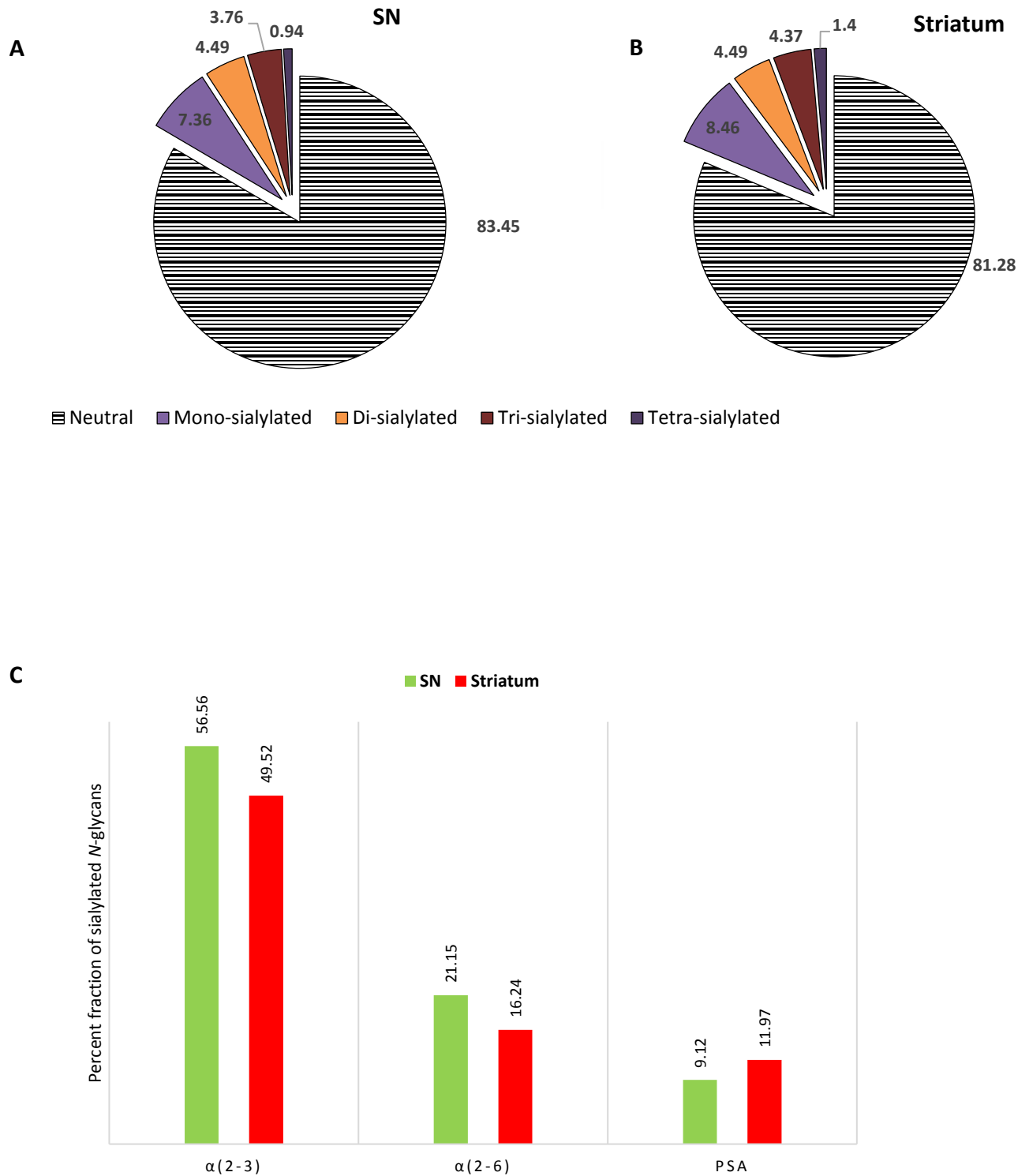


Figure 4.6 Percentage fractions of sialylated N-glycans. Sialylated N-glycans in the brain classified according to the degree of sialylation (mono-, di-, tri- and tetra-sialylated) in **A**) striatum and **B**) SN of the rat brain. **C**) Classification of sialylated N-glycans represented as percentages, according to linkage of the sialic acid to galactose residue indicative of the significantly high $\alpha(2-3)$ -linkage to galactose compared to that of $\alpha(2-6)$ -linkage.

4.4 Discussion

A small percentage (less than 5%) of the brain's dry weight is composed of carbohydrates. This represents a miniscule fraction when compared to the over 80% from lipids and proteins[33]. This represents a major limitation for development of glycoanalytical techniques focusing on whole brain tissue as they suffer from low sensitivity and high noise levels due to signal suppression. This study represents the first initiative to develop a glycoanalytical platform for the detailed assessment of the spatial regulation of *N*-glycosylation occurring in Parkinson's relevant regions of the brain. In detail, micro-biopsied tissue from rat brains using brain atlas was processed using Tris-SDS extraction followed by in gel blotting (IGB). The basis of selection of protein extraction method was the optimization performed using three extraction protocols using Tris-SDS buffer, RIPA buffer and Proteinase K (**Supplementary Fig. S2**). The criteria for opting the aforementioned method of extraction was the higher yield of tissue *N*-glycans and the ability to produce glycan peaks that were easy to resolve, reproduce and integrate.

Previous reports of brain glycosylation have used either the whole brain homogenates[20,21] or surgically dissected regions of brain[34–36]. Micro-biopsy of specific regions of brain from cryosectioned tissue facilitates an efficient collection of relatively smaller regions of the brain like SN for protein extraction. Higher specificity of the technique allows for a more defined spatial resolution of *N*-glycans when compared to tissue excision used in the previous studies. Immobilisation of the isolated glycoproteins in polyacrylamide gel pieces[37] minimises the concerns arising from the presence of contaminants in a sample by allowing efficacious removal of contaminants from buffers, denaturation, reduction and alkylation of the glycoproteins.

The next stage of this platform pertains to the release of *N*-glycans from the immobilised glycoproteins. Glycan release from the isolated glycoproteins can be performed using either an enzymatic or chemical protocol, each of which has its own merits and demerits. Takasaki et al.[38] described the use of anhydrous hydrazine for release of *N*-linked glycans for the first time and it remains the most frequently used technique for chemical release of glycans till date. Although, it is a well validated technique and has also been adapted for the release of *O*-glycan structures, enzymatic release is preferable when the proteins are difficult to purify or when the amount of sample available is restricted[39]. The latter was relevant in the current study given the limited amount of specific tissue samples available for protein extraction and glycan

release. Chemical release is further limited by the harsh reaction conditions involved, the release of glycans is usually affected by the salts and might result in the chemical modification of the released glycans. Due to the aforementioned reasons, the *N*-glycan moieties from the gel-entrapped proteins were then cleaved off with the endoglycosidase peptide: *N*-Glycosidase F (PNGase F). Preferential treatment with PNGase F is attributed to its broad specificity towards almost all *N*-glycans unless the core is modified with an α 1-3 fucose [40,41]. This is followed by labeling with 2-AB using reductive amination which in complex biological extracts like tissues might result in side-products and poor labeling efficiency. The immobilisation maximises the removal of by-products and contaminants prior to and after glycan fluorescence labeling. Labeled glycans were then analysed by UPLC and LC-MS with fluorescence detection.

Combined with LC-MS detection, HILIC-UPLC enabled simultaneous observation and quantification of both high- and low-abundance *N*-glycans. In this study, this multi-faceted analysis with a series of exoglycosidase digestions enabled the detection of over 170 *N*-glycan isomers for both striatum and SN, originating from over 100 distinct *N*-glycan compositions. The most abundant glycans in both striatum and SN were oligomannose or fucosylated complex type, though varying amounts of glycans were detected from all biosynthetic classes. An important feature for the hybrid neutral glycans detected in both striatum and SN was the presence of LewisX determinant characterised by the presence of outer arm α (1,3)-fucosylation. Major fraction of detected *N*-glycans for both striatum and SN were the fucosylated complex and hybrid type glycans (Striatum: 55%, SN: 53%). These included both unsialylated and sialylated fucosylated glycans and were followed in predominance by oligomannose type (Striatum: 36%, SN: 41%) and hybrid type (Striatum: 5%, SN: 3%). This reinforces the possibility of functional correlation of the glycosylation cues in different regions of brain. Spatial resolution of glycans has previously been investigated in a few studies where the resolved glycans are used as a marker for disease progression[42] or to identify specific regions in a tissue[43].

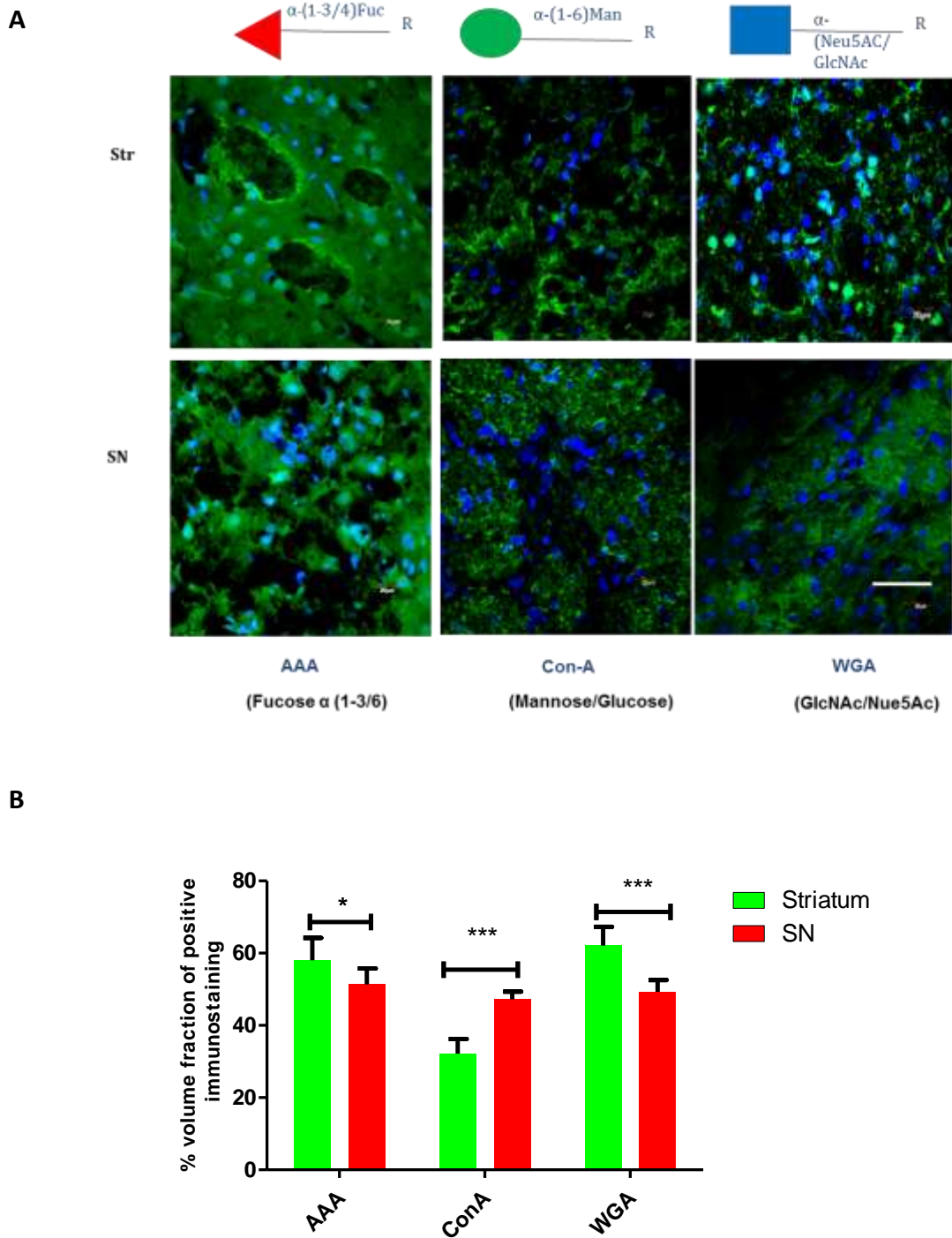


Figure 7 Lectin histochemical analysis for N-glycan modulation. A) Visual representation of the differential spatial distribution of N-glycans in rat brain through lectin histochemistry. Differential Con A, AAA and WGA binding aligns with the spatial resolution observed through HILIC-UPLC and LC-MS. B) Quantified lectin histochemistry results representing the spatial regulation of N-glycosylation in the rat brain.

Sialylation is known to be one of the most important forms of glycosylation in the CNS where it exists chiefly in the form of glycolipids[44], acting as receptors for toxins and pathogens [45] and mediates intercellular interactions through NCAMs [46]. There has been several studies that demonstrate the role of sialic acid-containing glycoconjugates in the differentiation and migration of neurons and axonal guidance[47,48]. Dietary supplementation of sialic acid leads to increases in sialic acid-containing glycoproteins in the frontal cortex and is reported to accelerate learning and memory in piglets[49]. Alterations in the sialome of neuronal glycoproteins translate into their structural and functional aspects as reflected by sialic acid removal from membrane proteins in primary neurons leading to actin depolymerization and axonal growth[50].

N-acetylneuraminic acid (Neu5Ac) and *N*-glycolylneuraminic acid (Neu5Gc) are the major sialic acids detected in most mammals. Neu5Gc is biosynthesized from Neu5Ac which acts as a sugar nucleotide donor and cytidine monophospho-*N*-acetylneuraminic acid hydroxylase (CMAH) mediates this conversion[51]. The gene for CMAH is mutated in humans resulting in the complete absence of endogenous Neu5Gc expression throughout the body. For other mammals, there are varied ratios of Neu5Ac to Neu5Gc detected in different tissues. However, the brain stands out an exception to this pattern where an extremely low expression of Neu5Gc is detected. In the current study, trace amounts of Nue5Gc (<3%) were detected in both striatum and SN of the adult rat brain. This is in compliance with the previous reports of minimal levels of Neu5Gc detection in mammalian brains including the rat brains [52,53]. However, contrary to the previous reports Ji *et al.* (2015) reported the complete absence of Neu5Gc sialylation in








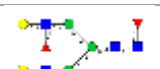




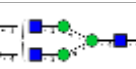






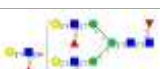






Glycan peak in SN	Composition	Structure	Peak area (%)	Glycan peak	Composition	Structure	Peak area (%)
GP1	M3		0.13	GP14	FA4F1G1		1.84
GP2	M3B		1.58	GP15	FM5A1G1F1		2.92
GP3	A1B		0.93	GP16	M8		8.70
GP4	FA2		6.00	GP17	FA2F2G2		2.51
GP5	FA3		17.18	GP18	FA3F1G2S1(3)		2.46
GP6	FA2G1		1.10	GP19	A2G2S2(3,6)		1.23
GP7	A2F1G1		0.21	GP20	M9		10.1 2
GP8	M6		9.48	GP21	A2F1G2S2(6,6)		1.06
GP9	FA2F1G1		3.94	GP22	M9P2		3.44
GP10	FA1BF1G1S 2(3,8P)		1.51	GP23	F(3)A3F3G3		4.38
GP11	FA3F1G1		3.55	GP24	FA4G4S(3,3,3)3		3.13
GP12	A2G2S1(6) Ac		1.97	GP25	FA4F3G4S1(3)		1.80
GP13	M7D1		7.63	GP26	FA4G4S(3,3,3.6)4		1.21

Table 4.1A: N-glycome of SN separated into 26 chromatographic peaks by HILIC chromatography. Structures of major glycans in each chromatographic peak and the average percentage of individual peak areas (%) as determined by HILIC-UPLC and validated by LC-MS have been represented here.

mouse brain[34]. The stringently conserved dichotomous expression of Neu5Gc in rat brain and the other tissues like liver, kidney etc. is suggestive of the probable adverse effects of Neu5Gc on neural development.

Another important feature detected was the presence of densely charged structures substituted with PSA. Polysialylation has been demonstrated to be an important factor in mediating neural cell interactions. A relatively higher fraction of polysialylation was detected in the striatal *N*-glycans (2%) when compared to SN (1%). In the present analysis, the results revealed that each glycan of this type contained one type-1 (Gal β 3GlcNAc) antenna in addition to type-2 (Gal β 4GlcNAc) chains which was found to be consistent with the studies on the polysialylated glycans of murine N-CAM[54]. Characterization of the differential expression of PSA in these regions of brain can be hypothesized to be correlated with processing of sensory information and neuronal plasticity. The homopolymers of α 2,8-linked sialic acid (PSA) have only been demonstrated to be present on the NCAM specifically in developing tissues such as brain [55], heart [56] and kidney [57] where it exhibits a highly regulated expression pattern. In brain, PSA expression is correlated to the regions that exhibit physiological plasticity suggesting that these might be related to developmental processes [58]. Interestingly, PSA-NCAM expression is induced ipsilaterally in SN of the 6-OHDA parkinsonian rats which serves as a marker for reactive astrocytes which was not detectable in the striatum containing the dopaminergic terminal fields[59]. This is indicative of the fact that regio-specific modulation of PSA expression in the brain can be well correlated to the state of proliferation and reactivity of the constituent cells and is usually over expressed in the areas of high plasticity like hypothalamo-neurohypophysial system[60].

A wide distribution of fucosylated *N*-glycans has been observed in mammalian tissues especially the brain[61]. Two major *N*-glycan structures found abundantly in neural tissues by Shimizu et al. were both fucosylated and showed a spatial regulation in their distribution across different regions of the brain. Interestingly, these structures were not detected in the glycans isolated from the blood. This reinforces the biological significance of the fucosylated glycans in regulating the neural functions. Another study by Ji *et al*[34] investigating the spatial resolution of *N*-glycans in mouse brain using a combination of tissue glyco-capture and nano LC-MS further supports extensive fucosylation in the mouse brain (up to 55%, almost 30% of which are multiply fucosylated). Earlier investigations of *N*-glycome from serum or other tissues[62,63] in mouse did not reveal such high levels of fucosylation which could be indicative of it being a typical 'brain trait'. Also, the observed fucosylation was chiefly












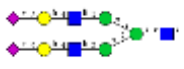
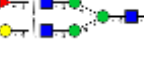













Glycan peak in striatum	Composition	Structure	Peak area (%)	Glycan peak	Composition	Structure	Peak area (%)
GP1	M3		0.13	GP14	A2G2S1(3)		1.84
GP2	M3B		1.58	GP15	FM5A1G1F1		2.92
GP3	A1B		0.93	GP16	M8		8.70
GP4	FA2		6.00	GP17	FA2F2G2		2.51
GP5	FA3		17.18	GP18	FA3F2G2		2.46
GP6	FA2G1		1.10	GP19	A2G2S2(3,6)		1.23
GP7	A2F1G1		0.21	GP20	M9		10.12
GP8	M6		9.48	GP21	A2F1G2S2(6,6)		1.06
GP9	FA2F1G1		3.94	GP22	FA3F2G3S1(3)		3.44
GP10	FA1BF1G1S2(3,8P)		1.51	GP23	F(3)A3F3G3		4.38
GP11	FA3F1G1		3.55	GP24	FA3F1G3S3(3,3,3)		3.13
GP12	A2G2S1(6)Ac		1.97	GP25	FA4F3G4S1(3)		1.80
GP13	M7D1		7.63	GP26	FA4F2G4S2(3,8,P)		1.21

Table 4.1B: N-glycome of striatum separated into 26 chromatographic peaks by HILIC chromatography. Structures of major glycans in each chromatographic peak and the average percentage of individual peak areas (%) as determined by HILIC-UPLC and validated by LC-MS have been represented here.

antennary contrary to core fucosylation observed in mouse serum glycoproteins. A metabolic study performed using radiolabelled fucose administered intracerebrally showed its incorporation exclusively into glycoproteins in the mouse. In a similar study with radiolabelled fucose in rats by Margolis et al[64] where tritium-labelled fucose was intra-peritoneally injected showed that a major proportion of tritium-labelled fucose was incorporated into the brain glycoproteins, but was absent in glycolipids or mucopolysaccharides. They also reported the slow turnover of fucosylated glycoproteins compared to sialylated glycoproteins. A study by Eshghi et.al[65] analysed brain section from 30 (71.4%) of which were fucosylated and 7 (16.7%) which were non-fucosylated complex glycans. As previously reported by Chen et al[21], analysed brain section from 30 (71.4%) of which were fucosylated and 7 (16.7%) which were non-fucosylated complex glycans. As previously reported by Chen et al[21], hybrid structures with $\alpha(1,3)$ - and core $\alpha(1,3)$ -fucosylation were detected in glycans isolated from both striatum and SN. However, contrary to their investigation, there were no hybrid components detected with outer arm fucosylation in the absence of core fucosylation. This is, therefore anticipated to be a regio-specific characteristic not detected in striatum or SN but in the other regions of the brain. However, in agreement to this report, the hybrid glycans from both striatum and SN were characterised by the presence of Lewis epitope (Le^x). Moreover, due to a stimulation of hippocampal dopamine receptor sites both an increase in the incorporation of 3H -fucose into glycoproteins mediated by receptor coupled events [66] and an improvement of the retention performance of rats in a discrimination reaction were observed. Finally, the improved retention of a learned behaviour in rats induced by an intracerebral injection of fucose itself [67] points to the assumed link between alterations in the fucosylation of brain glycoproteins and mechanisms involved in memory storage. The enhanced enrichment of fucosylated species in striatal *N*-glycans can be associated with its involvement in stimulus-response learning. Aberrant fucosylation of the neural glycoproteins attributed to the absence of $\alpha 1,6$ -fucosyltransferase is also known to result in the development of a schizophrenia-like phenotype in mice[68]. This highlights the significance of fucosylation of glycoproteins in regulating their biological functions and hence augments the concept of differential spatial regulation.

Oligomannose glycans are generally found in abundance among the neural *N*-glycans across different species. Previous studies have shown the significance of the cell surface expression of these glycans and their implication in neural tissue development[69]. It is well represented by the interaction between L1 and NCAM mediated by the recognition of oligomannose

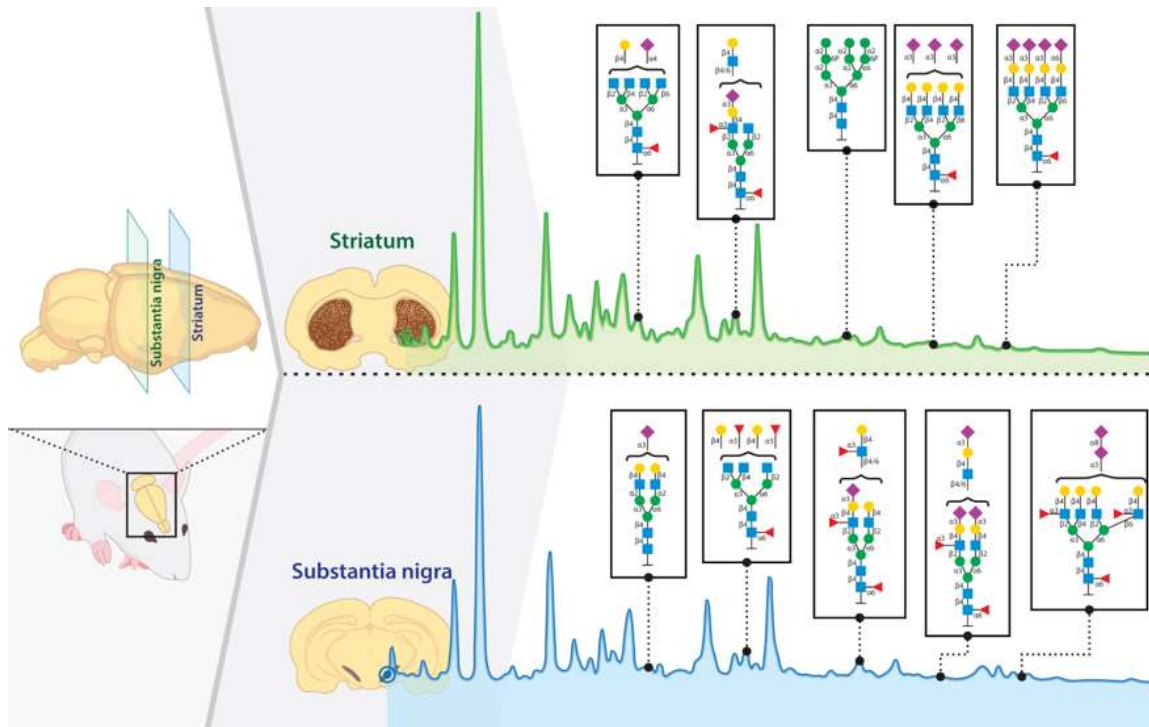


Figure 4.8 Schematic representation of spatial resolution of N-glycans in striatum and SN in the rodent brain.

Table 4.2: Summary of quantifiable differences in N-glycosylation patterns of striatum and SN detected using the elaborate glycoanalytical platform.

Glycan Peak	Striatum	Structure	m/z	SN	Structure	m/z
14	A2G2S1(3)		1024.8771	FA4F1G1		1147.4309
18	FA3F2G2		1199.9398	FA3F1G2S1(3)		1272.4739
22	FA3F2G3S(3)1		1426.5059	M9P2		1080.3519
24	FA3F1G3S3(3,3,3)		1096.0629	FA4G4S3(3,3,3)		1169.0634
26	FA4F2G4S2(3,8,P)		1169.4141	FA4G4S4(3,3,3,6)		1266.1017

of glycosylation. This post translational modification is correlated with the intracellular transport of soluble lysosomal enzymes. Majority of the Man 6-P glycoproteins have been found to be localized in the neuronal lysosomes which appears to be a brain-specific feature as Man 6-P lysosomal enzymes showed endosome-like localization in the liver[70]. Previous reports have suggested the enrichment of human brain proteome with Man 6-P modified lysosomal proteins with greater number of individual isoforms that could be implicated in various disease pathophysiology involving lysosomal dysfunction[71]. SN has been shown to have a high activity level for most lysosomal enzymes in previous studies[72] and this correlates well with the detection of Man 6-P as a chief glycosylation trait for *N*-glycans isolated from SN.

Lectins are the sugar-binding proteins of plant origin which can bind to the glycan moieties of several glyco-conjugates and used for their identification[73,74]. AAA lectin binding profile further supports our observation of the distinct spatial distribution of fucosylated *N*-glycans in the rodent brain. A region-specific differential binding of wheat germ agglutinin (WGA) binding was observed between the striatum and SN. The strong WGA localization could be potentially attributed to its interaction with the glial cells and astrocytes [75] which are densely present in the SN compared to the striatum. Concanavalin A (Con A) is known to bind to mannose motif and shows preferential binding to the oligomannose type *N*-linked glycosylation. The lectin histochemical analysis for ConA binding to SN and striatum further augments the spatial distribution of oligomannosidic *N*-glycans that was observed using HILIC-UPLC and LC-MS. The downside of lectin histochemistry is the semi-specific lectin binding to several glycan moieties. It, however, provides a very good qualitative evidence of the spatial resolution of *N*-glycosylation in the rat brain and the trends established through the more quantitative analyses performed earlier in this study. **Figure 4.8** summarises all the differential traits of *N*-glycosylation that were investigated and outlined in this study.

4.5 Conclusions

This study presents the development of an elaborate glycoanalytical platform for the detailed characterisation and investigation of spatial resolution of *N*-glycosylation in the rodent brains. In the course of this analysis, besides achieving a detailed glycoprofile for striatum and SN through the identification and profiling of more than a hundred glycan structures, novel glycan motifs and traits that have not been outlined till date were identified. Presence of Man 6-P amongst others represents a significant trait specific to SN which was not detected as a major

glycan in the striatum. There are significant functional and biological implications of this stringent spatial regulation of glycosylation that have been outlined in the study. More importantly, this comprehensive and reproducible regio-specific profiling of the brain glycome provides significant insights and serve as a baseline for the identification of biomarkers and their regulation in neurodegenerative diseases.

4.6 References

- [1] K.W. Moremen, M. Tiemeyer, A. V. Nairn, Vertebrate protein glycosylation: diversity, synthesis and function, *Nat. Rev. Mol. Cell Biol.* 13 (2012) 448–462. doi:10.1038/nrm3383.
- [2] Y. Zhang, H. Yin, H. Lu, Recent progress in quantitative glycoproteomics, *Glycoconj. J.* 29 (2012) 249–258. doi:10.1007/s10719-012-9398-x.
- [3] T.R. Henion, A.A. Faden, T.K. Knott, G.A. Schwarting, 3GnT2 maintains adenylyl cyclase-3 signaling and axon guidance molecule expression in the olfactory epithelium, *J. Neurosci.* 31 (2011) 6576–6586. doi:10.1523/JNEUROSCI.0224-11.2011.
- [4] B.D. Shur, S. Roth, Cell surface glycosyltransferases, *BBA - Rev. Biomembr.* 415 (1975) 473–512. doi:10.1016/0304-4157(75)90007-6.
- [5] S. Roseman, The synthesis of complex carbohydrates by multiglycosyltransferase systems and their potential function in intercellular adhesion, *Chem. Phys. Lipids.* 5 (1970) 270–297. doi:10.1016/0009-3084(70)90024-1.
- [6] E.C. Collin, M. Kilcoyne, S.J. White, S. Grad, M. Alini, L. Joshi, A.S. Pandit, Unique glycosignature for intervertebral disc and articular cartilage cells and tissues in immaturity and maturity, *Sci. Rep.* 6 (2016) 23062. doi:10.1038/srep23062.
- [7] R.S. Haltiwanger, J.B. Lowe, Role of glycosylation in development, *Annu. Rev. Biochem.* 73 (2004) 491–537. doi:10.1146/annurev.biochem.73.011303.074043.
- [8] S.D. Szajda, A. Jankowska, K. Zwierz, Carbohydrate markers in colon carcinoma., *Dis. Markers.* 25 (2008) 233–242. doi:10.1155/2008/206510.
- [9] S. Liedtke, H. Geyer, M. Wuhrer, R. Geyer, G. Frank, R. Gerardy-Schahn, U. Zahringer, M. Schachner, Characterization of N-glycans from mouse brain neural cell adhesion molecule, *Glycobiology.* 11 (2001) 373–384. doi:10.1093/glycob/11.5.373.
- [10] M. Natalia Lobanovskaya, Tamara Zharkovsky, Külli Jaako, A.Z. Jürgenson, *Anu*

- Aonurm-Helm, PSA modification of NCAM supports the survival of injured retinal ganglion cells in adulthood, *Brain Res.* 1625 (2015) 9–17. doi:10.1016/J.BRAINRES.2015.08.008.
- [11] P.T. Kelly, C.W. Cotman, Identification of glycoproteins and proteins at synapses in the central nervous system., *J. Biol. Chem.* 252 (1977) 786–793. <http://www.ncbi.nlm.nih.gov/pubmed/833152> (accessed October 5, 2017).
- [12] J.W. Gurd, S.C. Fu, Concanavalin A receptors associated with rat brain synaptic junctions are high mannose-type oligosaccharides, *J. Neurochem.* 39 (1982) 719–725. doi:10.1111/j.1471-4159.1982.tb07951.x.
- [13] Y. Takeuchi, J. Morise, I. Morita, H. Takematsu, S. Oka, Role of site-specific N-glycans expressed on GluA2 in the regulation of cell surface expression of AMPA-type glutamate receptors, *PLoS One.* 10 (2015) e0135644. doi:10.1371/journal.pone.0135644.
- [14] J. Hu, W. Reutter, H. Fan, Significance of N-glycosylation and sialylation of GABA Transporter 1, *J. Carbohydr. Chem.* 30 (2011) 206–217. doi:10.1080/07328303.2011.604455.
- [15] A.S. Kristensen, J. Andersen, T.N. Jorgensen, L. Sorensen, J. Eriksen, C.J. Loland, K. Stromgaard, U. Gether, SLC6 neurotransmitter transporters: structure, function, and regulation, *Pharmacol. Rev.* 63 (2011) 585–640. doi:10.1124/pr.108.000869.
- [16] M. Pučić, S. Pinto, M. Novokmet, A. Knežević, O. Gornik, O. Polašek, K. Vlahoviček, W. Wang, P.M. Rudd, A.F. Wright, H. Campbell, I. Rudan, G. Lauc, Common aberrations from the normal human plasma N-glycan profile, *Glycobiology.* 20 (2010) 970–975. doi:10.1093/glycob/cwq052.
- [17] S. Grünewald, The clinical spectrum of phosphomannomutase 2 deficiency (CDG-Ia), *Biochim. Biophys. Acta - Mol. Basis Dis.* 1792 (2009) 827–834. doi:10.1016/j.bbadis.2009.01.003.
- [18] M.A. Haeuptle, T. Hennet, Congenital disorders of glycosylation: an update on defects affecting the biosynthesis of dolichol-linked oligosaccharides, *Hum. Mutat.* 30 (2009) 1628–1641. doi:10.1002/humu.21126.
- [19] R. Kleene, M. Schachner, Glycans and neural cell interactions, *Nat. Rev. Neurosci.* 5

- (2004) 195–208. doi:10.1038/nrn1349.
- [20] S. Zamze, D.J. Harvey, Y.J. Chen, G.R. Guile, R.A. Dwek, D.R. Wing, Sialylated N-glycans in adult rat brain tissue--a widespread distribution of disialylated antennae in complex and hybrid structures., *Eur. J. Biochem.* 258 (1998) 243–70. doi:10.1046/j.1432-1327.1998.2580243.x.
- [21] Y.J. Chen, D.R. Wing, G.R. Guile, R.A. Dwek, D.J. Harvey, S. Zamze, Neutral N-glycans in adult rat brain tissue--complete characterisation reveals fucosylated hybrid and complex structures., *Eur. J. Biochem.* 251 (1998) 691–703. doi:10.1046/j.1432-1327.1998.2510691.x.
- [22] D.R. Wing, T.W. Rademacher, M.C. Field, R.A. Dwek, B. Schmitz, G. Thor, M. Schachner, Use of large-scale hydrazinolysis in the preparation of N-linked oligosaccharide libraries: application to brain tissue, *Glycoconj. J.* 9 (1992) 293–301. doi:10.1007/BF00731089.
- [23] S.T. Eshghi, S. Yang, X. Wang, P. Shah, X. Li, H. Zhang, Imaging of N-Linked glycans from formalin-fixed paraffin-embedded tissue sections using MALDI mass spectrometry, *ACS Chem. Biol.* 9 (2014) 2149–2156. doi:10.1021/cb500405h.
- [24] R. Raghunathan, N.K. Polinski, J.A. Klein, J.D. Hogan, C. Shao, K. Khatri, D. Leon, M.E. McComb, F.P. Manfredsson, C.E. Sortwell, J. Zaia, Glycomic and proteomic changes in aging brain nigrostriatal pathway, *Mol. Cell. Proteomics.* 17 (2018) 1778–1787. doi:10.1074/mcp.RA118.000680.
- [25] H. Stöckmann, R. O'Flaherty, B. Adamczyk, R. Saldova, P.M. Rudd, Automated, high-throughput serum glycoprofiling platform, *Integ.Biol.* 7 (2015) 1026–1032. doi:10.1039/x0xx00000x.
- [26] L. Royle, C.M. Radcliffe, R.A. Dwek, P.M. Rudd, Detailed Structural Analysis of N-Glycans Released From Glycoproteins in SDS-PAGE Gel Bands Using HPLC Combined With Exoglycosidase Array Digestions, in: *Glycobiol. Protoc.*, Humana Press, New Jersey, 2006: pp. 125–144. doi:10.1385/1-59745-167-3:125.
- [27] L. Royle, M.P. Campbell, C.M. Radcliffe, D.M. White, D.J. Harvey, J.L. Abrahams, Y.-G. Kim, G.W. Henry, N.A. Shadick, M.E. Weinblatt, D.M. Lee, P.M. Rudd, R.A. Dwek, HPLC-based analysis of serum N-glycans on a 96-well plate platform with dedicated

- database software, *Anal. Biochem.* 376 (2008) 1–12. doi:10.1016/j.ab.2007.12.012.
- [28] B. Küster, S.F. Wheeler, A.P. Hunter, R.A. Dwek, D.J. Harvey, Sequencing of N-linked oligosaccharides directly from protein gels: in-gel deglycosylation followed by Matrix-Assisted Laser Desorption/Ionization Mass Spectrometry and normal-phase High-Performance Liquid Chromatography, *Anal. Biochem.* 250 (1997) 82–101. doi:10.1006/abio.1997.2199.
- [29] J.C. Bigge, T.P. Patel, J.A. Bruce, P.N. Goulding, S.M. Charles, R.B. Parekh, Nonselective and efficient fluorescent labeling of glycans using 2-amino benzamide and anthranilic acid, *Anal. Biochem.* 230 (1995) 229–238. doi:10.1006/abio.1995.1468.
- [30] L. Royle, C.M. Radcliffe, R.A. Dwek, P.M. Rudd, Detailed structural analysis of N-glycans released from glycoproteins in SDS-PAGE gel bands using HPLC combined with exoglycosidase array digestions, in: *Glycobiol. Protoc.*, Humana Press, New Jersey, 2006: pp. 125–144. doi:10.1385/1-59745-167-3:125.
- [31] T. Krusius, J. Finne, Structural features of tissue glycoproteins. Fractionation and methylation analysis of glycopeptides derived from rat brain, kidney and liver., *Eur. J. Biochem.* 78 (1977) 369–379. doi:10.1111/j.1432-1033.1977.tb11749.x.
- [32] L.J. Lawson, V.H. Perry, P. Dri, S. Gordon, Heterogeneity in the distribution and morphology of microglia in the normal adult mouse brain., *Neuroscience.* 39 (1990) 151–170. doi:10.1016/0306-4522(90)90229-w.
- [33] R.L. Schnaar, A. Suzuki, P. Stanley, *Glycosphingolipids*, 2009. doi:doi:10.1101/glycobiology.3e.011.
- [34] I.J. Ji, S. Hua, D.H. Shin, N. Seo, J.Y. Hwang, I.-S. Jang, M.-G. Kang, J.-S. Choi, H.J. An, Spatially-resolved exploration of the mouse brain glycome by tissue glyco-capture (TGC) and Nano-LC/MS, *Anal. Chem.* 87 (2015) 2869–2877. doi:10.1021/ac504339t.
- [35] H. Shimizu, K. Ochiai, K. Ikenaka, K. Mikoshiba, S. Hase, Structures of N-Linked sugar chains expressed mainly in mouse brain, 1993. doi:10.1093/oxfordjournals.jbchem.a124177.
- [36] S. -i. Nakakita, S. Natsuka, J. Okamoto, K. Ikenaka, S. Hase, Alteration of brain type N-glycans in neurological mutant mouse brain, *J. Biochem.* 138 (2005) 277–283. doi:10.1093/jb/mvi125.

- [37] L. Royle, M.P. Campbell, C.M. Radcliffe, D.M. White, D.J. Harvey, J.L. Abrahams, Y.-G. Kim, G.W. Henry, N.A. Shadick, M.E. Weinblatt, D.M. Lee, P.M. Rudd, R.A. Dwek, HPLC-based analysis of serum N-glycans on a 96-well plate platform with dedicated database software, *Anal. Biochem.* 376 (2008) 1–12. doi:10.1016/j.ab.2007.12.012.
- [38] S. Takasaki, T. Mizuochi, A. Kobata, [17] Hydrazinolysis of asparagine-linked sugar chains to produce free oligosaccharides, *Methods Enzymol.* 83 (1982) 263–268. doi:10.1016/0076-6879(82)83019-X.
- [39] T. Merry, S. Astrautsova, Chemical and enzymatic release of glycans from glycoproteins, in: *Capill. Electrophor. Carbohydrates*, Humana Press, New Jersey, 2003: pp. 27–40. doi:10.1385/1-59259-294-5:27.
- [40] S.R. Kronewitter, M.L.A. de Leoz, K.S. Peacock, K.R. McBride, H.J. An, S. Miyamoto, G.S. Leiserowitz, C.B. Lebrilla, Human serum processing and analysis methods for rapid and reproducible N-glycan mass profiling., *J. Proteome Res.* 9 (2010) 4952–4959. doi:10.1021/pr100202a.
- [41] Y. Kita, Y. Miura, J. Furukawa, M. Nakano, Y. Shinohara, M. Ohno, A. Takimoto, S.-I. Nishimura, Quantitative glycomics of human whole serum glycoproteins based on the standardized protocol for liberating N-glycans, *Mol. Cell. Proteomics.* 6 (2007) 1437–1445. doi:10.1074/mcp.T600063-MCP200.
- [42] D.H. Dube, C.R. Bertozzi, Glycans in cancer and inflammation — potential for therapeutics and diagnostics, *Nat. Rev. Drug Discov.* 4 (2005) 477–488. doi:10.1038/nrd1751.
- [43] A. V Everest-Dass, M.T. Briggs, G. Kaur, M.K. Oehler, P. Hoffmann, N.H. Packer, N-glycan MALDI imaging mass spectrometry on formalin-fixed paraffin-embedded tissue enables the delineation of ovarian cancer tissues., *Mol. Cell. Proteomics.* 15 (2016) 3003–3016. doi:10.1074/mcp.M116.059816.
- [44] A. Varki, Sialic acids in human health and disease, *Trends Mol. Med.* 14 (2008) 351–360. doi:10.1016/J.MOLMED.2008.06.002.
- [45] Q. Chai, J.W. Arndt, M. Dong, W.H. Tepp, E.A. Johnson, E.R. Chapman, R.C. Stevens, Structural basis of cell surface receptor recognition by botulinum neurotoxin B, *Nature.* 444 (2006) 1096–1100. doi:10.1038/nature05411.

- [46] U. Rutishauser, A. Acheson, A. Hall, D. Mann, J. Sunshine, The neural cell adhesion molecule (NCAM) as a regulator of cell-cell interactions, *Science* (80-.). 240 (1988) 53–57. doi:10.1126/science.3281256.
- [47] T. Quirico-Santos, C.O. Fonseca, J. Lagrota-Candido, Brain sweet brain: importance of sugars for the cerebral microenvironment and tumor development., *Arq. Neuropsiquiatr.* 68 (2010) 799–803. doi:10.1590/S0004-282X2010000500024.
- [48] M. Kontou, W. Weidemann, K. Bork, R. Horstkorte, Beyond glycosylation: sialic acid precursors act as signaling molecules and are involved in cellular control of differentiation of PC12 cells., *Biol. Chem.* 390 (2009) 575–579. doi:10.1515/BC.2009.058.
- [49] B. Wang, Sialic acid is an essential nutrient for brain development and cognition, *Annu. Rev. Nutr.* 29 (2009) 177–222. doi:10.1146/annurev.nutr.28.061807.155515.
- [50] J.A. Rodriguez, E. Piddini, T. Hasegawa, T. Miyagi, C.G. Dotti, Plasma membrane ganglioside sialidase regulates axonal growth and regeneration in hippocampal neurons in culture., *J. Neurosci.* 21 (2001) 8387–8395. doi:10.1523/JNEUROSCI.21-21-08387.2001.
- [51] T. Kawano, S. Koyama, H. Takematsu, Y. Kozutsumi, H. Kawasaki, S. Kawashima, T. Kawasaki, A. Suzuki, Molecular cloning of cytidine monophospho-N-acetylneuraminic acid hydroxylase. Regulation of species- and tissue-specific expression of N-glycolylneuraminic acid., *J. Biol. Chem.* 270 (1995) 16458–63. doi:10.1074/jbc.270.27.16458.
- [52] L.R.L. Davies, O.M.T. Pearce, M.B. Tessier, S. Assar, V. Smutova, M. Pajunen, M. Sumida, C. Sato, K. Kitajima, J. Finne, P. Gagneux, A. Pshezhetsky, R. Woods, A. Varki, Metabolism of vertebrate amino sugars with N -glycolyl groups, *J. Biol. Chem.* 287 (2012) 28917–28931. doi:10.1074/jbc.M112.365056.
- [53] L.R.L. Davies, A. Varki, Why is N-Glycolylneuraminic acid rare in the vertebrate brain?, in: *Top Curr Chem*, Springer, Berlin, Heidelberg, 2013: pp. 31–54. doi:10.1007/128_2013_419.
- [54] H. Geyer, U. Bahr, S. Liedtke, M. Schachner, R. Geyer, Core structures of polysialylated glycans present in neural cell adhesion molecule from newborn mouse brain, 2001.

doi:10.1046/j.0014-2956.2001.02613.x.

- [55] J. Finne, Occurrence of unique polysialosyl carbohydrate units in glycoproteins of developing brain., *J. Biol. Chem.* 257 (1982) 11966–11970. <http://www.ncbi.nlm.nih.gov/pubmed/7118922> (accessed January 24, 2019).
- [56] P.M. Lackie, C. Zuber, J. Roth, Expression of polysialylated N-CAM during rat heart development, *Differentiation.* 47 (1991) 85–98. doi:10.1111/J.1432-0436.1991.TB00226.X.
- [57] J. Roth, D.J. Taatjes, D. Bitter-Suermann, J. Finne, Polysialic acid units are spatially and temporally expressed in developing postnatal rat kidney., *Proc. Natl. Acad. Sci. U. S. A.* 84 (1987) 1969–73. <http://www.ncbi.nlm.nih.gov/pubmed/3470771> (accessed January 24, 2019).
- [58] T. Seki, Y. Arai, Distribution and possible roles of the highly polysialylated neural cell adhesion molecule (NCAM-H) in the developing and adult central nervous system, *Neurosci. Res.* 17 (1993) 265–290. doi:10.1016/0168-0102(93)90111-3.
- [59] T. Nomura, T. Yabe, E.S. Rosenthal, M. Krzan, J.P. Schwartz, PSA-NCAM distinguishes reactive astrocytes in 6-OHDA-lesioned substantia nigra from those in the striatal terminal fields, *J. Neurosci. Res.* 61 (2000) 588–596. doi:10.1002/1097-4547(20000915)61:6<588::AID-JNR2>3.0.CO;2-M.
- [60] J.Z. Kiss, C. Wang, G. Rougon, Nerve-dependent expression of high polysialic acid neural cell adhesion molecule in neurohypophysial astrocytes of adult rats, *Neuroscience.* 53 (1993) 213–221. doi:10.1016/0306-4522(93)90299-U.
- [61] H. Shimizu, K. Ochiai, K. Ikenaka, K. Mikoshiba, S. Hase, Structures of N-linked sugar chains expressed mainly in mouse brain., *J. Biochem.* 114 (1993) 334–8. <http://www.ncbi.nlm.nih.gov/pubmed/8282722> (accessed February 26, 2019).
- [62] S. Hua, H.N. Jeong, L.M. Dimapasoc, I. Kang, C. Han, J.-S. Choi, C.B. Lebrilla, H.J. An, Isomer-specific LC/MS and LC/MS/MS profiling of the mouse serum N-glycome revealing a number of novel sialylated N-glycans., *Anal. Chem.* 85 (2013) 4636–43. doi:10.1021/ac400195h.
- [63] S.-Y. Lin, Y.-Y. Chen, Y.-Y. Fan, C.-W. Lin, S.-T. Chen, A.H.-J. Wang, K.-H. Khoo, Precise mapping of increased sialylation pattern and the expression of acute phase

- proteins accompanying murine tumor progression in BALB/c mouse by integrated sera proteomics and glycomics., *J. Proteome Res.* 7 (2008) 3293–303. doi:10.1021/pr800093b.
- [64] R.K. Margolis, R.U. Margolis, DISPOSITION OF FUCOSE IN BRAIN, *J. Neurochem.* 19 (1972) 1023–1030. doi:10.1111/j.1471-4159.1972.tb01422.x.
- [65] S. Toghi Eshghi, W. Yang, Y. Hu, P. Shah, S. Sun, X. Li, H. Zhang, Classification of Tandem Mass Spectra for Identification of N- and O-linked Glycopeptides, *Sci. Rep.* 6 (2016) 37189. doi:10.1038/srep37189.
- [66] F. Angenstein, H. Matthies, S. Staeck, K.G. Reymann, S. Staak, The maintenance of hippocampal long-term potentiation is paralleled by a dopamine-dependent increase in glycoprotein fucosylation., *Neurochem. Int.* 21 (1992) 403–8. <http://www.ncbi.nlm.nih.gov/pubmed/1338901> (accessed January 22, 2018).
- [67] W. Wetzel, N. Popov, B. Lössner, S. Schulzeck, R. Honza, H. Matthies, Effect of L-fucose on brain protein metabolism and retention of a learned behavior in rats, *Pharmacol. Biochem. Behav.* 13 (1980) 765–771. doi:10.1016/0091-3057(80)90204-X.
- [68] T. Fukuda, H. Hashimoto, N. Okayasu, A. Kameyama, H. Onogi, O. Nakagawasai, T. Nakazawa, T. Kurosawa, Y. Hao, T. Isaji, T. Tadano, H. Narimatsu, N. Taniguchi, J. Gu, α 1,6-Fucosyltransferase-deficient Mice Exhibit Multiple Behavioral Abnormalities Associated with a Schizophrenia-like Phenotype, *J. Biol. Chem.* 286 (2011) 18434–18443. doi:10.1074/jbc.M110.172536.
- [69] R. Horstkorte, M. Schachner, J.P. Magyar, T. Vorherr, B. Schmitz, The fourth immunoglobulin-like domain of NCAM contains a carbohydrate recognition domain for oligomannosidic glycans implicated in association with L1 and neurite outgrowth., *J. Cell Biol.* 121 (1993) 1409–21. doi:10.1083/JCB.121.6.1409.
- [70] M. Jadot, L. Lin, D.E. Sleat, I. Sohar, M.S. Hsu, J. Pintar, F. Dubois, S. Wattiaux-De Coninck, R. Wattiaux, P. Lobel, Subcellular localization of mannose 6-phosphate glycoproteins in rat brain., *J. Biol. Chem.* 274 (1999) 21104–13. <http://www.ncbi.nlm.nih.gov/pubmed/10409663> (accessed March 5, 2019).
- [71] D.E. Sleat, H. Lackland, Y. Wang, I. Sohar, G. Xiao, H. Li, P. Lobel, The human brain mannose 6-phosphate glycoproteome: A complex mixture composed of multiple

- isoforms of many soluble lysosomal proteins, *Proteomics*. 5 (2005) 1520–1532. doi:10.1002/pmic.200401054.
- [72] D. Chiasserini, S. Paciotti, P. Eusebi, E. Persichetti, A. Tasegian, M. Kurzawa-Akanbi, P.F. Chinnery, C.M. Morris, P. Calabresi, L. Parnetti, T. Beccari, Selective loss of glucocerebrosidase activity in sporadic Parkinson’s disease and dementia with Lewy bodies, *Mol. Neurodegener.* 10 (2015) 15. doi:10.1186/s13024-015-0010-2.
- [73] E.C. Collin, M. Kilcoyne, S.J. White, S. Grad, M. Alini, L. Joshi, A.S. Pandit, Unique glycosignature for intervertebral disc and articular cartilage cells and tissues in immaturity and maturity., *Sci. Rep.* 6 (2016) 23062. doi:10.1038/srep23062.
- [74] J.Q. Gerlach, M. Kilcoyne, S. Eaton, V. Bhavanandan, L. Joshi, Non-carbohydrate-Mediated Interaction of Lectins with Plant Proteins, in: *Adv. Exp. Med. Biol.*, 2011: pp. 257–269. doi:10.1007/978-1-4419-7877-6_12.
- [75] G. Szumanska, A.W. Vorbrodt, T.I. Mandybur, H.M. Wisniewski, Lectin histochemistry of plaques and tangles in Alzheimer’s disease, 1987. <https://link.springer.com/content/pdf/10.1007%2FBF00695495.pdf> (accessed May 14, 2019).

Chapter 5

Modulation of brain glyco-signature with the 6-OHDA induced Parkinsonism

Sections of this chapter are in preparation for submission:

Samal J., Abbah S.A., Black A., Saldova R., O'Flaherty R., Drake R., Pandit A.P., (2019).
"Spatio-temporal modulation of brain glycosignature with 6-OHDA induced Parkinsonism in rodent model"

5.1 Introduction

Glycosylation represents one of the most common post-translational modifications in the vast majority of mammalian proteins. Both secretory and membrane proteins are subject to glycosylation through the covalent linkage of the glycan moiety to either asparagine (N-linked) residues or serine/threonine (O-linked) [1]. As a post-translational modification, glycosylation has significant consequences in determining and altering the biochemical properties of a glycoprotein. These include its thermodynamic and kinetic properties as well as physical and conformational stability [2,3], isoelectric point [4], susceptibility to proteolysis [5] and lectin-binding [6]. The crucial impact and ubiquity of *N*-glycans in every biological process makes them a potential candidate for biomarker discovery. Several studies have investigated the roles played by *N*-glycans in chief biological processes like mediating cell–cell and cell–matrix interactions [7], guiding the protein folding [8], ligand-receptor binding and protein turnover [9].

Increasing links between glycans and the pathophysiology of several diseases have been forged over the years, correlating the states of protein glycosylation to the mild as well as severe syndromes, with varied onset times from the early neonatal to adult life. The most direct implication of aberrant glycosylation are manifested as diseases of glycosylation in the human population. A significant proportion of these diseases is represented by the congenital disorders of glycosylation (CDGs) including PMM2-CDG (CDG-Ia) and ALG6-CDG (CDG-Ic) where severe morphogenic and metabolic defects manifested by the patients have been linked to alterations in the distinct steps in glycan formation [10]. Previous studies have established that the biosynthesis of glycans is more significantly impacted by disease states than by protein production. It is also established that altered glycosylation is more pronounced than protein expression for cancer cells relative to the normal cells [11]. Small changes in the related protein expression can translate to amplified alterations in glycan production as metabolites. Also, localized production and modification of glycans in cells can impact a major proportion of glycoproteins produced by the diseased cells and result in the ‘mis-glycosylation’ of a bulk of the glycoproteins. This highlights the significance of glycosylation in disease pathophysiology and suggests its potential as disease biomarker.

The pathogenesis of most of the neurodegenerative disorders like Parkinson’s disease (PD), Alzheimer’s disease (AD), Amyotrophic Lateral Sclerosis (ALS) remains largely unknown despite our understanding of the pathway or mechanism oriented research [12,13]. A detailed proteomic study of cerebrospinal fluid in AD patients has revealed new potential biomarkers

for AD. Interestingly, a significant fraction of the altered proteins in the AD patients were isoforms of glycoproteins such as α -1-antitrypsin, apolipoprotein J and apolipoprotein E. This is suggestive of the changes in the protein glycosylation and their potential role in AD [14]. Another study by Zhang et al. [15] suggests the potential role of a specific molecular weight keratin sulfate (125–220 kDa) modified with sialic acids and its specific sulfotransferase GlcNAc6ST1 as both of these are upregulated during disease progression in brains of AD mouse models and AD patients. To date, the pathophysiological significance of the posttranslational modifications including glycosylation in most of the neurodegenerative diseases remains poorly understood. However, with the recent advances in glycoanalytical platforms e.g. LC-MS and MALDI-MSI analysis, some studies suggest a correlation between the glycosylation of AD-related molecules and investigating their involvement in the onset and progression of this disease [16].

PD is the second most prevalent progressive neurodegenerative disorder and currently affects more than 1% of the worldwide population over the age of 65 [17]. There are very limited studies to date that elucidate the correlation and the functional significance of glycosylation to the disease pathophysiology in PD. A study by Hwang et al. characterized the overlapping glycoproteins between the human brain and CSF using MALDI-TOF-TOF analysis several of which were linked to PD pathogenesis like neuroserpin and pentraxin [18]. Neuronal pentraxin II, a highly glycosylated protein, was found to be upregulated and was established as a component of the lewy bodies and lewy neurites. A study by Moran et al. (2008) shows a close association between pentraxin enriched- α -synuclein aggregates in the cortex and substantia nigra (SN) and dopaminergic cell death [19].

Another glycoprotein shown to have an increased expression in human PD brains is the β 4 subunit of the voltage gated sodium channels. These are known to contribute to neurite outgrowth, migration and axonal fasciculation [20,21]. In a study performed by Zhou et al. [22], the impact of the glycosylation of β 4 as a post translational modification on PD pathogenesis in Neuro2a cells through a comparison of the expression of the β 4-WT and β 4-MUT plasmids was characterized. An increase in the expression of β 4 in the neonatal PD transgenic mice and its developmental regulation was reported. The study also suggest that the sialic acid component of β 4 protein is imperative for proper physiological function, and its aberrant glycosylation might lead to neuritic degeneration. This study highlighted the significance of the alteration of glycosylation of sodium channel β 4 in the pathogenesis of PD. Another important implication of modulation of glycosylation in PD is represented by

immunoglobulin G (IgG). Immunoglobulins against alpha synuclein aggregates are found in both the blood plasma and CSF of the patients with familial PD[23]. It is well known that IgG can exert both anti-inflammatory and pro-inflammatory responses and it was shown by Russell et al. [24] that the switch between these phenotypes is regulated by the two *N*-glycans attached to the asparagine²⁹⁷ of both heavy chains in the fragment crystallizable (Fc) portion. This was an in-depth analysis of the changes in the traits of *N*-glycosylation of the alpha synuclein-reactive IgG where they reported a reduction in sialylation that translated to a reduced ability to counter the inflammatory activity mediated by antibody-dependent cell cytotoxicity (ADCC). However, no rigorous investigation into the modulation of the brain *N*-glycome with the induction and progression of Parkinson's has been performed to date.

Very recently, some studies have used the glycome as a source for disease markers. The progress on this front is severely limited by the inherent complexities of the glycan codes and the lack of suitable analytical methods to investigate glycan structures. However, over the last decade the availability and use of mass spectrometric techniques for identification and structural elucidation of glycans has intensified. MALDI-MSI allows for the robust and time-efficient collection of glycan information from both formalin-fixed paraffin-embedded (FFPE) [25] and snap-frozen [26] tissue sections. These methods obviate the need for multiple time-consuming processing steps like homogenization, fractionation or application of antibody-based extractions [27]. The seminal finding that the protein cross-links induced by formalin do not preclude the mapping and quantification of *N*-glycosylation has facilitated the retrospective analysis of several clinical tissue samples and identified the disease-associated glycan modifications using MALDI-MSI [28]. Furthermore, since the MALDI-MSI data is spatially annotated, it can be instrumental in the investigation of the spatial distribution of glycans over the different regions of the tissues [28]. The precision of the mass spectrometric techniques for structural analysis and the possibility of spatial resolution of glycans over the different pathologically relevant regions of the tissues makes it a very attractive tool for the investigation of disease biomarkers.

As discussed above, it is well established that the biosynthesis of *N*-glycans undergoes spatiotemporally controlled regulation within the tissue and shows distinct modulation in the diseased state. It is hypothesized that the spatiotemporal resolution of *N*-glycans isolated from striatum and substantia nigra (SN) over the time course of the disease progression in a Parkinson's model can give an insight into the structures and implications of the glycan cues in the pathophysiological degeneration of neural circuitry. In this study, spatio-specific

glycoanalytical technology was used to analyse the modulation of *N*-glycosylation of rodent brain with the progression of PD. Using a combination of Hydrophilic Interaction Chromatography (HILIC) ultra-performance liquid chromatography (UPLC), lectin histochemistry and MALDI-MSI, a detailed comparative spatio-temporal analysis of relative abundances of *N*-type glycans in the SN and striatum of 6-OHDA treated rat brains was presented. Analysis using this robust platform revealed regio-specific modulation of *N*-glycosylation in the rodent brains with the induction of PD as alterations of salient glycosylation features like sialylation and fucosylation and this was correlated to their projected biological significance and implications for motor function. This is the first study and most comprehensive elucidation of the spatiotemporal resolution of *N*-glycans in the rodent brains to extensively characterise and compare the *N*-glycome modulation of the striatum and SN in a PD model. This study is of significance in postulating the possible involvement of *N*-glycan cues and their modulation in the neurodegenerative disorders like Parkinson's disease.

5.2 Materials & Methods

The *in vivo* analysis and brain tissue collection and processing for protein extraction was performed at Centre for Research in Medical Devices (CÚRAM), National University of Ireland, Galway. The glyco-analytical platform was used for the investigation of the *N*-glycans in the striatum and substantia nigra of the rodent brains at The National Institute for Bioprocessing Research and Training (NIBRT), University College Dublin. This platform included multiple analytical techniques including HILIC-UPLC, WAX-UPLC, LC-MS/MS and exoglycosidase sequencing performed at NIBRT under the supervision of Dr. Roisin O'Flaherty and Dr. Radka Saldova Fahey. Lectin histochemical analysis was performed at CÚRAM, NUIG. MALDI-MSI analysis was performed by the author (Juhi Samal) under the supervision of Prof. Richard Drake at Medical University of South Carolina, USA.

5.2.1 Chemicals and Reagents

Formic acid (FA) and Tris were obtained from AnalaR, VWR. Sodium bicarbonate (NaHCO_3) and ammonium bicarbonate (NH_4HCO_3) were obtained from HiPerSolv, BDH. Protogel was purchased from National Diagnostics, Hesse, Hull, UK. Ammonium persulfate (APS) was purchased from AnalaR; BDH and *N,N,N',N'*-tetramethylethane-1,2-diamine (TEMED) from Sigma-Aldrich. Iodoacetamide (IAA) and dithiothreitol (DTT) were obtained from Sigma-Aldrich. Sodium dodecyl sulfate (SDS), acetonitrile and sucrose were obtained from Sigma Aldrich. Ultrapure water was obtained from arium[®] ProUV (Sartorius stedum). 2-

aminobenzamide (2-AB) labeling of *N*-glycans was performed using fluorescent labeling mix (50 μ L, 350 mM 2-AB (Sigma), 1 M sodium cyanoborohydride (Sigma) in acetic acid (Sigma)/dimethyl sulfoxide (Sigma) (30:70) [29]. The glycan standard NA2 was obtained from ProZyme (Hayward, CA). Trifluoroacetic acid, sodium hydroxide, dimethyl sulfoxide, iodomethane and α -cyano-4-hydroxycinnamic acid (CHCA) were obtained from Sigma-Aldrich (St. Louis, MO). HPLC grade methanol, ethanol, acetonitrile, xylene and water were obtained from Fisher Scientific (Pittsburgh, PA). SuperFrostTM Plus Adhesion slides were purchased from ThermoFischer Scientific (Dublin, IE). Citraconic anhydride for antigen retrieval was from ThermoFischer Scientific (Bellefonte, PA). Recombinant Peptide N-Glycosidase F (PNGaseF) was obtained from Bulldog Bio (Portsmouth, NH).

5.2.2 Animals

Female Sprague–Dawley rats (Charles River, UK) were used in this study (n=60), weighing 225–250 g at the start of the experiment. Only female rats were used in this study to minimise the total number of animals used in the study design, keeping in mind the associated cage expenditures. Animals were housed in groups of four per cage, on a 12:12-h light:dark cycle, at 19–23 °C, with the humidity level of the room maintained between 40% and 70%, and food and water available *ad libitum* throughout the experiment. All procedures were carried out in accordance with the European Union Directive 2010/73/EU and S.I. No. 543 of 2012, were completed under CAA license (B100/3827) issued to Dr Eilís Dowd by the Irish Department of Health and Children, and were reviewed and approved by The Animal Care and Research Ethics Committee of the National University of Ireland, Galway.

5.2.3 6-OHDA lesions and rotational behaviour

All surgeries were performed under isoflurane anaesthesia (5% in O₂ for induction and 2% in O₂ for maintenance) in a stereotaxic frame with the nose bar set at –4.5 (intra-MFB) or –2.3 (intra-striatal). The MFB was infused unilaterally at coordinates AP –4.0, ML –1.3 (from bregma) and DV –7.0 below dura. Infusions were completed at a total volume of 3 μ l (6-OHDA lesion) at a rate of 1 μ l/min with a further 2 min allowed for diffusion. Dopaminergic asymmetry in lesioned and transplanted rats was assessed via rotational behaviour using the dopaminergic stimulant apomorphine (1.5 mg/ml s.c.) as previously described [30].

5.2.4 Extraction of striatal and nigral tissues from rat brain for HILIC-UPLC

Intact brains from adult rats were snap frozen and lyophilized. Lyophilized brains were then sectioned into 300 μm slices using the Microm HM 505 E cryostat (GMI) after being mounted on the cryostat chuck using OCT. The sections were collected on SuperFrost™ Plus Adhesion slides (ThermoFischer Scientific). Relevant sections for striatum and nigra were identified using a brain atlas. Micron biopsy punches of 2 mm and 0.5 mm (Harvard apparatus) were used to punch out the striatum and nigra respectively from brain sections. The tissue punches were collected in microcentrifuge tubes and stored at $-80\text{ }^{\circ}\text{C}$ until processed further.

5.2.5 Perfusion

Rats were deeply anaesthetised with pentobarbital (1 ml/kg) and transcardially perfused with 100 ml of ice-cold heparinised saline (5000 U/L) followed by 150 ml of 4% paraformaldehyde (pH 7.4). Their brains were removed and placed into 4% paraformaldehyde overnight for post-fixation. Half of the brains were transferred to 30% sucrose. After 48 h equilibration in sucrose solution, 5 μm serial sections of the fixed brains were cut using a freezing sledge microtome and lectin staining was performed. The other half of the brains were paraffin embedded.

5.2.6 Tissue homogenization

Tissue homogenates for *N*-glycan isolation and profiling were obtained by using Tris-SDS lysis buffer [31]. Briefly, collected tissue samples were re-suspended in Tris-SDS lysis buffer (62.5 mM TRIS pH 6.6, 2% SDS) for 20 minutes on ice followed by aspiration three times and a further 20 minutes incubation. This was followed by homogenization using automated bead homogenizer (Qiagen TissueLyser LT) for complete lysis (40 Hz, six min). Supernatant was collected after centrifugation at 16,860 g for 20 minutes at $4\text{ }^{\circ}\text{C}$ and dried overnight under vacuum centrifugation. Protein concentration in the samples was estimated using bicinchoninic acid (BCA) protein assay (Pierce™ BCA Protein Assay Kit, ThermoFischer Scientific).

5.2.7 Release of *N*-glycans from striatal and nigral tissue homogenates

N-glycans were released from dried tissue samples using the high-throughput method described by Royle *et al* [32] with a slight modification in the protein extraction protocol. Briefly, samples were immobilized in SDS-gel blocks to minimise the sample

loss during transfer, reduced and alkylated in 96-well plates and then washed. The *N*-linked glycans were released using peptide *N*-glycanase F (500,000 U/ mL, NEB) as previously described [33].

5.2.8 2-AB labeling of *N*-glycans

N-glycans were fluorescently labeled with 2-AB by reductive amination [34]. Briefly, 2-AB labeling mixture was added to the released glycans, followed by agitation for five min to ensure proper mixing. This was followed by an incubation at 65°C for 30 min and five min agitation. The samples were then incubated at 65°C for 1.5 hours. Excess 2-AB reagent was removed on Whatman 3MM paper (Clifton, NJ) with acetonitrile and final elution of glycans was performed in water [31].

5.2.9 Ultra-Performance Liquid Chromatography (UPLC)

UPLC was performed using a BEH Glycan 1.7 μ m particles in 2.1 \times 150 mm column (Waters, Milford, MA) on an Acquity UPLC (Waters) equipped with a Waters temperature control module and a Waters Aquity fluorescence detector. Solvent A was 50 mM formic acid adjusted to pH 4.4 with ammonia solution. Solvent B was acetonitrile. The column temperature was set to 40 °C. A 30 min method was used with a linear gradient of 30–47% with buffer A at 0.56 mL/min flow rate for 23 min followed by 47–70% A and then to 30% A. Samples were injected in 70% acetonitrile. Fluorescence detection was performed using $\lambda_{\text{excitation}}$: 320 nm and $\lambda_{\text{emission}}$: 420 nm. The system was calibrated using an external standard of hydrolyzed and 2 AB-labeled glucose oligomers to create a dextran ladder, as described previously [31].

5.2.10 Tissue processing for MALDI-MSI

Brains were isolated from the animals post-perfusion and were stored in formalin overnight at 4 °C. The tissue was then removed from the formalin and rinsed with deionized H₂O before processing with Excelsior™ AS Tissue Processor (Thermo Scientific, Ireland). The protocol was as follows: 70 % EtOH for 5 min, 80 % EtOH for 2 h, 95 % EtOH for 2 h, 3 \times 100 % EtOH for 2 h each, 2 \times xylene for 2 h each, and 2 \times paraffin for 2 h each. A Leica EG1150 & EG1130 Cold Plate embedder (Leica Biosystems) was used to create paraffin-embedded tissue blocks. FFPE blocks were sectioned (6 μ m thick) on a Leica Microtome RM12235 and water bath mounted (39 °C) onto Superfrost™ Ultra Plus Adhesion Slides. Slides were left to dry at 37 °C for 1 h prior to storage at RT.

5.2.11 Deparaffinization and rehydration






Tissue blocks were sectioned at 5 μm and mounted on Bruker slide adaptor plate- compatible Superfrost™ Ultra Plus Adhesion Slides (25×75 mm). The slides were heated at 60°C for one hour. After cooling, the sections were deparaffinized by washing serially in xylene (3 minutes each). This was followed by rehydration by submerging the slide in progression: twice in 100% ethanol (1 minute each), once in 95% ethanol (one minute), once in 70% ethanol (one minute), and twice in water (3 minutes each). The slides were then subjected to antigen retrieval using citraconic anhydride buffer in a vegetable steamer for 25-30 minutes. Citraconic anhydride (Thermo) buffer was prepared by adding 25 μL citraconic anhydride in 50 mL water, and adjusted to pH 3 with HCl. After cooling, a series of three buffer exchanges was performed by replacing half of the buffer with water before eventually replacing it completely with water. The slides were then desiccated prior to the enzymatic digestion with PNGase F.

5.2.12 N- glycan MALDI-MSI

The slides were coated using an ImagePrep spray station (Bruker Daltonics) with a 0.2 ml aqueous solution of PNGaseF (20 μg total/slide) as previously described [25]. The slides were incubated at 37°C for two h in a humidified chamber and dried in a desiccator prior to matrix application. α -Cyano-4-hydroxycinnamic acid matrix (0.021 g CHCA in 3 ml 50% acetonitrile/50% water and 12 μL 25%TFA) was applied using the ImagePrep sprayer. Released glycan ions were detected using a SolariX dual source 7T FTICR mass spectrometer (Bruker Daltonics) ($m/z=690\text{--}5000$ m/z) with a SmartBeam II laser operating at 1000 Hz with a laser spot size of 25 μm . Images of differentially expressed glycans were generated to view the expression pattern of each analyte of interest using FlexImaging 4.0 software (Bruker Daltonics). Following MS analysis, data was loaded into FlexImaging Software focusing on the range $m/z=1000\text{--}4000$ and reduced to 0.95 ICR Reduction Noise Threshold. Observed glycans were searched against the glycan database provided by the Consortium for Functional Glycomics (www.functionalglycomics.org). Glycoworkbench was used to generate the glycan structures and represent putative structures determined by combinations of accurate m/z , CID fragmentation patterns and glycan database structures.

5.2.13 Glycan nomenclature

All *N*-glycans have two core GlcNAcs attached to trimannosyl; F at the start of the abbreviation indicates a core $\alpha(1,6)$ -fucose linked to the inner GlcNAc; otherwise F indicates an outer arm $\alpha(1,3)$ or $\alpha(1,4)$ -fucose linked to antenna or galactose; M_x, number (x) of mannose on core

GlcNAcs; Ax, number of antenna (GlcNAc) on trimannosyl core; A2, biantennary with both GlcNAcs as $\beta(1,2)$ -linked; A3, triantennary with a GlcNAc linked $\beta(1,2)$ - to both mannose and a third GlcNAc linked $\beta(1,4)$ - to the $\alpha(1,3)$ -linked mannose; A4, GlcNAcs linked as A3 with additional GlcNAc- $\beta(1,6)$ -linked to $\alpha(1,6)$ -mannose; Gx, number (x) of $\beta(1,4)$ -linked galactose on the antenna; Galx, number (x) of $\alpha(1,3/4/6)$ -linked galactose on $\beta(1,4)$ -linked galactose; Sx, number (x) of sialic acids linked to galactose; the number 3 or 6 in parentheses after S indicates whether the sialic acid is in an $\alpha(2,3)$ - or $\alpha(2,6)$ -linkage; Sx, number (x) of neuraminic acids linked to galactose; the number 3, 6 or 8 in parentheses after S indicates whether the sialic acid is in an $\alpha(2,3)$ -, $\alpha(2,6)$ - or $\alpha(2,8)$ - linkage; Gcx, number (x) of glycolylneuraminic acids linked to galactose; the number 3, 6 or 8 in parentheses after S indicates whether the sialic acid is in an $\alpha(2,3)$ -, $\alpha(2,6)$ - or $\alpha(2,8)$ - linkage; Acx, number (x) of acetyl groups; Lacx, the number (x) of repeating poly-N-acetylglucosamine repeats containing GlcNAc linked $\beta(1,4)$ - to Gal; Px, the number (x) of phosphorous groups. Symbols representative of different glycan moieties in the structures are represented as follows:  , N-acetylglucosamine;  , Mannose;  , Fucose;  , Galactose;  , N-acetylneuraminic acid (sialic acid).

5.2.14 Lectin histochemistry

Brains were dissected out and post-fixation was performed for four h at room temperature. They were then transferred to 25% sucrose in phosphate buffer. For lectin histochemistry, slides were washed with Tris-buffered saline supplemented with Ca^{2+} and Mg^{2+} (TBS; 20 mM Tris-HCl, 100 mM NaCl, 1 mM CaCl_2 , 1 mM MgCl_2 , pH 7.2) with 0.05% Triton X-100 (TBS-T) and then blocked with 2% periodate-treated BSA (Sigma-Aldrich[®]) in TBS for one hour. All washes were three times for five minutes each, all steps performed at room temperature in a humidity chamber unless otherwise stated. Sections were washed then incubated with four different fluorescein isothiocyanate (FITC)- conjugated lectins (EY Labs Inc.) in TBS for one h (**Appendices, Table A7**). Inhibitory controls were carried out in parallel to verify lectin binding specificity by pre- (for one hour) and co-incubating lectins in 100 mM of the appropriate haptenic sugar in TBS (**Appendices, Table A7**). Sections were washed five times with TBS-T and counterstained with 4' 6-diamidino-2-phenylindole dihydrochloride (DAPI) for 20 minutes. The slides were washed in TBS-T before mounting the coverslip with ProLong[®] Gold antifade (Life Technologies). Inhibition by the appropriate haptenic sugar was used as controls for all lectins in the study.

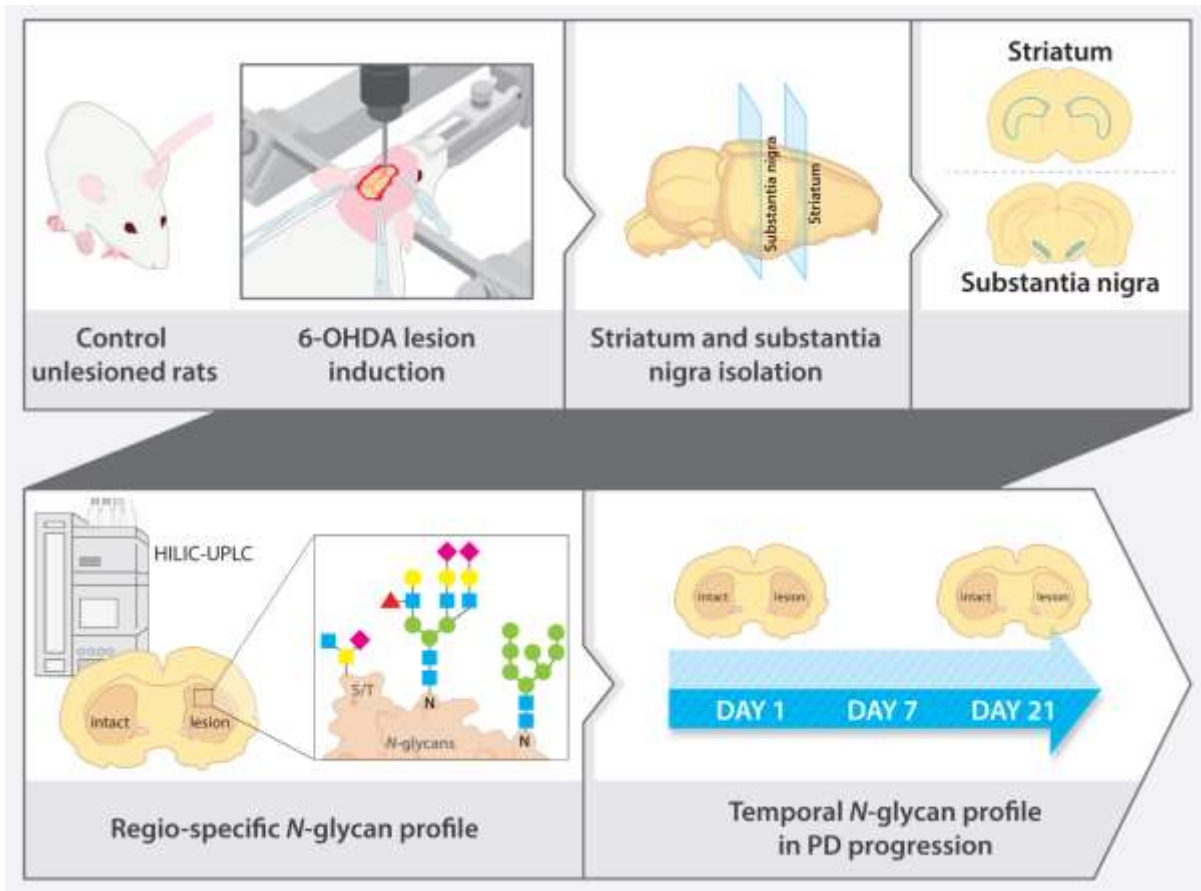
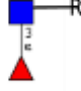





Figure 5.1: Schematic outline of the study to elucidate the spatio-temporal modulation of N-glycosylation in the 6-OHDA PD model. Study design for the detailed investigation of the brain N-glycosylation in the 6-OHDA rodent model of Parkinson’s over the time course of 21 days using the glyco-analytical platform described in Chapter 4.

Table 5.1: Summary of the lectins used for tissue histochemistry with their binding specificity, assay concentration and inhibitory carbohydrate (150 mM).

Lectin	Abbreviation	Binding specificity	Conc. (µg/ml)	Inhibitory carbohydrate	Structural specificity
<i>Anguilla anguilla</i> agglutinin	AAA	Fuc $\alpha(1,3/6)$ - GlcNAc	15	Fuc	
<i>Griffonia simplicifolia</i> lectin 1- β 4	GSA 1 β 4	Terminal α Gal	15	Gal	
Concanavalin A lectin	Con A	α -linked Man, Glc, or GlcNAc	10	Man	
Wheat germ agglutinin	WGA	GlcNAc, Neu5Ac/Glc	15	GlcNAc	

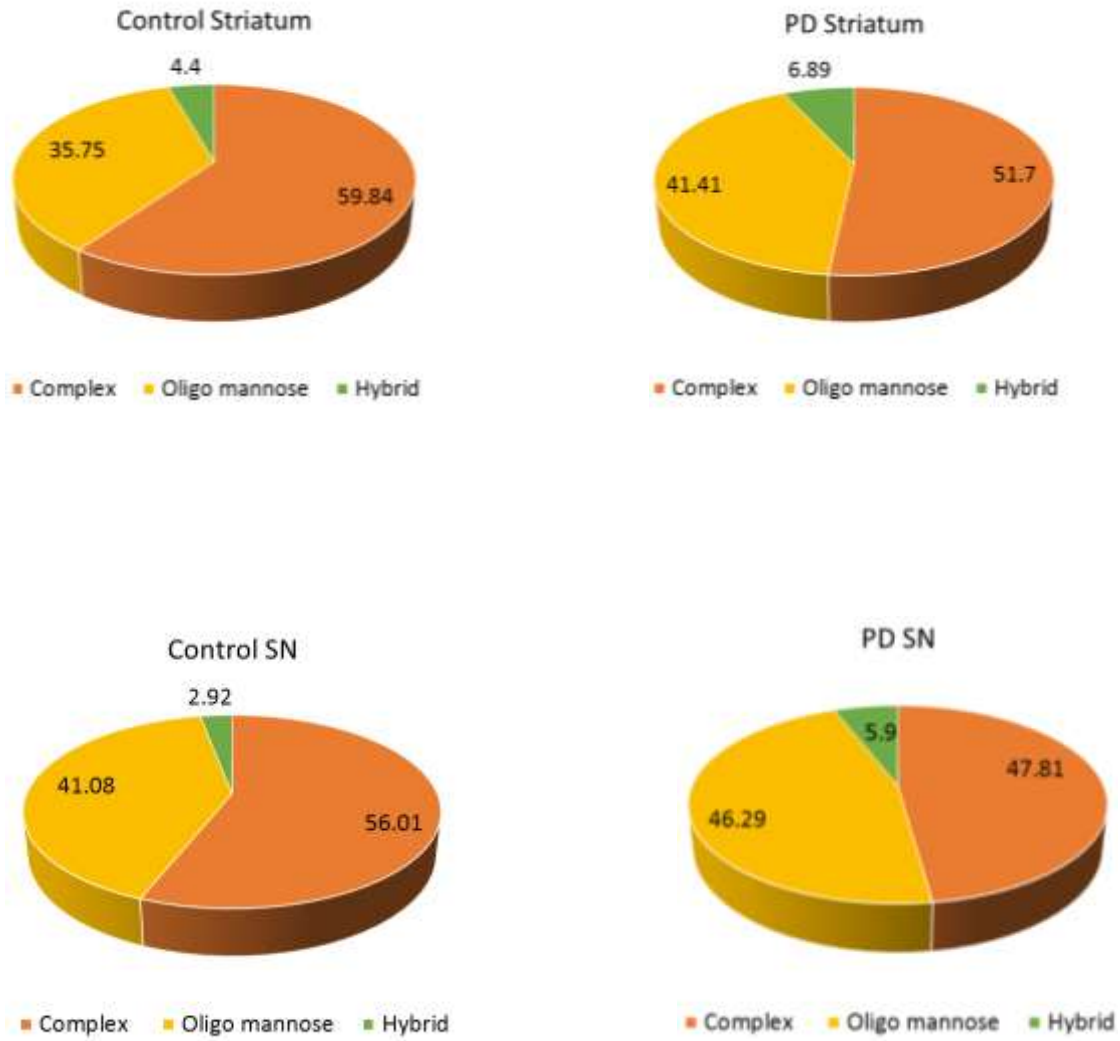


Figure 5.2: Overall modulation of major N-glycan classes. The trends of modulation of chief N-glycan classes in the rodent brain after 21 days of 6-OHDA lesioning compared to the healthy controls representing an overall increase in the hybrid and oligo-mannose N-glycans in the PD striatum and SN.

5.2.15 Statistical analysis

Statistical analyses were performed using GraphPad Prism[®] Version 5 (USA) and IBM SPSS[®] Version 21. Data were compared using one-way or two-way analysis of variance (ANOVA) based on the number of factors analysed, followed by a BonFerroni post-hoc comparison test. Statistical significance was set as * $p < 0.05$, ** $p < 0.01$, *** $p < 0.001$.

5.3 Results

5.3.1 Glycosylation trends in healthy vs diseased rodent brains

An *in vivo* analysis was performed to investigate the temporal changes in *N*-glycome of striatum and SN in the course of PD progression using the glyco-analytical platform developed earlier in this study as represented in **Figure 5.1**. This platform was able to reliably separate and individually quantify nearly all the *N*-glycans present in these two regions of the brain, in addition to elucidating the derived traits of glycosylation. In summary, six and five GPs (**Figure 5.3 A, B**) in the *N*-glycome of striatum and SN respectively showed statistically significant differences between the animals with PD and the controls. The trends of modulation of glycosylation were investigated and are represented as the percentage increase/decrease over the control peak areas for the respective peaks (**Figure 5.3C, D**). These GP's corresponded to oligomannose, fucosylated (both core and outer arm) and sialylated glycan species for striatum. However, in SN a distinct modulation of the hybrid *N*-glycans was also observed in addition to the above mentioned traits. An overall modulation of major *N*-glycan classes is represented in **Figure 5.2** for both striatum and SN for diseased and healthy brains.

5.3.2 Temporal modulation of glycosylation traits

In addition to outlining the changes in *N*-glycosylation typical of the eventual PD phenotype, the glycophenotype of a disease-intermediate state characterising the glycophenotype of disease progression was also profiled and mapped. As represented in **Figure 5.4 A, B**, we found that significant changes were detected in GP 20 and 25 for striatum and GP 24 for SN that are not detectable at day 21. Furthermore, GP 11 that was found to be significantly altered in both the striatum and SN at day 21 did not show any significant difference when analysed in the day 7 sample cohort. These trends are also represented as percentage increase/decrease over the control peak areas for the respective peaks in **Figure 5.4 C, D**. For the analysis of the temporal modulation of the glycosylation traits, all the features that were distinct at Day 21 post 6-OHDA treatment were selected for a time-course analysis of trends. For this analysis, only the animals that showed complete motor dysfunction as determined by apomorphine-induced

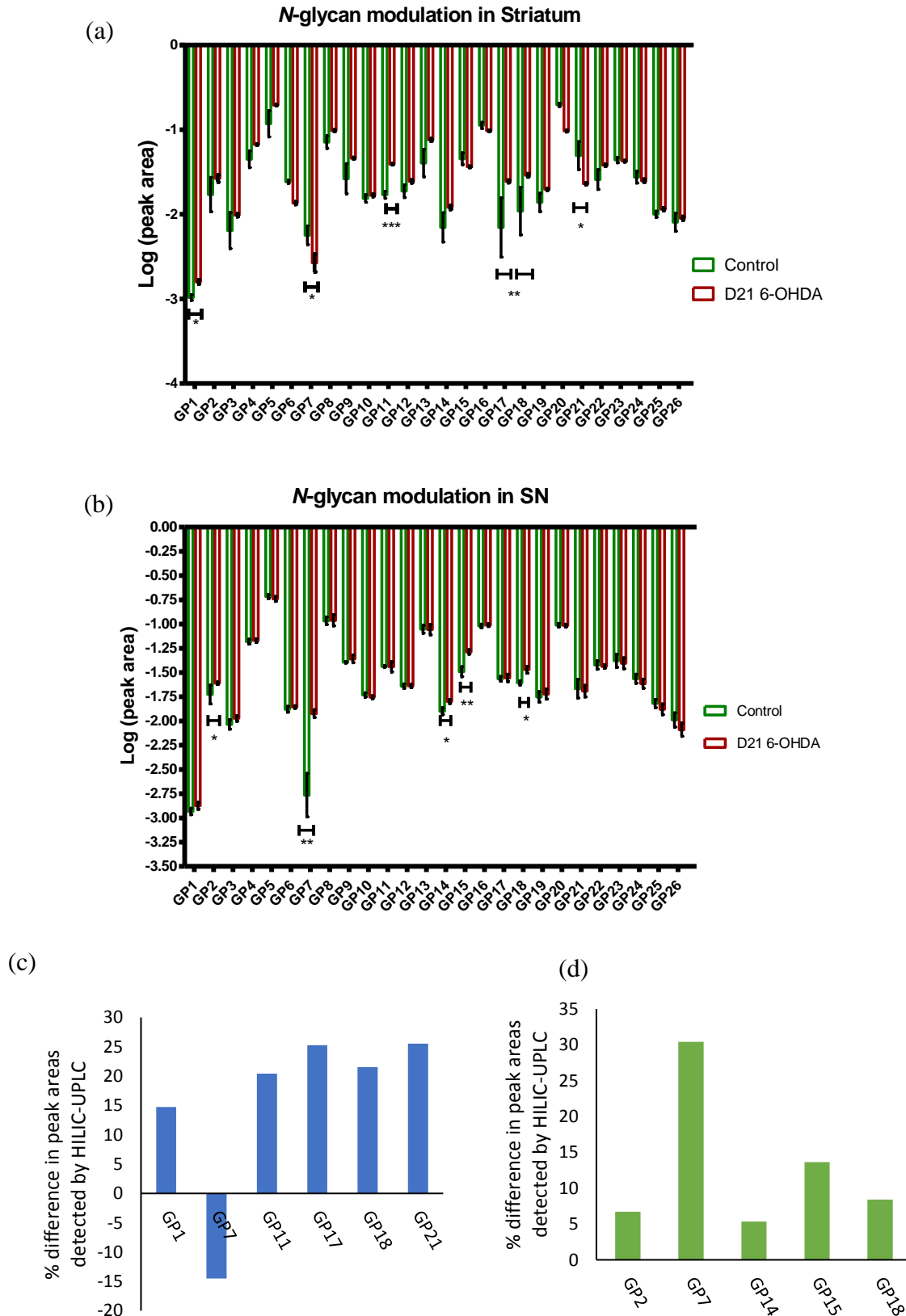


Figure 5.3: N-glycosylation modulation at Day 21. HILIC-UPLC detection of the N-glycosylation modulation at Day 21 post 6-OHDA treatment in (a) striatum and (b) SN of the rat brains (n=5, *p<0.05, **p<0.01, ***p<0.001). The percentage modulation of the respective glycan peak areas over healthy controls is represented for (c) striatum and (d) SN.

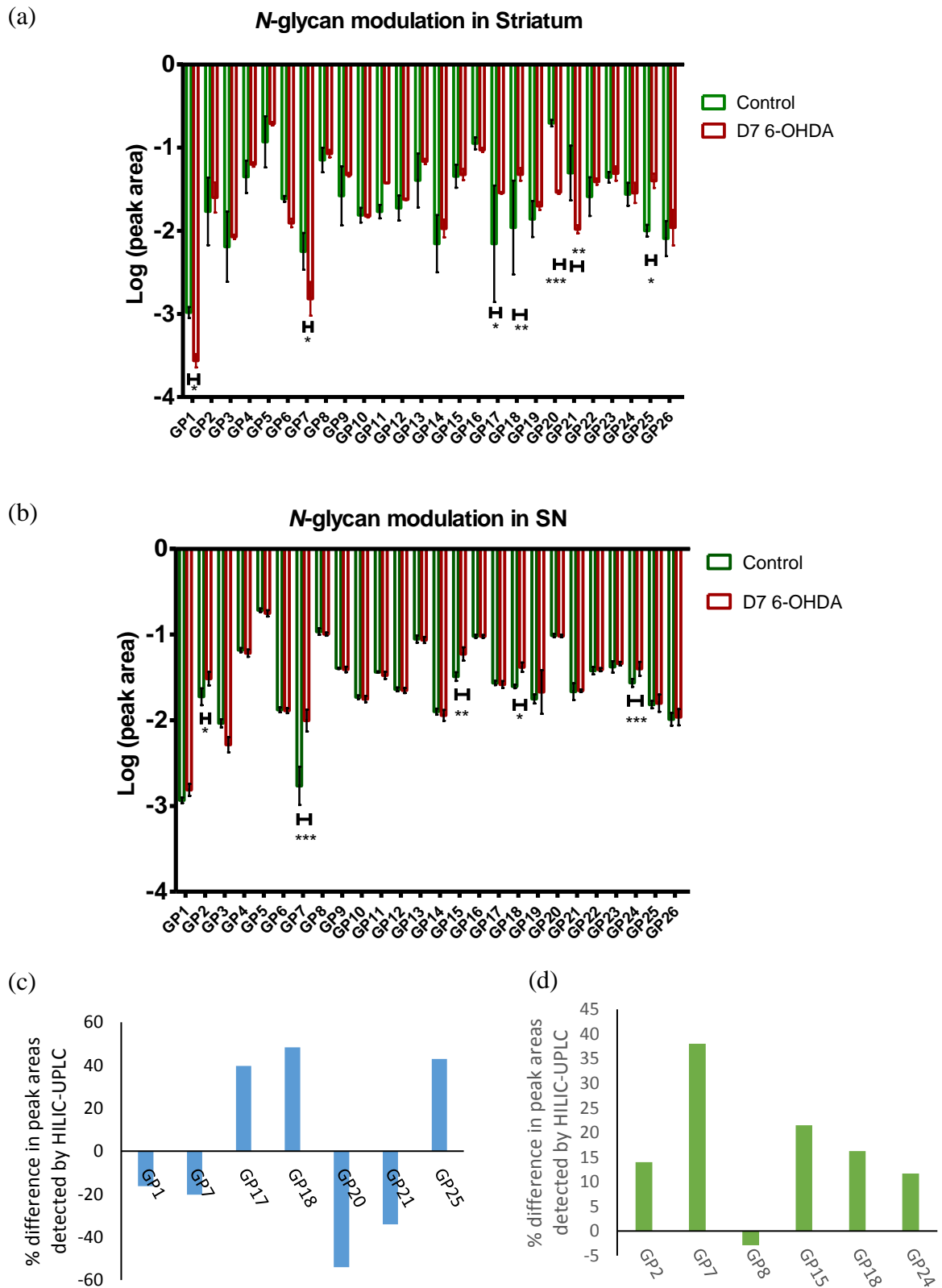


Figure 5.4: N-glycosylation modulation at Day 7. HILIC-UPLC detection of the N-glycosylation modulation at Day 7 post 6-OHDA treatment in (a) striatum and (b) SN of the rat brains (n=5, *p<0.05, **p<0.01, ***p<0.001). The percentage modulation of the respective glycan peak areas over healthy controls is represented for (c) striatum and (d) SN.

rotations were selected. There is an almost complete degeneration of TH-positive dopaminergic neurons that translates into the motor function impairment at day 21 post 6-OHDA administration.

Figure 5.5 represents the trends of temporal modulation for all the glycan species detected to be differentially regulated in the striatum of the Parkinsonian rats. Similar temporal analysis was performed for the glycan moieties detected in the SN of Parkinsonian rats and are represented in **Figure 5.6**. There was an observed increase in the fucosylation in both striatum and SN as represented in **Figure 5.5 & 5.6**. This correlates well with the trends observed in the human patients by Varadi et al [35]. This study investigated the application of a novel capillary electrophoresis (CE) method in combination with label-free quantitation to map the potential changes in serum N-glycans in the PD patients.

Another important observation made by the authors was the decrease in sialylation. The current study found this trend to be concomitant in the rodent brains as well where there was a significant decrease in sialylation associated with the tri-antennary glycan species. In addition to sialylation and fucosylation, there was a significant increase in the oligomannose glycans which was detected at both day 7 and day 21 post 6-OHDA administration in the rodent brains.

This trend was observed consistently in both the striatum and SN and could indicate its involvement in the neural degeneration processes characteristic of the disease pathophysiology.

5.3.3 Mannosylation

There were changes in the oligo mannose N-glycans that were detected in both the striatum and SN. In contrast to the changes in Alzheimer's Disease detected by Fang et al. [439], there was an evident increase in the oligomannose specifically in Man3B or Man3 that was detected by HILIC-UPLC for the striatum and SN respectively. However, MALDI-MSI analysis showed a significant increase in the oligomannose moieties for both the striatum and SN in the Parkinsonian brains that were not detected by the HILIC-UPLC. This trend was supported by the lectin histochemical analysis with Con A that showed an enhanced binding profile in the PD brains compared to the healthy controls.

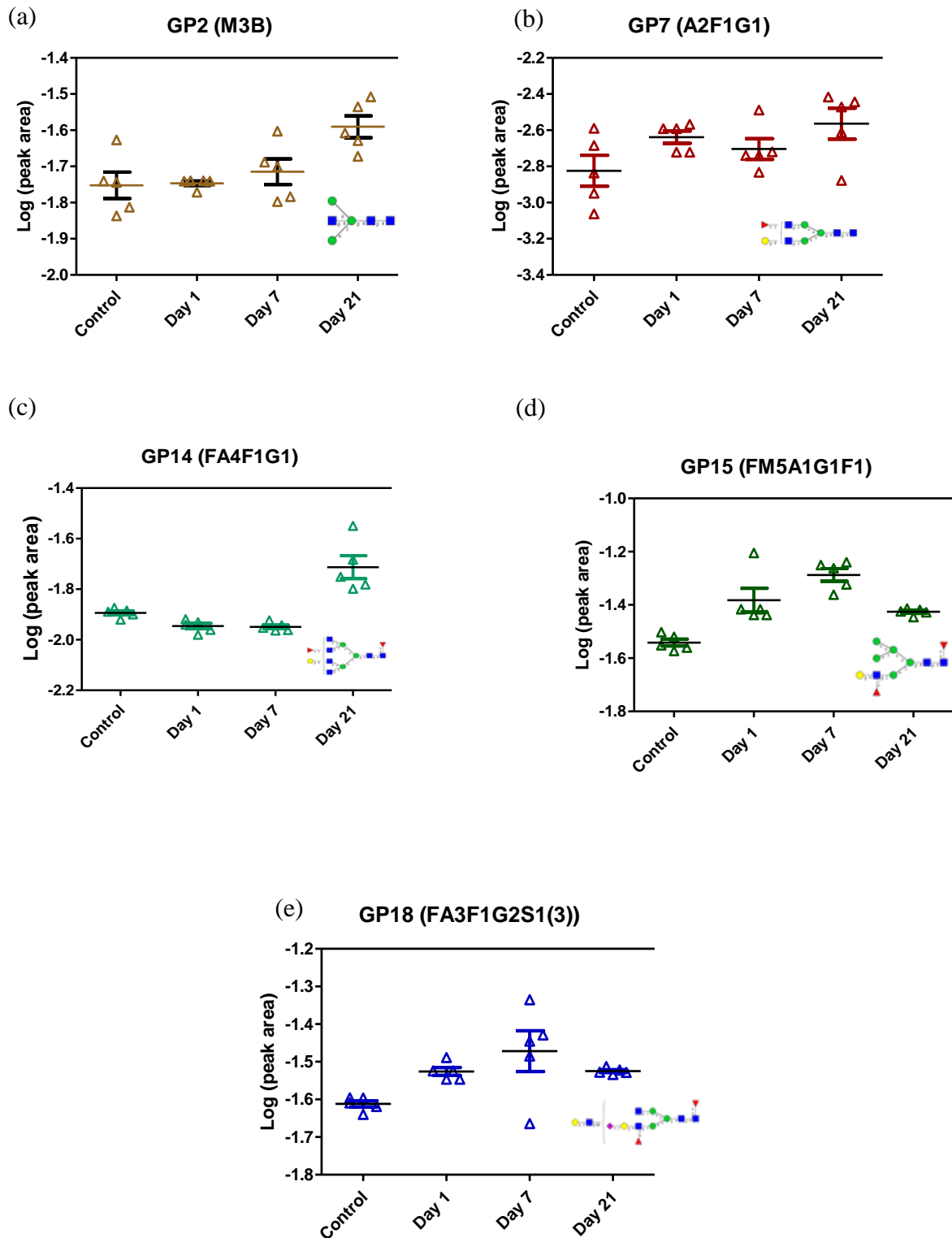


Figure 5.5: Temporal N-glycosylation modulation in SN. Temporal modulation of specific traits of glycosylation as detected by HILIC-UPLC in the SN of the PD rat brains represented over a period of 21 days post 6-OHDA treatment (n=5). The results are consistent with the end-point analysis represented in Figure 5.2 and Figure 5.3 and represent the time-course modulation in the five glycan peaks that were identified to show significant difference over the healthy controls.

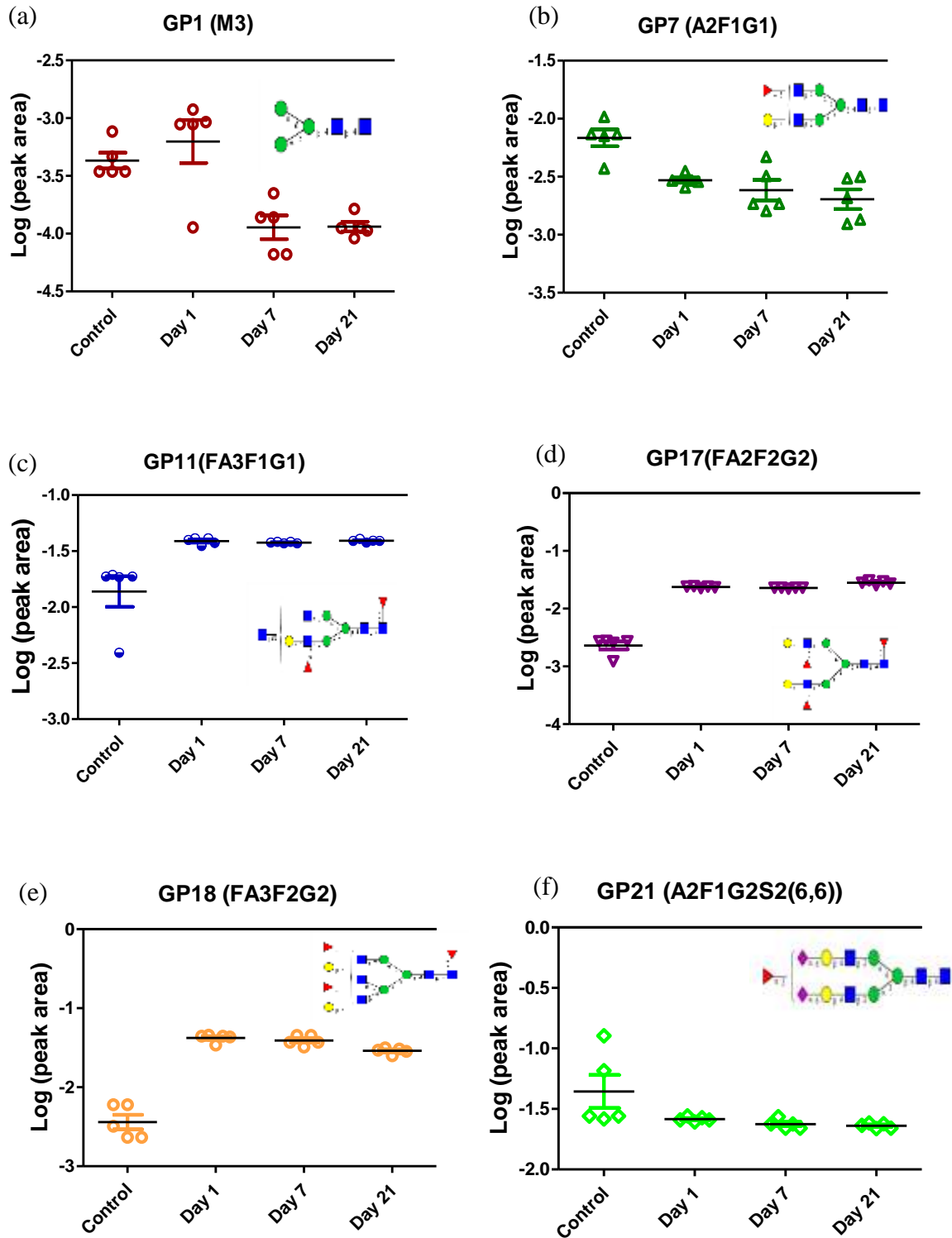


Figure 5.6: Temporal N-glycosylation modulation in striatum. Temporal modulation of specific traits of glycosylation as detected by HILIC-UPLC in the striatum of the PD rat brains represented over a period of 21 days post 6-OHDA treatment (n=5). The results are consistent with the end-point analysis represented in Figure 5.2 and Figure 5.3 and represent the time-course modulation in the six specific glycan peaks that were identified to show significant difference over the healthy controls.

5.3.4 Fucosylation

The trends for differential spatio-temporal modulation of fucosylation over the time course of PD induction was elucidated in **Figure 5.5 and 5.6**. There was also an overall change in fucosylation that is represented in **Figure 5.7 a, b**. There was an increase in fucosylation both core (Control: 51%; PD: 57%) and outer arm that was detected for SN (Control: 25%; PD: 29%). The major glycan species that showed modulation in SN were: A2F1G1, FA2G1, FM5A1G1F1 and FA3F1G2S1(3). An increased fucosylation was observed in the striatum (core fucose: Control: 52%; PD: 58%, outer arm: Control: 37%; PD: 43%) as compared to SN with an upregulation of A2F1G1, FA3F1G1, FA2F2G2, FA3F2G2 and A2F1G2S2(6,6). These results are consistent with the implied correlation of enhanced fucosylation with neuronal degradation as observed by Kollmann et al [440] which are indicative of the role of aberrant fucosylation in mediating neurodegeneration in PD.

5.3.5 Sialylation

A decrease in sialylation was observed for both striatum and SN. As represented in **Figure 5.7 d**, there was a particularly significant decrease in α -(2-3)-linked sialylation in SN associated with the tri-antennary glycans. For the striatum, this trend was detected more for α -(2-6)-linked sialylation as represented in **Figure 5.7 c**. There was an overall decrease in sialylation that is represented for the two regions of the brain. To the best of our knowledge, this is the first report of the observed changes in modulation of sialylation in the brain with the induction of PD in a rodent model. Interestingly, these changes were prominent in mono- and di-sialylated species in contrast to that of higher sialyl-substituted glycans for the SN and striatum respectively. Also, the sialyl groups were linked with fucosylated core structures for both regions of the brain.

5.3.6 Lectin histochemical characterisation of the disease glycophenotype

The panel of four lectins used to investigate and visually represent (**Figure 5.8a**) the differential modulation of glycan expression in the 6-OHDA treated rodent brains is represented in **Table 1** with their glycan-binding specificity. The basis of the lectins' selection is their ability to bind to general mammalian-type glycans and represent the region-specific modulation of *N*-glycosylation in diseased, injured and healthy animals. For fucosylation, a differential binding profile was detected with the *Anguilla anguilla* lectin (AAA) in the PD

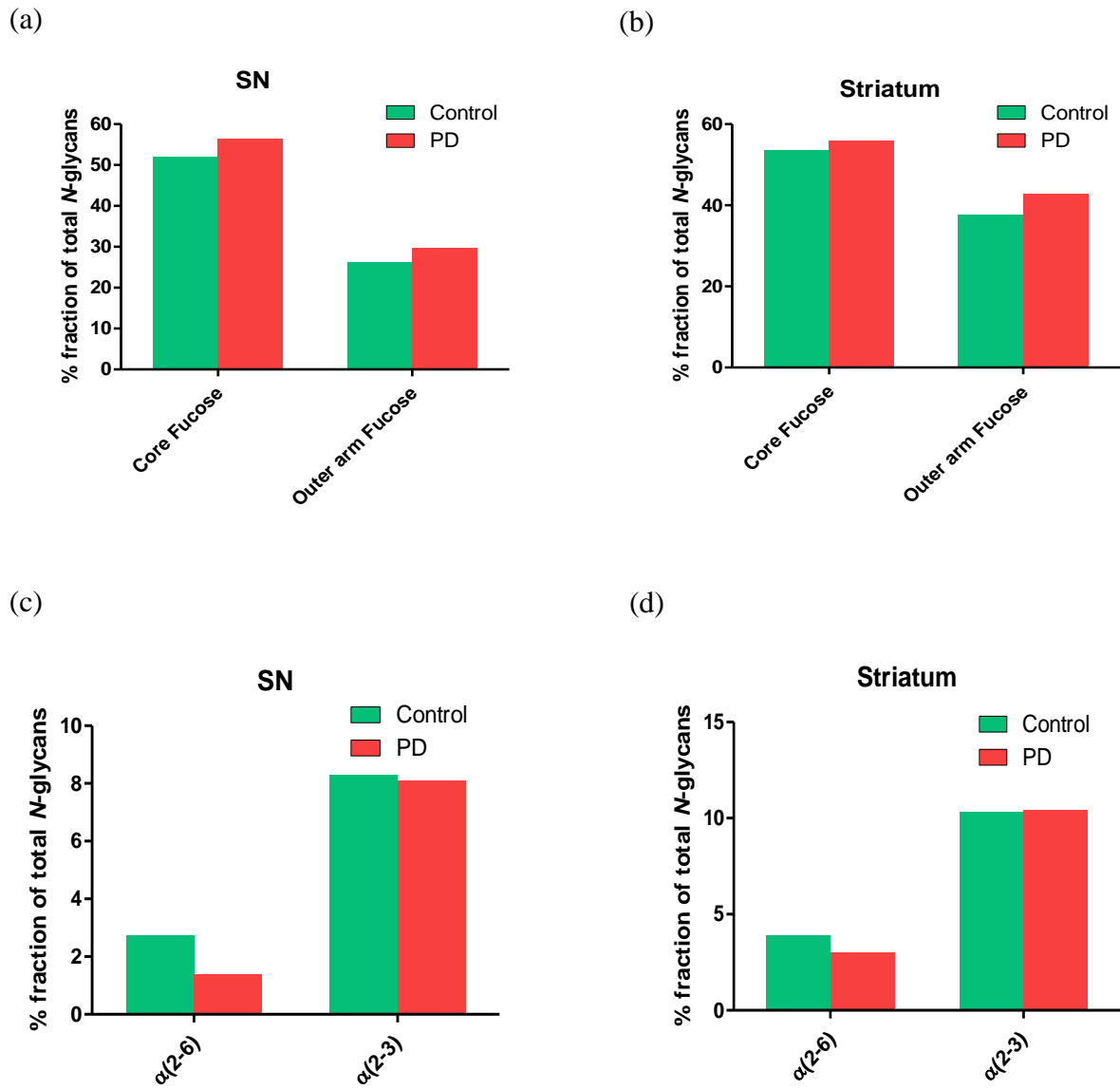


Figure 5.7: Modulation of fucosylation and sialylation in SN and striatum. Overall modulation of (a), (b) fucosylated and (c), (d) sialylated N-glycans in the rodent brain after 21 days of 6-OHDA lesioning compared to the healthy controls representing an overall increase in fucosylation and reduction in sialylation in striatum and SN of the PD brains.

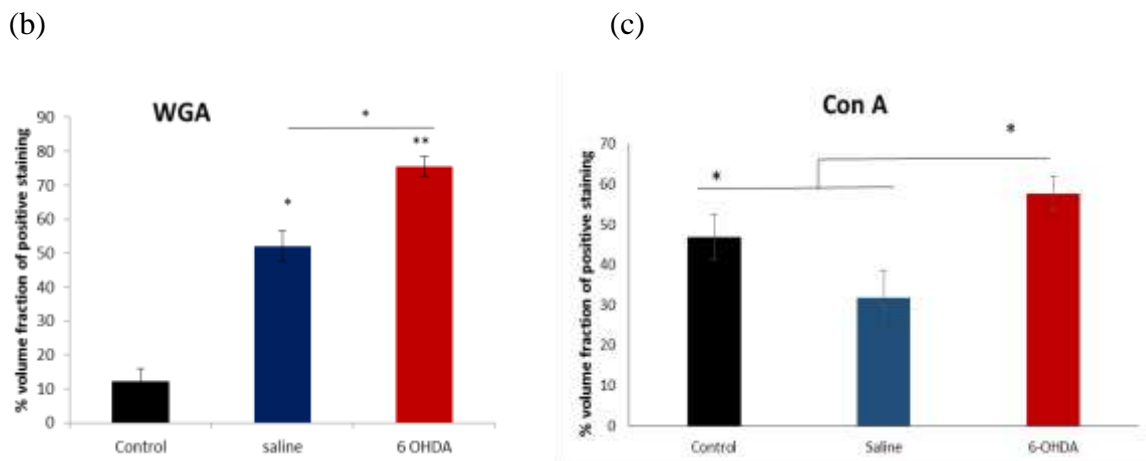
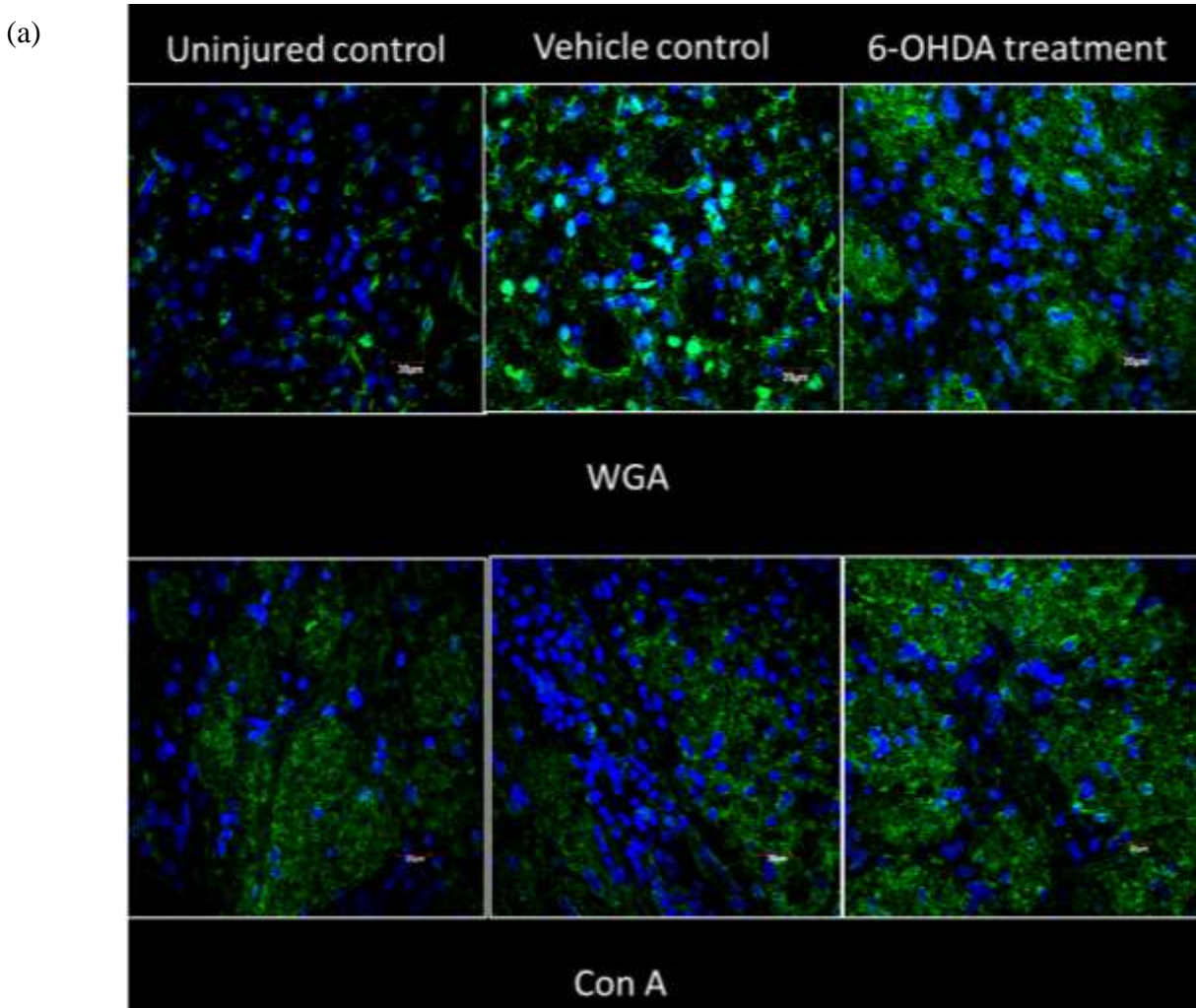


Figure 5.8: Lectin histochemical analyses for N-glycosylation modulation in PD. Representative images for WGA and ConA binding showing enhanced binding to the diseased brains compared to the healthy controls. All lectin binding intensities were background-subtracted and quantified by Image J (c, d). Data are shown as mean with standard deviation ($n = 4-6$ animals per group). Scale bar = 20 μm .

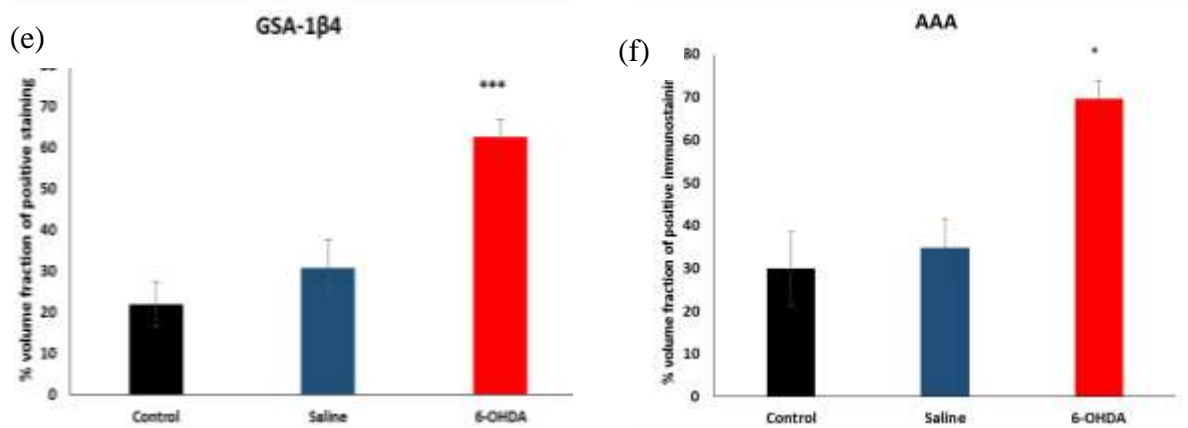
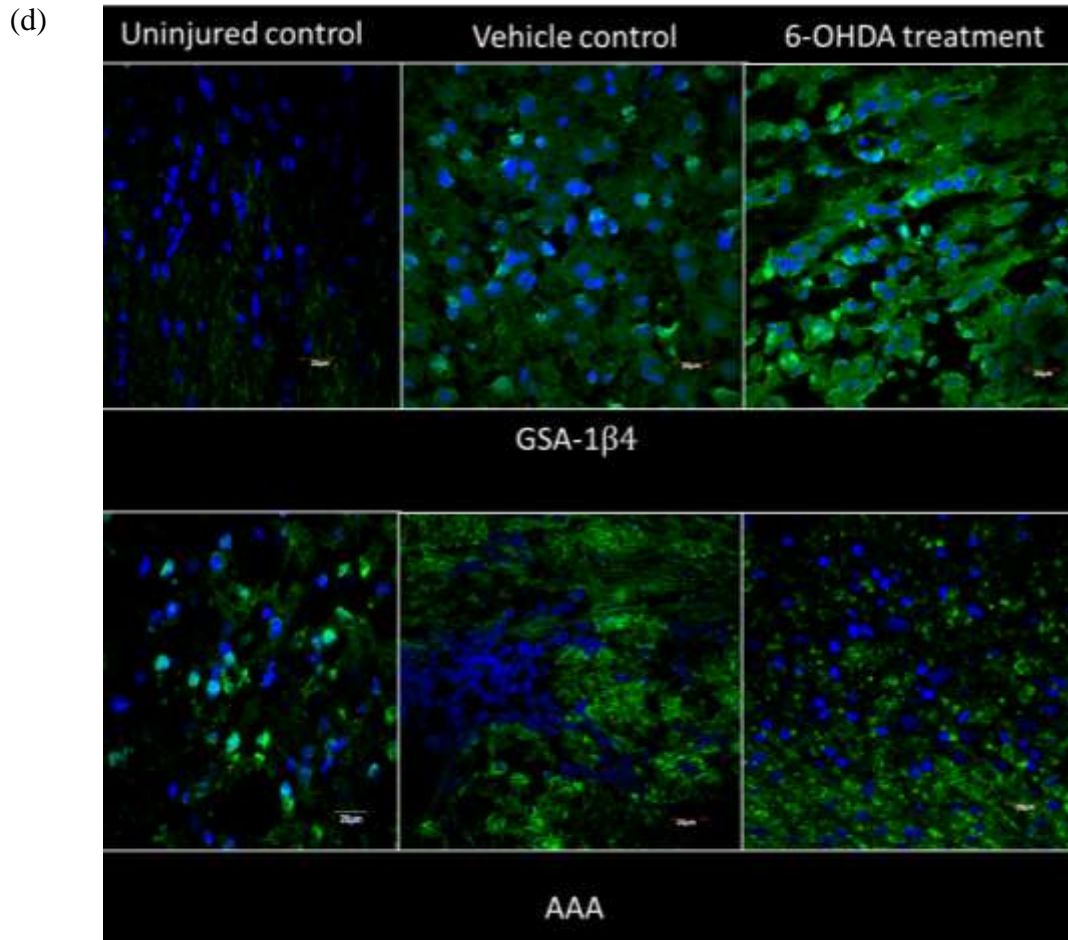


Figure 5.8: Lectin histochemical analyses for N-glycosylation modulation in PD. (d) Representative images for GSA 1 β 4 and AAA binding demonstrating the presence of α -gal epitope and enhanced binding of AAA to the diseased brains compared to that of the healthy controls. All lectin binding intensities were background-subtracted and quantified by Image J (e, f). Data are shown as mean with standard deviation ($n=4-6$ animals per group). Scale bar = 20 μ m.

brains compared to that of the healthy controls (**Figure 5.8 d**). This lectin binds to Fuc- α -(1-6) and Fuc- α -(1-3) glycan moieties. Interestingly, this modulation was assumed to be very disease-specific as there was a significant difference in the binding profiles of the lectin from that of the injured and PD brains. An increase in the overall fucosylation was most distinct in the lectin histochemistry where there was a significant increase in the lectin-positive staining (**Figure 5.8f**). In lectin histochemical analysis, Concanavalin A lectin (ConA) is usually employed to detect the presence and localisation of *N*-linked glycosylation in the tissue as it shows preferential binding (1.5-fold) to α -linked mannose (Man) residues in the core structures of all *N*-linked glycans. An enhanced binding of Con A (seven-fold) was detected in the diseased brains as compared to that of the healthy and injured controls as represented in **Figure 5.8c**. Wheat germ agglutinin (WGA) strongly binds to the microglial population [370] and hence it correlates well with the enhanced binding (seven-fold) to the PD brains as compared to that of the healthy controls. The quantified lectin histochemistry analysis is presented in **Figure 5.8b** which is in line with our previous analysis in this study. GSA 1 β ₄ shows strong binding to the microglia and has been shown previously to differentiate between the resting and activated microglia [441]. Consistent with this finding, an enhanced binding of GSA 1 β ₄ (three-fold) was observed in the 6-OHDA treated rat brains when compared to that of the healthy controls (**Figure 5.8e**). These trends of modulation of the *N*-glycosylation presents a very strong evidence about the speculated correlation of the glycosylation patterns in the brain with their biological functions and disease pathology.

5.3.7 MALDI-MSI analysis of the disease glycophenotype

Rat brains were fixed in formalin and processed using MALDI-IMS glycan imaging workflow followed for FFPE tissues as described by Powers et al [434]. The glycan cues differentially regulated in striatum and SN in response to disease induction are represented in **Figure 5.9, 5.10**. Brain slices were cut at 5 microns and deparaffinised. This was followed by rehydration in sequential xylene/ethanol/water rinses, and antigen retrieval in citraconic anhydride pH 3. The antigen-retrieved slices were then sprayed with PNGaseF to release the *N*-glycans followed by matrix spray and subsequent analysis by MALDI-MSI. The glycan peak composition analysis was performed by comparing the peak mass with a database of all possible mammalian *N*-glycan compositions in GlycoWorkBench and then refined by comparing the results with the Consortium for Functional Glycomics (www.functionalglycomics.org) databases followed by referencing to the previous studies to

remove the biologically irrelevant matches. Finally, the corresponding MS/MS spectra was used to confirm the peak glycan assignments.

The tissue section analysis using MALDI-MSI led to the identification of 17 differentially regulated N-glycans between the SN of the diseased animals and those of the healthy controls. Amongst the differentially regulated oligomannose glycans, M3 was detected in the HILIC-UPLC analysis. However, using the MALDI-MSI, differences in the expression of Man6, Man7, Man8, Man9 were also detected. There was also a very selective increase in the hybrid N-glycans detected by MALDI-MSI in the SN of the diseased animals as compared to those of the healthy controls. As a general observation, there was a loss of higher sialic acids when ionized by matrix-assisted laser desorption/ionization (MALDI) as the consequence of the labile carboxylic proton which is lost both in the ion source and during the flight to the detector [442]. There was a significant upregulation of the fucosylated N-glycans which was also detected using MALDI-MSI. This included both core and outer arm fucosylated N-glycans. An interesting finding of this analysis for SN was the upregulation of Lewis antigen^x and alpha-gal modified N-glycans in the diseased animals. The panel of MALDI-MSI images representative of these changes in SN and the glycan species implicated are represented in **Figure 5.9**.

As with the SN, 17 differentially regulated glycans were detected in the striatum of diseased and healthy animals. Interestingly, all the oligomannose N-glycans (Man5, Man6, Man7, Man8 and Man9) showed a differential regulation in the striatum as compared to the SN where Man5 did not show any alteration with the disease induction. In line with the observation for SN, Lewis antigen^x modified N-glycans showed distinct modulation in the brains of the PD model. A significant upregulation of alpha-gal modified N-glycans was also detected in the striatum of the diseased animals which could indicate its role in the disease pathophysiology. An upregulation of fucosylated N-glycans was detected in the striatum of the disease model when compared to the healthy controls. The panel of MALDI-MSI images representative of these changes in the striatum and the glycan species implicated are represented in **Figure 5.10**.

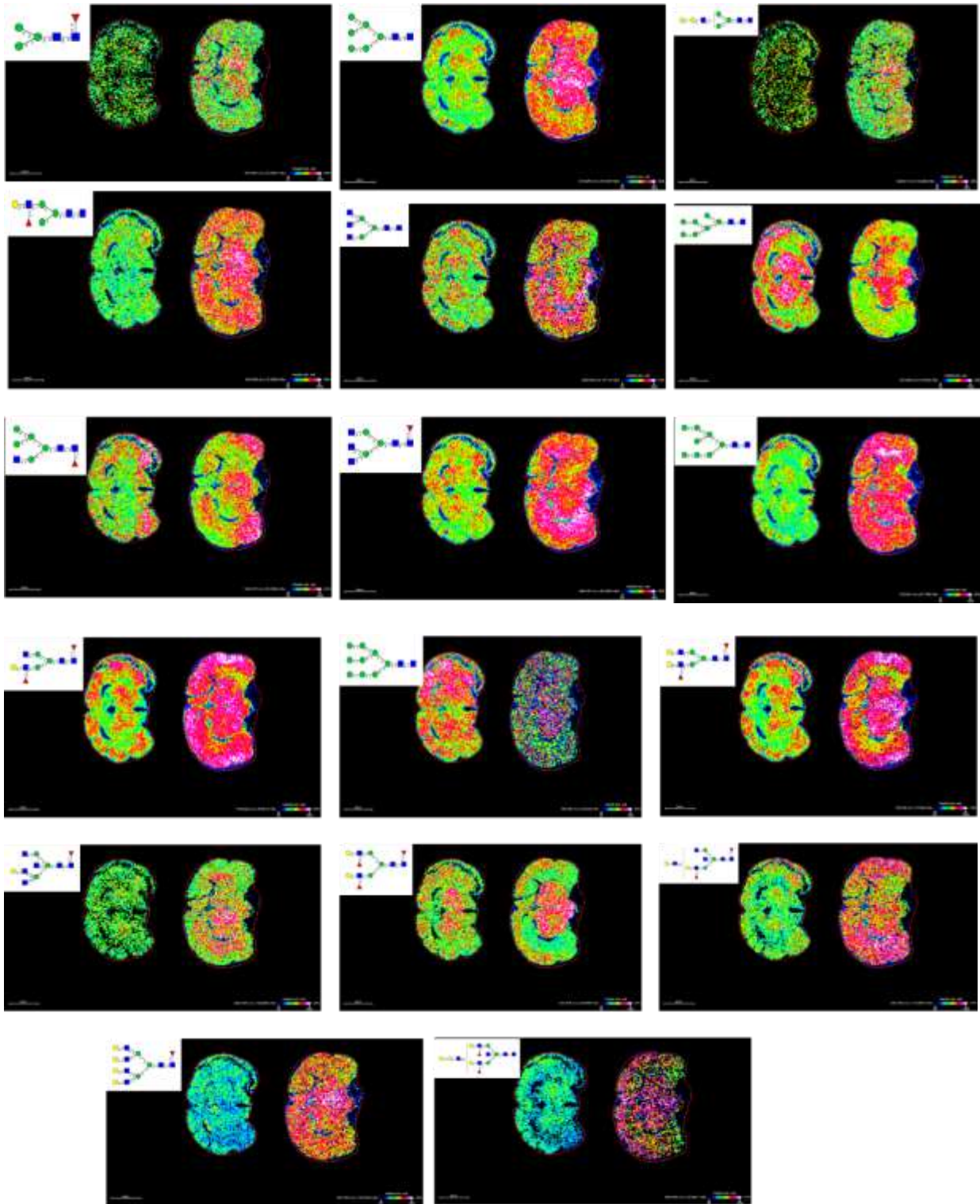


Figure 5.9: MALDI-MSI resolution of N-glycan modulation in SN in the healthy vs diseased brains. An FFPE block of rat brain tissue sectioned coronally at 5 μm and sections with SN were subjected to MALDI-MSI. MALDI-MSI was able to distinguish 17 glycans that were differentially expressed based off of specific ions after MALDI-MSI detected in healthy and diseased tissues. Image spectra were acquired at 150 μm raster. The panel shows representative individual glycan images for the brain FFPE tissue slice alongside the putative structures determined by combinations of accurate m/z , CID fragmentation patterns and glycan database structures. (Left: Healthy, Right: 6-OHDA lesioned)

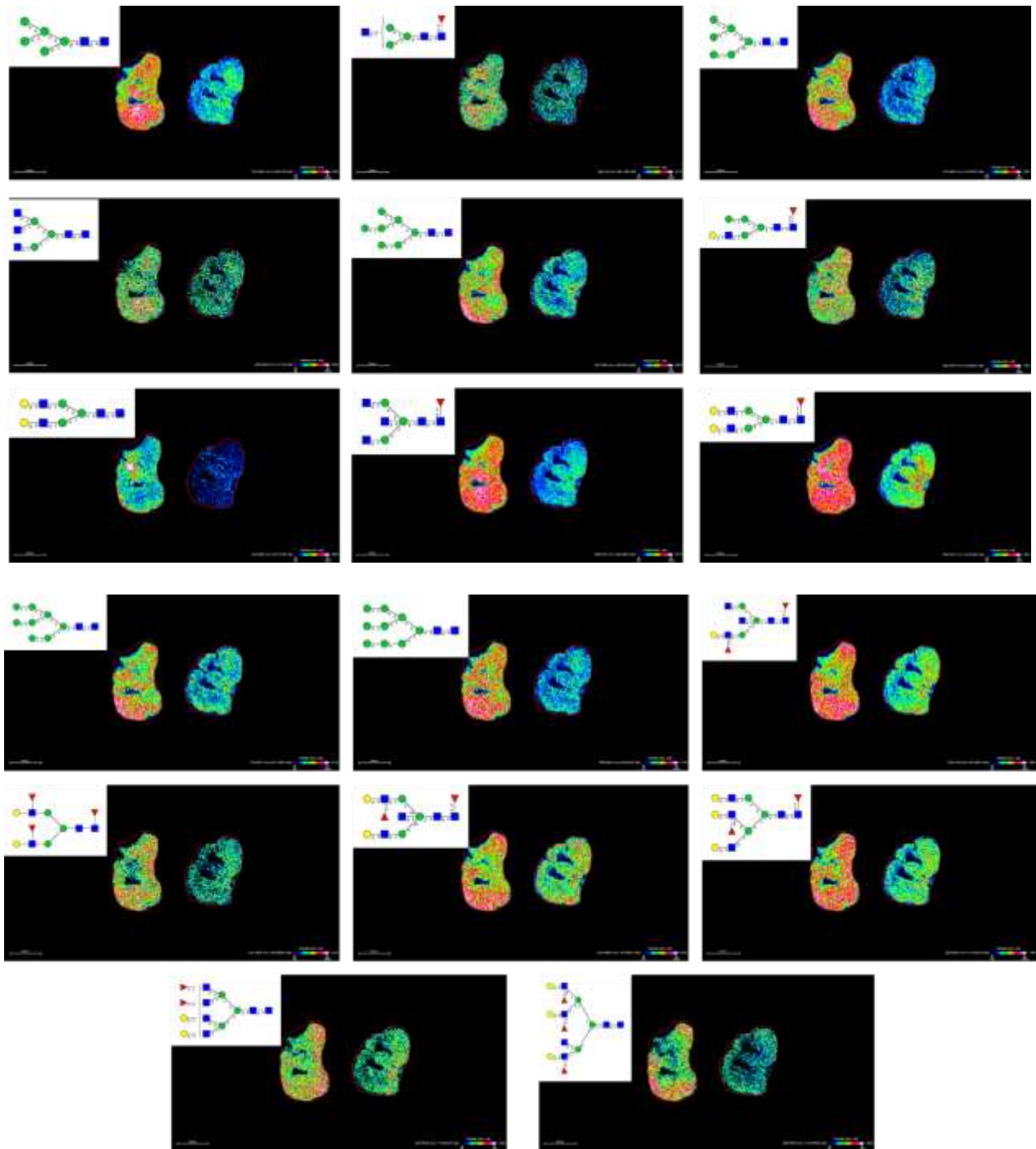


Figure 5.10: MALDI-MSI resolution of N-glycan modulation in striatum in the healthy vs diseased brains. An FFPE block of rat brain tissue sectioned coronally at 5 μm and sections with striatum were subjected to MALDI-MSI. MALDI-MSI was able to distinguish 17 glycans that were differentially expressed based off of specific ions after MALDI-MSI detected in healthy and diseased tissues. Image spectra were acquired at 150 μm raster. The panel shows representative individual glycan images for the brain FFPE tissue slice alongside the putative structures determined by combinations of accurate m/z , CID fragmentation patterns and glycan database structures. (Left: 6-OHDA lesioned, Right: Healthy).

5.4 Discussion

This was the first study to investigate the overall N-glycome for striatum and SN in a rodent model of PD over the time course of disease induction. It was hypothesized that there would be a distinct modulation of the overall N-glycosylation in both regions of the brain that could be involved in the disease pathophysiology and motor dysfunctions. Indeed, this study demonstrated that in the 6-OHDA rat model, the glycosylation profile compared with the controls shows significant differences. A detailed glyco-analytical platform combining HILIC-UPLC, LC-MS/MS and exoglycosidase digestions to map the N-glycosylation in the striatum and SN in a healthy rodent brain was developed. This was followed by the current study where an *in vivo* analysis was performed to track the changes in the N-glycome of these two regions of the brain during the disease progression. Derived from the classification model, the animals with PD had an increased relative abundance of GP1, GP11, GP17, GP18 and GP21 and a reduced relative abundance of GP7 in striatum. There was an increased abundance of GP2, GP7, GP8, GP15, GP18 and GP24 in SN in the animals with PD.

Aberrant protein glycosylation has been implicated in several diseases including neurodegenerative disorders like Parkinson's disease. In the current study, the temporal modulation of different traits of N-glycosylation in a rodent model of PD was elucidated. As a common observation, a decrease in overall sialylation for both the striatum and SN in the PD brains when compared to that of the healthy controls was detected. Similar trends were observed in human sera by Varadi et al. (2019) [35] where the authors reported a decreased sialylation on tri- and tetra- antennary glycans mainly detected in the samples from the male patients (age average 66.8 years).

Microglia are the immune cells that play a key role in the development of pro-inflammatory or anti-inflammatory phenotypes in response to the cues they are presented with in the CNS. Sialic-acid-binding immunoglobulin superfamily (Siglec) and their ligands play a crucial role in the regulation of microglia activation[41]. Sialic acids are the most frequent terminal glycan residues for extracellular proteins that function as docking sites for Siglecs masking the immune recognition sites and promoting complement inhibition [42]. Therefore, alterations in the sialome plays an important part in the development of immune responses [41,42] and potentiate the exacerbated immune response. This justifies the decrease in sialylation that was observed in the current study and correlates well to its biological involvement in promoting the inflammatory phenotype characteristic of Parkinson's.

Another significant implication of the altered sialylation can be correlated to the specific protein glycosylation. Prior glycoproteomic analysis has shown that amongst the various glycoproteins found to be differentially regulated in the PD patient brains, sodium channel $\beta 4$ subunit could be involved in PD and other neurodegenerative disorders [21,22]. Disruption of parkin and an increased $\beta 4$ expression mediates the excitatory response that may contribute to the pathophysiology of PD. Voltage-gated sodium channels are complex glycoproteins comprising a large, pore-forming α subunit and often one to several regulating β subunits responsible for initiation and propagation of nerve action potentials which is crucial for neuronal excitability. Fully sialylated $\beta 1$ subunit was found to impact the kinetic gating of the two neuronal α subunit isoforms [43]. However, the loss of this glycosylation was observed to be correlated with the loss of all effects of $\beta 1$ subunit on channel gating, thereby impacting neuronal excitability [43]. The extent and type of glycosylation of $\beta 4$ during different developmental stages and in the course of disease progression may be important for their ability to modulate channel activities. The glycosylation of the different β subunits by different mechanisms regulates its activity [43], so differential glycosylation of auxiliary subunits could be postulated to interfere with neuronal function at multiple levels [44].

Several studies have suggested the involvement of the immune mechanisms of the host in the degeneration of dopaminergic neurons [45,46]. It has been shown previously that the serum IgG of the PD patients can induce selective degeneration of dopaminergic neurons through the microglial activation via the Fc γ receptors both *in vitro* and *in vivo* [47]. However, IgG is a densely glycosylated protein and a detectable change was seen in the glycosylation state of IgG in the serum of PD patients [35]. These changes are postulated to be salient in mediating the inflammatory activity by ligating to the Fc γ receptors on the natural killer cells as well as on the microglia. An overall reduction in sialylation of the IgG has been shown to enhance the microglia-mediated toxicity to dopaminergic neurons, which explains the impact of the modulation of N-glycosylation of glycoproteins on the disease pathophysiology in PD.

Fucose is one of the most prominent deoxyhexoses expressed at the cell surface. Fucosylated N-glycans are widely distributed in mammalian tissues, with a specific enrichment in brain tissue [48]. Previous studies have shown that the majority of N-glycans present in mouse brain tissue are $\alpha 1,6$ - fucosylated [49]. Fucosylated glycan structures play various roles in mammals from cell adhesion, inflammation, host response mediation to regulating angiogenesis and tumor metastases [50]. Several studies have indicated the involvement of altered fucosylation in disease pathogenesis. A seminal study by Fukuda et al. has shown the translation of $\alpha 1,6$ -

fucosyltransferase deficiency into the manifestation of schizophrenia-like phenotype and significant behavioural impairment [36]. In the early stages of organ development, compartmentalisation outside the nervous system is determined by O-fucose- β 1,3-N-acetylglucosaminyl-transferase-dependent signal transduction between cell surface Notch receptors and their ligands [51].

Another pathway implicated in translating the aberrant fucosylation into neurodegeneration was explained by Kollmann et al. [37] while investigating neurodegeneration in mucopolipidosis. The study reported that the loss of Man 6-P impacted the processing of several lysosomal proteins which led to the accumulation of fucosylated N-glycans. This was well correlated with enhanced astrogliosis, accumulation of storage materials in axons and the formation of neuronal aggregates followed by the loss of Purkinje cells. These examples highlight the significance of N-glycans in mediating intercellular interactions in CNS. This is the first study, to date, investigating the modulation of fucosylation in the striatum and SN of a Parkinson's model.

These results were further augmented by MALDI imaging analysis and were in agreement with the HILIC-UPLC analysis. However, there were certain other traits that were revealed as a part of the MALDI imaging analysis that were not detected using the HILIC-UPLC analysis because for feature analysis, only the major glycan constituents of each peak were considered to be representative features for that peak. This results in a partial loss in the detection of certain traits of glycosylation as these were not representative for different peaks of the UPLC chromatogram. This limitation in the current analyses was circumvented by the use of MALDI-MSI wherein a panel of more than 50 glycans that were expressed in the striatum and SN and investigated their modulation in Parkinsonism was detected.

The analysis of brain sections from the striatum and SN of diseased and healthy animals using MALDI-MSI resulted in the detection and analysis of 48 and 52 N-glycans respectively. The largest identified N-linked glycan for both the striatum and SN was a highly branched structure with $[M + Na]^+$ theoretical mass of 3124.133 Da. Amongst these, a differential modulation was observed in the diseased and healthy animals for 17 glycans in the striatum and SN. Some of these trends in the modulation of glycosylation characteristic of the disease phenotype were not elucidated in the HILIC-UPLC studies since the mode of analysis took into account only the major glycan species per chromatographic peak. There was a noticeable modulation in the oligomannose glycans both in the striatum and SN. However, in the striatum, a modulation was

observed for all the oligomannose groups whereas no distinct modulation of Man5 was observed in the SN. This study provides further evidence that N-glycans can be directly released and identified *in situ* from the tissue glycoproteins immobilized on slides.

Another significant trait of N-glycosylation that was upregulated was that of LewisX in both the striatum and SN of the diseased brains. LewisX is the predominant fucosylated antigen synthesized primarily by fucosyl transferase-9 (FUT9) in the brain and it is known to mediate the intercellular communication involved in neuronal development [52]. It is also used as a surface marker for neuronal stem cells [53]. The complete lack of LewisX expression in the mouse brain that is devoid of the *Fut9* gene gives rise to an enhanced anxiety-like behaviour compared to the wild type mice [54]. It has also been shown in previous studies that LewisX colocalizes with the GFAP-positive cells with a fibroblast-like morphology typical of the Type-1 astrocytes and plays a crucial role in mediating the neuroglial interactions [55]. An enhanced expression of the LewisX antigens could therefore be attributed to the increased migration of the inflammatory cells that is reflective of the neuro-inflammatory phenotype in PD.

Lectins are proteins, mostly of plant origin, which recognize specific glycan structures. This makes them valuable tools in studying glycan structures and as mediators of the modulation of glycosylation [56,57]. The specificity of glycan-lectin interactions is usually less than that for protein-protein interactions. However, the lectin-glycan interactions have a higher avidity as most lectins can bind multiple glycan moieties with considerable specificity. Therefore, a panel of lectins was used in this study to elucidate the brain glycophenotype of the 6-OHDA-induced rat PD model. There was an enhanced binding of Con A in the PD brains which was consistent with the HILIC-UPLC and MALDI-MSI analysis that reveals a significant increase in oligomannose glycans in the disease phenotype. Increased migration and activation of the microglial cells due to the 6-OHDA lesioning was represented by the enhanced binding of WGA and GSA1 β ₄. In an MPTP induced PD model, an enhanced binding of GSA 1 β ₄ was detected in the striatum of the mice [39]. GSA 1 β ₄ showed an enhanced binding profile (two-fold) and represented the morphological changes indicative of the microglial activation. This was suggestive of microglial involvement in the pathological sequence leading to the loss of dopaminergic neurons.

Taken together, the findings of this study used the elaborate glyco-analytical platform discussed in Chapter-4 in combination with MALDI-MSI to decipher carefully the N-glycophenotype characteristic of 6-OHDA induced Parkinsonism in a rodent model.

5.5 Conclusions

An elaborate glyco-analytical platform was used in this study to investigate the modulation of the rodent brain *N*-glycosylation during PD progression. The developed platform was employed to annotate the *N*-glycans from the striatum and SN of healthy and diseased controls through a combination of HILIC-UPLC, exoglycosidase digestions and MALDI-MSI fragmentation. Altered levels of sialylation, fucosylation and mannosylation were found to be most significant in PD animals. Future studies will involve glyco-proteomic analysis to investigate and correlate the glycomic changes with the proteomic alterations to identify chief targets for biomaterial therapy.

5.6 References

- [1] R.K.T. Kam, T.C.W. Poon, The potentials of glycomics in biomarker discovery, *Clin. Proteomics*. 4 (2008) 67–79. doi:10.1007/s12014-008-9017-9.
- [2] S. Barbarić, V. Mrsa, B. Ries, P. Mildner, Role of the carbohydrate part of yeast acid phosphatase., *Arch. Biochem. Biophys.* 234 (1984) 567–75. doi:10.1016/0003-9861(84)90305-9.
- [3] Y. Tsuji, K. Yamamoto, T. Tochikura, Formation of deglycosylated alpha-L-fucosidase by endo-beta-N-acetylglucosaminidase in *Fusarium oxysporum*., *Appl. Environ. Microbiol.* 56 (1990) 928–33. doi:10.1074/jbc.M114.583286.
- [4] V. Belalcazar, R. Gutiérrez Gallego, E. Llop, J. Segura, J.A. Pascual, Assessing the instability of the isoelectric focusing patterns of erythropoietin in urine, *Electrophoresis*. 27 (2006) 4387–4395. doi:10.1002/elps.200500891.
- [5] F.K. Chu, F. Maley, Stabilization of the structure and activity of yeast carboxypeptidase Y by its high-mannose oligosaccharide chains., *Arch. Biochem. Biophys.* 214 (1982) 134–9. doi:10.1016/0003-9861(82)90015-7.
- [6] K. Sarter, C. Mierke, A. Beer, B. Frey, B.G. Führrohr, C. Schulze, S. Franz, Sweet clearance: Involvement of cell surface glycans in the recognition of apoptotic cells, *Autoimmunity*. 40 (2007) 345–348. doi:10.1080/08916930701356804.
- [7] J. Gu, T. Isaji, Q. Xu, Y. Kariya, W. Gu, T. Fukuda, Y. Du, Potential roles of *N*-glycosylation in cell adhesion, *Glycoconj. J.* 29 (2012) 599–607. doi:10.1007/s10719-012-9386-1.
- [8] D. Shental-Bechor, Y. Levy, Folding of glycoproteins: toward understanding the biophysics of the glycosylation code, *Curr. Opin. Struct. Biol.* 19 (2009) 524–533.

- doi:10.1016/j.sbi.2009.07.002.
- [9] M.N. Fukuda, H. Sasaki, L. Lopez, M. Fukuda, Survival of recombinant erythropoietin in the circulation: the role of carbohydrates., *Blood*. 73 (1989) 84–9. <http://www.ncbi.nlm.nih.gov/pubmed/2910371> (accessed June 12, 2019).
- [10] J. Jaeken, H. Carchon, Congenital disorders of glycosylation: a booming chapter of pediatrics., *Curr. Opin. Pediatr.* 16 (2004) 434–9. doi:10.1097/01.mop.0000133636.56790.4a.
- [11] M.M. Fuster, J.D. Esko, The sweet and sour of cancer: glycans as novel therapeutic targets, *Nat. Rev. Cancer*. 5 (2005) 526–542. doi:10.1038/nrc1649.
- [12] B. Thomas, M.F. Beal, Parkinson’s disease, *Hum. Mol. Genet.* 16 (2007) R183–R194. doi:10.1093/hmg/ddm159.
- [13] M.R. Cookson, THE biochemistry of Parkinson’s Disease, *Annu. Rev. Biochem.* 74 (2005) 29–52. doi:10.1146/annurev.biochem.74.082803.133400.
- [14] P. Davidsson, A. Westman-Brinkmalm, C.L. Nilsson, M. Lindbjer, L. Paulson, N. Andreasen, M. Sjögren, K. Blennow, Proteome analysis of cerebrospinal fluid proteins in Alzheimer patients., *Neuroreport*. 13 (2002) 611–615. <http://www.ncbi.nlm.nih.gov/pubmed/11973456> (accessed June 13, 2019).
- [15] Z. Zhang, Y. Takeda-Uchimura, T. Foyez, S. Ohtake-Niimi, H. Akatsu, K. Nishitsuji, M. Michikawa, T. Wyss-Coray, K. Kadomatsu, K. Uchimura, Deficiency of a sulfotransferase for sialic acid-modified glycans mitigates Alzheimer’s pathology, *Proc Natl Acad Sci U S A*. 114 (2017) E2947–E2954. doi:10.1073/pnas.1615036114.
- [16] P. Regan, P.L. McClean, T. Smyth, M. Doherty, Early stage glycosylation biomarkers in Alzheimer’s Disease, *Medicines*. 6 (2019) 92. doi:10.3390/medicines6030092.
- [17] J.M. Hatcher, K.D. Pennell, G.W. Miller, Parkinson’s disease and pesticides: a toxicological perspective, *Trends Pharmacol. Sci.* 29 (2008) 322–329. doi:10.1016/J.TIPS.2008.03.007.
- [18] H. Hwang, J. Zhang, K.A. Chung, J.B. Leverenz, C.P. Zabetian, E.R. Peskind, J. Jankovic, Z. Su, A.M. Hancock, C. Pan, T.J. Montine, S. Pan, J. Nutt, R. Albin, M. Gearing, R.P. Beyer, M. Shi, J. Zhang, Glycoproteomics in neurodegenerative diseases, 29 (2010) 79–125. doi:10.1002/mas.20221.
- [19] L.B. Moran, L. Hickey, G.J. Michael, M. Derkacs, L.M. Christian, M.E. Kalaitzakis, R.K.B. Pearce, M.B. Graeber, Neuronal pentraxin II is highly upregulated in Parkinson’s disease and a novel component of Lewy bodies, *Acta Neuropathol.* 115 (2008) 471–478. doi:10.1007/s00401-007-0309-3.

- [20] W.J. Brackenbury, T.H. Davis, C. Chen, E.A. Slat, M.J. Detrow, T.L. Dickendesher, B. Ranscht, L.L. Isom, Voltage-gated Na⁺ channel 1 subunit-mediated neurite outgrowth requires Fyn Kinase and contributes to postnatal CNS development in vivo, *J. Neurosci.* 28 (2008) 3246–3256. doi:10.1523/JNEUROSCI.5446-07.2008.
- [21] H. Miyazaki, F. Oyama, H.-K. Wong, K. Kaneko, T. Sakurai, A. Tamaoka, N. Nukina, BACE1 modulates filopodia-like protrusions induced by sodium channel β 4 subunit, *Biochem. Biophys. Res. Commun.* 361 (2007) 43–48. doi:10.1016/j.bbrc.2007.06.170.
- [22] T. Zhou, Z. Zhang, J. Liu, J. Zhang, B. Jiao, Glycosylation of the sodium channel β 4 subunit is developmentally regulated and involves in neuritic degeneration, *Int. J. Biol. Sci.* 8 (2012) 630–639. doi:10.7150/ijbs.3684.
- [23] A. Russell, A. Drozdova, W. Wang, M. Thomas, The impact of dementia development concurrent with Parkinson's disease: a new perspective., *CNS Neurol. Disord. Drug Targets.* 13 (2014) 1160–1168. doi:10.2174/1871527313666140917122739.
- [24] A.C. Russell, M. Šimurina, M.T. Garcia, M. Novokmet, Y. Wang, I. Rudan, H. Campbell, G. Lauc, M.G. Thomas, W. Wang, The N-glycosylation of immunoglobulin G as a novel biomarker of Parkinson's disease, *Glycobiology.* 27 (2017) 501–510. doi:10.1093/glycob/cwx022.
- [25] T.W. Powers, B.A. Neely, Y. Shao, H. Tang, D.A. Troyer, A.S. Mehta, B.B. Haab, R.R. Drake, MALDI imaging mass spectrometry profiling of N-glycans in formalin-fixed paraffin embedded clinical tissue blocks and tissue microarrays, *PLoS One.* 9 (2014) e106255. doi:10.1371/journal.pone.0106255.
- [26] T.W. Powers, E.E. Jones, L.R. Betesh, P.R. Romano, P. Gao, J.A. Copland, A.S. Mehta, R.R. Drake, Matrix assisted laser desorption ionization imaging mass spectrometry workflow for spatial profiling analysis of N-linked glycan expression in tissues, *Anal. Chem.* 85 (2013) 9799–9806. doi:10.1021/ac402108x.
- [27] D.S. Cornett, M.L. Reyzer, P. Chaurand, R.M. Caprioli, MALDI imaging mass spectrometry: molecular snapshots of biochemical systems, *Nat. Methods.* 4 (2007) 828–833. doi:10.1038/nmeth1094.
- [28] O.J.R. Gustafsson, M.T. Briggs, M.R. Condina, L.J. Winderbaum, M. Pelzing, S.R. McColl, A. V. Everest-Dass, N.H. Packer, P. Hoffmann, MALDI imaging mass spectrometry of N-linked glycans on formalin-fixed paraffin-embedded murine kidney, *Anal. Bioanal. Chem.* 407 (2015) 2127–2139. doi:10.1007/s00216-014-8293-7.
- [29] H. Stöckmann, R. O'flaherty, B. Adamczyk, R. Saldova, P.M. Rudd, Automated, high-throughput serum glycoprofiling platform, *Integ.Biol.* 7 (2015) 1026–1032.

- doi:10.1039/x0xx00000x.
- [30] U. Ungerstedt, G.W. Arbuthnott, Quantitative recording of rotational behavior in rats after 6-hydroxy-dopamine lesions of the nigrostriatal dopamine system., *Brain Res.* 24 (1970) 485–493. doi:10.1016/0006-8993(70)90187-3.
- [31] L. Royle, C.M. Radcliffe, R.A. Dwek, P.M. Rudd, Detailed structural analysis of N-glycans released from glycoproteins in SDS-PAGE gel bands using HPLC combined with exoglycosidase array digestions, in: *Glycobiol. Protoc.*, Humana Press, New Jersey, 2006: pp. 125–144. doi:10.1385/1-59745-167-3:125.
- [32] L. Royle, M.P. Campbell, C.M. Radcliffe, D.M. White, D.J. Harvey, J.L. Abrahams, Y.-G. Kim, G.W. Henry, N.A. Shadick, M.E. Weinblatt, D.M. Lee, P.M. Rudd, R.A. Dwek, HPLC-based analysis of serum N-glycans on a 96-well plate platform with dedicated database software, *Anal. Biochem.* 376 (2008) 1–12. doi:10.1016/j.ab.2007.12.012.
- [33] B. Küster, S.F. Wheeler, A.P. Hunter, R.A. Dwek, D.J. Harvey, Sequencing of N-linked oligosaccharides directly from protein gels: in-gel deglycosylation followed by Matrix-Assisted Laser Desorption/Ionization Mass Spectrometry and normal-phase High-Performance Liquid Chromatography, *Anal. Biochem.* 250 (1997) 82–101. doi:10.1006/abio.1997.2199.
- [34] J.C. Bigge, T.P. Patel, J.A. Bruce, P.N. Goulding, S.M. Charles, R.B. Parekh, Nonselective and efficient fluorescent labeling of glycans using 2-amino benzamide and anthranilic acid, *Anal. Biochem.* 230 (1995) 229–238. doi:10.1006/abio.1995.1468.
- [35] C. Váradi, K. Nehéz, O. Hornyák, B. Viskolcz, J. Bones, C. Váradi, K. Nehéz, O. Hornyák, B. Viskolcz, J. Bones, Serum N-glycosylation in Parkinson’s Disease: A novel approach for potential alterations, *Molecules.* 24 (2019) 2220. doi:10.3390/molecules24122220.
- [36] T. Fukuda, H. Hashimoto, N. Okayasu, A. Kameyama, H. Onogi, O. Nakagawasai, T. Nakazawa, T. Kurosawa, Y. Hao, T. Isaji, T. Tadano, H. Narimatsu, N. Taniguchi, J. Gu, α 1,6-Fucosyltransferase-deficient mice exhibit multiple behavioral abnormalities associated with a schizophrenia-like phenotype, *J. Biol. Chem.* 286 (2011) 18434–18443. doi:10.1074/jbc.M110.172536.
- [37] K. Kollmann, M. Damme, S. Markmann, W. Morelle, M. Schweizer, I. Hermans-Borgmeyer, A.K. Röchert, S. Pohl, T. Lübke, J.-C. Michalski, R. Käkelä, S.U. Walkley, T. Braulke, Lysosomal dysfunction causes neurodegeneration in mucopolipidosis II ‘knock-in’ mice, *Brain.* 135 (2012) 2661–2675. doi:10.1093/brain/aws209.
- [38] L.J. Lawson, V.H. Perry, P. Dri, S. Gordon, Heterogeneity in the distribution and

- morphology of microglia in the normal adult mouse brain., *Neuroscience*. 39 (1990) 151–170. doi:10.1016/0306-4522(90)90229-w.
- [39] A. Członkowska, M. Kohutnicka, I. Kurkowska-Jastrzebska, A. Członkowski, Microglial reaction in MPTP (1-methyl-4-phenyl-1,2,3,6-tetrahydropyridine) induced Parkinson's disease mice model., *Neurodegeneration*. 5 (1996) 137–143. doi:10.1006/neur.1996.0020.
- [40] S.F. Wheeler, P. Domann, D.J. Harvey, Derivatization of sialic acids for stabilization in matrix-assisted laser desorption/ionization mass spectrometry and concomitant differentiation of α (2 \rightarrow 3)- and α (2 \rightarrow 6)-isomers, *Rapid Commun. Mass Spectrom.* 23 (2009) 303–312. doi:10.1002/rcm.3867.
- [41] B. Linnartz, L.-G. Bodea, H. Neumann, Microglial carbohydrate-binding receptors for neural repair, *Cell Tissue Res*. 349 (2012) 215–227. doi:10.1007/s00441-012-1342-7.
- [42] H.J. Crespo, J.T.Y. Lau, P.A. Videira, Dendritic cells: a spot on sialic acid, *Front. Immunol.* 4 (2013). doi:10.3389/fimmu.2013.00491.
- [43] D. Johnson, M.L. Montpetit, P.J. Stocker, E.S. Bennett, The sialic acid component of the beta1 subunit modulates voltage-gated sodium channel function., *J. Biol. Chem.* 279 (2004) 44303–10. doi:10.1074/jbc.M408900200.
- [44] T.H. Davis, C. Chen, L.L. Isom, Sodium channel β 1 subunits promote neurite outgrowth in cerebellar granule neurons, *J. Biol. Chem.* 279 (2004) 51424–51432. doi:10.1074/jbc.M410830200.
- [45] X.-J. Wang, Z.-Q. Yan, G.-Q. Lu, S. Stuart, S.-D. Chen, Parkinson disease IgG and C5a-induced synergistic dopaminergic neurotoxicity: Role of microglia, *Neurochem. Int.* 50 (2007) 39–50. doi:10.1016/J.NEUINT.2006.07.014.
- [46] S.H. Appel, W.-D. Le, J. Tajti, L.J. Haverkamp, J.I. Engelhardt, Nigral damage and dopaminergic hypofunction in mesencephalon-immunized guinea pigs, *Ann. Neurol.* 32 (1992) 494–501. doi:10.1002/ana.410320403.
- [47] Y. He, W.-D. Le, S.H. Appel, Role of Fc γ receptors in nigral cell injury induced by Parkinson Disease immunoglobulin injection into mouse substantia nigra, *Exp. Neurol.* 176 (2002) 322–327. doi:10.1006/EXNR.2002.7946.
- [48] N. Uozumi, S. Yanagidani, E. Miyoshi, Y. Ihara, T. Sakuma, C.-X. Gao, T. Teshima, S. Fujii, T. Shiba, N. Taniguchi, Purification and cDNA cloning of porcine brain GDP-L-Fuc: N -Acetyl- β -D-Glucosaminide α 1 \rightarrow 6Fucosyltransferase, *J. Biol. Chem.* 271 (1996) 27810–27817. doi:10.1074/jbc.271.44.27810.
- [49] S. i. Nakakita, S. Natsuka, K. Ikenaka, S. Hase, Development-dependent expression of

- complex-type sugar chains specific to mouse brain, *J. Biochem.* 123 (1998) 1164–1168. doi:10.1093/oxfordjournals.jbchem.a022056.
- [50] D.J. Becker, J.B. Lowe, Fucose: biosynthesis and biological function in mammals, *Glycobiology.* 13 (2003) 41R–53R. doi:10.1093/glycob/cwg054.
- [51] T. Okajima, A. Xu, L. Lei, K.D. Irvine, Chaperone activity of protein O-fucosyltransferase 1 promotes notch receptor folding., *Science.* 307 (2005) 1599–603. doi:10.1126/science.1108995.
- [52] S. Nishihara, H. Iwasaki, K. Nakajima, A. Togayachi, Y. Ikehara, T. Kudo, Y. Kushi, A. Furuya, K. Shitara, H. Narimatsu, alpha1,3-Fucosyltransferase IX (Fut9) determines Lewis X expression in brain, *Glycobiology.* 13 (2003) 445–455. doi:10.1093/glycob/cwg048.
- [53] J. Pruszek, W. Ludwig, A. Blak, K. Alavian, O. Isacson, CD15, CD24 and CD29 define a surface biomarker code for neural lineage differentiation of stem cells, *Stem Cells.* 27 (2009) 2928–2940. doi:10.1002/stem.211.
- [54] T. Kudo, T. Fujii, S. Ikegami, K. Inokuchi, Y. Takayama, Y. Ikehara, S. Nishihara, A. Togayachi, S. Takahashi, K. Tachibana, S. Yuasa, H. Narimatsu, Mice lacking α 1,3-fucosyltransferase IX demonstrate disappearance of Lewis x structure in brain and increased anxiety-like behaviors, *Glycobiology.* 17 (2007) 1–9. doi:10.1093/glycob/cwl047.
- [55] E.M. Sajdel-Sulkowska, Immunofluorescent detection of CD15-fucosylated glycoconjugates in primary cerebellar cultures and their function in glial-neuronal adhesion in the central nervous system., *Acta Biochim. Pol.* 45 (1998) 781–790. <http://www.ncbi.nlm.nih.gov/pubmed/9918505> (accessed July 29, 2019).
- [56] P. Contessotto, B.W. Ellis, C. Jin, N.G. Karlsson, P. Zorlutuna, M. Kilcoyne, A. Pandit, Distinct glycosylation in membrane proteins within neonatal versus adult myocardial tissue, *Matrix Biol.* (2019). doi:10.1016/J.MATBIO.2019.05.001.
- [57] N. Sharon, H. Lis, History of lectins: from hemagglutinins to biological recognition molecules, *Glycobiology.* 14 (2004) 53R–62R. doi:10.1093/glycob/cwh122.

Chapter 6

Fibrin-in-fibrin intervention for enhanced graft survival and glyco-modulation in 6-OHDA Parkinson's model

Sections of this chapter are in preparation for publication:

Samal J., Abbah S.A., Lucia A.R., Black A., Drake R., Pandit A. "Fibrin-in-fibrin intervention for enhanced graft survival in Parkinson's disease: Special focus on brain N-glycans".

6.1 Introduction

Parkinson's disease (PD) is the second most prevalent chronic neurodegenerative disorder characterized by the impairment in motor functions manifested as tremors, rigidity and akinesia. The selective degeneration of dopaminergic neurons in substantia nigra *pars compacta* mediates the underlying PD pathology due to aberrant dopamine (DA) signalling. Several studies aimed at addressing the off-base DA transmission by direct injections of L-Dopa in the animal models and patients but long-term administration in patients was found to cause side effects like dyskinesia, inflammation and toxicity [1]. This makes PD an ideal candidate for cell replacement therapies to compensate for the loss of dopaminergic neurons and reinstate the striatal DA transmission [2,3]. The chief focus of the cell therapies in Parkinson's disease is to restore normal motor function by striatal re-innervation following the engraftment of the dopaminergic precursors. There has been a progressive shift in the field of cellular therapies in PD towards more readily available dopaminergic cell sources, such as embryonic stem cells and induced pluripotent stem cells [4]. However, their translation to the clinical settings has still not been realised fully and their use is still in the experimental settings. Therefore in this study, the dopaminergic neuron-enriched foetal ventral mesencephalic (VM) grafts are used as a cell source to test the potential of biomaterial therapy in improving the survival and efficacy of cellular therapies.

VM grafts are a mixed cell population, about 10% of which is constituted by dopaminergic neurons. Several studies have confirmed the survival rate of the grafted dopaminergic neurons to be in the range of 1-20% [5–7] after the initial proposed rate of around 10% survival [8]. VM tissue from about 4-8 embryos are required per grafted hemisphere to observe a significant clinical improvement in PD patients, which represents a limiting step for clinical translation [4]. The ethical concerns stemming from the use of embryonic tissue mandates the search for strategies to increase the survival of grafted dopaminergic neurons, which in turn would substantially reduce the amount of embryonic tissue needed per patient. There are four different phases that have been identified to significantly contribute to the death of engrafted dopaminergic cells encompassing the extraction, transplantation and development of the grafts in the host brain. The chief modes of induction of cell death in all these phases is necrosis and apoptosis. Detachment of the embryos from the maternal blood supply subjects them to a hypoxic and hypoglycemic insult causing an oxidative damage [9]. This is followed by the axotomy and mechanical damage during tissue dissociation which result in a significant neuronal damage. The process of implantation and subjecting the cells to a new adult host

environment may constitute a period of further death and recruitment of host neuro-immune cells to the exogenous graft [10]. Other factors contributing to the reduced survival of the engrafted neurons include oxidative stress and the expression of pro-inflammatory cytokines as a result of the brain damage [11–13]. Another significant contributing factor to the progressive cell death post-implantation is the lack of the neurotrophic support for maturation of the developing neurons in the adult host environment [14].

Several different approaches have been adopted over the recent years to improve the graft survival by intervening at each of these checkpoints limiting the successful clinical translation of VM cell therapy in PD. Biomaterial therapy is particularly significant in improving the graft survival post-transplantation. Injectable, natural biopolymeric scaffolds, such as *in situ* forming hydrogels, provide a delivery platform to improve grafted cell survival after transplantation. These scaffolds can also act as local depots for neurotrophic factors to promote the survival and integration of the engrafted neurons in the host neuronal circuitry. Besides, these platforms could potentially enhance cell survival by providing a multi-faceted solution to several problems encountered during cellular transplantation. They provide a supportive matrix for cellular adhesion and protect the engrafted cells by creating a physical barrier for the host immune cells.

There has been a growing interest in the development of extracellular matrix (ECM)-based cell and therapeutic delivery systems which can modulate cellular signalling while delivering therapeutic molecules. Fibrin has been used as a surgical sealant for over two decades and also as an encapsulation platform for cells owing to its ability to support cell growth and direct their differentiation to different phenotypes [15,16]. The injectability and tuneability of the mechanical properties, particularly the stiffness, of the fibrin gel makes fibrin a promising candidate for cell and growth factor delivery in the brain. Besides, the degradability of the fibrin gels to allow for tissue regeneration also supports the use of fibrin as a biomaterial of choice in this study.

This study aims at the assessment of the fibrin-in-fibrin intervention for the controlled delivery of glial cell derived neurotrophic factor (GDNF) in fibrin hollow microspheres towards the transplantation of primary dopaminergic neurons to the Parkinsonian brain using a fibrin hydrogel. GDNF was opted as the model growth factor in this study as it is a very potent neurotrophic factor with growth- and survival-promoting capabilities for developing dopaminergic neurons [17,18]. We hypothesised that a tuneable fibrin-in-fibrin intervention

would act as a temporally-controlled local GDNF reservoir and immunoprotect the transplanted cells, thereby improving the overall survival and re-innervation of primary dopaminergic neurons after intra-striatal transplantation and lead to motor function recovery in a 6-OHDA PD model while modulating the brain glyco-signature. Specific objectives of this study were to fabricate and test the fibrin-in-fibrin system in a 6-OHDA rat model for the survival of dopaminergic cells, host immune response and functional recovery followed by the investigation of the impact of the aforementioned intervention on the N-glycosignature of the rodent brains through MALDI-MSI and lectin histochemistry.

6.2 Materials & Methods

The *in vivo* study was performed at the Centre for Research in Medical Devices (CÚRAM), National University of Ireland, Galway by Juhi Samal and Dr. Sunny-Abbah. The immunohistochemical analyses and lectin histochemical analysis was performed at CÚRAM, NUIG by Juhi Samal. MALDI-MSI analysis was performed by Juhi Samal under the supervision of Prof. Richard Drake at Medical University of South Carolina, USA.

6.2.1 Fabrication of fibrin hollow microspheres

Fibrin hollow microspheres were fabricated via the LbL approach using CaCO₃ microbeads as a sacrificial template and polyarginine (PAR) (Sigma-Aldrich, Dublin) and dextran sulfate (DS) (Sigma-Aldrich, Dublin) as polyelectrolytes. For the fabrication of the sacrificial microbead templates, 0.66 mL of a 1 M Na₂CO₃ solution was mixed with an equal volume of 1 M CaCl₂ solution. After vigorous stirring of these solutions together for 30 s, the obtained dispersion was centrifuged to collect the microbeads followed by washing them three times with a 0.005 M NaCl (wash buffer). This was followed by coating the particles with a 2 mg/mL PA solution of pH 6.5 while stirring. After 15 minutes of incubation, the particles were centrifuged and washed three times with the wash buffer. Then, particles were stirred in a 2 mg/mL DS solution at pH 6.5 for 15 minutes. This process was repeated until two layers of DS and two layers of PA were alternately deposited rendering PA as the pre-final layer to electrostatically support the final layer of fibrinogen. Finally, the particles were suspended in a 3 mg/mL fibrinogen solution at pH 6.5 and incubated for 30 minutes. This was followed by three washes and suspension of the coated particles in 0.1 M EDTA solution for template dissolution. The particles were collected by centrifugation after incubation with EDTA solution for five minutes. This was repeated three times to ensure complete template removal. This was followed by cross-linking the fibrinogen layer on the hollow microspheres with thrombin by

incubating them in the cross-linking solution (40 U/ml in TBS and 50 mM CaCl₂) for 10 minutes at 37°C. The resulting fibrin hollow microspheres were washed three times with PBS before the morphological and physiochemical characterization.

6.2.2 Loading of hollow fibrin microspheres with GDNF

Microspheres were loaded with GDNF by re-suspending 1 mg of hollow fibrin spheres in 300 µl of PBS–0.05% Tween solutions (loading buffer) containing 10 µg of GDNF. The hollow fibrin spheres were then incubated on a shaker at room temperature for 24 h to allow the growth factor to diffuse into the hollow spheres. Samples were then spun down for 20 minutes at 14000 rpm to collect the loaded hollow spheres and supernatant was analysed using GDNF-ELISA (R&D Systems, Abingdon, U.K.).

6.2.3 Fabrication of the fibrin-in fibrin intervention

The fibrin-in-fibrin (FNF) platform was designed by reconstituting human fibrinogen (20 mg/ml) in TBS (1X) with a defined concentration of GDNF-loaded microspheres and VM cells. The FNF gels were then fabricated by cross-linking the fibrinogen component by an equal volume of thrombin crosslinking solution (40 U/ml of human thrombin in TBS with 50 mM CaCl₂). The gels were then allowed to incubate at 37°C for ten minutes to stabilize the cross-linking. The volume of the gels (6 µl) designed were kept consistent with that used in the preclinical model of PD to improve the *in vivo* translation of the *in vitro* optimized parameters. To fabricate and collect the gels efficiently, they were micro-dispensed on a hydrophobic (commercial Teflon[®] tape) and incubated there for stable cross-linking. The gels were then collected by scraping off the hydrophobic surface using a sterile spatula. The microgels were then resuspended in the cell culture media to incubate them with the VM cells for further experiments.

6.2.4 Isolation of VM cells

For E14 VM cultures, E14 embryos were obtained by laparotomy from time-mated female Sprague-Dawley rats following quick decapitation under isoflurane (5% in 0.5 L O₂). The VM was micro-dissected from each embryo as previously described [478]. Dissected VM tissue was centrifuged at 1100 rpm for five mins at 4 °C. The tissue pellet was incubated in 40% trypsin-Hank's balanced salt solution (HBSS) for 4 min, at 37 °C with 5% CO₂. Foetal calf serum (FCS) was then added to the tissue and centrifuged at 1100 rpm for 5 min at 4 °C. The cell pellet was then resuspended in 1 ml of plating media (Dulbecco's modified Eagle's

medium/F12, 0.6% D-glucose, 1% L-glutamine, 1% FCS and 2% B27), and dissociated first using a P1000 Gilson pipette, followed by a 25 gauge needle and syringe. Cell density was estimated using a haemocytometer. For the *in vivo* analyses, the cells were re-suspended at 5×10^5 cells/5 μ l.

6.2.5 *In vivo* study

All procedures were carried out in accordance with the Cruelty to Animals Act 1876 under an animal licence (B100/3827) by the Irish Department of Health and Children and the Irish Health Products Regulatory Authority. Procedures were carried out in accordance with European Union Directive 2010/63/EU and S.I. No. 543 of 2012, and were approved by the Animal Ethics Committee of the National University of Ireland, Galway. Male Sprague-Dawley rats (weighing 200–225 g on arrival) and time-mated female Sprague-Dawley rats were sourced from Charles River, UK. Animals were housed in groups of four per cage, on a 12:12 h light/dark cycle, at 19–23 °C, with relative humidity levels maintained between 40 and 70%. For the duration of the experiment, animals were allowed food and water *ad libitum*. Behavioural testing was carried out by an experimenter who was blind to the treatment of the animals. All the animals with successful lesion induction were divided into six treatment groups per time point (week 1 post-lesion and week 6 post-lesion, n=7).

6.2.6 6-OHDA lesion and transplant surgery

All surgeries were performed under isoflurane anaesthesia (5% in O₂ for induction and 2% in O₂ for maintenance) in a stereotaxic frame with the nose bar set at –4.5 (intra-MFB) or –2.3 (intra-striatal). The striatum was infused unilaterally at coordinates Anterior-Posterior (AP) = 0.0, Medial-Lateral (ML) \pm 3.7 (from bregma) and Dorsal-Ventral (DV) –5.0 below dura, while the MFB was infused unilaterally at coordinates AP –4.0, ML –1.3 (from bregma) and DV –7.0 below dura. Infusions were completed at a total volume of either three μ l (6-OHDA lesion) or six μ l (VM transplants and fibrin hydrogels) at a rate of 1 μ l/min with a further two mins allowed for diffusion.

6.2.7 Behavioural analysis

The Cylinder Test of forelimb use asymmetry was used as previously described [20]. Briefly, the rat was placed into a clear cylinder for 5 min and the number of times it touched the side walls with the impaired or unimpaired forelimb or both simultaneously was recorded. Each individual rearing episode was counted by a blinded researcher. The scores were

calculated by the following asymmetry ratio: $\text{Left-right}/(\text{right} + \text{left} + \text{both})$. Scores on the forelimb asymmetry ratio range from -1 to 1 . The positive ratio was reflective of the greater use of the unimpaired forelimb over the impaired forelimb. By contrast, the negative asymmetry ratio was suggestive of an enhanced use of the impaired forelimb in comparison to the unimpaired one. Therefore, a high positive ratio would be consistent with a unilateral lesion and the reduction in the positive scores would be anticipated for the therapeutic interventions. Dopaminergic asymmetry in lesioned and transplanted rats was assessed via rotational behaviour using the dopaminergic stimulant apomorphine. Rotation was expressed as net contralateral turns/min over 60 min post-injection, as previously described [21]. Briefly, 2 weeks after surgery, all animals were injected subcutaneously with apomorphine hydrochloride (0.5 mg/kg; Sigma-Aldrich) and individually placed in the test cylinder. Rats that rotated in excess of 60 turns/30 min were considered to be the PD unilateral models. The drug-induced rotation was re-examined at 2, 4 and 6 weeks after surgery.

6.2.8 Peroxidase-based immunohistochemistry

Animals were sacrificed by terminal anaesthesia (50 mg/kg pentobarbital intraperitoneal (i.p)) and transcardially perfused with 100 ml heparinised saline followed by 150 ml of 4% PFA. Brains were rapidly removed and placed in 4% PFA overnight before being paraffin embedded. Serial coronal sections (5 μm) were cut using a microtome and immunohistochemical analysis for TH, GDNF, fibrin, microglial activation (Iba-1) and astrocyte recruitment (GFAP) was performed. In short, endogenous peroxidase activity was quenched using a solution of 3% hydrogen peroxidase and 10% methanol in distilled water. Non-specific binding was blocked using 3% normal goat in TBS with 0.2% Triton-X-100. Primary antibody (Mouse anti-TH, 1:1000, Millipore; Mouse anti-fibrin, 1:500, Abcam; Mouse anti-GDNF, 1:200, R & D systems; Rabbit anti-Iba-1, 1:400, Millipore; Rabbit anti-GFAP, 1:2000, Dako) was diluted in TBS with 0.2% triton-X-100, added to sections and incubated at room temperature overnight. Sections were incubated in secondary antibody (Horse anti-mouse, 1:200, Vector; Goat anti-rabbit, 1:200, Jackson ImmunoResearch) for 2 h at room temperature. A streptavidin-biotin-horseradish peroxidase solution (Vector, UK) was subsequently added to sections and allowed to incubate for 2 h. The development of staining was carried out using a 0.5% solution of diaminobenzidine tetra hydrochloride (DAB, Sigma, Ireland) in TBS containing 0.3 $\mu\text{l}/\text{ml}$ of hydrogen peroxide. Sections were

dehydrated in a series of ascending alcohols, cleared in xylene and finally coverslipped using DPX mountant for DAB stained sections (Sigma, Dublin, Ireland).

6.2.9 Tissue processing for MALDI-MSI

Brains were isolated from the animals post-perfusion and were stored in formalin overnight at 4 °C. The tissue was then removed from the formalin, rinsed with deionized H₂O before processing with Excelsior™ AS Tissue Processor (Thermo Scientific, Ireland). The protocol was as follows: 70 % EtOH for 5 min, 80 % EtOH for 2 h, 95 % EtOH for 2 h, 3× 100 % EtOH for 2 h each, 2× xylene for 2 h each, and 2× paraffin for 2 h each. A Leica EG1150 & EG1130 Cold Plate embedder (Leica Biosystems) was used to create paraffin-embedded tissue blocks. FFPE blocks were sectioned (6 µm thick) on a Leica Microtome RM12235 and water bath mounted (39 °C) onto Superfrost™ Ultra Plus Adhesion Slides. Slides were left to dry at 37 °C for 1 h prior to storage at 4 °C.

6.2.10 Deparaffinization and Rehydration

Tissue blocks were sectioned at 5 µm and mounted on Bruker slide adaptor plate- compatible Superfrost™ Ultra Plus Adhesion Slides (25×75 mm). The slides were heated at 60°C for one hour. After cooling, the sections were deparaffinized by washing serially in xylene (3 minutes each). This was followed by rehydration by submerging the slide in progression: twice in 100% ethanol (1 minute each), once in 95% ethanol (one minute), once in 70% ethanol (one minute), and twice in water (3 minutes each). The slides were then subjected to antigen retrieval using citraconic anhydride buffer in a vegetable steamer for 25-30 minutes. Citraconic anhydride (Thermo) buffer was prepared by adding 25 µL citraconic anhydride in 50 mL water, and adjusted to pH 3 with HCl. After cooling, a series of three buffer exchanges was performed by replacing half of the buffer with water, before eventually replacing it completely with water. The slides were then desiccated prior to the enzymatic digestion with PNGase F.

6.2.11 In vitro glycan MALDI-MSI

The slides were coated using an ImagePrep spray station (Bruker Daltonics) with a 0.2 ml aqueous solution of PNGaseF (20 µg total/slide) as previously described [22]. The slides were incubated at 37°C for two h in a humidified chamber and dried in a desiccator prior to matrix application. α -Cyano-4-hydroxycinnamic acid matrix (0.021 g CHCA in 3 ml 50% acetonitrile/50% water and 12 µL 25%TFA) was applied using the ImagePrep sprayer. Released glycan ions were detected using a Solarix dual source 7T FTICR mass spectrometer

(Bruker Daltonics) ($m/z=690-5000$ m/z) with a SmartBeam II laser operating at 1000 Hz with a laser spot size of 25 μm . Images of differentially expressed glycans were generated to view the expression pattern of each analyte of interest using FlexImaging 4.0 software (Bruker Daltonics). Following MS analysis, data was loaded into FlexImaging Software focusing on the range $m/z=1000-4000$ and reduced to 0.95 ICR Reduction Noise Threshold. Observed glycans were searched against the glycan database provided by the Consortium for Functional Glycomics (www.functionalglycomics.org). Glycoworkbench was used to generate the glycan structures and represent putative structures determined by combinations of accurate m/z , CID fragmentation patterns and glycan database structures.

6.2.12 Glycan nomenclature

All *N*-glycans have two core GlcNAcs attached to trimannosyl; F at the start of the abbreviation indicates a core $\alpha(1,6)$ -fucose linked to the inner GlcNAc; otherwise F indicates an outer arm $\alpha(1,3)$ or $\alpha(1,4)$ -fucose linked to antenna or galactose; M_x, number (x) of mannose on core GlcNAcs; A_x, number of antenna (GlcNAc) on trimannosyl core; A2, biantennary with both GlcNAcs as $\beta(1,2)$ -linked; A3, triantennary with a GlcNAc linked $\beta(1,2)$ - to both mannose and a third GlcNAc linked $\beta(1,4)$ - to the $\alpha(1,3)$ -linked mannose; A4, GlcNAcs linked as A3 with additional GlcNAc- $\beta(1,6)$ -linked to $\alpha(1,6)$ -mannose; G_x, number (x) of $\beta(1,4)$ -linked galactose on the antenna; Gal_x, number (x) of $\alpha(1,3/4/6)$ -linked galactose on $\beta(1,4)$ -linked galactose; S_x, number (x) of sialic acids linked to galactose; the number 3 or 6 in parentheses after S indicates whether the sialic acid is in an $\alpha(2,3)$ - or $\alpha(2,6)$ -linkage; S_x, number (x) of neuraminic acids linked to galactose; the number 3, 6 or 8 in parentheses after S indicates whether the sialic acid is in an $\alpha(2,3)$ -, $\alpha(2,6)$ - or $\alpha(2,8)$ - linkage; Gc_x, number (x) of glycolylneuraminic acids linked to galactose; the number 3, 6 or 8 in parentheses after S indicates whether the sialic acid is in an $\alpha(2,3)$ -, $\alpha(2,6)$ - or $\alpha(2,8)$ - linkage; Ac_x, number (x) of acetyl groups; Lac_x, the number (x) of repeating poly-*N*-acetyllactosamine repeats containing GlcNAc linked $\beta(1,4)$ - to Gal; P_x, the number (x) of phosphorous groups.

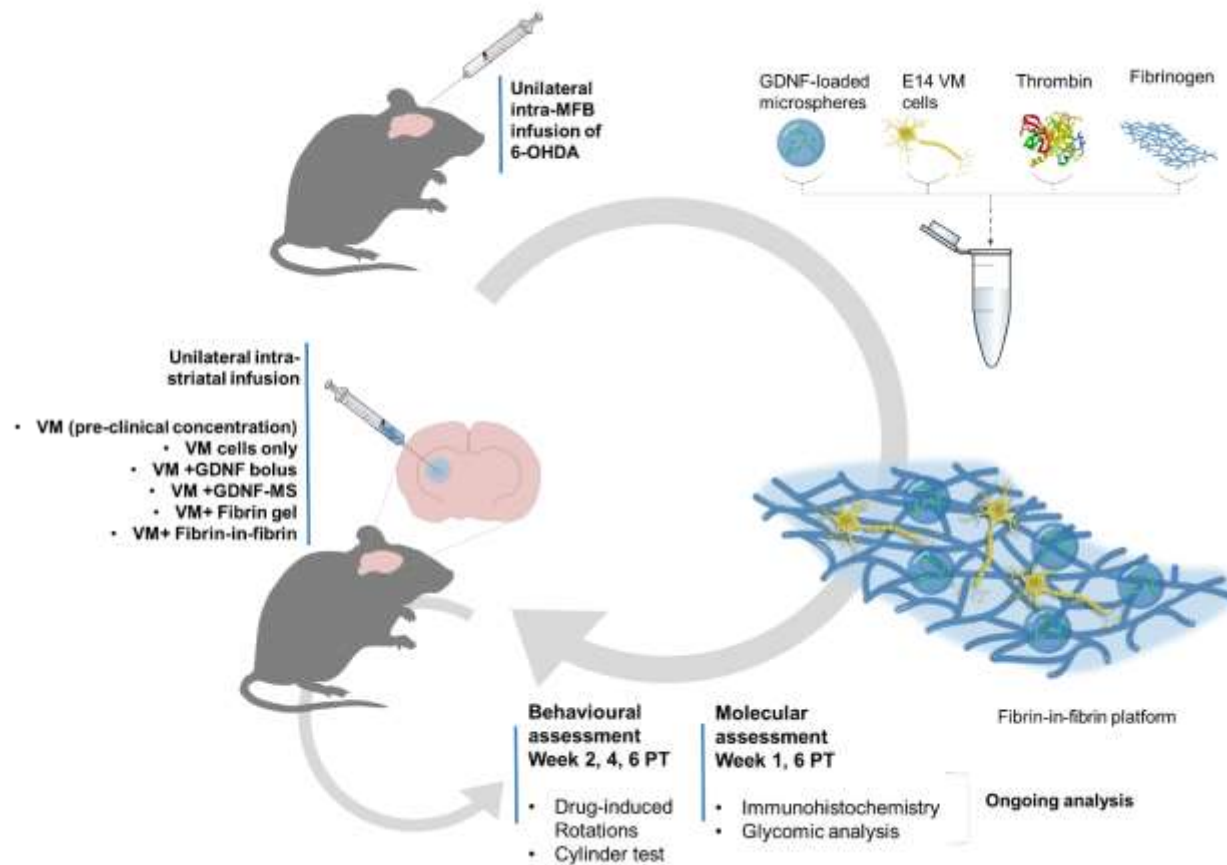


Figure 6.1 *In vivo* assessment of the impact of a GDNF-loaded fibrin-in-fibrin platform on the survival and efficacy of primary dopaminergic neurons. Schematic representation of the delivery of E14 VM cells in a GDNF-loaded fibrin-in-fibrin platform. E14 VM cells (500,000 cells/6 μ l) were encapsulated in a GDNF (5000 ng)-loaded fibrin microspheres embedded hydrogel and delivered to the unilaterally 6-OHDA lesioned striatum. Graft survival, neural outgrowth and the host immune response were assessed at six weeks post-transplantation (PT)

6.2.13 Statistical analysis

Statistical analyses were performed using GraphPad Prism[®] Version 5 (USA) and IBM SPSS[®] Version 21. Data were compared using one-way or two-way analysis of variance (ANOVA) based on the number of factors analysed, followed by a BonFerroni post-hoc comparison test. Statistical significance was set as * $p < 0.05$, ** $p < 0.01$, *** $p < 0.001$.

6.3 Results

6.3.1 *In vivo experimental design*

The study presented in this chapter was designed to assess the long-term effect of a GDNF-loaded fibrin-in-fibrin intervention on the survival and efficacy of encapsulated primary dopaminergic neurons. To this end, 90 adult male Sprague-Dawley rats received a unilateral intra-MFB 6-OHDA lesion (3 μ l). Two weeks later, rats underwent post-lesion apomorphine-induced rotations (0.5 mg/kg). Based on these results, rats were performance matched into six groups to receive intra-striatal transplants of E14 VM cells alone (500,000 per 6 μ l), E14 VM cells in the pre-clinical standard concentration (100,000 per 6 μ l), E14 VM cells with GDNF (5000 ng), E14 VM cells encapsulated in a fibrin hydrogel, E14 VM cells with GDNF-loaded fibrin microspheres and E14 VM cells with GDNF-loaded fibrin-in-fibrin platform. Apomorphine-induced rotations resumed three weeks post-transplantation and were carried out at two week intervals for a total of six weeks. The animals were then sacrificed for *post mortem* assessment. A schematic of this experimental design is shown in **Figure 6.1**.

6.3.2 *Impact of the fibrin-in-fibrin intervention on the motor function recovery*

The ability of the transplanted graft to restore motor function to the unilaterally lesioned animals was assessed at biweekly intervals for six weeks post-transplantation using apomorphine-induced rotations. In line with previous results, we found that the delivery of VM cell grafts significantly reduced the number of contralateral rotations in each group (**Figure 6.2A**). Although, a significant reduction in the number of rotations was observed for the GDNF-loaded fibrin microspheres treatment as well, a higher functional recovery was

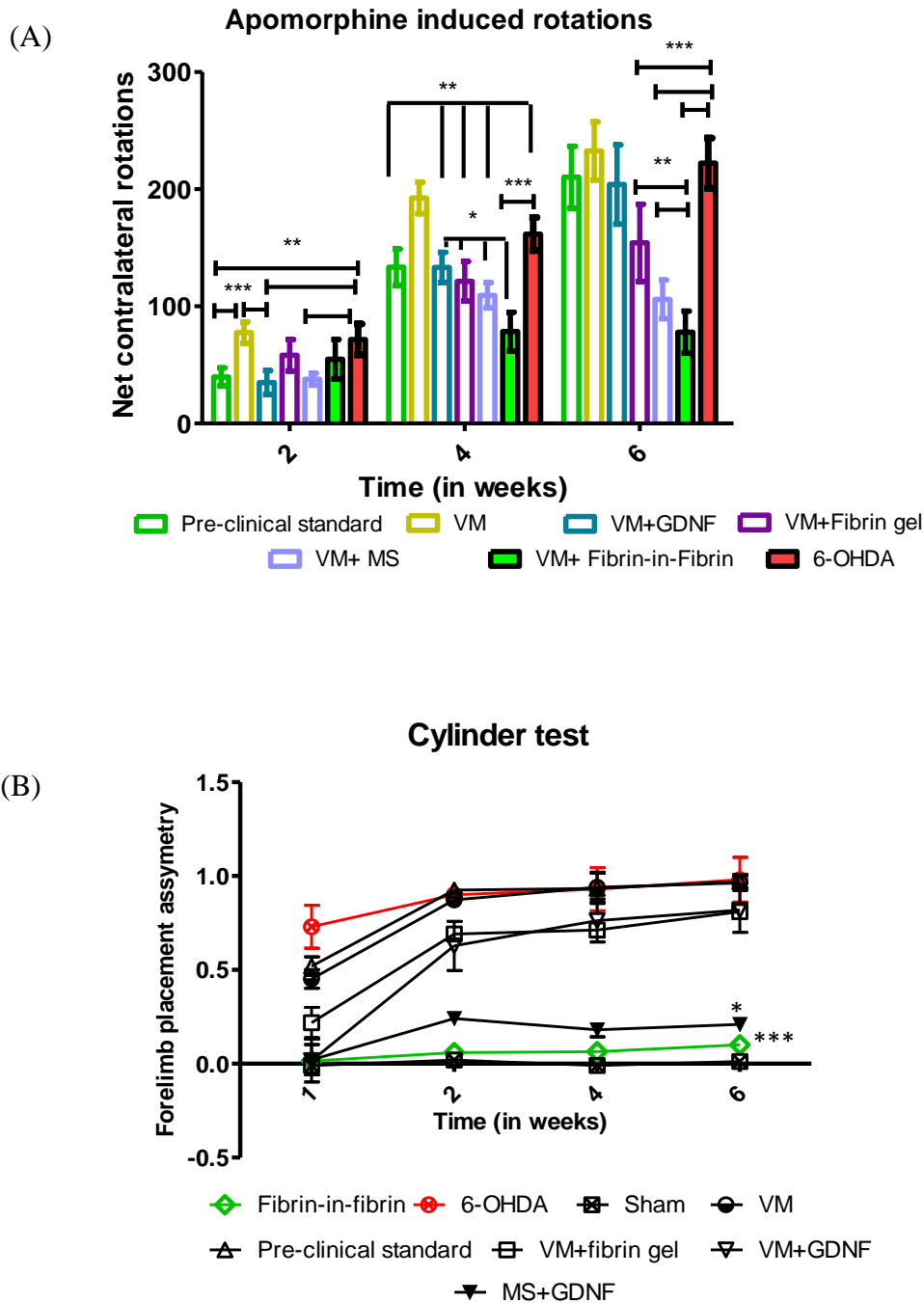


Figure 6.2: Impact of the GDNF-loaded collagen hydrogel on graft functionality (A) Transplantation of VM grafts significantly decreased the number of contralateral turns made in each group. However, the delivery of cells in a fibrin-in-fibrin platform resulted in a significantly greater level of functional recovery post-transplantation. **(B)** Enhanced functional recovery detected in the fibrin-in-fibrin treatment when compared to other groups in the limb placement asymmetry investigated using the cylinder test. Data are represented as mean \pm SD and were analysed by two-way repeated measures ANOVA with *post-hoc* Bonferroni. (* $p < 0.05$, ** $p < 0.01$, *** $p < 0.001$)

observed in GDNF-loaded fibrin-in-fibrin intervention in the rotation analysis. Also, the encapsulation of VM cells in a fibrin-in-fibrin platform provided a significantly greater level of functional recovery at all the corresponding time points post-transplantation in the cylinder test (**Figure 6.2B**)

6.3.3 Impact of the fibrin-in-fibrin intervention on striatal microgliosis

The process of transplantation of VM cells elicited a host immune response in the striatum surrounding the site of implantation. Iba-1 staining was performed to investigate the microglial response to the different therapeutic implantations at week 1 (**Figure 6.3A**) and week 6 (**Figure 6.3B**) post-implantation. It was observed that when the VM cells were delivered encapsulated in a fibrin hydrogel or a GDNF-loaded fibrin-in-fibrin intervention there was a significant decrease in striatal microgliosis. There was a significant reduction in the volume of the Iba-1 positive immunostaining at week 6 for the fibrin hydrogel and fibrin-in-fibrin intervention as compared to other treatments indicating that the loading of a fibrin hydrogel with GDNF-microspheres does not hinder its ability to act as a protective shield to the grafted cells, thereby reducing the host immune response. Quantification of the volume of microgliosis showed a significant three-fold reduction in the treatment with the fibrin hydrogel and fibrin-in-fibrin intervention as compared to the cells only treatment (**Figure 6.3C**).

6.3.4 Impact of the fibrin-in-fibrin intervention on striatal astrocytosis

The astrocytic response to different therapeutic implantations was measured by the GFAP immunohistochemistry. As represented in **Figure 6.4 A, B**, the striatal astrocytic migration was attenuated at both week 1 and week 6 in the treatment groups with fibrin hydrogel and GDNF-loaded fibrin-in-fibrin intervention. The significant reduction in the volume of GFAP-positive immunostaining at week-6 post-implantation in the groups with fibrin hydrogel and fibrin-in-fibrin intervention was indicative of the effective shielding of the engrafted cells from the host response by the biomaterial matrix (**Figure 6.4B**). The quantification of the volume of striatal astrocytosis represented a significant three-fold reduction in the treatments with fibrin hydrogel and fibrin-in-fibrin intervention as compared to the treatment with cells only (**Figure 6.4C**). This effective masking of the encapsulated cells from the surrounding host response protects the transplanted cells and enhances the graft survival post-implantation.

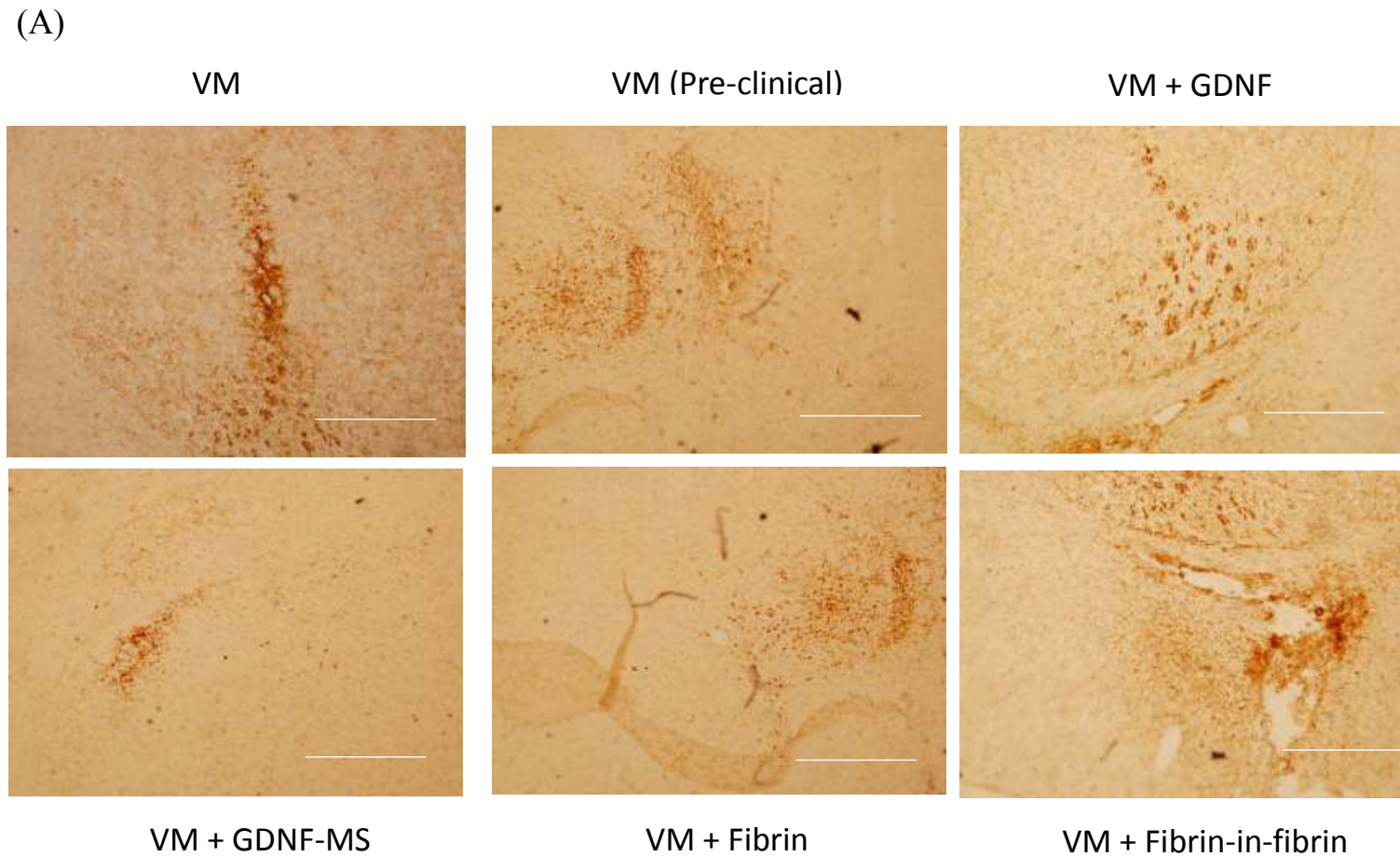
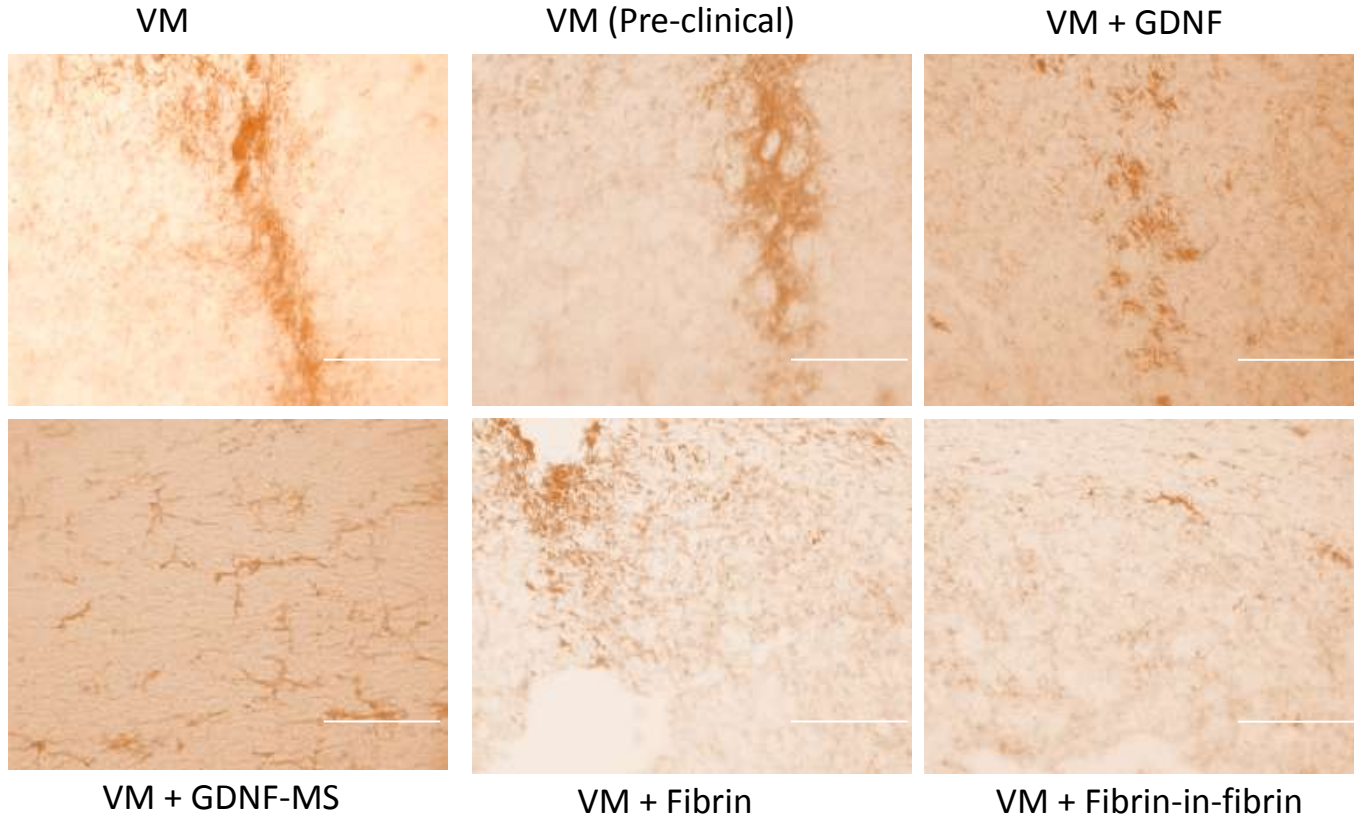


Figure 6.3 Microglial response to the biomaterial intervention. (A) Iba-1 immunohistochemical analysis for microglial recruitment one week post-therapeutic implantation representing the attenuation of host response in the presence of the biomaterial intervention (scale bar= 100 μ m, n=7)

(B)



(C)

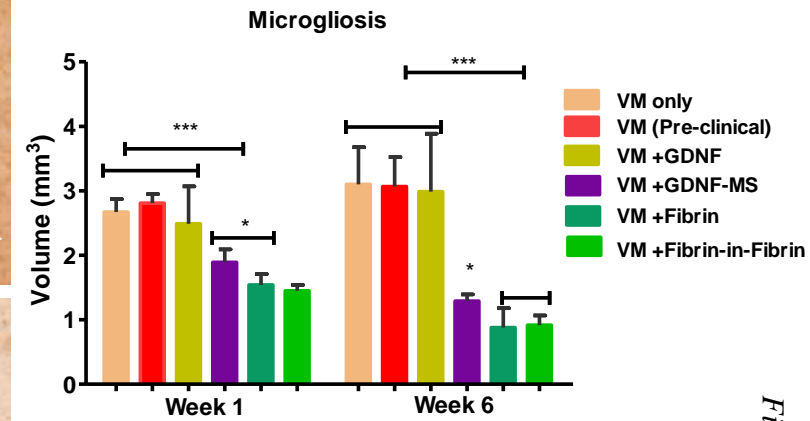


Figure 6.3 Microglial response to the biomaterial intervention. (B) Iba-1 immunohistochemical analysis for microglial recruitment six weeks post-therapeutic implantation representing the significant attenuation of host response in the presence of the fibrin-in-fibrin intervention as compared to the other treatments (scale bar= 100 μ m, n=7) , (C) Volume of microgliosis significantly reduced with the encapsulation of cells in a fibrin hydrogel and a GDNF-loaded fibrin-in-fibrin intervention. Data are represented as mean \pm SEM and analysed using two-way ANOVA with Bonferroni post-hoc test (* p < 0.05, ** p <0.01, *** p < 0.001)

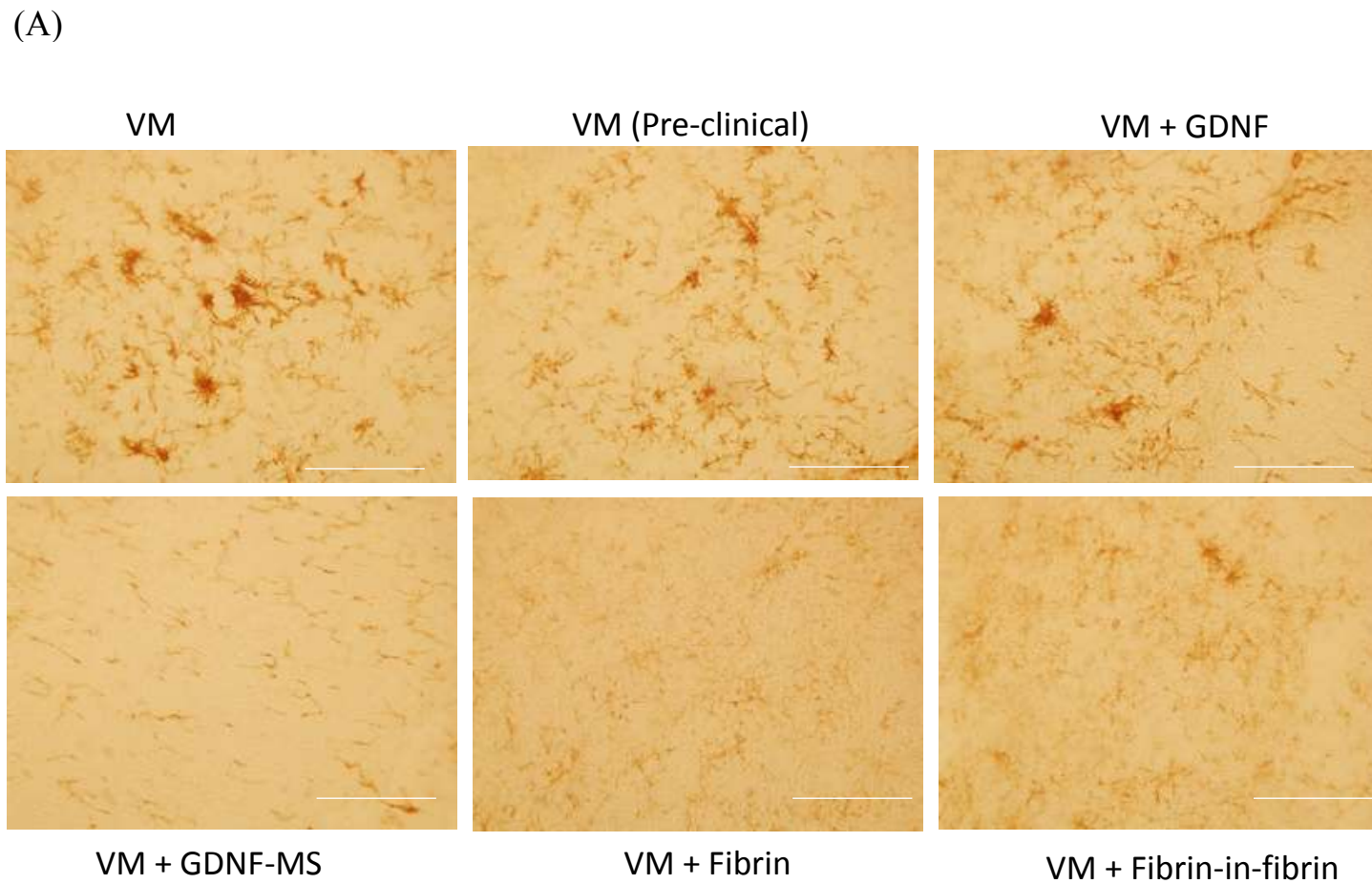
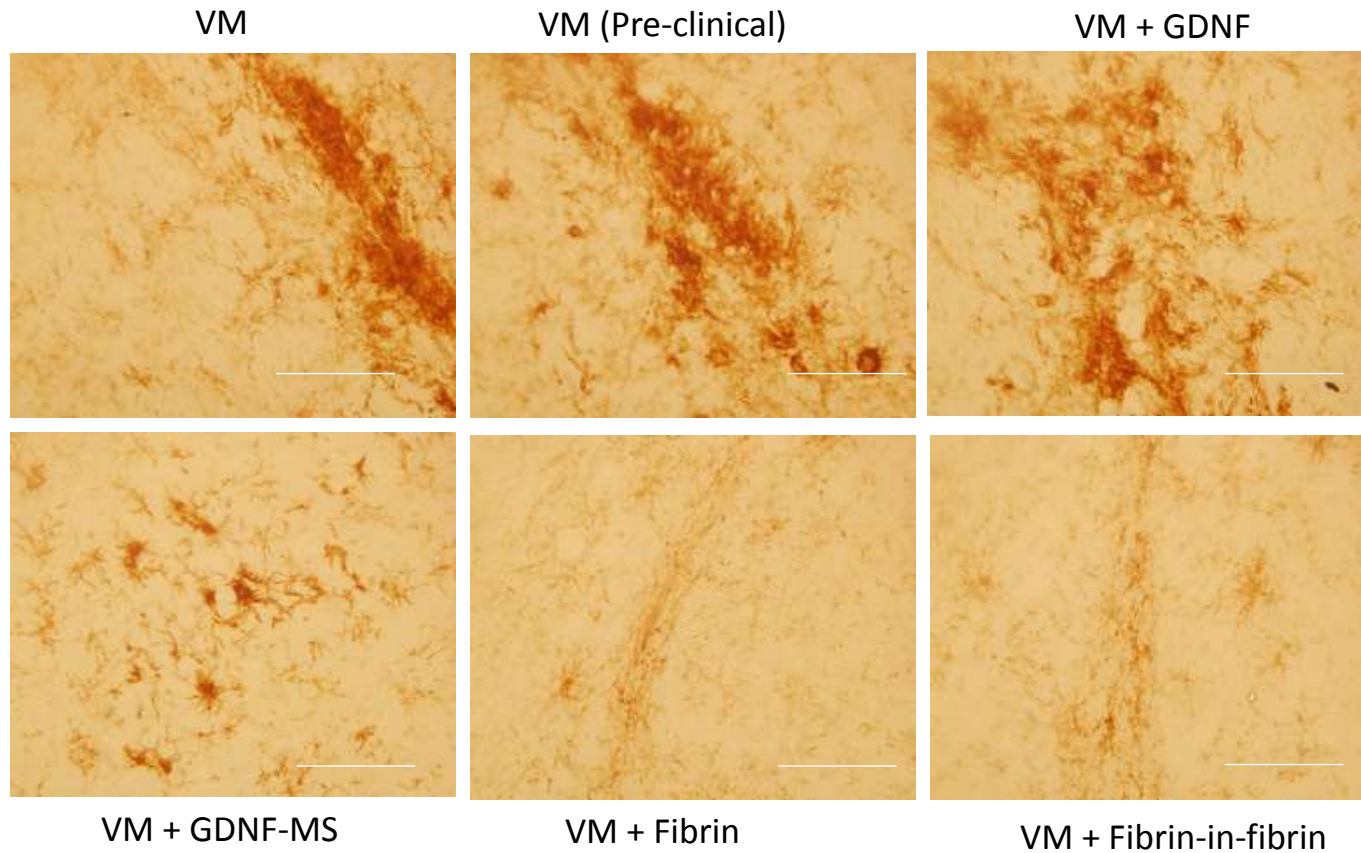


Figure 6.4 Astrocytic response to the biomaterial intervention. (A) GFAP immunohistochemical analysis for astrocytic recruitment one week post-therapeutic implantation representing the attenuation of host response in the presence of the biomaterial intervention (scale bar= 100 μ m, n=7)

(B)



(C)

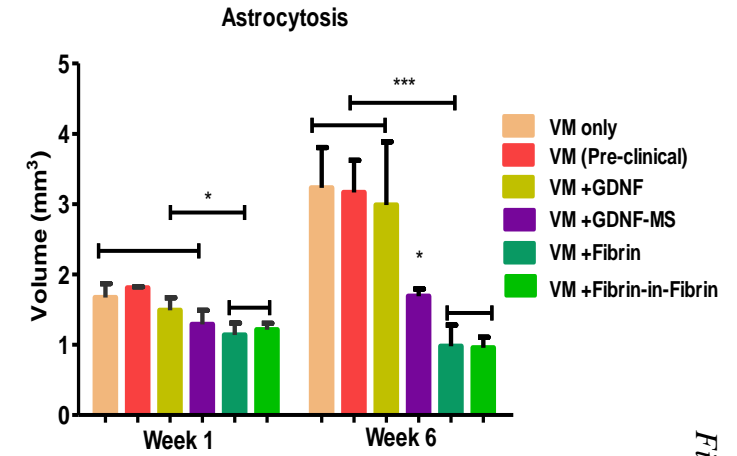


Figure 6.4 Astrocytic response to the biomaterial intervention. (B) GFAP immunohistochemical analysis for astrocytic recruitment six weeks post-theapeutic implantation representing the significant attenuation of host response in the presence of the fibrin-in-fibrin intervention as compared to the other treatments (scale bar= 100 μ m, n=7) , (C) Volume of astrocytosis significantly reduced with the encapsulation of cells in a fibrin hydrogel and a GDNF-loaded fibrin-in-fibrin intervention. Data are represented as mean \pm SEM and analysed using two-way ANOVA with Bonferroni post-hoc test (* $p < 0.05$, ** $p < 0.01$, *** $p < 0.001$)

6.3.5 Biodegradability of the fibrin-in-fibrin intervention

Degradation of the biomaterial intervention *in vivo* was determined using the fibrin immunohistochemistry. At one week post-implantation, there was a significantly higher volume of positive immunostaining in the groups with biomaterial treatments as represented in **Figure 6.5A**. This was significantly reduced at six weeks post-implantation of the therapeutic interventions as represented in **Figure 6.5B**. This is indicative of the fact that the fibrin-in-fibrin intervention is biodegradable. There was almost a complete absence of the positive immunostaining for the treatment with fibrin microspheres at six weeks when compared to fibrin hydrogel or fibrin-in-fibrin intervention, indicating a higher persistence of the modular biomaterial format than the microspheres alone.

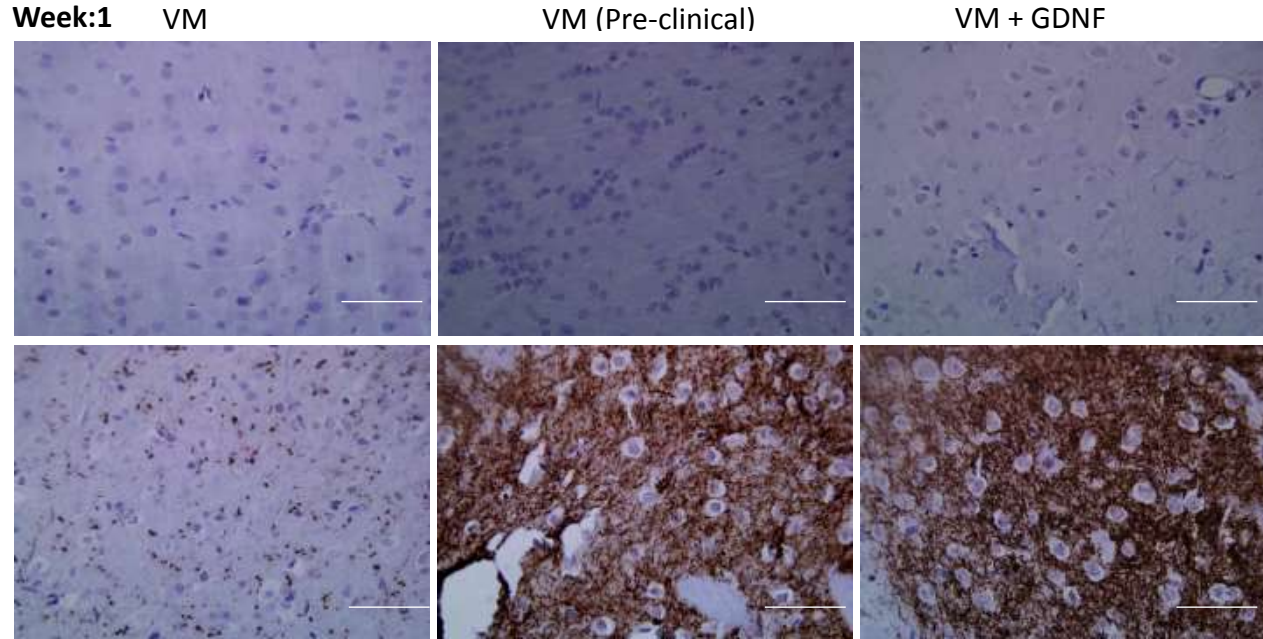
6.3.6 GDNF release from the fibrin-in-fibrin intervention *in vivo*

The human GDNF immunohistochemical analysis was performed to detect the release of GDNF from the biomaterial interventions *in vivo*. As represented in **Figure 6.6A**, there was a significant increase in the positive immunostaining at one week post-implantation in the GDNF-loaded fibrin microspheres and fibrin-in-fibrin intervention. Interestingly, bolus GDNF injection showed a complete lack of immunostaining at one week post-implantation indicating the rapid clearance post-injection. Contrarily, there was a significantly higher (**Figure 6.6B**) positive-immunostaining detected at one week post-implantation in the GDNF-loaded biomaterial treatments, indicating that the both the microspheres and fibrin-in-fibrin intervention showed a sustained growth factor release. There was an absence of human-GDNF immunohistochemical staining six weeks post intra-striatal delivery showed that the transplanted GDNF was cleared from the brain in that time frame.

6.3.7 Improvement in striatal re-innervation using fibrin-in-fibrin intervention

The ability of engrafted cells to form neural outgrowths *in situ* and re-innervate the striatum post-transplantation was investigated in all the treatment groups. Using TH immunostaining, the volume of striatal tissue occupied by innervation from the transplanted dopaminergic cells was calculated. Investigation of striatal re-innervation six weeks post-transplantation of the E-14 embryonic grafts shows a significant increase in the fibrin-in-fibrin treatment group with a five-fold increase when compared to the VM cells only. Although there was an initial improvement in re-innervation observed with GDNF treatment, this impact failed to last for six weeks post-treatment owing to the short half-life of the GDNF bolus.

(A)

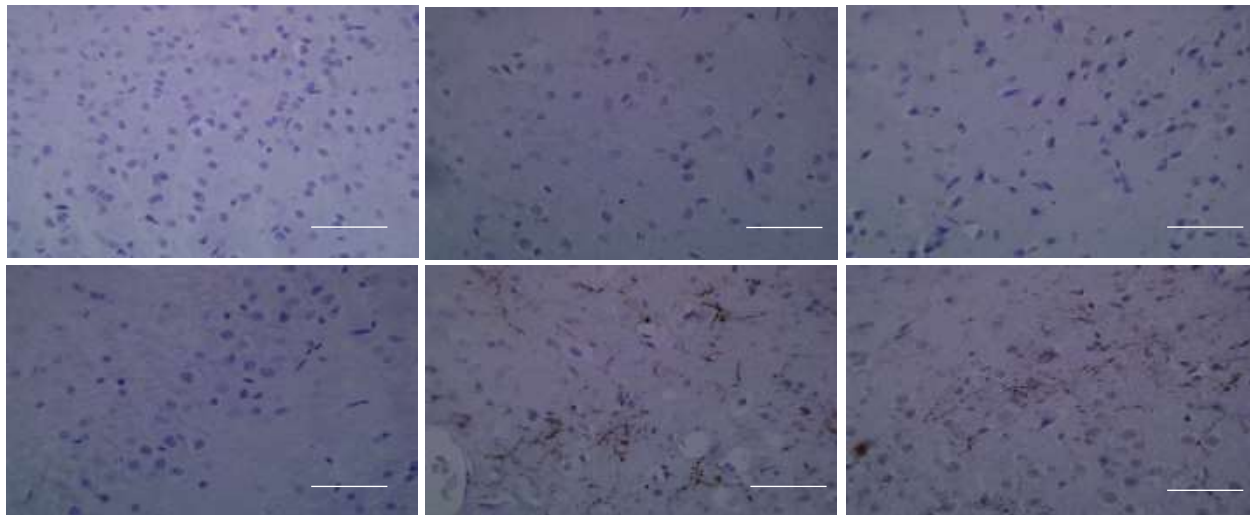


VM + GDNF-MS

VM + Fibrin

VM + Fibrin-in-fibrin

Week:6 VM VM (Pre-clinical) VM + GDNF



VM + GDNF-MS

VM + Fibrin

VM + Fibrin-in-fibrin

(B)

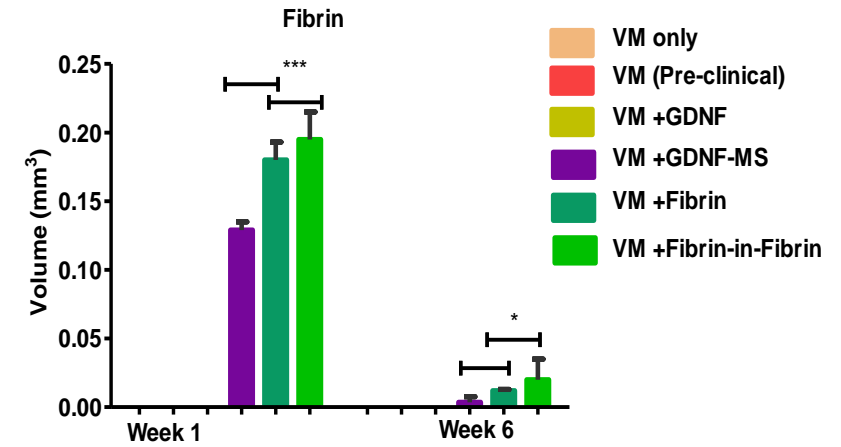
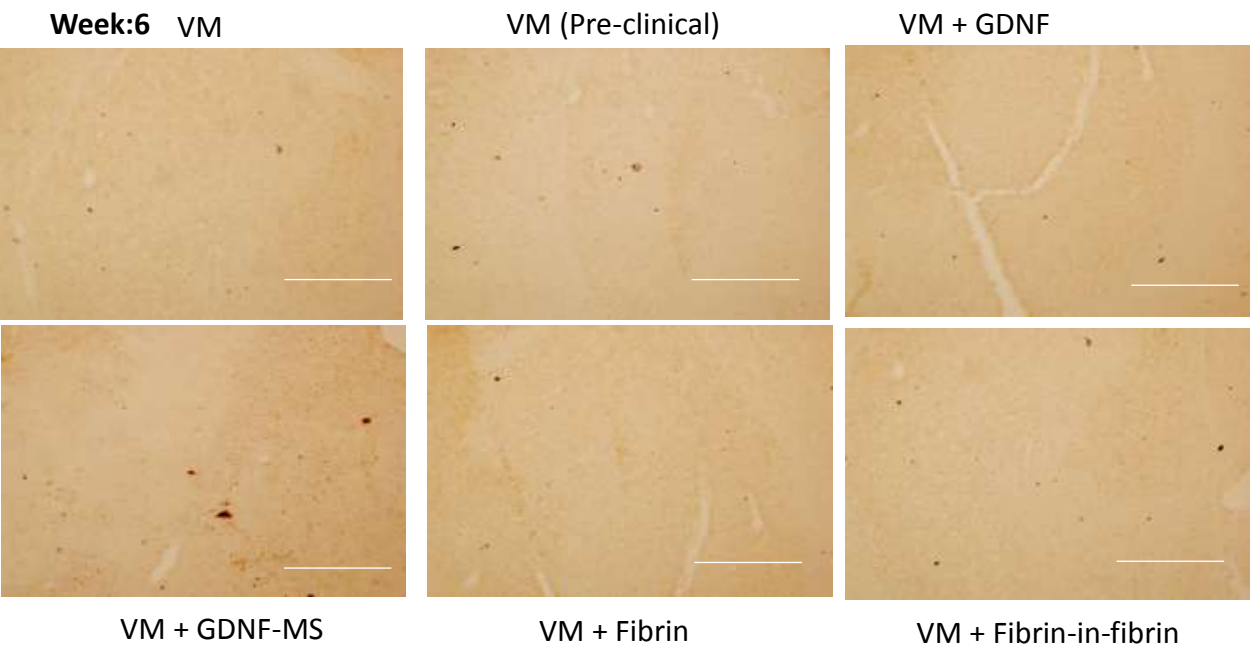
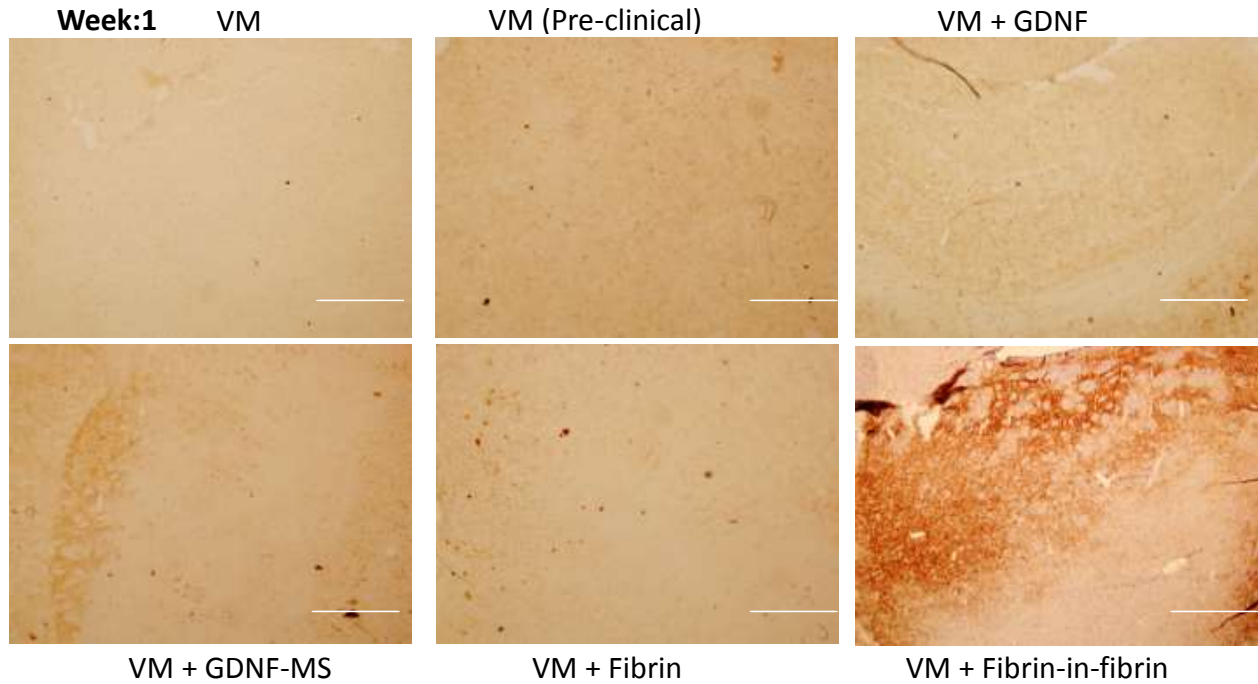


Figure 6.5 Biodegradability of the fibrin-in-fibrin intervention. (A) Fibrin immunohistochemical analysis to determine the degradation of the biomaterial intervention *in vivo* at one and six weeks post-implantation (scale bar= 100 μ m, n=7) , (B) Volume of fibrin-positive immunostaining significantly reduced at six weeks post-implantation in the fibrin hydrogel and GDNF-loaded fibrin-in-fibrin intervention treatments. Data are represented as mean \pm SEM and analysed using two-way ANOVA with Bonferroni post-hoc test (* $p < 0.05$, ** $p < 0.01$, *** $p < 0.001$)

(A)



(B)

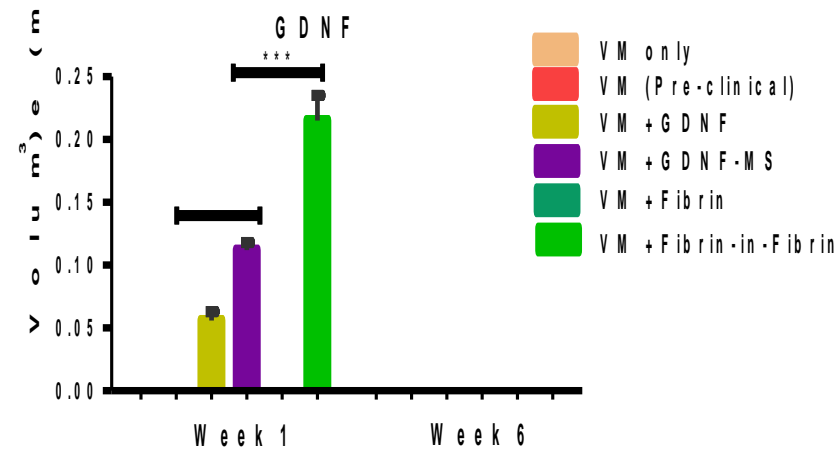


Figure 6.6 GDNF release *in vivo*. (A) GDNF immunohistochemical analysis to detect GDNF release at one and six weeks post-implantation (scale bar= 100 μm, n=7) , (B) Volume of GDNF-positive immunostaining was reduced to null at six weeks post-implantation in all treatments indicative of GDNF clearance. Data are represented as mean ± SEM and analysed using two-way ANOVA with Bonferroni post-hoc test (* $p < 0.05$, ** $p < 0.01$, *** $p < 0.001$)

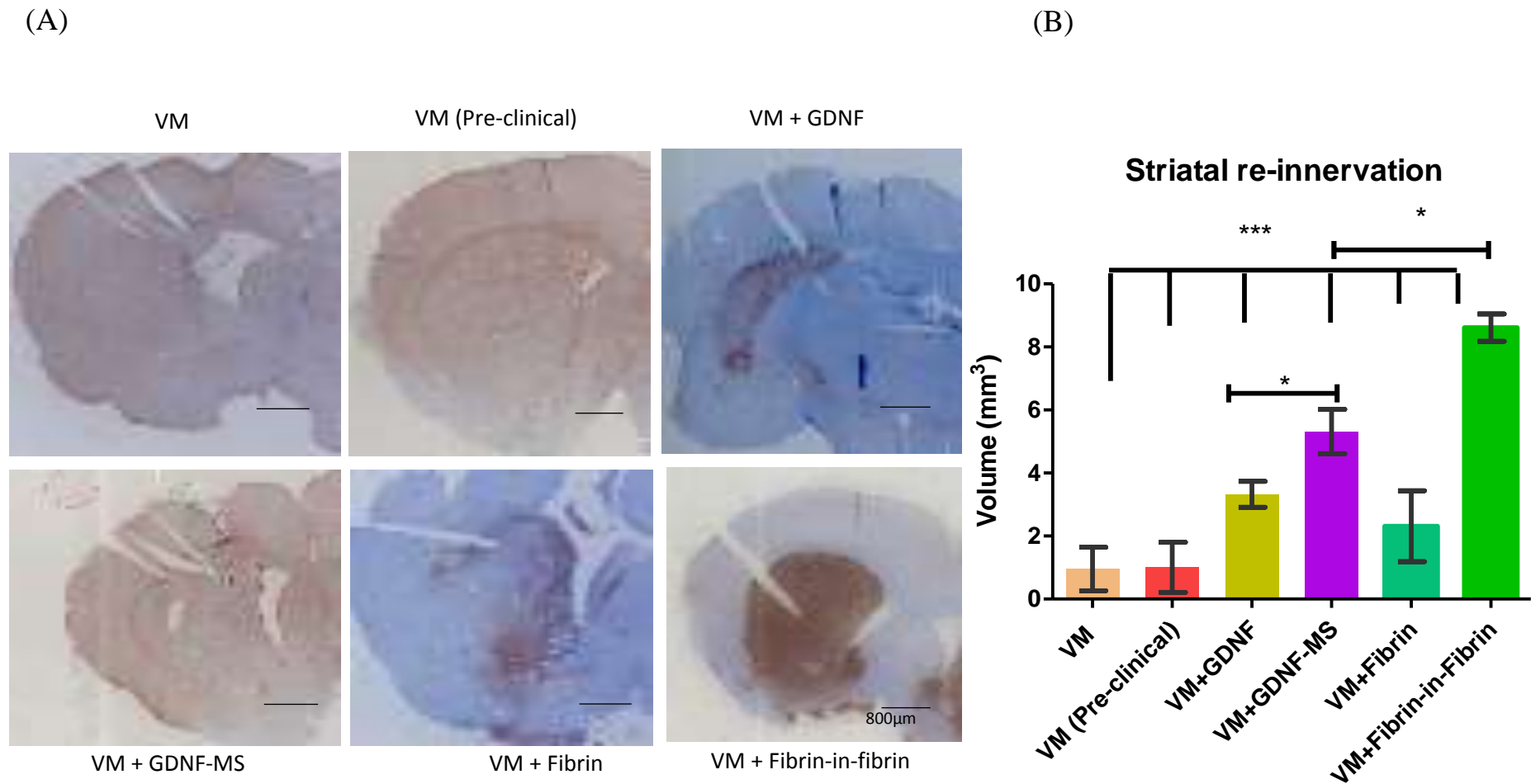


Figure 6.7 Enhanced striatal re-innervation by fibrin-in-fibrin intervention. (A) TH immunostaining showing that all groups did successfully re-innervate a portion of the denervated striatum. The fibrin-in-fibrin intervention treatment shows an enhanced striatal re-innervation compared to the other treatments. Scale bar represents 800 μm , $n=7$ (B) The magnitude of striatal re-innervation was significantly greater (five-fold vs. VM alone) as represented by the volume of TH-positive immunostaining at six weeks post-implantation in all treatments. Data are represented as mean \pm SEM and analysed using two-way ANOVA with Bonferroni post-hoc test (* $p < 0.05$, ** $p < 0.01$, *** $p < 0.001$)

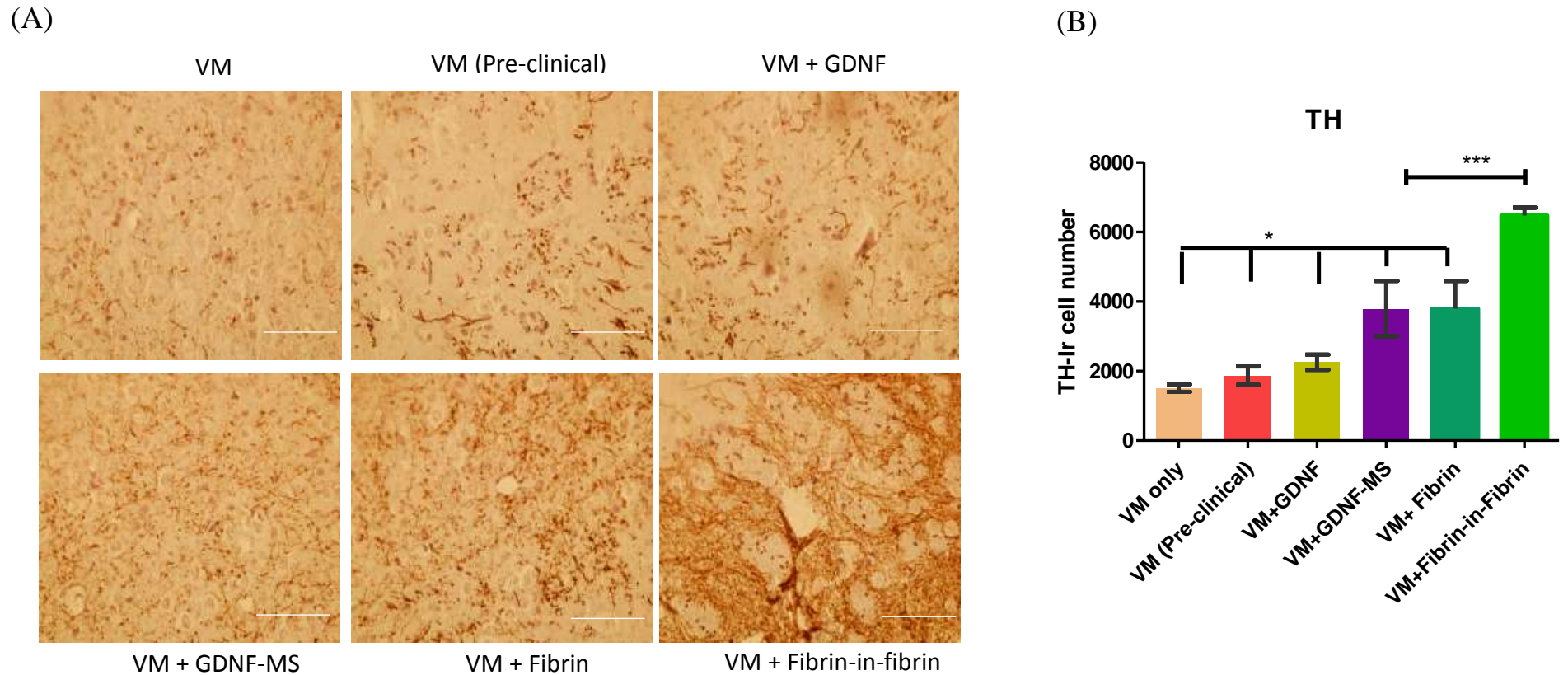


Figure 6.8 Enhanced dopaminergic cell survival by fibrin-in-fibrin intervention. (A) TH immunostaining demonstrating the presence of surviving dopaminergic cell bodies in each treatment group. The fibrin-in-fibrin intervention shows higher number of surviving dopaminergic cells when compared to the other treatments. Scale bar represents 800 μm , $n=7$ (B) The delivery of VM cells in a GDNF-loaded fibrin-in-fibrin intervention showed a greater yield of surviving TH-positive cells at six weeks post-implantation in all treatments (five-fold higher than VM only treatment). Data are represented as mean \pm SEM and analysed using two-way ANOVA with Bonferroni post-hoc test (* $p < 0.05$, ** $p < 0.01$, *** $p < 0.001$)

Interestingly, the magnitude of striatal re-innervation was also significantly greater (five-fold) from the delivery of cells alone or when cells were co-delivered with the GDNF-loaded fibrin microspheres (**Figure 6.7A**). The quantified results from immunohistochemical analysis as represented in **Figure 6.7B** show a five-fold increase in striatal re-innervation in the fibrin-in-fibrin treatment as compared to the VM cells only, thereby illustrating the efficacy of the biomaterial intervention in successfully promoting the graft integration and re-innervation of the host brain.

Furthermore, striatal re-innervation from cells in the GDNF-loaded fibrin-in-fibrin platform was significantly greater than that of cells delivered with GDNF alone (two-fold) and GDNF-loaded fibrin spheres (1.5-fold), showing that the fibrin-in-fibrin intervention can successfully increase the volume of innervation from the encapsulated cells. Interestingly, the cells encapsulated in fibrin gel alone didn't show any significant difference in striatal re-innervation compared to the VM cells (**Figure 6.7A**).

6.3.8 Improvement in dopaminergic cell survival using fibrin-in-fibrin intervention

The successful survival of the transplanted cells was investigated by counting the number of surviving TH⁺ dopaminergic cells throughout the striatum. TH immunostaining identified the successful transplantation of dopaminergic neurons in each group (**Figure 6.8A**), however, not all groups expressed the same number of surviving neurons (**Figure 6.8B**). A significant increase in the number of surviving dopaminergic neurons was observed with the delivery of GDNF with VM cells. However, interestingly, when cells were delivered in a GDNF-loaded fibrin-in-fibrin intervention, there was a significant (five-fold) increase in the number of surviving cells when compared to the delivery of VM cells alone (**Figure 6.8B**). Additionally, cell survival in a GDNF-loaded collagen hydrogel was significantly greater than that of the VM & GDNF group (1.5 fold).

6.3.9 Impact of the fibrin-in-fibrin intervention on the modulation of host brain glyco-phenotype

The tissue section analysis using MALDI-MSI led to the identification of 10 differentially regulated N-glycans between the SN of the diseased, biomaterial-treated and healthy controls. The summary of these glycans alongside their compositions are represented in **Table 6.1**. **Figure 6. 9A and 6.10A** represent the overall segmental analysis of the N-glycan distribution in striatum and SN for healthy, diseased and biomaterial-treated brains. There was a selective

Table 6.1: MALDI-MSI detection of N-glycan modulation: Summary of N-glycan species and their compositions modulated by the induction of PD and counter-modulated by the application of fibrin-in-fibrin intervention in the SN and striatum of the rodent brains.

[m/z]	Glycan composition in SN
1079.3861	Hex3dHex1HexNAc2 + 1Na
1444.5205	Hex4dHex1HexNAc3 + 1Na
1606.5707	Hex5dHex1HexNAc3 + 1Na
1793.6424	Hex4dHex2HexNAc4 + 1Na
1955.692	Hex5dHex2HexNAc4 + 1Na
2361.8934	Hex5dHex2HexNAc6 + 1Na
2539.9389	Hex7dHex1HexNAc6 + 1Na
2757.926	Hex6dHex3HexNAc5NeuAc1 + 1Na
2758.9933	Hex8HexNAc7 + 1Na
2815.0777	Hex6dHex2HexNAc6NeuAc1 + 1Na
[m/z]	Glycan composition in Striatum
1079.3861	Hex3dHex1HexNAc2 + 1Na
1095.3954	Hex4HexNAc2 + 1Na
1257.4305	Hex5HexNAc2 + 1Na
1298.4504	Hex4HexNAc3 + 1Na
1419.4993	Hex6HexNAc2 + 1Na
1444.5205	Hex4dHex1HexNAc3 + 1Na
1501.5606	Hex4HexNAc4 + 1Na
1590.5882	Hex4dHex2HexNAc3 + 1Na
1606.5707	Hex5dHex1HexNAc3 + 1Na
1704.6037	Hex4HexNAc5 + 1Na
1850.66	Hex4dHex1HexNAc5 + 1Na
1996.7794	Hex4dHex2HexNAc5 + 1Na
2012.7193	Hex5dHex1HexNAc5 + 1Na
2053.7605	Hex4dHex1HexNAc6 + 1Na
2115.7043	Hex5dHex1HexNAc4NeuGc1 + 1Na
2157.7935	Hex5HexNAc5NeuAc1 + 1Na
2319.8343	Hex6HexNAc5NeuAc1 + 1Na
2466.8792	Hex6dHex3HexNAc5 + 1Na
2523.9296	Hex6dHex2HexNAc6 + 1Na
2539.9389	Hex7dHex1HexNAc6 + 1Na
2669.9993	Hex6dHex3HexNAc6 + 1Na
2832.0586	Hex7dHex3HexNAc6 + 1Na

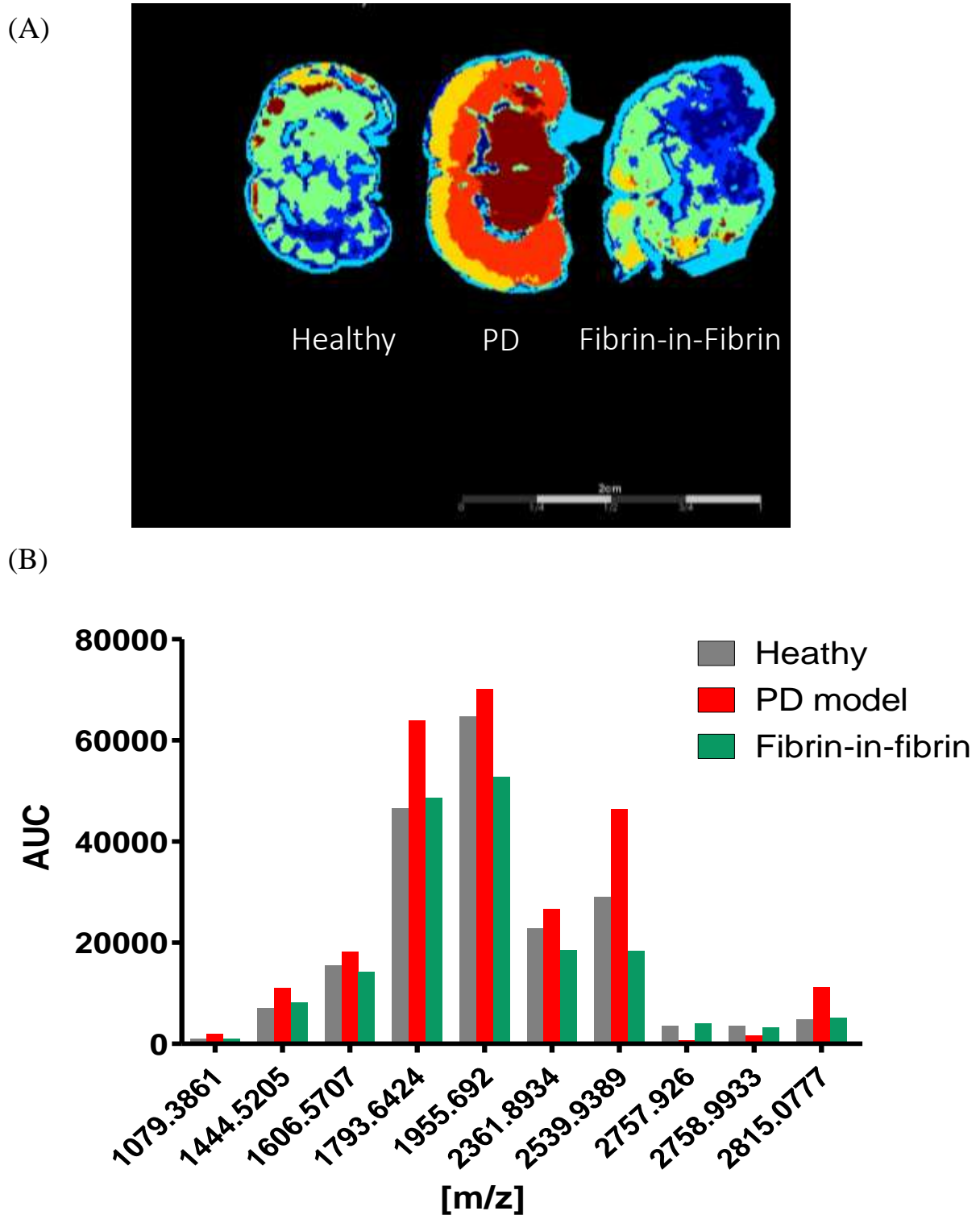


Figure 6.9: Modulation of SN glyco phenotype: (A) Segmentation analysis of overall N-glycosylation showing the differential modulation of glycosylation by the induction of PD and impact of the biomaterial intervention on this modulation. (B) Quantified changes in expression of different N-glycan species as detected by MALDI-MSI representing the chief glycan players in the PD pathophysiology. There is a significant upregulation in the mannosylation, sialylation, terminal α -Gal and fucosylation in the PD brains which is targeted by the biomaterial therapy.

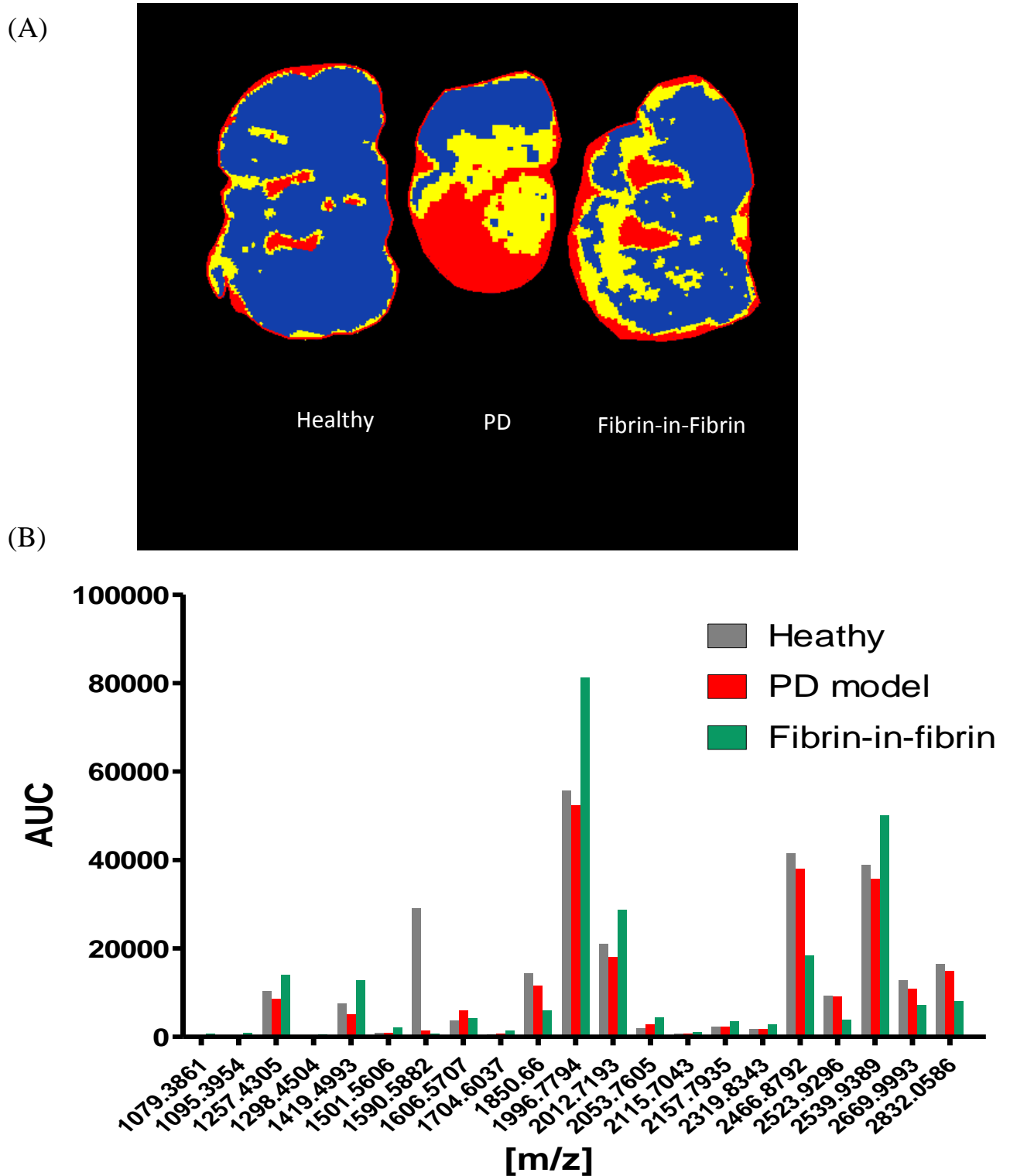


Figure 6.10: Modulation of striatal glyco phenotype: (A) Segmentation analysis of overall N-glycosylation showing the differential modulation of glycosylation by the induction of PD and impact of the biomaterial intervention on this modulation. (B) Quantified changes in expression of different N-glycan species as detected by MALDI-MSI in striatum representing the chief glycan players in the PD pathophysiology. Significant downregulation of mannosylation and sialylation was detected in the biomaterial treatment group.

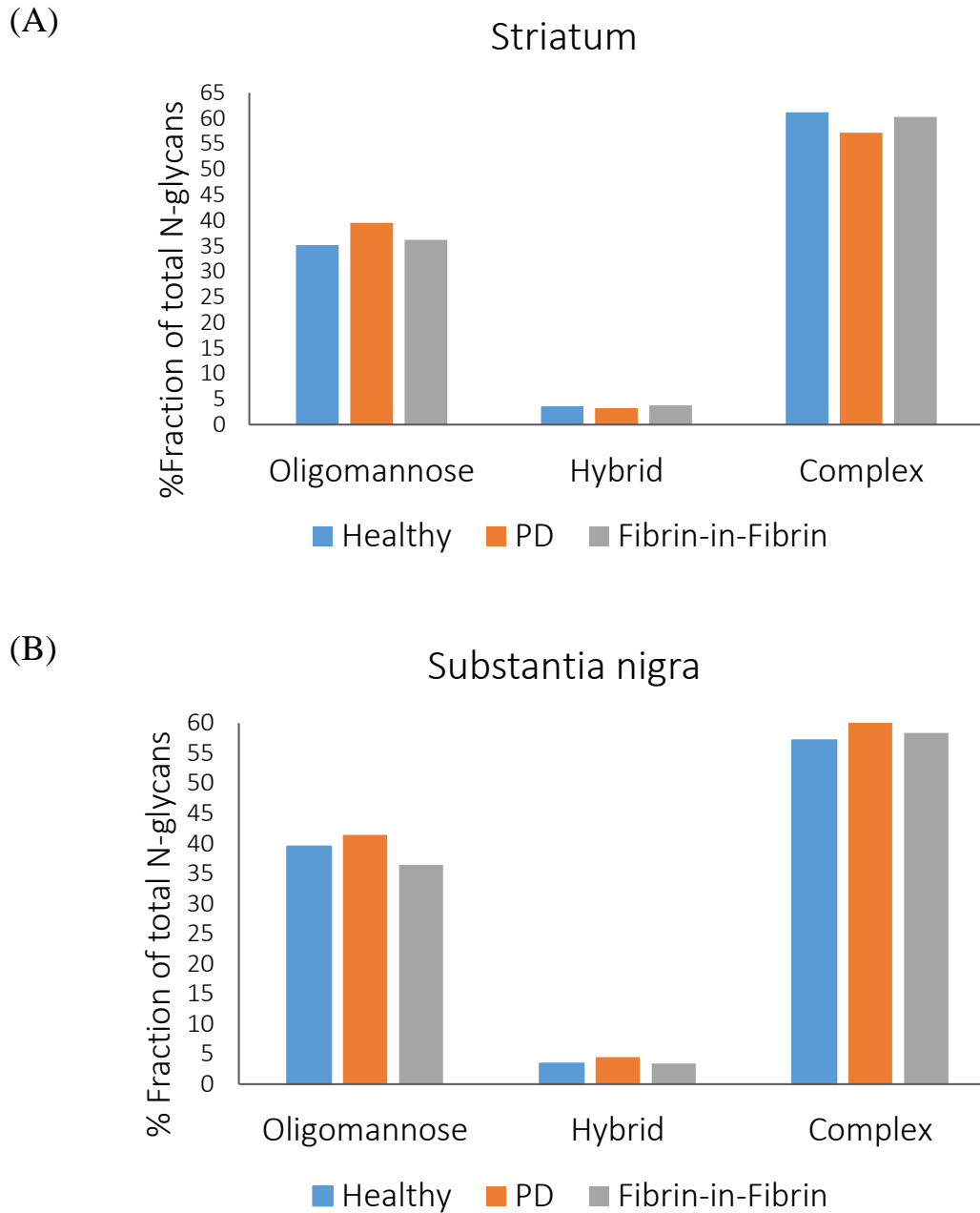


Figure 6.11: Modulation of major N-glycan classes in response to the biomaterial intervention: Modulation of oligomannose, complex and hybrid glycans in (A) Striatum and (B) SN detected by MALDI-MSI representing the restoration of the brain glycophenotype towards the ‘healthy’ spectrum post-treatment with biomaterial intervention.

targeting of the oligomannose N-glycans by the biomaterial intervention as is represented in the MALDI-MSI quantifications. As a general observation, there was a loss of higher sialic acids when ionized by matrix-assisted laser desorption/ionization (MALDI) as the consequence of the labile carboxylic proton which is lost both in the ion source and during the flight to the detector [39]. An intriguing observation that stemmed from this analysis was the downregulation of Lewis antigen^x, sialyl Lewis antigen^x and alpha-gal modified N-glycans in the diseased animals by the biomaterial intervention. The panel of MALDI-MSI images representative of these changes in SN is shown in supplementary data. However, contrary to the lectin histochemical analysis, MALDI-MSI picked up a significant downregulation of fucosylation with the fibrin-in-fibrin treatment, which included both core and outer arm fucosylated N-glycans.

There were about 21 differentially regulated glycans were detected in the striatum of diseased, biomaterial-treated and healthy animals as represented in **Figure 6.10B**. In addition to the oligomannose moieties, a differential regulation in the striatum was observed for Lewis antigen^x and Sialyl Lewis antigen^x modified N-glycans showed distinct modulation in the striatum of the PD model. A significant upregulation of alpha-gal modified N-glycans as detected in the striatum of the diseased animals was downregulated post- biomaterial treatment indicative of the implication of alpha-Gal in the reparative mechanisms initiated by the biomaterial intervention. A summary of the variation in the chief classes of glycosylation in striatum and SN in response to the biomaterial treatment are represented in **Figure 6.11 A, B**. In the striatum, there is an attenuation of the increase in the oligomannose and the decrease in the complex N-glycans observed as a result of 6-OHDA lesioning due to the treatment with the fibrin-in-fibrin intervention. Similarly, in the SN, there is an attenuation of the increase in both the oligomannose and complex N-glycans observed as a result of 6-OHDA lesioning due to the treatment with the fibrin-in-fibrin intervention. This is indicative of the glycan-based reparative impact of the fibrin-fibrin intervention.

6.4 Discussion

Cellular regenerative therapies offer a promising solution for progressive neurodegenerative disorders like PD where cardinal pathology is the loss of dopaminergic neurons in SN. Progenitor cell therapies in PD aiming at replacement of lost dopaminergic neurons have shown their ability to re-innervate the striatum and attenuate motor function deficits in

various rodent and non-human primate models [25–27]. Although, several clinical trials have highlighted the effective reversal in motor function deficits by the transplantation of VM tissue [28–30], the rapid cell-death post-transplantation calls for multiple fetal donors to ensure a certain level of cell survival necessary to cause a functional impact. This poses a significant constraint to the clinical translation of the VM cell therapy due to the associated ethical and logistical constraints. Therefore, this chapter evaluated the potential of a multi-modal trophic factor-loaded fibrin-in-fibrin intervention to enhance the survival of the primary dopaminergic precursors and their ability to reverse the functional deficits to lessen the ethical and logistical burden associated with the use of fetal donors.

The overarching aim of this study was to emphasize the potential of trophic support enriched biomaterial intervention in promoting the graft survival to enhance the efficacy of cell therapies. Necrosis appears to be the key player in the poor viability of the fetal dopaminergic cells occurring as a result of the physiological insult born by the cells during the tissue dissection, preparation and transplantation process. However, a sizable fraction of these progenitor cells are lost post-transplantation through apoptosis which is driven predominantly driven by factors in the cell microenvironment [31,32]. As described by Sortwell et al (2000), there are several stages of the transplantation protocol that can evoke an apoptotic response in the engrafted cells [32], first of which is the cell dissection/dissociation promoting anoikis (detachment from extracellular matrix). Secondly, the switch of the cellular microenvironment from a trophic factor rich-embryonic brain to trophic factor-devoid adult striatum results in a significant cell death post-transplantation. Finally, another leading reason of the cell death post-transplantation is the host immune response evoked against the established graft. Intriguingly, each of these stages could be successfully intervened by a carefully deigned biomaterial therapy to approach the problem in a multi-faceted way. The fibrin-in-fibrin system includes a hydrogel component which can serve as a supplementary matrix to restore the normal cell-matrix interactions and prevent the ensuing cell death due to anoikis [33]. Fibrin scaffolds offer an inherent advantage over several other biomaterial scaffolds that require chemical manipulation to improve cell adherence as it contains the natural Arg-Gly-Asp (RGD) tripeptide and enables the integrin-mediated cellular adhesion while acting as a natural anchor for cell delivery [34–36]. The work described in this chapter shows that the encapsulation of cells derived from the E14 VM in a fibrin-in-fibrin intervention resulted in a five-fold increase in primary dopaminergic neuron survival and a five-fold increase in striatal re-innervation, which correlated with a significantly greater level of functional recovery.

A very important concern about the longevity of the engrafted neurons is the exposure to the hostile host immune response. Several studies have demonstrated that the grafting of exogenous cells in the brain evokes an elevated host response [28,37]. It is crucial here that the aforementioned fibrin-in-fibrin intervention effectively shields the engrafted from the exposure to the immune cells in the brain. By, itself the biomaterial intervention was found to be immune-neutral, not eliciting an exaggerated host response. This was in line with the primary observation with the fibrin hollow microspheres as tested in Chapter 1 [38]. The host response at one and six weeks post-treatment represent the effective shielding of the encapsulated cells from the host immune system and a three-fold reduction in the microgliosis and astrogliosis in the fibrin-in-fibrin treatment group. As previously reported by Dunn et al. (1995), the vast extent of cell death seen within the first four days after transplantation owing to the increase in microglial activation, lymphocyte infiltration and MHC expression [39]. Consequently, the presence of the fibrin-in-fibrin platform as an attenuating barrier between the engrafted cells and host neuro-immune cells facilitates the maturation and establishment of a new terminal network. It is hypothesized that the mature cells that are integrated with the host system might be more resistant to the host immune system. A major loophole of this immuno-histological analysis is that it only provides a gross measure of astrogliosis and microgliosis which pictures the overall immune response generated, but it fails to provide any information about the immune cell activation and the pathways involved.

A crucial factor in the therapeutic application of the fibrin-in-fibrin platform is the multimodal approach to counter the apoptotic triggers discussed earlier. Although, no GDNF staining was detected six weeks post-transplantation due to the short half-life of the GDNF, preliminary analysis performed using NGF in chapter-1 showed that the encapsulation of neurotrophic factor in the fibrin microspheres significantly retained and provided a sustained release in the striatum post-transplantation. This controlled release profile was further modulated using the fibrin gels which achieved an enhanced, site-specific retention of GDNF in the striatum providing the engrafted primary dopaminergic neurons with critical trophic support upon transplantation and throughout target innervation. The improved trophic support resulted in an enhanced graft survival which was reflected in the improvement in the functional outcomes.

There is an established relationship between the degeneration of the dopaminergic system and the disruption of motor function. A unilateral loss of DA system in hemiparkinsonian models can recreate an experimental scenario where pharmacologically induced DA release occurs only on one side. In various rodent models, this imbalance is manifested as a vigorous rotational behaviour after treatment with amphetamine or apomorphine. Spiking of unilateral DA

transmission triggered by the administration of these drugs induces a rotational behaviour towards the side ipsilateral (amphetamine) or contralateral (apomorphine) to the DA abundance. These two drugs are most commonly used to relate the behavioural impact to the extent of lesioning and consequently to test the efficacy of various neuro-reparative and neuro-restorative therapeutics. DA receptor agonists like apomorphine cause the direct stimulation of supersensitive postsynaptic receptors on the lesioned side, which results in contralateral rotations [41]. The elicited rotational behaviour is quantified as turns per minute versus time either manually or in a specially designed 'rotometer' where the animal moves on a spherically shaped surface while connected to the registering device by a thin wire [42–44]. A major proportion of the studies investigating the functional recovery post-treatment with biomaterial interventions have used apomorphine induced rotations for behavioural assessment [42,45–47]. A major drawback of the rotational analysis is the ambiguity resulting from sensitization, conditioning or priming effects and compensation in the rotational behaviour by grafts or therapeutics while the other deficits remain unaddressed [48,49]. Simplicity, reproducibility and ease of automation are the most important advantages of rotation tests which makes them the most frequently used means of behavioural assessment for Parkinson's and its therapy.

A significant reduction in apomorphine-induced contralateral rotations was observed in 6-OHDA lesioned animals after the treatment with lactoferrin (Lf) conjugated PEG-PLGA nanoparticles (Lf-NP) [45]. These nanoparticles were loaded with urocortin peptide which has been reported to arrest the development of 6-OHDA induced PD pathophysiology as reported by Abuirmelh *et al.* [50]. The current study implemented a MFB lesion model of Parkinson's disease where a single injection of the neurotoxin 6-OHDA is usually sufficient to degenerate >90% of dopaminergic neurons [51]. The impact on functional deficits was assessed using apomorphine-induced rotational behaviour as it is a widely used measure of striatal dopamine depletion. The increase in the graft survival was well correlated with the increase in graft functionality in this study. As expected, the delivery of VM cells in the fibrin-in-fibrin intervention group and GDNF-loaded fibrin microspheres resulted in significant behavioural recovery after six weeks post-transplantation, suggesting that all grafts were successfully producing dopamine upon transplantation. The other groups showed an initial improvement in functional analyses, however, there were no significant differences detected between the 6-OHDA treatment and other treatments at six weeks post-implantation. This re-emphasizes the correlation between this enhanced functional recovery and the observed increase in the cell survival and the striatal re-innervation. Similar results were observed for the cylinder test which investigates the spontaneous activity and can be used to investigate the impact of the neuro-

reparative therapies [52]. Similarly, in the spontaneous paw placement tested using the cylinder test, fibrin-in-fibrin treatment group shows significantly less bias in paw-placement as compared to the other treatments. From this functional analyses, it can be concluded that GDNF-loaded fibrin-in-fibrin intervention restores the functional deficits in the parkinsonian model through the protection of engrafted dopaminergic progenitors and successful striatal re-innervation.

Interestingly, this data is in line recent studies of biomaterial approaches to dopaminergic neuron survival after transplantation in the brain. Adil et al. (2017) PNIPAAm-PEG 3D gels to differentiate the hPSCs into dopaminergic neurons which showed a 30 fold increase in survival *in vivo* as compared to the 2D differentiated cells [53]. Another seminal analysis in this field was performed by Moriarty et al. (2017) where they showed the efficacy of the GDNF-functionalized collagen gels for enhancing the survival of dopaminergic progenitors in the 6-OHDA model [38]. However, the multi-modular system applied in the current study provides more control and fine-tuning of the release profile of GDNF, thereby making a longer, sustained release of the neurotrophic factors feasible *in vivo*.

This is the first study to date investigating the impact of a biomaterial system on modulating the tissue glyco-phenotype while mediating a therapeutic impact. This study elaborates on the general trends of glycosylation impacted by the application of the biomaterial intervention. For both striatum and SN, there was a consistent downregulation in sialyl Lewis^x, Lewis^x and alpha-gal linked N-glycans. These moieties have been implicated as key regulators of inflammation and hence, it is hypothesized that the biomaterial intervention maximises the graft survival by modulating the neuro-inflammation promoting glycan cues. With the MALDI-imaging analysis, it was feasible to determine the impact of the fibrin-in-fibrin system on the overall distribution of chief N-glycan biosynthetic classes. As a general observation, the treatment with the therapeutic fibrin-in-fibrin intervention effectively reversed the changes in the brain glyco-phenotype observed as a result of 6-OHDA lesioning.

6.5 Conclusions

A combinatorial, biomaterial-based approach to tackle each of apoptotic triggers post-transplantation harnessing the ability of the scaffold to provide a supportive matrix, increased trophic factor support and the attenuation of the immune response results in a significant improvement in dopaminergic cell survival and effectively reverses the motor function deficits in Parkinson's model. The outcomes of this study highlights the potential of biomaterial

hydrogel scaffolds to improve the functional outcomes of regenerative cell therapies for Parkinson's disease.

6.6 References

- [1] J. Dorszewska, M. Prendecki, M. Lianeri, W. Kozubski, Molecular effects of L-dopa therapy in Parkinson's Disease., *Curr. Genomics.* 15 (2014) 11–7. doi:10.2174/1389202914666131210213042.
- [2] O. Lindvall, A. Björklund, Cell therapy in Parkinson's disease., *NeuroRx.* 1 (2004) 382–93. doi:10.1602/neurorx.1.4.382.
- [3] J.L. Eriksen, Z. Wszolek, L. Petrucelli, Molecular pathogenesis of Parkinson Disease, *Arch. Neurol.* 62 (2005) 353. doi:10.1001/archneur.62.3.353.
- [4] S. Tabbal, S. Fahn, S. Frucht, Fetal tissue transplantation in Parkinson's disease, *Curr. Opin. Neurol.* 11 (1998) 341–349. doi:10.1097/00019052-199808000-00010.
- [5] S.R. Sinclair, J.W. Fawcett, S.B. Dunnett, Delayed implantation of nigral grafts improves survival of dopamine neurones and rate of functional recovery, *Neuroreport.* 10 (1999) 1263–1267. doi:10.1097/00001756-199904260-00020.
- [6] S.R. Sinclair, C.N. Svendsen, E.M. Torres, D. Martin, J.W. Fawcett, S.B. Dunnett, GDNF enhances dopaminergic cell survival and fibre outgrowth in embryonic nigral grafts, *Neuroreport.* 7 (1996) 2547–2552. doi:10.1097/00001756-199611040-00029.
- [7] A.M. Sullivan, J. Pohl, S.B. Blunt, Growth/differentiation factor 5 and glial cell line-derived neurotrophic factor enhance survival and function of dopaminergic grafts in a rat model of Parkinson's disease., *Eur. J. Neurosci.* 10 (1998) 3681–3688. doi:10.1046/j.1460-9568.1998.00378.x.
- [8] P. Brundin, A. Björklund, Survival, growth and function of dopaminergic neurons grafted to the brain., *Prog. Brain Res.* 71 (1987) 293–308. doi:10.1016/S0079-6123(08)61832-4.
- [9] S. Glozman, E. Yavin, Lipid peroxides are generated by the fetal rat brain after episodes of global ischemia in utero, *Neurochem. Res.* 22 (1997) 201–208. doi:10.1023/A:1027371725159.
- [10] R.A. Barker, H. Widner, Immune problems in central nervous system cell therapy,

- NeuroRX. 1 (2004) 472–481. doi:10.1602/neurorx.1.4.472.
- [11] D.R. Lynch, T.M. Dawson, Secondary mechanisms in neuronal trauma, *Curr. Opin. Neurol.* 7 (1994) 510–516. doi:10.1097/00019052-199412000-00007.
- [12] R.S. Ghirnikar, Y.L. Lee, L.F. Eng, Inflammation in traumatic brain injury:role of cytokines and chemokines, *Neurochem. Res.* 23 (1998) 329–340. doi:10.1023/A:1022453332560.
- [13] R.D. Azbill, X. Mu, A.J. Bruce-Keller, M.P. Mattson, J.E. Springer, Impaired mitochondrial function, oxidative stress and altered antioxidant enzyme activities following traumatic spinal cord injury., *Brain Res.* 765 (1997) 283–90. doi:10.1016/s0006-8993(97)00573-8.
- [14] T.J. Collier, C.E. Sortwell, Therapeutic Potential of Nerve Growth Factors in Parkinson's Disease, *Drugs Aging.* 14 (1999) 261–287. doi:10.2165/00002512-199914040-00003.
- [15] C. Mouritzen, M. Drömer, H.O. Keinecke, The effect of fibrin glueing to seal bronchial and alveolar leakages after pulmonary resections and decortications., *Eur. J. Cardiothorac. Surg.* 7 (1993) 75–80. doi:10.1016/1010-7940(93)90184-d.
- [16] G. Zhang, C.T. Drinnan, L.R. Geuss, L.J. Suggs, Vascular differentiation of bone marrow stem cells is directed by a tunable three-dimensional matrix, *Acta Biomater.* 6 (2010) 3395–3403. doi:10.1016/j.actbio.2010.03.019.
- [17] L. Andereggen, M. Meyer, R. Guzman, A.D. Ducray, H.R. Widmer, Effects of GDNF pretreatment on function and survival of transplanted fetal ventral mesencephalic cells in the 6-OHDA rat model of Parkinson's disease, *Brain Res.* 1276 (2009) 39–49. doi:10.1016/j.brainres.2009.04.021.
- [18] M. Espejo, B. Cutillas, E. Arenas, S. Ambrosio, Increased survival of dopaminergic neurons in striatal grafts of fetal ventral mesencephalic cells exposed to Neurotrophin-3 or Glial Cell Line-Derived Neurotrophic Factor, *Cell Transplant.* 9 (2000) 45–53. doi:10.1177/096368970000900107.
- [19] S.B. Dunnett, A. Björklund, Basic neural transplantation techniques. I. Dissociated cell suspension grafts of embryonic ventral mesencephalon in the adult rat brain, *Brain Res. Protoc.* 1 (1997) 91–99. doi:10.1016/S1385-299X(96)00015-3.

- [20] T. Schallert, S.M. Fleming, J.L. Leasure, J.L. Tillerson, S.T. Bland, CNS plasticity and assessment of forelimb sensorimotor outcome in unilateral rat models of stroke, cortical ablation, parkinsonism and spinal cord injury, *Neuropharmacology*. 39 (2000) 777–787. doi:10.1016/S0028-3908(00)00005-8.
- [21] R.-J. Su, J.-L. Zhen, W. Wang, J.-L. Zhang, Y. Zheng, X.-M. Wang, Time-course behavioral features are correlated with Parkinson's disease-associated pathology in a 6-hydroxydopamine hemiparkinsonian rat model., *Mol. Med. Rep.* 17 (2018) 3356–3363. doi:10.3892/mmr.2017.8277.
- [22] T.W. Powers, B.A. Neely, Y. Shao, H. Tang, D.A. Troyer, A.S. Mehta, B.B. Haab, R.R. Drake, MALDI imaging mass spectrometry profiling of N-glycans in formalin-fixed paraffin embedded clinical tissue blocks and tissue microarrays, *PLoS One*. 9 (2014) e106255. doi:10.1371/journal.pone.0106255.
- [23] L.J. Lawson, V.H. Perry, P. Dri, S. Gordon, Heterogeneity in the distribution and morphology of microglia in the normal adult mouse brain., *Neuroscience*. 39 (1990) 151–170. doi:10.1016/0306-4522(90)90229-w.
- [24] A. Członkowska, M. Kohutnicka, I. Kurkowska-Jastrzebska, A. Członkowski, Microglial reaction in MPTP (1-methyl-4-phenyl-1,2,3,6-tetrahydropyridine) induced Parkinson's disease mice model., *Neurodegeneration*. 5 (1996) 137–143. doi:10.1006/neur.1996.0020.
- [25] S.F. Wheeler, P. Domann, D.J. Harvey, Derivatization of sialic acids for stabilization in matrix-assisted laser desorption/ionization mass spectrometry and concomitant differentiation of α (2 \rightarrow 3)- and α (2 \rightarrow 6)-isomers, *Rapid Commun. Mass Spectrom.* 23 (2009) 303–312. doi:10.1002/rcm.3867.
- [26] P. Brundin, O.G. Nilsson, R.E. Strecker, O. Lindvall, B. Astedt, A. Björklund, Behavioural effects of human fetal dopamine neurons grafted in a rat model of Parkinson's disease., *Exp. Brain Res.* 65 (1986) 235–40. doi:10.1007/bf00243848.
- [27] A. Björklund, S.B. Dunnett, U. Stenevi, M.E. Lewis, S.D. Iversen, Reinnervation of the denervated striatum by substantia nigra transplants: Functional consequences as revealed by pharmacological and sensorimotor testing, *Brain Res.* 199 (1980) 307–333. doi:10.1016/0006-8993(80)90692-7.

- [28] E. Dowd, S.B. Dunnett, Deficits in a lateralized associative learning task in dopamine-depleted rats with functional recovery by dopamine-rich transplants, *Eur. J. Neurosci.* 20 (2004) 1953–1959. doi:10.1111/j.1460-9568.2004.03637.x.
- [29] C.W. Olanow, C.G. Goetz, J.H. Kordower, A.J. Stoessl, V. Sossi, M.F. Brin, K.M. Shannon, G.M. Nauert, D.P. Perl, J. Godbold, T.B. Freeman, A double-blind controlled trial of bilateral fetal nigral transplantation in Parkinson's disease, *Ann. Neurol.* 54 (2003) 403–414. doi:10.1002/ana.10720.
- [30] Z. Kefalopoulou, M. Politis, P. Piccini, N. Mencacci, K. Bhatia, M. Jahanshahi, H. Widner, S. Rehncrona, P. Brundin, A. Björklund, O. Lindvall, P. Limousin, N. Quinn, T. Foltynie, Long-term clinical outcome of fetal cell transplantation for Parkinson disease: two case reports., *JAMA Neurol.* 71 (2014) 83–87. doi:10.1001/jamaneurol.2013.4749.
- [31] O. Lindvall, S. Rehncrona, P. Brundin, B. Gustavii, B. Astedt, H. Widner, T. Lindholm, A. Björklund, K.L. Leenders, J.C. Rothwell, R. Frackowiak, D. Marsden, B. Johnels, G. Steg, R. Freedman, B.J. Hoffer, A. Seiger, M. Bygdeman, I. Strömberg, L. Olson, Human fetal dopamine neurons grafted into the striatum in two patients with severe Parkinson's Disease, *Arch. Neurol.* 46 (1989) 615. doi:10.1001/archneur.1989.00520420033021.
- [32] T.J. Mahalik, W.E. Hahn, G.H. Clayton, G.P. Owens, Programmed cell death in developing grafts of fetal substantia nigra, *Exp. Neurol.* 129 (1994) 27–36. doi:10.1006/EXNR.1994.1144.
- [33] C.E. Sortwell, M.R. Pitzer, T.J. Collier, Time course of apoptotic cell death within mesencephalic cell suspension grafts: implications for improving grafted dopamine neuron survival, *Exp. Neurol.* 165 (2000) 268–277. doi:10.1006/EXNR.2000.7476.
- [34] P.J. Reddig, R.L. Juliano, Clinging to life: cell to matrix adhesion and cell survival, *Cancer Metastasis Rev.* 24 (2005) 425–439. doi:10.1007/s10555-005-5134-3.
- [35] T.A.E. Ahmed, R. Ringuette, V.A. Wallace, M. Griffith, Autologous fibrin glue as an encapsulating scaffold for delivery of retinal progenitor cells, *Front. Bioeng. Biotechnol.* 2 (2015) 85. doi:10.3389/fbioe.2014.00085.
- [36] M.A. Chernousov, D.J. Carey, α V β 8 integrin is a Schwann cell receptor for fibrin, *Exp.*

- Cell Res. 291 (2003) 514–524. doi:10.1016/S0014-4827(03)00409-9.
- [37] A. Salsmann, E. Schaffner-Reckinger, F. Kabile, S. Plançon, N. Kieffer, A new functional role of the fibrinogen RGD motif as the molecular switch that selectively triggers integrin α IIb β 3-dependent RhoA activation during cell spreading., *J. Biol. Chem.* 280 (2005) 33610–9. doi:10.1074/jbc.M500146200.
- [38] N. Moriarty, A. Pandit, E. Dowd, Encapsulation of primary dopaminergic neurons in a GDNF-loaded collagen hydrogel increases their survival, re-innervation and function after intra-striatal transplantation, *Sci. Rep.* 7 (2017) 16033. doi:10.1038/s41598-017-15970-w.
- [39] J. Samal, D.B. Hoban, C. Naughton, R. Concannon, E. Dowd, A. Pandit, Fibrin-based microsphere reservoirs for delivery of neurotrophic factors to the brain, *Nanomedicine.* 10 (2015) 765–783. doi:10.2217/nmm.14.221.
- [40] W.M. Duan, H. Widner, P. Brundin, Temporal pattern of host responses against intrastriatal grafts of syngeneic, allogeneic or xenogeneic embryonic neuronal tissue in rats., *Exp. Brain Res.* 104 (1995) 227–42. doi:10.1007/bf00242009.
- [41] U. Ungerstedt, Postsynaptic supersensitivity after 6-Hydroxy-dopamine induced degeneration of the nigro-striatal dopamine system, *Acta Physiol. Scand.* 82 (1971) 69–93. doi:10.1111/j.1365-201X.1971.tb11000.x.
- [42] Z. Wen, Z. Yan, K. Hu, Z. Pang, X. Cheng, L. Guo, Q. Zhang, X. Jiang, L. Fang, R. Lai, Odorranalectin-conjugated nanoparticles: Preparation, brain delivery and pharmacodynamic study on Parkinson's disease following intranasal administration, *J. Control. Release.* 151 (2011) 131–138. doi:10.1016/J.JCONREL.2011.02.022.
- [43] U. Ungerstedt, G.W. Arbuthnott, Quantitative recording of rotational behavior in rats after 6-hydroxy-dopamine lesions of the nigrostriatal dopamine system, *Brain Res.* 24 (1970) 485–493. doi:10.1016/0006-8993(70)90187-3.
- [44] R. Iancu, P. Mohapel, P. Brundin, G. Paul, Behavioral characterization of a unilateral 6-OHDA-lesion model of Parkinson's disease in mice, *Behav. Brain Res.* 162 (2005) 1–10. doi:10.1016/J.BBR.2005.02.023.
- [45] K. Hu, Y. Shi, W. Jiang, J. Han, S. Huang, X. Jiang, Lactoferrin conjugated PEG-PLGA nanoparticles for brain delivery: Preparation, characterization and efficacy in

- Parkinson's disease, *Int. J. Pharm.* 415 (2011) 273–283. doi:10.1016/J.IJPHARM.2011.05.062.
- [46] C. Saraiva, J. Paiva, T. Santos, L. Ferreira, L. Bernardino, MicroRNA-124 loaded nanoparticles enhance brain repair in Parkinson's disease, *J. Control. Release.* 235 (2016) 291–305. doi:10.1016/J.JCONREL.2016.06.005.
- [47] Y.-Z. Zhao, R.-R. Jin, W. Yang, Q. Xiang, W.-Z. Yu, Q. Lin, F.-R. Tian, K.-L. Mao, C.-Z. Lv, Y.-X.J. Wáng, C.-T. Lu, Using gelatin nanoparticle mediated intranasal delivery of neuropeptide Substance P to enhance neuro-recovery in hemiparkinsonian rats, *PLoS One.* 11 (2016) e0148848. doi:10.1371/journal.pone.0148848.
- [48] S.B. Dunnett, I.Q. Whishaw, D.C. Rogers, G.H. Jones, Dopamine-rich grafts ameliorate whole body motor asymmetry and sensory neglect but not independent limb use in rats with 6-hydroxydopamine lesions., *Brain Res.* 415 (1987) 63–78.
- [49] J.M. Klug, A.B. Norman, Long-term sensitization of apomorphine-induced rotation behavior in rats with dopamine deafferentation or excitotoxin lesions of the striatum., *Pharmacol. Biochem. Behav.* 46 (1993) 397–403.
- [50] A. Abuirmeileh, R. Lever, A.E. Kingsbury, A.J. Lees, I.C. Locke, R.A. Knight, H.S. Chowdrey, C.S. Biggs, P.S. Whitton, The corticotrophin-releasing factor-like peptide urocortin reverses key deficits in two rodent models of Parkinson's disease, *Eur. J. Neurosci.* 26 (2007) 417–423. doi:10.1111/j.1460-9568.2007.05653.x.
- [51] E.B. Torres, K.M. Heilman, H. Poizner, Impaired endogenously evoked automated reaching in Parkinson's disease., *J. Neurosci.* 31 (2011) 17848–17863. doi:10.1523/JNEUROSCI.1150-11.2011.
- [52] K.E. Glajch, S.M. Fleming, D.J. Surmeier, P. Osten, Sensorimotor assessment of the unilateral 6-hydroxydopamine mouse model of Parkinson's disease., *Behav. Brain Res.* 230 (2012) 309–316. doi:10.1016/j.bbr.2011.12.007.
- [53] M.M. Adil, G.M.C. Rodrigues, R.U. Kulkarni, A.T. Rao, N.E. Chernavsky, E.W. Miller, D. V. Schaffer, Efficient generation of hPSC-derived midbrain dopaminergic neurons in a fully defined, scalable, 3D biomaterial platform, *Sci. Rep.* 7 (2017) 40573. doi:10.1038/srep40573.

Chapter 7

Summary and Future Directions

7.1 Introduction

Parkinson's disease is the second most prevalent, chronic neurodegenerative disorder affecting about 0.1 and 0.2% of the population [1]. PD affects 1% of the population above 60 years and its prevalence increases with the increase in age with males being more susceptible to PD than females. The underlying neuropathology involves the formation of α -synuclein-containing proteomic inclusions called Lewy bodies and loss of dopaminergic neurons in the substantia nigra (SN) translating to reduced facilitation of voluntary movements. Unfortunately, to date, all the available treatments for Parkinson's disease are solely symptomatic and do not address the underlying process of neurodegeneration. The current 'platinum standard' in this area for PD treatment is the dopamine precursor, Levodopa which came into the therapeutic arena over 60 years ago [2]. The most significant impediment to successful long-term therapeutic use of Levodopa, despite of its cost-effectiveness and excellent results in the early stage disease management, is its failure to address the full spectrum of parkinsonian symptoms, as well as its declining effectiveness over time [3]. This highlights the major unmet clinical need for new and improved therapies to repair the prevailing neurodegenerative milieu in the brain and provide significant motor function recovery in the patients.

The relatively selective loss of dopaminergic neurons from the nigrostriatal pathway makes Parkinson's disease an ideal candidate for cell replacement therapies. To date, several cell sources have been investigated as potential candidates for cellular therapy in PD. However, the transplantation of dopamine neuron-rich fetal ventral mesencephalon (VM) grafts which have been shown to both survive and re-innervate the striatum post-transplantation, whilst also restoring motor function [4–6] remains the gold standard. A major obstacle in the translation of VM cells as a potential restorative approach for Parkinson's disease despite long-term symptomatic relief in patients is poor survival post-transplantation, which calls for an unethically high number of fetal donors for a successful transplant.[7]. An effective rejoinder to this issue can be the use of biomaterial therapy to augment the cell survival *in vivo* and improve the brain repair approaches for Parkinson's disease. Biomaterials refer to the engineered materials designed to interact with cellular/living for therapeutic purposes, have the potential to substantially enhance the engrafted cell survival. Carefully tailored biomaterials can serve as an ambidextrous solution to provide a supportive matrix to the transplanted cells, and can also be functionalised for the delivery of therapeutic molecules to promote the survival, axonal outgrowth and connectivity of transplanted cells. In particular, natural biomaterials,

such as fibrin, collagen etc. have the leverage of being remarkably similar to the body's native tissue, are biodegradable, and able to promote the cellular adhesion and proliferation. Fibrin is also capable of forming *in situ* gelling (and therefore injectable) hydrogels, thus making it an attractive candidate for improving cell replacement therapies in neurodegenerative disorders such as PD. Furthermore, fibrin-derived biomaterials have the benefit of already having clinical approval for a wide variety of applications. Keeping this in mind, the project described in this thesis sought to determine the impact of an injectable, growth factor-loaded fibrin-in-fibrin intervention on the survival, integration and efficacy of transplanted dopaminergic neurons and thus to highlight on the neuroreparative potential of biomaterials to improve cellular therapies in PD and other neurodegenerative diseases.

A better knowledge of the tissue glycoenvironment in both the healthy and the neurodegenerative brain is imperative to design a responsive biomaterial intervention to provide an optimal regenerative microenvironment. Such an environment will facilitate regeneration by maximising the cell-cell and cell-matrix interactions and minimising the inflammatory signalling. The overall goal of this project was to develop a regenerative strategy for enhancing the graft survival in a PD model by using biomaterials that aim at promoting the survival and integration of engrafted neurons in the host neural circuitry while attenuating inflammation in a relevant *in vivo* disease model and subsequently modulating the brain glycoenvironment, inflammatory and regulatory signalling to bring about motor function recovery in the 6-OHDA PD model (**Figure 7.1**).

7.2 Summary

7.2.1 Phase I- Fibrin-based hollow reservoirs for neurotrophic factor delivery

The *in vivo* therapeutic potential of neurotrophic factors to modify neuronal dysfunctions is limited by the short half-life of these factors. A biomaterials-based intervention, which protects these factors and allows a controlled release, is therefore required. Fibrin as a biomaterial offers the advantage of being an autologous substrate where the rate of polymerization and degradation can be well controlled. This study (**Chapter 2**) was aimed at using the template charge manipulation [8] to fabricate hollow fibrin microspheres as a reservoir for controlled delivery of the neurotrophins *in vivo*. The hollow microspheres were physically characterized and protein loading and release from the microspheres were demonstrated using NGF as a model neurotrophin. Fibrin microspheric reservoirs showed high loading efficiency (>80%) for the different sizes and dosage of NGF tested. No adverse impact of fibrin microspheres on cell

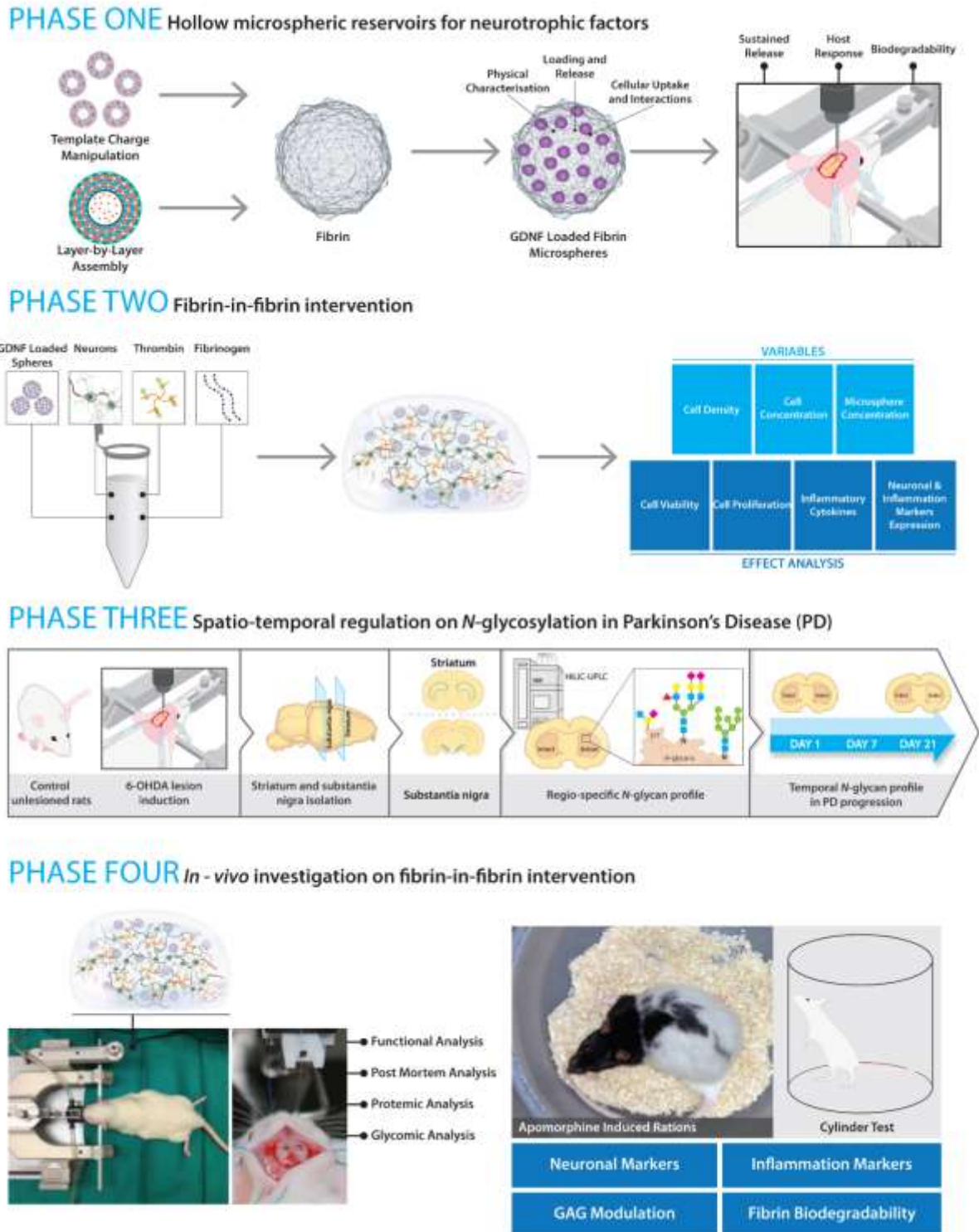


Figure 7.1: Schematic representation of the milestones achieved during the study. Each phase of study is correlated towards the development of a biomaterial intervention to promote graft survival in a PD model

viability was detected with rat mesenchymal stem cells (rMSCs), PC-12 and foetal ventral mesencephalon (VM) cells. Bioactivity of the released NGF was demonstrated by neuronal outgrowth assay in PC-12 cells followed by *in vivo* assessment for NGF release and host response. Neurotrophin encapsulation into the microspheres did not alter its bioactivity. Controlled release of NGF was observed from hollow fibrin spheres in the *in vivo* study over a period of 14 days. Very importantly, the immune response obtained in response to NGF, spheres and NGF-loaded spheres was comparable demonstrating the absence of any exaggerated host response to the microspheres in the brain.

7.2.2 Phase II- Fibrin-in-fibrin intervention for enhanced VM graft survival

Progenitor cell therapies in PD aiming at replacement of lost dopaminergic neurons are limited by poor cell survival and limited reinnervation of host tissue following transplantation. This hinders their clinical progression. To address this limitation, the modification of the cellular milieu in terms of biophysical properties and/or biochemical cues like neurotrophins could enhance the survival of transplanted cells in the host. This study (**Chapter 3**) aimed at developing an injectable biomaterial-based intervention which would improve the survival of engrafted dopaminergic progenitor cells by providing adequate physical and trophic support through controlled spatio-temporal release of glial-cell derived neurotrophic factor (GDNF). The therapeutic potential of GDNF, one of the most effective neuroprotective trophic factor identified through preclinical trials [9,10], is limited by its short half-life. This study catered to the fabrication and characterisation of a fibrin-based reservoir system using layer-by-layer assembly, investigating the loading and release of GDNF using ELISA and to examine the cellular behaviour on tuneable parameters such as hydrogel concentration, cell density and microsphere concentration. Fibrin hydrogel of different concentrations (10, 20, 30 and 60 mg/ml) were embedded with varied concentrations of microspheres (0.05, 0.1, 1 and 10 $\mu\text{g/gel}$) to obtain an ECM-based controlled release system. Cell densities $0.1 \times 10^5/\text{mL}$, $1 \times 10^5/\text{mL}$, $5 \times 10^5/\text{mL}$ and $10 \times 10^5/\text{mL}$ VM cells were embedded in the fibrin hydrogel. Cells were tested for viability, proliferation and apoptosis using flow cytometry. Morphology and survival of dopaminergic neurons and inflammatory cells was investigated by immunostaining for cellular markers (tyrosine hydroxylase (TH), β -Tubulin, glial fibrillary acidic protein (GFAP) followed by confocal microscopy and RT-PCR. The modulation of the pro-and anti-inflammatory cytokine profile of VM cells in hydrogel was analysed using an inflammation array to select an optimally supportive ECM-based tuneable biomaterial platform for delivery of VM cells in a Parkinson's model. The hydrogel microenvironment was optimized in terms of the hydrogel

(20mg/ml), cells (5×10^5 cells/gel) and microsphere concentration (1 μ g/gel) to best support the survival of VM grafts by providing sustained trophic support and modulating the interplay of pro-and anti-inflammatory cytokines. This study describes the characterization of the fibrin-in-fibrin intervention as a 3D cell culture tool to assess the CNS-tailored biological response as a function of cell-matrix and cell–cell interactions.

7.2.3 Phase III- Complete spatial resolution of rodent brain N-glycans

Cell surface *N*-glycans are involved in several essential cellular functions including cellular and cell–matrix interactions. Alteration in *N*-glycosylation could fundamentally alter the structure and function of the glycoprotein. The cardinal role of *N*-glycans for the nervous system is brought forth by congenital glycosylation diseases, resulting in different neuropathological symptoms like mental retardation, seizures and epilepsy. Previous studies have reported the conservation of *N*-glycan processing in rodents [11]. However, there was a lack of spatial resolution of these glycan profiles as the tissue samples were homogenized intact for these studies or specific proteins were picked up for analysis of glycosylation. Since the biosynthesis of *N*-glycans undergoes a stringent spatio-temporal regulation within the tissue, this study (**Chapter 4**) aimed at the spatial resolution of *N*-glycans isolated from the striatum and SN to give an insight into their involvement in regulation of striatal and nigral cues for establishment and pathophysiological degeneration of neural circuitry in Parkinson's disease. This is the first spatio-specific glyco-analytical platform to thoroughly describe both neutral and charged *N*-glycans in both the striatum and SN of the rodent brain. Combined with LC-MS detection, HILIC-UPLC enabled simultaneous observation and quantification of both high- and low-abundance *N*-glycans. In this study, this multi-faceted analysis with a series of exoglycosidase digestions enabled the detection of over 170 *N*-glycan isomers for both the striatum and SN, originating from over 100 distinct *N*-glycan compositions. The most abundant glycans in both the striatum and SN were oligomannose or fucosylated complex type, though varying amounts of glycans were detected from all biosynthetic classes. A very important feature for the hybrid neutral glycans detected in both the striatum and SN was the presence of Lewis^x determinant characterised by the presence of outer arm $\alpha(1,3)$ -fucosylation. A major fraction of detected *N*-glycans for both the striatum and SN was the fucosylated complex and hybrid type glycans (Striatum: 55%, SN: 53%). These included both unsialylated and sialylated fucosylated glycans and were followed in predominance by oligomannose type (Striatum: 36%, SN: 41%) and hybrid type (Striatum: 5%, SN: 3%). More importantly, this comprehensive and reproducible regio-specific profiling of the brain glycome could provide significant insights

and serve as a baseline for the identification of biomarkers and their regulation in neurodegenerative diseases.

7.2.4 Phase IV- Modulation of brain glyco- signature with the 6-OHDA induced Parkinsonism

The time course modulation *N*-glycosylation was further investigated using an *in vivo* study using Sprague–Dawley rats over a period of 21 days. Both the striatum and SN from diseased animals and healthy controls were analysed using HILIC-UPLC and the trends of *N*-glycosylation were visually represented and quantified by using matrix-assisted laser desorption ionization –mass spectrometric imaging (MALDI-MSI). These results were then counter-confirmed using lectin histochemistry. In addition to outlining the changes in *N*-glycosylation typical of the eventual PD phenotype, the glycophenotype of a disease-intermediate state characterising the glycophenotype of disease progression was also profiled and mapped. Significant changes were detected in GP 20 and 25 for the striatum and GP 24 for the SN that are not detectable at day 21. Furthermore, GP 11 that was found to be significantly altered in both the striatum and SN at day 21 did not show any significant difference when analysed in the day 7 sample cohort. There was an observed increase in the fucosylation in both the striatum and SN. Another important observation in this analyses was the decrease in sialylation. The current study found this trend to be concomitant in the rodent brains as well where there was a significant decrease in sialylation associated with the tri-antennary glycan species. In addition to sialylation and fucosylation, there was a significant increase in the oligomannose glycans which was detected at both day 7 and day 21 post 6-OHDA administration in the rodent brains. To the best of our knowledge, this is the first study that elucidate the spatio-temporal changes in overall *N*-glycosylation in the striatum and SN of the 6-OHDA PD model.

7.2.5 Phase V- Fibrin-in-Fibrin intervention for enhanced graft survival and glyco-modulation in 6-OHDA Parkinson's model

Cellular regenerative therapies offer a promising solution for progressive neurodegenerative disorders like Parkinson's disease (PD) where the cardinal pathology is the loss of dopaminergic neurons in the SN. Extensive pre-clinical and clinical assessment has shown that, when transplanted into the Parkinsonian brain, primary dopaminergic neurons can survive, integrate with the host system, produce dopamine and provide functional recovery. However, their widespread use as a routine clinical procedure is hindered by their extremely poor survival after transplantation and the subsequent requirement to use multiple fetal donors for each

Parkinson's disease patient. Injectable biomaterial scaffolds, particularly collagen hydrogels, have the potential to improve the engraftment of encapsulated cells through the provision of a supportive and growth factor-rich environment while providing the necessary immunoisolation. In this study (**Chapter 6**) the effect of a glial-derived neurotrophic factor (GDNF)-loaded fibrin-in-fibrin injectable system on the survival and efficacy of dopaminergic neurons after transplantation into the Parkinsonian brain is investigated. The fibrin-in-fibrin platform fabricated and characterized in Chapter 3 was tested in a 6-OHDA PD model. In brief, we found that the fibrin-in-fibrin platform did not evoke an unfavourable, exaggerated host response in the brain and supported the survival and neural outgrowth of encapsulated cells. The encapsulation of GDNF in fibrin microspheres and further in fibrin gel resulted in a significantly greater retention of striatal GDNF immediately post-transplantation. There was a significant five-fold increase in the embryonic day (E) 14 VM cells in a GDNF-loaded fibrin-in-fibrin intervention and functional recovery observed in the rotational and limb placement analyses. In conclusion, GDNF functionalized fibrin-in-fibrin intervention can improve the efficacy of primary dopaminergic neuron cell replacement therapies in Parkinson's disease by providing cells with a supportive matrix, trophic factor support upon transplantation and the attenuation of the host immune response to help the transplanted neurons survive and integrate into the host neuronal circuitry.

7.3 Limitations

7.3.1 Phase I- Fibrin-based hollow reservoirs for neurotrophic factor delivery

This chapter dealt with the fabrication and characterisation of hollow fibrin microspheres as reservoirs for neurotrophic factors for the *in vivo* delivery. The template method was used to form fibrin hollow spheres. A coating of fibrin is formed around a polystyrene bead, which is then removed by washing with a solvent, THF. FTIR measurements showed that the characteristic peaks of polystyrene were removed by THF treatment. However, FTIR is a surface measurement, with a depth typically on the order of about 1 μm . Thus, if there were any polystyrene remnants left behind due to the partial dissolution by THF treatment, these may not show up on the FTIR analysis. To minimise this possibility, multiple THF washes were performed. In addition, SEM and TEM analysis showed the absence of a solid core, consistent with the removal of polystyrene. Despite this, the possibility that small amount of polystyrene was not removed cannot be discounted.

The method for fabrication of microspheres was not pursued further in the studies due to the unforeseen changes in the template properties, due to which the batch-to-batch variation

amongst the microspheres was very high. However, similar hollow fibrin microspheres were fabricated using the layer-by-layer assembly (Chapter 3) and were thoroughly characterized before application in an *in vivo* setting. These microspheres showed comparable loading and release profiles and did not have any adverse impact on the cellular survival or metabolic activity.

7.3.2 Phase II- Fibrin-in-fibrin intervention for enhanced VM graft survival

In phase II, a fibrin-in-fibrin intervention to maximise the graft survival was optimized *in vitro*. Here, the *in vitro* release profile of the fibrin-in-fibrin intervention was characterised. However, the presence of a plethora of enzymes and proteases capable of degrading the implanted fibrin system *in vivo* will accelerate the release. A definitive link between the *in vitro* and *in vivo* release profile will aid in future optimisation of the system. An *in vivo* release analysis using *in vivo* imaging techniques would establish a definitive correlation between *in vitro* and *in vivo* release kinetics, and enable further development and optimisation of the system *in vitro*. GDNF release *in vivo* from fibrin-in-fibrin system was however quantified in the 6-OHDA model in Chapter-6.

7.3.3 Phase III & IV- Complete spatial resolution of rodent brain N-glycans and Modulation of brain glyco- signature with the 6-OHDA induced Parkinsonism

Phase III and IV investigated the overall N-glycome and its modulation in the striatum and SN of the healthy animals and the PD model. The chief limitation of the HILIC-UPLC analysis performed for feature analysis was that only the major glycan constituents of each peak were considered the representative feature for that peak. The glycosylation traits were calculated from the sum of glycan peaks (GP1-GP26) each of which combined the glycans with the same structural features. An inherent limitation of such an approach is the inability to include the features detected in trace amounts like phosphorylation etc. However, such features were reported based on the exoglycosidase and an extensive MALDI-MSI analyses in Chapter-4. Also, due to the incomplete digestion by some exoglycosidases, it was difficult to identify the bisects from the antenna as well as $\alpha(1-3/4)$ linked fucose from $\alpha(1-2)$ fucose.

An inherent limitation of the MALDI analyses is the generation of structural fragments due to in source decay. While performing a spot MALDI analyses of glycans, this can be leveraged as pseudo MS3 for structural elucidation [12]. This is particularly challenging in the imaging studies, as it is practically impossible to determine an intact structure produced by the native protein versus the fragmented structure caused by instrumentation. Detection of the sialic acids is a particularly difficult as these readily cleave under even low source energy. MALDI-FT-

ICR instruments usually compensate for this problem by incorporating a built-in cooling nitrogen gas stream into the source, limiting the loss of labile sialic acid by in source decay [13,14]. Further investigation into the impact of the ipsilateral vs contralateral N-glycosylation due to the 6-OHDA lesioning would give an insight into the lesion-specific changes in brain glycosylation.

7.3.4 Phase V- Fibrin-in-Fibrin Intervention for Enhanced Graft Survival and Glyco-modulation in 6-OHDA Parkinson's Model

This phase dealt with the investigation of the optimised fibrin-in-fibrin system in a PD model and investigates the modulation of the tissue glycome by the biomaterial intervention. The chief limitation in this analysis was the inability to quantify the exact implanted neurons survival except with a correlation to increased striatal reinnervation and functional improvement. This is slightly offset by the fact that there was an almost complete loss of TH+ cells in the 6-OHDA treatment without any therapeutic intervention. All the analyses were performed with the diseased controls as the baseline.

Another very important limitation of this study was the disease model used for the investigation. As it has been well established in the previous studies, the 6-OHDA model does not manifest all pathological and clinical features of human parkinsonism [15]. The chief pathological hallmark of human PD, i.e. the formation of cytoplasmatic inclusions (Lewy bodies), is not manifested in the 6-OHDA lesions. A major issue with the 6-OHDA as a neurotoxin is that it does not affect other brain areas involved in PD, such as in anterior olfactory structures or lower brain stem areas [16]. The motor dysfunctions typical of PD such as parkinsonian-like tremor are rarely expressed in the studies of 6-OHDA-lesioned rodents with the occasional akinesia and rigidity in the rats [17]. The limitation of the disease model is well acknowledged in the study. The 6-OHDA rat model is, however, the most suited model to validate our experimental therapies because it is the best characterised animal model of Parkinson's disease. There are several behavioural tests in place for testing motor impairments and brain repair in this model.

The modulation of N-glycosylation was investigated through the MALDI-MSI and thus the inherent limitations of the instrumentation and methodology were applicable here. However, the trends of glycosylation were also counter-confirmed by lectin histochemistry in the current analysis.

7.4 Future directions

Several research questions have stemmed from the results obtained in this project that need further investigation to explicate the mechanistic aspects. The first project involves the application of the fibrin-in-fibrin system for the therapeutic delivery of exosomes to promote neuro-regeneration in pre-clinical models of PD. The second project describes the development of the iPSCs-seeded 3D fibrin microgels to direct their differentiation into dopaminergic neurons. Third project deals with the development of more reactive and progressive delivery systems using glycan functionalisation to promote tissue repair and graft survival. A quantitative glycoproteomic analysis will be very instrumental in identifying the suitable disease markers that can be potentially modulated using biomaterial therapy.

7.4.1 Delivery of Mesenchymal Stem Cell (MSCs) and Dendritic Cell (DC) Derived Exosomes

A significant obstacle for about 98% of all potent drugs that may improve therapy for various central nervous system (CNS) disorders to be clinically translated is their inability to cross the BBB [18]. Multiple drug nanoformulations have been designed to overcome the BBB for the therapeutic delivery to the brain [19]. Unfortunately, dispensing of drug-delivery systems in the bloodstream has two major issues: systemic toxicity and rapid clearance by the mononuclear phagocyte system [20]. Ideal brain-delivery systems should elude the immune system and have a longer half-life in the circulation system for therapeutic cargo delivery. Interestingly enough, all these desired characteristics are found in the exosomes which may function as a “stealth cloak” for effective therapeutic delivery to the brain; minimise the clearance by MPS and increase drug transport to the brain [21,22].

Exosomes derived from different cellular sources (bone marrow, mesenchymal stem cells, dendritic cells and others) or engineered to deliver select cargo (therapeutic proteins, RNA and others) effectively deliver the cargo across the blood-brain barrier to the brain while affecting immunomodulation. The ability of exosomes to act as a highly efficient reservoir for therapeutic delivery in both local and systemic settings makes them an ideal delivery platform to alleviate a wide range of neuropathologies. Exosomes can be genetically tailored to package mRNA, siRNA, proteins, and drugs and subsequently be used for the RNAi therapy, immunotherapy, and drug delivery. A detailed study of the engineering of natural exosomes for targeted delivery to the brain was performed by Alvarez-Erviti et al where they provided the proof-of-concept that exogenous RNA could be efficiently delivered using the RNA

transporting characteristic of exosomes. The cell source in this case was immature DCs which were transfected with a plasmid coding for the exosomal membrane protein, Lamp2b, with the RVG targeting peptide inserted in the frame between amino acid residues 39 and 40 [23]. When this cascade is expressed, RVG derived from the rabies virus glycoprotein binding to acetylcholine receptors expressed on the BBB and on neuronal cells is expressed on the surface of exosomes in association with Lamp2b [24]. Exosomes were then purified using the self-derived DCs transfected with this fusion plasmid and GAPDH siRNA cargo was loaded onto them using electroporation which, upon administration, resulted in specific knockdown of GAPDH in the cortex, striatum and midbrain. The reproducibility and efficacy of this approach was further tested by the delivery of BACE-1 siRNA. This resulted in specific and highly significant BACE-1 gene knockdown (60%) which correlated with reduced accumulation of A β 1-42 produced by BACE-1 in the mouse brain cortex. Being derived from immature DCs, these exosomes showed negligible toxicity or immunogenicity on repeated administration, which is a very important advantage considering that the clinical applications would require multiple administrations of the therapeutic cargo. Exosomal cargo has been shown to mediate neuronal protection, regeneration and synaptic plasticity while delivering the regulatory elements to neurological injury sites that promote tissue regeneration and cause functional recovery [25–28]. The potential of exosomes to attenuate the neuro-inflammation and/ mediate the modulation of the active genetic players in PD pathophysiology can be harnessed in a modular hydrogel-based platform (**Figure 7.2**). MSC- and DC- derived exosomes embedded in a three-dimensional hydrogel can be tested for dose-dependent enhancement of neuro-reparative strategies for PD.

7.4.2 Directed Differentiation of Human-Induced Pluripotent Stem Cells to Dopaminergic Cells on Microgels

Induced pluripotent stem (iPS) cells are the outcome of somatic cell reprogramming that brings back cells like fibroblasts to an embryonic-like state by the introduction of a carefully optimised set of transcription factors and culture conditions [29]. A major appeal of the use of the iPSC- cell technology is that it obviates the use of embryonic cells by direct conversion of somatic cells into pluripotent cells. This is a very exciting avenue for cellular therapies as it eliminates any ethical issues associated with the procurement of the embryonic cells. Besides, it opens up a whole new arena of patient-specific cell therapies given that iPS cells can be derived from the patient to be treated and thus are genetically identical cells that would avoid immune rejection.

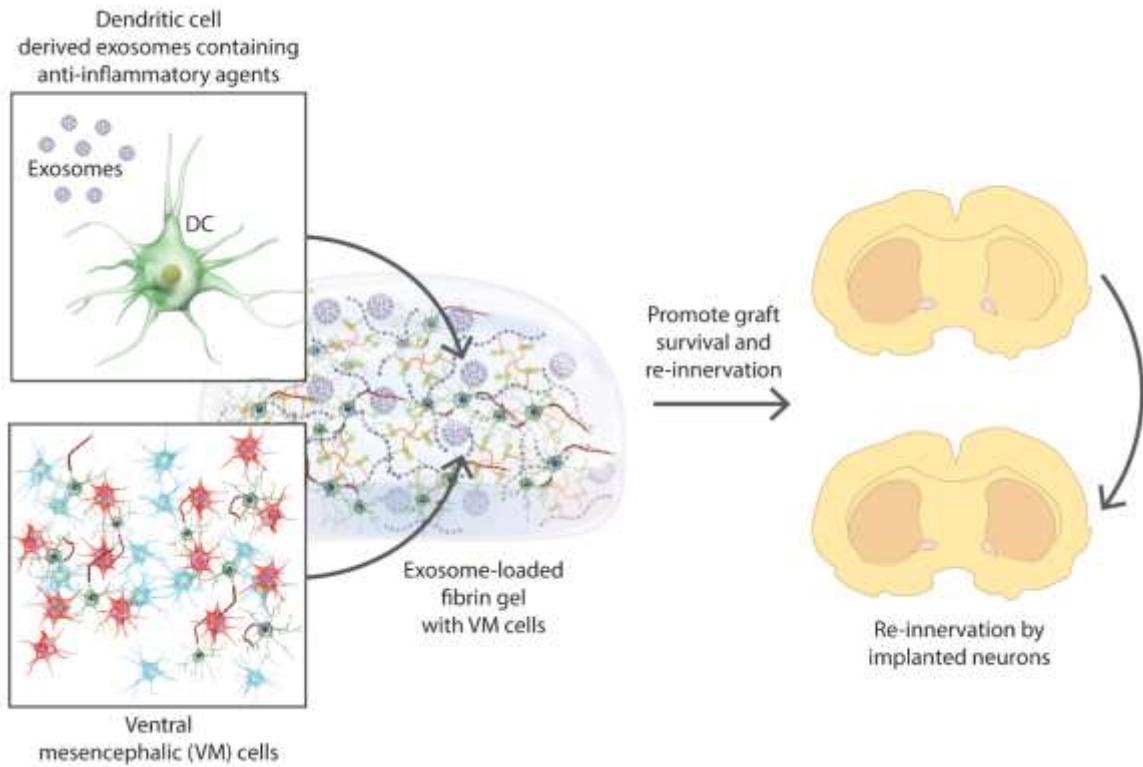


Figure 7.2: Schematic representing the combinatorial biomaterial therapy for augmenting the VM cell survival and promoting functional repair by minimising the neuro-inflammation by modulating the cellular paracrine response.

A pioneering study by Wernig et al. (2008) showed that iPSCs can differentiate into dopamine neurons of midbrain character through reprogramming, and that they restored the normal rotational behaviour in an 6-OHDA rat model of Parkinson's disease after intra-striatal transplantation with enhanced survival and integration with the host system [29]. Another seminal study by Kikuchi *et al.* (2017) reported a long-term analysis of human iPS cell-derived dopaminergic neurons in MPTP non-human primate PD model [30]. Functional analyses revealed an increase in spontaneous movement of the monkeys after transplantation and consistent striatal innervation was detected irrespective of the cell sources (healthy vs diseased animals). A major issue related to the use of iPSC-derived transplants is the use of viral vectors to insert the relevant genes into the genome at multiple sites during re-programming, significantly impairing iPSCs' clinical compatibility. Soldner et al (2009) circumvented this issue by manufacturing hiPSCs free of viral reprogramming using Cre-recombinase excisable viruses and the hiPSCs maintained a pluripotent state with a global gene expression profile closer to that of hESCs . Since a specific differentiation of iPSCs into A9 dopaminergic neurons is feasible, it gives iPSCs an unequalled advantage of biological relevance for use as a PD model to verify the understanding of disease mechanisms operative in PD harvested from cellular or animal models and pathological studies in live DA neurons [29]. Using iPSC-derived DA neurons from PD patients with mutations in the genes implicated in PD neuropathology, several mechanistic insights into how mutations of these genes are linked to PD have been deduced. The derivation of the midbrain dopaminergic neurons on a 3-D microgel platform can therefore be used as a human disease model for PD. 3D-platform propagated iPSCs can be also utilised to probe the mechanism, and serve as an 'in vivo' platform for drug screening and for cell-replacement therapies (**Figure 7.3**).

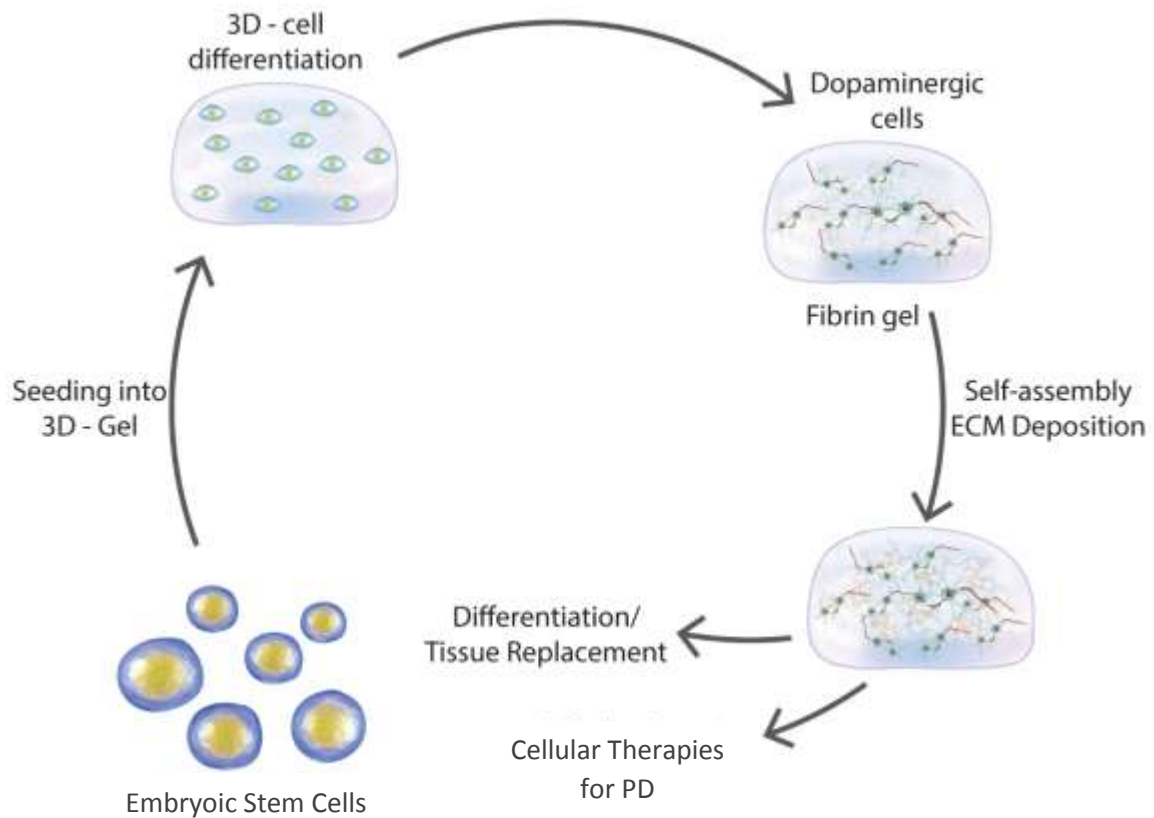


Figure 7.3: Schematic representing the directed differentiation of human iPSCs on a 3D fibrin gel platform to VM cells to form a cellular ‘micro-graft’ for testing the potency of cellular therapies in a PD model.

7.4.3 Glyco-engineered Hydrogel System

Glycans mediate several crucial physiological activities where they act as bearer of bio-code, immune recognition executors and functional regulators. There is increasing evidence that glycans and their interactions with glycan-specific binding proteins regulate and mediate several important physiological processes including cellular communication and adhesion, immune response, metabolism and so forth. A minor alteration in the glycan composition or structure could result in significant modulation of the protein conformation and function as represented by the terminal saccharides of the glycoprotein antigen identifying the blood groups [31] or by inhibition of branching of N-glycans retarding the tumor development [32].

To elucidate the role of glycosylation on cell fate regulation, there are several studies that have used mono-, di- and oligosaccharides to functionalise synthetic or natural bioactive materials and investigated the biological significance of the functionalisation as therapy. Intriguing results were obtained by glycosylating collagen by reductive amination with maltose where the exposed α -Glc residue induced differentiation in F11 neuroblastoma cells and restored the functional neuronal activity with the transmission of the electric signal [33]. A forthcoming challenge is to construct of glyco-engineered materials capable of recognizing and responding to these tissue-specific glycan cues. The intrinsically complicated compositions and structures as well as the high microheterogeneity of glycans makes the development of glycan-responsive materials with a high sensitivity, reproducibility and specificity an especially challenging goal.

A significant aspect addressed in this thesis (Chapter 4 & 5) was investigation of the glycosylation profiles of both healthy and Parkinsonian brains that gave ample information about the differential modulation of traits of glycosylation in the diseased brains. Once identified, these glycans can be orchestrated as heterogenous glycoclusters and delivered for burst release or controlled release using fibrin microspheres. Another approach to address the aberrant glycosylation patterns prevalent in PD brains will be the use of these glycan-bioengineered microgels as cell delivery vehicles. Yet another way to approach the therapeutic glyco-modulation to assist tissue repair will be the encapsulation and localized delivery of the 'glycozymes' (**Figure 7.4**). A number of metabolic enzymes like sialyltransferases, fucosyltransferases etc. have been shown to be implicated in neurodegenerative disease pathophysiology [34,35] and their therapeutic delivery using a biomaterial platform could be a way to tune the glyco-environment towards the regenerative side.

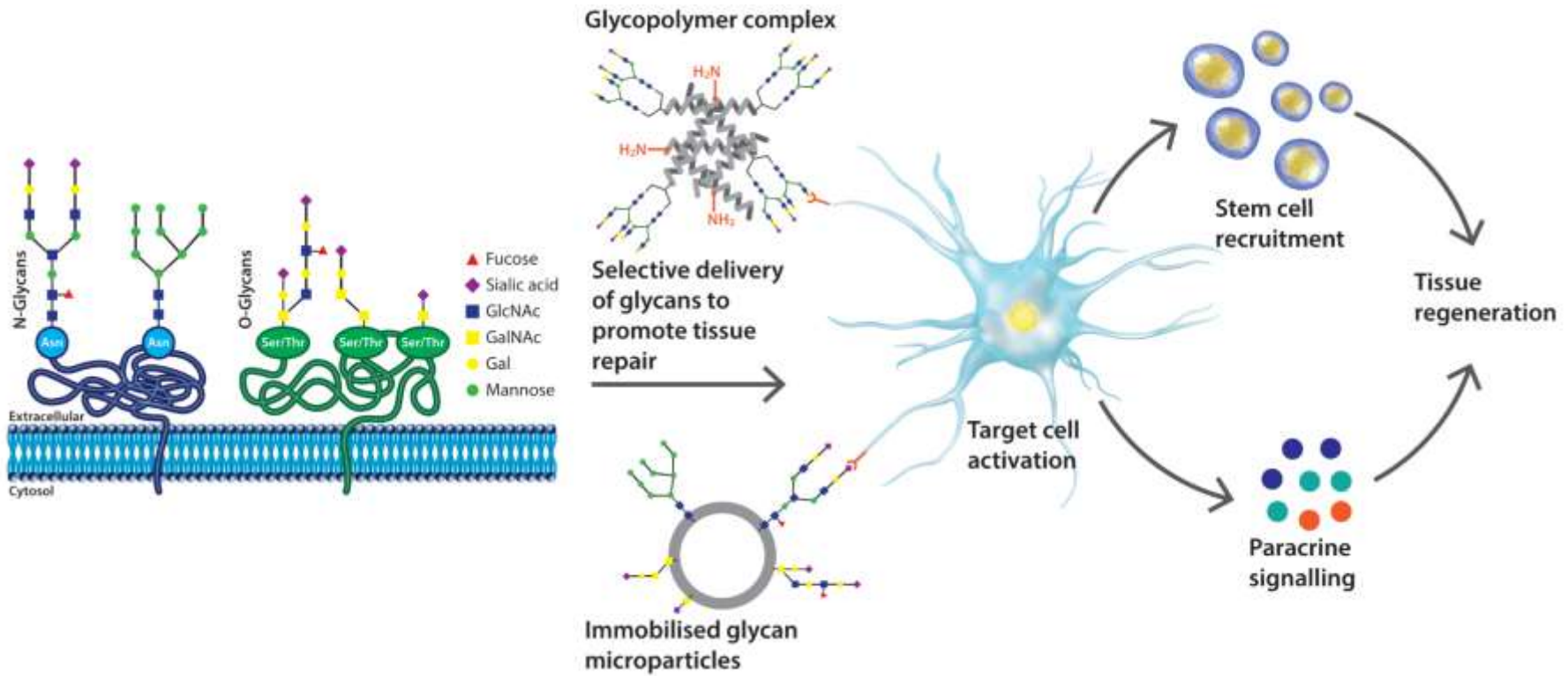


Figure 7.4: Schematic representation of the glycosylation approaches targeted by the biomaterial therapies to ‘tune’ the paracrine profile of the target cells to promote tissue repair.

7.4.4 Spatio-temporal proteomic analysis for PD progression

Biomaterial interventions are often used in combination with ‘targets’ which were identified or validated to be of therapeutic significance in basic pathophysiological studies of disease. However, these studies seldom consider the consequences of a biomaterial’s interaction with the tissue, in both a beneficial and an undesirable way. Therefore, it will prove useful to identify therapeutic targets using a biomaterial-specific approach by performing protein and RNA arrays on diseased models both in the presence of and without a biomaterial. Certain biomaterials have an intrinsic therapeutic value for certain disease targets like HA gels in the prevention of the development of the pain phenotype [36]. A detailed proteomic and transcriptomic analysis to elucidate the spatio-temporal patterns of modulation of the proteomic and genomic markers with the progression of PD can corroborate the glycomic data gathered in this study to pick specific therapeutic targets for PD. Such analysis could also give several mechanistic insights into the development and progression of Parkinson’s. In the course of this study, LC-MS/MS analysis of the proteomic modulation in response to the disease induction and biomaterial treatment was performed as a response to both collagenase C3 and trypsin treatments. To date, this is the first analysis which is underway, that took into consideration the peptides generated using C3 treatment.

7.5 References

- [1] O.-B. Tysnes, A. Storstein, Epidemiology of Parkinson’s disease, *J. Neural Transm.* 124 (2017) 901–905. doi:10.1007/s00702-017-1686-y.
- [2] P.A. LeWitt, Levodopa therapy for Parkinson’s disease: pharmacokinetics and pharmacodynamics, *Mov. Disord.* 30 (2015) 64–72. doi:10.1002/mds.26082.
- [3] M.A. Hely, J.G.L. Morris, W.G.J. Reid, R. Trafficante, Sydney multicenter study of Parkinson’s disease: Non-L-dopa-responsive problems dominate at 15 years, *Mov. Disord.* 20 (2005) 190–199. doi:10.1002/mds.20324.
- [4] O. Lindvall, S. Rehnström, P. Brundin, B. Gustavii, B. Astedt, H. Widner, T. Lindholm, A. Björklund, K.L. Leenders, J.C. Rothwell, R. Frackowiak, D. Marsden, B. Johnels, G. Steg, R. Freedman, B.J. Hoffer, A. Seiger, M. Bygdeman, I. Strömberg, L. Olson, Human fetal dopamine neurons grafted into the striatum in two patients with severe Parkinson’s Disease, *Arch. Neurol.* 46 (1989) 615. doi:10.1001/archneur.1989.00520420033021.
- [5] P. Brundin, R.E. Strecker, O. Lindvall, O. Isacson, O.G. Nilsson, G. Barbin, A. Prochiantz, C. Forni, A. Nieoull, H. Widner, F.H. Gage, A. Björklund, Intracerebral grafting of dopamine neurons., *Ann. N. Y. Acad. Sci.* 495 (1987) 473–495. doi:10.1111/j.1749-6632.1987.tb23695.x.
- [6] C.W. Olanow, C.G. Goetz, J.H. Kordower, A.J. Stoessl, V. Sossi, M.F. Brin, K.M. Shannon, G.M. Nauert, D.P. Perl, J. Godbold, T.B. Freeman, A double-blind controlled

- trial of bilateral fetal nigral transplantation in Parkinson's disease, *Ann. Neurol.* 54 (2003) 403–414. doi:10.1002/ana.10720.
- [7] R.A. Barker, J. Barrett, S.L. Mason, A. Björklund, Fetal dopaminergic transplantation trials and the future of neural grafting in Parkinson's disease, *Lancet Neurol.* 12 (2013) 84–91. doi:10.1016/S1474-4422(12)70295-8.
- [8] S. Browne, G. Fontana, B.J. Rodriguez, A. Pandit, A protective extracellular matrix-based gene delivery reservoir fabricated by electrostatic charge manipulation, *Mol. Pharm.* 9 (2012) 3099–3106. doi:10.1021/mp300231d.
- [9] A.E. Lang, S. Gill, N.K. Patel, A. Lozano, J.G. Nutt, R. Penn, D.J. Brooks, G. Hotton, E. Moro, P. Heywood, M.A. Brodsky, K. Burchiel, P. Kelly, A. Dalvi, B. Scott, M. Stacy, D. Turner, V.G.F. Wooten, W.J. Elias, E.R. Laws, V. Dhawan, A.J. Stoessl, J. Matcham, R.J. Coffey, M. Traub, Randomized controlled trial of intraputamenal glial cell line-derived neurotrophic factor infusion in Parkinson disease, *Ann. Neurol.* 59 (2006) 459–466. doi:10.1002/ana.20737.
- [10] R.M. Richardson, A.P. Kells, K.H. Rosenbluth, E.A. Salegio, M.S. Fiandaca, P.S. Larson, P.A. Starr, A.J. Martin, R.R. Lonser, H.J. Federoff, J.R. Forsayeth, K.S. Bankiewicz, Interventional MRI-guided putaminal delivery of AAV2-GDNF for a planned clinical trial in Parkinson's disease., *Mol. Ther.* 19 (2011) 1048–1057. doi:10.1038/mt.2011.11.
- [11] A.F. Williams, R.B. Parekh, D.R. Wing, A.C. Willis, A.N. Barclay, R. Dalchau, J.W. Fabre, R.A. Dwek, T.W. Rademacher, Comparative analysis of the *N*-glycans of rat, mouse and human Thy-1. Site-specific oligosaccharide patterns of neural Thy-1, a member of the immunoglobulin superfamily, *Glycobiology.* 3 (1993) 339–348. doi:10.1093/glycob/3.4.339.
- [12] Y. Mechref, M. V. Novotny, C. Krishnan, Structural characterization of oligosaccharides using Maldi-TOF/TOF tandem mass spectrometry, *Anal. Chem.* 75 (2003) 4895–4903. doi:10.1021/ac0341968.
- [13] P.B. O'Connor, E. Mirgorodskaya, C.E. Costello, High pressure matrix-assisted laser desorption/ionization Fourier transform mass spectrometry for minimization of ganglioside fragmentation, *J. Am. Soc. Mass Spectrom.* 13 (2002) 402–407. doi:10.1016/S1044-0305(02)00351-3.
- [14] P.B. O'Connor, C.E. Costello, A high pressure matrix-assisted laser desorption/ionization Fourier transform mass spectrometry ion source for thermal stabilization of labile biomolecules, *Rapid Commun. Mass Spectrom.* 15 (2001) 1862–1868. doi:10.1002/rcm.447.
- [15] A. Schober, Classic toxin-induced animal models of Parkinson's disease: 6-OHDA and MPTP, *Cell Tissue Res.* 318 (2004) 215–224. doi:10.1007/s00441-004-0938-y.
- [16] R. Betarbet, T.B. Sherer, J.T. Greenamyre, Animal models of Parkinson's disease, *BioEssays.* 24 (2002) 308–318. doi:10.1002/bies.10067.
- [17] M.A. Cenci, I.Q. Whishaw, T. Schallert, Animal models of neurological deficits: how relevant is the rat?, *Nat. Rev. Neurosci.* 3 (2002) 574–579. doi:10.1038/nrn877.
- [18] W.M. Pardridge, Drug transport across the blood-brain barrier., *J. Cereb. Blood Flow Metab.* 32 (2012) 1959–1972. doi:10.1038/jcbfm.2012.126.

- [19] G.A. Silva, Nanotechnology applications and approaches for neuroregeneration and drug delivery to the central nervous system., *Ann. N. Y. Acad. Sci.* 1199 (2010) 221–230. doi:10.1111/j.1749-6632.2009.05361.x.
- [20] Q. Peng, S. Zhang, Q. Yang, T. Zhang, X.-Q. Wei, L. Jiang, C.-L. Zhang, Q.-M. Chen, Z.-R. Zhang, Y.-F. Lin, Preformed albumin corona, a protective coating for nanoparticles based drug delivery system., *Biomaterials.* 34 (2013) 8521–8530. doi:10.1016/j.biomaterials.2013.07.102.
- [21] R.C. Lai, R.W.Y. Yeo, K.H. Tan, S.K. Lim, Exosomes for drug delivery - a novel application for the mesenchymal stem cell., *Biotechnol. Adv.* 31 (2013) 543–51. doi:10.1016/j.biotechadv.2012.08.008.
- [22] Y. Tian, S. Li, J. Song, T. Ji, M. Zhu, G. Anderson, J. Wei, G. Nie, A doxorubicin delivery platform using engineered natural membrane vesicle exosomes for targeted tumor therapy., *Biomaterials.* 35 (2014) 2383–2390. doi:10.1016/J.BIOMATERIALS.2013.11.083.
- [23] L. Alvarez-Erviti, Y. Seow, H. Yin, C. Betts, S. Lakhal, M.J.A. Wood, Delivery of siRNA to the mouse brain by systemic injection of targeted exosomes., *Nat. Biotechnol.* 29 (2011) 341–5. doi:10.1038/nbt.1807.
- [24] T.L. Lentz, Rabies virus binding to an acetylcholine receptor alpha-subunit peptide., *J. Mol. Recognit.* 3 (1990) 82–88. doi:10.1002/jmr.300030205.
- [25] K. Hira, Y. Ueno, R. Tanaka, N. Miyamoto, K. Yamashiro, T. Inaba, T. Urabe, H. Okano, N. Hattori, Astrocyte-derived exosomes treated with a Semaphorin 3A inhibitor enhance stroke recovery via Prostaglandin D2 synthase., *Stroke.* 49 (2018) 2483–2494. doi:10.1161/STROKEAHA.118.021272.
- [26] M.A. Lopez-Verrilli, A. Caviedes, A. Cabrera, S. Sandoval, U. Wyneken, M. Khoury, Mesenchymal stem cell-derived exosomes from different sources selectively promote neuritic outgrowth, *Neuroscience.* 320 (2016) 129–139. doi:10.1016/J.NEUROSCIENCE.2016.01.061.
- [27] J. Wei, Y. Chen, C. Xue, B. Ma, Y. Shen, J. Guan, X. Bao, H. Wu, Q. Han, R. Wang, C. Zhao, Protection of nerve injury with exosome extracted from mesenchymal stem cell., *Zhongguo Yi Xue Ke Xue Yuan Xue Bao.* 38 (2016) 33–36. doi:10.3881/j.issn.1000-503X.2016.01.006.
- [28] J.P. de Rivero Vaccari, F. Brand, S. Adamczak, S.W. Lee, J. Perez-Barcena, M.Y. Wang, M.R. Bullock, W.D. Dietrich, R.W. Keane, Exosome-mediated inflammasome signaling after central nervous system injury, *J. Neurochem.* 136 (2016) 39–48. doi:10.1111/jnc.13036.
- [29] K. Takahashi, S. Yamanaka, Induction of pluripotent stem cells from mouse embryonic and adult fibroblast cultures by defined factors, *Cell.* 126 (2006) 663–676. doi:10.1016/j.cell.2006.07.024.
- [30] T. Kikuchi, A. Morizane, D. Doi, H. Magotani, H. Onoe, T. Hayashi, H. Mizuma, S. Takara, R. Takahashi, H. Inoue, S. Morita, M. Yamamoto, K. Okita, M. Nakagawa, M. Parmar, J. Takahashi, Human iPS cell-derived dopaminergic neurons function in a primate Parkinson's disease model, *Nature.* 548 (2017) 592–596. doi:10.1038/nature23664.

- [31] K. Landsteiner, C.P. Miller, Serological studies on the blood of the primates : II. The blood groups in anthropoid apes., *J. Exp. Med.* 42 (1925) 853–862. doi:10.1084/jem.42.6.853.
- [32] X. Yang, J. Tang, C.E. Rogler, P. Stanley, C. Rogler, P. Stanley, Reduced hepatocyte proliferation is the basis of retarded liver tumor progression and liver regeneration in mice lacking N-acetylglucosaminyltransferase III., *Cancer Res.* 63 (2003) 7753–7759. doi:10.1158/0008-5472.can-09-2719.
- [33] L. Russo, A. Sgambato, M. Lecchi, V. Pastori, M. Raspanti, A. Natalello, S.M. Doglia, F. Nicotra, L. Cipolla, Neoglycosylated collagen matrices drive neuronal cells to differentiate, *ACS Chem. Neurosci.* 5 (2014) 261–265. doi:10.1021/cn400222s.
- [34] A. Didonna, F. Benetti, Post-translational modifications in neurodegeneration, *AIMS Biophys.* 3 (2015) 27–49. doi:10.3934/biophy.2016.1.27.
- [35] Y. Li, G. Wu, G.S. Dawe, L. Zeng, S. Cui, G. Loers, T. Tilling, L. Sun, M. Schachner, Z.-C. Xiao, Cell surface sialylation and fucosylation are regulated by L1 via phospholipase C γ and cooperate to modulate neurite outgrowth, cell Survival and migration, *PLoS One.* 3 (2008) e3841. doi:10.1371/journal.pone.0003841.
- [36] I.L. Mohd Isa, S.A. Abbah, M. Kilcoyne, D. Sakai, P. Dockery, D.P. Finn, A. Pandit, Implantation of hyaluronic acid hydrogel prevents the pain phenotype in a rat model of intervertebral disc injury, *Sci. Adv.* 4 (2018) eaaq0597. doi:10.1126/sciadv.aaq0597.

Appendices

A. List of reagents

Materials/Reagents	Catalogue #	Supplier
Tween20®	BP337-500	Fisher Scientific, Ireland
Phosphate buffer saline (PBS)	1282-1680	
Donkey anti-mouse antibody Alexa Fluor® 488 conjugate	ab150110	Abcam, UK
Donkey anti-rabbit antibody Alexa Fluor® 594 conjugate	ab150066	
Rneasy® Mini Kit	74106	Qiagen, Germany
SYBR® green PCR Master Mix	330500	
OCT embedding medium	4583	Thermofisher Scientific, Ireland
Pierce® BCA Assay	23235	
Chamber slide, Lab-Tek II, 8-wells	12852794	
Lactose	61339	Sigma-Aldrich, Ireland
GlcNAc	A3286-25G	
Galactose	G0750	
Mannose	M2069	
Sucrose	S0389	
Isopentane	M32631-1L	
Molecular grade ethanol	459844-1L-D	
Molecular grade chloroform	C2432-25ML	
Triton™ X-100	T9284-500ML	
Paraformaldehyde (PFA)	158127	
Penicillin/streptomycin (P/S)	P4458-100ML	
Fetal bovine serum (FBS)	F2442-500ML	
Trypsin	T4174-100ML	
NaCl	S7653-5KG	
CaCl ₂	C1016-500G	
MgCl ₂	M2670-1KG	
Bovine serum albumin	A6003-100G	
HCl	31894-9	
Hanks' balanced salt solution (HBSS)	H8264-6X500ML	
Xylene	534056-4L	
Ethanol	459844-1L-D	
25-G needle		
Dulbeco modified eagle's media (DMEM)	D6429-6X500ML	
DPX mounting media	06522-500ML	
Glucose	G7021	
Normal goat serum	G9023-10ML	
Hematoxylin Gill no.2	GHS232	
Hoescht	14533	
L-glutamine	G7513-100ML	
Poly-L-lysine	P7886-10MG	

Trypsin-EDTA	T4174-100ML	
Anti-fibrinogen antibody (produced in goat)	F8512-2ML	
Thrombin from bovine plasma	T1063-250UN	
Fibrinogen, human plasma	F4883-500MG	Merck Milipore, USA
Anti-Tyrosine Hydroxylase antibody	MAB318	
Anti-tubulin beta III antibody	MAB1637	
Anti-Iba1 antibody	019-19741	Wako chemicals, Germany

B. Fibrin hydrogel fabrication

- Wrap the PTFE tape around the microscopic slides and place them on the petri-dishes with 70% ethanol. Leave them overnight in a hood for the ethanol to evaporate and then UV sterilize the slide surface for 30 mins.
- Reconstitute the fibrinogen fraction of microgel with desired concentration of the microspheres/cells in a final volume of 6 μ L per gel.
- Drop the 6 μ L using a P20 micropipette.
- Cross link the fibrinogen using 2 μ L of the thrombin stock solution using P10 micropipette.
- Incubate at 37°C for 5-6 mins.
- Collect the gels by scrapping off the hydrophobic surface using the sterile spatula and resuspend the microgels in sterile PBS with aprotinin for long term storage to prevent rapid degradation.

C. Isolation of VM cells

a. Preparation of complete media

- Out of cell culture hood, weigh 3 g of D-glucose in a 50 mL tube.
- In cell culture hood, add 20 mL warmed Dulbecco's modified Eagle's medium/F12 (DMEM) to D-glucose. Invert to dissolve D-glucose in DMEM.
- Using a 0.2 micron filter and 5 mL syringe, steri-filter the 20 mL D-glucose-DMEM solution back into the 500 ml bottle of DMEM.
- Defrost 5 mL Penicillin/Streptomycin (P/S) and 5 mL L-glutamine aliquots. Invert aliquots to mix, ensuring L-glutamine turns from cloudy to clear, before adding to 500 mL bottle of D-glucose-DMEM solution.
- Label the bottle of DMEM-D-glucose-AAS-L-glutamine complete media with, your initials, the date and ingredients in media. Complete media can be stored at 4°C.

b. Plating media for E14 rat VM cultures

- To prepare plating media, mix the following: Complete media + 1% Fetal calf serum (FCS) + 2% B27 supplement

Notes: Make plating media fresh every time. B27 supplement is light sensitive - cover aliquots in tin foil and turn lights off in hood when in use. B27 supplement and FCS aliquots stored at -20°C, once defrosted dated and stored at 4°C.

c. Poly-d-lysine coating

- Reconstitute 5 mg lyophilized poly-d-lysine in 50 mL sterile cell culture grade water to make a 0.1 mg/mL working solution. Aliquot poly-d-lysine solution and store at -20°C.
- In cell culture hood, pipette 130 µL poly-d-lysine to centre of each well of 24-well plate.
- Leave to incubate, covered for 5-20 minutes in cell culture hood, before removing.
- Wash surface of wells 3 times with sterile cell culture grade water. Allow plates to dry for 1-2 h before introducing cells and media.

Notes: Poly-d-lysine solution can be reused up to ~3 times when stored at 4°C

d. Ventral mesencephalon dissection

- E14 Sprague-Dawley rat embryos are obtained by laparotomy from time-mated female Sprague-Dawley rats (plug day counted as E1) following decapitation under terminal anaesthesia induced by the inhalation of isoflurane (Isoflo®).
- The embryonic sacs are placed in a petri dish containing ice-cold Hank's Balanced Salt Solution (HBSS).
- The embryos are removed from their yolk sac and their crown-to-rump length was measured to verify their embryonic ages.
- The embryonic brains are isolated from the heads in ice-cold HBSS, the mesencephalon is excised from the brains, an incision was made along the dorsal midline and the dorsal portion of the mesencephalon is discarded, the meninges removed, leaving the VM.

Notes: Dissection instruments sterilised in ethanol and washed in HBSS prior to dissections. Keep dissected VM tissue in HBSS on ice prior to cell culture procedure.

e. E14 rat VM cultures

- Prior to dissections, poly-d-lysine coat a 24-well plate, and warm plating media, FCS and trypsin aliquots at 37°C.
- Centrifuge dissected VM tissue in HBSS at 1100 revolutions per minute (rpm) for 5 minutes at 4°C. Discard HBSS from tube.
- Add 3 ml of HBSS to 2 mL of trypsin aliquot (warmed). Add 1.5 mL HBSS-trypsin solution to tube containing VM tissue. Incubate for 4 minutes at 37°C with 5% CO₂.
- Discard 1 mL HBSS-trypsin solution and add 500 µL FCS. Centrifuge at 1100 rpm for 5 minutes at 4°C. Discard HBSS-trypsin-FCS solution from tube.
- Resuspend cell pellet in 1 mL of plating media using a P1000 pipette (set at 500 µL), followed by a 25 gauge needle and 1 mL syringe, ensuring not to add air bubbles into the cell suspension. Media should turn cloudy.
- Estimate cell density using a haemocytometer, as follows: dilute 10 µL of cell suspension 1:10 in 45 µL of plating media and 45 µL of trypan blue. Pipette 10 µL of cell solution under cover slip on haemocytometer. Count number of alive cells in 5 squares.
- The total number of cells in the cell suspension was calculated using the formula:

- Cells/ml = (number of cells counted in 5 squares/5) x 10⁴ x dilution factor*
- Dilution factor = Total Volume/Volume of sample = 100 µL /10 µL = 10
- Calculate volume of cell suspension and volume of plating media needed to seed 100,000 cells per well of a 24-well plate.
- Pipette 50 µL of cell-plating media mix into the centre of each well.
- Leave 24-well plate for 60 minutes at 37°C with 5% CO₂.
- After 60 min, examine cells under microscope to ensure cells have plated down and flood each well with 500 µL of plating media (aimed at side of well - added gently).
- Feeding E14 rat VM cultures: On day 2 in vitro, discard 250 µL media from each well and replace with 300 µL of fresh warmed plating media.

D. Immunocytochemistry

- Fix the cells for 10 min using 100% ice-cold methanol
- Wash the cells 3x with 10 mM phosphate-buffered saline (PBS) containing 0.02% Triton X (PBS-Tx), for 5 minutes each wash.
- Block non-specific antibody binding for 1 h using 5% bovine serum albumin in 10 mM PBS at room temperature.
- Incubate cells overnight at 4°C in the desired primary antibodies (Table A1) in antibody diluent (1% bovine serum albumin in 10 mM PBS).
- Wash the cells 3x 5 minutes using PBS-T.
- Incubate the cells for 2 h at room temperature in the appropriate secondary antibodies in antibody diluent (1% bovine serum albumin in 10 mM PBS).
- Wash the cells 3x 5 minutes using PBS-T.
- Counterstain the cells for 5 minutes using DAPI in 10 mM PBS.
- Wash the cells 3x 5 minutes using PBS-T.
- Images were taken in 40X.

Table A1: Summary of the phenotypic markers and antibodies used for detection.

Marker	Antibody	Dilution
TH	Mouse-anti TH (Millipore, MAB318)	1:200
GFAP	Rabbit-anti-GFAP (Sigma-Aldrich, G3893)	1:500
βIII-Tubulin	Mouse-anti βIII-Tubulin (Millipore, MAB1637)	1:200

E. RNA extraction (*in vitro* study)

a. Cell lysis

- Remove media from cells, but do not wash.
- Add 1 mL of Trizol[®] reagent for every 10 cm² (1 well of 6-well plate) of culture disc area.
- Use pipette to help lyse the cells in culture dish.

- Incubate cell lysate at room temperature for five minutes.
- Remove all the Trizol[®] and cell lysate mixture into 2 mL appendorf tubes.
- Add 200 μ L of chloroform without isoamyl alcohol for every 1 mL of Trizol[®].
- Vortex the mixture for fifteen seconds and incubate at room temperature for five minutes.
- Centrifuge at 13,300 rpm for fifteen minutes at 4°C (do not exceed 8°C which can cause some DNA partition in the aqueous phase).

b. RNA isolation

- Transfer 600 μ L of mixture into RNAeasy[®] mini/micro column (Qiagen, Germany) to remove genomic DNA.
- Centrifuge at 10,000 rpm for fifteen seconds at room temperature and discard flow through.
- Repeat step two if necessary.
- Add 700 μ L of RW1 to wash and centrifuge at 10,000 rpm for fifteen seconds at room temperature and discard flow through.
- Add 500 μ L of RPE and centrifuge at 10,000 rpm for fifteen seconds at room temperature and discard flow through.
- Add 500 μ L of RPE and centrifuge at 10,000 rpm for two minutes at room temperature and discard flow through.
- Place column in a new collection tube and add 30 μ L RNase free water and centrifuge at 10,000 rpm for one minute at room temperature.
- Pipette eluted 30 μ L into column again and centrifuge at 10,000 rpm for one minute at room temperature.
- Check RNA concentration by dropping 2 μ L in NanoDrop[™] spectrophotometer (Thermo Fisher Scientific).
- Keep RNA in -80°C.

c. RNA quantification

- Calibrate the spectrometer with RNase free water.
- Measure the absorbance of the RNA at 230nm, 260nm and 280nm.
- 1 unit of A260 = 40 μ g/mL of RNA
- Concentration of RNA sample = 40 x A260 x dilution factor = x μ g/mL
- Quantity of RNA = concentration x volume of sample in mL = x μ g
- The reading at ratio 260/280 close to 2.00 indicates a good grade RNA and the ratio at 230/260 close to 2.00 remarks little protein.

Note: The ratio at A260/A280 provides an estimation of the purity of RNA with respect to contaminants that absorb in the UV such as protein; and the ratio at A230/A260 provides an estimation of the purity of RNA with respect to organic contaminant.

F. Synthesis of cDNA by Reverse Transcription

Note: For the entire procedure, use filter tips, sterile and nuclease-free tubes pre-chilled on ice.

- Dilute RNA with RNase free water to a final concentration of 100 ng/ μ L.

- For 20 μL reverse transcription reaction, mix 1 μL of RNA with 1 μL random primer, and then RNase free water to a final volume of 5 μL in PCR tube 0.2 mL.
- Incubate at 70°C for five minutes, for the denaturation of the RNA template and the primers in DNA engine.
- Quick chill at 4°C for five minutes and hold on ice (or direct in the bath of ice).

Note: Keep on ice during the preparation of the reverse transcription mix.

1. Prepare reverse transcription mix as Table A2.
2. Dispense 15 μL of the mix into the reaction tubes onto the 5 μL template/primers mix.
3. Mix gently and run the program described in Table A3, A4 after addition of the tube onto a DNA engine.
4. After this step, keep samples at -20°C until further PCR analysis.

Table A2: Master mix composition of reverse transcription

Component	Volume per one reaction (μL)	Final concentration
RNase free water	5.34	-
ImProm-II TM 5x reaction buffer	4.4	1x
MgCl ₂ (25mM)	2.64	3mM
dNTP mix (10mM)	1.1	0.5mM
Recombinant RNasin Ribonuclease inhibitor (20/40U/ μL)	1.1	1U/ μL
ImProm-II TM reverse transcriptase	1.1	
Final volume for 20 μL reaction	15	

Table A3: Reverse transcription program in DNA engine

Step	Temperature	Time
Steps temperature time annealing	25°C	5 minutes
Extension heat inactivation	42°C	60 minutes
Reverse transcriptase	70°C	15 minutes

G. RT-qPCR Analysis

Prepare PCR master mix as Table A4.

2. Add 2 μL of cDNA template into each well of PCR 96-well plate in triplicate.
3. Mix well with 18 μL of master mix to obtain a final volume of 20 μL by pipetting and adding into well containing cDNA.

4. Seal the plate with plastic cover.
5. If any bubbles are seen, centrifuge the plate at 2000 rpm for five minutes.
6. In StepOnePlus™ Real-Time PCR software, configure plate setup and PCR experiment according to program described in Table A5.
7. Insert PCR plate into StepOnePlus™ Real-Time PCR machine and run the instrument accordingly e.g. fast rpm speed and analysis methods via quantitative comparative C_T .

Table A4: PCR master mix for SYBR® Green

Component	Volume per reaction (µL)	Final concentration
QuantiFast SYBR® Green PCR kit 2X	10	1.2 mM
Forward primer	0.1	500 nM
Reverse primer	0.1	500 nM
RNase free water	7.8	
Total volume	18	

Table A5: qPCR program for TH, B-tubulin, GFAP and 18s primers

Step	Temperature	Time	Number of cycles
Holding stage			
Initial denaturation	95°C	5 minutes	1 Cycle
Cycling stage			
Denaturation	95°C	15 minutes	40 Cycles
Annealing	60°C	30 minutes	
Melt curve stage			
Denaturation	95°C	15 minutes	1 Cycle
Final extension	60°C	60 minutes	

Table A6: qPCR primers for TH, B-tubulin, GFAP and GAPDH

Cells	Gene	Forward (5'-3')	Reverse (5'-3')
Neurons	β-Tubulin	gtttgtgatgggtgtgaacc	tcttctgagtggcagtgatg
Dopaminergic neurons	TH	cagggctgctgtcttctac	gggctgtccagtagtcaat
Astrocytes	GFAP	agggacaatctcacacagg	gactcaaccttctctcca

H. 6-OHDA rat model induced by stereotactic injection

- Under isoflurane gaseous anaesthesia, secure the rat's head on the stereotaxic apparatus using non-rupture ear bars and nose bars to allow for accurate targeting of the specific brain regions relevant to Parkinson's disease (i.e. the cell bodies, axons or terminals of the nigrostriatal pathway).
- Make an incision (~2 cm) through the skin using a scalpel and a tissue retractor, and make 1-2 (depending on the site of administration) small burr holes (~2 mm diameter) using a dental drill at the appropriate point(s) on the skull surface on one side of the skull only.
- Lower a stainless-steel cannula slowly through the burr hole to the site of administration in the brain and administer 10 μg of 6-OHDA per site (no more than 6 μL of any solution is infused at any one site). 6-Hydroxydopamine is a neurotoxin which causes selective lesion of the targeted dopaminergic neurons.
- After the administration, leave the cannula in place for a further 2-5 minutes to allow for diffusion after which it is slowly retracted. Then suture the wound and treat with local anaesthetic.

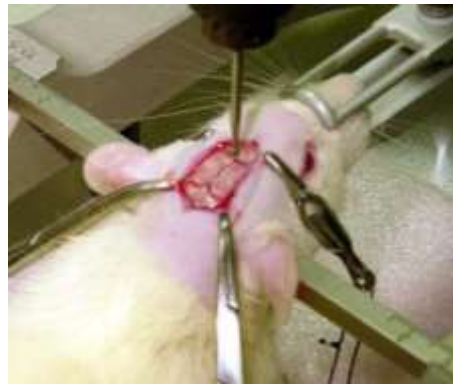


Figure. A1 Photo of rat undergoing stereotaxic surgeries

I. Injection of fibrin hydrogel in 6-OHDA Parkinsonian rat model

- Under isoflurane gaseous anaesthesia, secure the rat's head on the stereotaxic apparatus using non-rupture ear bars and nose bars to allow for accurate targeting of the specific brain regions relevant to Parkinson's disease (i.e. the cell bodies, axons or terminals of the nigrostriatal pathway).
- Make an incision (~2 cm) through the skin using a scalpel and a tissue retractor, and make 1-2 (depending on the site of administration) small burr holes (~2 mm diameter) using a dental drill at the appropriate point(s) on the skull surface on one side of the skull only.
- Lower a stainless steel cannula slowly through the burr hole to the site of administration in the brain and administer the relevant biomaterial-based therapy under investigation (no more than 6 μL of any solution/suspension is infused into the brain).
- Human fibrin (20mg/mL human fibrinogen with up to 4 IU human thrombin) will be infused as hydrogels and/or microspheres (<10 μm in diameter).

- The hydrogels will be used to encapsulate primary dopaminergic neurons dissected from the developing rat mesencephalon for brain repair. Up to 3.0×10^5 cells will be implanted at each site of administration.
- The hydrogels will be functionalised for sustained delivery of GDNF. This will be infused at up to 100 μg per site of administration.
- After the administration, leave the cannula in place for a further 2-5 minutes to allow for diffusion after which it is slowly retracted. Then suture the wound and treat with local anaesthetic.

J. Behavioural analysis

a) Drug induced rotations

- Inject the rats intraperitoneally with apomorphine (0.5 mg/kg s.c. in 0.9% saline).
- Place the rats in a cylindrical bowl and count the number of full turns they make in each direction for 1 minute every 10 minutes up to 90 minutes after injection.



Figure A2: Parkinsonian rat exhibiting turning behaviour

b) Cylinder test

- Since this test takes advantage of an animal's drive to explore a novel environment by standing on the hindlimbs and leaning towards the enclosing walls of a cylinder, no habituation to the test itself is required.
- To perform this test, animals are placed individually into a glass cylinder (4L beaker: 17cm diameter and 27cm height).
- The number of wall contacts performed independently with the left and the right forepaw are counted per rat.
- The test is deemed complete once a total of 20 wall contacts have been made or until an allotted time of 5 minutes has elapsed.
- The number of wall contacts per forelimb and the time taken are recorded.



Figure A3: Cylinder test for Parkinsonian rats

K. Tissue processing

a. Preparation of 4% paraformaldehyde solution

To make up a solution (1 L) of 4% paraformaldehyde (PFA) perform the following procedure in a fume hood.

- Weigh out 40 g of paraformaldehyde powder wearing a nasal mask.
- Dissolve powder in 800 ml dH₂O.
- Heat the solution using a hotplate/stirrer to approximately 60°C. Once this temperature is reached, turn off the hotplate. Do not allow the solution to reach 65°C or greater.
- Using a plastic pipette, slowly add 1M NaOH dropwise to the solution until it clears.
- Make up the solution to a final volume of 1 L and allow to cool to RT.
- Filter and store the solution at RT.
- Aliquot and store at -80°C if the solution is not used within the following two weeks.

b. Tissue processing for cryopreservation

- Fix each sample with freshly prepared PFA 4% overnight at 4°C (approx.10 mL for each specimen).
- Wash each sample with PBS three times for 10minuteseach.
- Incubate each sample in 30% sterile-filtered sucrose solution (approx. 10 mL for each specimen).
- Proceed when the specimen sinks to the bottom of the tube or leave overnight at 4°C.
- Remove the excess of sucrose solution on filter paper.
- Leave all the samples to equilibrate in OCT compound for 5-10 min.
- Meanwhile, fill a polystyrene contained with liquid nitrogen until around 3 cm.
- Position a small metal container filled with isopentane (2 cm) in the middle of the polystyrene box.
- If possible, check the temperature inside the metal container using an ethanol thermometer to check that it is at least below -100°C. The solution should look turbid and whitish on the bottom and sides of the container once it reaches that temperature.
- Firmly hold the cryomold vertically using a pair of tweezers and carefully submerge only the bottom and sides of the mold. Do not submerge completely the cryomold to avoid cracking inside the OCT-embedded sample.

- Once the OCT turned its color to white, remove the specimen from the plastic mold and quickly transfer it on ice.
- Do not leave the OCT embedded blocks for more than 5 minutes on ice and store them at -80°C .

c. Tissue processing for embedding in paraffin

- Each tissue sample was fixed in 4% PFA overnight at 4°C .
- Wash each sample with PBS three times for 10 minutes each.
- Place each sample in a plastic cassette and label it with a pencil, keep the cassettes submerged in 70% ethanol solution.
- Set the overnight processing using an Excelsior™ AS Tissue Processor (Thermo Fisher Scientific, USA), as detailed in Table A7.
- The following day, collect the samples from the paraffin wax bath (still at 62°C) and keep them in hot wax bath to avoid solidifying.
- Quickly remove each sample from the cassette and place it in a plastic mold for embedding with fresh paraffin wax using an EG1150 Modular Tissue Embedding Center (Leica, Germany).
- During the embedding procedure, make sure that the specimen has a thin layer of paraffin above the bottom of the plastic mold where it is embedded.
- Leave the embedded samples to solidify for at least one h on the refrigerated surface of the Tissue Embedding Center.

d. Tissue sectioning using the cryostat

- Take the samples (OCT blocks) out of the -80°C freezer and place them at -20°C to equilibrate for at least 1 h.
- Set the temperature inside the CM1850 cryostat (Leica, Germany) chamber at -25°C and move the required equipment for cutting inside the chamber (blades, brush, specimen stage).
- Put a drop of OCT compound on the specimen stage and quickly position the samples embedded in OCT on the top of that. Leave the assembled specimen stage inside the chamber for 5 minutes.
- Fix the specimen stage in the arm and use the motorised controls to adjust the distance between the blade and the OCT block.
- Set the cutting angle between 1° and 5° and cut specimens into $5\ \mu\text{m}$ -thick sections.
- Avoid wrinkles and disruptions in the sections. After a prolonged use, move the blade laterally or change it.
- Lift the cutting glass and quickly make the section adhere on the charged side of a SuperFrost Plus™ slide.
- When applying serial sectioning, calculate at least $100\ \mu\text{m}$ distance between the first section series and the following one. At the end of the sectioning, three sections taken at $100\ \mu\text{m}$ -distance apart should be present on the same slide.
- Label the slides and store at -80°C .

Table A7. Routine program overnight for tissue processor

Reagent	Duration (min)	Temperature (°C)
Ethanol 70%	Until start	RT
Ethanol 70%	45	RT
Ethanol 90%	45	RT
Ethanol 100% (1)	45	RT
Ethanol 100% (2)	60	RT
Ethanol 100% (3)	60	RT
Xylene (1)	45	RT
Xylene (2)	60	RT
Xylene (3)	75	RT
Paraffin wax (1)	60	62
Paraffin wax (2)	60	62
Paraffin wax (3)	60 - until collection	62

e. *Tissue sectioning using the microtome*

- Leave the samples embedded in paraffin wax on the refrigerated surface of the Tissue Embedding Center for at least 1 h before starting to section. The face of the block which will be cut needs to lay on the refrigerated surface.
- Fill the water bath with distilled water at an approximate height of 5 cm and set the temperature to 50°C.
- Position the paraffin block on the sample holder of a RM2235 microtome (Leica, Germany).
- Set the cutting angle at 3° and cut specimens into 5 µm-thick sections.
- Section a ribbon including three sections and transfer it onto the water bath using forceps. Collect the floating sections submerging SuperFrost Plus™ slides.
- Leave the glasses to dry the excess of water and store at RT until use.
- Before histological staining, make the section to adhere by incubating the glasses at 60°C for 10 min.

L. **Tissue histochemistry**

a. *Periodate treatment of bovine serum albumin (3%) for lectin histochemistry*

- Use high grade BSA (purity >99%) and 10 mM periodic acid in 0.1 M sodium acetate, pH 4.5 made up fresh.
- Dissolve BSA in the freshly made periodic acid solution (approx 5g/100 mL).
- Incubate at RT for 6 h.
- Dialyse against dH₂O (or PBS) with four changes over two days at 4 °C.
- Lyophilise and store at 4 °C.

b. Lectin histochemistry on cryosections

- Leave the sections to warm at RT for 15-20 min.
- Circle the sections using a hydrophobic marker (PAP pen).
- Place the sections in a glass staining jar and wash with TBS-T three times (3minuteseach wash, gentle shaking).
- Lay all the slides on a slide staining tray and incubate with 3% BSA (periodate-treated, high grade, made in TBS).
- Wash with TBS twice (3minuteseach wash, gentle shaking).
- From this point onwards, avoid exposure to direct light.
- Incubate with the lectin solution (in TBS) (lectins used are listed in Table A5).
- Wash with TBS three times (3minuteseach wash, gentle shaking).
- If staining with antibody, should be done after lectin incubation.
- Counterstain each section with one drop of with ProLong™ Gold Antifade Mountant with DAPI and coverslip.
- Leave to cure in the dark for one day. Image within three days after curing.

Table A8: Binding specificity and haptenic sugars of lectins for profiling of tissue glycosylation.

Lectin	Binding specificity	Haptenic sugar (100 mM)
SNA-I (Sambucus nigra agglutinin I)	Sialic acid- α -(2,6)-GalNAc-R	Lactose
MAA (Maackia amurensis agglutinin)	Sialic acid- α -(2,3)-GalNAc-R	Lactose
WGA (Wheat germ agglutinin)	Sialic acid, GlcNAc	GlcNAc
PNA (Peanut agglutinin)	Gal- β -(1,3)-GalNAc (T-antigen), > GalNAc > lactose > Gal, terminal β -Gal, non-sialylated	Gal
GS-I-B4 (Griffonia simplicifolia isolectin)	Terminal α -linked Gal	Gal
Con A (Concanavalin A)	α -linked mannose, glucosamine and GlcNAc	Mannose
UEA-I (Ulex europaeus agglutinin I)	α -(1,2)-linked fucose	Fucose
WFA (Wisteria floribunda agglutinin)	GalNAc and chondroitin sulfate	GalNAc
A haptenic sugar is a monosaccharide or disaccharide that can inhibit binding of a lectin. Abbreviations: Gal, galactose; GalNAc, N-acetylgalactosamine; GlcNAc, N-acetylglucosamine.		

c. *Immunohistochemistry on paraffin-embedded sections*

- Antigen retrieval
 - I. Preheat the vegetable steamer for 5 minutes prior to retrieval.
 - II. Add around ~10 mL of the buffer to a 5 slide mailer with side opening.
 - III. Place no more than 3 slides per 5 slide mailer with side opening. Slides should be placed with tissue facing outward to the solution in positions 1 and 5, and NOT facing the slide mailer walls. Position 3 may face either way.
 - IV. Completely fill the slide mailer the rest of the way with the antigen retrieval buffer.
 - V. If the mailer has no holes punched in the lid, only snap close one corner of the mailer.
 - VI. Place the mailer in the center of the vegetable steamer.
 - VII. Set heating for 25 minutes.

- Circle the sections using a hydrophobic marker (PAP pen).
- Lay all the slides on a slide staining tray and incubate with 0.3% hydrogen peroxide in 70% MeOH in PBS for 20 minutes to block endogenous peroxidase.
- Wash slides 2 x 5 minutes in PBS.
- Block the slides with 5% Normal Goat Serum (NGS) in PBS-Tx for 20 minutes at room temperature
- Incubate the slides overnight at 4°C with the primary antibody solution made in 5% NGS in PBS-Tx.
- On the second day, wash 2x 5 minutes in PBS.
- Incubate the slides in biotinylated secondary antibody made up in PBS for 30 minutes at room temperature.
- Wash 2x 5 minutes in PBS
- Incubate slides in Streptavidin ABS HRP-complex (Vector Labs®) (made up 30 minutes before and left at room temperature to homogenise)
- Wash 2x 5 minutes in PBS
- Incubate slides with 3,3'-Diaminobenzidine tetrahydrochloride hydrate (DAB) (2mg/mL), activated with 30% hydrogen peroxide (2µL per 1ml of DAB), for 5 minutes.
- Stop the reaction with tap water.
- Counterstain the slides with Hematoxylin Gill no. 2 for 40 seconds.
- Wash 3x 5 minutes in tap water.
- Dehydrate in 100% ethanol, 3x 2 minutes.
- Clear in xylene 2x 5 minutes.
- Mount with DPX and let the slides dry.

M. Lectin microarray on brain samples

All lectin microarrays were printed with 48 lectins (EY laboratories, USA) according to an established protocol [Kilcoyne]. Each lectin microarray slide had a unique barcode indicating the printing batch. All the procedures described here prior to scanning needed to be performed in a dark room with red light. Membrane protein samples labelled with Alexa Fluor® 555 Succinimidyl Ester were thawed and a titration experiment using a concentration of protein from 1 to 10 µg/mL was run to assess the optimum binding intensity of the sample to the printed lectins and to avoid saturation signals; therefore the chosen concentration was 5 µg/mL for all samples. The procedure of the lectin microarray analysis is detailed below here.

- Thaw labelled membrane protein samples on ice and dilute in TBS-T (0.01% of Tween-20) to the optimal concentration in a final volume of 70 µL in a rubber eight-well gasket (Agilent Technologies, USA).
- Carefully assemble each slide (lectin-printed side) on the top of the loaded gaskets to avoid splashing of the samples.
- Incubate with gentle rotation (4 rpm) in a hybridization oven at 23°C for 1 hour.
- Carefully disassemble the slide and quickly submerge it in TBS-T buffer.

- Place the slides in a glass staining jar filled with TBS-T with and wash three times (3minuteseach wash, gentle shaking).
- Do a final wash in TBS without Tween-20 before transferring the slides in empty falcon tubes. Centrifuge at 1500 g for 5 min.
- Scan the slides immediately using a G2505 microarray scanner (Agilent Technologies, USA) at 90% laser power.
- Process image files showing the scanned lectin microarrays using GenePix Pro v6.1.0.4 software (Molecular Devices, UK). Superimpose grids having an adaptive diameter circular alignment based on 230 μm features in the options on the subarrays.
- Extract background-corrected median feature intensity data for analysis.
- Normalise data to the median total intensity value of six replicate microarray slides.
- Run clustering of the normalised data using Hierarchical Clustering Explorer v3.5 (HCE 3.5, University of Maryland). Select Euclidean distance with complete linkage in the clustering options.

N. Glycoprotein extraction

- To a 2ml round bottom eppendorf tube add:
 - 500 μL of Sample Buffer (62.5 mM Tris pH6.6, 2%SDS) for brain samples of 30-45 mg
 - One bead –5mm stainless steel (Qiagen)
- -Tissue sample - tissue sample had previously been snap frozen on dry ice, stored at -80°C . Allowed to thaw on ice for 1hour.
- Homogenise using Qiagen TissueLyser LT (ideally this equipment should be cold) at speed of 40/s during 8 mins.
- Centrifuge at 16,000 x g (=13,400 rpm), at 4°C , for 20 mins.

O. N-glycans isolation and detection

- Make gel around dried tissue homogenate:
 1. To each sample tube add 22.5 μL (5 μL) Protogel + 11.25 μL (22.5 μL) gel buffer +1 μL (2 μL) 10% SDS.
 2. Mix by vortexing and by agitating with pipette tip.
 3. Add 1 μL (2 μL) APS and 1 μL (2 μL) TEMED to each sample.
 4. Allow gels to set for approx. 10-20 mins.
 5. Remove gels and chop into 1mm³ pieces on clean glass plate with clean scalpel.
- Wash gels:
 1. 1 mL 20 mM NaHCO₃ – 20minutesshaking (400 rpm), spin and remove all liquid.
 2. 1 mL Acetonitrile – 10minutesshaking, spin and remove all liquid.
- Reduce and alkylate:
 1. Add 100 μL 50 mM DTT added to each tube (in the hood)

2. Incubate for 15minutes@ 65°C
 3. Add 100 µL 20mM IAA solution to each tube on top of DTT solution (final 10 mM concentration)
 4. Incubate for 30minutes@ room temp in the dark
 5. Remove all liquid
- Wash gels:
 1. 1 mL Acetonitrile – shake for 10 mins, spin and remove liquid
 2. 1 mL 20mM NaHCO₃ – shake for 10 mins, spin and remove liquid
 3. 1 mL Acetonitrile – shake for 10 mins, spin and remove liquid
 4. 1 mL 20mM NaHCO₃ – shake for 10 mins, spin and remove liquid
 5. 1 mL Acetonitrile – shake for 10 mins, spin and remove liquid
 6. Dry in speed vac (15-20minutes until dry)
 - Digest *N*-glycans with PNGaseF:
 1. Add 50 µL PNGaseF 1:400 solution (in 20 mM NaHCO₃ buffer) to each tube, leave for 15minutesfor gel to absorb solution.
 2. Add a further 50 µL PNGaseF solution to each tube.
 3. Top up with further 50 µL approx. 20mM NaHCO₃ so that there is approx. 1mm visible above the gels.
 4. Incubate at 37°C overnight.
 - Elute glycans:

Keep precipitation plate on collection block.

1. Add 200 µL H₂O to each gel, sonicate for 30 mins, spin, move all liquid into a new tube and start drying
2. Add 200 µL H₂O to each gel, sonicate for 30 mins, spin, move all liquid into a new tube and continue drying
3. Add 200 µL H₂O to each gel, sonicate for 30 mins, spin, move all liquid into a new tube and continue drying
4. Add 200 µL Acetonitrile to each gel, sonicate for 30 mins, spin, move all liquid into a new tube and continue drying
5. Add 200 µL H₂O to each gel, sonicate for 30 mins, spin, move all liquid into a new tube and continue drying
6. Add 200 µL Acetonitrile to each gel, sonicate for 30 mins, spin, move all liquid into a new tube and continue drying

After completion of all sonications, filter the supernatant into a fresh tube using 0.45 µm LH Millipore filter and a 1mL syringe. Wash old tube with 100 µL water and filter this into fresh tube as well (using the same syringe/filter).

Dry completely in vacuum centrifuge – overnight.

- Label with 2AB:

1. Add 20 μL 1% formic acid (in MilliQ) to each sample (it needs to cover the sample, use more if needed); vortex and spin.
 2. Incubate for 40 minutes at room temperature.
 3. Dry completely in speed vac (approx. 1hr).
 4. Check that 2AB solution is still fluorescent under UV lamp.
 5. Add 5 μL 2AB labelling mixture to each well (use more if needed, the sample needs to be dissolved/covered).
 6. Shake for 5 mins.
 7. Incubate at 65°C for 30 minutes (cover with foil adhesive cover).
 8. Shake for 5 mins.
 9. Incubate at 65°C for 1.5 hours.
 10. Freeze at -20°C for a minimum of 5 minutes or overnight.
- Clean up excess 2AB:
 1. Condition wells fresh wells of glass fibre plate: 200 μL acetonitrile (vacuum to waste); 200 μL water (vacuum to waste).
 2. Transfer chromatography paper squares, folded into half and half again to plate wells.
 3. Apply samples (in labelling mixture, approx. volume = 5 μL) to middle of chromatography paper.
 4. Allow to dry/bind for 15 mins.
 - Wash off excess 2AB:
 1. Add 1.7 mL acetonitrile to each well, shake for 15 mins, vacuum to waste.
 2. Add 1.7 mL acetonitrile to each well, shake for 15 mins, vacuum to waste.
 3. Add 1.7 mL acetonitrile to each well, shake for 15 mins, vacuum to waste.
 4. Add 1.7 mL acetonitrile to each well, shake for 15 mins, vacuum to waste.
 5. Add 1.7 mL acetonitrile to each well, shake for 15 mins, vacuum to waste.
 - Elute labelled glycans:
 1. Move the papers with clean forceps to clean 2 mL Eppendorf tubes.
 2. Add 900 μL water to tube with paper, shake for 30 mins, move the liquid into the new tube.
 3. Add 900 μL water to tube with paper, shake for 30 mins, move the liquid into the new tube and together with the previous 900 μL .
 4. Dry overnight in speed vac.

P. Exoglycosidase digestion of N-glycans

- In a PCR tube, add sample, enzymes (according to Table A9, A10), 10x buffer (500 mM sodium acetate pH5.5) up to a volume of 10 μL .
- Vortex and spin the samples.
- Incubate for 16h (overnight) at 37°C.
- Inactivate exoglycosidase(s) by incubating each digest at 65°C for 15 min.

- Load 500 μ L of MilliQ water into the microcentrifuge filter and centrifuge at 13,000 rpm (approx. 16,000 g) for 10 min.
- Discard flow through (by pipetting it out).
- Repeat steps 2 and 3.
- Apply digestion to centre of filter ensuring that the pipette tip does not contact the filter (keep the digestion eppendorfs, you will use them in step 7).
- Centrifuge at 13,000 rpm for 2 min. Do not discard flow through.
- Use 20 μ L of MilliQ water to wash digestion eppendorf and apply this 20 μ L to the microcentrifuge filter.
- Centrifuge at 13,000 rpm for 2 min.
- Use 100 μ L of MilliQ water to wash digestion and apply this 100 μ L to the microcentrifuge filter.
- Centrifuge at 13,000 rpm for 5 min.
- Discard filter and retain collection eppendorf (a total of 130 μ L should be present in this Eppendorf).
- Dry down the glycans in speed vac and resuspend in a predetermined volume of MilliQ water in preparation for HPLC or UPLC (if running HILIC-UPLC, you resuspend the samples in 6 μ L MilliQ water, move to the UPLC vial and add 14 μ L acetonitrile)

Table A9: List of enzymes used for exoglycosidase digestions

Enzymes	Supplier	Catalog
ABS	Prozyme (Dublin, Irealnd)	GK80041
NAN1	Prozyme (Dublin, Irealnd)	GK80021
BTG	Prozyme (Dublin, Irealnd)	GKX-5013
SPG	Prozyme (Dublin, Irealnd)	GKX-5014
CBG	Prozyme (Dublin, Irealnd)	GKK-5007
AMF	NEB (Dublin, Irealnd)	P0769L
BKF	Prozyme (Dublin, Irealnd)	GKX-5006
GUH	NEB (Dublin, Irealnd)	P044S
JBH	Prozyme (Dublin, Irealnd)	
JBM	NEB (Dublin, Irealnd)	P0768L

Table A10: Digestion volumes used per tube for exoglycosidase digestions

TUBE	Amount used (µl)											Sample	
	ABS	NAN1	CBG	BTG	AMF	BKF	JBH	JBM	GUH	Buffer	MiliQ		
Sample+ABS	1										1	6	2
Sample + NAN1		2									1	5	2
Sample+ABS+SPG	1										1	4	2
Sample+ABS+CBG	1		2.5								1	3.5	2
Sample+ABS+JBH	1						2					4	2
Sample+ABS+BTG	1			2							1	4	2
Sample+ABS+BTG+JBH	1			2			2				1	2	2
Sample+ABS+BTG+AMF	1			2	1						1	3	2
Sample+ABS+BTG+BKF	1			2		1					1	3	2
Sample+ABS+BTG+AMF+BKF+GUH	1			2	1	1			1		1	1	2
Sample+ABS+BTG+AMF+BKF+GUH+JBM	1			2	1	1		(2) (added on 2 nd day)	1		1	1	2

Abbreviations: ABS, *Arthrobacter ureafaciens* sialidase; NAN-1, Recombinant sialidase; BTG, Bovine testes Beta-galactosidase; CBG, Coffee bean alpha-galactosidase; AMF, Almond meal alpha-fucosidase; BKF, Bovine kidney alpha-fucosidase; JBM, Jack bean mannosidase; JBH, Jack bean beta-acetylhexoaminidase

Q. MALDI imaging

- a) For MALDI-FT-ICR, standard microscope slides (*Tissue Tack*, Polyscientific preferred) are suitable as long as they fit into the 25 x 75 mm slide holder for the instrument.
- b) Dewax slides:
 1. Heat slides at 60°C for one hour.
 2. Remove and cool to room temperature, usually 5 minutes.
 3. Dewax washes:
 - Xylenes 3 minutes, repeating a total of two times.
 - 100% ethanol 1 minute, repeating a total of two times.
 - 95% ethanol 1 minute
 - 70% ethanol 1 minute
 - Distilled water 3 minutes, repeating a total of two times.
 - Slides may be stored overnight in desiccator prior to completion.
 - If continuing, dry slides in desiccator 5 minutes prior to scanning.
 - Scan each slide, minus the surrounding sample holder, at a minimum of 1200 ppi resolution. Samples for higher resolution will require a higher resolution scanned image. For example, images acquired with a ≤ 50 µm stepsize require a 2400 dpi scanned image.
 - Save the images to a folder for the project.

c) *Antigen retrieval prep:*

1. Prepare Citraconic buffer:
 - 25 mL distilled water or HPLC grade water into a 50 mL falcon tube.
 - Add 25 μ L of Citraconic buffer to the water.
 - Add 2 μ L of 12 M HCl.
 - Agitate tube after capping.
 - Add water to a total of 50 mL.
 - Agitate tube to mix.
 - Check that pH is around 3.0 ± 0.5 by spotting 2 μ L of the prepared buffer onto a pH strip.

2. Heat slides in vegetable steamer:
 - Preheat the vegetable steamer for 5 minutes prior to retrieval.
 - Add around ~10 mL of the buffer to a 5 slide mailer with side opening.
 - Place no more than 3 slides per 5 slide mailer with side opening. Slides should be placed with tissue facing outward to the solution in positions 1 and 5, and NOT facing the slide mailer walls. Position 3 may face either way.
 - Completely fill the slide mailer the rest of the way with the buffer.
 - If the mailer has no holes punched in the lid, only snap close one corner of the mailer.
 - Place the mailer in the center of the vegetable steamer.
 - Set heating for 30 minutes.

3. Cool the slides after antigen retrieval:
 - Remove mailer and place in a tub with cool water from the faucet. Water should not go over the top of the mailer.
 - Allow to cool for 5 minutes.
 - Remove half the buffer from the mailer and replace with distilled water.
 - Allow to cool 5 minutes on countertop.
 - Repeat removal of half the buffer two more times, each with 5 minutes of cooling.
 - Complete by rinsing in 100% distilled water.
 - Dry the slides 5 minutes in the desiccator.
 - Check to ensure scanning of the slides has been performed.
 - For scanning, scan one slide each at 1200 dpi.

d) *Application of PNGase F:*

1. Prepare PNGase F solution:
 - Prepare 0.1 μ g/ μ L PNGaseF in water using aliquots from the -20°C freezer. Ensure that enough solution is prepared, e.g, three full slides takes approximately 1 mL of solution, spraying at 25 μ L/min.

2. Spray the PNGase F solution:

- Using the syringe dedicated to PNGase F enzyme solution, rinse the syringe with water by screwing in the needle tip, filling with 3 or more mL of water, and aspirating into waste.
- Fill with PNGase F solution ensuring that there are no bubbles in syringe. Tip: After loading all the PNGase F solution required, pull a small volume of air into the syringe. Gently dispense the syringe until the large air bubble is gone.
- Remove the needle tip and fasten the syringe to the TMSprayer line used for PNGaseF. Place the syringe onto the red syringe pump. Check that the syringe head is snug against the dispense head of the syringe pump. Ensure that the diameter is set appropriate to the syringe and the rate is set at 25 $\mu\text{L}/\text{min}$. Do not start the pump at this time.
- Place the samples in the TMSprayer tray, fastening them with tape.
- Set up TM sprayer, referring to the guide for the TMSprayer. Temperature should be set to 45°C with 15 passes, velocity of 1200, and 3 mm offset.
- Pressure reading on the front of the TMSprayer should be 10 psi.
- Start the syringe pump.
- Use a dummy slide to check the TMSprayer nozzle for spraying of solution. It generally takes about 1-3 minutes to start spraying.
- Once moisture is detected on the dummy slide, press Start on the TMSprayer. PNGase F solution will be applied in a thin layer onto target tissues.
- While the PNGase F is being applied, set up the incubation chambers.

e) Set up incubation chambers for PNGase F digest:

- Obtain a 100 x 15 mm cell culture dish with lid.
- Cut a paper towel (Wypex60 preferred) to fit to the bottom of the cell culture dish and place in bottom of dish.
- Take an 11x21 mm Kimwipe (Kimtech) and fold it in half along the creased line. Roll up the Kimwipe lengthwise forming a roll about 10 mm in diameter.
- Place the rolled Kimwipe on one end of the paper towel. You may need to squirt a little DI water on it to make sure it stays rolled.
- Place a second rolled Kimwipe at the other end.
- Saturate the paper towel and Kimwipes with water. Typically, this takes around 5 mL DI water. To perform this, simply hold the incubation dish at an angle and squirt DI water onto the towels and Kimwipes until water starts seeping out from under the towel, indicating saturation. Discard excess water that is not absorbed by the towels and Kimwipe.
- Pre-warm the incubation dish in a $38.5 \pm 1.5^\circ\text{C}$ oven at least half an hour. Light condensation should be observable on the lid of the dish.
- After application of PNGase F onto the slide, place the slide into the incubation dish using the Kimwipes as rests. Gently push the slide down slightly so that when the cover is placed on, the tissue does not touch the incubation dish cover.
- Incubate 2 hours.

- When removing, be aware that heavy condensation will have developed underneath the slide. Remove the slide slowly while holding it parallel with the countertop. Wipe off the condensation before rotating the slide.
- Store the slide in a 5 slide mailer to protect the released glycans. If matrix cannot be sprayed the same day, store at -20°C. It is preferred to immediately spray matrix onto the slide.

f) Application of Matrix:

1. Prepare the CHCA matrix:

- Prepare CHCA matrix at 7 mg/mL in 50% acetonitrile/0.1% TFA. Add 0.042g CHCA to 6 mL 50% acetonitrile/0.1% TFA. Prepare fresh each time in a 50 mL falcon tube.
- Vortex briefly and sonicate 5 minutes.
- Small chunks may remain in the bottom of the falcon tube. Make sure that these are not loaded into the TM sprayer loop as they will clog components of the TMSprayer.
- Filter CHCA solution using Millex (Millipore) 0.2 µm syringe filter.

g) Spray the CHCA matrix:

- Fill the glass 5-mL syringe with CHCA solution ensuring that there are no bubbles in syringe. Tip: After loading all the solution required, pull a small volume of air into the syringe. Gently dispense the syringe until the large air bubble is gone.
- Remove the needle tip and fasten the syringe to the TMSprayer line going to the 6-port valve.
- Move the switch to “LOAD” and steadily depress the syringe until all the sample is loaded. Note: Do not load air bubbles or undissolved matrix.
- Make sure that the pump is flowing at 0.1 mL/min. Pump pressure should be 30-40 psi when flowing at 0.1 mL/min.
- Place the samples in the TMSprayer tray, fastening them with tape.
- Set up TMSprayer referring to the guide for the TMSprayer. Temperature should be set to 80°C with 10 passes, velocity of 1300, and 2.5 mm offset.
- Pressure reading on the front of the TMSprayer should be 10 psi.
- Move the 6-port valve switch to “Spray”.
- Use a dummy slide to check the TMSprayer nozzle for spraying of solution. It generally takes about one minute to start spraying matrix.
- Once matrix is detected as an opaque solution on the dummy slide, press Start on the TMSprayer. CHCA solution will be applied in a thin layer onto target tissues.
- When finished, matrix coated slides may be imaged immediately or stored in a desiccator.

R. Supplementary data

1) Chapter 4:

Table S4.1: Calculation of derived traits

SN	GROUP	HEADINGS	DESCRIPTION	FORMULA	VALUES
Initial Profile	Glycan Peaks	GP1	<i>The percentage of M3 (major glycan) in total glycans</i>	GP1	0.13
		GP2	<i>The percentage of M3B glycan in total glycans</i>	GP2	1.58
		GP3	<i>The percentage of A1B glycan in total glycans</i>	GP3	0.93
		GP4	<i>The percentage of FA2 glycan in total glycans</i>	GP4	6.00
		GP5	<i>The percentage of FA3 glycan in total glycans</i>	GP5	17.18
		GP6	<i>The percentage of FA2G1 glycan in total glycans</i>	GP6	1.10
		GP7	<i>The percentage of A2FIG1 glycan in total glycans</i>	GP7	0.21
		GP8	<i>The percentage of M6 glycan in total glycans</i>	GP8	9.48
		GP9	<i>The percentage of FA2FIG1 glycan in total glycans</i>	GP9	3.94
		GP10	<i>The percentage of FA1BF1G1S2(3,8,P) glycan in total glycans</i>	GP10	1.51
		GP11	<i>The percentage of FA3FIG1 glycan in total glycans</i>	GP11	3.55
		GP12	<i>The percentage of A2G2S1Ac glycan in total glycans</i>	GP12	1.97
		GP13	<i>The percentage of M7D1 glycan in total glycans</i>	GP13	7.63
		GP14	<i>The percentage of FA4FIG1 glycan in total glycans</i>	GP14	1.84
		GP15	<i>The percentage of FM5A1FIG1 glycan in total glycans</i>	GP15	2.92
		GP16	<i>The percentage of M8 glycan in total glycans</i>	GP16	8.70
		GP17	<i>The percentage of FA2F2G2 glycan in total glycans</i>	GP17	2.51
		GP18	<i>The percentage of FA3FIG2S1(3) glycan in total glycans</i>	GP18	2.46
		GP19	<i>The percentage of A2G2S2(3,6) glycan in total glycans</i>	GP19	1.23
		GP20	<i>The percentage of M9 glycan in total glycans</i>	GP20	10.12
		GP21	<i>The percentage of A2FIG2S2(6,6) glycan in total glycans</i>	GP21	1.06

SN	GROUP	HEADINGS	DESCRIPTION	FORMULA	VALUES
		GP22	<i>The percentage of M9P2 glycan in total glycans</i>	GP22	3.44
		GP23	<i>The percentage of FA3F3G3 glycan in total glycans</i>	GP23	4.38
		GP24	<i>The percentage of FA4G4S3(3,3,3) glycan in total glycans</i>	GP24	3.13
		GP25	<i>The percentage of FA4F3G4S1(3) glycan in total glycans</i>	GP25	1.80
		GP26	<i>The percentage of FA4G4S4(3,3,3,6) glycan in total glycans</i>	GP26	1.21
		GPTotal	<i>The sum of total glycans</i>	SUM (GP1:GP26)	100.01
Derived Traits	Charge analysis	N1	<i>The percentage of total neutral glycans in total glycans</i>	SUM(GP1:9,GP11,GP13:GP17, GP20, GP23)	82.20
		STotal	<i>The percentage of total sialylated glycans in total glycans</i>	SUM(GP10,GP12,GP18,GP19,GP21,GP24:26)	14.37
		S1	<i>The percentage of mono-sialylated glycans in total glycans</i>	SUM(GP12, GP18, GP25)	6.23
		S2	<i>The percentage of di-sialylated glycans in total glycans</i>	SUM(GP10, GP19, GP21)	3.80
		S3	<i>The percentage of tri-sialylated glycans in total glycans</i>	SUM(GP24)	3.13
		S4	<i>The percentage of tetra-sialylated glycans in total glycans</i>	SUM(GP26)	1.21
		Phos	<i>The percentage of phosphorylated glycans in total glycans</i>	SUM(GP22)	3.44
		SAc	<i>The percentage of acetylated charged species</i>	SUM (GP12)	1.97
		Total charged species	<i>The percentage of total charged species in total glycans</i>	SUM(GP10,GP12,GP18,GP19,GP21,GP22, GP24:26)	17.81
	Poly	<i>The percentage of polysialic acids in total glycans</i>	SUM (GP10)	1.51	
	Branching	A1	<i>The percentage of monoantennary glycans in total glycans</i>	SUM(GP15)	2.92
		A2 or A1B	<i>The percentage of biantennary (or bisecting monoantennary) glycans in total glycans</i>	SUM(GP3,GP4,GP6,GP7,GP9, GP10, GP12, GP17, GP19, GP21)	20.46
		A3 or A2B	<i>The percentage of triantennary (or bisecting diantennary) glycans in total glycans</i>	SUM(GP5, GP11, GP18, GP23)	27.57
		A4 or A3B	<i>The percentage of tetraantennary (or bisecting triantennary) glycans in total glycans</i>	SUM(GP14,GP24:GP26)	7.98

SN	GROUP	HEADINGS	DESCRIPTION	FORMULA	VALUES
	High Mannose	Total high mannose	<i>The percentage of high mannose structures in total glycans</i>	SUM(GP1,GP2, GP8, GP13, GP16, GP20, GP22)	41.08
		Lower order high mannose	<i>The percentage of high mannose structures from M1-M5 in total glycans</i>	SUM(GP1, GP2)	1.71
		Higher order high mannose	<i>The percentage of high mannose structures from M6-M9 in total glycans</i>	SUM(GP8, GP13, GP16, GP20, GP22)	39.37
	Hybrid	Total hybrid glycans	<i>The percentage of hybrid structures in total glycans</i>	SUM (GP15)	2.92
	Galactosylation	G0	<i>The percentage of agalactosylated glycans in total glycans</i>	SUM(GP1:GP5,GP8, GP13, GP16, GP20, GP22)	65.19
		G1	<i>The percentage of monogalactosylated glycans in total glycans</i>	SUM(GP6,GP7, GP9, GP10, GP11, GP14, GP15)	15.07
		G2	<i>The percentage of digalactosylated glycans in total glycans</i>	SUM(GP12, GP17, GP18, GP19,GP21)	9.23
		G3	<i>The percentage of trigalactosylated glycans in total glycans</i>	SUM(GP23)	4.38
		G4	<i>The percentage of tetragalactosylated glycans in total glycans</i>	SUM(GP24:GP26)	6.14
		G0/G1	<i>The ratio of agalactosylated glycans to monoglaactosylated glycans</i>	G0/G1	4.33
		G0/G2	<i>The ratio of agalactosylated glycans to diglaactosylated glycans</i>	G0/G2	7.06
	Core fucosylation	Core Fucose Total	<i>The percentage of core fucosylated glycans in total glycans</i>	SUM(GP4: GP6, GP9: GP11,GP14, GP15, GP17, GP18, GP23:GP26)	53.53
		FG0	<i>The percentage of core fucosylated agalactosylated structures in total glycans</i>	SUM(GP4, GP5)	23.18
		FG1	<i>The percentage of core fucosylated monogalactosylated structures in total glycans</i>	SUM(GP6, GP9, GP10, GP11, GP14, GP15)	14.86
		FG2	<i>The percentage of core fucosylated digalactosylated structures in total glycans</i>	SUM(GP17, GP18)	4.97

SN	GROUP	HEADINGS	DESCRIPTION	FORMULA	VALUES
		FG3	<i>The percentage of core fucosylated trigalactosylated structures in total glycans</i>	GP23	4.38
		FG4	<i>The percentage of core fucosylated tetragalactosylated structures in total glycans</i>	SUM(GP24, GP25, GP26)	6.14
		Hybrid glycans	<i>The percentage of core fucosylated hybrid structures in total glycans</i>	SUM (GP15)	2.92
	Outer arm fucosylation	Outer armFTotal	<i>The percentage of outer arm fucosylated glycans in total glycans</i>	SUM(GP7, GP9, GP10, GP11, GP14, GP15, GP17, GP18, GP21, GP23, GP25)	26.18
		G0F	<i>The percentage of outer arm fucosylated agalactosylated structures in total glycans</i>	nd	0.00
		G1F	<i>The percentage of outer arm fucosylated monogalactosylated structures in total glycans</i>	SUM (GP7, GP9: GP11, GP14, GP15)	13.97
		G2F	<i>The percentage of outer arm fucosylated digalactosylated structures in total glycans</i>	SUM(GP17, GP18, GP21)	6.03
		G3F	<i>The percentage of outer arm fucosylated trigalactosylated structures in total glycans</i>	GP23	4.38
		G4F	<i>The percentage of outer arm fucosylated tetragalactosylated structures in total glycans</i>	GP25	1.80
		Hybrid glycans	<i>The percentage of hybrid (high mannose and complex glycans) outer arm fucosylated structures in total glycans</i>	GP15	2.92
	Alpha galactosylation	αGal	<i>The percentage of α-galactosylated glycans in total glycans</i>	nd	0.00

SN	GROUP	HEADINGS	DESCRIPTION	FORMULA	VALUES
Initial Profile	Glycan Peaks	GP1	<i>The percentage of M3 (major glycan) in total glycans</i>	GP1	0.14
		GP2	<i>The percentage of M3B glycan in total glycans</i>	GP2	1.77
		GP3	<i>The percentage of A1B glycan in total glycans</i>	GP3	0.88
		GP4	<i>The percentage of FA2 glycan in total glycans</i>	GP4	5.60
		GP5	<i>The percentage of FA3 glycan in total glycans</i>	GP5	16.86
		GP6	<i>The percentage of FA2G1 glycan in total glycans</i>	GP6	1.25
		GP7	<i>The percentage of A2F1G1 glycan in total glycans</i>	GP7	0.24
		GP8	<i>The percentage of M6 glycan in total glycans</i>	GP8	8.52
		GP9	<i>The percentage of FA2F1G1 glycan in total glycans</i>	GP9	4.56
		GP10	<i>The percentage of FA1BF1G1S2(3,8,P) glycan in total glycans</i>	GP10	1.55
		GP11	<i>The percentage of FA3F1G1 glycan in total glycans</i>	GP11	4.08
		GP12	<i>The percentage of A2G2S1Ac glycan in total glycans</i>	GP12	2.16
		GP13	<i>The percentage of M7D1 glycan in total glycans</i>	GP13	7.23
		GP14	<i>The percentage of A2G2S1(3) glycan in total glycans</i>	GP14	2.86
		GP15	<i>The percentage of FM5A1F1G1 glycan in total glycans</i>	GP15	4.40
		GP16	<i>The percentage of M8 glycan in total glycans</i>	GP16	9.01
		GP17	<i>The percentage of FA2F2G2 glycan in total glycans</i>	GP17	2.61
		GP18	<i>The percentage of FA3F2G2 glycan in total glycans</i>	GP18	2.28
		GP19	<i>The percentage of A2G2S2(3,6) glycan in total glycans</i>	GP19	1.27
		GP20	<i>The percentage of M9 glycan in total glycans</i>	GP20	9.08
		GP21	<i>The percentage of A2F1G2S2(6,6) glycan in total glycans</i>	GP21	1.77
		GP22	<i>The percentage of FA3F2G3S1(3) glycan in total glycans</i>	GP22	3.08
		GP23	<i>The percentage of FA3F3G3 glycan in total glycans</i>	GP23	4.13
		GP24	<i>The percentage of FA3F1G3S3(3,3,3) glycan in total glycans</i>	GP24	2.80
		GP25	<i>The percentage of FA4F3G4S1(3) glycan in total glycans</i>	GP25	1.17
		GP26	<i>The percentage of FA4F2G4S2(3,8,P) glycan in total glycans</i>	GP26	0.69
		GPTotal	<i>The sum of total glycans</i>	SUM (GP1:GP26)	99.99

SN	GROUP	HEADINGS	DESCRIPTION	FORMULA	VALUES
Derived Traits	Charge analysis	N1	<i>The percentage of total neutral glycans in total glycans</i>	SUM(GP1:9,GP11,GP13, GP15:GP18, GP20, GP23)	82.64
		STotal	<i>The percentage of total sialylated glycans in total glycans</i>	SUM(GP10,GP12, GP14, GP19,GP21, GP22, GP24:26)	17.35
		S1	<i>The percentage of mono-sialylated glycans in total glycans</i>	SUM(GP12, GP14, GP22, GP25)	9.27
		S2	<i>The percentage of di-sialylated glycans in total glycans</i>	SUM(GP10, GP19, GP21, GP26)	5.28
		S3	<i>The percentage of tri-sialylated glycans in total glycans</i>	SUM(GP24)	2.80
		S4	<i>The percentage of tetra-sialylated glycans in total glycans</i>	nd	0.00
		Phos	<i>The percentage of phosphorylated glycans in total glycans</i>	nd	0.00
		SAc	<i>The percentage of acetylated charged species</i>	SUM (GP12)	2.16
		Total charged species	<i>The percentage of total charged species in total glycans</i>	SUM(GP10,GP12, GP14, GP19,GP21,GP22, GP24:26)	17.35
		Poly	<i>The percentage of polysialic acids in total glycans</i>	SUM (GP10, GP26)	2.24
	Branching	A1	<i>The percentage of monoantennary glycans in total glycans</i>	SUM(GP15)	4.40
		A2 or A1B	<i>The percentage of biantennary (or bisecting monoantennary) glycans in total glycans</i>	SUM(GP3,GP4,GP6,GP7,G P9, GP10, GP12, GP14, GP17, GP19, GP21)	24.75
		A3 or A2B	<i>The percentage of triantennary (or bisecting diantennary) glycans in total glycans</i>	SUM(GP5, GP11, GP18, GP22, GP23, GP24)	33.23
		A4 or A3B	<i>The percentage of tetraantennary (or bisecting triantennary) glycans in total glycans</i>	SUM(GP25, GP26)	1.86
	High Mannose	Total high mannose	<i>The percentage of high mannose structures in total glycans</i>	SUM(GP1,GP2, GP8, GP13, GP16, GP20)	35.75
		Lower order high mannose	<i>The percentage of high mannose structures from M1-M5 in total glycans</i>	SUM(GP1, GP2)	1.91

SN	GROUP	HEADINGS	DESCRIPTION	FORMULA	VALUES
		Higher order high mannose	<i>The percentage of high mannose structures from M6-M9 in total glycans</i>	SUM(GP8, GP13, GP16, GP20)	33.84
	Hybrid	Total hybrid glycans	<i>The percentage of hybrid structures in total glycans</i>	SUM (GP15)	4.40
	Galactosylation	G0	<i>The percentage of agalactosylated glycans in total glycans</i>	SUM(GP1:GP5,GP8, GP13, GP16, GP20)	59.09
		G1	<i>The percentage of monogalactosylated glycans in total glycans</i>	SUM(GP6,GP7, GP9, GP10, GP11, GP15)	16.08
		G2	<i>The percentage of digalactosylated glycans in total glycans</i>	SUM(GP12, GP14, GP17, GP18, GP19,GP21)	12.95
		G3	<i>The percentage of trigalactosylated glycans in total glycans</i>	SUM(GP22: GP24)	10.01
		G4	<i>The percentage of tetragalactosylated glycans in total glycans</i>	SUM(GP25, GP26)	1.86
		G0/G1	<i>The ratio of agalactosylated glycans to monogalactosylated glycans</i>	G0/G1	3.67
		G0/G2	<i>The ratio of agalactosylated glycans to digalactosylated glycans</i>	G0/G2	4.56
	Core fucosylation	Core Fucose Total	<i>The percentage of core fucosylated glycans in total glycans</i>	SUM(GP4: GP6, GP9: GP11, GP15, GP17, GP18, GP22:GP26)	55.06
		FG0	<i>The percentage of core fucosylated agalactosylated structures in total glycans</i>	SUM(GP4, GP5)	22.46
		FG1	<i>The percentage of core fucosylated monogalactosylated structures in total glycans</i>	SUM(GP6, GP9, GP10, GP11, GP15)	15.84
		FG2	<i>The percentage of core fucosylated digalactosylated structures in total glycans</i>	SUM(GP17, GP18)	4.89
		FG3	<i>The percentage of core fucosylated trigalactosylated structures in total glycans</i>	SUM(GP22:GP24)	10.01
		FG4	<i>The percentage of core fucosylated tetragalactosylated structures in total glycans</i>	SUM(GP25, GP26)	1.86

SN	GROUP	HEADINGS	DESCRIPTION	FORMULA	VALUES
		Hybrid glycans	<i>The percentage of core fucosylated hybrid structures in total glycans</i>	SUM (GP15)	4.40
	Outer arm fucosylation	Outer arm Fucose Total	<i>The percentage of outer arm fucosylated glycans in total glycans</i>	SUM(GP7, GP9, GP10, GP11, GP15, GP17, GP18, GP21:GP25)	33.36
		G0F	<i>The percentage of outer arm fucosylated agalactosylated structures in total glycans</i>	nd	0.00
		G1F	<i>The percentage of outer arm fucosylated monogalactosylated structures in total glycans</i>	SUM (GP7, GP9: GP11, GP15)	14.83
		G2F	<i>The percentage of outer arm fucosylated digalactosylated structures in total glycans</i>	SUM(GP17, GP18, GP21)	6.66
		G3F	<i>The percentage of outer arm fucosylated trigalactosylated structures in total glycans</i>	SUM(GP23, GP24)	6.93
		G4F	<i>The percentage of outer arm fucosylated tetragalactosylated structures in total glycans</i>	SUM (GP25, GP26)	1.86
		Hybrid glycans	<i>The percentage of hybrid (high mannose and complex glycans) outer arm fucosylated structures in total glycans</i>	GP15	4.40
	Alpha galactosylation	α Gal	<i>The percentage of α-galactosylated glycans in total glycans</i>	nd	0.00

Table S4.2: Mass spectrometry tables for glycan peak identification

SN: t _R (min)	Peak	Experimental mass (m/z)	Theoretical mass (m/z)	Error (ppm)	Ion	Assignment	Monosaccharide composition	Monoisotopic mass
7.39	1	nd	514.1910		[M-2H] ⁻²	M3	HexNAc ₂ Hex ₃	1030.3965
8.14	2	nd	615.7307		[M-2H] ⁻²	M3B,A1	HexNAc ₃ Hex ₃	1233.4759
8.92	3	717.2723	717.2704	2.65	[M-2H] ⁻²	A1B	HexNAc ₄ Hex ₃	1436.5553
9.51	4	790.2977	790.2993	2.02	[M-2H] ⁻²	FA2, FA1B	dHex ₁ HexNAc ₄ Hex ₃	1582.6132
		1581.6016	1581.6059	2.72	[M-H] ⁻¹			
		688.7602	688.7566	5.23	[M-2H] ⁻²	FA1	dHex ₁ HexNAc ₃ Hex ₃	1379.5338
		818.8132	818.8100	3.91	[M-2H] ⁻²	A3	HexNAc ₅ Hex ₃	1639.6345
10.78	5	891.8362	891.8390	3.14	[M-2H] ⁻²	FA3	dHex ₁ HexNAc ₅ Hex ₃	1785.6926
		1784.6782	1784.6926	8.07	[M-1H] ⁻¹			
		676.2537	676.2438	14.64	[M-2H] ⁻²	M5	HexNAc ₂ Hex ₅	1354.5422
		1353.4977	1353.4949	2.07	[M-1H] ⁻¹			
		769.7871	769.7860	1.43	[M-2H] ⁻²			
12.07	6	871.3132	871.3257	14.35	[M-2H] ⁻²	FA2G1, A2F1G1, FA1BG1	dHex ₁ HexNAc ₄ Hex ₄	1744.6660
		749.2681	749.2728	6.27	[M-2H] ⁻²	FM5	dHex ₁ HexNAc ₂ Hex ₅	1500.5601
12.88	7	871.3132	871.3257	14.35	[M-2H] ⁻²	A2F1G1	dHex ₁ HexNAc ₄ Hex ₄	1744.6660
		777.7692	777.7835	18.39	[M-2H] ⁻²	M5A1	HexNAc ₃ Hex ₅	1557.5815
13.59	8	757.2618	757.2702	11.09	[M-2H] ⁻²	M6	HexNAc ₂ Hex ₆	1516.5550
		1515.5400	1515.5477	5.08	[M-1H] ⁻¹			
		972.8723	972.8654	7.09	[M-2H] ⁻²	FA3G1, A3F1G1	dHex ₁ HexNAc ₅ Hex ₄	1947.7454
		850.8018	850.8125	12.58	[M-2H] ⁻²	FM5A1, FM4A1G1,M4A1F1G1	dHex ₁ HexNAc ₃ Hex ₅	1703.6395
		879.3174	879.3232	6.60	[M-2H] ⁻²	A2G1Gal1	HexNAc ₄ Hex ₅	1703.6395
		842.8217	842.815	7.95	[M-2H] ⁻²	FA1F1G1	HexNAc ₂ Hex ₆	1687.6445

SN: t _R (min)	Peak	Experimental mass (m/z)	Theoretical mass (m/z)	Error (ppm)	Ion	Assignment	Monosaccharide composition	Monoisotopic mass
14.66	9	944.3465	944.3547	8.68	[M-2H] ⁻³	FA2F1G1	dHex ₂ HexNAc ₄ Hex ₄	1890.7239
		850.8018	850.8099	9.52	[M-2H] ⁻²	M6A1, FM5A1, FA1G1Gal1	dHex ₁ HexNAc ₃ Hex ₅	1719.6344
		1016.8818	1016.8734	8.26	[M-2H] ⁻²	FA1BG1S1	dHex ₁ HexNAc ₄ Neu5Ac ₁ Hex ₄	2035.7614
		972.8594	972.8654	6.17	[M-2H] ⁻²	FA3G1	dHex ₁ HexNAc ₅ Hex ₄	1947.7454
14.99	10	944.3528	944.3547	2.01	[M-2H] ⁻²	FA2F1G1	dHex ₂ HexNAc ₄ Hex ₄	1890.7239
		1016.8688	1016.8734	4.52	[M-2H] ⁻²	FA2G1S1	dHex ₁ HexNAc ₄ Neu5Ac ₁ Hex ₄	2035.7614
		1235.4397	1235.4501	8.42	[M-H] ⁻¹	FA1BF1G1S2(P), FA2F1G1S2(P)	dHex ₂ HexNAc ₄ Neu5Ac ₂ Hex ₄	2472.9147
		952.3621	952.3521	10.50	[M-2H] ⁻²	FA2G2,A2F1G2	dHex ₁ HexNAc ₄ Hex ₅	1906.7188
15.27	11	1045.8645	1045.8944	28.59	[M-2H] ⁻²	FA3F1G1	dHex ₂ HexNAc ₅ Hex ₄	2093.8033
		952.3494	952.3521	2.84	[M-2H] ⁻²	FA2G1Gal1	dHex ₁ HexNAc ₄ Hex ₅	1906.7188
		1016.8622	1016.8734	11.01	[M-2H] ⁻²	FA1BG1S1	dHex ₁ HexNAc ₄ Neu5Ac ₁ Hex ₄	2035.7614
		1118.4080	1118.4131	4.56	[M-2H] ⁻²	FA3G1S1	dHex ₁ HexNAc ₅ Neu5Ac ₁ Hex ₄	2238.8408
		944.3528	944.3547	2.01	[M-2H] ⁻²	FA2F1G1	dHex ₂ HexNAc ₄ Hex ₄	1890.7239
15.98	12	1045.8844	1045.8944	9.56	[M-2H] ⁻²	FA3F1G1	dHex ₂ HexNAc ₅ Hex ₄	2093.8033
		1045.8711	1045.8762	4.88	[M-2H] ⁻²	A2G2S1Ac	HexNAc ₄ Neu5Ac ₁ Hex ₅ Ac	2093.7669
		1064.8613	1064.8493	11.27	[M-2H] ⁻²	A2Sul1G2S1	HexNAc ₄ Neu5Ac ₁ Hex ₅ Sul	2131.7132
		923.8229	923.8414	20.03	[M-2H] ⁻²	FM4A1F1G1	dHex ₂ HexNAc ₃ Hex ₅	1849.6974
		996.3636	996.3602	3.41	[M-2H] ⁻²	FA1F1G1Gc1, FM4A1G1S1	dHex ₂ HexNAc ₃ Hex ₄ Neu5Gc ₁ /dHex ₁ Hex NAc ₃ Neu5Ac ₁ Hex ₅	1994.7349
		1118.4354	1118.4131	19.94	[M-2H] ⁻²	A3F1G1S1, FA3G1S1	dHex ₁ HexNAc ₅ Neu5Ac ₁ Hex ₄	2238.8408
		1053.8795	1053.8918	11.67	[M-2H] ⁻²	FA3G2	dHex ₁ HexNAc ₅ Hex ₅	2109.7982

SN: t _R (min)	Peak	Experimental mass (m/z)	Theoretical mass (m/z)	Error (ppm)	Ion	Assignment	Monosaccharide composition	Monoisotopic mass
16.84	13	838.2903	838.2966	7.52	[M-2H] ⁻²	M7	HexNAc ₂ Hex ₇	1678.6078
		1677.5890	1677.6005	6.86	[M-1H] ⁻¹			
		1025.3894	1025.3811	8.09	[M-2H] ⁻²	A2G2F2, FA2F1G2	dHex ₂ HexNAc ₅ Hex ₅	2052.7767
		1045.8778	1045.8944	15.87	[M-2H] ⁻²	A3F2G1	dHex ₂ HexNAc ₅ Hex ₄	2093.8033
		1118.4216	1118.4131	7.60	[M-2H] ⁻²	FA3G1S1	dHex ₁ HexNAc ₅ Neu5Ac ₁ Hex ₄	2238.8408
17.86	14	1147.4309	1147.4341	2.79	[M-2H] ⁻²	FA4F1G1	dHex ₂ HexNAc ₆ Hex ₄	2296.8827
		1118.4148	1118.4131	1.52	[M-2H] ⁻²	A3F1G1S1, FA3G1S1	dHex ₁ HexNAc ₅ Neu5Ac ₁ Hex ₄	2238.8408
		1219.9666	1219.9528	11.31	[M-2H] ⁻²	FA3BG1S1	dHex ₁ HexNAc ₆ Neu5Ac ₁ Hex ₄	2411.9202
		1024.8574	1024.8709	13.17	[M-2H] ⁻²	A2G2S1	HexNAc ₄ Neu5Ac ₁ Hex ₅	2051.7563
18.37	15	1191.4359	1191.4421	5.20	[M-2H] ⁻²	A3F2G1S1, FA3F1G1S1	dHex ₂ HexNAc ₅ Neu5Ac ₁ Hex ₄	2384.8987
		1191.4005	1191.4239	19.64	[M-2H] ⁻²	A2G2S2Ac	HexNAc ₄ Neu5Ac ₂ Hex ₅ Ac	2384.8623
		1162.4175	1162.4393	18.75	[M-2H] ⁻²	FA2G1S2 (P)	dHex ₁ HexNAc ₄ Neu5Ac ₂ Hex ₄	2326.8568
		1004.8760	1004.8678	8.16	[M-2H] ⁻²	FM5A1F1G1	dHex ₂ HexNAc ₃ Hex ₆	2011.7502
		1097.9175	1097.8998	16.12	[M-2H] ⁻²	FA2G2S1, FA2F1G1Gc1	dHex ₁ HexNAc ₄ Neu5Ac ₁ Hex ₅ /dHex ₂ HexNAc ₄ Neu5Gc ₁ Hex ₄	2197.8142
19.85	16	919.3210	919.3230	2.18	[M-2H] ⁻²	M8	HexNAc ₂ Hex ₈	1840.6606
		1839.6235	1839.6105	7.07	[M-1H] ⁻¹			
		1170.9155	1170.9288	11.36	[M-2H] ⁻²	FA2F1G2S1	dHex ₂ HexNAc ₄ Neu5Ac ₁ Hex ₅	2343.8722
		1106.4060	1106.4075	1.36	[M-2H] ⁻²	M4A2F2G2	dHex ₂ HexNAc ₄ Hex ₆	2214.8296
		1243.4044	1243.3972	5.79	[M-2H] ⁻²	FA2G2S2, A2F1G2S2,FA2F1G1Gc1S1	dHex ₁ HexNAc ₄ Neu5Ac ₂ Hex ₅ / dHex ₂ HexNAc ₄ Neu5Gc ₁ Neu5Ac ₁ Hex ₄	2488.9097

SN: t _R (min)	Peak	Experimental mass (m/z)	Theoretical mass (m/z)	Error (ppm)	Ion	Assignment	Monosaccharide composition	Monoisotopic mass
		1199.4282	1199.4395	9.42	[M-2H] ⁻²	FA3G2S1,FA3F1G1Gc1	dHex ₁ HexNAc ₅ Neu5Ac ₁ Hex ₅ / dHex ₂ HexNAc ₅ Neu5Gc ₁ Hex ₄	2400.8936
		1264.4382	1264.4528	11.55	[M-2H] ⁻²	FA2G2S2Ac	dHex ₁ HexNAc ₄ Neu5Ac ₂ AcHex ₅	2530.9202
20.38	17	1098.4001	1098.4100	9.01	[M-2H] ⁻²	FA2F2G2, A2F3G2	dHex ₃ HexNAc ₄ Hex ₅	2198.8346
		1170.9086	1170.9288	17.25	[M-2H] ⁻²	FA2F1G2S1, FM4A1BF1G1S1, FA2F2G1Gc1, FA2F1G2S1	dHex ₂ HexNAc ₄ Neu5Ac ₁ Hex ₅ /dHex ₃ HexNAc ₄ Neu5Gc ₁ Hex ₄	2343.8722
		1243.3972	1243.3972	0.00	[M-2H] ⁻²	FA2G2S2, A2F1G2S2,FA2F1G1Gc1S1	dHex ₁ HexNAc ₄ Neu5Ac ₂ Hex ₅ / dHex ₂ HexNAc ₄ Neu5Gc ₁ Neu5Ac ₁ Hex ₄	2488.9097
		919.3086	919.3230	15.66	[M-2H] ⁻²	M8	HexNAc ₂ Hex ₈	1840.6606
20.85	18	1272.4739	1272.4685	4.24	[M-2H] ⁻²	FA3F1G2S1	dHex ₂ HexNAc ₅ Neu5Ac ₁ Hex ₅	2546.9515
		1199.9540	1199.9497	3.58	[M-2H] ⁻²	FA3F2G2, A2F2G1F1L1	dHex ₃ HexNAc ₅ Hex ₅	2401.9140
		1106.4020	1106.4075	4.97	[M-2H] ⁻²	FA2F1G2Gal	dHex ₂ HexNAc ₄ Hex ₆	2214.8296
		1284.4720	1284.4741	1.63	[M-2H] ⁻²	FA2GalNAc2S2	dHex ₁ HexNAc ₆ Neu5Ac ₂ Hex ₃	2570.9628
21.65	19	1199.9469	1199.9497	2.33	[M-2H] ⁻²	A2F3G1L1, A3F3G2	dHex ₃ HexNAc ₅ Hex ₅	2401.9140
		1170.4103	1170.4186	7.09	[M-2H] ⁻²	A2G2S2	HexNAc ₄ Neu5Ac ₂ Hex ₅	2342.8518
		1373.9714	1373.9900	13.54	[M-2H] ⁻²	FA4F1G2S1	dHex ₂ HexNAc ₆ Neu5Ac ₁ Hex ₅	2751.0513
		1243.4623	1243.4476	11.82	[M-2H] ⁻²	FA2G2S2	dHex ₁ HexNAc ₄ Neu5Ac ₂ Hex ₅	2488.9097
		1272.4739	1272.4685	4.24	[M-2H] ⁻²	FA3F1G2S1,FA3F2G1Gc1	dHex ₂ HexNAc ₅ Neu5Ac ₁ Hex ₅ /dHex ₃ Hex NAc ₅ Neu5Gc ₁ Hex ₄	2546.9515
22.22	20	1000.3493	1000.3495	0.20	[M-2H] ⁻²	M9	HexNAc ₂ Hex ₉	2002.7135
		1301.4772	1301.4894	9.37	[M-2H] ⁻²	A4F3G2,FA4F2G2, FA2BF2G1L1	dHex ₃ HexNAc ₆ Hex ₅	2604.9904

SN: t _R (min)	Peak	Experimental mass (m/z)	Theoretical mass (m/z)	Error (ppm)	Ion	Assignment	Monosaccharide composition	Monoisotopic mass
		1374.0018	1373.9900	8.59	[M-2H] ⁻²	A3G3S2Ac,FA4F1G2S1,A4F2G2S1	dHex ₂ HexNAc ₆ Neu5Ac ₁ Hex ₅ / HexNAc ₅ Neu5Ac ₂ AcHex ₆	2750.0309
		1243.9397	1243.9578	14.55	[M-2H] ⁻²	FA2F2G2S1	dHex ₃ HexNAc ₄ Neu5Ac ₁ Hex ₅	2489.9301
		1316.4845	1316.4765	6.08	[M-2H] ⁻²	FA2F1G2S2, A2F2G2S2	dHex ₂ HexNAc ₄ Neu5Ac ₂ Hex ₅	2634.9676
		1170.4296	1170.4186	9.40	[M-2H] ⁻²	A2G2S2	HexNAc ₄ Neu5Ac ₂ Hex ₅	2342.8518
24.16	21	1316.4548	1316.4765	16.48	[M-2H] ⁻²	FA2F1G2S2, A2F2G2S2	dHex ₂ HexNAc ₄ Neu5Ac ₂ Hex ₅	2634.9676
		1389.9839	1390.0031	13.81	[M-2H] ⁻²	A4G4S1, FA4G3Gc1, A3BG3GalS1	HexNAc ₆ Neu5Ac ₁ Hex ₇ /dHex ₁ HexNAc ₆ Neu5Gc ₁ Hex ₆	2782.0207
		1243.4261	1243.4476	17.29	[M-2H] ⁻²	A2F1G2S2	dHex ₁ HexNAc ₄ Neu5Ac ₂ Hex ₅	2488.9097
		925.6566	925.6611	4.86	[M-3H] ⁻³	FA2G2S3(P), A2F1G2S3	dHex ₁ HexNAc ₄ Neu5Ac ₃ Hex ₅	2780.0051
24.37	22	1426.5369	1426.5239	9.11	[M-2H] ⁻²	FA2F2G2L1S1, FA3F2G3S1	dHex ₃ HexNAc ₅ Neu5Ac ₁ Hex ₆	2855.0623
		1499.0245	1499.0426	12.07	[M-2H] ⁻²	FA3F1G3S2,FA2F1G2L1S2	dHex ₃ HexNAc ₅ Neu5Ac ₁ Neu5Gc ₁ Hex ₅	3000.0998
		1080.3519	1080.3158	33.42	[M-2H] ⁻²	M9P2	HexNAc ₂ Hex ₉	2162.6464
26.14	23	1354.0109	1354.0051	4.28	[M-2H] ⁻²	FA3F3G3	dHex ₄ HexNAc ₅ Hex ₆	2710.0248
		1047.3575	1047.3718	13.65	[M-3H] ⁻³	A3F2G2Gc1S2(P),A3G3F1 S3,FA3G3S3,FA3F1G2Gc1 S2(P)	dHex ₂ HexNAc ₅ Neu5Gc ₁ Neu5Ac ₂ Hex ₅ / dHex ₁ HexNAc ₅ Neu5Ac ₃ Hex ₆	3145.1373
		1571.5760	1571.5614	9.29	[M-2H] ⁻²			
		1499.0166	1499.0426	17.34	[M-2H] ⁻²	FA3F1G3S2,FA2F1G2L1S2	dHex ₂ HexNAc ₅ Neu5Ac ₂ Hex ₆	3000.0998
		1115.0631	1115.0649	1.61	[M-3H] ⁻³	FA3BG3S3	dHex ₁ HexNAc ₆ Neu5Ac ₃ Hex ₇	3348.2166
		1528.0542	1528.0635	6.09	[M-2H] ⁻²	FA4F2G3S1	dHex ₃ HexNAc ₆ Neu5Ac ₁ Hex ₆	3058.1416
30.06	24	1169.0634	1169.0825	16.34	[M-3H] ⁻³	FA4G4S3, FA3G3L1S3,FA4F1G3Gc1S 2(P)	dHex ₁ HexNAc ₆ Neu5Ac ₃ Hex ₇ / dHex ₂ HexNAc ₆ Neu5Gc ₁ Neu5Ac ₂ Hex ₆	3510.2695
		1754.1617	1754.1275	19.50	[M-2H] ⁻²			
		1096.0562	1096.0494	6.20	[M-3H] ⁻³	FA3F1G3S3	dHex ₂ HexNAc ₅ Neu5Ac ₃ Hex ₆	3291.1952

SN: t _R (min)	Peak	Experimental mass (m/z)	Theoretical mass (m/z)	Error (ppm)	Ion	Assignment	Monosaccharide composition	Monoisotopic mass
		1217.7324	1217.7324	0.00	[M-3H] ⁻³	FA4F1G4S3,FA4F2G3Gc1S 2	dHex ₂ HexNAc ₆ Neu5Ac ₃ Hex ₇ / dHex ₃ HexNAc ₆ Neu5Gc ₁ Neu5Ac ₂ Hex ₆	3656.3274
		1681.1024	1681.0985	2.32	[M-2H] ⁻²	A4G4S3	HexNAc ₆ Neu5Ac ₃ Hex ₇	3364.2116
		1120.3706	1120.3966	23.21	[M-3H] ⁻³			
		1115.0838	1115.0649	16.95	[M-3H] ⁻³	FA3BG3S3	dHex ₁ HexNAc ₆ Neu5Ac ₃ Hex ₇	3348.2166
		1681.5735	1681.6087	20.93	[M-2H] ⁻²	FA4F1G4S2,FA4F2G3Gc1S 1	dHex ₂ HexNAc ₆ Neu5Ac ₂ Hex ₇ / dHex ₃ HexNAc ₆ Neu5Gc ₁ Neu5Ac ₁ Hex ₆	3365.2320
30.58	25	1169.0845	1169.0825	1.71	[M-3H] ⁻³	FA4G4S3, FA3G3L1S3	dHex ₁ HexNAc ₆ Neu5Ac ₃ Hex ₇	3510.2695
		1754.1617	1754.1275	19.50	[M-2H] ⁻²			
		1266.1017	1266.1144	10.03	[M-3H] ⁻³	FA4G4S4, A4F1G4S4	dHex ₁ HexNAc ₆ Neu5Ac ₄ Hex ₇	3801.3649
		1682.1118	1682.1189	4.22	[M-2H] ⁻²	FA4F3G4S1	dHex ₄ HexNAc ₆ Neu5Ac ₁ Hex ₇	3366.2524
		1121.0916	1121.0768	13.20	[M-3H] ⁻³			
		1217.7180	1217.7324	11.83	[M-3H] ⁻³	FA4F1G4S3,FA4F2G3Gc1S 2(P)	dHex ₂ HexNAc ₆ Neu5Ac ₃ Hex ₇ / dHex ₃ HexNAc ₆ Neu5Gc ₁ Neu5Ac ₂ Hex ₆	3656.3274
31.34	26	1266.1017	1266.1144	10.03	[M-3H] ⁻³	FA4G4S4	dHex ₁ HexNAc ₆ Neu5Ac ₄ Hex ₇	3801.3649
		1217.7252	1217.7324	5.91	[M-3H] ⁻³	FA4F1G4S3 (P), FA4F2G3Gc1S2 (P)	dHex ₂ HexNAc ₆ Neu5Ac ₃ Hex ₇ / dHex ₃ HexNAc ₆ Neu5Gc ₁ Neu5Ac ₂ Hex ₆	3656.3274
		1314.8032	1314.8003	2.21	[M-3H] ⁻³	FA4F1G4S4	dHex ₂ HexNAc ₆ Neu5Ac ₄ Hex ₇	3801.3649
		1169.4352	1169.4227	10.69	[M-3H] ⁻³	FA4F2G4S2 (P)	dHex ₃ HexNAc ₆ Neu5Ac ₂ Hex ₇	3511.2899

Striatum tr (min)	Peak UPLC	Experimental mass (m,z)	Theoretical mass (m,z)	Error (ppm)	Ion	Assignment	Monosaccharide composition	Monoisotopic mass
7.39	1	nd	514.1910		[M-2H] ⁻²	M3	HexNAc ₂ Hex ₃	1030.3965
8.14	2	nd	615.7307		[M-2H] ⁻²	M3B, A1	HexNAc ₃ Hex ₃	1233.4759
8.92	3	717.2723	717.2704	2.65	[M-2H] ⁻²	A1B	HexNAc ₄ Hex ₃	1436.5553
9.51	4	790.2977	790.2993	2.02	[M-2H] ⁻²	FA2, FA1B	dHex ₁ HexNAc ₄ Hex ₃	1582.6132
		1581.6016	1581.6059	2.72	[M-H] ⁻¹			
		688.7602	688.7566	5.23	[M-2H] ⁻²	FA1	dHex ₁ HexNAc ₃ Hex ₃	1379.5338
		818.8132	818.8100	3.91	[M-2H] ⁻²	A3	HexNAc ₃ Hex ₃	1639.6345
10.78	5	891.8362	891.8390	3.14	[M-2H] ⁻²	FA3	dHex ₁ HexNAc ₅ Hex ₃	1785.6926
		1784.6782	1784.6926	8.07	[M-1H] ⁻¹			
		676.2537	676.2438	14.64	[M-2H] ⁻²	M5	HexNAc ₂ Hex ₅	1354.5422
		1353.4977	1353.4949	2.07	[M-1H] ⁻¹			
		769.7871	769.7860	1.43	[M-2H] ⁻²	FA1G1, FM4A1, A1F1G1	dHex ₁ HexNAc ₃ Hex ₄	1541.5866
12.07	6	871.3132	871.3257	14.35	[M-2H] ⁻²	FA2G1, A2F1G1, FA1BG1	dHex ₁ HexNAc ₄ Hex ₄	1744.6660
		749.2681	749.2728	6.27	[M-2H] ⁻²	FM5	dHex ₁ HexNAc ₂ Hex ₅	1500.5601

Striatum tr (min)	Peak UPLC	Experimental mass (m,z)	Theoretical mass (m,z)	Error (ppm)	Ion	Assignment	Monosaccharide composition	Monoisotopic mass
12.88	7	871.3132	871.3257	14.35	[M-2H] ⁻²	A2F1G1	dHex ₁ HexNAc ₄ Hex ₄	1744.6660
		777.7692	777.7835	18.39	[M-2H] ⁻²	M5A1	HexNAc ₃ Hex ₅	1557.5815
13.59	8	757.2618	757.2702	11.09	[M-2H] ⁻²	M6	HexNAc ₂ Hex ₆	1516.5550
		1515.5400	1515.5477	5.08	[M-1H] ⁻¹			
		972.8723	972.8654	7.09	[M-2H] ⁻²	FA3G1, A3F1G1	dHex ₁ HexNAc ₅ Hex ₄	1947.7454
		850.8018	850.8125	12.58	[M-2H] ⁻²	FM5A1, FM4A1G1, M4A1F1G1	dHex ₁ HexNAc ₃ Hex ₅	1703.6395
		879.3174	879.3232	6.60	[M-2H] ⁻²	A2G1Gal1	HexNAc ₄ Hex ₅	1703.6395
		842.8217	842.815	7.95	[M-2H] ⁻²	FA1F1G1	HexNAc ₂ Hex ₆	1687.6445
14.66	9	944.3465	944.3547	8.68	[M-2H] ⁻³	FA2F1G1	dHex ₂ HexNAc ₄ Hex ₄	1890.7239
		850.8018	850.8099	9.52	[M-2H] ⁻²	M6A1, FM5A1, FA1G1Gal1	dHex ₁ HexNAc ₃ Hex ₅	1719.6344
		1016.8818	1016.8734	8.26	[M-2H] ⁻²	FA1BG1S1	dHex ₁ HexNAc ₄ Neu5Ac ₁ Hex ₄	2035.7614
		972.8594	972.8654	6.17	[M-2H] ⁻²	FA3G1	dHex ₁ HexNAc ₅ Hex ₄	1947.7454
14.99	10	944.3528	944.3547	2.01	[M-2H] ⁻²	FA2F1G1	dHex ₂ HexNAc ₄ Hex ₄	1890.7239
		1016.8688	1016.8734	4.52	[M-2H] ⁻²	FA2G1S1	dHex ₁ HexNAc ₄ Neu5Ac ₁ Hex ₄	2035.7614

Striatum tr (min)	Peak UPLC	Experimental mass (m,z)	Theoretical mass (m,z)	Error (ppm)	Ion	Assignment	Monosaccharide composition	Monoisotopic mass
		1235.4397	1235.4501	8.42	[M-H] ⁻¹	FA1BF1G1S2(P), FA2F1G1S2(P)	dHex ₂ HexNAc ₄ Neu5Ac ₂ Hex ₄	2472.9147
		952.3621	952.3521	10.50	[M-2H] ⁻²	FA2G2,A2F1G2	dHex ₁ HexNAc ₄ Hex ₅	1906.7188
15.27	11	1045.8645	1045.8944	28.59	[M-2H] ⁻²	FA3F1G1	dHex ₂ HexNAc ₅ Hex ₄	2093.8033
		952.3494	952.3521	2.84	[M-2H] ⁻²	FA2G1Gal1	dHex ₁ HexNAc ₄ Hex ₅	1906.7188
		1016.8622	1016.8734	11.01	[M-2H] ⁻²	FA1BG1S1	dHex ₁ HexNAc ₄ Neu5Ac ₁ Hex ₄	2035.7614
		1118.4080	1118.4131	4.56	[M-2H] ⁻²	FA3G1S1	dHex ₁ HexNAc ₅ Neu5Ac ₁ Hex ₄	2238.8408
		944.3528	944.3547	2.01	[M-2H] ⁻²	FA2F1G1	dHex ₂ HexNAc ₄ Hex ₄	1890.7239
15.98	12	1045.8844	1045.8944	9.56	[M-2H] ⁻²	FA3F1G1	dHex ₂ HexNAc ₅ Hex ₄	2093.8033
		1045.8711	1045.8762	4.88	[M-2H] ⁻²	A2G2S1Ac	HexNAc ₄ Neu5Ac ₁ Hex ₅ Ac	2093.7669
		1064.8613	1064.8493	11.27	[M-2H] ⁻²	A2Sul1G2S1	HexNAc ₄ Neu5Ac ₁ Hex ₅ Sul	2131.7132
		923.8229	923.8414	20.03	[M-2H] ⁻²	FM4A1F1G1	dHex ₂ HexNAc ₃ Hex ₅	1849.6974
		996.3636	996.3602	3.41	[M-2H] ⁻²	FA1F1G1Gc1, FM4A1G1S1	dHex ₂ HexNAc ₃ Hex ₄ Neu5Gc ₁ /dHex ₁ HexNAc ₃ Neu5Ac ₁ Hex ₅	1994.7349
		1118.4354	1118.4131	19.94	[M-2H] ⁻²	A3F1G1S1, FA3G1S1	dHex ₁ HexNAc ₅ Neu5Ac ₁ Hex ₄	2238.8408
		1053.8795	1053.8918	11.67	[M-2H] ⁻²	FA3G2	dHex ₁ HexNAc ₅ Hex ₅	2109.7982

Striatum tr (min)	Peak UPLC	Experimental mass (m,z)	Theoretical mass (m,z)	Error (ppm)	Ion	Assignment	Monosaccharide composition	Monoisotopic mass
16.84	13	838.2903	838.2966	7.52	[M-2H] ⁻²	M7	HexNAc ₂ Hex ₇	1678.6078
		1677.5890	1677.6005	6.86	[M-1H] ⁻¹			
		1025.3894	1025.3811	8.09	[M-2H] ⁻²	A2G2F2, FA2F1G2	dHex ₂ HexNAc ₅ Hex ₅	2052.7767
		1045.8778	1045.8944	15.87	[M-2H] ⁻²	A3F2G1	dHex ₂ HexNAc ₅ Hex ₄	2093.8033
		1118.4216	1118.4131	7.60	[M-2H] ⁻²	FA3G1S1	dHex ₁ HexNAc ₅ Neu5Ac ₁ Hex ₄	2238.8408
17.86	14	1147.4309	1147.4341	2.79	[M-2H] ⁻²	FA4F1G1	dHex ₂ HexNAc ₆ Hex ₄	2296.8827
		1118.4148	1118.4131	1.52	[M-2H] ⁻²	A3F1G1S1, FA3G1S1	dHex ₁ HexNAc ₅ Neu5Ac ₁ Hex ₄	2238.8408
		1219.9666	1219.9528	11.31	[M-2H] ⁻²	FA3BG1S1	dHex ₁ HexNAc ₆ Neu5Ac ₁ Hex ₄	2411.9202
		1024.8574	1024.8709	13.17	[M-2H] ⁻²	A2G2S1	HexNAc ₄ Neu5Ac ₁ Hex ₅	2051.7563
18.37	15	1191.4359	1191.4421	5.20	[M-2H] ⁻²	A3F2G1S1, FA3F1G1S1	dHex ₂ HexNAc ₅ Neu5Ac ₁ Hex ₄	2384.8987
		1191.4005	1191.4239	19.64	[M-2H] ⁻²	A2G2S2Ac	HexNAc ₄ Neu5Ac ₂ Hex ₅ Ac	2384.8623
		1162.4175	1162.4393	18.75	[M-2H] ⁻²	FA2G1S2 (P)	dHex ₁ HexNAc ₄ Neu5Ac ₂ Hex ₄	2326.8568
		1004.8760	1004.8678	8.16	[M-2H] ⁻²	FM5A1F1G1	dHex ₂ HexNAc ₃ Hex ₆	2011.7502
		1097.9175	1097.8998	16.12	[M-2H] ⁻²	FA2G2S1, FA2F1G1Gc1	dHex ₁ HexNAc ₄ Neu5Ac ₁ Hex ₅ /dHex ₂ HexNAc ₄ Neu5Gc ₁ Hex ₄	2197.8142

Striatum tr (min)	Peak UPLC	Experimental mass (m,z)	Theoretical mass (m,z)	Error (ppm)	Ion	Assignment	Monosaccharide composition	Monoisotopic mass
19.85	16	919.3210	919.3230	2.18	[M-2H] ⁻²	M8	HexNAc ₂ Hex ₈	1840.6606
		1839.6235	1839.6105	7.07	[M-1H] ⁻¹			
		1170.9155	1170.9288	11.36	[M-2H] ⁻²	FA2F1G2S1	dHex ₂ HexNAc ₄ Neu5Ac ₁ Hex ₅	2343.8722
		1106.4060	1106.4075	1.36	[M-2H] ⁻²	M4A2F2G2	dHex ₂ HexNAc ₄ Hex ₆	2214.8296
		1243.4044	1243.3972	5.79	[M-2H] ⁻²	FA2G2S2, A2F1G2S2, FA2F1G1Gc1S1	dHex ₁ HexNAc ₄ Neu5Ac ₂ Hex ₅ / dHex ₂ HexNAc ₄ Neu5Gc ₁ Neu5Ac ₁ Hex ₄	2488.9097
		1199.4282	1199.4395	9.42	[M-2H] ⁻²	FA3G2S1, FA3F1G1Gc1	dHex ₁ HexNAc ₅ Neu5Ac ₁ Hex ₅ / dHex ₂ HexNAc ₅ Neu5Gc ₁ Hex ₄	2400.8936
		1264.4382	1264.4528	11.55	[M-2H] ⁻²	FA2G2S2Ac	dHex ₁ HexNAc ₄ Neu5Ac ₂ AcHex ₅	2530.9202
20.38	17	1098.4001	1098.4100	9.01	[M-2H] ⁻²	FA2F2G2, A2F3G2	dHex ₃ HexNAc ₄ Hex ₅	2198.8346
		1170.9086	1170.9288	17.25	[M-2H] ⁻²	FA2F1G2S1, FM4A1BF1G1S1, FA2F2G1Gc1, FA2F1G2S1	dHex ₂ HexNAc ₄ Neu5Ac ₁ Hex ₅ / dHex ₃ HexNAc ₄ Neu5Gc ₁ Hex ₄	2343.8722
		1243.3972	1243.3972	0.00	[M-2H] ⁻²	FA2G2S2, A2F1G2S2, FA2F1G1Gc1S1	dHex ₁ HexNAc ₄ Neu5Ac ₂ Hex ₅ / dHex ₂ HexNAc ₄ Neu5Gc ₁ Neu5Ac ₁ Hex ₄	2488.9097
		919.3086	919.3230	15.66	[M-2H] ⁻²	M8	HexNAc ₂ Hex ₈	1840.6606
20.85	18	1272.4739	1272.4685	4.24	[M-2H] ⁻²	FA3F1G2S1	dHex ₂ HexNAc ₅ Neu5Ac ₁ Hex ₅	2546.9515
		1199.9540	1199.9497	3.58	[M-2H] ⁻²	FA3F2G2, A2F2G1F1L1	dHex ₃ HexNAc ₅ Hex ₅	2401.9140

Striatum tr (min)	Peak UPLC	Experimental mass (m,z)	Theoretical mass (m,z)	Error (ppm)	Ion	Assignment	Monosaccharide composition	Monoisotopic mass
		1106.4020	1106.4075	4.97	[M-2H] ⁻²	FA2F1G2Gal	dHex ₂ HexNAc ₄ Hex ₆	2214.8296
		1284.4720	1284.4741	1.63	[M-2H] ⁻²	FA2GalNAc2S2	dHex ₁ HexNAc ₆ Neu5Ac ₂ Hex ₃	2570.9628
21.65	19	1199.9469	1199.9497	2.33	[M-2H] ⁻²	A2F3G1L1, A3F3G2	dHex ₃ HexNAc ₅ Hex ₅	2401.9140
		1170.4103	1170.4186	7.09	[M-2H] ⁻²	A2G2S2	HexNAc ₄ Neu5Ac ₂ Hex ₅	2342.8518
		1373.9714	1373.9900	13.54	[M-2H] ⁻²	FA4F1G2S1	dHex ₂ HexNAc ₆ Neu5Ac ₁ Hex ₅	2751.0513
		1243.4623	1243.4476	11.82	[M-2H] ⁻²	FA2G2S2	dHex ₁ HexNAc ₄ Neu5Ac ₂ Hex ₅	2488.9097
		1272.4739	1272.4685	4.24	[M-2H] ⁻²	FA3F1G2S1,FA3F2G1Gc1	dHex ₂ HexNAc ₅ Neu5Ac ₁ Hex ₅ /dHex ₃ HexNAc ₅ Neu5Gc ₁ Hex ₄	2546.9515
22.22	20	1000.3493	1000.3495	0.20	[M-2H] ⁻²	M9	HexNAc ₂ Hex ₉	2002.7135
		1301.4772	1301.4894	9.37	[M-2H] ⁻²	A4F3G2,FA4F2G2,FA2BF2G1L1	dHex ₃ HexNAc ₆ Hex ₅	2604.9904
		1374.0018	1373.9900	8.59	[M-2H] ⁻²	A3G3S2Ac,FA4F1G2S1,A4F2G2S1	dHex ₂ HexNAc ₆ Neu5Ac ₁ Hex ₅ /HexNAc ₅ Neu5Ac ₂ AcHex ₆	2750.0309
		1243.9397	1243.9578	14.55	[M-2H] ⁻²	FA2F2G2S1	dHex ₃ HexNAc ₄ Neu5Ac ₁ Hex ₅	2489.9301
		1316.4845	1316.4765	6.08	[M-2H] ⁻²	FA2F1G2S2, A2F2G2S2	dHex ₂ HexNAc ₄ Neu5Ac ₂ Hex ₅	2634.9676
		1170.4296	1170.4186	9.40	[M-2H] ⁻²	A2G2S2	HexNAc ₄ Neu5Ac ₂ Hex ₅	2342.8518
24.16	21	1316.4548	1316.4765	16.48	[M-2H] ⁻²	FA2F1G2S2, A2F2G2S2	dHex ₂ HexNAc ₄ Neu5Ac ₂ Hex ₅	2634.9676

Striatum tr (min)	Peak UPLC	Experimental mass (m,z)	Theoretical mass (m,z)	Error (ppm)	Ion	Assignment	Monosaccharide composition	Monoisotopic mass
		1389.9839	1390.0031	13.81	[M-2H] ⁻²	A4G4S1, FA4G3Gc1, A3BG3GalS1	HexNAc ₆ Neu5Ac ₁ Hex ₇ /dHex ₁ HexNAc ₆ Neu5Gc ₁ Hex ₆	2782.0207
		1243.4261	1243.4476	17.29	[M-2H] ⁻²	A2F1G2S2	dHex ₁ HexNAc ₄ Neu5Ac ₂ Hex ₅	2488.9097
		925.6566	925.6611	4.86	[M-3H] ⁻³	FA2G2S3(P), A2F1G2S3	dHex ₁ HexNAc ₄ Neu5Ac ₃ Hex ₅	2780.0051
24.37	22	1426.5369	1426.5239	9.11	[M-2H] ⁻²	FA2F2G2L1S1, FA3F2G3S1	dHex ₃ HexNAc ₅ Neu5Ac ₁ Hex ₆	2855.0623
		1499.0245	1499.0426	12.07	[M-2H] ⁻²	FA3F1G3S2,FA2F1G2L1S2	dHex ₃ HexNAc ₅ Neu5Ac ₁ Neu5Gc ₁ Hex ₅	3000.0998
		1080.3519	1080.3158	33.42	[M-2H] ⁻²	M9P2	HexNAc ₂ Hex ₉	2162.6464
26.14	23	1354.0109	1354.0051	4.28	[M-2H] ⁻²	FA3F3G3	dHex ₄ HexNAc ₅ Hex ₆	2710.0248
		1047.3575	1047.3718	13.65	[M-3H] ⁻³	A3F2G2Gc1S2(P),A3G3F1S3,F A3G3S3,FA3F1G2Gc1S2(P)	dHex ₂ HexNAc ₅ Neu5Gc ₁ Neu5Ac ₂ Hex ₅ /dHex ₁ HexNAc ₅ Neu5Ac ₃ Hex ₆	3145.1373
		1571.5760	1571.5614	9.29	[M-2H] ⁻²			
		1499.0166	1499.0426	17.34	[M-2H] ⁻²	FA3F1G3S2,FA2F1G2L1S2	dHex ₂ HexNAc ₅ Neu5Ac ₂ Hex ₆	3000.0998
		1115.0631	1115.0649	1.61	[M-3H] ⁻³	FA3BG3S3	dHex ₁ HexNAc ₆ Neu5Ac ₃ Hex ₇	3348.2166
		1528.0542	1528.0635	6.09	[M-2H] ⁻²	FA4F2G3S1	dHex ₃ HexNAc ₆ Neu5Ac ₁ Hex ₆	3058.1416
30.06	24	1169.0634	1169.0825	16.34	[M-3H] ⁻³	FA4G4S3, FA3G3L1S3,FA4F1G3Gc1S2(P)	dHex ₁ HexNAc ₆ Neu5Ac ₃ Hex ₇ /dHex ₂ HexNAc ₆ Neu5Gc ₁ Neu5Ac ₂ Hex ₆	3510.2695

Striatum tr (min)	Peak UPLC	Experimental mass (m,z)	Theoretical mass (m,z)	Error (ppm)	Ion	Assignment	Monosaccharide composition	Monoisotopic mass
		1754.1617	1754.1275	19.50	[M-2H] ⁻²			
		1096.0562	1096.0494	6.20	[M-3H] ⁻³	FA3F1G3S3	dHex ₂ HexNAc ₅ Neu5Ac ₃ Hex ₆	3291.1952
		1217.7324	1217.7324	0.00	[M-3H] ⁻³	FA4F1G4S3,FA4F2G3Gc1S2	dHex ₂ HexNAc ₆ Neu5Ac ₃ Hex ₇ / dHex ₃ HexNAc ₆ Neu5Gc ₁ Neu5Ac ₂ Hex ₆	3656.3274
		1681.1024	1681.0985	2.32	[M-2H] ⁻²	A4G4S3	HexNAc ₆ Neu5Ac ₃ Hex ₇	3364.2116
		1120.3706	1120.3966	23.21	[M-3H] ⁻³			
		1115.0838	1115.0649	16.95	[M-3H] ⁻³	FA3BG3S3	dHex ₁ HexNAc ₆ Neu5Ac ₃ Hex ₇	3348.2166
		1681.5735	1681.6087	20.93	[M-2H] ⁻²	FA4F1G4S2,FA4F2G3Gc1S1	dHex ₂ HexNAc ₆ Neu5Ac ₂ Hex ₇ / dHex ₃ HexNAc ₆ Neu5Gc ₁ Neu5Ac ₁ Hex ₆	3365.2320
30.58	25	1169.0845	1169.0825	1.71	[M-3H] ⁻³	FA4G4S3, FA3G3L1S3	dHex ₁ HexNAc ₆ Neu5Ac ₃ Hex ₇	3510.2695
		1754.1617	1754.1275	19.50	[M-2H] ⁻²			
		1266.1017	1266.1144	10.03	[M-3H] ⁻³	FA4G4S4, A4F1G4S4	dHex ₁ HexNAc ₆ Neu5Ac ₄ Hex ₇	3801.3649
		1682.1118	1682.1189	4.22	[M-2H] ⁻²	FA4F3G4S1	dHex ₄ HexNAc ₆ Neu5Ac ₁ Hex ₇	3366.2524
		1121.0916	1121.0768	13.20	[M-3H] ⁻³			
		1217.7180	1217.7324	11.83	[M-3H] ⁻³	FA4F1G4S3,FA4F2G3Gc1S2(P)	dHex ₂ HexNAc ₆ Neu5Ac ₃ Hex ₇ / dHex ₃ HexNAc ₆ Neu5Gc ₁ Neu5Ac ₂ Hex ₆	3656.3274

Striatum tr (min)	Peak UPLC	Experi mental mass (m,z)	Theoreti cal mass (m,z)	Error (ppm)	Ion	Assignment	Monosaccharide composition	Monoisotopic mass
31.34	26	1266.10 17	1266.114 4	10.03	[M-3H] ⁻³	FA4G4S4	dHex ₁ HexNAc ₆ Neu5Ac ₄ Hex ₇	3801.3649
		1217.72 52	1217.732 4	5.91	[M-3H] ⁻³	FA4F1G4S3 (P), FA4F2G3Gc1S2 (P)	dHex ₂ HexNAc ₆ Neu5Ac ₃ Hex ₇ / dHex ₃ HexNAc ₆ Neu5Gc ₁ Neu5Ac ₂ Hex ₆	3656.3274
		1314.80 32	1314.800 3	2.21	[M-3H] ⁻³	FA4F1G4S4	dHex ₂ HexNAc ₆ Neu5Ac ₄ Hex ₇	3801.3649
		1169.43 52	1169.422 7	10.69	[M-3H] ⁻³	FA4F2G4S2 (P)	dHex ₃ HexNAc ₆ Neu5Ac ₂ Hex ₇	3511.2899

S4.3 Summary of the techniques used in the glyco-analytical platform

Techniques	Analysis performed
HILIC-UPLC	Resolution of N-glycans, both neutral and charged, in different glycan peaks based on their differential elution
WAX-UPLC	Resolution and quantification of charged N-glycans
LC-MS	Cross-confirmation of the N-glycan moieties detected using HILIC-UPLC
Exoglycosidase digestions	Elucidation of the glycosidic linkages in the N-glycan moieties detected in HILIC-UPLC
Lectin histochemistry	Semi-quantitative and visual representation of modulation of N-glycosylation
MALDI-MSI	Visual and quantitative representation of the spatial resolution of N-glycosylation

2) Chapter 5:

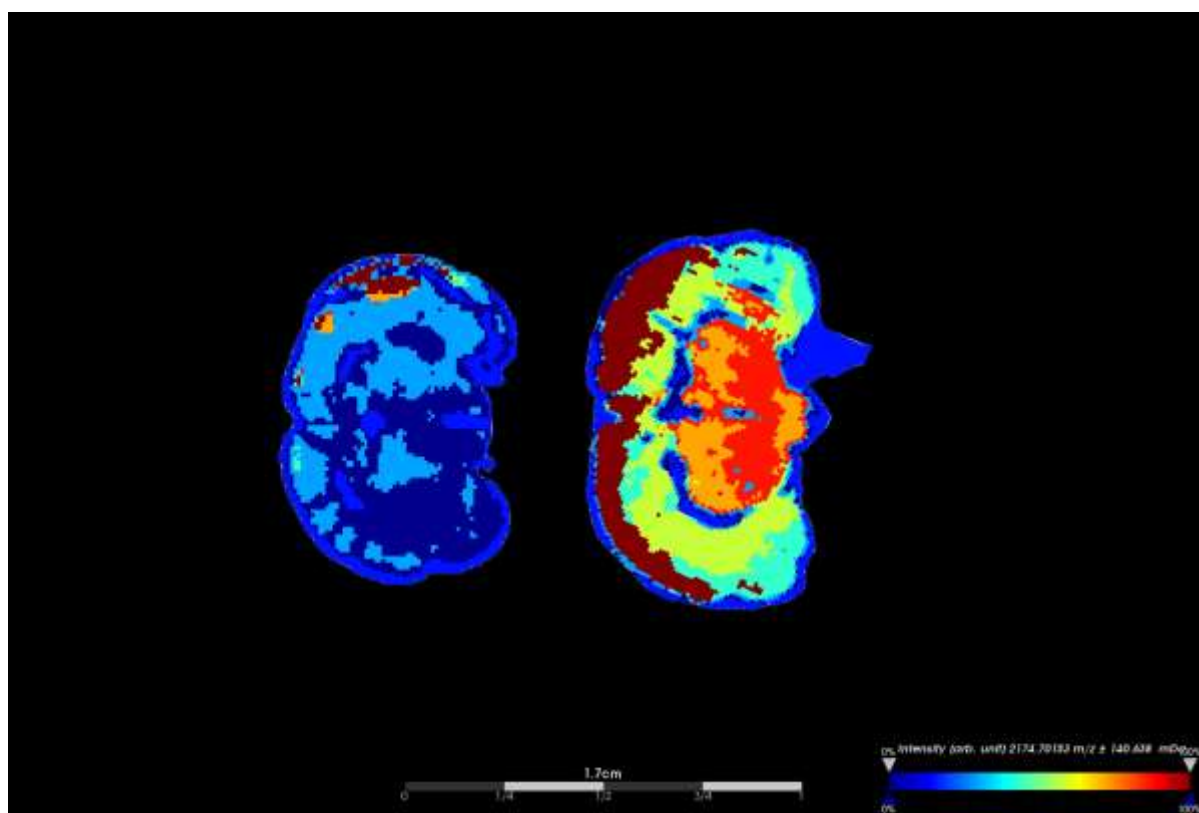


Figure S 5.1: **Segmentation analysis in SN for comparison between healthy and diseased brains.** Segmentation analysis representative of the differences in the N-glycan profiles of healthy and 6-OHDA PD brains. All the detected glycan classes have been regionally classified in the brain sections. The representative images are indicative of the significant shift in the glyco-phenotype of the PD brain from the healthy rodent brain.

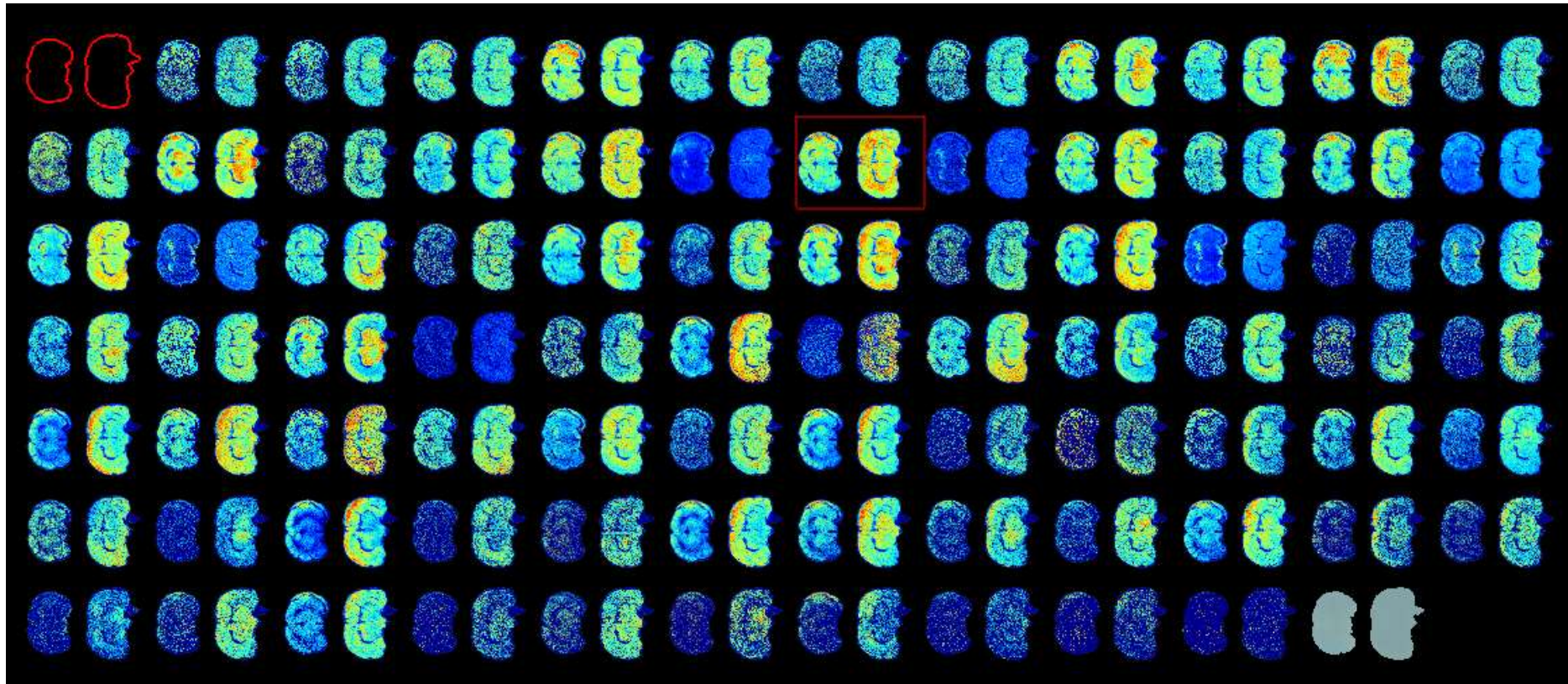


Figure S 5.2: **MALDI-MSI analysis of SN glyco-phenotype between healthy and diseased brains.** Panel of 83 N-glycans compared between healthy and Parkinsonian brains using MALDI-MSI showing the modulation of glyco-phenotype due to disease induction. Each set of two brains represents a healthy vs diseased control for each glycan that was investigated. Specific differences in the glycan expression patterns were quantified and reported based on this analysis (n=3). The image raaster was 150 μm .

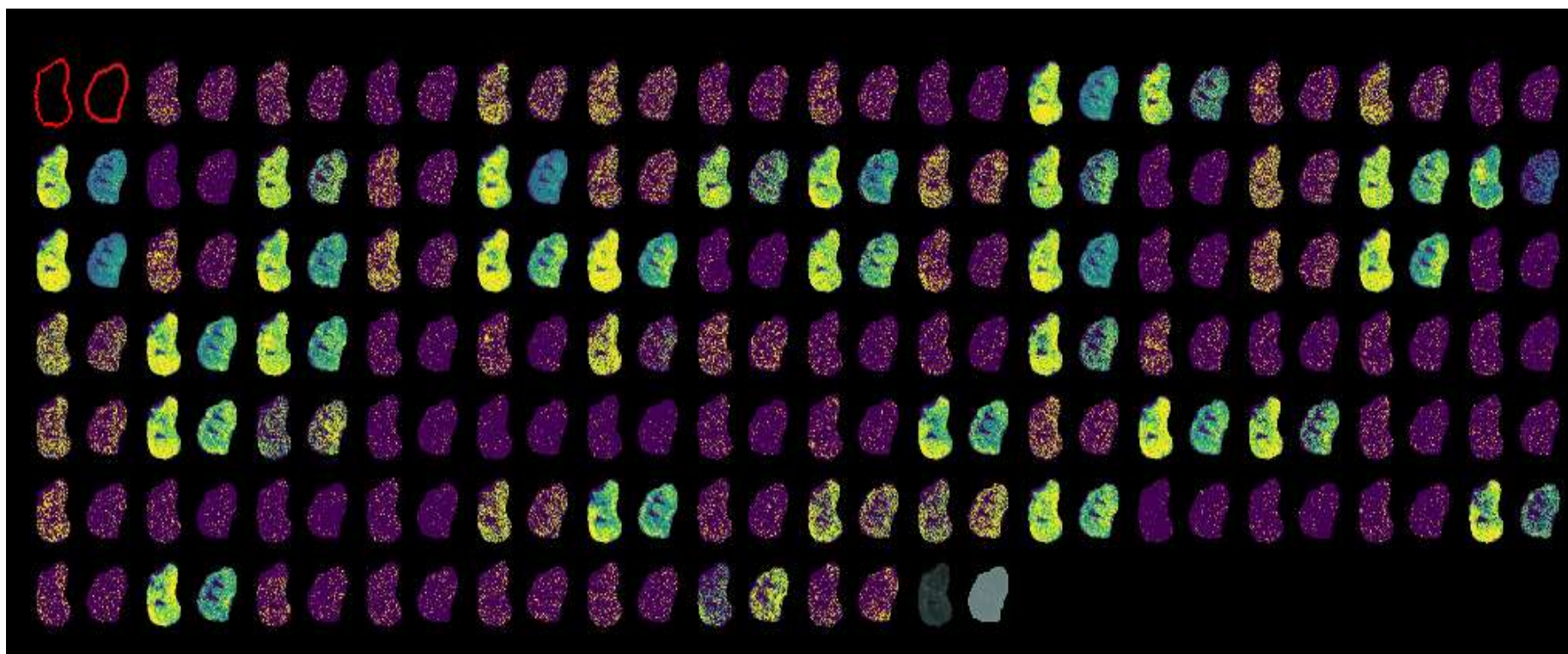


Figure S 5.3: **MALDI-MSI analysis of striatum glyco-phenotype between healthy and diseased brains.** Panel of 83 N-glycans compared between healthy and Parkinsonian brains using MALDI-MSI showing the modulation of glyco-phenotype due to disease induction. Each set of two brains represents a healthy vs diseased control for each glycan that was investigated. Specific differences in the glycan expression patterns were quantified and reported based on this analysis (n=3). The image raaster was 150 μ m.

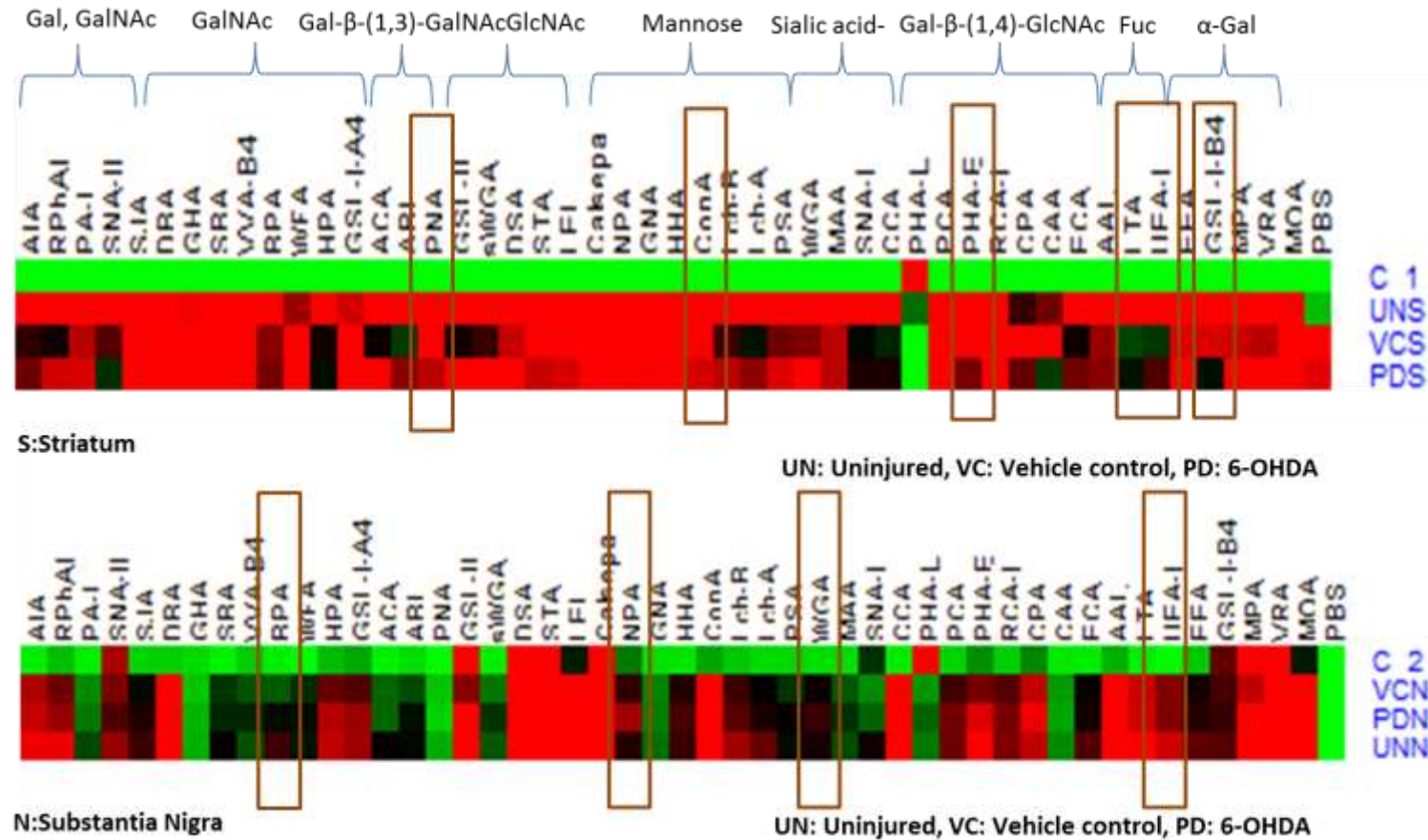


Figure S 5.4: **Lectin microarray analysis of glyco-phenotype between healthy and diseased rodent brains.** Lectin microarray analysis between the healthy and Parkinsonian brains representative of the N-glycan modulation with the induction of PD (S: Striatum, N: Substantia nigra; UN: Uninjured, VC: Vehicle control, PD: 6-OHDA Parkinsonian model)

3) Chapter 6:

6.6 Lectin histochemistry

Brains were dissected out and post-fixation was performed for four h at room temperature. They were then transferred to 25% sucrose in phosphate buffer. For lectin histochemistry, slides were washed with Tris-buffered saline supplemented with Ca^{2+} and Mg^{2+} (TBS; 20 mM Tris-HCl, 100 mM NaCl, 1 mM CaCl_2 , 1 mM MgCl_2 , pH 7.2) with 0.05% Triton X-100 (TBS-T) and then blocked with 2% periodate-treated BSA (Sigma-Aldrich) in TBS for one hour. All washes were three times for five minutes each, all steps performed at room temperature in a humidity chamber unless otherwise stated. Sections were washed then incubated with four different fluorescein isothiocyanate (FITC)- conjugated lectins (EY Labs Inc.) in TBS for one hour. Inhibitory controls were carried out in parallel to verify lectin binding specificity by pre- (for one hour) and co-incubating lectins in 100 mM of the appropriate haptenic sugar in TBS. Sections were washed five times with TBS-T and counterstained with 4' 6-diamidino-2-phenylindole dihydrochloride (DAPI) for 20 minutes. The slides were washed in TBS-T before mounting the coverslip with ProLong[®] Gold antifade (Life Technologies). Inhibition by the appropriate haptenic sugar was used as controls for all lectins in the study.

Lectin histochemical analysis

A panel of four lectins was selected based on their ability to bind to general mammalian-type glycans and represent the region-specific modulation of N-glycosylation in diseased, fibrin-in-fibrin intervention-treated and healthy animals. Lectin binding profiles to the PD brains and biomaterial-treated PD brains were used to investigate the modulation of glycosylation by the biomaterial intervention. For fucosylation, a differential binding profile was detected with the *Anguilla anguilla* lectin (AAA) in the PD brains compared to that of the healthy controls which remained unaffected with the fibrin-in-fibrin treatment (**Figure 6.9**). This lectin binds to Fuc- α -(1-6) and Fuc- α -(1-3) glycan moieties. Interestingly, this modulation was assumed to be very disease-specific as there was a significant difference in the binding profiles of the lectin from that of the injured and PD brains as elucidated in Chapter 5. This is suggestive of the fact that the biomaterial therapy might operate in a fucose-independent regulation pathway to mediate the functional recovery in the rodent model.

In lectin histochemical analysis, Concanavalin A lectin (ConA) is usually employed to detect the presence and localisation of N-linked glycosylation in the tissue as it shows preferential binding to α -linked mannose (Man) residues in the core structures of all N-linked glycans. An enhanced binding of Con A was detected in the diseased brains as compared to that of the healthy and injured controls. This lectin-binding profile was returned to a near-healthy spectrum through the application of the biomaterial intervention. Wheat germ agglutinin

(WGA) strongly binds to the microglial population [23] and hence it was upregulated in the PD brains. However, with the downregulation of the immune response as observed after the application of the biomaterial intervention, the WGA-binding profile was found to be very close to the healthy brains. GSA 1 β ₄ shows strong binding to the microglia and has been shown previously to differentiate between the resting and activated microglia [24]. Very interestingly, a downregulation of this lectin-binding was observed in the fibrin-in-fibrin treatment which also correlates well to the platform's ability to modulate terminal α -gal expression, which is a chief player in mediating the neuro-inflammation. This provides a fundamental proof-of-concept of the role of the *N*-glycosylation in the disease pathophysiology of PD and also represents the disease-attenuating interactions of the biomaterial intervention with the glycans cues in the brain to tune the glyco-phenotype towards a reparative spectrum.

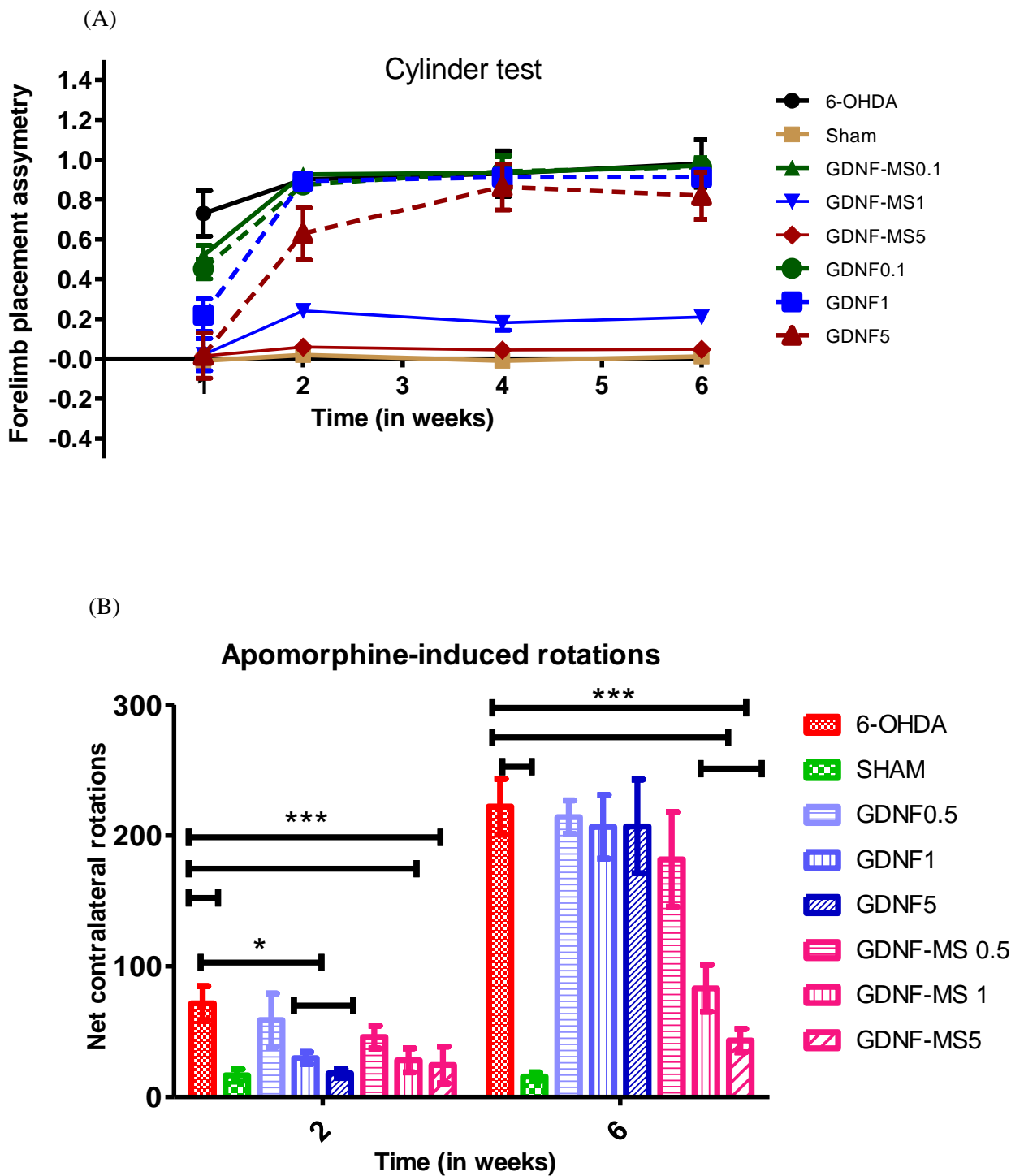


Figure S 6.1: Motor function analysis for the pilot study to investigate an optimal dose of GDNF-loaded microsphere-in-fibrin gel for promoting graft survival (a) Cylinder test and (b) Apomorphine-induced rotations demonstrating that microspheres loaded with 5 μ g of GDNF result in a better functional recovery when compared to bolus GDNF injections and the other encapsulated and bolus doses.

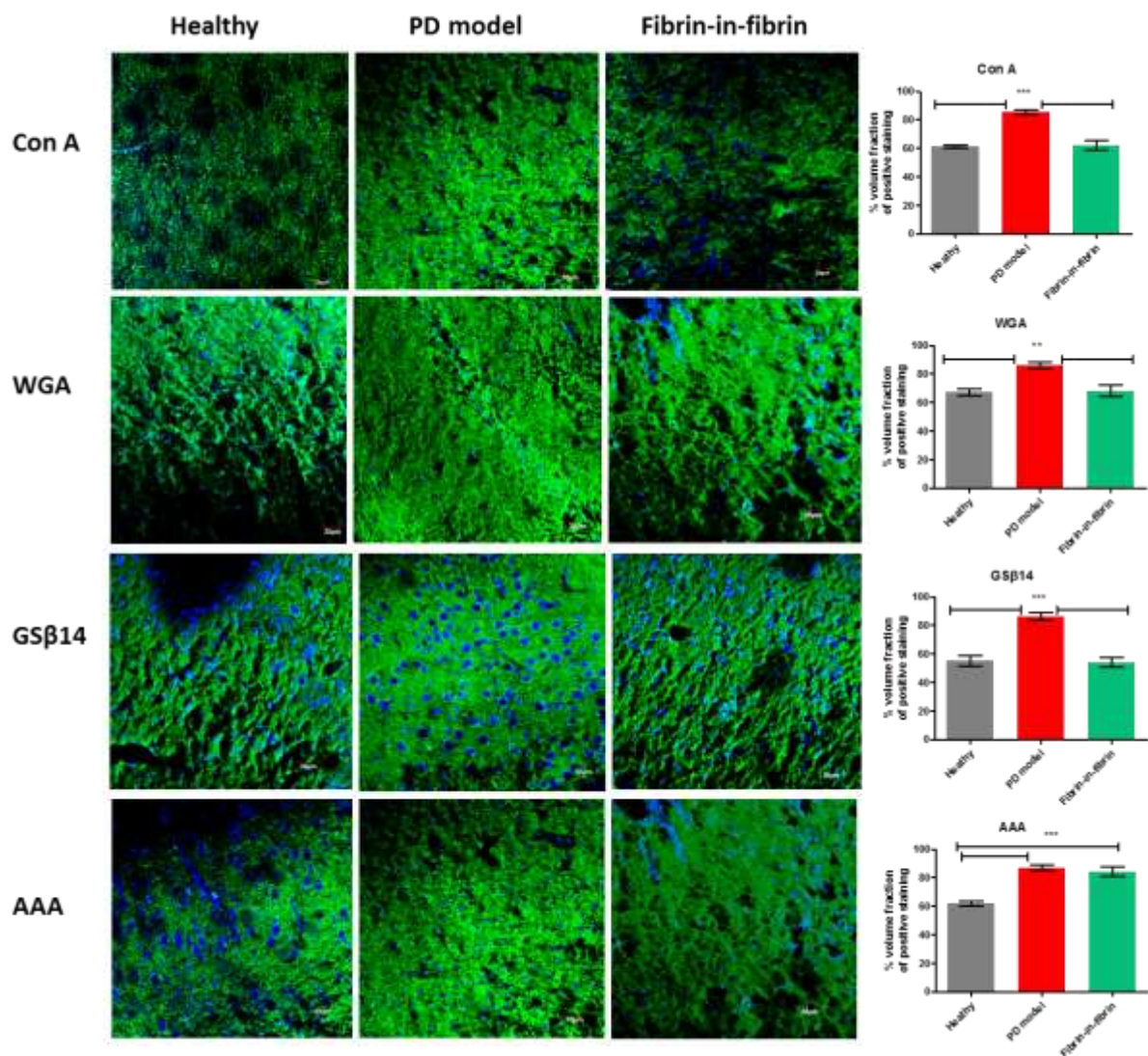


Figure S 6.2: Lectin histochemical analysis for N-glycosylation modulation by the biomaterial intervention. Representative lectin micrographs and quantified positively stained volumetric analysis showing the differential modulation of glycosylation by the induction of PD and impact of the biomaterial intervention on this modulation. There is a significant upregulation in the mannosylation, sialylation, terminal α -Gal and fucosylation as detected by enhanced Con A, WGA, GS-1 β 4 and AAA binding to the PD brains. Therapeutic fibrin-in-fibrin intervention restores the glyco-phenotype towards the healthy brain with the exception of the modulation of fucosylation, where it has no apparent impact. Data are represented as mean \pm SD and were analysed by one-way repeated measures ANOVA with *post-hoc* Dunnett's test. (* p <0.05, ** p <0.01, *** p <0.001)

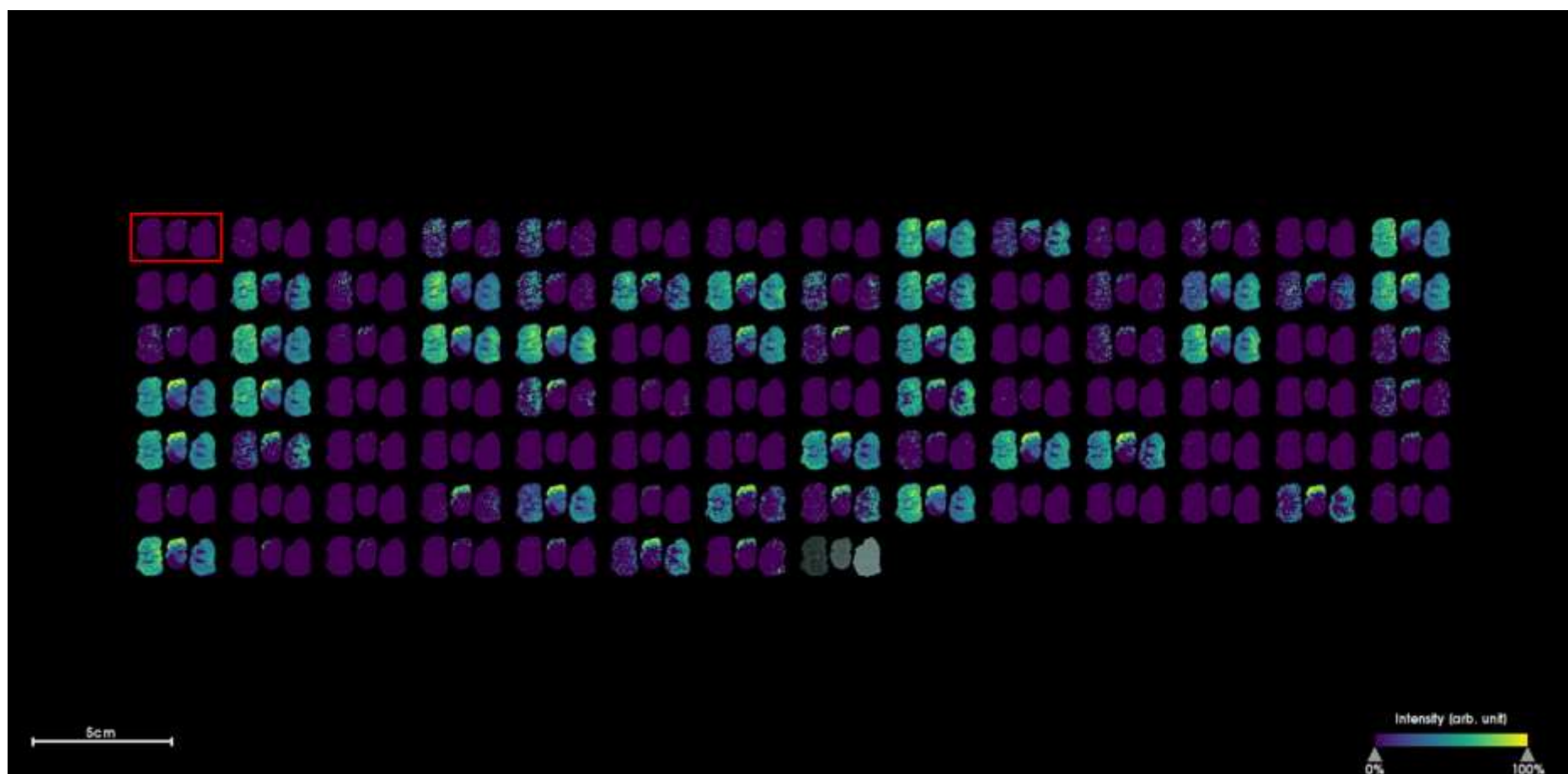


Figure S 6.3: **MALDI-MSI analysis for N-glycosylation modulation in striatum by the biomaterial intervention.** Panel of 83 N-glycans compared between healthy, Parkinsonian and fibrin-in-fibrin treated rat brains using MALDI-MSI showing the modulation of glyco phenotype due to disease induction. Each set of three brains represents a healthy, diseased and biomaterial-treated rat brain for each glycan that was investigated. Specific differences in the glycan expression patterns were quantified and reported based on this analysis (n=3). The image raster was 150 μm .

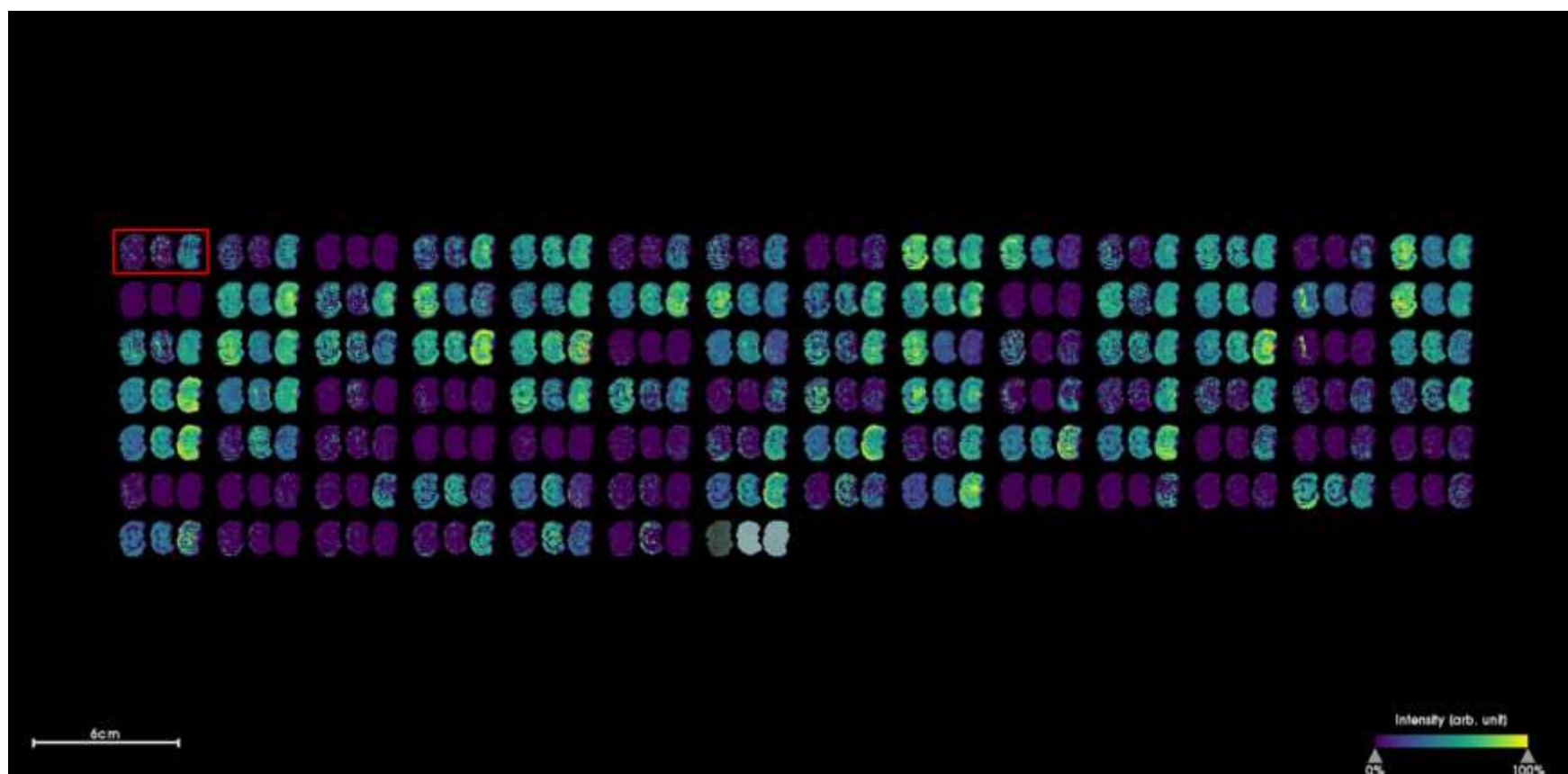


Figure S 6.4: MALDI-MSI analysis for N-glycosylation modulation in SN by the biomaterial intervention. Panel of 83 N-glycans compared between healthy, Parkinsonian and fibrin-in-fibrin treated rat brains using MALDI-MSI showing the modulation of glyco phenotype due to disease induction. Each set of three brains represents a healthy, diseased and biomaterial-treated rat brain for each glycan that was investigated. Specific differences in the glycan expression patterns were quantified and reported based on this analysis (n=3). The image raaster was 150 μm .

S. Journal Publications, Conference Proceedings and Awards*Journal Publications (published)*

1. **Samal J**, Hoban DB, Naughton C, Concannon R, Dowd E, Pandit A (2015). Fibrin-based microsphere reservoirs for delivery of neurotrophic factors to the brain. *Nanomedicine* 10 (5), 765-783.
2. Murab S, **Samal J**, Shrivastava A, Ray AR, Pandit A, Ghosh S (2015). Glucosamine loaded injectable silk-in-silk integrated system modulate mechanical properties in bovine ex-vivo degenerated intervertebral disc model. *Biomaterials* 55, 64-83.
3. **Samal J**, Rebelo AL, Pandit A (2019). A window into the brain: tools to assess preclinical efficacy of biomaterials-based therapies on central nervous system disorders. *Advanced Drug Delivery Reviews* (in press).

Journal Publications (in preparation)

1. Samal J., Saldova R., Pandit A., Flaherty R.O'. Complete spatial characterisation of rodent brain N-glycans
2. Samal J., Black A., Cabre S., Flaherty R.O', Dowd E., Drake R., Pandit A. Modulation of brain glycosylation with induction of Parkinsonism
3. Samal J., Abbah S.A., Lucia A.R., Black A., Drake R., Pandit A. Fibrin-in-fibrin intervention for enhanced graft survival in PD: Special focus on brain N-glycans.

Book Chapter:

1. **Samal J**, Demir S, Pandit A (2018). Cellular Capsules for Drug Delivery in Parkinson's disease In *Drug Delivery Nanosystems for Biomedical Applications*, 91-151

Conference Proceedings

1. Samal J, Moriarty N, Cabre S, Alamilla V, Saldova R, Rudd PM, O'Flaherty R, Dowd E, Pandit A. Tuneable Fibrin-in-Fibrin System for Improved Survival of Dopaminergic Progenitors with a Focus on Spatial Characterisation and Modulation of Brain N-Glycans in Response to 6-OHDA Induced Parkinsonism. **Gordon Research Conference** in Signal Transduction by Engineered Extracellular Matrices, Andover, USA, 2018 (Oral presentation in associated GRS).
2. Samal J, O'Flaherty R, Saldova R, Rudd PM, Pandit A. Complete Spatial Characterization of N-glycans in an Adult Rat Brain. 29th ICS Lisbon, Portugal, 2018 (Oral presentation)
3. Samal J, O'Flaherty R, Saldova R, Rudd PM, Pandit A. Complete Spatial Characterisation of N-glycans in an Adult Rat Brain. Matrix Biology Ireland, Trinity College Dublin, Dublin, Ireland (Rapid-Fire presentation).

4. Samal J, Hoban DB, Moriarty N, Naughton C, Concannon R, Pandit A. Tuneable Fibrin-In-Fibrin System for Improved Survival of Dopaminergic Progenitors. Gordon Research Conference in Biomaterials & Tissue Engineering, Holderness School, Holderness, NH, 2017 (Accepted for poster presentation)
5. Samal J, Moriarty N, Kilcoyne M, Dowd E, Pandit A. Characterization of Tissue Glycosignature in Healthy, Injured and 6-OHDA-induced Parkinsonian Brains. Matrix Biology Ireland, 2016 (Oral presentation)
6. Samal J, Hoban DB, Naughton C, Concannon R, Dowd E, Pandit A. Delivery of Neurotrophic Factors to the Brain using Fibrin-based Hollow Microsphere Reservoirs. 27th European Conference on Biomaterials ESB2015, Krakow, Poland (Oral presentation)
7. Samal J, Moriarty N, Hoban DB, Naughton C, Concannon R, Dowd E, Pandit A. Fibrin-based Hollow Microsphere Reservoirs for Controlled Delivery of Neurotrophic Factors to the Brain. 4th TERMIS World Congress, Boston, USA (Oral presentation)
8. Samal J, Dowd E, Pandit A. Fibrin-based Microsphere Reservoirs for Delivery of Neurotrophic Factors. 26th Annual conference, European Society of Biomaterials. Liverpool,UK,2014 (Oral presentation)
9. Samal J, Dowd E, Pandit A. Fibrin-based Microsphere Reservoirs for Delivery of Neurotrophic Factors. 24th annual meeting, Network for European CNS Transplantation & Restoration, NECTAR(Data Blitz)
10. Samal J, Hoban DB, Naughton C, Concannon R, Dowd E, Pandit A. Fibrin-based Microsphere Reservoirs for Delivery of Neurotrophic Factors to the Brain. Biochemical society Annual meeting, protein interactions in biology, 2015 (Oral presentation)
11. S Murab, J Samal, A Shrivastava, AR Ray, A Pandit, S Ghosh. Injectable Silk-In-Silk System Loaded with Glucosamine Modulate Mechanical Properties in Bovine Exvivo Degenerated Intervertebral Disc (IVD) Model. 4th TERMIS World Congress, Boston, USA, 2015 (Poster presentation)
12. S Murab, J Samal, A Shrivastava, AR Ray, A Pandit, S Ghosh. An Injectable Silk-in-Silk System for Enhanced Proteoglycan Production. 26th Annual conference, European Society of Biomaterials. Liverpool,UK,2014 (Oral presentation)

Awards

1. Registration award from GRC at STEEM GRC, Andover, NH (2018)
2. Hardiman Fellowship (NUIG, Ireland), 2013-2017
- 3.
4. Best Rapid-fire Presentation Award in Matrix Biology Ireland, Trinity College Dublin, Dublin, Ireland (2017)

5. Best Oral Presentation Award amongst over 400 podium presentations in 27th European Conference on Biomaterials (ESB), Krakow, Poland (2015)
6. Awardee of NSF Travel Grant for 2015 TERMIS World Congress, Boston, USA